

**EVALUATING THE POTENTIAL FLAVONOIDS  
BASED NANO-FORMULATIONS AS ANTICANCER  
ACTIVITY AGAINST LUNG CANCER**

Thesis Submitted for the Award of the Degree of

**DOCTOR OF PHILOSOPHY**

in

**Bioinformatics**

By

**Swati Arora**

**Registration Number: 12009878**

**Supervised By**

**Dr. Himanshu Singh (11691)**

**School of Bioengineering and  
Biosciences (Associate Professor &  
Head)**

**Lovely Professional University**

**Supervised By**

**Dr. Sugunakar Vuree**

**Indo-American Cancer Research  
Foundation, Basavatarakam Indo-  
American Cancer Hospital and  
Research Institute, Hyderabad  
(Principal Scientist & Liaison  
Officer)**



**LOVELY PROFESSIONAL UNIVERSITY, PUNJAB**

**2024**

## **DECLARATION**

I, hereby declare that the presented work in the thesis entitled “**Evaluating the Potential Flavonoids based Nano-formulations as Anticancer Activity against Lung Cancer**” in fulfilment of the degree of **Doctor of Philosophy (Ph.D.)** is the outcome of research work carried out by me under the supervision of **Dr. Himanshu Singh**, working as **Associate Prof.** in the **School of Bioengineering and Biosciences** of **Lovely Professional University, Punjab, India**. In keeping with the general practice of reporting scientific observations, due acknowledgements have been made whenever the work described here has been based on the findings of other investigators. This work has not been submitted in part or full to any other University or Institute for the award of any degree.



**(Signature of Scholar)**

Name of the scholar: Swati Arora

Registration No.: 12009878

Department/School: School of Bioengineering and Biosciences

Lovely Professional University,

Punjab, India

## CERTIFICATE

This is to certify that the work reported in the Ph.D. thesis entitled “**Evaluating the Potential Flavonoids based Nano-formulations as Anticancer Activity against Lung Cancer**” submitted in fulfilment of the requirement for the award of the degree of **Doctor of Philosophy (Ph.D.)** in the **Bioinformatics** Discipline, **School of Bioengineering and Biosciences**, is a research work carried out by **Swati Arora, 12009878**, is a bonafide record of his/her original work carried out under my supervision and that no part of the thesis has been submitted for any other degree, diploma or equivalent course.



**(Signature of Supervisor)**

Name of supervisor: Dr. Himanshu Singh

Designation: Associate Professor

Department/School: SBES

University: LPU, Jalandhar



**(Signature of Co-Supervisor)**

Name of Co-Supervisor: Dr. Sugunakar

Vuree

Designation: Principal Scientist & Liason  
Officer

University: Indo-American Cancer  
Research Foundation, Basavatarakam  
Indo-American Cancer Hospital and  
Research Institute, Hyderabad

## ABSTRACT

Lung cancer (LC) is the most commonly diagnosed form of cancer and the leading contributor to cancer-related fatalities across the globe. In India, LC represents 5.9% of all cancer cases and contributes to 8.1% of all cancer-related deaths. Notably, approximately 80% of LC patients have a smoking history. Within the realm of lung cancer, pivotal components of cellular signalling pathways, such as receptor tyrosine kinases (RTKs), protein kinase C (PKC), and the Ras/mitogen-activated protein kinase (MAPK) systems, are frequently disrupted in lung cancer cells due to oncogene-driven overexpression or mutations. This disruption results in the dysregulation of cell signalling and uncontrolled cell proliferation. While the national and international markets offer a range of treatment options, including antagonists and agonists, they often induce severe side effects and can ultimately lead to remission and resistance. Therefore, the imperative lies in exploring innovative, side-effect-free approaches to effectively combat LC, overcoming the challenges.

Phytomedicines are renowned for their multifaceted impact on cellular biomarkers linked to various stages of carcinogenesis. These compounds are celebrated for their health-enhancing properties. Consequently, our study sought to investigate the chemo preventive capabilities of specific flavonoids. However, these promising agents face low bioavailability, solubility issues, and short half-life. To surmount these hurdles, we turned to nano-based emulsions as a source of drug administration for increased efficacy. By leveraging nano-based emulsions, we aimed to enhance the effectiveness and delivery of these flavonoids, thereby addressing their limitations and optimizing their potential.

Nanoformulation provide self-assembled and building materials that could develop entirely innovative devices, which may lessen the noxiousness along the development of drug delivery treatments and their efficacies. It provides us with the platform to study these nanomaterials during the early stages of cancer progression. Tremendous applications of metal nanoparticles are envisaged in anticancer, antibacterial, antioxidant, antidiabetic, and anti-inflammatory activities, as well as for drug delivery and bioimaging applications. Nano-sized molecular tools can



potentially increase the selectivity and potency of chemical, physical, and biological approaches for stimulating cancer cell death while minimizing toxicity to healthy cells.

Molecular docking is a two-step technique that starts with ligand conformational changes in the active area of the receptors. Then, depending on the relative interaction conformational energy for each interaction confirmation, as per their binding score and affinity. We employ GOLD and GLIDE for molecular docking because of their performance, precision, adaptability, and extensive analysis. Our virtual screening tests are premised on the hypothesis that flavonoids may decrease LC genesis and progression by interfering with objectives. We deploy flavonoids against specific targets, such as EGFR and ROS1.

When designing novel pharmaceutical substances, pharmacokinetic variables are among the most crucial things to consider. Any product intended for use as a medication must possess the highest levels of biological activity and pharmacokinetic properties. Pgp (p-glycoprotein), found in the liver and vital for drug discovery and development, functions as an efflux pump regarding pharmacokinetic properties. They permit the prioritisation and selection of interesting molecules for future experimental study. Adhering to Lipinski's rule facilitates the identification of substances with better odds of favourable pharmacokinetic characteristics and increased possibilities of drug development success. Molecular dynamic simulations have been undertaken to evaluate the dynamic and solvent influence of the ligands-receptor complex.

The present work identified a novel flavonoid, Diosmin and Hesperidin, as a potential candidate against LC. This study investigates anticancer activity by employing Insilico and In vitro techniques. We used Molecular Docking analysis, suggesting that Diosmin and Hesperidin inhibit ROS1 and EGFR, respectively. Further, we used ADME and drug-like properties and found it obeys all the Lipinski rules and has efficacy in inhibiting Pgp protein. Pgp protein is located in the liver and works as an efflux pump. If the drug candidate inhibits Pgp, it has high bioavailability and a high half-life. Further, Nano-formulations, i.e., Silver, Zinc and Graphene oxide, are utilised to enhance the efficiency of Diosmin and Hesperidin

and tested on A549 cell lines by performing MTT assay and Scratch assay and found  $IC_{50}$  25 $\mu$ g/ml on A549 for both the compounds. In case of scratch assay, we induced 25 $\mu$ g/ml and it stops the migration at 24hr time interval. So, we conclude that both the compounds having potential to inhibit LC and also migration of cancer cells.

Moreover, following a thorough cytotoxicity evaluation, we chose Hesperidin for expression analysis utilizing LC-MS, the applications for LC-MS can be categorized as either quantitative or qualitative. In qualitative analysis, unknown components found in often complicated sample combinations are separated and identified. Quantitative analysis counts the amounts of particular, well-known chemical substances. Our inquiry delved into network pharmacology, shedding light on the intricate interplay between flavonoids and molecular targets, emphasizing their relevance in the context of LC.

In summary, our comprehensive data analysis strongly suggests that Hesperidin holds promise as a ground breaking therapeutic avenue for LC. It has the potential to serve as a more effective and better-tolerated alternative to existing treatment methods, offering a significant advancement in the field of cancer therapeutics.

## PREFACE

The present thesis entitled “**Evaluating the Potential Flavonoids based Nano-formulations as Anticancer Activity against Lung Cancer**” encompasses the details of the studies undertaken and analyses of results obtained under 5 major chapters as described below:

**Chapter 1 - Introduction & Objectives:** This chapter includes a brief introduction and objectives designed to address the novel treatment option to treat lung cancer, the Hypothesis and objectives of the study.

**Chapter 2 - Review of Literature:** This chapter summarizes the present literature available, anatomy of the lung cancer, cause and risk factors, and flavonoids utilized for the treatment of lung cancer.

**Chapter 3 - Methodology:** It includes the details of various experimental materials, procedures and protocols that were employed in order to accomplish the objectives.

**Chapter 4- Results And Discussion:** It includes the details of the results of the experiments and the conclusion of the study.

**Chapter 5 – Significance of the study:** This chapter briefly tells the significance of the work that has been presented in this thesis.

**Bibliography:** This chapter contains citations of references used in the present investigation.

## ACKNOWLEDGMENTS

Completing my Ph.D. thesis was an incredibly challenging journey, akin to riding a roller coaster. However, the experience was immensely rewarding. Today, I stand with a deep sense of privilege as I express my heartfelt gratitude to all those who played a part, big or small, in helping me achieve this milestone. Their support and contributions have transformed my Ph.D. experience into a cherished memory that I will carry with me forever.

Foremost, my gratitude extends to the divine presence of God Almighty, whose intricate plan has guided every step of my journey.

I extend my deepest gratitude to my Co-supervisor, **Dr. Sugunakar Vuree**, Principal Scientist at Indo-American Cancer Research Foundation, Basavatarakam Indo-American Cancer Hospital and Research Institute, Hyderabad and my Supervisor, **Dr. Himanshu Singh**, Associate Professor at the School of Bioengineering and Biosciences, Lovely Professional University (LPU), Punjab, India. I consider myself incredibly fortunate to have had a supervisor and Co-supervisor of such exceptional calibre. Their unwavering support granted me the freedom to explore and work independently, shaping my research in ways that were truly my own.

**Dr. Vuree's** efforts, motivation, and patience were instrumental in helping me surmount numerous challenges throughout my Ph.D. journey. His constructive criticism not only honed my research skills but also provided a delicate balance between my professional and personal life. The impact of their contributions on every aspect of my research and Ph.D. thesis writing is immeasurable. Words, no matter how heartfelt, can scarcely capture the depth of my gratitude for their invaluable guidance and unwavering support.

I am deeply indebted to my supervisor, **Dr. Himanshu Singh**, and my co-supervisor, **Dr. Sugunakar Vuree**, whose unwavering encouragement, guidance, and steadfast support have been the cornerstone of this endeavour. Their invaluable contributions have been instrumental in shaping this work into its final form. I hold profound respect for their expertise and insight, and I am truly grateful for the transformative

suggestions provided during our scientific discussions. These interactions have played a pivotal role in my growth as an independent researcher. This work stands as a testament to their mentorship and dedication, and I recognize the significant debt of gratitude I owe to them.

I am also deeply thankful for the invaluable assistance provided by **Dr. Atul Kumar Upadhyay**, Assistant Professor at TIET, Patiala, Punjab, India, during my project training, particularly in the realm of Insilco work. His guidance was indispensable, and I am truly indebted for his unwavering support, encouraging words, and timely discussions whenever I sought his expertise. His contributions significantly enriched my research experience, and I am sincerely appreciative of his generosity and mentorship.

I am profoundly grateful for the guidance and supervision provided by **Dr. Neeraj Kumar Kamra**, Assistant Professor at Bhuple's Nobel College of Pharmacy, Udaipur, Rajasthan, India, **Dr. Dhamodharan Prabhu**, Assistant Professor at Karpagam Academy of Higher Education, Coimbatore especially in the realm of Molecular Simulation work. His expertise and support have been invaluable, and I am deeply indebted for his kind words, timely discussions, and unwavering assistance whenever I needed guidance. His mentorship has significantly enhanced my understanding of the subject, and I am sincerely appreciative of his contributions to my research journey.

I am sincerely thankful to **Dr. Tushinder Preet Kaur**, Professor and Assistant Dean at Mittal School of Business LPU, for her invaluable support and motivation during the crucial final stages of my Doctoral journey.

I extend my heartfelt gratitude to **Dr. Neeta Raj Sharma**, Associate Dean of the School of Bioengineering and Biosciences, for her unwavering support and guidance. Additionally, my sincere thanks go to the esteemed leaders of Lovely Professional University, including **Mr. Ashok Mittal**, Chancellor of LPU, **Mrs. Rashmi Mittal**, Pro Chancellor of LPU, **Dr. Lovi Raj Gupta**, Pro Vice Chancellor of LPU, and **Dr. Monica Gulati**, Registrar of LPU. Their visionary approach encapsulated in the motto 'Think Big,' coupled with their motivation and support, have been

instrumental in shaping my academic journey. I am truly appreciative of their inspiring leadership and encouragement.

I wish to extend my deepest gratitude to my family for their unwavering financial support, constant encouragement, and loving presence throughout my academic journey. My heartfelt thanks go to my mother, **Mrs. Sucheta Kumari**, and my father, **Mr. Rajinder Kumar**, whose unconditional love, sacrifices, and nurturing care have been my pillars of strength. They have surrounded me with warmth, provided me with every opportunity, and supported me in ways words can hardly express, allowing me to pursue my dreams with confidence and determination.

I am sincerely grateful to my Badi Maa (Nani), **Pushpa Rani**, whose constant hope and eagerness to hear positive updates about my doctoral journey inspired me to keep striving for success.

I am deeply grateful to my elder brother, **Mr. Kunal Kumar**, whose cheerful presence, unwavering support, and heartfelt prayers for my success inspired me to give my best throughout my doctoral journey. Additionally, I want to express my sincere appreciation to my lab mates, **Sumit Sheoran, Dinesh Bejanki** and others. Their care, love, and unwavering support were instrumental in creating a positive and nurturing environment, allowing me to thrive. Their presence made my academic journey not just bearable but enjoyable, and for that, I am profoundly thankful.

I would like to extend my sincere gratitude to our diligent lab attendants, **Ms. Sandeep Kour** and **Mr. Parveen**, for their exceptional cooperation and invaluable guidance. I consider myself privileged to work alongside **Mr. Sumit Sheoran**, whose unwavering support has been a constant source of motivation. Furthermore, I express my heartfelt thanks to **Ms. Sandeep Kour, Mr. Kuldeep Singh**, and **Mr. Sunny Gupta** for their prompt and efficient supply of essential lab materials and glassware for our experiments. Their timely assistance has significantly contributed to the smooth progress of our research endeavours.

  
**Swati Arora**

## TABLE OF CONTENTS

Title	i
Declaration	ii
Certificate	iii
Abstract	iv
Preface	vii
Acknowledgement	viii
Table of Contents	xi
List of Tables	xvi
List of Figures	xxi

S.No.	Title	Page No.
<b>1.</b>	<b>Chapter 1 – Introduction</b>	<b>1 – 33</b>
1.1	Cancer	1
1.2	Causes of Cancer	1
1.3	Types of Cancer	3
1.4	Cancer Cycle	4
1.5	Lung Cancer	6
1.6	Phytomedicines and Lung Cancer	16
1.7	Role of Flavonoids in Cancer Chemoprevention	17
1.8	Bioavailability and Metabolism of FL	18
1.9	The Epidemiology of Flavonoids in Relation to Cancer	23
1.10	Are Flavonoids Safe for Human Use?	25
1.11	Diosmin	28
1.12	Hesperidin	30
1.13	Hypothesis	31
1.14	Aim & Objective	32

<b>S.No.</b>	<b>Title</b>	<b>Page No.</b>
<b>2.</b>	<b>Chapter 2 – Review of Literature</b>	<b>34 – 63</b>
2.1	Carcinogens	35
2.2	Carcinogenesis	36
2.3	Cell Cycle	36
2.4	Induction of Apoptosis in Human Cancer Cells	37
2.5	Lung Cancer	38
2.6	Epidemiology	40
2.7	Etiology	40
2.8	Types and Staging of LC	41
	2.8.1 NSCLC	42
	2.8.2 SCLC	43
2.9	LC and Grading	44
2.10	Pathogenesis	45
2.11	Risk Factors	46
2.12	Symptoms of LC	48
	2.12.1 Symptoms related to Metastasis	49
	2.12.2 Paraneoplastic Symptoms	49
	2.12.3 Non-Specific Symptoms	49
2.13	Prevention	50
2.14	Diagnosis of LC	51
2.15	Histological Confirmation	52
2.16	Evaluating the Extent of Disease	52
2.17	Treatment of NSCLC	53
	2.17.1 Treatment of Early Stage (Stage I and Stage II) NSCLC	54



<b>S.No.</b>	<b>Title</b>	<b>Page No.</b>
2.17.2	Treatment of Stage III NSCLC	54
2.17.3	Treatment of Stage IV Non-Small Cell LC	55
2.17.4	Towards EGFR Tyrosine Kinase Inhibitors (first line)	55
2.18	EGFR Inhibitors for Recurrent NSCLC	56
2.19	Treatment of SCLC	56
2.19.1	Targeted therapies in SCLC	58
2.20	Prognosis	58
<b>3.</b>	<b>Chapter 3: Methodology</b>	<b>64 – 91</b>
3.1	Introduction	64
3.2	Materials	65
3.3	Cell Culture Maintenance	66
3.4	Collection of Compounds	66
3.4.1	Diosmin	67
3.4.2	Hesperidin	67
3.4.3	ROS1	68
3.4.4	EGFR	68
3.5	In Silico Studies	69
3.5.1	Introduction	69
3.5.2	Computational Studies for Drug Analysis	71
3.5.3	Natural Compounds	71
3.6	Methods utilized for In-silico Analysis	71
3.6.1	ROS1	71
3.6.2	EGFR	72
3.7	Methods Utilized for In-vitro Analysis	79

<b>S.No.</b>	<b>Title</b>	<b>Page No.</b>
3.7.1	Materials and Instruments	79
3.7.2	Nano-formulation	80
3.7.3	Characterization of the developed Nano-formulation	83
3.7.4	Biological Assays	84
3.7.5	LCMS Analysis	89
<b>4.</b>	<b>Chapter 4 – Results and Discussions</b>	<b>92 – 195</b>
4.1	In silico Studies	92
4.1.1	ADMET and Drug related Properties of Hesperidin	92
4.1.2	Virtual Screening and Molecular Docking Analysis (ROS1)	95
4.1.3	DFT Analysis	97
4.1.4	ADME Analysis	98
4.1.5	Boiled Egg Plot Analysis	99
4.1.6	Molecular Simulation Evaluation	100
4.1.7	Protein Secondary Structure	103
4.1.8	Virtual Screening and Molecular Docking Analysis (EGFR)	105
4.1.9	DFT Analysis	107
4.1.10	ADME Evaluation	108
4.1.11	Boiled Egg Plot Analysis	110
4.1.12	Evaluation of Molecular Dynamics Simulation	111
4.1.13	Ligand Torsion Profile and Properties	114
4.1.14	Protein Secondary Structure	116
4.2	Characterization of Diosmin	118

<b>S.No.</b>	<b>Title</b>	<b>Page No.</b>
4.2.1	FTIR (Fourier Transform Infrared)	118
4.2.2	NMR	119
4.2.3	DSC	120
4.2.4	XRD	121
4.2.5	Characterization of Hesperidin	123
4.2.6	Pre-Nano Formulations	128
4.3	Biological Assay of (Pure) Diosmin	153
4.4	Biological Assay of (Pure) Hesperidin	154
4.5	Biological Assay of nano-Formulations	154
4.5.1	Biological Assay for Graphene Conjugate nano-formulations	154
4.5.2	Biological Assay for Silver Conjugate nano-formulations	155
4.5.3	Biological Assay for Zinc Conjugate nano-formulations	156
4.6	Scratch Assay	157
4.7	LCMS Analysis	158
<b>5.</b>	<b>Chapter 5 – Significance of the Study</b>	<b>196 – 197</b>
<b>6.</b>	<b>References</b>	<b>198 – 213</b>
	<b>Annexures</b>	

## LIST OF FIGURES

<b>S.No.</b>	<b>Title</b>	<b>Page No.</b>
1.1	Cancer growth and development	1
1.2	Causes of Cancer	2
1.3	The types of cancer	4
1.4	Cell Division	5
1.5	Cell Growth	6
1.6	Graph source GLOBOCAN 2020, showing new cases of Lung cancer	7
1.7	Landscape of treatment option in LC depending on the stage of Lung cancer	8
1.8	Cancer survival rate by SEER	9
1.9	Mutations in NSCLC	11
1.10	Molecular compositions of flavonoids and their corresponding classes	15
1.11	Flavonoids impact on cellular signaling pathway	16
1.12	Natural compounds modulate the TME	17
1.13	In vitro and in vivo preclinical cancer research	18
1.14	Phytochemicals chemo sensitize cancer treatment resistance	19
1.15	Metabolism of Flavonoids	21
1.16	The molecular actions of FL in cell signalling in cancer	24
1.17	Role of flavonoids in cancer as well as in other illnesses	25
1.18	Chemical Structure of Diosmin	28
1.19	The diversified effects of Diosmin	29
1.20	Chemical structure of Hesperidin	30

<b>S.No.</b>	<b>Title</b>	<b>Page No.</b>
1.21	MOA of Diosmin in cancer prevention	30
1.22	Role of Hesperidin activity in various cancer type	31
1.23	Hypothesis of study	32
2.1	The cancer progression process	34
2.2	Cancer Pathogenesis	35
2.3	Different phases of carcinogenesis	36
2.4	The epidemiology of cancers	40
2.5	Different stages of lung cancer	41
2.6	Types of LC	41
2.7	Gleason Grading	45
2.8	Pathogenesis in Lung cancer as point of immunology	46
2.9	Risk factor of LC	47
2.10	Symptoms of LC	48
2.11	The preventive measures against lung cancer	50
2.12	The diagnosis of Lung Cancer	51
2.13	Various treatment option of LC	53
3.1	Workflow	65
3.2	Conceptual illustration of in-silico methods	70
3.3	SwissADME web server snapshot of Diosmin	75
3.4	SwissADME web server snapshot of Hesperidin	79
3.5	Workflow of Nanoformulation	80
3.6	Formation of MTT into Formazen crystal	86
3.7	Schematic representation of workflow of the scratch assay	88

<b>S.No.</b>	<b>Title</b>	<b>Page No.</b>
4.1	Boiled egg prediction of Hesperidin	92
4.2	Bioavailability Radar prediction of Hesperidin	93
4.3	2D and 3D image of interaction with ROS1 and Diosmin	96
4.4	Schrodinger docking complex	97
4.5	HOMO LOMO Chemical orbitals of Diosmin	98
4.6	Boiled egg graph for Diosmin	99
4.7	MD simulation by Schrodinger	100
4.8	PSA, MOLsa, SASA, RMSD, RGyr	101
4.9	Protein secondary structure of ROS1-Diosmin	102
4.10	RMSF of ligand 2D structure of Diosmin	103
4.11	Secondary structure of protein	104
4.12	Total number of residues of chain A of protein ROS1	104
4.13	2D and 3D interaction of EGFR- Hesperidin	106
4.14	Docking complex of EGFR-Hesperidin	107
4.15	HOMO LOMO Chemical orbitals of Hesperidin	108
4.16	Boiled egg plot of Hesperidin	110
4.17	RMSD graph of Hesperidin using Desmond	111
4.18	Ligand RMSF of Hesperidin	112
4.19	Visualization of protein's secondary structure dynamics	114
4.20	2D 3D compound torsional patterns	115
4.21	RMSD, RGYR, IntraHB, MolSA, SASA and PSA	116
4.22	Secondary Protein structure of EGFR	117
4.23	Total number of residues of chain A of EGFR	117

<b>S.No.</b>	<b>Title</b>	<b>Page No.</b>
4.24	FTIR analysis of Diosmin	119
4.25	NMR results of Diosmin	120
4.26	DSC analysis of Diosmin	121
4.27	XRD results of Diosmin	122
4.28	FTIR of Hesperidin	124
4.29	NMR results of Hesperidin	125
4.30	DSC analysis of Hesperidin	126
4.31	XRD results of Hesperidin	127
4.32	UV lambda max. graph for Diosmin	128
4.33	Straight line graph for Diosmin	129
4.34	UV lambda max. graph for Hesperidin	130
4.35	Straight line graph for Hesperidin	130
4.36	Workflow of Nanoformulation	131
4.37	FTIR graph of Graphene Hesperidin	132
4.38	FTIR graph of Graphene Diosmin	132
4.39	FTIR graph of Graphene conjugates	134
4.40	FTIR graph of Silver Hesperidin	135
4.41	FTIR graph of Silver Diosmin	135
4.42	FTIR graph of Silver conjugates	136
4.43	FTIR graph of Zinc Hesperidin	137
4.44	FTIR graph of Zinc Diosmin	138
4.45	FTIR graph of Zinc conjugates	139
4.46	FESEM images of graphene Hesperidin nano-formulation	140

<b>S.No.</b>	<b>Title</b>	<b>Page No.</b>
4.47	FESEM images of graphene Diosmin nano-formulation	141
4.48	FESEM images of graphene conjugates nano-formulation	143
4.49	FESEM images of Ag Hesperidin nano-formulation	144
4.50	FESEM images of Ag Diosmin nano-formulation	145
4.51	FESEM images of Ag conjugates nano-formulation	147
4.52	FESEM images of Zinc Hesperidin nano-formulation	148
4.53	FESEM images of Zinc Diosmin nano-formulation	150
4.54	FESEM graph of Zinc conjugates nano-formulation	151
4.55	Zeta Potential images of all conjugates	152
4.56	IC <sub>50</sub> graph of Diosmin	153
4.57	Cytotoxicity of Hesperidin	154
4.58	Cytotoxicity of Graphene nano-formulation	155
4.59	Cytotoxicity of silver nano-formulation	156
4.60	Cytotoxicity of Zinc nano-formulation	157
4.61	Scratch Assay images	158
4.62	MSTIC graph of LCMS analysis	159
4.63	MS spectrum graph of LCMS analysis	192



## LIST OF TABLES

S.No.	Title	Page No.
2.1	Anatomic stage/ Prognostic groups	43
4.1	Top 10 compounds having high GOLD scores with ROS1	96
4.2	Top 10 compounds having high GOLD scores with EGFR	105
4.3	ADME characteristics of the Hesperidin and Diosmin	109
4.4	Drug-like properties of Hesperidin and Diosmin	109
4.5	Solubility of Diosmin	128
4.6	Solubility of Hesperidin	129
4.7	Nano-encapsulation of drug	153
4.8	The identified proteins from LCMS analysis	160

## Chapter – 1

# INTRODUCTION

## 1.1 CANCER

Gene alterations of somatic cells and proliferation of abnormal cells which led to Cancer. The formed abnormal cells will be spread different parts of the body (*Figure 1.1*). Cancerous cells which form neoplasm or tumour. Neoplasm is a group of cells which may exhibit abnormal growth. Neoplasm produce a bulk mass and it can easily distribute by simple diffusion (Riaz et al., 2017). Disorder of cancer was projected by GDC (Global demographic characteristics), is about 420 million novel cases by 2025 yearly, that the rate of incidence growing gradually with time to time. In 2018, over 18 million new cases were reported Globally; it further in female is around 8.5 and in male is around 9.5 million respectively.

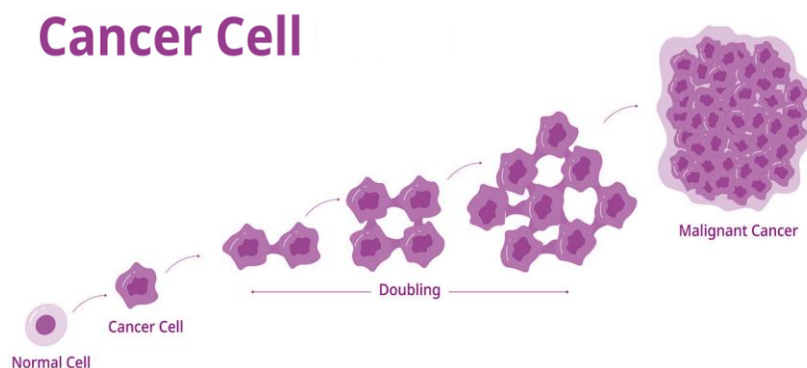


**Figure 1.1 : Cancer growth and development**

Total 9.6 million deaths may be expected through worldwide with cancer (Ferlay et al., 2015). More commonly observed cancers are prostate, breast, colorectal, stomach and non-melanoma skin malignancies (respectively 1.28, 2.09, 1.1, 1.03, 1.04 million) (Fitzmaurice et al., 2019).

## 1.2 CAUSES OF CANCER (Baylin & Jones, 2016)

- Most of the cancers are caused by different factors such as consumption of tobacco (22%), poor intake of diet (10%), less physical activity, over consumption of alcohol, obesity or other related factors.

- Some other infectious diseases also may produce (15%) of cancers through globally they are including hepatitis b & c, human papillomavirus infection, helicobacter pylori, and HIV, Epstein - Barr virus.
- Genetic abnormalities of parents are also producing about 5-10% of cancer.
- Different types of carcinogens also cause cancers when consuming externally they are:
  - Physical Carcinogens:** Radiations like radon (Ionising), UV, uranium, alpha, gamma, beta, and X-rays.
  - Chemical Carcinogens:** Chemical substances like N-nitrosamines, asbestos, cadmium, benzene, vinyl chloride, nickel, and benzidine, drinking water contaminant (arsenic), a food contaminant (aflatoxin).
  - Biological Carcinogens: Micro-organisms like** bacteria, viruses, or parasites and Pathogens like HPV, EBV, hepatitis B and C, Kaposi's sarcoma-associated herpesvirus (KSHV). One of the other causes is Aging. It is more common incidence, in which it drastically increases.

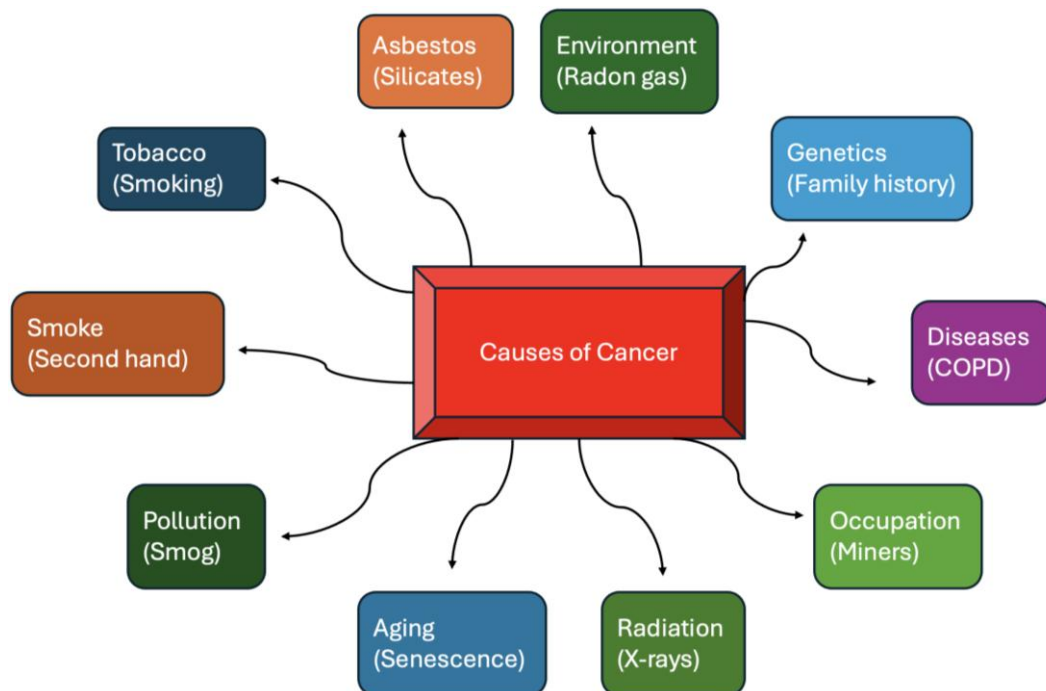


**Figure 1.2 : Causes of Cancer.**

### 1.3 TYPES OF CANCER

Cancers are further classified into different types they are: [cancerresearchuk.org updated, 2024]

- a) **Carcinomas (Starts in cells)** - Breast cancer, prostate cancer, colorectal cancer, lung cancer.
- b) **Sarcomas (Starts in the tissues)** - Nerves, tendons, joints, fat, blood vessels, bone, lymph vessels, muscles, or cartilage.
- c) **Leukaemia's (Blood-forming tissue)** - Myeloid leukaemia, lymphocytic leukaemia.
- d) **Lymphomas (Lymphatic cells)** - Hodgkin lymphoma and non-Hodgkin lymphoma.
- e) **Central Nervous System Cancers (Brain & Spinal)** - CNS lymphomas, vestibular schwannomas, gliomas, pituitary adenomas, primitive neuro-ectodermal tumors, meningiomas, and vestibular schwannomas.
- f) **Multiple Myeloma (Plasma & Immune Cells)** - Kahler disease.
- g) **Melanoma (Melanocytes)** – Skin cancer.
- h) **Other Types of Cancers:**

**Germ Cell (Reproductive cells)** – Growth of Tumor cells from reproductive cells.

**Neuroendocrine (Neuroendocrine cells)** - It may be either benign or malignant.

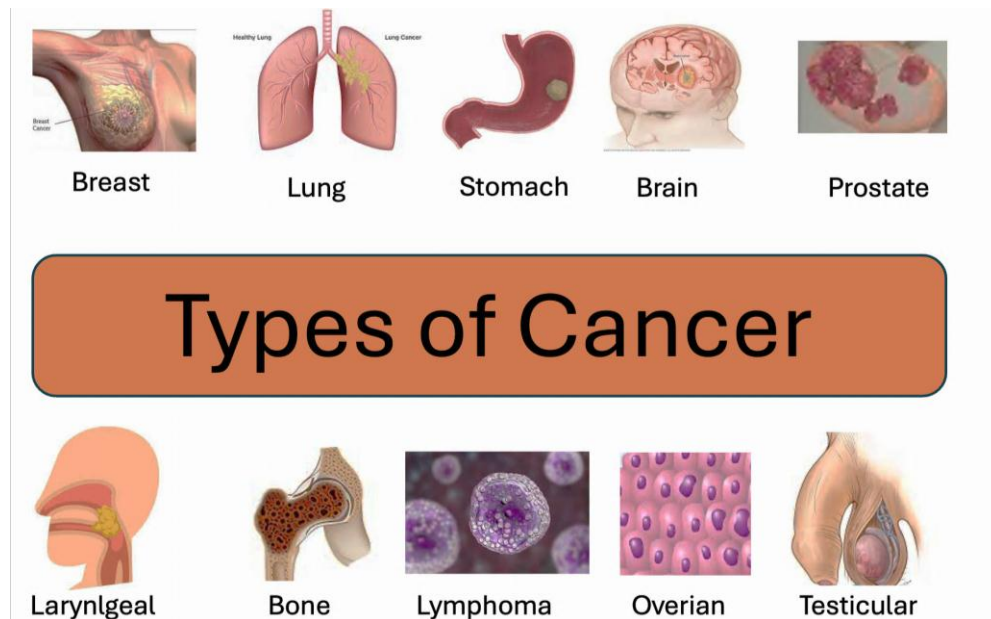


**Figure 1.3 : Types of Cancer**

## **1.4 CANCER CYCLE**

The following steps are help to understand how the cancer begins: (McGuire, 2016)

### **a) Changes in the Cell**

Body is composed by very tiny functional units known as cells, a greater number of cells which joins with each other and to form body. Initially, Changes in the cell is more common in cancers. Mostly cells are involved in signal transduction processes. Any disruption in the cell signalling pathway than the cells undergo uncontrol proliferation and this proliferation may lead to the formation bulk mass is known as tumor. There are some other mechanisms also possible that depends on the type of cancer.

### **b) Cell Division**

Structurally, cells are quite similar but specific cells may exhibit specific functions in our body. For all functions of the cell, responsible unit is gene which is present in the nucleus. It is made up of long chain polynucleotides in the form DNA. Every cell has nucleus, which regulate the cell functions. Nucleus contains chromosomes these are composed by many numbers of genes. Every gene is coded a signal, which says to the

cell how to perform or division. During the cell division, the parent cells divide into two similar identical cells, and then these two cells divide into four and so on.

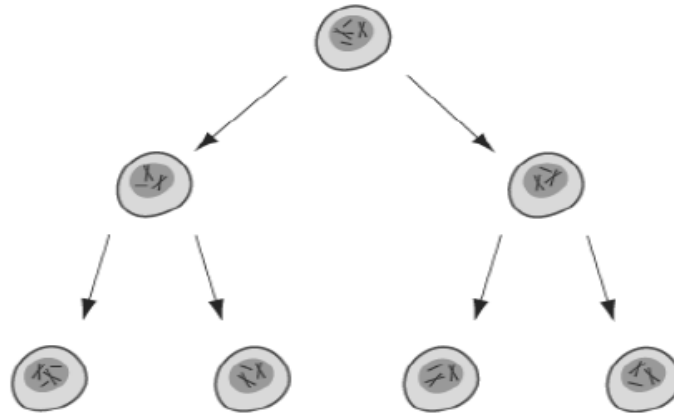


**Figure 1.4 : Cell Division**

#### **c) Mutations**

During the cell division there are changes within the gene sequence due to chemical changes which may come from external factors like smoking. Mutation is nothing but a sudden change in nucleotide base pair sequence. By Mutation genes lose their original function. Mutations also cause abnormalities in their function regulation like cell growth control. Due to this the cell may undergo uncontrolled proliferation. Mutation of genes also does not produce the actual required proteins which may stop the cell division and there may be a chance of producing a high number of proteins, which may help to rapid cell division. This is another cause to the formation of a tumor.

#### **d) Growth of Cancer**

Cancer cells may function in a different manner than that of normal cells. Cancer cells also require the substances for their survival like that of normal cells. Due to this function, it will grow continually.

By the following characters the cancer cells are varied from normal cells:

- Cell division is uncontrolled.
- They are functionally immature.

- They do not recognize the original signals like cell division controlling signals.
- Cancer cells easily spread different parts throughout the body by using circulatory systems.
- They will injure different tissues and organs.

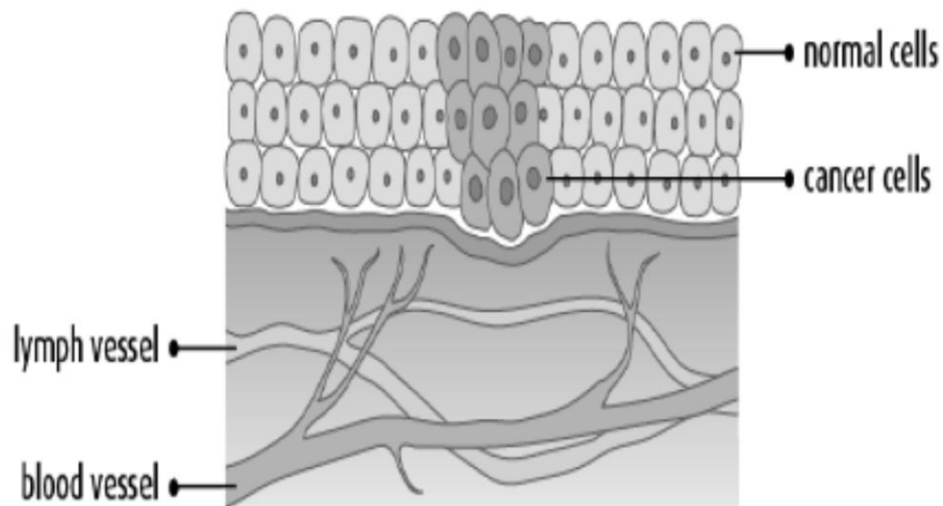


**Figure 1.5 : Cancer growth** Adopted from (<https://cancer.ca/en/cancer-information/what-is-cancer/how-cancer-starts-grows-and-spreads>)

#### e) Spreading

During the growing stage, they are distributed to the different parts of the body by circulatory systems like systemic or lymphatic. Proliferation of new cancerous cells is known as metastasis.

### 1.5 LUNG CANCER

According to current figures (Fitzmaurice et al., 2019) Lung Cancer (LC) is at the forefront of worldwide cancer occurrence and fatalities. This disease is categorized into two primary types: small-cell LC (SCLC) and non-small-cell LC (NSCLC). The non-small-cell LC (NSCLC) category can be further divided into several subtypes. In 2020 alone, 2,206,771 new instances of LC were recorded globally, cementing its status as the most diagnosed disease (see Figure 1.6). It ranks as the second most common cancer in men, trailing only prostate cancer, and holds the same position as

the second most prevalent disease in women. Surprisingly, males have a 14.3% lifetime chance of developing LC, whereas women have a 8.4% of the total risk (Bray et al., 2018; Organization, 2019) . LC is more common in poorer nations wherein tobacco use is prevalent, resulting in a more than 20-fold disparity in occurrence rates across locations. This highlights the important relationship between LC and cigarette smoking behaviours, making it a worldwide public health problem.

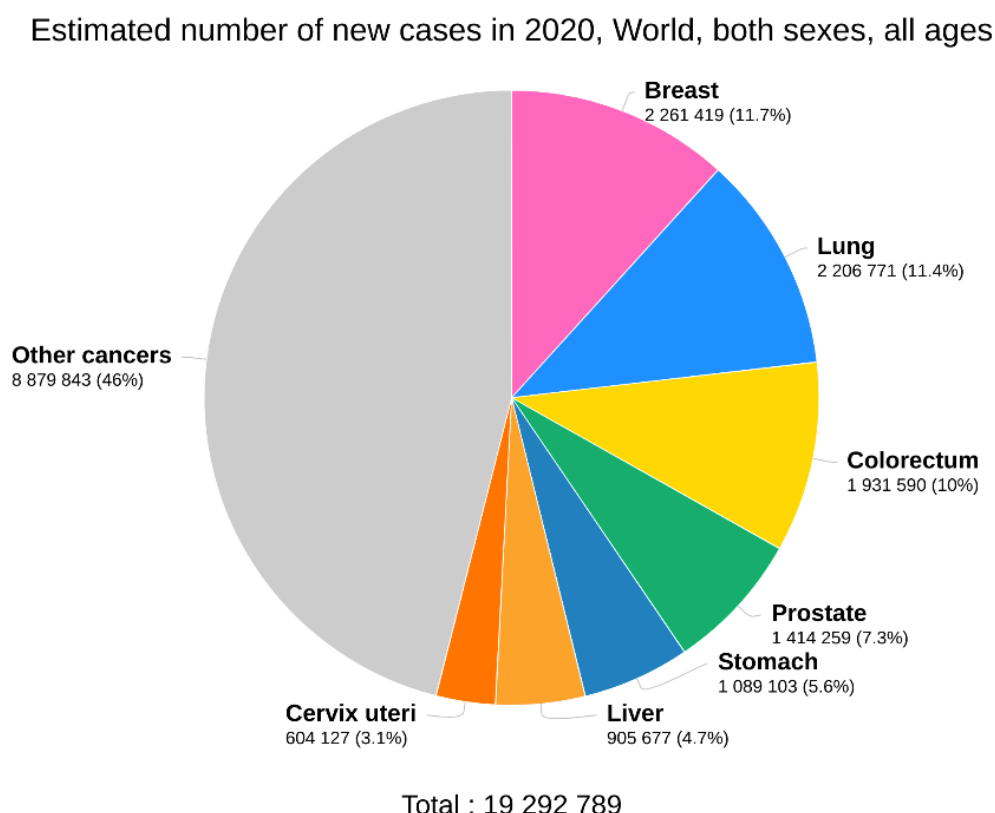


**Figure 1.6 : Graph source GLOBOCAN 2020, showing new cases of LC.**

LC stands as the foremost contributor to cancer-related deaths on a global scale, affecting both men and women at an equal rate. In the year 2020 alone, LC accounted for 1,796,144 casualties, accounting for 18% of all cancer-related deaths globally. This illness has the unfortunate distinction of being the greatest cause of mortality in males, contributing to 21.5% of male related to cancer fatalities, and 13.7% in women (Organization, 2019). These troubling numbers highlight the huge toll that LC exacts on human lives, underscoring the critical need for ongoing studies, prevention, and awareness initiatives.



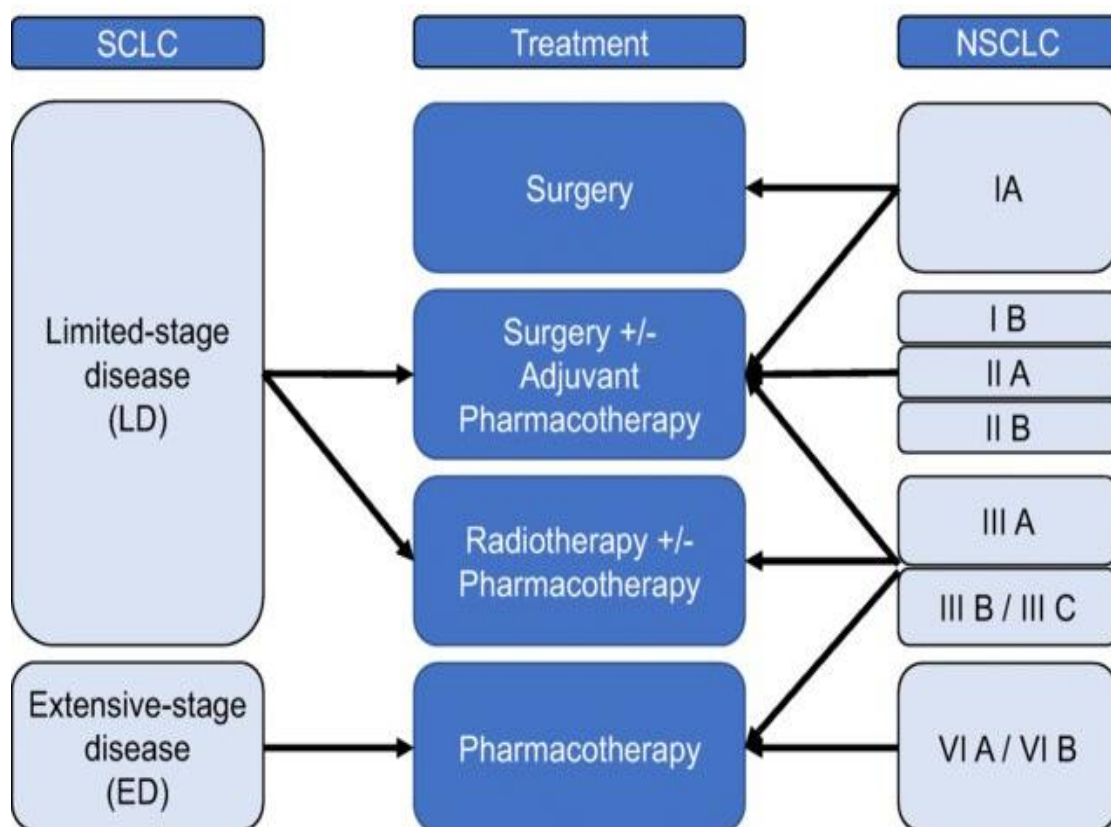


**Figure 1.7 : Landscape of treatment options in Lung Cancer depending on the stage of Lung Cancer (Sase et al., 2021).**

Latest 5-year survival rate for LC, according to SEER (from 2013–2019) was 24.3% with estimated cases 3,94,312 in both sexes (Thandra et al., 2021). Out of which the 5-year survival rate for women is 29.6% (1,91,855 cases) and males is 21.3% (2,02,457 cases). Early detection measures, such as the suggested computed tomography (CT) screening, may be credited to improvements in LC survival rates, particularly for persons with a strong history of smoking. Furthermore, the progress in treatment options has made a significant impact, particularly with the introduction of targeted therapies along with immunotherapies inhibitors. Additionally, developed countries enjoy a distinct advantage due to their superior access to state-of-the-art diagnostic tools and advanced treatment methods. This enhanced accessibility correlates with higher survival rates among LC patients, underscoring the pivotal role economic factors play in healthcare outcomes (Barta et al., 2019).

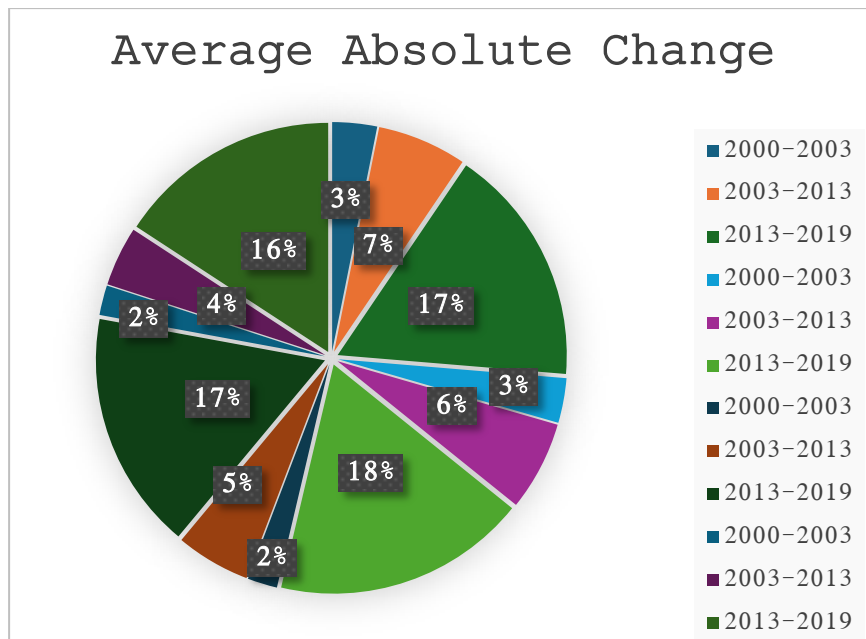


**Figure 1.8 : Recent trends in lung and bronchus cancer survival rates from 2013 to 2019, as reported by the SEER database, encompass data across all genders, races (including Hispanic ethnicity), age groups, and disease stages over a span of five years. (P. Liu et al., 2012).**

The world health organization, in 2022, classified LC into distinct categories (Travis et al., 2015) and in the Western world, more than 80% of LC cases are directly linked to cigarette smoking. Efforts to curb smoking, including successful smoking cessation programs, have led to a decline in both the number of new cases and mortality rates associated with LC. However, in poor nations, the scenario is different. Persistent tobacco use remains widespread, and there are additional health risks stemming from factors such as prolonged exposure to industrial substances like asbestos and combustion fumes. Despite progress in some areas, these ongoing challenges highlight the complex interplay of social, economic, and environmental factors in the global fight against LC.

Well-known genetic modification in LC, such as EGFR, BRAF and KRAS, EGFR have been confirmed in recent genomic research. Furthermore, these investigations have revealed previously unreported uncommon but recurrent mutations in LC, such as amenable to targeting changes in genes including RET, ERBB4, JAK2 and fibroblast growth factor receptor 1 (FGFR1) (“Comprehensive Genomic

Characterization of Squamous Cell Lung Cancers.” 2012; Ding et al., 2008; Govindan et al., 2012; Ju et al., 2012; Kohno et al., 2012; Lipson et al., 2012; P. Liu et al., 2012). Understanding the complex landscape of LC epidemiology or risk factors is critical. This understanding not only informs preventative initiatives, but it also plays a vital responsibility in minimizing the disease's rising worldwide burden (“Global Burden of 87 Risk Factors in 204 Countries and Territories, 1990-2019: A Systematic Analysis for the Global Burden of Disease Study 2019.” 2020).

Significant progress in the understanding and treatment of LC has been achieved in recent years due to the finding of mutational catalyst such as ROS1, EGFR, ALK and BRAF. In patients meeting the criteria, targeted therapies utilizing small molecule inhibitors targeting specific mutations in receptor tyrosine kinases, along with immunotherapies have emerged as potent alternatives to or supplements for traditional chemotherapy (Denisenko et al., 2018).

EGFR, an important player in cancer cell signaling, activates pathways such as PI3K-AKT-mTOR, RAS-RAF-MAPK, and JAK-STAT, controlling crucial oncogenic processes such as cell proliferation, cell viability, cellular specialization, new blood vessel formation, cellular infiltration and Disease spreading or distant migration (Sordella et al., 2004; Yarden & Sliwkowski, 2001). EGFR activating genetic alteration cause continuous tyrosine kinase activation and the transformation of lung epithelial cells into malignant forms (Greulich et al., 2005; Sordella et al., 2004). Similarly, ROS1 activation activates signaling pathways such as PI3K-AKT-mTOR, STAT3, and RA-/MAPK-ERK. ROS1 gene rearrangements have been found, including 5' fusion partners such as KDEL2, FIG, SDC4, TPM3,EZR,CD74, SLC34A2, albeit the specific involvement of these partners in the integration of kinase's oncogenic activity remains unknown (Govindan et al., 2012; Rikova et al., 2007; Takeuchi et al., 2012). This expanding knowledge of individual abnormalities and their associated pathways not only provides insight on the molecular processes behind LC, but it also informs the development of tailored medications, resulting in more precise and successful treatments for patients. These mutations and alterations lead to resistance and reoccurrence, which cause DNA damage leading to apoptosis, clonality and LC (Figure 1.9).

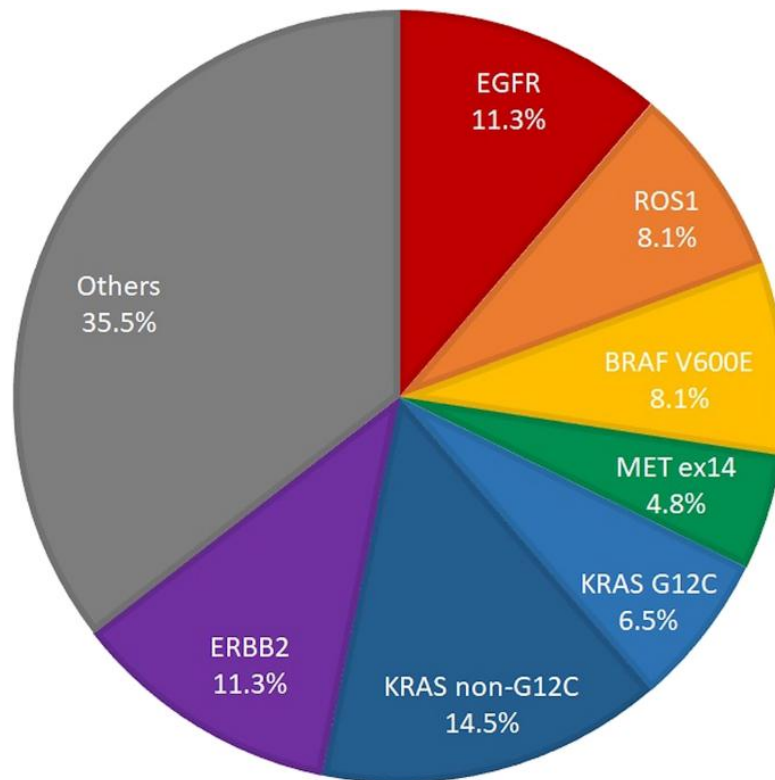


**Figure 1.9: Mutations in NSCLC (Shen et al., 2022).**

SCLC, which accounts for roughly 14% of all lung malignancies (Sharp et al., 2016) is a violent, neuro-endocrine neoplasm with a quick doubling period, fast expansion rate, and early metastasis initiation (Pietanza et al., 2015; Waqar & Morgensztern, 2017). For SCLC, no particular protein biomarkers have been discovered. Because of the poor prevalence and survival rates of SCLC (Y. Zhang & He, 2013), little is called about the driving iterations that link cancer formation and development.

When assessing tumor heterogeneity, it is crucial to consider that the cumulative presence of co-occurring genomic alterations in NSCLC can have a more significant impact than individual mutations within oncogenic driver genes. In comparison to many other types of tumors, both LUADs and LUSCs exhibit a notably higher average number of somatic mutations per mega base. While a substantial portion of these mutations may be considered as passenger mutations, its noteworthy that combinations of somatic mutations within cancer driver genes have been identified in a significant proportion of LUADs and a considerable fraction of LUSCs. (Skoulidis & Heymach, 2019)

EGFR is the central concept of molecular targeted treatment in LC, which is currently widely employed in clinical trials throughout the globe (Lynch et al., 2004; Paez et al., 2004; Pao et al., 2004). The majority of EGFR mutations discovered in NSCLC were determined to be somatic, with just a few, like T790M, being germline in origin. Exons 18 to 21 in the tyrosine kinase domain were the most thoroughly sequenced because they are thought to include mutational hot spots. Other EGFR variants exist outside of these hot area exons, with some having a distinct influence on TKI sensitivity, although at a lesser frequency; for example, the E884K mutation in exon 22 can be more sensitizing to gefitinib but imparts insensitivity to erlotinib (Choong et al., 2006; Tang et al., 2009). The bulk (85%) of the recently discovered EGFR kinase mutations are due to the L858R missense substitution in exon 21 and short in-frame deletions variants in exon 19, (Gazdar et al., 2004; Greulich et al., 2005) both of which have been demonstrated to be EGFR TKI sensitizing.

The ROS-1 protein consists of an extracellular domain featuring a hydrophobic segment, allowing for permeability passage. Its intracellular region contains a tyrosine-kinase domain with a terminal carboxyl group (Roskoski, 2017). While the exact physiological role of ROS-1 is yet unknown, research suggests that the wild-type ROS plays a crucial role in embryonic growth, activating signaling processes essential for the differentiation of epithelial tissues (Acquaviva et al., 2009). ROS-1 is pivotal in activating multiple signaling pathways crucial for cell proliferation, differentiation, developmental processes, and cell survival. Rearrangements of ROS-1 occur at specific points within the gene, including the 5' end of exons 32, 34, 35, or 36, or introns 31 or 33 (Cui et al., 2020; Davies & Doebele, 2013). Common fusion partners include CD74 (38-54%), EZR (13%-24%), SDC4 (9-13%), and SLC34A2 (5-10%) (Cui et al., 2020; Huang et al., 2021). Notably, lung adenocarcinomas with ROS1 mutations have been found to be associated with EGFR mutations, suggesting a complex interplay of genetic factors in these cancer cases.

Despite rising interest in the research of targeted medicines, chemotherapy remains the basis of NSCLC treatment. However, chemotherapy resistance restricts our capacity to treat advanced LC successfully. Some LCs are fundamentally resistant to treatment, and in nearly all instances acquired resistance quickly. While targeting

histology may result in increased tumor sensitivity to a certain chemotherapeutic treatment, a greater knowledge of the molecular drivers of chemotherapy sensitivity/resistance is necessary. Some potential options for overcoming chemotherapy resistance in LC include the discovery of predictive biomarkers for personalizing chemotherapeutic drugs and the combination of new medicines targeting particular resistance pathways with conventional chemotherapy (Kim, 2016).

Despite significant developments in treatment technologies and a better knowledge of LC, which led to the development of tailored medicines, chemotherapy remains the cornerstone of NSCLC treatment. Several chemotherapeutic drugs with various modes of action are now being utilized to treat LC. Almost all cancers, however, acquire resistance to all of these drugs (Kim, 2016). Persistent research is required to understand the molecular causes of chemotherapy resistance and to identify biomarkers that are predictive for chemotherapy sensitivity. Improved molecular knowledge of resistance mechanisms may open up potential to combine chemotherapeutic medicines with molecularly targeted therapies, which might be a viable method for overcoming chemotherapy resistance and optimizing treatment for LC patients.

The initial therapies for LC, according to FDA-approved medications, were mostly connected to chemical components like cisplatin, known to be capable of inducing apoptosis. However, adverse effects, limited particularity, and resistance have prompted the development of new medicines. Interestingly, cisplatin remains the simplest synthetic chemical utilized as a chemotherapeutic therapy, with less side effects arose in the subsequent decades. The growth of technology then led to a pivotal discovery, which resulted in the creation of novel anti-cancer medicines (Ruiz-Casado et al., 2017).

Aside from the expense of therapy, patients often endure consequences of the illness itself as well as adverse effects of cancer treatment. The combined impact of the illness and hazardous medications reduces patients' quality of life and may make therapy difficult for them. Another critical concern among the individual receiving therapy and the treating physician is the emergence of resistance of malignant cells to

medication treatment. After a lengthy period of treatment, the tumor may grow resistant to chemotherapy, resulting in a poor response to the chemotherapeutic medicines. Because cancer treatment is a burden globally, several solutions have proposed to reduce the expense of treatment options while improving the result (Kolodziej et al., 2011; Siddiqui & Rajkumar, 2012).

One of the ways mentioned is the incorporation of phytomedicine with conventional treatment. Phytomedicine is a herbal-based ancient medical practice that employs a variety of plant materials in preventative and therapeutic methods. Clinical trials investigating the effectiveness of herbal medications in patients with cancer have shown mixed findings (Hamilton-Reeves et al., 2013; Tröger et al., 2014). A primary problem in this objective is the search for medications with less toxicity. Natural products have significant anti-cancer activities with fewer side effects than conventional chemotherapeutic medicines owing to chemoresistance and high cytotoxicity.

The majority of the phytochemicals categories have remarkable pleiotropic activities that are being investigated for potential anti-tumor activities (Berk et al., 2022). Flavonoids are most significant and ubiquitous types of phytochemicals, present in most of the eatable items as well as several drinks. Flavonoids are primarily generated in certain organs of plants to help development and defend against infections, to colour and provide scent, and to entice pollinators (Dias et al., 2021). Flavonoids also protect plants from biotic and abiotic stresses and function as distinctive UV filters (Takahashi & Ohnishi, 2004). Flavonoids' exceptional antioxidant and anti-inflammatory properties have made them an essential component of a wide range of nutraceutical, pharmaceutical, medical, and cosmetic goods. Furthermore, flavonoids are appealing molecules because of their pharmaceutical and bioactivities characteristics (Figure 1.10). (Falcone Ferreyra et al., 2012; Walker et al., 2000).

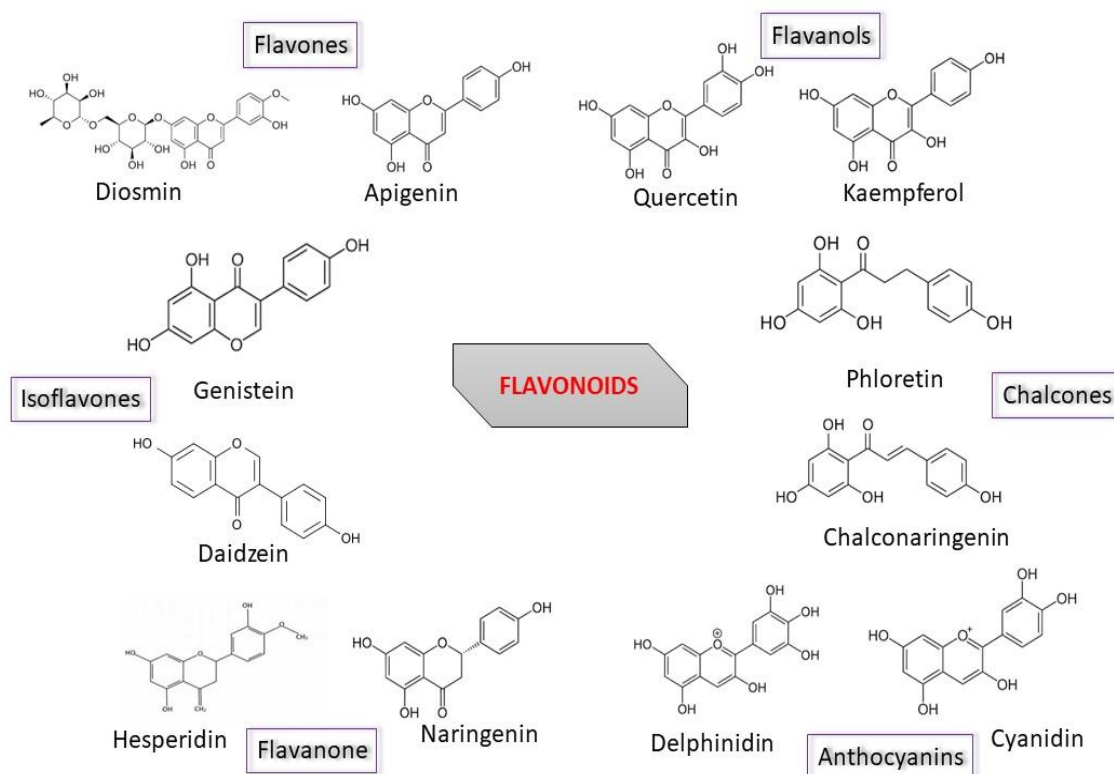


**Figure 1.10 : Molecular compositions of flavonoids and their corresponding classes (Berk et al., 2022)**

Flavonoids' major biological activity is to suppress the creation of ROS, and this ability may modify a broad range of key cellular processes that influence multiple molecular pathways in tumor cells (Batra & Sharma, 2013; Budisan et al., 2017). Modulation of cell signaling pathways and suppression of critical transcription factor activity are examples of these strategies. (Braicu et al., 2017; Khan & Mukhtar, 2013). These pathways are directly relevant to the prevention or treatment of LC. The impact of the flavonoids on enzyme functions might be separate from their primary function as antioxidant effects, however they could also be linked with the ROS triggered MAPK (mitogen-activated protein kinase) cascade, PI3K (phosphatidylinositol 3-kinase)/Akt(serine/ threonine kinase 1) or Janus kinase/signal conversion devices and activators of transcription (JAK/STAT) pathways (Shanmugam et al., 2016; H. Zhang et al., 2018) (Figure 1.11).



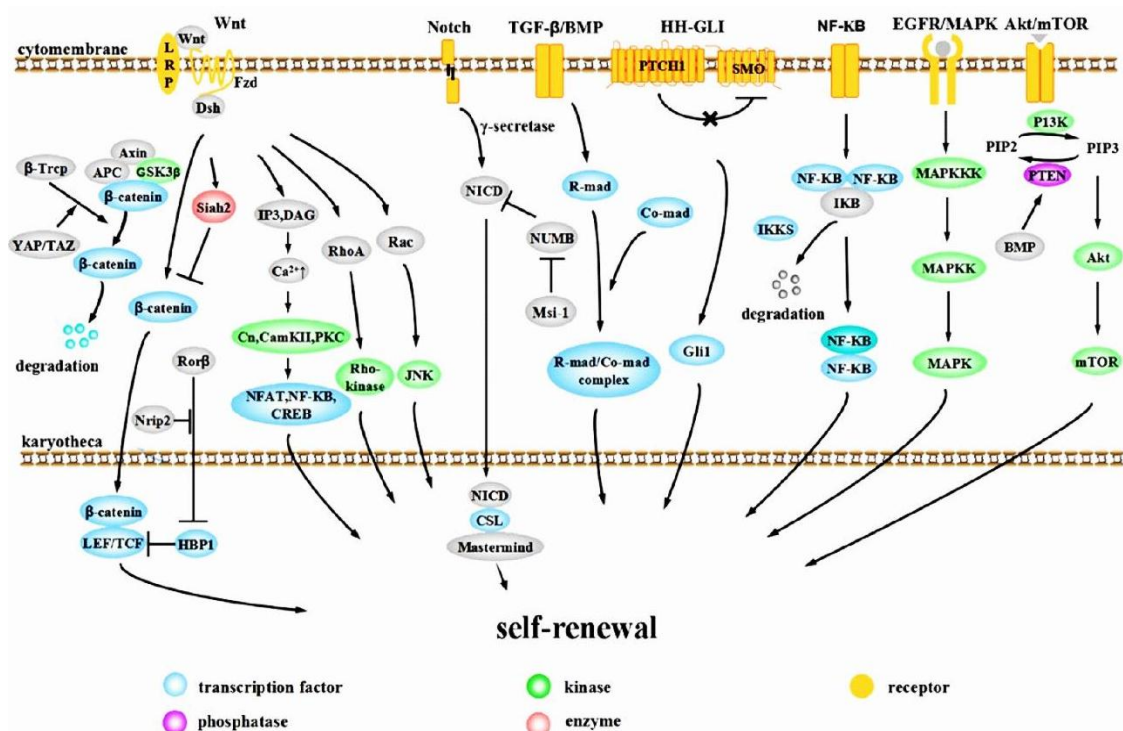


**Figure 1.11. Flavonoids impact cellular signaling pathways by targeting various components disrupted in LC, including protein kinase C (PKCs) and integrin. Integrin, a key regulator of cancer cell proliferation and adhesion, is influenced by flavonoids, leading to modulation of these crucial pathways (H. Chen et al., 2022) (Kopustinskiene et al., 2020).**

### 1.6 PHYTOMEDICINES AND LUNG CANCER

Natural commodities are valuable offerings from nature to humans. They comprise plants and animals extracts, insect, oceanic, and microbial metabolic products, and also a variety of chemical components found naturally in humans and animals. Furthermore, traditional Chinese medicine (TCM) is based on a mix of natural ingredients and TCM philosophy. Natural products have traditionally been a valuable source for medication development. According to the most recent data on pharmaceuticals authorised by the Food and Drug Administration (FDA) in the United States, many prescription medicines for treatment are derived from natural ingredients. From 1946 to 2019, almost half of newly authorised medications were natural small molecules (Newman & Cragg, 2020). Plant preparations and Chinese

medicines are products that have several components, channels, and targets. Natural products remain to pique researchers' interest because of their various forms and functions. Although the TME has been extensively explored, the natural compounds that target and modulate the TME of lung cancer have not been well reviewed.

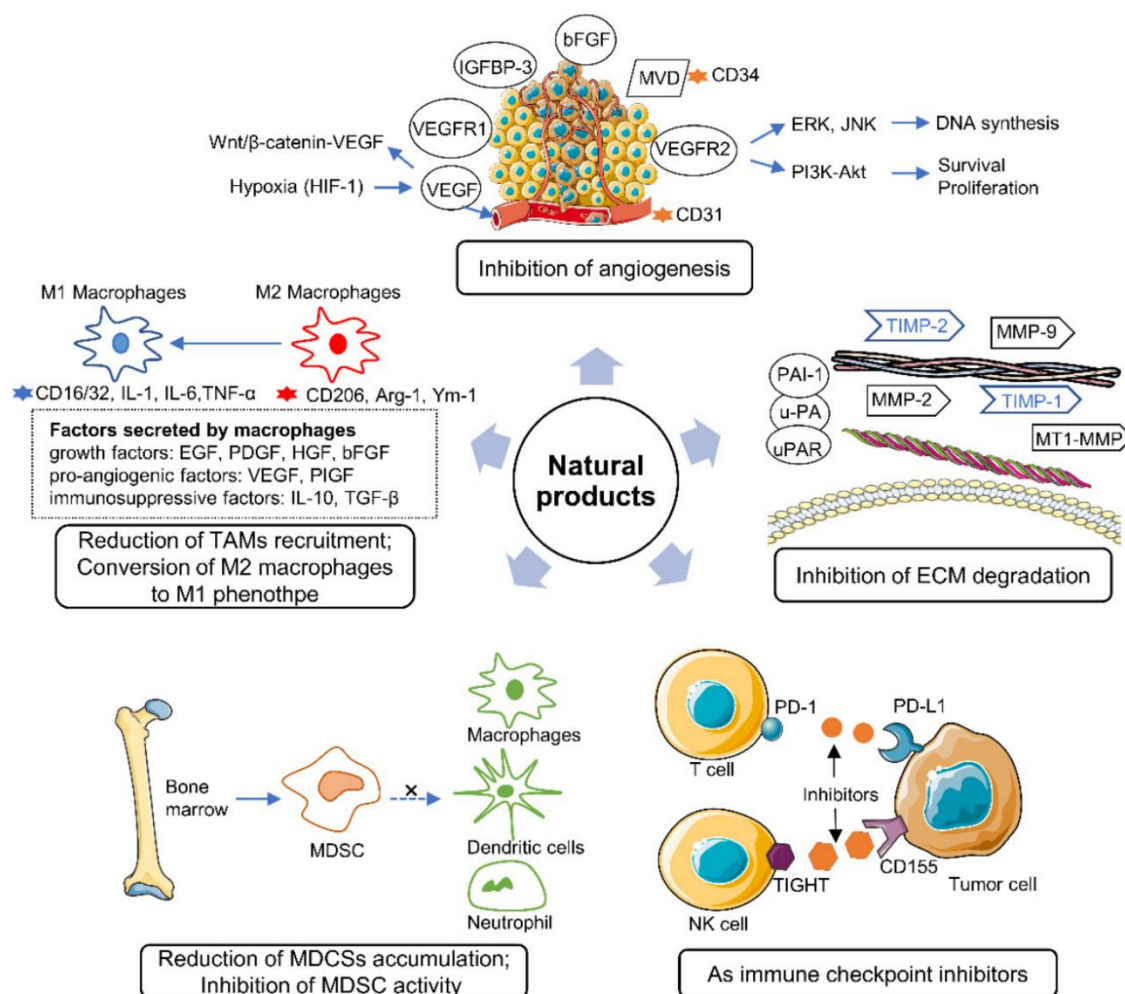


**Figure 1.12. : Natural compounds modulate the TME (Shen et al., 2022)**

## 1.7 ROLE OF FLAVONOIDS IN CANCER CHEMOPREVENTION

Natural chemicals are the most pervasive family of plant chemicals and include molecules having a -OH connected to an aromatic hydrocarbon. They are an exceptional variety of FL. The term "flavonoids" encompasses a diverse group of compounds that share a common structure known as C6-C3-C6, also referred to as a phenyl benzopyran structure (Kumar & Pandey, 2013). The fundamental framework

of all FL consists of two aromatic rings denoted as the A and B rings, interconnected by a three-carbon bridge. In most FL, this three-carbon bridge connects with oxygen and the "a" ring to form the "c" ring, which is a pivotal ring structure. This central ring configuration is referred to as a chromane ring, and it is a shared feature with FL and tocopherols. Notably, chalcones, a specific subclass of FL, lack the essential "c" ring. FL, isoFL, and neoFL are categorized as distinct classes based on their structural characteristics, as outlined by Kumar and Pandey in 2013. Within the core chromane ring structure of essential FL, further subgroups are defined by variations in chromane ring saturation. Flavanones and flavanols, characterized by the absence of carbon-carbon double bonds within the central ring, are differentiated from flavones.

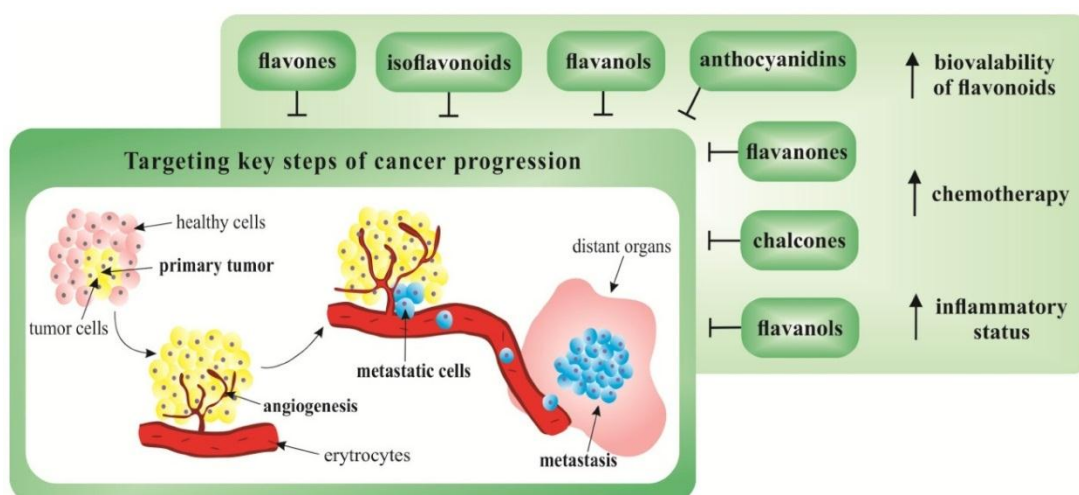


**Figure 1.13 : In vitro and in vivo preclinical cancer research, flavonoids show significant anti-cancer actions that target crucial stages of metastatic development (Liskova et al., 2020)**

The realm of FL encompasses approximately 9000 identified compounds in nature, with the potential for many more due to the vast array of possible substitutions at various positions on the FL carbon framework. Furthermore, each hydroxyl group and certain carbons can be further modified with a variety of sugars, which can, in turn, be substituted by a range of organic and aliphatic acids. This intricate diversity contributes to the extensive spectrum of FL. Due to their widespread prevalence in plant life, FL are an essential element of the human diet, with daily consumption estimates ranging from 50 to 1,000 mg. The enormous discrepancies in predicted FL

intake are attributable in part to the assessment of different FL types based on separate studies.

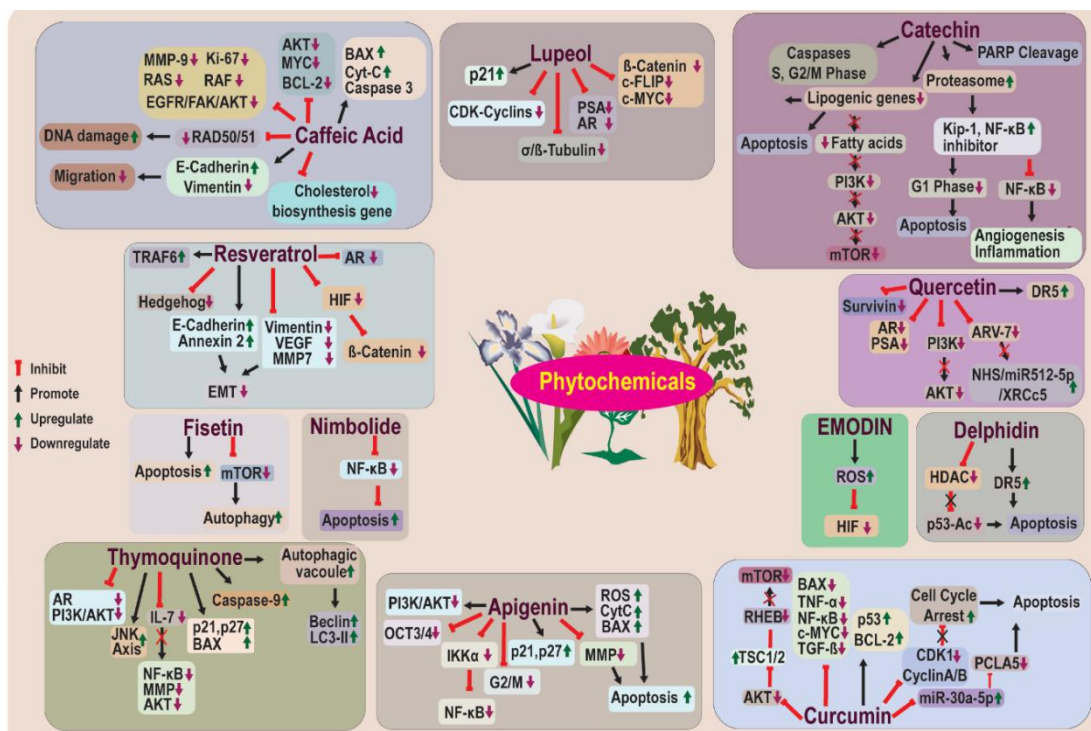


**Figure 1.14 : Phytochemicals are used to chemo sensitize cancer treatment resistance. By targeting numerous signalling molecules and pathways, phytochemicals extracted from diverse plants help to sensitise resistant cells to various anti-cancer therapy (Jameel et al., 2023).**

Because the bulk of FL in nature are glycosylated, studies assessing FL glycoside intake vastly overstate FL consumption compared to researchers assessing aglycone consumption. Regardless of estimates, the intake of FL in the Western diet, which is low in fruits and vegetables, much outweighs that of other phytochemicals like vitamin E and -carotene. Because of the widespread use of FL, it is critical that we investigate their safety and underlying impacts on human health and illness.

The range of FL effects on mammalian biological structures is very remarkable. In vitro, FL influence a broad spectrum of cell techniques. Numerous thousands of studies on this topic have shown a number of concerns. First, the impressive in vitro effects of FL have not been confirmed in the in vivo setting. This will be explained by a variety of variables, including poor FL absorption, high metabolism, and the

complexity of the *in vivo* environment, which is difficult to reproduce *in vitro*. Secondly, the research considers the relevance of FL form in relation to their biological effects, such that positive systems (e.g. flavonols) have a much stronger organic impact than others (e.g. Flavanones). One source of this latter impact may be the additional planar structure of flavonols (due to the double bond inside the c-ring) that makes these molecules considerably more likely to bind with active locations on enzymes.

## **1.8 BIOAVAILABILITY AND METABOLISM OF FL**

The primary site of FL absorption is the small intestine, with only minimal absorption occurring through the stomach mucosa. The process of FL absorption is significantly influenced by their glycosylation status. It is important to note that a large proportion of naturally occurring FL exist in glycoside forms. Initial investigations proposed that FL glycosides might not be absorbed intact in the human intestine due to their high hydrophilicity. However, subsequent studies have raised questions about this assumption.

Further investigations have revealed that certain FL glycosides, particularly quercetin glycosides, are not only absorbed but are absorbed more efficiently than their aglycone counterparts. Typically, the initial step in FL glycoside absorption involves the hydrolysis of the sugar moiety, primarily occurring in the colon, leading to the formation of FL aglycones. It was previously believed that this hydrolysis was solely facilitated by colonic microorganisms due to the absence of the necessary enzymes for breaking  $\beta$ -glycosidic bonds of FL glycosides in the small intestine.

However, recent findings suggest that extensive-specificity glucosidase enzymes present in lactase phlorizin hydrolase and enterocytes is found in the small intestine brush border may also participate in the hydrolysis of such  $\beta$ -glycosidic bonds, indicating a more complex and dynamic process of FL glycoside absorption than initially thought.

The hydrolysis of FL glycosides has also been demonstrated to occur in the oral cavity (Walle et al., 2005), indicating that the process of FL transformation begins



earlier in the digestive system than previously understood. The conversion of FL glycosides into aglycone forms, initiated by the cleavage of sugar moieties, results in the formation of aglycones that exhibit significantly higher lipid solubility. This increased lipid solubility facilitates their absorption in the colon through passive diffusion.

FL that successfully reach the colon encounter the action of bacterial glucosidases, leading to further transformations. Post-sugar hydrolysis, FL undergo aromatic ring scission, culminating in the generation of simpler phenolic molecules.

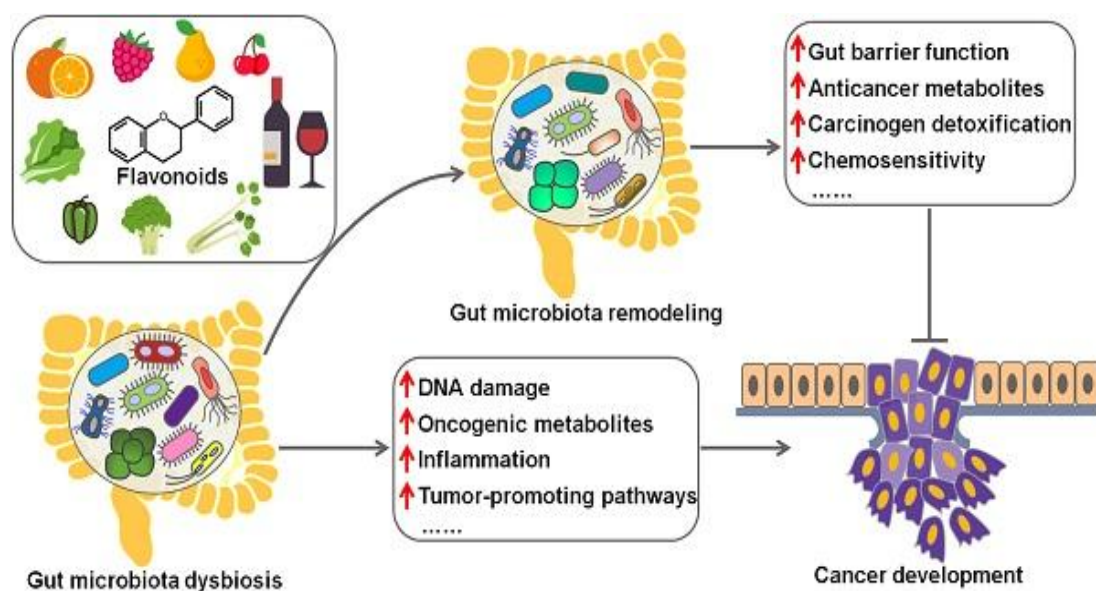


**Figure 1.15 : Metabolism of FL (M. Wang et al., 2022) .**

FL-glucosides exhibit higher absorption rates in comparison to FL-rutinosides. Furthermore, among FL, methoxylated derivatives are more readily absorbed than their hydroxylated counterparts due to their increased lipophilicity. The absorption of FL primarily occurs through passive diffusion, a more environmentally efficient process, especially for hydrophobic FL (Walle, 2007). FL absorption is subject to several other influencing factors, including the protein content of concurrently ingested foods. Given that FL tend to bind to proteins, their absorption remains limited until the concurrent dietary protein undergoes digestion. This dynamic interaction underscores the intricacies of FL absorption within the gastrointestinal tract. (Prasain & Barnes, 2007).

Continued biotransformation of FL in enterocytes. The key metabolic changes consist of glucuronidation, methylation, and sulphation. These conjugations are essentially phase II detoxification processes that increase the molecular mass and solubility of the drug, hence facilitating its excretion in bile and urine. Consequently, the enterocyte is necessary for FL metabolism. Certain FL aglycones that enter circulation are bound to albumin. Evidently, binding to albumin has no effect on the antioxidant Capacity of FL, which is significant in terms of the potential biological effects of FL that are absorbed (Janisch et al., 2004).

Finally, FL entering the bloodstream undergo segment ii liver detoxification. Formation of FL-glutathione adducts inside the liver contributes to more appropriate excretion (Spencer et al., 2004). Additionally, FL are excreted in bile and urine. For quercetin and other FL, the absorption and metabolic kinetics in humans have been examined. Hollman et al. (Hollman et al., 2001) demonstrated that subjects consuming 33.3 grammes of fried onion attained peak plasma levels of quercetin in 2.9 hours.

A flavonol, is thought to have unique immersion and dynamics relative to other classes. Anthocyanins are evaluated to be poorly absorbed and rapidly eliminated through urine. Citrus flavanones are efficiently absorbed but exhibit relatively short half-lives in the plasma (Manach et al., 2004). The pharmacokinetic characteristics of different FL are expected to display significant variability. Similar to many other orally ingested compounds, inter-individual differences play a crucial role in shaping the pharmacokinetic profiles of FL in the human body. Moreover, dietary instructions can exert variable effects on the bioavailability of FL. For example, the removal of peels from fruits and vegetables significantly reduces the FL concentration, as these peels often contain substantial amounts of FL.

For example, cooked onion, while onions are being cooked, FL diffuse out into the broth, enriching it with FL. Forty minutes of frying onions had no effect on the total quercetin content. Microwaving is associated with an increase in quercetin due to increased extractability (Nemeth & Piskula, 2007). Consumption of FL and protein together, although hypothesised to inhibit FL absorption, is no longer supported by

evidence. Accordingly, cooking seems to increase the FL availability of foods, as is now trendy.

## **1.9 THE EPIDEMIOLOGY OF FLAVONOIDS IN RELATION TO CANCER**

Extensive epidemiological research has provided substantial evidence supporting the health benefits associated with FL consumption, with particular emphasis on their anticancer effects. Cancer has drawn significant consideration in this context due to considerable disparities in mortality between populations with high FL consumption (e.g., China) and those with low consumption (e.g., North America and Europe). This phenomenon has been substantiated through numerous epidemiological studies, including both case-control and cohort investigations. It is noteworthy that, among the seven case-control studies conducted, two did not yield evidence supporting a protective relationship between FL consumption and the risk of cancers (Bosetti et al., 2006).

Even at the greatest levels of FL consumption, chemo preventive levels were not reached in any of these studies. These studies also vary from the study that demonstrated a strong negative correlation between FL consumption and mortality by virtue of their very long pattern duration. The chemo preventive potential of FL in the context of various cancer has garnered substantial support through extensive studies. These studies have consistently revealed a noteworthy contrary relationship between FL consumption and the risk of developing cancer.

It is important to underscore the scientific rigor and statistical significance of these large-scale prospective cohort studies, which have robustly demonstrated the inverse correlation between FL intake and cancer risk. Such findings underscore the considerable potential for FL to serve as chemo preventive agents against cancer, offering valuable insights for both clinical and epidemiological research in the field.



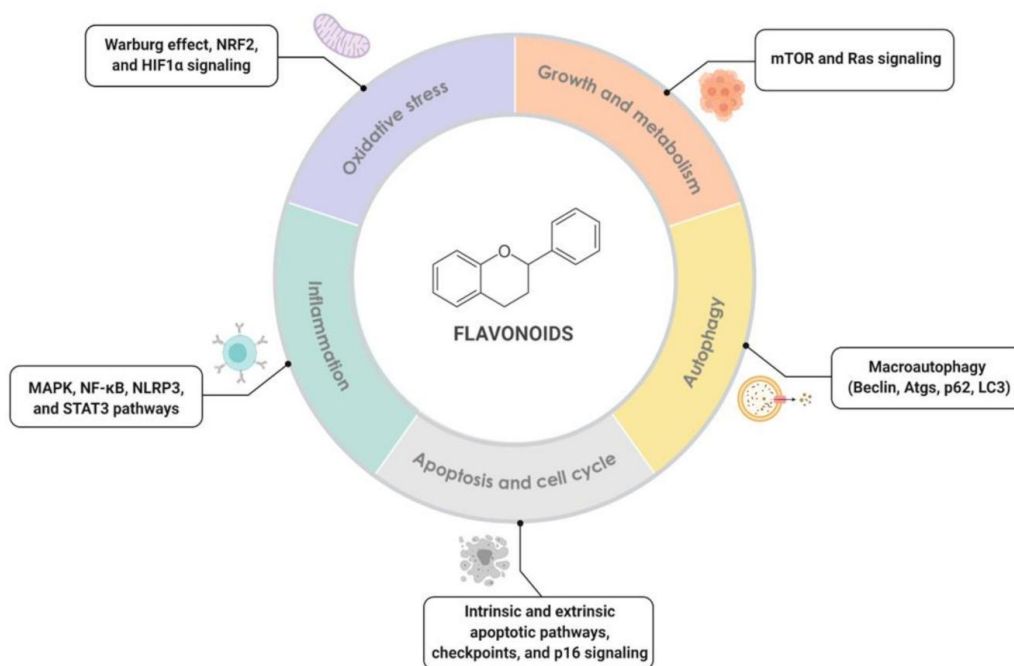


**Figure 1.16 : Molecular actions of FL in cell signaling in cancer (Ponte et al., 2021).**

In various studies, the consumption of soy isoflavones and green tea has shown significant reductions (Kurahashi et al., 2008) in the risk of cancer.

The favourable impact of FL on cancer extends beyond different malignancies. These bioactive compounds have demonstrated their potential as beneficial agents in the prevention and management of various cancer types. It is imperative to acknowledge that the scope of FL' anti-cancer effects encompasses a broader spectrum of malignancies, underlining their versatility and significance in oncological research and potential clinical applications.

This broad-spectrum effect of FL in countering cancer underscores the need for comprehensive investigation and exploration across diverse cancer types. The diverse mechanisms through which FL exert their anti-cancer properties further emphasize their potential for broader therapeutic applications. Consequently, understanding these mechanisms and their impact on different cancer forms can lead to valuable insights for cancer prevention and treatment strategies. Studies investigating the relationship between FL intake and the consequence of colon, stomach, and pancreatic cancer have yielded inconsistent results (Zeng et al., 2014). Variability in the methods used

for estimating FL intake in nutritional assessments has contributed to these discrepancies within the scientific literature. Furthermore, higher intake of isoflavones, black tea, and specific flavonols such as kaempferol and luteolin has been associated with a reduced risk of ovarian cancer (Ide et al., 2007). Despite the predominant evidence of FL anticancer properties, there is a unique case where an increase in FL intake connected with a reduced the cases of bladder cancer.

## 1.10 ARE FLAVONOIDS SAFE FOR HUMAN USE?

The availability of a wide variety of FL as nonprescription dietary supplements to the majority of the population brings FL protection to the forefront of public health concern. Numerous studies have examined the protective properties of FL, including in vitro and in vivo genotoxicity experiments that have been used to explore the impact of these FL (Yamakoshi et al., 2002).

In an in vitro salmonella mutagenicity experiment, studies assessing the toxicity of EGCG revealed no mutagenicity; nevertheless, dosages of 210 m were clastogenic. EGCG became non-toxic to rats at 50 mg/kg as an intravenous bolus and at 500 mg/kg/day after 13 weeks of treatment. Rats can only survive a lethal oral dosage of 2 mg/kg (Isbrucker et al., 2006). To determine procreant noxiousness, 14000ppm EGCG was supplied to pregnant mice throughout the course of gestation. Even though domestic pup growth and mortality had decreased, there was no evidence of teratogenicity.

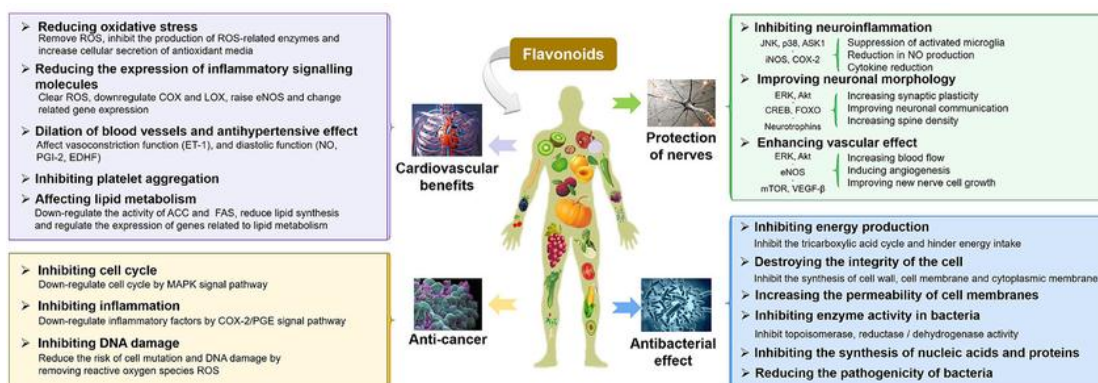


**Figure 1.17: Role of flavonoids in cancer as well as in other illnesses (L. Wang et al., 2021).**

There have been no abnormalities in haematology or serum chemistry. In vitro, EGCG does not seem to be mutagenic even at very high levels. At some time during pregnancy, EGCG must be avoided. ((Michael McClain et al., 2006). Similar to EGCG, treatment of genistein during gestation (1 g/kg) increased pup mortality without causing teratogenic effects (Ode et al., 2017). No adverse effects on growth, development, or subsequent reproduction have been confirmed by research on the effects of soy-based infant formula (Testa et al., 2018). Following administration of 600 mg of genistein per day to people for many weeks, neither micronucleus production nor rearrangement of the MLL gene occurred.

McClain and colleagues conducted an investigation to assess the impact of both short-term and long-term treatment with genistein at a dosage of 500 mg/kg/day in rats. Their findings revealed that this dosage had adverse effects on the rats, manifested by a decline in body weight and a decrease in food intake. The prolonged administration of genistein for a duration of 52 weeks revealed certain notable effects. It was associated with an improvement in liver gamma glutamyl transferase levels and a reduction in bile duct proliferation, indicative of a beneficial impact on liver health. However, the observations also pointed towards potential effects on hormone-sensitive tissues.

These consequences on hormone-subtle tissues were characterized by ovarian shrinkage. These findings collectively suggest that high-dose genistein has estrogenic effects on these tissues (Spagnuolo et al., 2015).

In summary, genistein did not exhibit genotoxicity in vivo when administered at high doses over a short term (2 mg/kg). However, in in vitro assessments, it displayed clastogenic properties. At significantly higher dosages, particularly at 500 mg/kg, toxic effects of genistein were observed, encompassing estrogenic side effects. It is noteworthy that a safe dosage for human consumption is determined to be 600 mg per day. Nevertheless, it is essential to underscore that the potential adverse effects on fetal development should discourage the use of genistein during pregnancy.

In conclusion, the amount of FL toxicity is dose-dependent. Extremely high dosages (>1 gramme per kilogramme) may cause hazardous adverse effects. FL supplements

sold over-the-counter are recommended at roughly 14 mg per kilogramme. However, FL self-supplementation is unlikely to have adverse effects in people. Although large dosages of FL were not teratogenic in the majority of trials, there was an increase in foetal loss and a decrease in pup weight. For these reasons, excessive FL consumption during pregnancy should be avoided.

In the present study, we employed an in-silico and in-vitro approach to evaluate the potential of Diosmin (DS) and Hesperidin (HS) as a ROS1 and EGFR in LC therapy. DS and HS are naturally occurring flavonoids found in citrus fruits and has been shown to possess anticancer properties in different cancer types (Patel et al., 2013),(Sheoran et al., 2023). Therefore, we aimed to investigate the binding affinity of DS and HS with ROS1 and EGFR associated with LC, assess its drug-like properties, and evaluate its stability during molecular dynamics simulations. Additionally, we analysed DS and HS absorption, distribution, metabolism, and excretion (ADME) properties as well as In-vitro analyses to gauge its potential as a lead compound for further development.

By employing Computational analysis, we aimed to provide a comprehensive understanding of the potential of Diosmin and Hesperidin as a ROS1 and EGFR in LC therapy. The findings from this in silico investigation can serve as a basis for future experimental analysis to validate and expand upon the computational results. Furthermore, successfully identifying DS and HS as a promising lead compound could pave the way for developing novel targeted therapies against LC, offering new treatment options for patients facing this challenging disease.

Molecular docking is a sophisticated process involving two stages. Initially, it focuses on the ligand's conformational changes within the active site of receptors. These conformations are then ranked based on their respective interaction energies, as outlined by Seyedi et al. in 2016 (Seyedi et al., 2016). To assess the interaction affinity between various ligand-receptor conformations, widely used tools like Auto-Dock, Swiss-Dock and GOLD are employed, as highlighted by Lounnas et al. in 2013 (Lounnas et al., 2013). In our research, we opt for GOLD and GLIDE for molecular docking due to their superior performance, accuracy, flexibility, and comprehensive

analytical capabilities. These tools enable us to delve deeply into the intricate interactions between ligands and receptors, providing valuable insights for our studies.

Pharmacokinetic factors are among the most essential features to consider while developing new medication compounds. Any medicinal substance produced as a medicine must have the best biological activity and pharmacokinetic qualities. Regarding pharmacokinetic characteristics, Pgp (p-glycoprotein), which is present in the liver and essential for drug discovery and creation, serves as an efflux pump. ROS1 gene rearrangement have been observed with different 5' fusion partners, including CD74, SLC34A2, KDELR2, FIG, TPM3, SDC4, EZR and LRIG3. However, the specific role, if any, that these partners play in the oncogenic function of the fusion kinase remains unclear (Govindan et al., 2012; Rikova et al., 2007; Takeuchi et al., 2012). In order to account for the dynamic nature and solvent effects of the ligand-receptor complex, molecular dynamic simulations were conducted. We performed Nano-formulations to enhance the efficacy and bioavailability of our chosen flavonoids.

### 1.11 DIOSMIN

Diosmin, a naturally occurring flavonoid found in citrus fruits, has gained significant interest for its diverse biological activities beyond its well-established role in improving venous health. Recent research suggests promising potential for diosmin in the realm of cancer prevention and treatment.

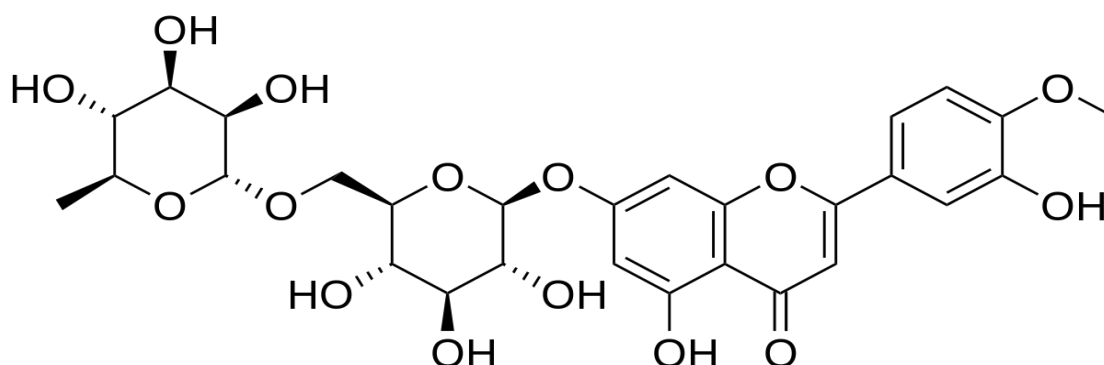


**Figure 1.18 : Chemical Structure of Diosmin**

Studies have revealed diosmin ability to interfere with various hallmarks of cancer, including uncontrolled cell proliferation, invasion, and metastasis. One mechanism involves its interaction with signaling pathways crucial for cancer cell growth and survival. Diosmin has been shown to downregulate the expression of specific proteins involved in these pathways, leading to cell cycle arrest and apoptosis (programmed cell death) in cancer cells (J. Liu et al., 2016). Previously, Diosmin is known for its bioactivities like, antioxidants, anti-inflammatory, neuro-protective, anti-diabetic, anti-pain and anti-mutagenic (Rahman et al., 2024).

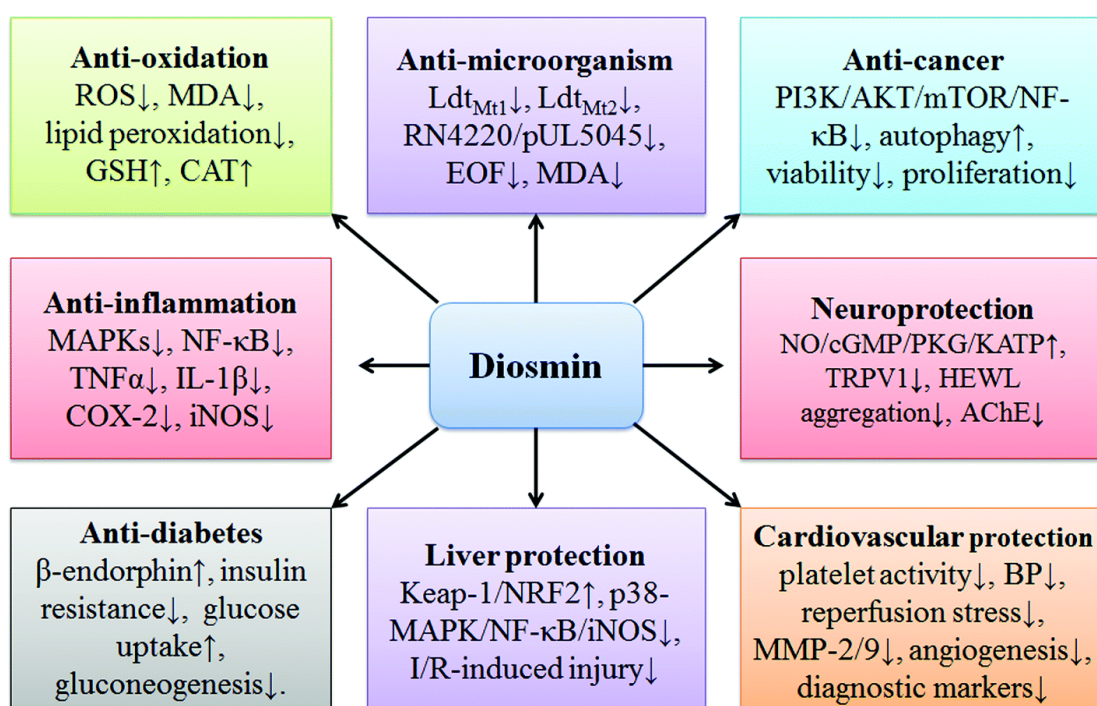


**Figure 1.19. Diversified effects of Diosmin.**

Furthermore, diosmin exhibits anti-angiogenic properties, hindering the formation of new blood vessels that tumors require for growth and dissemination. This disrupts the tumors ability to obtain essential nutrients and oxygen, ultimately leading to its demise. Additionally, diosmin antioxidant and anti-inflammatory effects are believed to contribute to its potential anticancer activity by mitigating oxidative stress and inflammatory processes that can promote tumorigenesis (Liskova et al., 2020).

While these findings are encouraging, it's important to note that most current evidence comes from preclinical studies conducted in cell lines and animal models.

## 1.12 HESPERIDIN

Hesperidin, a flavanone found abundantly in citrus fruits, exhibits a range of biological activities beyond its established role in improving vascular health. Recent research has shed light on its potential as a promising candidate in cancer prevention and treatment strategies.

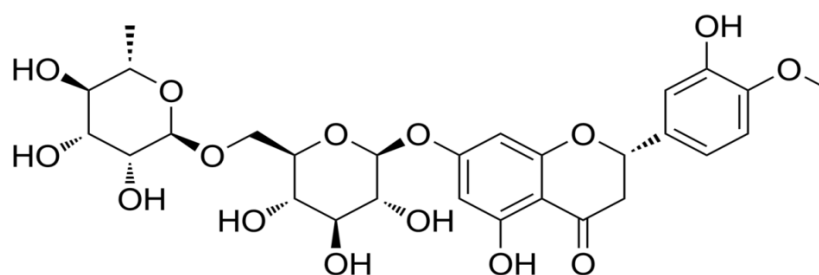


**Figure 1.20 : Chemical structure of Hesperidin**

Hesperidin's anticancer properties are attributed to its multifaceted approach, targeting various hallmarks of cancer progression. Studies suggest its ability to inhibit uncontrolled cell proliferation, a key driver of tumor growth. This effect is achieved through multiple mechanisms, including cell cycle arrest, induction of apoptosis (programmed cell death), and suppression of pro-angiogenic factors that promote blood vessel formation essential for tumor sustenance (Aggarwal et al., 2020) (Rahmani et al., 2023).

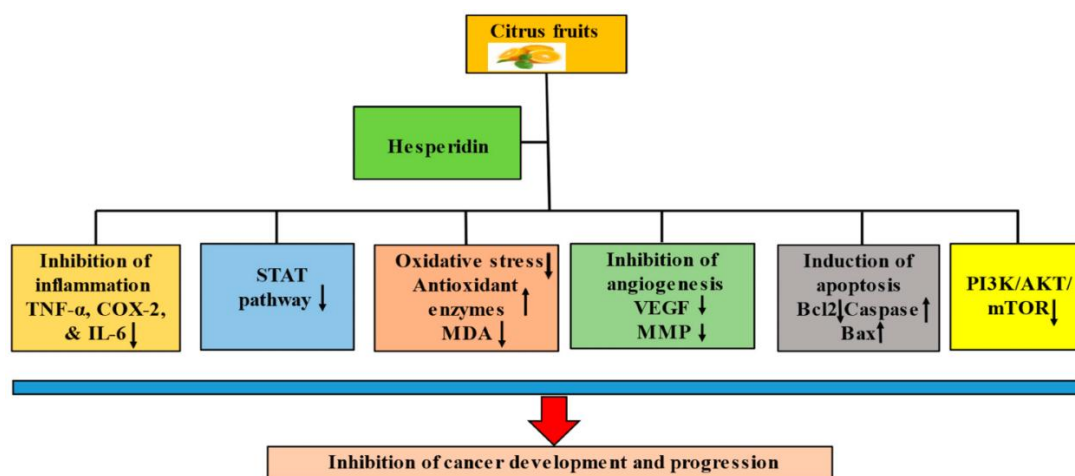


**Figure 1.21 : Mechanism of action of Diosmin in cancer care or prevention**  
(Rahmani et al., 2023).



Furthermore, hesperidin's antioxidant and anti-inflammatory properties contribute to its potential anticancer activity. By scavenging free radicals and modulating inflammatory pathways, hesperidin helps mitigate oxidative stress and chronic inflammation, both of which are implicated in tumorigenesis (Qiu et al., 2023).

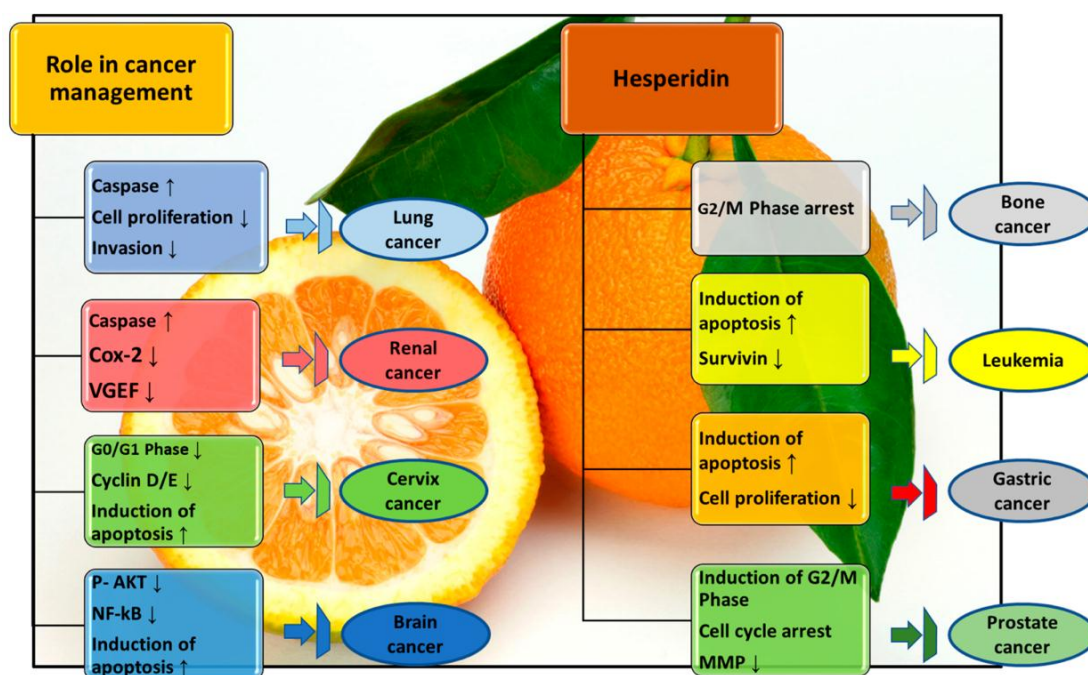


**Figure 1.22 : Role of Hesperidin activity in various cancer type.**

While preclinical studies in cell lines and animal models demonstrate promising results, further research is crucial. Well-designed clinical trials are needed to definitively establish the efficacy and safety of hesperidin in human cancer prevention and treatment. Nevertheless, the current evidence highlights the exciting potential of hesperidin as a natural compound with promising anticancer properties.

### 1.13 HYPOTHESIS

During the preliminary stages of LC, a complex interplay of causative agents, both endogenous and exogenous, sets the groundwork for the proliferation of this deadly disease. These factors trigger a chain reaction, leading to genomic instability and the failure of apoptosis, a natural process where damaged cells are programmed to self-destruct. Consequently, the intricate cellular surveillance system, designed to detect and eliminate abnormal cells, becomes compromised.



In this compromised state, the affected cells gain clonality, forming a genetically identical group. This clonality, coupled with a newfound survival advantage, propels the progression of the disease towards a more aggressive form—metastatic LC. This metastasis, where cancer cells spread from their original site to other parts of the body, marks a critical juncture, often significantly reducing the chances of successful treatment.

Understanding this intricate process is crucial in developing targeted therapies and interventions that can disrupt these pathways, offering hope to patients grappling with the challenges of LC.

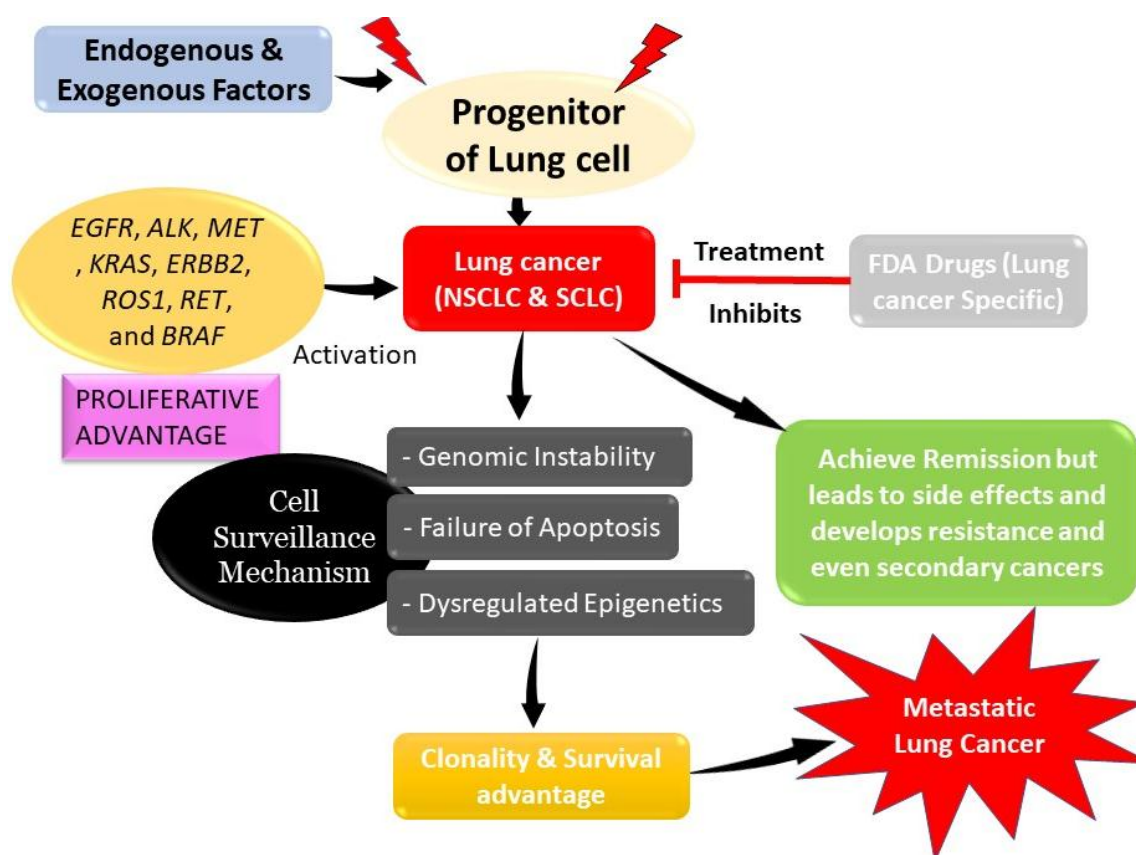


**Figure 1.23 : Hypothesis of Study**

## 1.14 AIM & OBJECTIVE

Evaluating the potential Flavonoids-Based-Nano-formulation as anticancer activity against LC

### **Research Objectives**

1. To screen the anti-cancer Flavonoids using Insilco based approaches
2. To evaluate the selected molecules based nano formulations against LC
3. To examine the qualitative and quantitative assessment of altered proteins through system biology-based approaches.

## Chapter – 2

### REVIEW OF LITERATURE

Cancer is a normal phrase used as malignant modes of pathological cell development when identifying a population of at least 100 diseases in one or more organs. In a series of genetic mutations, cancer creates and kills natural cell growth regulators. This cancer cells also divide and grow to tumors. Cancer cells may infiltrate and spread through the lymph or blood to distant organs. Biochemical pathways are understood to convert a regular cell into a cancer cell, but some of them are unclear (Fitzmaurice et al., 2019) Cancer is a metabolic disease explained by the dynamic relationship of carcinogenesis triggers with the hereditary and environmental influences. It is one of the world's most extreme diseases (Schiliro & Firestein, 2021). Cancer is a disease of cellular structure abnormalities. Mutual events involving the genetic material of a cell are known to deregulate the pathways of cell most critical processes. In fact, there have been many genetic defects prior to cancer (Pistritto et al., 2016); contributing to de-regulation of cell growth, apoptosis and repair mechanisms of signal DNA. Cancer cells will proliferate and expand until converted to suppress cell regulation effects in the absence of usual restrictions. There are several well-developed methods to transform normal cells into cancer cells. Oncological studies in the latter half of this century found that nearly all cancer cells had very low genetic and biochemical and cellular characteristics arising from significant routes of alteration (Kreeger & Lauffenburger, 2010).

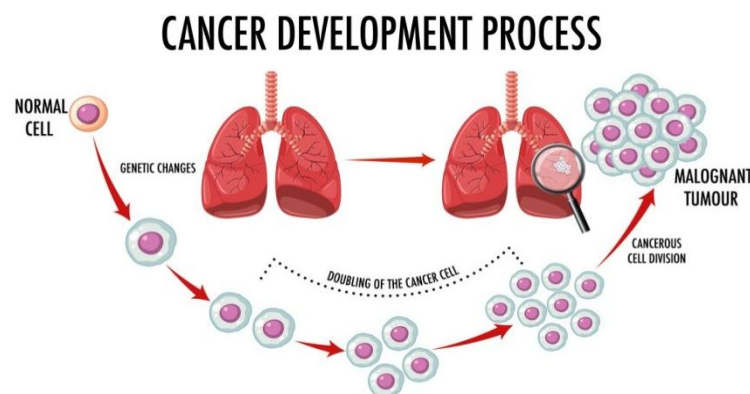


**Figure 2.1 : The cancer progression process.**

Angiogenesis facilitates the growth of primary tumors, enabling them to expand within the organ of origin and metastasize to distant parts of the body through the circulatory system.

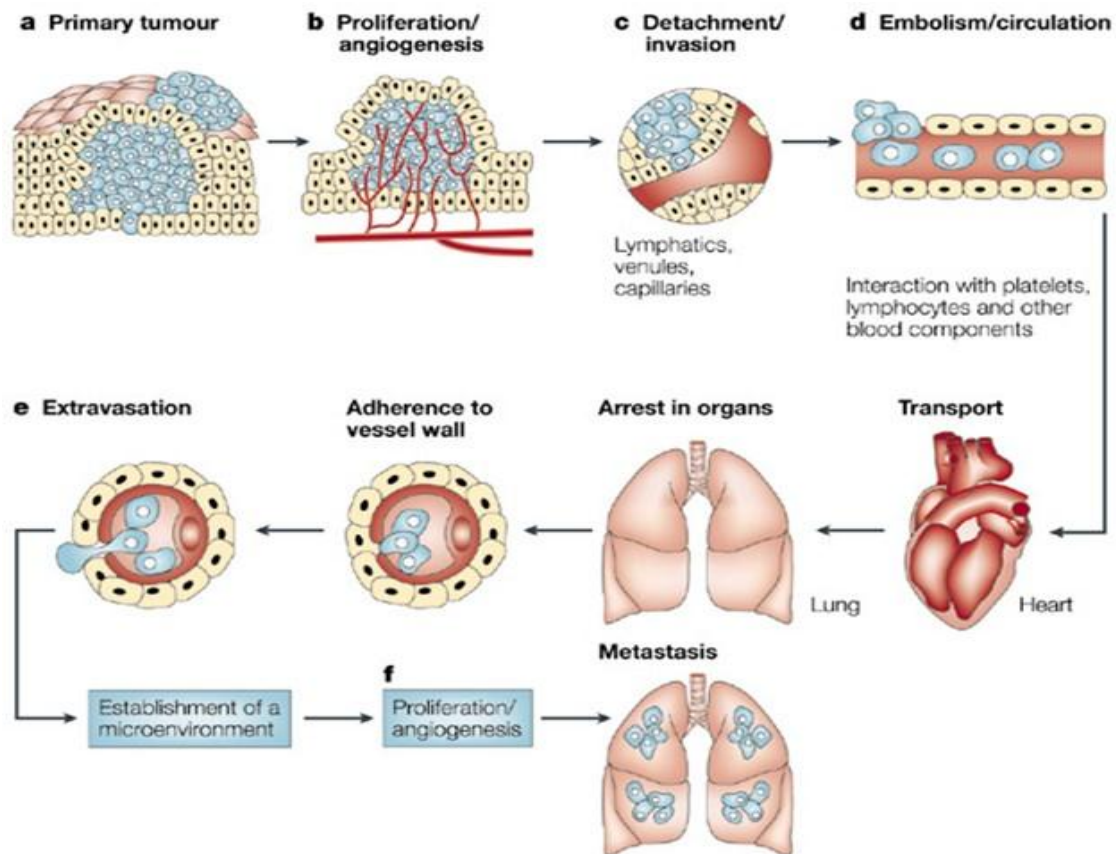


**Figure 2.2 : Cancer Pathogenesis (Fidler, 2003).**

## 2.1 CARCINOGENS

The bulk of human cancers are induced by the reaction to industrial cancer from both common and human-made toxins, radiation and viruses. Can be split into many carcinogenic groups (Timbrell 2000). Genotoxic cancerous acids or main cancerous acids are influenced, and cell components are reacted to. Alternatively, procarcinogens and non-genotoxic carcinogenic may require carcinogenesis with mitochondrial activation. The molecular forms of substances that cause cancer range considerably from metals to complex organic chemicals. The variations in shape and intensity suggest that carcinogenesis involves more than one direction. Original levels of carcinogenicity in diets are mold and aflatoxin, romantic fats, frying oils, smoking

and other foodstuffs, cigarettes, chemicals and preservatives. If deficient foods are added in the adverse setting, a food combination is blended in because of DNA and cancer damages, smoking, ultraviolet radiation, free radicals, lack of exercise and tension.

## 2.2 CARCINOGENESIS

It is understood that a regular cell will sometimes grow into a cancer cell over years or even decades. The cancerous stage consists of initiation, induction, and growth. The first step requires a reaction between the cancer agent (carcinogen) of the tissue cell and DNA. Genetic vulnerabilities can occur (Torgovnick & Schumacher, 2015). This is an idle time and only at a later stage is the individual at risk of cancer. The second phase takes place very progressively over many months or years. A shift in nutrition and lifestyle can have a beneficial influence now such that people cannot grow cancer during their lives. The third and final stage consists of cancer growth and distribution, such that the diet has less effect.

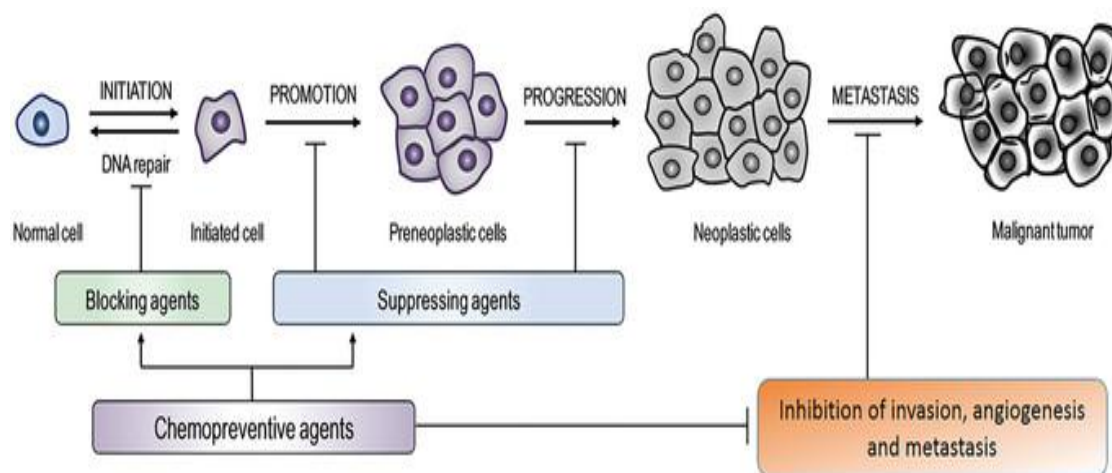


**Figure 2.3 : Different phases of carcinogenesis (I. A. Siddiqui et al., 2015)**

## 2.3 CELL CYCLE

Improved growth and impaired apoptotic activity of cancer cells. In a cell for DNA propagation, sufficient cell organs, membranes, soluble protein, etc. should be reliably reproduced, and the daughter's cell should likewise be divided between two daughter cells. This method needs immense guidance control to ensure the systematic

and precise synchronization of molecular activities. The inability to control the function of the cell cycle is quite expensive. Top eukaryotes have a defensive network where their basic life programme will display apoptosis. Cell multiplication is a process that has been tightly controlled and involves many control points to control the continuation of the unpredictable cell cycle. The cyclin, cyclin-dependent kinase (CDK) and CDK (CKI) inhibitors are regulated by transformations in the G1, S and G2/M phases modulated by a different transmission of the extracellular growth cue in an intracellular signal (Obaya & Sedivy, 2002). Using a minimal (R) or S phase feedback, transformations from G1 into S have been shown to be regulated until now by mitogenic reagents, intact cyto-skeletal network and cell obedience (Assoian & Zhu, 1997). In addition to the G1 control level, cell systems often prevent weak or abnormally synthesized DNA for girls at the G2 surveillance phase. (Kermi et al., 2019). One of the involving cell growth molecules is P53, a cell cycle receptor inhibition such as p21Waf1 CKI (J. Chen, 2016). The CKI p21Waf1 inhibits CDC2-cylinder B G2arrest complex (Hitomi et al., 1998).

## **2.4 INDUCTION OF APOPTOSIS IN HUMAN CANCER CELLS**

Cells which are no longer required or pose a hazard to the species are killed in multicellular creatures by a tightly controlled suicide of cells procedure referred to as programmable cell death or apoptosis. Apoptosis is generally seen throughout embryonic stages during growth to maintain homeostasis and verify the integrity of cell fractions. Another role of apoptosis has been characterized as a defensive mechanism that safeguards the immune system from injury or sickness. The process of apoptosis is characterized by specific cellular events, including membrane blebbing, DNA fragmentation, and condensation of both the nucleus and cytoplasm. These changes are accompanied by various phenomena and cellular activities, making apoptotic cells recognizable and eventually leading to their phagocytosis. This fundamental biological phenomenon occurs in a range of histo-physiological contexts, including tumor regression, regulation of damaged cell proliferation, and tissue remodeling (Sundarraaj et al., 2012). Apoptosis plays a crucial role in maintaining cellular balance and is essential in various biological processes, contributing significantly to the overall understanding of cell biology. Tissue

homeostasis and proper growth is involved in apoptosis (Kaziet al., 2004). Autoimmunity, neurodegenerative diseases, immune disorder, and any cancer may contribute to apoptotic disruption. The p53 protein plays an important role in neoplasm pathogenesis (Greenblatt et al., 1994). The mechanism involved rapidly raises p53 protein levels and mediates numerous cellular reactions, including the arrest of G1, corrective action to avoid degradation of DNA and activation of apoptosis (Bhaumik et al., 2000). Intracellular caspases (Salvesen and Dixit 1997), a class of systemic cysteine proteases, are one of the key symptoms of apoptotic cell death. Caspase operations are responsible for the cleavage of the regular cell-protein proteolysis, direct or indirect during apoptosis; for example, Caspases —2, -3, -6, -7 and —9 can be cleavage polymerase (PARP) polymerase (ADP-ribose). Bcl-2 is now recognized as one of the apoptosis regulators. A central control point for most apoptotic forms is the homologous protein Bcl-2, which is responsible for irreversible harm to the cell portion upstream (Adams and Cory, 1996).

## **2.5 LUNG CANCER**

LC, a highly aggressive and swiftly spreading malignancy, stands as the topmost cause of mortality in America. The likelihood of developing tobacco-induced LC is determined by intricate gene-enzyme interactions. These interactions influence the activation or detoxification of carcinogens, as well as the formation of DNA adducts, highlighting the complexity of the biological processes underlying susceptibility to this disease. Additionally, it is influenced by the effectiveness of the body's mechanisms for repairing DNA lesions. Notably, LC exhibits significant heterogeneity, emerging from various sites within the bronchial tree. Consequently, its symptoms and signs vary widely depending on its specific location. Alarming, 70% of LC cases are diagnosed at advanced stages (III or IV), underscoring the urgency for early detection and improved therapeutic interventions.

LC is one of the deadliest tumors for men and women (Fitzmaurice et al., 2019). The death risk is linked with three of the most common cancers (colon, breast and pancreas). More than half of those afflicted in one year after death was about 17.8 lakh, about five years after LC mortality and recovery. LC is also one of the leading

causes of tumor death linked with slow post-operative healing. Almost half of stage I patients and one third of stage II patients had primary treatment for an average of 5 years. But the NSCLC population is particularly heterogeneous relative to adenocarcinomas (ADCs), pseudo-cell carcinomas (SCC), large cells and anaplastic carcinomas.

Small lung carcinoma and non-small lung carcinoma are two main types of LC, inducing respectively 15 and 85% of all lung cell cancers (Sher et al., 2008). (Sher et al. 2008). 2008. NSCLC is further categorized in three classes as squamous cell carcinoma, adenocarcinoma and large cell carcinoma. Squamous cell carcinoma accounts for approximately 25% and 30% in all cases of LC. Early copies of the spinal cells are found in the bronchial tubes in the center of the epithelial lungs. This subtype of NSCLC shows a strong smoking cigarette link. (Kenfampet al. 2009).

Adenocarcinoma is the most frequent type of LC, involving around 40% of all LC. It is derived from small alveolar cells of the type II epithelial airways which secrete mucus and other materials (Noguchi et al., 1995). Adenocarcinoma in smokers and non-smokers, regardless of age, is the most prevalent type of LC (Curaud et al. 2012). This is obviously the case at the outskirts of the pulmonary system (Travis et al., 1995) due to the presence of smoke filters which prevent the penetration of the palm by large particles. This contributes to stronger smoke inhalation from peripheral lesions (Stellman et al., 1997). Adenocarcinoma also develops more steadily than most types of LC and is most often diagnosed before it grows outside of the lungs. 10% of pulse tumors are severe (undifferentiated cell carcinomas); no squamous or glandular maturation of this carcinoma type and therefore other alternatives may be considered mostly chance through elimination. Significant cell carcinoma begins mainly in the central lung, especially in surrounding lymphatic nodes, chest walls and remote bodies (Brambilla). In specific, smoking-related large-cell carcinoma tumors are (Muscat et al., 1997). The most prominent malignant tumor in the pulmonary system is by far, LC. Roughly 30% of LC is histologically multiple. The sporadic reaction to chemotherapy and comparatively low survival of neuroendocrine dysfunction will directly diagnose small cell LC. (Brambilla et al., 2009).



## 2.6 EPIDEMIOLOGY

LC is the third most often identified gene carcinoma in Germany. There is a net incidence of men and women in Germany of 65 per 100,000 and 21 per 100,000. The peak incidence is 75 to 80 years. Men are stable or marginally lower, but the trend is growing for women. The human community's prevalence and death rates about 20 years ago reflect the use of tobacco.

In LC development, exogenous agents, especially cigarette smoke, which can adversely affect the body, play a vital role. This trigger will connect approximately 90 percent of LCs. The risk of contracting LC reduced in the post-smoking age (Batzler et al. 2008). LC can appear years or decades after cancer. In infected cells, there are several genetic variations that ultimately contribute to invasive lung carcinoma.

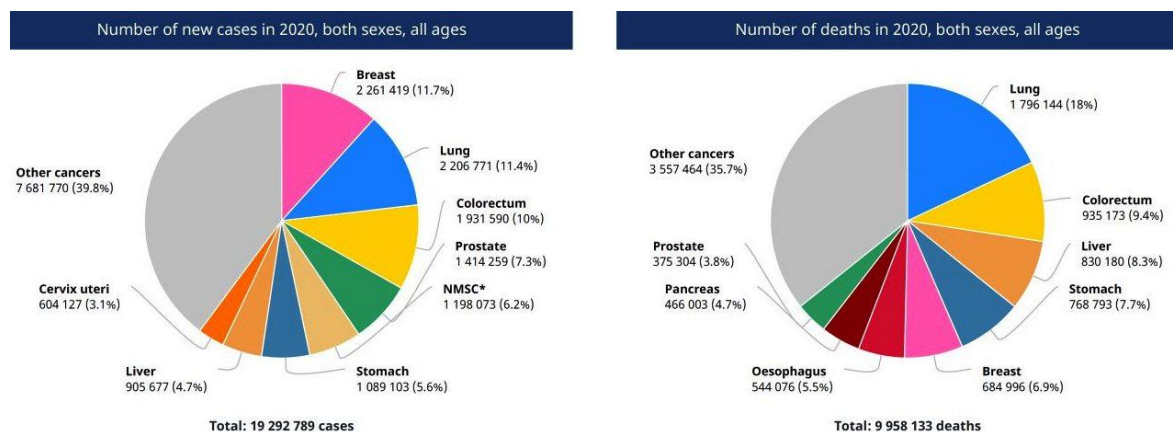


Figure 2.4 : The Epidemiology of Cancers (Globocon, 2020)

## 2.7 ETIOLOGY

A blend of critical factors and carcinogenic agents at work is part of the pathogenesis of LC. Pre-invasive lesions, including adenocarcinoma and adenocarcinoma with reduced invasion, have demonstrated a steady rise in malignant dysplasia (Alberg et al., 2013). Non-smokers with a lung disorder will also suffer from family and hereditary changes. In tumours, multiple genetic variants were reported. For example, an EGFR gene for EGFR (erlotinib [ Tarceva] and afatinib [Gilotrif]) or the EGFR monoclonal antibody (cetuximab [erbitux]) mutates 20 percent of adenocarcinoma. EGFR is an EGFR limited counselling applicant. The tumour mutations required for a

future analysis may also predict certain reactions or chemotherapy toxicity (Amann et al. 2005).

## 2.8 TYPES AND STAGING OF LC

Two primary forms of LC exist, NSLC and small cell LC (SCLC). Pulmonary condition depends on the locality of the cancer or when lymph nodes or pulmonary organs have spread. Since the lungs are huge, tumors can occur even before they are detected. And although there are signs such as coughing and exhaustion, other factors can be attributed. Early LC (stages I and II) is difficult to classify for this cause (Wistuba et al. 2019).

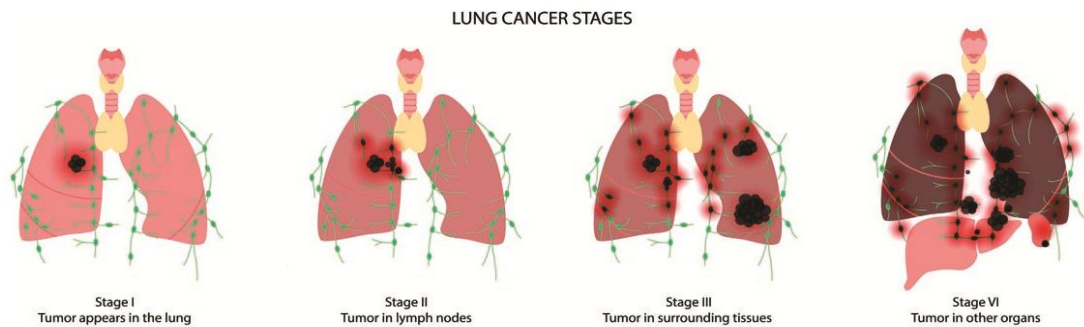


**Figure 2.5 : Different Stages of Lung Cancer.**

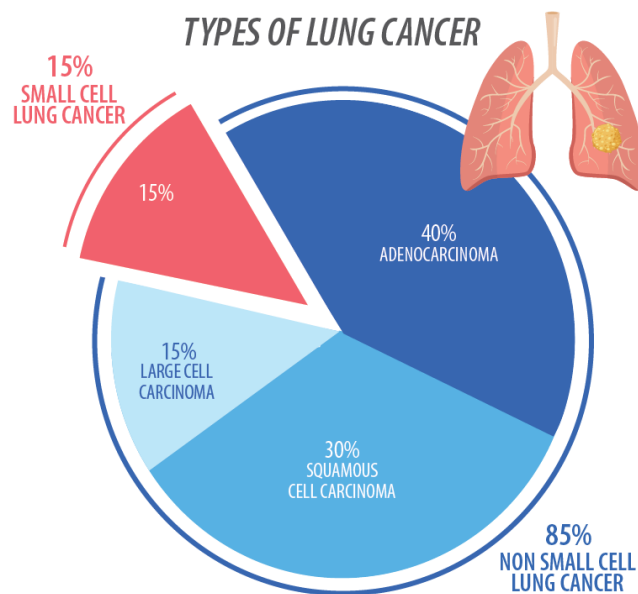


**Figure 2.6 : Types of Lung Cancer.**

### **2.8.1 NSCLC**

NSCLC makes up 85% of the total number of LCs, including: adenocarcinoma, the most frequent kind of LC in both the sexes in the United States.

- Squamous cell carcinoma, which is responsible for 25% of all lung malignancies; These, referred to as epidermoid carcinomas, accounting for about 30-40% of all primary lung malignancies. This form of cancer often develops in the core regions around large bronchi in a tiered configuration.
- Large-cell carcinoma, which accounts for around 10% of NSLC tumors, has epithelial tissue development and individual cell keratinization. (Becket et al. 2017) are huge and without any distinguishing physical characteristics. They are the least prevalent kind of NSCLC and commonly referred to as undifferentiated carcinomas.

#### **2.8.1.1 Stages of NSCLC Cancer**

Step I: Instead of all lymph nodes, cancer formed only in the lung.

Step II: lung and lymph nodes with tumours all over.

Step III: lung and lymph node cancer, also known as progressive disease, is in the centre of the abdomen. Step III consists of two subtypes:

Step IIIA notes that cancer has recently spread to the lymph nodes on the same side of the chest in which cancer has begun.

Step IIIB is called as cancer spreads through the chest or the lymph nodes' collar bone.

Step IV: This is the current form of LC that is now known as advanced. Cancer travels through the abdomen, the lungs or some other section of the body, such as the liver or other glands (Kay et al., 2018).

## 2.8.2 SCLC

The remaining 15% of lung tumors in the US are a small cell lung disorder. They tend to develop faster than NSCLC tumors. SCLC is typically more tolerant than NSCLC of chemotherapy.

**2.8.2.1. Stages of SCLC :** Restricted stage: at this phase, cancer arises on one side of the thorn and occupies just one section of the lung and the lymph nodes surrounding it.

Extensive step : Cancer has at this point spread to other chest or other sections of the body (Lovly et al., 2019).

The American Joint Committee on Cancer established a more elaborate staging system which uses roman numerals and letters (e.g. process IIA) for the identification of the LC of small cells. This mechanism is the same as for non-small cell LC development and proliferation (Rami-Porta et al. 2017). Cancer's anatomical staging is elucidated through a set of descriptive criteria. in **Table 2.1**

**Table 2.1 :Anatomic Stage/ Prognostic Groups**

Stage	Metastasis	Node	Tumor
Ia	M0	N0	T1a
	M0	N0	T1b
Ib	M0	N0	T2a
IIa	M0	N1	T1a
	M0	N1	T1b
	M0	N1	T2a
	M0	N0	T2b
IIb	M0	N1	T2b
	M0	N0	T3

<b>Stage</b>	<b>Metastasis</b>	<b>Node</b>	<b>Tumor</b>
IIIa	M0	N2	T1
	M0	N2	T2
	M0	N2	T3
	M0	N1	T3
	M0	N0	T4
	M0	N1	T4
IIIb	M0	N2	T4
	M0	N3	T1
	M0	N3	T2
	M0	N3	T3
	M0	N3	T4
IV	M1a or 1b	N Any	T Any

## 2.9 LC AND GRADING

Cancer grading assesses the appearance and behavior of cells in tumors and neoplasms when examined under a microscope. It differs from staging, indicating the degree to which the cancer has spread. The grade is assigned numerical values, representing the extent of cellular differentiation and the tumor cells' spread compared to their healthy counterparts. This standardized grading system, recommended by organizations like the American Joint Commission on Cancer, provides valuable information for understanding the cancer's aggressiveness and planning appropriate treatments.

## Gleason's Pattern Scale

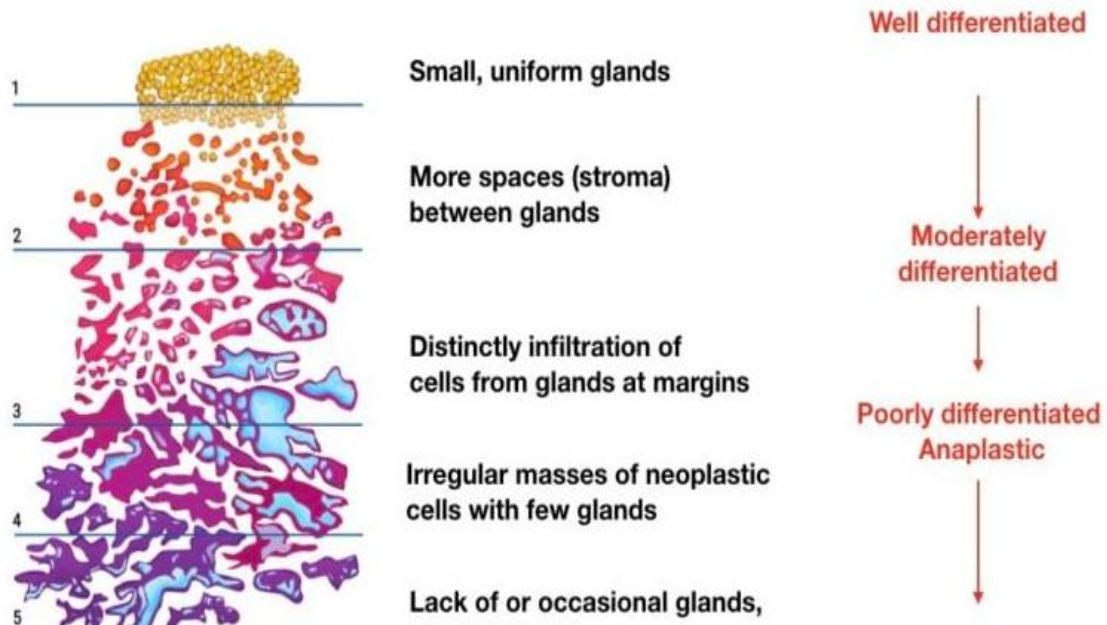


**Figure 2.7 : Gleason Grading**

### 2.10 PATHOGENESIS

LC, like other cancers, is driven by the activation of oncogenes or the suppression of tumor suppressor genes in the lungs, often due to mutations caused by carcinogenic agents. Notably, K-ras mutations contribute to a significant portion of lung adenocarcinomas, while the EML4 ALK tyrosine kinase fusion gene is found in a small percentage of non-small lung cell carcinomas. Inactivation of tumor suppressor genes can lead to changes in DNA methylation, histone modifications, and microRNA regulation. The epidermal growth factor receptor (EGFR) plays a crucial role in regulating cell processes and is commonly mutated in non-small-cell lung carcinoma, making it a target for treatment with EGFR inhibitors. Additionally, several other genes, such as C-MET, NKX2-1, LKBI, PIK3CA, and BRAF, are often mutated and amplified in LC. The role of stem cells in LC development is not fully understood, but they are implicated, particularly Keratin-5 stem cells, which are associated with squamous carcinoma in the proximal respiratory system. Metastasis in LC involves a transition from epithelial to mesenchymal cells, driven by signals like Akt/GSK3Beta, MEK-ERK, Fas, and Par6.

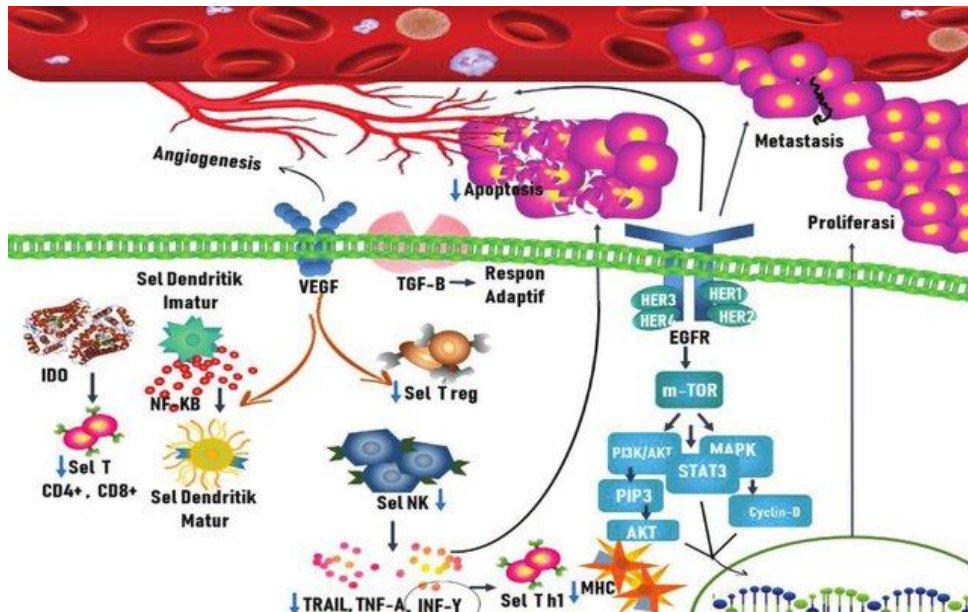


**Figure 2.8. The Pathogenesis in Lung Cancer as Point of Immunology (Anggaraditya et al., 2019).**

## 2.11 RISK FACTORS

DNA and epigenetic alterations were caused by cancer after genetic disorders. This influences natural cell functions such as cell division, cell death (apoptosis) programming and DNA repair. The higher the chance, the higher the incidence of cancer (Brown et al. 2010).

1. **Tobacco:** Smoking, particularly tobacco, is the greatest risk to LC. At least 73 documented carcinogenic compounds like benzo[ $\alpha$ ] pyrene are present in smoke. NNK, 1, 3-butadiene polonium isotope and 210 nuclear polonium (HechSS 2012, Kumar et al 2013). 90% (7% in women) of the men who died of LC arose in the industrialized world in 2000 (Peto et al., 2006). Smoking represents 85 percent of deaths from LC. Passive smoke - another individual smoking causes non-smoking LC. Almost 3,400 deaths from lung disease are suspected of passive smoking in the United States. Smoking pot is a significant source of carcinogenic chemicals, including tobacco smoke.
2. **Carbon Radon:** Radon gas is an odorless, colorless, radiation-declining gas that decreases the atomic uranium in the surface of the planet. The radiation



materials ionize genetic material and trigger cancer mutations. Radon is the second primary indicator of LC in the United States and induces about 21,000 deaths annually. For each 100 Bq/m<sup>3</sup> radon the risk improves by 8-16 percent. The amount of radon gas varies according to area, soil and rock. Roughly one household out of 15 has radon levels above appropriate per liter (pCi/l) (148Bq/m<sup>3</sup>) picocurie criteria (Schmid et al. 2010).

3. **Air and Asbestos Exposure :** The quality of external contamination has a minor influence on the high rate of LC. Small particulate matter (PM<sub>2.5</sub>) and sulphate sprays emitted by the traffic from the pollution fumes are highly probable. The chance of LC with nitrogen dioxide is 14 percent higher by 10 per billion. The quality of outdoor exposure is estimated to account for 1 to 2 percent of LC. A range of lung disorders, including LC, can be related to asbestos. Tobacco and asbestos affect the growth of LC synergistically.
4. **Genetics and Complex Risk Generators:** Residual conditions cause nearly 8 percent of LC. The frequency is doubled in households of lung disease. The gene mixture may be related to this (Dela Cruz et al., 2015). Polymorphism is known to impair LC in chromosomes 5, 6 and 15.

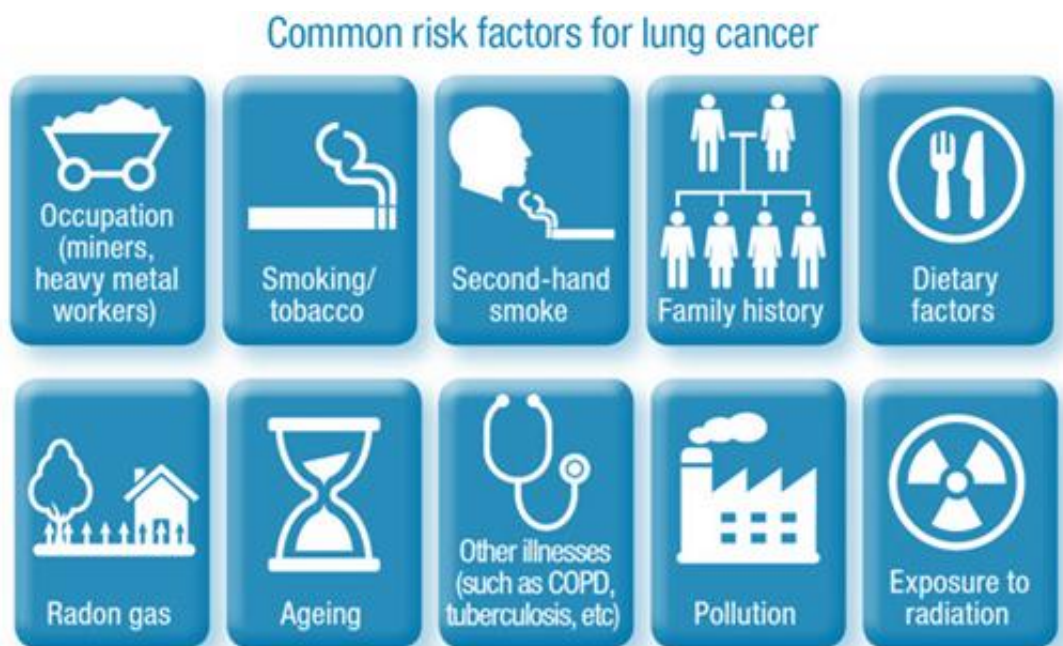


**Figure 2.9 : The Risk Factors of Lung Cancer.**



## 2.12 SYMPTOMS OF LC

Cases with LC are almost always symptomatic due to diagnosis. Primary tumors might cause symptoms (e.g., coughing, hemoptysis), spreading intrathoracic (e.g. Horner syndrome, upper-vein cava obstruction) and remote (e.g., bone pain). Tables 2 and 3 summaries these signs. Paraneoplastic syndromes may also cause symptoms, such as excessive anti-diuretic hormone syndrome (Table 4). These effects are a direct result of the tumor hormone ectopic or the body's response to the tumor. About 10 percent of patients with paraneoplastic syndrome have the most stable SCLC medicine for paraneoplastic syndromes. Wireless clubbing is a general misconception in paraneoplastic Syndrome that is most observed with NSCLC (Beckles et al. 2003).



**Figure 2.10 : Symptoms of Lung Cancer.**

Many records of symptoms of LC originate from referral facilities, which renders extrapolating primary treatment challenging. Hemoptysis and digital clubbing are two

separate symptoms (Hamilton et al., 2005; Shapley et al., 2010, Schim et al., 2014). These independent LC predictors include appetite drop, weightlessness, nausea, exhaustion, dyspnea, chest and rib pain. Patients seldom experience a special, stronger symptom when two or three signs are known. For example, the combination of weight loss and hemoptysis is 9.2% essential (Hamilton and Sharp. 2004). LC is expected to develop in patients 40 years of age who have risk factors and symptoms. Doctors might be aware, but LC develops without established risk factors for younger adults and individuals.

Dysphagia (difficulty swallowing) may result from esophageal invasion. Large blockages may cause lung collapse in extreme instances, raising the possibility of pneumonia (Mavros et al., 2011). These symptoms reflect the diverse and frequently severe effect of LC on the respiratory system and overall health.

### **2.12.1 Symptoms related to Metastasis**

If LC cells migrate to the bones, they may cause agonizing pain. When bone metastasis occurs, it may induce a variety of neurologic symptoms such as seizures, headache, altered vision, or signs of stroke (Horn et al., 2012).

### **2.12.2 Paraneoplastic Symptoms**

Most lung tumors tend to be accompanied by symptoms caused by the tumor cells' release of hormone-like chemicals. The paraneoplastic syndromes are most typically associated with SCLC, although they may also occur with other kinds of cancers in certain situations. The most common paraneoplastic symptom found with NSCLC is the production of a parathyroid hormone-like substance (Horn et al., 2012).

### **2.12.3. Non-Specific Symptoms**

Weight loss and weariness are two non-specific symptoms of LC. Many individuals (approximately 25%) have no indications of LC, yet the illness is diagnosed as a single lump on a routine chest X-ray or CT scan. At the time of diagnosis, some of these individuals with tiny and/or single masses had no symptoms (Alberg and Samet, 2010).

### 2.13 PREVENTION

The widespread use of cigarettes in the 20th century contributed to the 21st century outbreak of LC. >1.3 million worldwide LC deaths in 2001 are estimated. The identification of LC was limited to advanced methods of identification and improvement in local and systemic procedures. In all phases of LC, the average survival rate of 5 years was 5 percent in the 1950's equivalent to 14.5 percent in 1992–97 (Ries et al., 2001, Khuri et al., 2001).

These sober findings have contributed to greater consideration being given to clinical methodologies for avoidance of health and LC by reduction of cancer through stopping smoking, and to pharmacological attacks directed at multi-stage tumor-original pathways induced by cancer of tobacco. More commonly recognized as chemoprevention, this latter approach was marked by a combination of achievements and failures affecting tobacco-related epithelial cancers.



**Figure 2.11 : The preventive measures against lung cancer.**

Specifically, 13 cis-retinoic acids are used to control pre-malignant oral lesions and to prevent primary cancer of the head and neck (Hong et al., 2000). This technique was

nonetheless related to considerable toxicity, which excludes extended administration and does not preserve the feasibility of discontinuation. Several clinical studies have found that NSCLC chemical avoidance has either been ineffective or has possible harmful consequences in retinoids, alpha-tocopherol and  $\beta$ -carotenes (Lippman et al., 2001, Tockman et al., 2001).

## 2.14 DIAGNOSIS OF LC

The diagnosis of LC involves histological examination validation, determining the tumor's distribution (staging), and assessing the patient's overall health for further treatment decisions. The course of action depends on the patient's general condition and prognosis. In cases with confirmed distant metastases, complex diagnostic procedures for precise staging are not typically initiated. Managing non-small cell LC effectively hinges on accurately determining the cancer's stage and evaluating the patient's health status.

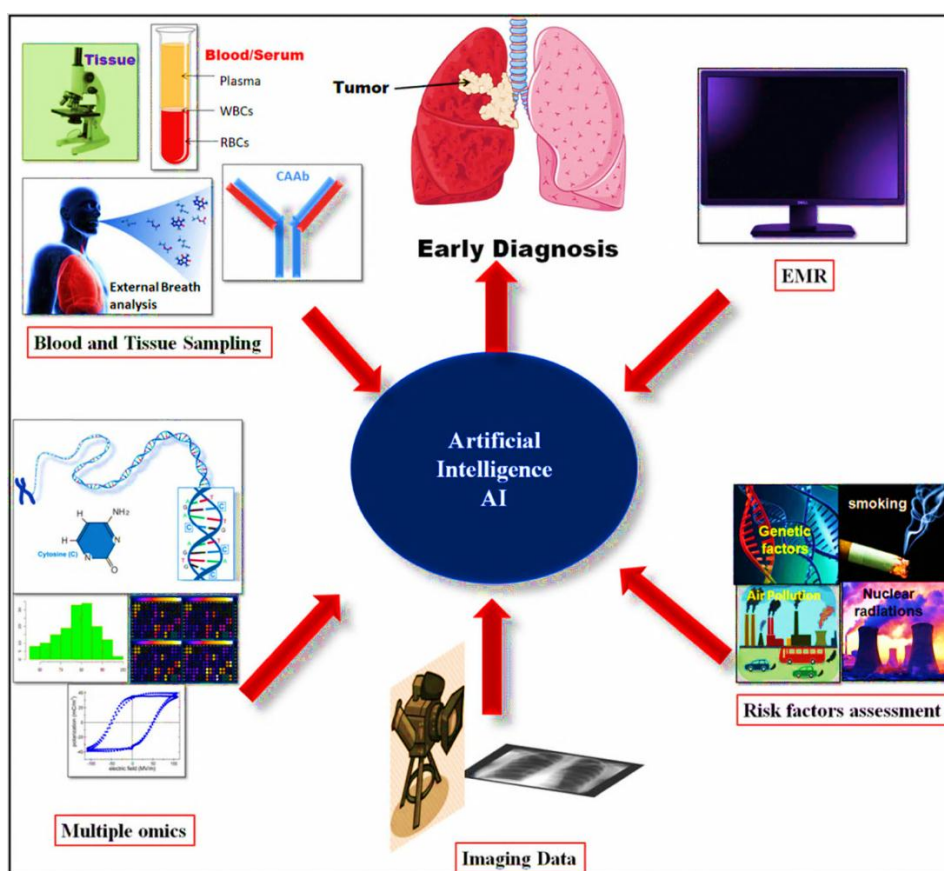


Figure 2.12 : Diagnosis of Lung Cancer.

## 2.15 HISTOLOGICAL CONFIRMATION

The crucial aspect in LC treatment is distinguishing between SCLC and NSCLC. Differentiating subtypes of NSCLC is increasingly important because to licensing variations and the effectiveness of various chemotherapies and targeted drugs. In both cases, histological proof may be necessary, but clear cytological findings can suffice when a biopsy is not feasible. Diagnostic tools such as bronchoscopy, ultrasound, fluoroscopy, or CT scans are used to determine tumor characteristics and lymph node involvement. Preferably, histological confirmation is based on a metastatic sample, minimizing damage to the lung tissue.

## 2.16 EVALUATING THE EXTENT OF DISEASE

The international stage treatment is used for cancer of small cells and non-small cells of the lung. A separation between 'limited illness' (i.e., one hemithorax-only disorder) and a 'extensive disease' (expansion outside one hemithorax) is created with small cell LC (Simon et al. 2007).

**T Descriptor :** CT enhanced contrast is the most important T-descriptor measurement measure. MRI may provide more specific information about the penetration of thoracic structures in a few instances. (Silvestri et al. 2007). 2007. 2007. 2007. MRI is of paramount significance in the examination of invasion of brachial plexus vascular and neural structures in patients with Pancoast tumors.

**N Descriptor :** Contractually improved chest CT is sensitive to mediastinum alone in patients without remote metastasis between 51 and 64 percent, and has a vulnerability between 74 and 86 percent, which is inadequate to assess mediastinum alone. Positron emission tomography (PET) or PET-CT has become the most effective, non-invasive therapy for mediastinal N-staging, but it is not optimal at least with a sensitivity of 74% and a precision of 85%. When the lymph node is extended (>1cm), the immunity of PET/PET-CT is up to 100% with a precision of 78% (Gould et al. 2003). The PET-positive mediastinal lymph knots are biopsied for final inspection if curative treatment is intended. Mediastinoscopy (includes lymphadenectomy aided on media), endobronchial, esophageal, and transbronchial (TBNA), based on where the

goal lymph node is situated, are important (Dette becket al., 2007). PET and PET-CT allow the accurate identification of the target node for lymph node stadium biopsy validation.

**M Descriptor:** Far metastases typically talk against healing medication. Far metastases in the brain, liver, skeleton, lung and surreal are more frequently found.

## 2.17 TREATMENT OF NSCLC

In this segment, normal and new therapies will be addressed for early, advanced and persistent NSCLC and brain metastasis.

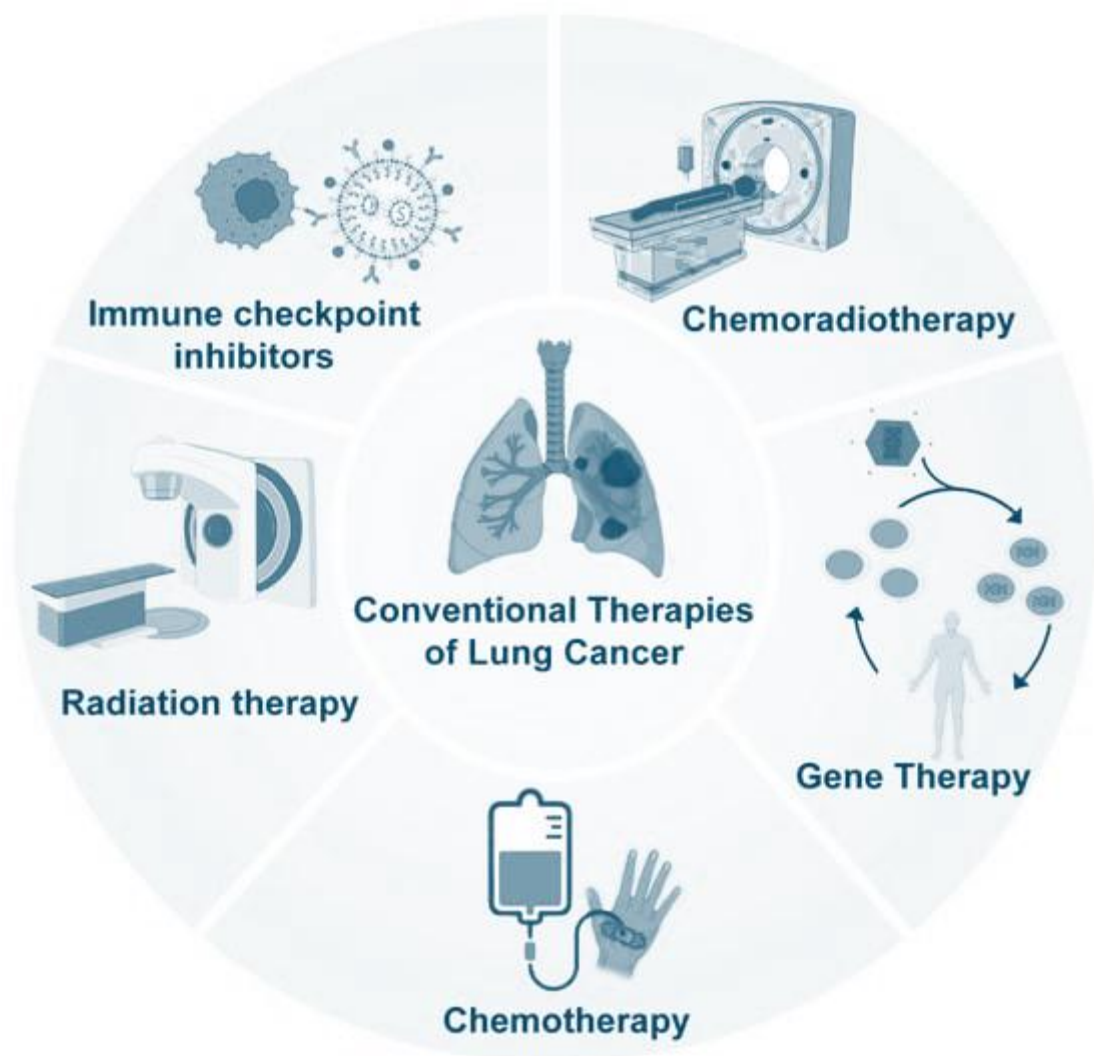


Figure 2.13 : Treatment options of lung cancer.

### **2.17.1 Treatment of Early Stage (Stage I and Stage II) NSCLC**

Surgery was used to treat early-stage cancer and operational disease (stages I & II), which is the greatest option for prolonged survival (Sangha et al., 2010). The 5-year average recovery rate following surgery is 60%-80% for stage I NSCLC patients and 30%-50% for stage II NSCLC patients (Tanoue & Detterbeck. 2009). In situations of rejection or unresectable tumors in high-risk patients, key radiology, including stereotactic body radiation treatment (SBRT), may be employed. However, post-operative radiation treatment is not recommended for patients in Phase I or Phase II (Howington et al., 2013). Adjuvant platinum-based chemotherapy has been demonstrated to be effective in stage II patients with NSCLC (Pignon et al. 2008), and therapeutic approaches for totally resected patients have been proposed. Step I adjuvant chemotherapy, on the other hand, may not give a clear benefit in patients with NSCLC (Group et al., 2010).

### **2.17.2 Treatment of Stage III NSCLC**

Roughly 70 percent of NSCLC cases are identified in early phases (Travis et al. 2013), as well as in metastatic diseases (stages III and IV). NSCLC Step III is a multi-node multiple microscopic tamp heterogeneous disorder (Winton et al. 2005). The five-year OS occurrence ranges for Stage IIIA N2 from 10 to 15 percent and for Stage IIIA bulk mediastis from 2 to 5 percent (Scagliottiet al., 2003). The clinical approaches, including radiation therapy, chemotherapy and surgical resection, are chosen and resistible in this heterogeneous population of patients with NSCLC. (Hottaet al. 2004). 2004.

Operation is the standard care of resectable stage IIIA patients with NSCLC with the following chemical treatment (Arriagada et al., 2004, Edell et al., 1992). Adjuvant chemotherapy revealed that clinical evidence indicates major increases in OS levels and better control of resected stage IIIA-N2 disease by adjuvant therapy (Group PM-aT., 2005). Meta-analysis of many clinical trials reveals that during the past five years, survival by neoadjuvant chemotherapy increased moderately by 5 to 6 percent (Gilligan et al., 2007).

Unresectable stage IIIA patients may receive conventional drugs for patients that cannot be handled with combination therapy, with either concomitant or combined combination chemotherapy and radiation (chemoradiation) or with external care. Meta-analysis of multiple randomized clinical studies indicated that platinum chemoradiation therapy significantly reduced the likelihood of death by 10 percent in contrast with radiation treatment alone (Auperinet al. 2006, Rowell et al. 2004). Several clinical tests have demonstrated that drastic intervention may offer up to 50% for stage IIA patients with dense primary tumors of the five-year survival rate in comparison to incomplete patients with resection (Doddoliet al. 2005, Faccioloet al. 2001, Matsuokaet al. 2004). Phase IIIB NSCLC accounts for about 17.6% of all LCs with an estimated 5-year survival of between 3% and 7%. Step IIIB NSCLC care options and sequence are focused on the position of the tumor presence and patient condition (PS). In addition, the treatment itself would not support patients with Step IIIB NSCLC. Standard care comprises either of a sequential chemotherapy cocktail or external radiation treatment in these situations. NSCLC Stage IIIB should only be treated as external radiation treatment to reduce discomfort and other symptoms and enhance quality of life.

### **2.17.3 Treatment of Stage IV Non-Small Cell LC**

Step IV NSCLC accounts for 40% of newly diagnosed NSCLC patients. The choice of phase IV NSCLCs is dictated by different factors, including variations of external radiation care, merged chemotherapy, blended chemotherapy and internal or laser treatment, including co-orbidity, PS, histology and molecular genetic features of patients with phase IV NSCLC disorder. Operation can often be utilized in some cases to control disease-related conditions close to radiation therapy.

### **2.17.4 Towards EGFR Tyrosine Kinase Inhibitors (first line)**

The first NSCLC approved medicines for use in agents such as inhibitor tyrosine kinase (TKI) Erlotinib (Tarceva) and gefitinib (Iressa), which directly block EGFR. This recipient will lead irregularly to EGFR mutations that cause unregulated cell proliferation that is responsible for several cancer subsets, including NSCLC (Maemondoet al., 2010).



Several randomized clinical test data suggest that first-line treatment may be administered with a single-agent gefitinib for patients with EGFR active mutations, especially for platinum contraindications. (Swedish and some, 2011). 2012. 2012. Conversely, it facilitates cytotoxic chemical care if the position of an EGFR mutation is unacceptable or unknown. Three large randomized controlled experiments have shown that fitinib or erlotinib is better in Eastern Asia than first-line phase III or IV platinum compound chemotherapy for non-smokers or former bright smokers (Mitsudomiet al. 2010). It has been demonstrated that fitinib or erlotinib improves PFS, not OS, and favorable toxicity profiles were reported in a large European randomized clinical trial for EGFR-negative and adenocarcinoma patients. Comparable benefits against platinum-driven chemotherapy were recorded early in the early phase (PFS: 9.7 versus 5.2 months; neither erlotinib nor gefitinib in conjunction with cytotoxic chemotherapy was reported as initial treatment.

## **2.18 EGFR INHIBITORS FOR RECURRENT NSCLC**

Erlotinib has been shown to improve survival in the randomized Phase III trial to contrast gefitinib and placebo in chronic patients with NSCLC, suggested as a valid treatment of NS CLCC patients with improved placebo survival in non-smokers (median 8.9 MB versus 6.1 MB) and in Asian patients (median 9.5 MB versus 4.5 MB) (Thatcher et al. 2005). (Thatcher et al., 2005). In comparison, erlotinib therapy has improved the outcomes of patients rather than placebo, for example contaminants, discomfort and breathing difficulties. Erlotinib has not increased survival of standard second-line docetaxel or pemetrexed chemotherapy in the first-line platinum combination treatment in recurrent NSCLC patients (Ciuleanuet al., 2012).

## **2.19 TREATMENT OF SCLC**

About 15 per cent of all lung carcinomas are represented by Small Cell LC (SCL4\*56742C). Smoking is the highest risk factor for growth of SCLC, and a reduction in smoking and tobacco intake per person in the US could account for the recent decrease in the rate of SCLC (Murray et al. 1993). Limited-stage illness (LS-SCLC) is diagnosed to be 30 per cent of patients in SCLC who have cancer-confined

hemithorax, mediastinum or supraclavicular lymph nodes. In 70 per cent of SCLC cases, tumors that reach into supraclavicular regions are diagnosed with large-stage cancer (ES-SCLC). While SCLC is at first more sensitive to chemotherapy and radiation than any other type of LC, its rapid growth and widespread diagnosis are exceedingly challenging to handle. Govindan et al., 2006.

The care options of SCLC patients are like other LCs, depending on the histology, degree, general health and patient comorbidities. Standard LS-SCLC care options involve platinum chemotherapy and radiation, combination chemotherapy alone, surgery accompanied by chemotherapy, or chemoradiation, as well as cranial prophylaxis (Joshi et al., 2013). Chemotherapy and palliative care are the therapeutic methods for persistent SCLC. Whereas chemotherapy and radiation therapy may lead to extreme initial reactions in SCLC, disease recurrence is common. The overall forecast for SCLC patients, considering the improvements in research and treatment during the past two decades, is still below average. Untreated SCLC, with median diagnostic survival of just 2-4 months, is the most aggressive of all LCs. The two-year DFS remains decreased by 10 percent after the care of SCLC patients (Johnson et al., 1990). In comparison, the operational system of each patient aged 5 to 10 percent (Fry et al. 1996, Lassen et al. 1995) of every 5-year-old SCLC patient is greater than the ES-SCLC patient (a 14% five-year survival) (Janne et al. 2002, Turrisi et al. 1999). Cranial prophylactic radiation can prevent recurrence of brain metastases in fully-chemo treated cases, thereby improving patient safety (Auperin et al., 1999, Slotman et al., 2007).

Although LS-SCLC-patients may gain from surgery or chemotherapy alone, combination treatment has demonstrated increased survival (Videtic et al. 2003, Janne et al. 2002). Especially the combination of chemotherapy and thoracic radiation therapy (TRT) improves OS by five percent in comparison to chemotherapy alone (Pignon et al., 1992, Warde and Payne, 1992). Although the median survival in ES-SCLC patients can be maintained for 6-12 months, long-term DFS is uncommon in ES-SCLC patients (Perry et al., 1987, Takada et al., 2002).

### **2.19.1 Targeted therapies in SCLC**

#### **a) EGFR inhibitors**

EGFR mutation is less prevalent in SCLC than NSCLC, with just about 4 percent of patients exhibiting a mutation (Tatematsu et al., 2008). The patients have been stratified and treated with gefitinib in a phase II study focused on chemosensitizer or chemical-refractory SCLC. However, in SCLC patients, the above research did not show a gefitinib benefit (Moore et al., 2006).

#### **b) VEGF inhibitors**

ES-SCLC investigated the circulation of VEGF inhibition with bevacizumab. Cisplatin, irinotecan and bevacizumab in previously untreated patients seeking chemotherapy, 75% ORR had 11.6 months of median OS and 7.0 months of median PFS (Ready et al. 2011). A study of cisplatin, etoposide and bevacizumab research showed that the elevated baseline levels of vascular molecular adhesion (VCAM) but no other biomarker may be correlated with the clinical result of previously untreated ES-SCLC patients (Horn et al., 2009). Other VEGF antagonists, including sorafenib, sunitinib and cediranib multikinase inhibitors, are also studied on a clinical basis (Gitlitz et al., 2010). Aflibercept (AVE0005) is a completely humanized immunoglobulin protein that fuses in the IgG1 constant area of both VEGF VEGFR1/2 receptors. These soluble receptors function as a VEGFR trap and prohibit VEGF from connecting to its normal receptors. Aflibercept is being tested in combination with topotecan in ES-SCLC (Joshi et al., 2013).

### **2.20 PROGNOSIS**

Of all patients with LC in the United States, 16.8% remain after diagnosis for a five-year duration (Ridge et al. 2013). Total LC mortality in England and Wales was measured at 9.5 percent between 2010 and 2011. Outcomes in developed nations are usually poorer. Diagnosis has even improved. In the NSCLC situations generally, 30%–40% is in stage IV and 60% is in stage IV.

The NSCLC's predictive variables are the lung signs, large tumors (> 3 cm), cell form non-squamous (histology), stage (proliferation) and numerous lymphatic and vascular

invasion metastasis. The outcomes for those with poor efficiency and weight reduction was greater by more than 10% than those with inoperative diseases. The prognostic factors for small lung cells include diagnostic performance, biologic sex, illness and central nervous system or liver involvement.

The highest prediction for NSCLC is full operative resection with a survival of up to 70% of stage IA cancer over five years. (Spiro SG. 2010) The average survival rate for individuals with large-scale SCLCs for five years is less than 1 per cent. The total remission time for limited-stage diseases is 20 months, with a survival rate of five years of 20 percent. According to National Cancer Center, the median age of diagnosing LC is 70years in the USA and the median age of death is 72 years. In the US, individuals with medical insurance are more likely to receive positive performance. (Slatore et al., 2010).

In 2021, Melosky and others reported that a complete review of accessible data, as well as an easy-to-use interface to the present state of new targeted treatment in oncogene-driven advanced NSCLC This rapidly growing area has yielded several new targeted therapeutic options and encouraging results have resulted to the FDA approval of 7 novel medicines for use in advanced NSCLC. Several phase III studies are under ongoing to completely examine novel potential medicines under development for enhancing outcomes in patients with NSCLC having various molecular subgroups. Advances in NSCLC molecular characterization have resulted in a more rapid capacity to precisely block molecular changes of concern. As a result, there has been an explosion of innovative target chosen therapy for oncogene-driven advanced NSCLC, resulting in a slew of new therapeutic choices for advanced NSCLC. Despite the challenges of remaining on top of this ever-changing therapy environment, these discoveries help us get closer to our goal: better treatment for cancer sufferers (Melosky et al., 2021).

In 2021, Cong Zhang and colleagues reported that, Cox15 emerged as a promising prognostic molecule for LC patients. Identified as a novel oncogene, Cox15 plays a crucial role in promoting the growth of LC cells. Notably, Aripiprazole, a potent Cox15 inhibitor, demonstrated substantial inhibitory effects on LC cell proliferation

and tumor development both in vivo and in vitro, showcasing its therapeutic potential. The study also revealed that Cox15 expression profiles are correlated with overall survival rates in LC patients, indicating its significance as a potential prognostic biomarker. Targeting Cox15 in future treatments holds promise for highly effective and specific therapeutic approaches in LC patients. However, it's important to note a limitation of this study: there is still a lack of comprehensive understanding regarding the underlying processes through which Cox15 enhances LC growth [11]. Despite this, the findings provide substantial evidence linking Cox15 to LC progression, paving the way for further research and potential targeted therapies in the future (Zhang et al., 2021).

In 2021, Pratibha Pandey and others stated that Hesperidin has the potential to be a powerful and attractive option for medications and cancer care. Hesperidin works by influencing many pathways in cancer cells, including cell cycle arrest, apoptosis, antiangiogenic, ant metastaticity, and DNA repair. Hesperidin has been shown to affect a variety of carcinogenic molecular targets. Combining chemotherapy medications with phytoconstituents would be a more effective strategy to treating cancer. In most cases, hesperidin has little effect on the action of chemo medicines when used in combination, however it does slightly augment drug-induced cytotoxicity in organ tissues. Hesperidin has been shown to have both chemo preventive and chemotherapeutic actions against a variety of carcinomas. Hesperidin may influence numerous cells signaling pathways linked to cancer growth. Several techniques, such as combining hesperidin with some other phytochemicals, chemotherapeutic medicines, irradiation, and nano-formulations, might be used to boost its bioavailability and antitumor potency. Nonetheless, hesperidin's anticancer activity has been determined solely in preclinical research using in vivo and in vitro cancer models. However, due to the scarcity of clinical investigations on the pharmacological characteristics of hesperidin, it is difficult to develop a clear picture of the therapeutic dose for cancer control in the human body. As a result, further research is needed to determine the most effective dosages for future clinical trials in cancer patients to verify hesperidin's position as one of the prospective and successful therapeutic options for cancer treatment (Rahmani et al., 2023) .

In 2021, Atefeh Satari et al., stated that the impact of rutin, which may be a suitable option for cancer therapy in vitro in combination with other anticancer drugs or alone, were investigated. Furthermore, rutin has been demonstrated to lessen medicine resistance and the side effects of chemotherapy. Rutin has been demonstrated to inhibit the development of several cancers. Furthermore, rutin has been shown to modulate several signaling pathways such as the Ras/Raf and PI3K/Akt, MAPK, and TGF2/Smad2/3Akt/PTEN, amongst others, which are involved with carcinogenesis and apoptosis induction, either alone or in combination with other pharmacological therapies. Pairing rutin alongside additional chemotherapy drugs may aid in tumor cell prevention by decreasing drug resistance and the side effects of chemotherapy. Furthermore, rutin causes apoptosis in conjunction with the medicinal medication. It has been shown that it inhibits cell proliferation, regulates mortality and the cell phase in cancer cell lines, and assists in the creation of the most effective treatment choices. However, further study is required to fully comprehend the process of action of rutin on cancer cell lines in the future. Furthermore, further study is required to establish the impact of rutin on the generation of anti- or proapoptotic pathways and genes, either alone or in conjunction with other components (Satari et al., 2021) .

In 2021, Y. Lee and others stated that Flavonoids' anticancer impact is due to both their antioxidative activity and their prooxidative activity. This study aims to conduct a thorough examination of the findings of distinct and separate studies on the modification of redox status in cancer cells by flavonoids. It focuses on the mechanism of action of anti-cancer flavonoids (Lee et al., 2021)

In 2020, Xuewen Wang and others reported that the link between flavonoids' anti-cancer properties and their potential regulatory functions in specific types of mutations that might lead to EGFR-TKI resistance in NSCLC EGFR-TKIs (EGFR-TKIs) are widely utilized in the treatment of NSCLC with EGFR mutations. Patients treated with EGFR-TKI, on the other hand, acquire resistance with time. Flavonoids, as prospective adjuvants for cancer treatment, shown anticancer effects such as suppression of chemoresistance by interfering with ABC transporter induced drug efflux, inhibition of c-MET amplification, and reversal of T790M mutation mediated resistance in laboratory experiments. Furthermore, flavonoids may be a beneficial

option to help prevent side effects during cancer therapy, with findings from randomized clinical trials supporting the usefulness of Delica flavone, a component of SDEA extract. However, pharmacokinetic data on flavonoids is still insufficient, and most research have focused on in vitro NSCLC models rather than flavonoids' clinical use. As a result, more work is still necessary in these sectors (*Pmc\_7603574*, n.d.)

In 2020, Kopustinskiene, D. M. et.al. stated that flavonoids' biochemical characteristics and bioavailability, anticancer potency, and mechanisms of action Numerous investigations have demonstrated their potent anti-inflammatory, immune-modulating, and cell-supporting and cellular-restoration properties. Flavonoids have a wide spectrum of anticancer properties, making them ideal substances for future research into the creation of new cancer chemo preventive medicines and understanding their exact mechanisms of action. Furthermore, regular use of flavonoids as in form of flavonoid-rich foodstuffs or flavonoid fortified foods may elicit beneficial changes in the gut flora, lowering the risk of cancer and restoring critical processes at the cellular level (*Pmc\_7071196*, n.d.).

In 2019, P. Aiello, and others stated that the anticancer efficacy of nanoparticles (NPs) generated from food-derived flavonoids has been studied in vivo. A total of 60 studies were discovered through a comprehensive search. The flavanols EGCG & quercetin were studied extensively in delivery and combined delivery (with other medicines of cancer) systems. Moreover, other investigations investigated the effects of other flavonoids. In both xenograft and chemical induced animal models of carcinogenesis, NPs suppressed tumor development (Aiello et al., 2021)

In 2019, Haroon Khan and others stated that the influence of nano-formulated flavonoids on the enhancement of their bioavailability, therapy, and less side effects will provide new insights in the field of cancer therapeutic drug research. Flavonoids have showed considerable promise in the treatment of several forms of cancer; however, the primary problem is their low bioavailability, non-specificity at specific sites, and propensity to interact with other therapeutic drugs. These problems can be solved by creating flavonoids nanoparticles. Similarly, in vitro and in vivo research have demonstrated the applications and advantages of nanoparticle-based

formulations of flavonoids alone or in combination in cancer therapy, but relatively few clinical trials have been conducted. Given the positive results, clinical investigations to thoroughly examine nanoparticle formulations of flavonoids in cancer therapy may be encouraged (31374244, n.d.).

In 2019, Imran, M. and others stated that eating and intake of bioactive chemicals derived from natural sources have been linked to a lower risk of several human illnesses, including tumor. The inhibitory effects of phytochemicals present in plants on major illnesses are widely recognized in the literature. Because of its natural origin, safety, and cheap cost in comparison to manufactured cancer medications, luteolin has the potential to be an essential supplemental therapy for the prevention and treatment of several types of malignancies. More research on different parameters is required in the future before this substance becomes a prescribed drug. Furthermore, clinical trials might be used to investigate the creation of uniform dose (S. A. Siddiqui et al., 2023).

In 2019, M. ERSOZ and team reported that the encapsulation of hesperetin into PLGA nanoparticles and the subsequent detailed characterization of these HspNPs proved to be highly effective. Moreover, in vitro testing of the antitumor activity of HspNPs was conducted, comparing it with free hesperetin. Remarkably, this study marks a significant milestone as it is the first to demonstrate that both hesperetin and hesperetin-loaded PLGA nanoparticles exhibit anti-proliferative, apoptotic, and antioxidant effects in C6 glioma cells (Ersoz et al., 2019a)

In 2018, Civiletto et al., reported that Cox15 was shown to be participate in the stimulation of autophagic flux, and cellular metabolism contributes to the efficient clearance of defective mitochondria, suggesting that Cox15 promotes LC development by activating autophagy (Ersoz et al., 2019b)

In 2017, D. Raffa and team reported that the most recent breakthroughs in anticancer activity of the family of naturally occurring flavonoids, spanning the previous five years, as well as the targets and methods of action, as well as the molecules' structure-activity connections The most promising anticancer flavonoids are still being researched, and none are currently being utilised in clinical trials (Raffa et al., 2017)



## Chapter – 3

# METHODOLOGY

### 3.1 INTRODUCTION

*LC* is the most dangerous after heart disease [1] and has a high fatality rate, making it critical to find potential treatment options [2]. However, there are numerous treatment options present in International as well as National markets, like agonists and antagonists to treat the malady [3] [5], [6]. But they have various side effects. Researchers are trying hard to develop advanced therapies for treating *LC*, but these have not been discovered over the past 40 years. *LC* was responsible for 9.3% of cancer fatalities in India, affecting both male and female patients [4]. Many individuals diagnosed with metastatic *LC* contribute to poor survival rates (57%). *LC* remains a significant global health challenge, with non-small cell lung carcinoma (NSCLC) accounting for approximately 85% of cases and exhibiting a high mortality rate [1]. Small cell lung carcinomas (SCLCs) account for 35% of the population [2]. The dysregulated activation of these signaling cascades leads to abnormal cell growth, whereas the inhibition of apoptosis activates oncogenic pathways, thereby exacerbating the severity of the pathological condition [3]. Although numerous pharmaceutical agents are available for cancer treatment, their high cost, the challenge of developing resistance, and the increased toxicity following drug administration are substantial obstacles to achieving effective therapy. Furthermore, these issues have adverse effects on non-malignant cells. So, there is a significant effort to prioritize the development of novel therapeutic agents that exhibit low cost and high bioavailability to address these challenges in the field of therapeutics.

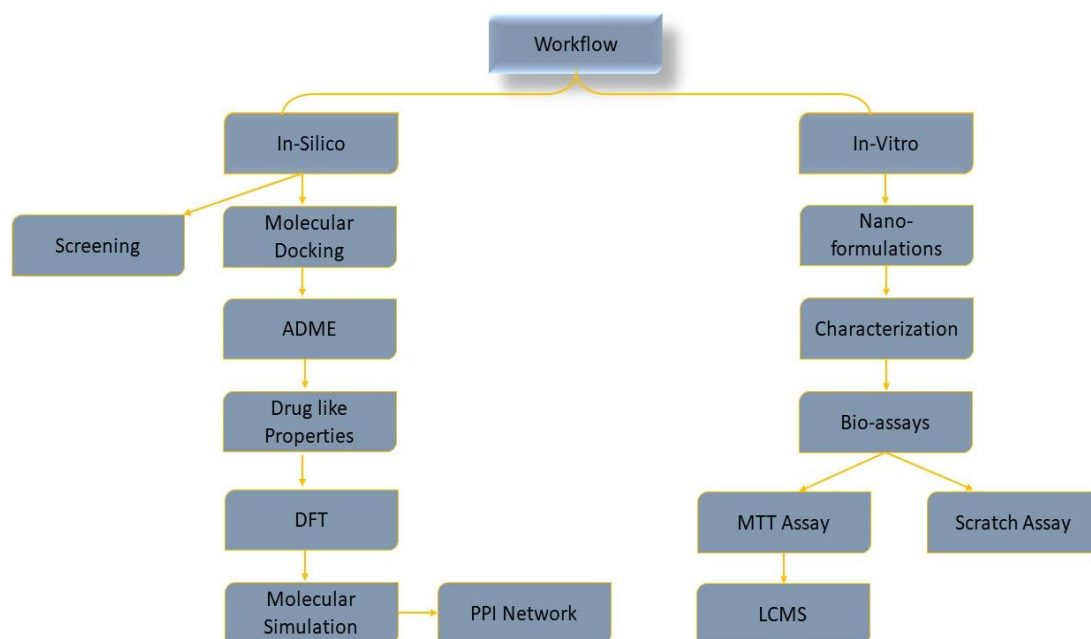


**Figure 3.1: Workflow**

### 3.2 MATERIALS

Standard laboratory-grade chemicals/ reagents were used for the study. Chloroform (CHCl<sub>3</sub>), methanol (CH<sub>3</sub>OH), ethyl acetate (C<sub>4</sub>H<sub>8</sub>O<sub>2</sub>), petroleum ether, ethanol (C<sub>2</sub>H<sub>5</sub>OH), DMEM high glucose media, FBS, Silver nitrate (AgNO<sub>3</sub>) was purchased from HI Media, Mumbai, India. MTT dye was purchased from Thermofischer Scientific, U.S. and dimethyl sulphoxide (DMSO) was purchased from LobaChemie Pvt. Ltd., Colaba, Mumbai. All other solvents and reagents were of analytical grade.

#### Utensils and Instrument Utilised:

1. Beakers
2. Separating Funnel
3. Pipette
4. Pipette tips
5. Centrifuge tubes (50 ml)
6. Eppendorf tubes (2ml)
7. Magnetic Stirrers

8. Glass tubes
9. Petri plates
10. Spatula
11. 96 well plates
12. 24 well plates
13. 6 well plates
14. Weighing machine
15. Centrifuge
16. Autoclave
17. Air flow Laminar
18. Incubator
19. UV visible spectrophotometer
20. -80-degree Celsius freeze
21. CO<sub>2</sub> incubator
22. Hot air oven
23. Probe Sonicator
24. Microscope
25. Elisa reader

### **3.3 CELL CULTURE MAINTENANCE**

A549 (LC) cell lines were obtained from NCCS, Pune, India. They were sustained in DMEM with 10 % (v/v) FBS and 1 % penicillin/streptomycin solution (10,000 Units/ml penicillin and 10,000 µg/ml streptomycin) in a humidified atmosphere of 5 % CO<sub>2</sub> at 37 °C temperature.

### **3.4. COLLECTION OF COMPOUNDS**

We collect Diosmin and Hesperidin from otto Kemi Pvt. Ltd. Mumbai and Protein structures from PDB database.

### **3.4.1 Diosmin**

Diosmin, a naturally occurring flavonoid found in citrus fruits, exhibits a diverse range of bioactivities with intriguing implications for human health. Studies have revealed its potent anti-inflammatory, antioxidant, and antimicrobial properties, highlighting its potential as a therapeutic candidate for various ailments.

Particularly captivating is diosmin potential role in cancer prevention and treatment. Research suggests it can modulate multiple cellular pathways involved in carcinogenesis, including cell proliferation, apoptosis (programmed cell death), and angiogenesis (blood vessel formation). Diosmin has been shown to suppress the growth and induce apoptosis in various cancer cell lines, including those of breast, colon, and prostate cancers. Additionally, it may hinder tumor progression by interfering with the formation of new blood vessels that tumors rely on for sustenance.

While the precise mechanisms underlying diosmin anticancer effects are still being unravelled, exploring its efficacy in combination with conventional therapies and delving deeper into its molecular targets hold promise for developing novel strategies in cancer management.

### **3.4.2 Hesperidin**

Hesperidin, a naturally occurring flavanone found abundantly in citrus fruits, boasts a diverse range of bioactivities with significant implications for human health. Studies have demonstrated its potent anti-inflammatory, antioxidant, and antimicrobial properties, making it a potential candidate for various therapeutic applications.

However, hesperidin's potential extends beyond these established benefits. Recent research has shed light on its intriguing potential as a promising player in cancer prevention and treatment strategies. Hesperidin's multifaceted approach targets various hallmarks of cancer progression, offering a unique advantage.

Studies suggest hesperidin's ability to inhibit uncontrolled cell proliferation, a key driver of tumor growth. It achieves this effect through multiple mechanisms, including inducing apoptosis (programmed cell death), arresting the cell cycle, and

suppressing the production of factors that promote blood vessel formation, crucial for tumor sustenance.

Furthermore, hesperidin's antioxidant and anti-inflammatory properties contribute to its potential anticancer activity. By scavenging free radicals and modulating inflammatory pathways, hesperidin helps mitigate oxidative stress and chronic inflammation, both of which are implicated in tumorigenesis.

### **3.4.3 ROS1**

The ROS-1 gene plays a pivotal role in the development of various tumors, particularly in non-small-cell lung cancers (NSCLCs), where ROS-1 rearrangements are found in 0.9% to 2.6% of cases, predominantly in lung adenocarcinomas. This genetic alteration is notably more common in women, non-smokers, and younger individuals. Extensive research has firmly established ROS-1 as a genuine oncogenic driver, and the use of tyrosine kinase inhibitors (TKIs) specifically designed to target ROS-1 has proven remarkably effective in halting tumor growth and delivering significant clinical benefits to patients.

The ROS-1 gene encodes a transmembrane protein consisting of 2347 amino acids. Interestingly, this protein shares structural similarities with both insulin receptors and the ALK family. The ROS-1 protein is composed of an extracellular domain that contains a hydrophobic segment, aiding in its transmembrane function. Additionally, it possesses an intracellular component housing a tyrosine-kinase domain with a terminal carboxyl. Notably, ROS-1 plays a crucial role in activating multiple signaling pathways associated with processes such as differentiation, proliferation, cell growth, and overall cellular survival.

### **3.4.4 EGFR**

For advanced non-small cell LC (NSCLC) patients with EGFR mutations, (EGFR-TKIs) are the preferred treatment choices. Osimertinib is a powerful irreversible third-generation EGFR-TKI that targets EGFR mutations but has no impact on wild-type EGFR. Because of its outstanding effectiveness and manageable toxicity, Osimertinib has been recommended as the usual first-line therapy for progressed or metastatic non-small-cell LC patients with mutations in the EGFR. Priority is given

to patients with EGFR-sensitizing mutations, such as EGFR exon 19 deletions (Ex19del) and L858R variants.

### **3.5 IN SILICO STUDIES**

#### **3.5.1 Introduction**

In recent years, there has been a radical transformation from traditional drug design methodologies to Computer Aided Drug Design (CADD) as a viable tool for predicting biological activity. Rational drug design methodologies combined with structural biology have a lot of potential for facilitating the development of new therapeutic medicines [Rao, V. S., & Srinivas, K, 2011]. Computational drug discovery is a good way to speed up and save money on the drug research and development process. Because of the dramatic increase in the availability of biological information at the macro and micro levels, computational drug discovery has been extended and widely applied to nearly every stage of the drug discovery and development workflow, including target identification and validation, lead discovery and optimization, and preclinical tests.

Computational drug discovery approaches such as molecular docking, pharmacophore modelling and mapping, de novo design, molecular similarity computation, and sequence-based high - throughput screening have all made substantial developments during the past few decades [Ou-Yang, S. S *et al.*, 2012]. Advancements in pharmacology, biochemical, molecular genetics, and biomedical sciences, together with developments in genomic technologies, have resulted in a large number of new biological targets that might be used for treatments, encouraging this trend.

Integrating experimental and theoretical approaches has shown it is very useful in identifying and developing new promising compounds. Molecular docking is becoming a more important method in drug development. The goal of this section is to look at current molecular modelling procedures in drug development and medicinal chemistry, as well as the advances in the area and the role that structure, and ligand-based methods play.

The relevant basic information including the structures, physicochemical and toxicological molecular properties, pharmacokinetics, drug-likeness and medicinal chemistry friendliness of small molecules and target protein are summarized with different software and an online free web-server tools. This project outlines molecular docking and structure based virtual screening protocols used to predict the interaction of small molecules with the molecular targets for cancer diseases. An elaborate procedure on how to carry out a molecular docking for the candidate compounds with a wonderful software known as Schrodinger tools was discussed. A detailed description of the molecular docking and structure based virtual screening procedures and an evaluation of the results are provided.

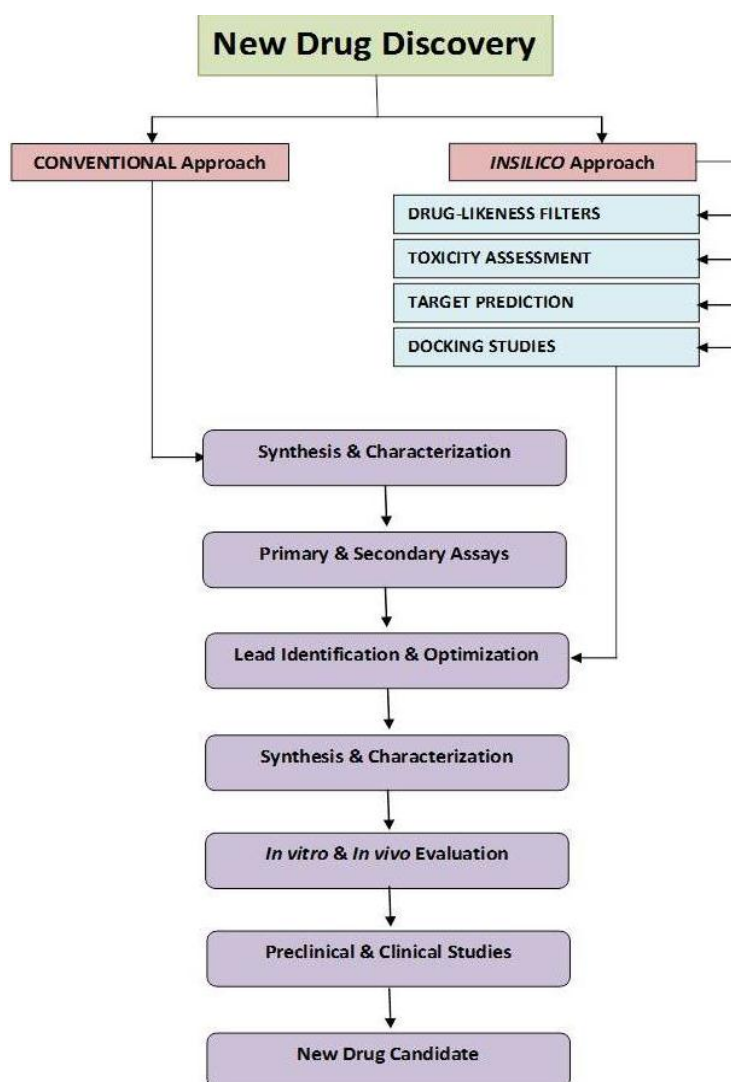


**Figure 3.2 : Conceptual illustration of in-silico methods and traditional drug discovery procedure.**

### **3.5.2 Computational Studies for Drug Analysis**

Exploring cancer pathways reveals a complex network of interconnected markers driving oncogenesis. Identifying a suitable target for therapy amid this complexity can be daunting. Docking, a method predicting how molecules bind to each other to create a stable complex, offers valuable insights. Researchers employ diverse experimental and computational techniques to pinpoint potential protein binding partners. The prediction of these protein-ligand interactions, studied through computational docking methods, has become increasingly vital in the realm of structure-based drug design.

### **3.5.3 Natural Compounds**

Natural substances have been shown to have anti-cancer properties due to their capacity to lower reactive oxygen species and preserve essential cellular components including lipids, proteins, and DNA from oxidative damage. They may also interfere with intracellular signaling networks that govern proliferation, apoptosis induction, and oxidative stress response. The current study's goal is to look into the anti-LC effects of Diosmin and Hesperidin using in-silico and in-vitro research.

## **3.6. METHODS UTILIZED FOR IN-SILICO ANALYSIS**

### **3.6.1. ROS1**

**3.6.1.1. Preparation of ligand for docking study :** The molecular structures of ligand, i.e., Diosmin were retrieved from the PubChem database in the SDF 3D file format (Ali et al., 2019; Patidar et al., 2019; Sweta et al., 2019; Yadav et al., 2019). The Avogadro program and the MMF (Molecular Mechanics Force field) minimised the ligands' energy. The steepest descent technique was applied with 200 rounds to achieve optimisation, and RMS gradients were set to 0.1. This process allowed for the refinement of the ligand structures, ensuring their stability and reliability for further analyses. Subsequently, the minimized ligands underwent docking studies, which involved predicting their binding interactions with specific target proteins or receptors.



**3.6.1.2. Preparation of Protein for Docking Study :** The three-dimensional structures of the chosen protein targets for LC, namely ROS1, were acquired from the Protein Data Bank (PDB) database and prepared for further investigation. Using the software Chimera, all extraneous water molecules were removed from the protein structures, and polar hydrogens were added to the molecules to ensure a biologically relevant environment. Energy optimization was carried out to enhance the structural accuracy to address any potential localised strain arising from minor imperfections in the initial protein models, such as suboptimal Van der Waals interactions. The energy optimization was performed under a vacuum hypothesis to eliminate loosely bound connections and achieve a more energetically favourable protein conformation.

Chimera was utilized for energy minimization by generating optimized protein structures with partial atomic charges. These optimised protein structures and their respective atomic charges were subsequently employed in docking analyses. The docking studies aimed to predict and estimate the optimal orientations of the ligand-receptor complexes within the active sites of the ROS1. Moreover, the docking analysis identified essential amino acid residues involved in specific interactions with the ligand molecules, providing valuable insights into the molecular basis of ligand-protein interactions.

**3.6.1.3. Molecular Docking Protocol :** The glide modules was employed to investigate the binding mechanism and selectivity of target proteins with various drugs. It was also employed to distribute hydrogen molecules and active peptide torsions, which were attached farther into binding pockets, according to the literature. Within a 5-Å distance range, the binding site region was constructed. Water molecules and undesirable ligands were removed after choosing binding sites or atomic ligands. We next choose a binding energy score, use the standard generic algorithm, and execute. To categorize and analyse the generated structures, a scoring function was utilized. Finally, the docking findings were compared to excellent conformation posture, and the group of groups with the greatest docked value were selected for further investigation.

**3.6.1.4. Drug-like & pharmacokinetic properties :** Pharmacokinetic factors are among the most essential features to consider while developing new medication

compounds. Any medicinal substance produced as a medicine must have the best biological activity and pharmacokinetic qualities. Regarding pharmacokinetic characteristics, Pgp (p-glycoprotein), found in the liver and plays a vital role in drug discovery and development, functions as an efflux pump (Muthumanickam et al., 2020). If the drug molecule inhibits the Pgp, it is a good candidate and vice versa.

**3.6.1.5. Drug-like properties :** Lipinski's rule was applied to evaluate the drug-like properties of the compounds, which encompasses the assessment of several critical molecular characteristics. Molecular weight (MW), partition coefficient (Log P), hydrogen bond donors (HBD), hydrogen bond acceptors (HBA), and the number of rotatable bonds were predicted using two online tools, namely the zinc online server and SwissADME. Utilising the zinc online server and SwissADME facilitated the accurate prediction of these drug-like properties, enabling prioritising and selecting of promising compounds for further experimental investigations. Adhering to Lipinski's rule aids in identifying compounds with higher probabilities of favourable pharmacokinetic profiles and improved chances of successful drug development.

**3.6.1.6. Swiss ADME :** Molecules may be submitted to this publicly accessible web server for ADME, physiochemistry, drug-likeness, pharmacology, and pharmaceutical applications compatibility estimation. [Kassel Database, 2004]

Deploying the web server Molecular and physicochemical characteristics such molecular weight (MW), molecular refractivity (MR), molecular formula, and the number of heavy atoms The number of aromatic heavy atoms, the number of rotatable bonds, the number of H-bond acceptors and donors, the Molar Refractivity count of certain atom types, and the polar surface area (PSA) may all be calculated.

**3.6.1.7. The Bioavailability Radar :** The Bioavailability Radar is provided to quickly assess drug-likeness. The radar examines six physicochemical characteristics. The pink coloured region represents the ideal values for the six parameters listed above

**3.6.1.8. Molecular Simulation :** Desmond software was employed to perform molecular dynamics simulations on an Acer workstation running the Ubuntu 22.04

operating system. In order to create the topology of the molecular complex under examination, the OPLS-2005 force field was used. The complex was constructed via the use of a system builder platform. This included the integration of explicit water models, which were represented as basic point charges, into an orthorhombic simulation box.

To emulate physiological conditions, the solvated complex system was neutralised by the addition of appropriate Na<sup>+</sup> and Cl<sup>-</sup> counterions, resulting in the formation of a 0.15 M salt concentration. The ligand-receptor complex was simulated using the OPLS-2005 force field, and a transparent fluid model consisting of SPC water atoms was inserted into an orthorhombic simulation box.

Subsequently, Desmond simulations were carried out for a total duration of 200 nanoseconds, maintaining a temperature of 300 Kelvin and a pressure of 1.0325 bar. Prior to the simulation runs, the system underwent a minimization process for 100 picoseconds, followed by system relaxation using the default approach.

**3.6.1.9. BOILED EGG plot analysis :** The Estimate D permeation technique, commonly referred to as the BOILED-Egg model, stands as a reliable predictive tool for the assessment of ligand lipophilicity and polarity within the context of brain or intestinal tract permeation. This model offers a structured statistical framework for the comprehensive analysis of the bioavailability characteristics exhibited by various ligand molecules.

The underlying principle of the BOILED-Egg model draws an analogy to the physicochemical properties of cooked eggs, which can be correlated to important aspects of drug development, including gastrointestinal absorption and blood-brain barrier permeability. It is worth noting that the Swiss ADME online service is proficient in generating BOILED plots (Figure 5), which serve as indispensable resources in the field of drug research and discovery. These plots facilitate a deeper understanding of the critical factors governing ligand permeation and guide the development of pharmacologically effective compounds. (Daina et al., 2017).

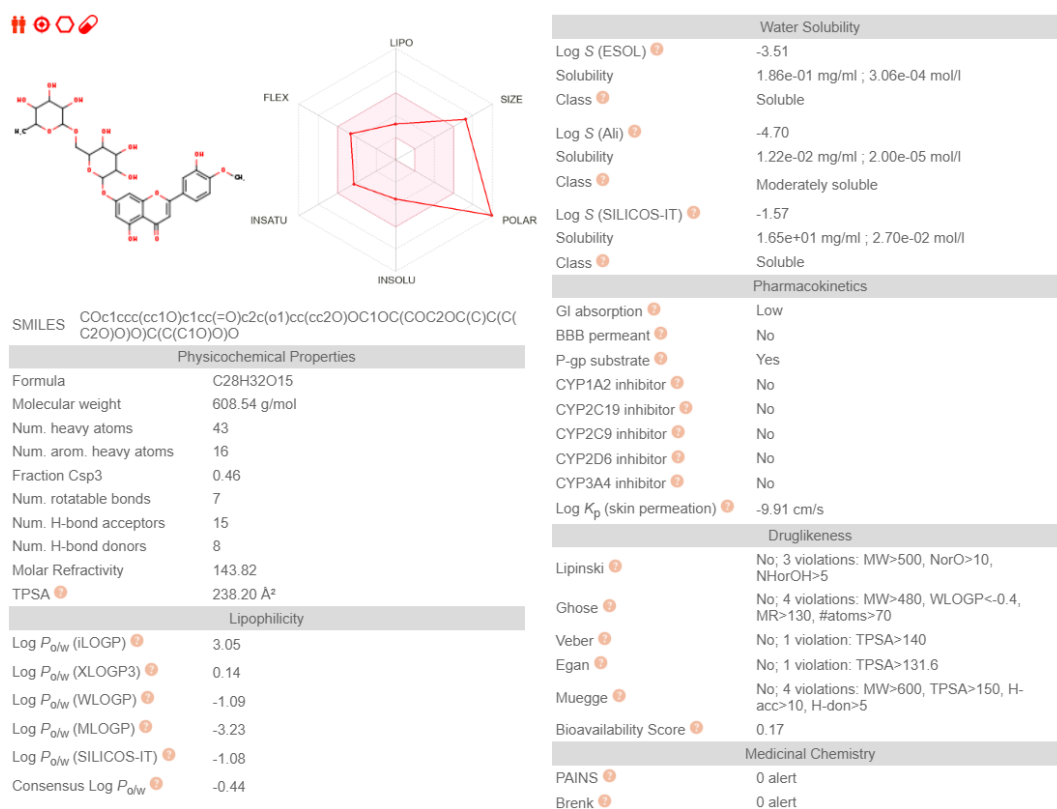


**Figure 3.3 : SwissADME web server snapshot of Diosmin.**

### 3.6.2. EGFR

**3.6.2.1. Preparation of ligand for docking study :** The molecular structures of ligand, i.e., Hesperidin, were retrieved from the PubChem database in the SDF 3D file format (Ali et al., 2019; Patidar et al., 2019; Sweta et al., 2019; Yadav et al., 2019). The Avogadro program and the MMF (Molecular Mechanics Force field) minimised the ligands' energy. The steepest descent technique was applied with 200 rounds to achieve optimisation, and RMS gradients were set to 0.1. This process allowed for the refinement of the ligand structures, ensuring their stability and reliability for further analyses. Subsequently, the minimized ligands underwent docking studies, which involved predicting their binding interactions with specific target proteins or receptors.

**3.6.2.2. Preparation of Protein for Docking Study :** The three-dimensional structures of the chosen protein targets for LC, namely EGFR, were acquired from the Protein Data Bank (PDB) database and prepared for further investigation. Using

the software Chimera, all extraneous water molecules were removed from the protein structures, and polar hydrogens were added to the molecules to ensure a biologically relevant environment. Energy optimization was carried out to enhance the structural accuracy to address any potential localised strain arising from minor imperfections in the initial protein models, such as suboptimal Van der Waals interactions. The energy optimization was performed under a vacuum hypothesis to eliminate loosely bound connections and achieve a more energetically favourable protein conformation.

Chimera was utilized for energy minimization by generating optimized protein structures with partial atomic charges. These optimised protein structures and their respective atomic charges were subsequently employed in docking analyses. The docking studies aimed to predict and estimate the optimal orientations of the ligand-receptor complexes within the active sites of the EGFR. Moreover, the docking analysis identified essential amino acid residues involved in specific interactions with the ligand molecules, providing valuable insights into the molecular basis of ligand-protein interactions.

**3.6.2.3. Molecular Docking Protocol :** The glide modules was employed to investigate the binding mechanism and selectivity of target proteins with various drugs. It was also employed to distribute hydrogen molecules and active peptide torsions, which were attached farther into binding pockets, according to the literature. Within a 5-Å distance range, the binding site region was constructed. Water molecules and undesirable ligands were removed after choosing binding sites or atomic ligands. We next choose a binding energy score, use the standard generic algorithm, and execute. To categorize and analyze the generated structures, a scoring function was utilized. Finally, the docking findings were compared to excellent conformation posture, and the group of groups with the greatest docked value were selected for further investigation.

**3.6.2.4. Drug-like & pharmacokinetic properties :** Pharmacokinetic factors are among the most essential features to consider while developing new medication compounds. Any medicinal substance produced as a medicine must have the best biological activity and pharmacokinetic qualities. Regarding pharmacokinetic

characteristics, Pgp (p-glycoprotein), found in the liver and plays a vital role in drug discovery and development, functions as an efflux pump (Muthumanickam et al., 2020). If the drug molecule inhibits the Pgp, it is a good candidate and vice versa.

**3.6.2.5. Drug-like properties :** Lipinski's rule was applied to evaluate the drug-like properties of the compounds, which encompasses the assessment of several critical molecular characteristics. Molecular weight (MW), partition coefficient (Log P), hydrogen bond donors (HBD), hydrogen bond acceptors (HBA), and the number of rotatable bonds were predicted using two online tools, namely the zinc online server and SwissADME. Utilising the zinc online server and SwissADME facilitated the accurate prediction of these drug-like properties, enabling prioritising and selecting of promising compounds for further experimental investigations. Adhering to Lipinski's rule aids in identifying compounds with higher probabilities of favourable pharmacokinetic profiles and improved chances of successful drug development.

**3.6.2.6. Swiss ADME :** Molecules requiring ADME estimation, drug-likeness, pharmacokinetics, and medicinal chemistry friendliness qualities may be submitted to this publicly accessible online site. [DB Kassel, 2004]

Implementing a web server Descriptors at the molecular and physicochemical levels, including the number of heavy atoms, molecular weight (MW), and molecular refractivity (MR). The following may be calculated: polar surface area (PSA), number of aromatic heavy atoms, number of rotatable bonds, number of H-bond acceptors, number of H-bond donors, and a polar refractivity count of certain atom types.

**3.6.2.7. The Bioavailability Radar :** By using the Bioavailability Radar, a rapid assessment of the drug-likeness may be achieved. The radar takes six physicochemical characteristics into account. Flexibility, size, polarity, solubility, and saturation are among them. A significant deviation from any of these parameters would suggest that the ligand lacks oral bioavailability [Daina, A et al, 2017].

**3.6.2.8 Molecular Simulation :** Desmond software was employed to perform molecular dynamics simulations on an Acer workstation running the Ubuntu 22.04

operating system. The OPLS-2005 force field was selected for constructing the topology of the molecular complex under investigation. The complex was generated using a system builder platform, which involved the incorporation of explicit water models represented as simple point charges within an orthorhombic simulation box.

To mimic physiological conditions, the solvated complex system was neutralized by introducing appropriate Na<sup>+</sup> and Cl<sup>-</sup> counter ions, resulting in a salt concentration of 0.15 M. The receptor-ligand complex was modeled utilizing the OPLS-2005 force field, and an orthorhombic simulation box was filled with a transparent fluid model composed of SPC water atoms.

Subsequently, Desmond simulations were carried out for a total duration of 200 nanoseconds, maintaining a temperature of 300 Kelvin and a pressure of 1.0325 bar. Prior to the simulation runs, the system underwent a minimization process for 100 picoseconds, followed by system relaxation using the default approach.

**3.6.2.9. BOILED EGG plot analysis :** The Estimate D permeation technique, commonly referred to as the BOILED-Egg model, stands as a reliable predictive tool for the assessment of ligand lipophilicity and polarity within the context of brain or intestinal tract permeation. This model offers a structured statistical framework for the comprehensive analysis of the bioavailability characteristics exhibited by various ligand molecules.

The underlying principle of the BOILED-Egg model draws an analogy to the physicochemical properties of cooked eggs, which can be correlated to important aspects of drug development, including gastrointestinal absorption and blood-brain barrier permeability. It is worth noting that the Swiss ADME online service is proficient in generating BOILED plots (Figure 5), which serve as indispensable resources in the field of drug research and discovery. These plots facilitate a deeper understanding of the critical factors governing ligand permeation and guide the development of pharmacologically effective compounds. (Daina et al., 2017).

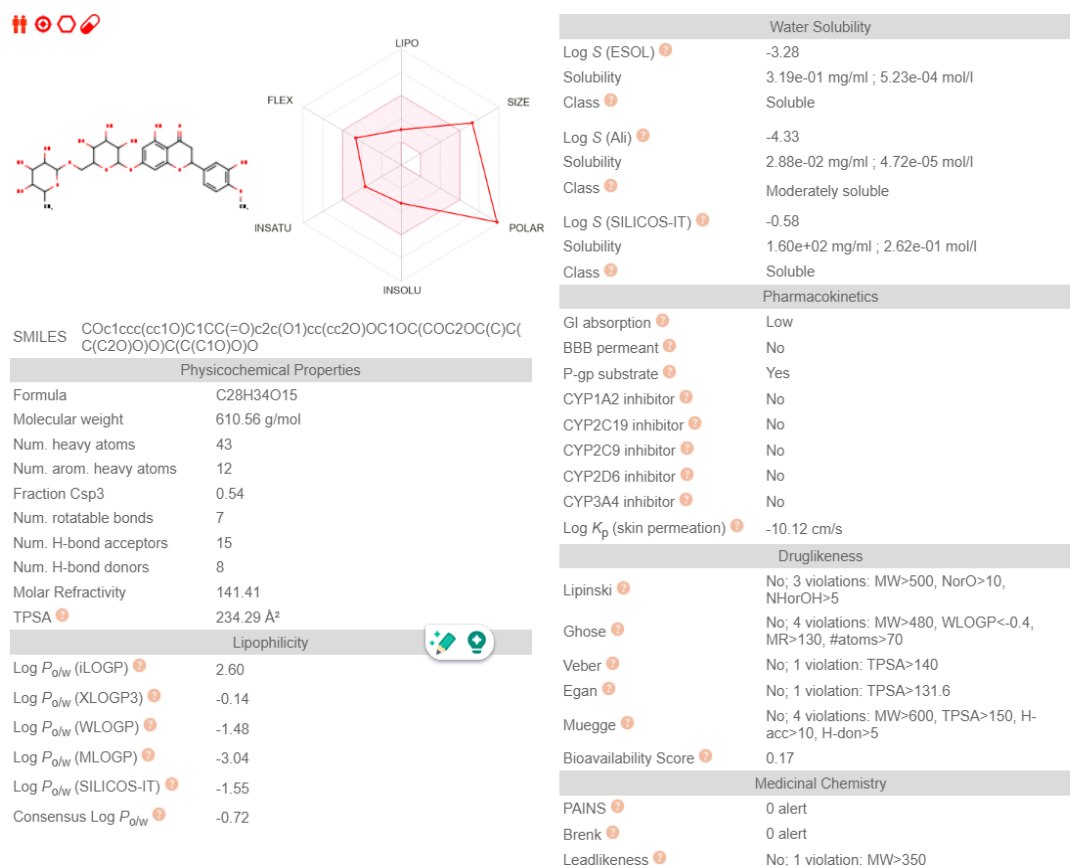


**Figure 3.4 : SwissADME web server snapshot of Hesperidin.**

### 3.7. METHODS UTILIZED FOR IN-VITRO ANALYSIS

#### 3.7.1. Materials and Instruments

Eppendorf centrifuge 5810R, roto shake-Genie, Sigma4k15 centrifuge, Labtech water bath, Thermo electron corporation sterically CO<sub>2</sub> incubator, Sigma 1-18k centrifuge, Nikon Eclipse TE 2000-S electron microscope, innovative air systems laminar air flow hood, New Brunswick Galaxy170S Eppendorf CO<sub>2</sub> incubator, TKA-GenPure water unit, Spectra ax M5 Elisa plate multimode reader.

DMEM (Dulbecco's Modified Eagle Medium), Fetal Bovine Serum (Gibco, U.S Origin), antibiotic solution (Gibco), sodium bicarbonate (Sigma), DMSO (Sigma), MTT reagent (SRL), propidium iodide (sigma), 10x PBS (Sigma), 0.5% Trypsin-EDTA solution (Lonza), tritonX100, tween20 (sigma) were procured from BD Biosciences and conjugated was purchased from Santacruz.



Sterile cell culture plastic ware such as T-25 flasks, T-75 flasks, 6well plates, 12 well plates, 96 well plates, 1.7ml, 5ml, 15ml, 50ml centrifuge tubes were purchased from Eppendorf, Micropipette tips 1.0ml, 200  $\mu$ l, 10  $\mu$ l (Tarsons), 2.0ml, 1.5ml, 0.6ml, 0.2ml microcentrifuge tubes (Axygen Inc), 0.2 $\mu$ m Polyether sulfone (PES) syringe filters and 60 $\mu$ m Nylon net filters (Merck, Millipore).

### 3.7.2 Nano-formulation

To develop a nano-formulation, firstly we performed some pre-formulation studies i.e., Solubility studies, Lambda max, and straight-line graph.

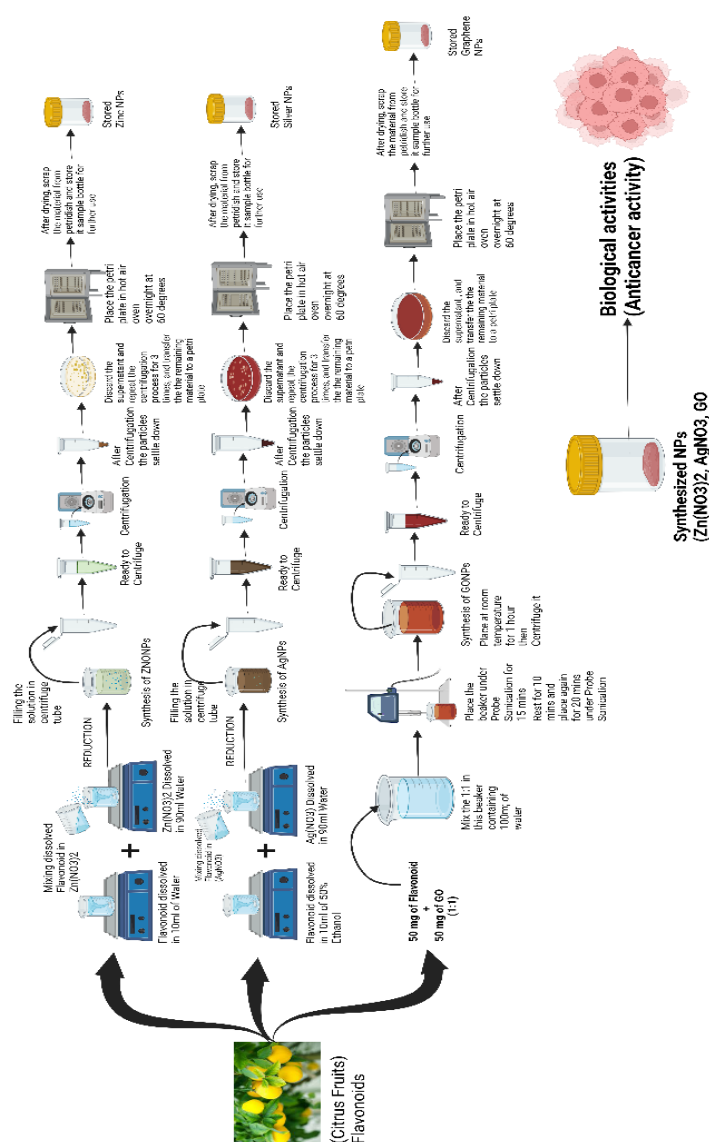


Figure 3.5 : Workflow of Nano formulation.

### **3.7.2.1. Zinc Diosmin Nano-formulation**

#### **Methodology**

We adopt methodology as per MA Saleemi 2022 published in antioxidants 2022 with some modifications (Saleemi et al., 2022). Further, we take 15mg of Zinc acetate and 30 Mg of Diosmin. Moreover, we dissolve Zinc acetate (1.5 Gms) in 90ml Distilled water and placed it on a Magnetic stirrer. After that Diosmin (30mg) is dissolved in 10 ml of Distilled water in a separate beaker and Use NaOH and HCL if flavonoids in not dissolved properly. pH 7. After that, mix the solutions and place them on a magnetic stirrer at 800-1000 RPM and temp 50-60 degrees Celsius. Colour change indicates the starting point of the reaction. After yellow or white colour appears after approx. 4 hrs. stop the stirrer. Placed at room temperature for 1 hour, let the particles settle and then, centrifuge at 2000 RPM for 10 minutes for cleaning or removing unwanted chemicals. After cleaning store, it for further use.

### **3.7.2.2. Zinc Hesperidin Nano-formulation**

#### **Methodology**

We adopt methodology as per MA Saleemi 2022 published in antioxidants 2022 with some modifications (Saleemi et al., 2022). Further, we take 15mg of Zinc acetate and 30 Mg of Hesperidin. Moreover, we dissolve Zinc acetate (1.5 Gms) in 90ml Distilled water and placed it on a Magnetic stirrer. After that Hesperidin (30mg) is dissolved in 10 ml of Distilled water in a separate beaker and Use NaOH and HCL if flavonoids in not dissolved properly. pH 7. After that, mix the solutions and place them on a magnetic stirrer at 800-1000 RPM and temp 50-60 degrees Celsius. Colour change indicates the starting point of the reaction. After yellow or white colour appears after approx. 4 hrs. stop the stirrer. Placed at room temperature for 1 hour, let the particles settle and then, centrifuge at 2000 RPM for 10 minutes for cleaning or removing unwanted chemicals. After cleaning store, it for further use.

### **3.7.2.3. Silver Diosmin Nano-formulation**

#### **Methodology**

We adopt methodology from Zhao et. Al. 2020 published in ACS Omega with some modifications (Li et al., 2020). We take 15mg of silver nitrate and 30 Mg of Diosmin.

Further, we dissolve Silver Nitrate (1.5 Gms) in 90ml Distilled water and placed it on a Magnetic stirrer. Then we add Diosmin (30mg) in 10 ml of 1:1 ethanol and water in a separate beaker. Use NaOH if flavonoids in not dissolved properly. pH 8. After that, mix the solutions and place on a magnetic stirrer at 800 RPM and temp 50 degrees Celsius. Note for Colour change starts after 10-15 minutes indicating the starting point of the reaction. Continue stirrer for 3-4 hrs. After the brick red/brown colour appears stop the stirrer. Placed at room temperature for 1 hour, let the particles settle and centrifuge at 2000 RPM for 10 minutes 3 times to clean or remove unwanted chemicals. After cleaning store, it for further use.

#### **3.7.2.4. Silver Hesperidin Nano-formulation**

##### **Methodology**

We adopt methodology from Zhao et. Al. 2020 published in ACS Omega with some modifications (Li et al., 2020). We take 15mg of silver nitrate and 30 Mg of Hesperidin. Further, we dissolve Silver Nitrate (1.5 Gms) in 90ml Distilled water and placed it on a Magnetic stirrer. Then we add Hesperidin (30mg) in 10 ml of 1:1 ethanol and water in a separate beaker. Use NaOH if flavonoids in not dissolved properly. pH 8. After that, mix the solutions and place on a magnetic stirrer at 800 RPM and temp 50 degrees Celsius. Note for Colour change starts after 10-15 minutes indicating the starting point of the reaction. Continue stirrer for 3-4 hrs. After the brick red/brown colour appears stop the stirrer. Placed at room temperature for 1 hour, let the particles settle and centrifuge at 2000 RPM for 10 minutes 3 times to clean or remove unwanted chemicals. After cleaning store, it for further use.

#### **3.7.2.5. Graphene oxide Diosmin nano-formulation**

##### **Methodology**

We adopt methodology from Nazanin Rahmanian et. al. 2014 in colloidal and surfaces B: Bio interfaces with some modifications (Rahmanian et al., 2014). We take 50 Mg of Graphene Oxide and 50 Mg of Diosmin (1:1). Then we dissolve both in 100 ml distilled water and placed them under probe sonication for 15 minutes. Further rest for 10 minutes and then places again for 20 minutes under probe sonication. Once

both the chemicals dissolved and dark black colour appears stop the probe sonication. After this Placed at room temperature for 1 hour, let the particles settle and centrifuge at 3000 RPM for 15 minutes to clean or remove unwanted chemicals. After cleaning, store it for further use.

### **3.7.2.6. Graphene oxide Hesperidin nano-formulation**

#### **Methodology**

We adopt methodology from Nazanin Rahmanian et. al. 2014 in colloidal and surfaces B: Bio interfaces with some modifications (Rahmanian et al., 2014). We take 50 Mg of Graphene Oxide and 50 Mg of Hesperidin (1:1). Then we dissolve both in 100 ml distilled water and placed them under probe sonication for 15 minutes. Further rest for 10 minutes and then places again for 20 minutes under probe sonication. Once both the chemicals dissolved and dark black colour appears stop the probe sonication. After this Placed at room temperature for 1 hour, let the particles settle and centrifuge at 3000 RPM for 15 minutes to clean or remove unwanted chemicals. After cleaning, store it for further use.

### **3.7.3. Characterization of the developed Nano-formulation**

For characterization we utilise FTIR, XRD, and FESEM.

**3.7.3.1. Fourier transform infrared (FT-IR) :** To analyse the functional groups present on the biosynthesized AgNP, Zinc NP, and GoNP, Fourier-transform infrared spectroscopy (FTIR) analysis was meticulously performed employing the advanced Perkin Elmer Spectrum 400 instrument. The analytical procedure involved the application of the KBr pellet method, encompassing a broad wavelength range from 4000 to 400  $\text{cm}^{-1}$ , with a spectral resolution finely set at 4  $\text{cm}^{-1}$ .

**3.7.3.2. X-Ray diffraction (XRD) :** The investigation into the crystalline properties of nanoparticles (NPs) was conducted through X-ray diffraction (XRD) analysis, employing the XPERT-PRO instrument located at Panjab University, Chandigarh. The XRD analysis was performed utilizing Cu  $\text{K}\alpha$  radiation with a wavelength ( $\lambda$ ) of 1.5406 Å, operating at 45 kilovolts (kV) and 40 milliamperes (mA), under ambient conditions at 25°C, employing a 2 $\theta$ / $\theta$  scanning mode.

Data acquisition encompassed a diffraction angular range ( $2\theta$ ) spanning from  $10^\circ$  to  $89.99^\circ$ , with a finely resolved step size of  $0.017^\circ$  and a scan step time of 29.85 seconds. This meticulous XRD procedure enabled a comprehensive exploration of the structural characteristics of the nanoparticles under investigation.

**3.7.3.3. FESEM & EDS-mapping :** The surface morphology of nanoparticles (NPs) was examined and characterized through the utilization of Field Emission Scanning Electron Microscopy (FE-SEM), specifically employing the FESEM SU8010 Scanning Electron Microscope. This analysis was conducted under an accelerated voltage of 10 kilovolts (kV).

Additionally, the elemental composition of the NPs was thoroughly assessed using Energy-Dispersive X-ray Spectroscopy (EDS) with the Bruker X Flash 6130 system. The EDS analysis included mapping to provide detailed insights into the spatial distribution of elements, enhancing our understanding of the elemental makeup of the NPs' surface structure.

#### **3.7.4. Biological Assays**

**3.7.4.1. Human lung cancer cells :** A549 (human lung cancer) cells were procured from the cell repository of the National Centre for Cell Sciences, Pune, India.

##### **3.7.4.2. Reagent Preparation**

**3.7.4.2.1. Phosphate Buffered Saline (PBS) :** Ready to use potassium phosphate buffer salts (PBS) was dissolved into 800mL of autoclaved milli Q water and the pH was adjusted to 7.4 and the volume was made up to 1 litre with water. The PBS solution was passed through 0.22-micron filter and stored at  $4^\circ\text{C}$ .

**3.7.4.2.2. MTT reagent preparation :** 5mg/ml primary stock of MTT reagent was prepared in sterile PBS and stored at  $-20^\circ\text{C}$  until use. The final working concentration was 0.5mg/mL in the wells.

##### **3.7.4.3. In vitro cell culture procedures**

**3.7.4.3.1. Cell culture of A549 :** A549 were grown in DMEM medium containing 10% heat-inactivated FBS along with 1% Pen-Strep antibiotic solution. Cells were

grown at 37°C at a relative humidity of 85% containing 5% CO<sub>2</sub>. lung cancer cells were expanded and frozen each one million cells per vial of 20 were cryopreserved in liquid nitrogen for future usage.

**3.7.4.3.2. *Micro culture tetrazolium (MTT) assay*** : Anti-cancer drug development is carried out in four distinct phases include drug discovery, in-vitro screening, pre-clinical tests on animal models and clinical trials. The first two phases are aimed to find out the efficiency of the drug and the last two phases are to find out both efficiency and safety or toxicity. Cytotoxic chemotherapeutic drugs are used in the treatment of certain types of Cancer [Koch S.et.,al 2003].Cytotoxicity of the newly synthesized anticancer drugs can be evaluated by in-vitro methods rather than by in-vivo methods using animal models. In-vitro methods provide more rapid and precise information than in-vivo methods [Person RM et.,al 1986].Cell based assays are useful in determining the potency of the chemotherapeutic anti-cancer agents [Carmichael Jet.,al 1987 and Alami N et.,al 2007].

Various physical and chemical agents such as pesticides drugs induce cytotoxicity by different mechanisms such as disruption of cell membrane, inhibition of DNA synthesis protein synthesis and enzymatic reactions [IshiyamaM et.,al 1996]. Anticancer agents can kill cancer cells by causing cytotoxicity to cancer cells specifically. Cytotoxicity of chemotherapeutic agents designed used for treatment of can be assessed by cell viability tests and cytotoxicity assays. Cytotoxicity assays plays an important role in toxicology, oncology and pharmacology. These cell viability / cytotoxicity assays are more rapid, inexpensive and reliable than in-vivo tests [Chrzanowska C et.,al 1990],Drugs are screened for their cytotoxicity by cytotoxicity assays and cell viability tests on cultured cell lines. Cell viability tests are based on various cellular functions such as enzyme activity, cell membrane permeability, cell adherence, ATP production, co-enzyme production, and nucleotide uptake activity. There are various cell viability tests.

MTT assay is one of the most frequently used cell viability assay. MTT assay is sensitive and quantitative colorimetric assay used to determine the cell viability [Mosmann et al., 1983]. MTT assay is based on metabolic activity of the cell which

determines the functional state of the Mitochondria. Apart from cell viability studies, MTT assay is also used to study the cytotoxic potential of the drugs. MTT assay is most widely used assay to evaluate the anticancer properties of drugs. MTT assay measures the cell proliferation rate. MTT assay is more sensitive method for study of cell viability when compare to determining the LDH levels for assessment of cell viability. (Fotakis and Timbrell et al., 2006).

MTT assay depends on biochemical reduction of yellow tetrazolium MTT [3-(4, 5-dimethylthiazolyl-2)-2,5-diphenyltetrazolium bromide] into insoluble purple (E,Z)-5-(4,5-dimethylthiazol-2-yl)- 1,3-diphenylformazan (formazan) by mitochondrial NAD(P)H-dependent oxidoreductase[Berridge et al., 2005].

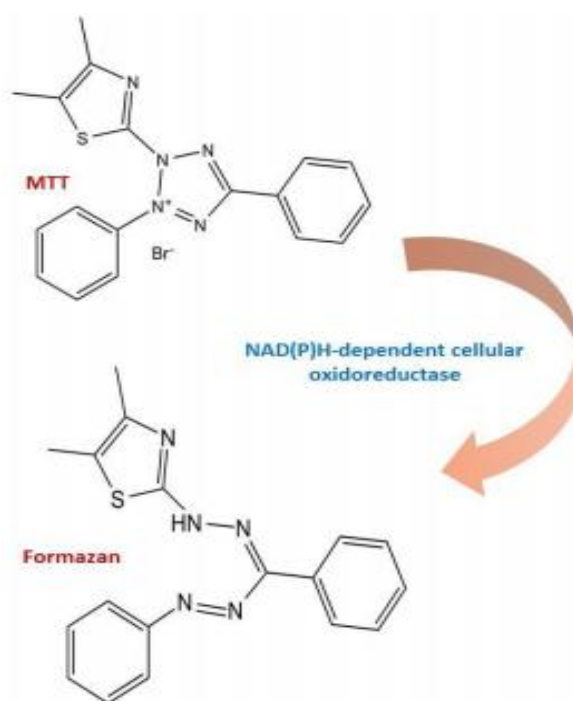


**Figure 3.6 : Formation of MTT into Formazan crystals.**

Cell viability by MTT assay is studied by determining the amount of formazan formed by reading its absorbance at 540nm. There is linear relationship between the cell proliferation and the purple colour formazan formed (van de Loosdrecht et al., 1994). The cell viability is directly proportional to the intensity of the purple colour. Less intensity of purple colour formazan indicates cell death of drug treated cells due to cytotoxicity. MTT assay is most widely used screening test to determine anti-

proliferative activity of newly synthesized drugs on cell cultures [Wang, P., Henning, S. M. et al., 2010]. In cell cultures the MTT assay results depend on cell culture conditions which in turn affect the metabolic activity of the cells [Magaud et al., 1988 and Tagaki et al., 1993].

#### **3.7.4.4. Cell growth inhibition assay (MTT assay)**

**3.7.4.4.1. Principle :** Mitochondrial dehydrogenase is responsible for catalysing the transformation of the yellow-coloured tetrazolium salt, MTT, into a purple-coloured complex known as formazan. The intensity of this resultant coloration is directly correlated with mitochondrial activity and serves as a reliable indicator of cell viability.

**3.7.4.4.2. Procedure :** The human lung cancer cell line A549 was sourced from the National Centre for Cell Science (NCCS) located in Pune. These cells were maintained in Dulbecco's Modified Eagle's Medium (DMEM) supplemented with 10% foetal bovine serum (FBS). For experimental purposes, the cells were seeded into 96-well plates at a density of 10,000 cells per well in a total volume of 100  $\mu$ l of the respective medium, which also contained 10% FBS. The plates were then incubated at 37°C with a 5% CO<sub>2</sub> atmosphere for 24 hours, allowing the cells to adhere overnight. Subsequently, a serum-starvation period of 6 hours was imposed prior to the commencement of the experiment.

Diosmin and Hesperidin, a pharmacological agent, was initially dissolved in dimethyl sulfoxide and subsequently diluted in serum-free culture medium. To evaluate the influence of both the compounds on cell viability, the culture medium in the wells was replaced with a medium containing 1% FBS, which was supplemented with varying concentrations of drug candidate (ranging from 200 to 2  $\mu$ g/ml). Following this, the cells were incubated at 37°C in a 5% CO<sub>2</sub> environment for an additional 24 hours. Each concentration was tested in triplicate, while wells containing medium devoid of drug served as the control. After the incubation period, 10  $\mu$ l of a 5 mg/ml MTT (3-(4,5-dimethylthiazol-2-yl)-2,5-diphenyl tetrazolium bromide) solution in phosphate-buffered saline was added to each well and incubated at 37°C for 4 hours, resulting in the formation of dark blue crystals.



To dissolve these crystals, 10 µl of a solubilizing solution was introduced and meticulously mixed. Following thorough dissolution of all crystals at room temperature, the plates were subjected to optical density measurement at 570 nm using a microplate reader. Percentage cell viability was computed using the prescribed formula. A graphical representation was established, correlating percentage cell viability with drug concentrations, and the half-maximal inhibitory concentration (IC50) was determined according to the method elucidated by Mossman in 1983. The inhibitory rate of cell proliferation was quantified using the subsequent formula :

$$\text{Growth inhibition} = \frac{\text{OD control} - \text{OD treated}}{\text{OD Control}} * 100$$

**3.7.4.4.3. Scratch/wound healing assay :** A total of 0.25 million A549 cells were seeded into 24-well plates and allowed to grow until reaching full confluency. To create a controlled wound, a scratch was made in the cell monolayer using a P200 pipette tip. Following a gentle wash and media change, images were captured at both the start (0 hours) and after 24 hours, using an inverted microscope (Ziess, Germany). The analysis of cell migration was performed using NIH ImageJ software, which calculated the percentage of the open wound area. Each cell line was analysed in a minimum of three independent repetitions, ensuring the reliability of the results.

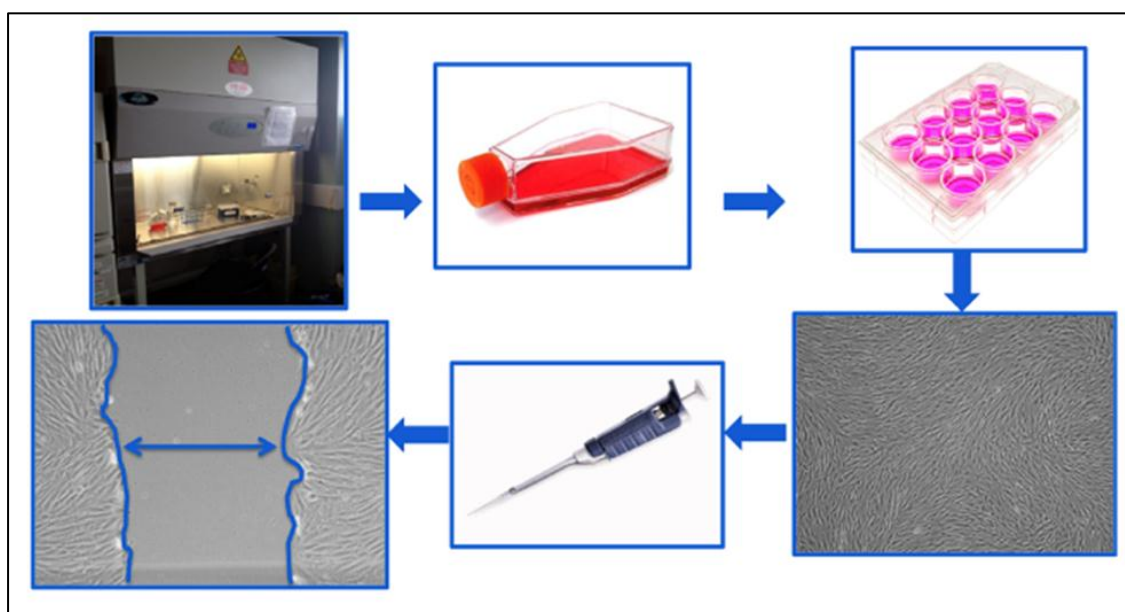


**Figure 3.7 : Schematic representation of workflow of the scratch assay.**

**3.7.4.4.4. Statistical analysis :** The data presented in this study is expressed in terms of the mean value accompanied by the standard deviation (SD) as a measure of data variability. To evaluate the statistical significance of the observed results, a widely recognized analytical approach known as one-way analysis of variance (ANOVA) was applied. This statistical test, executed through GraphPad Prism software, serves the purpose of comparing means derived from multiple groups to ascertain whether significant differences exist among them.

In the context of result interpretation, a significance threshold of  $p < 0.05$  was adopted. In essence, when the calculated  $p$  value falls below 0.05, it signifies that the observed differences among the groups are unlikely to be attributed to random chance. This outcome underscores the presence of meaningful and noteworthy findings within the scope of the study.

### **3.7.5. LCMS Analysis**

**Sample preparation:** 200 $\mu$ L of chilled acetone was added to 200 $\mu$ L of the sample (AgH) and incubated at -20°C for 2hours to precipitate the proteins. After incubation the sample was centrifuged at 10000 rpm for 10 mins. The pellet was dissolved in 200 $\mu$ L of 50mM Ammonium Bicarbonate and used for further processing.

#### **SDS page:**

Resolving gel : 12%

Stacking gel : 5%

Volume of sample used : 10 $\mu$ l

Staining : Coomassie Brilliant Blue

#### **Sample digestion:**

1. 100 $\mu$ g of the sample was taken for digestion.
2. The sample is diluted with 100mM  $\text{NH}_4\text{HCO}_3$  and treated with 100mM DTT at 95°C for 1hr followed by 250mM IDA at room temperature in dark for 45min.

3. The sample is then digested with Trypsin (1:20) sample: Enzyme and incubated over night at 37°C.
4. The resulting sample was vacuum dried and dissolved in 50µl of 0.1% formic acid in water
5. After centrifugation at 10000g the supernatant was collected into a separate tube
6. 8µL of sample was injected on BEH C18PeptideUPLC column for separation of peptides
7. The peptides separated on the column were directed to Waters XevoG2Q-TOF instrument for MS analysis.

**Instrument Settings:**

**LC Method Conditions:**

Buffer A : 0.1% FA in MS Grade water

Buffer B : 0.1%FA in ACN

Run Time : 60mins

Flow Rate : 0.3mL/min

Injection Volume : 8.0 µL

Column : AcquityUPLCBEHPeptideC18,150X2.1,1.7µ,300A°

**Gradient :**

Time	%A	%B
Initial	95.0	5.0
5.00	95.0	5.0
35.00	55.0	45.0
52.00	0.0	100.0
56.00	0.0	100.0
56.10	98.0	2.0
60.00	98.0	2.0

**MS Method Conditions**

Ionization Mode	: Positive
Scan Range	: 50-3000 m/z
Capillary Voltage	: 3 kV
Source Temperature	: 100 <sup>C</sup>
Desolation Gas Flow	: 900L/Hr
Desolation Temperature	: 300 <sup>C</sup>
Cone Voltage	: 25V
Reference lock Mass Compound	: Leucine Enkephalin

## Chapter – 4

# RESULTS AND DISCUSSION

**Objective 1:** To screen the anti-cancer Flavonoids using *Insilco*-based approaches.

### 4.1. *In silico* STUDIES

#### 4.1.1. ADMET and Drug related Properties of Hesperidin

The prediction of whether or not chosen and developed compounds possess the characteristics of drug-like molecules is achieved using Lipinski's rule of five. This is contingent upon the chosen molecule meeting the five criteria outlined in this regulation: molecular weight below 500 Da, log P below 5, number of H-bond donors and acceptors below 5, refractivity between 40 and 130 molar, and total polar surface area below 140. Hesperidin went past Lipinski filters with just one or two identified breaches. The expected drug-like compounds were shown in Table 1, as indicated by the following studies: Christopher AL et al. (2001), Kent B et al. (2004), Philip JH et al. (2000), and Lakshmi S et al. (1986). The molecular weight of the molecule is 610.6g/mol. Each compound is composed of less than five HBDs and ten HBAs. Each compound consists of a minimum of four and a maximum of seven rotatable bonds. The compounds were discovered to include 'N' and 'O' heteroatoms.

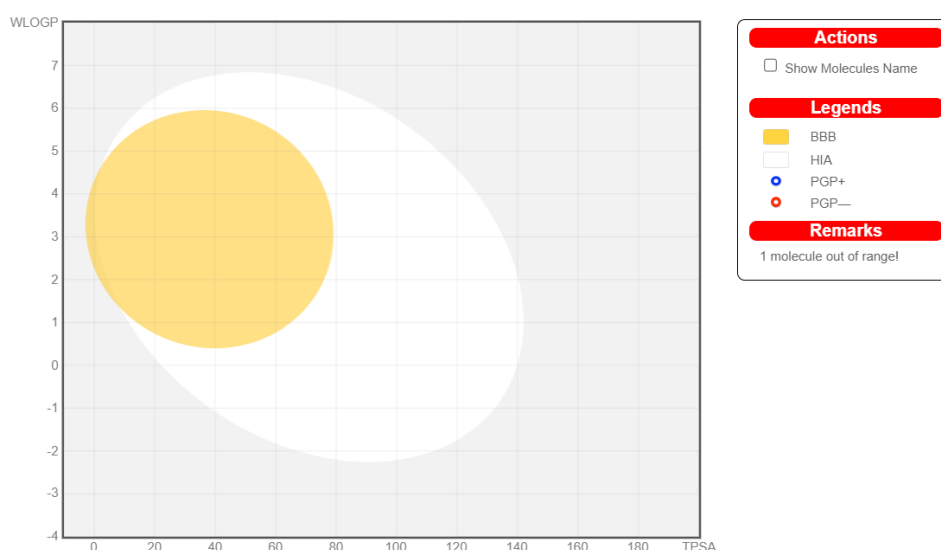


**Figure 4.1 : BIOLLED Egg prediction of Hesperidin**

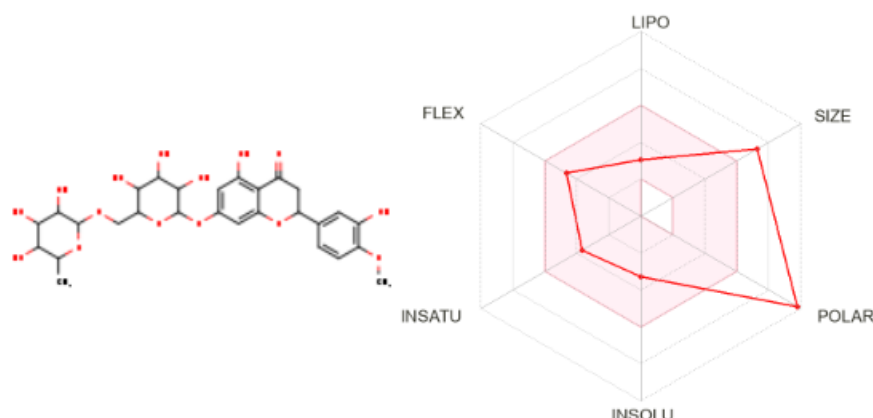


**Figure 4.2 : Bioavailability Radar Prediction of Hesperidin.**

The distribution of a molecule inside a biological system is significantly influenced by its log P, or partition coefficient, which it utilises to traverse membranes and dissolve in bodily fluids. The prediction of LogP was performed on a subset of flavonoids using a variety of algorithms and calculating methods (Table 2). The first approach is LogP, a physics-based technique that was introduced by Daina A et al. It was observed that the evaluated compounds had LogP values ranging from 2.68 to 3.26 [Daina A et al. 2014]. The compounds exhibited XLOGP3 values ranging from 2.63 to 4.14, as determined by the XLOGP software using both atomic and knowledge-based methods [Fik-Jaskółka, M. A et al., 2020]. In a similar vein, the WLOGP3 atomic technique, which was developed by Wildman SA and Crippen GM in 1999, determined the present compounds to have a range of 3.16 to 4.1 [Wildman, S. A et al., 1999]. Moriguchi et al. (1992) and Lipinski PA et al. (2001) developed the topical MLOGP technique; the compounds were determined to have a minimum of 1.39 and a maximum of 2.76 [Moriguchi, I. et al., 1992; Lipinski, C. A et al., 1997]. SILICOS-IT is an alternative approach that utilises a hybrid fragmental/topological technique for computation. It was computed using the FILTER-IT software with the assistance of SILICOS-IT. The resulting value was about 2.4 to 3.07 [Daina, A et al., 2014]. It was noted that the predictions of the various compounds varied among programmes and algorithms; hence, a Consensus Log P ranging from 2.47 to 3.05 was calculated as the mean of the five techniques [Plante, J et al., 2018]. It was noted that the LogP value of each compound is less than 5, indicating compliance with the Lipinski RO5 criterion.

The prediction of water solubility was exclusively performed using the Swiss ADME online tool, using several calculation methodologies, as shown in Table 3. In accordance with the ESOL predicted by Delaney JS et al. (2004), it was determined that compounds 5a and 5b were soluble at 0.0567 mg/ml with a LogS value of -3.78; compounds 5c to 5g were moderately soluble at 0.00691 to 0.027 mg/ml with LogS values ranging from -4.14 to -4.69 [Delaney JS et al. 2004]. All compounds were moderately soluble, with LogS values ranging from -4.43 to -5.58 and solubility values between 0.0009 and 0.0126 mg/ml, according to Ali et al. (2012). All the compounds were expected to be weakly soluble by Silicos-IT calculations, with LogS values ranging from -6.17 to -6.58; their solubility was determined to range between 0.000088 and 0.00027 mg/ml. On the basis of the ESOL and Ali projections, it was hypothesised that the proposed compounds had a moderate solubility in water, notwithstanding the uncertainty around the water solubility in the data.

In addition to skin penetration, the pharmacokinetic features of absorption, distribution, and protein binding were anticipated. As determined by the BOILED EGG technique, all of the examined compounds exhibited a high degree of gastrointestinal absorption. The compounds exhibited non-permeability across the blood-brain barrier and did not function as substrates for p-Glycoprotein. The majority of the substances were hypothesised to block CYP enzymes, including CYP1A2, CYP2C19, CYP2C9, CYP2D6, and CYP3A4, which are accountable for the metabolism of xenobiotics. Based on the skin permeation predictions made by Potts RO and Guy RH in 1992, it was determined that the logKp values for the compounds ranged from -5.42 to -6.45 cm/s, indicating their suitability for topical administration on the skin.

It was determined that none of the compounds violated the drug likeness standards, as proposed by Lipinski, Ghose, Veber, Egan, and Muegge. A estimated bioavailability of 0.55 was attributed to each component. Non-brenk and PAINS warnings were generated in response to any of the substances that were evaluated. [Mitragotri, S. et al., 2011] projected that every chemical would resemble lead, and their synthetic feasibility was estimated to be between 2.7% and 3.04%, indicating that they are readily synthesizable.

By using the Bioavailability Radar, a rapid assessment of the drug-likeness may be achieved. The radar system incorporates the analysis of six physicochemical characteristics. Flexibility, size, polarity, solubility, and saturation are among them. The region coloured in pink indicates the ideal values for the six factors listed above. The specific parameter's range is defined as follows: The ligand should possess the following characteristics: lipophilicity: XLOGP3; size: MW; polarity: TPSA; valence: 20–130 Å; solubility: molar solubility in water (log S) should not exceed 6; saturation: fraction of carbons in the sp<sup>3</sup> hybridization should be 0.25 or greater; and flexibility: a maximum of 9 rotatable bonds. A significant deviation from any of these parameters would suggest that the ligand lacks oral bioavailability. Each molecule has shown physical qualities that are ideal. With the exception of the proportion of sp<sup>3</sup> hybridization carbons, all other parameters fall within acceptable limits. The chemicals are thus safe for consumption orally.

The capacity of tiny compounds to enter the brain and passive gastrointestinal absorption were evaluated using the BOILED-EGG technique for prediction. Compounds having a high possibility of penetrating the BBB and entering the CNS are often denoted by a yellow ellipse (i.e. the yolk). In contrast, the white ellipse represents substances that have a high possibility of being passively absorbed by the gastrointestinal system. Those compounds that do not penetrate BBB molecules and are not efficiently absorbed by the GIT are located in the grey zone. It was determined that every molecule that underwent testing had white space characteristics and passive GIT absorption, indicating their potential inability to traverse the BBB. Compounds shown by red colour spots are incapable of functioning as substrates for the P-glycoprotein (PGP-).

#### **4.1.2. Virtual Screening and Molecular Docking Analysis (ROS1)**

Diosmin exhibits greater binding energy (64.57 kcal/mol) with the drug target protein ROS1 (PDB ID: 3ZBF) (Figures. 4.3 and 4.4), suggesting the potential of Diosmin's binding affinity and possible anti-LC effect. Moreover, to validate the result, we utilized Glide, molecular docking of diosmin with the receptor ROS1, showing the Glide XP score of -11.24 kcal/mol with a glide energy of -57.04 kcal/mol. *Table 4.1*



shows the top 10 compounds with their GOLD score. The binding of Diosmin within the active site of ROS1 was stabilized by six hydrogen bonds with the residues Lys1980, Glh1997, Arg2083, Met2029, and Glu2030. Higher energy and XP scores depict the favorable and stable binding of Diosmin in the receptor protein.

**Table 4.1 : Top 10 compounds having high GOLD scores with ROS1.**

S.no.	Compound Name	GOLD score
1.	Diosmin	64.57
2.	Myrciacitrin V	52.15
3.	Pedalitin	51.32
4.	Velutin	48.81
5.	Wogonin	48.54
6.	Tricin	47.23
7.	Rhamnetin	45.35
8.	Myricetin	44.74
9.	Naringenin	44.20
10.	Sorbifolin	43.94

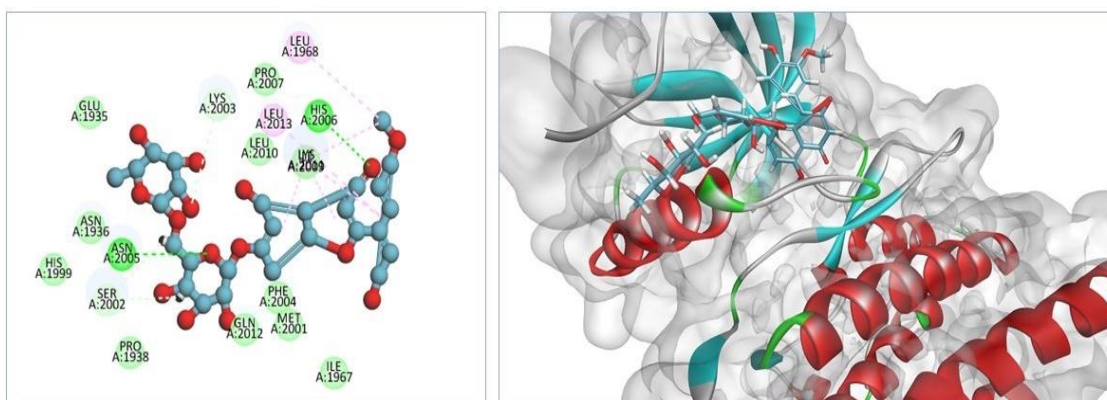


**Figure 4.3 : 2D and 3D images of interactions with *ROS1* and Diosmin, in green color, showing hydrogen bonding.**

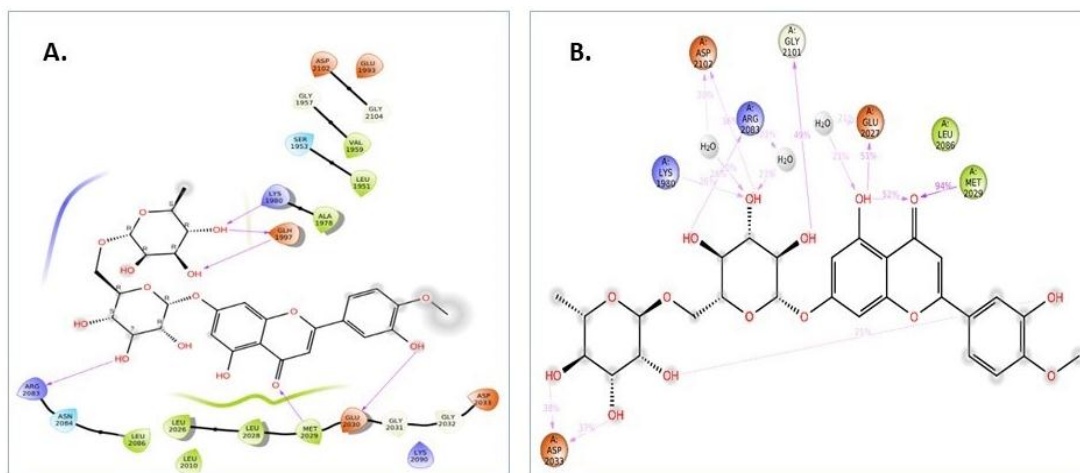


**Figure 4.4 : A. Schrodinger's docking complex is shown to have a Glide energy of -57.044 and an Xp score of -11.239. 3B. Demonstrating the precise connections between all atoms of diosmin and protein sites throughout the 100ns simulation.**

### 4.1.3 DFT Analysis

DFT calculation was carried out to understand the molecular structure, geometry and electron distribution (figure 4.5), which also predicts the stability and reactivity of the compound. The characters of the electron donors and electron acceptors in the diosmin are explained by the frontier molecular orbitals HOMO energy and LUMO energy, respectively. The higher values of HOMO and LUMO energies correspond to the higher capacity of electron donors and acceptors in the molecule. The HOMO and LUMO values of the Diosmin are -0.230962eV and -0.081269 eV, respectively. The smaller HOMO and LUMO values predicted from DFT analysis show the Diosmin compound's limited electron donor and electron acceptors. However, Diosmin has higher electron-donating groups than the electron-accepting group, evident from the HOMO (-0.230962eV) and LUMO (-0.081269 eV) values. The predicted energy gap of the Diosmin compound is 0.149693 eV, a relatively tiny energy gap. The smaller energy gap predicted for the Diosmin compound shows that the molecule is highly polarizable and reactive.

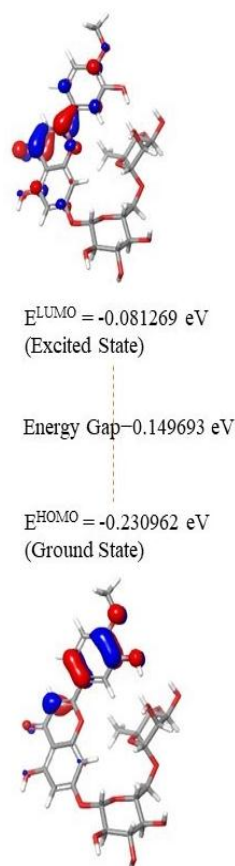


**Figure 4.5 : HOMO-LUMO border chemical orbitals of diosmin and the associated transition energies.**

#### 4.1.4. ADME Analysis

ADME prediction is crucial to the pharmaceutical research and development processes to forecast in-vivo pharmacokinetics. ADME analyses are done in conjunction with molecular docking studies to categories the safety and efficacy of a pharmaceutical compound [30]. It depicts the process of Absorption, Distribution, Metabolism, and Excretion of any drug. CYP and P-gp protein play a vital role in this process, while if the compound inhibits the P-gp protein, it has high bioavailability and vice-versa. At last, we found that diosmin inhibits the Pgp and cannot inhibit other important targets i.e., Cyp Substrate and inhibitions.

We predicted Lipinski's rule of 5 using the online zinc server, including other properties. With one or two exceptions, the findings showed that all the compounds adhered to the Lipinski rule. Furthermore, the results indicated that the compounds

possess a drug-like characteristic that may be able to produce oral bioavailability. DIOSMIN has Log P 2.66, Molecular Weight is 608.54 and has 8 Hydrogen bond donors and 15 acceptors, and last, it has 7 rotatable bonds.

#### 4.1.5. BOILED Egg Plot Analysis

Aside from ADME prediction, failures due to undesirable pharmacokinetic features include small molecule toxicity and efficacy. The BBB and gastrointestinal absorption are two advantageous pharmacokinetic characteristics of the DIOSMIN Boiled Egg plot. In contrast, the blood-brain barrier and gastrointestinal absorption rate of DIOSMIN are not seen in the white and yellow zones of the egg, respectively (Figure 4.6). Consequently, the brain cannot pass through the DIOSMIN molecule. These observations suggest potential limitations regarding the compound's distribution and absorption in these regions. Overall, our investigation showed that DIOSMIN was the most successful anti-cancer drug. Further, pre-clinical analysis is required.

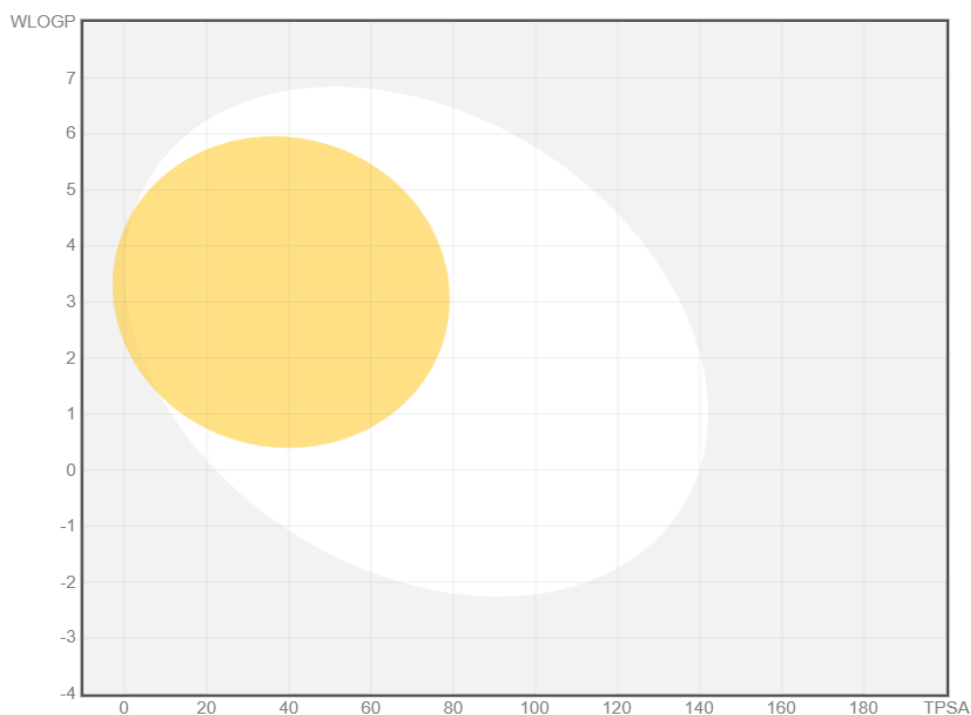


**Figure 4.6 : The graph- as shown, diosmin is not present in the white or yellow center, so it has no or moderate gastrointestinal absorption rate and BBB permeability.**

#### 4.1.6. Molecular Simulation Evaluation

Studying the behavior of a protein and its ligand over a certain period is the focus of MD simulation. The production phase of the ligand complex was exposed to the whole simulation for 100 ns. The structural and dynamic properties of the protein-ligand complexes were investigated as RMSD over the 100 ns simulation period and according to the RMSD plot for DIOSMIN bound with ROS1 in Figure 4.7, the ligand-binding protein displayed substantial stability in the range of 1.6 - 3.2nm over the 100ns of the MD simulation. However, it becomes stable after 10ns at 2.4nm as the median throughout the 100ns. The RMSD result decodes that diosmin did not dissociate from the protein during the 100 ns simulation, and the relationship between ROS1 and diosmin remained stable.

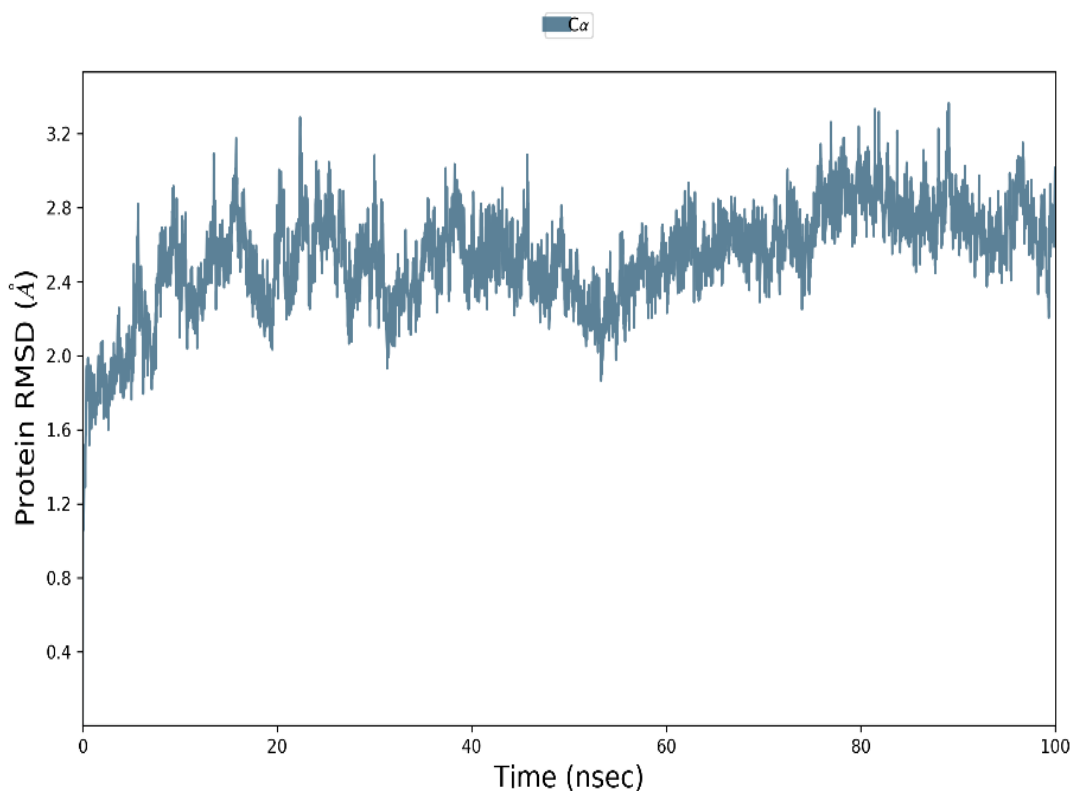


**Figure 4.7 : MD simulation by employing Schrodinger.**

### Ligand Properties

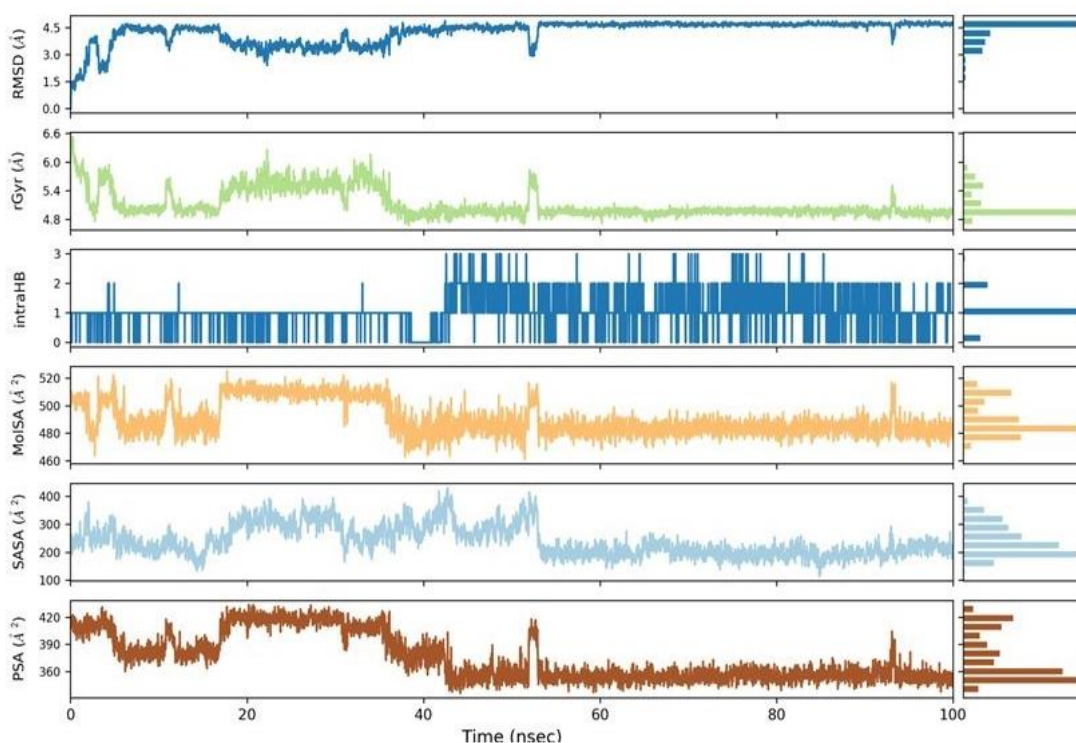


**Figure 4.8 : PSA, RGYR, MolSA, SASA, RMSD, and IntraHB.**

The MD simulation (Figure 4.8) also looked at rGyr, MolSA, SASA, and PSA variations. Figure 4.8 shows the ligands' root-mean-square deviations. rGyr serves as a representation of the ligands' "extendedness". Calculating the molecular surface area with a 1.4 probe radius is called molecular surface area (MolSA). The reciprocal of this number is a van der Waals surface area. SASA refers to the surface area of each ligand that a water molecule may reach. Oxygen and nitrogen are the only atoms in the ligands that provide solvent-accessible surface area. This is known as PSA.

The Root Mean Square Deviation (RMSD) value of the ligand remained relatively stable within the range of 1.5 to 4.3 Å over the course of the simulation. The radius of gyration exhibited minor fluctuations but predominantly fluctuated within the range of 4.8 to 6.0 Å. The molecular surface area also displayed variations, primarily within the range of 475 to 510 Å<sup>2</sup> during most of the simulation.

Moreover, the solvent-accessible area underwent dynamic changes, commencing at approximately 200 Å<sup>2</sup>, increasing to 380 Å<sup>2</sup> within the first 50 ns, and subsequently stabilizing at around 200 Å<sup>2</sup> for the remaining 100 ns with minimal fluctuations. Similarly, the polar surface area experienced fluctuations, initially ranging from 360 to 420 Å<sup>2</sup> during the first 50 ns, followed by reaching an equilibrium state at approximately 360 Å<sup>2</sup> for the subsequent 100 ns.

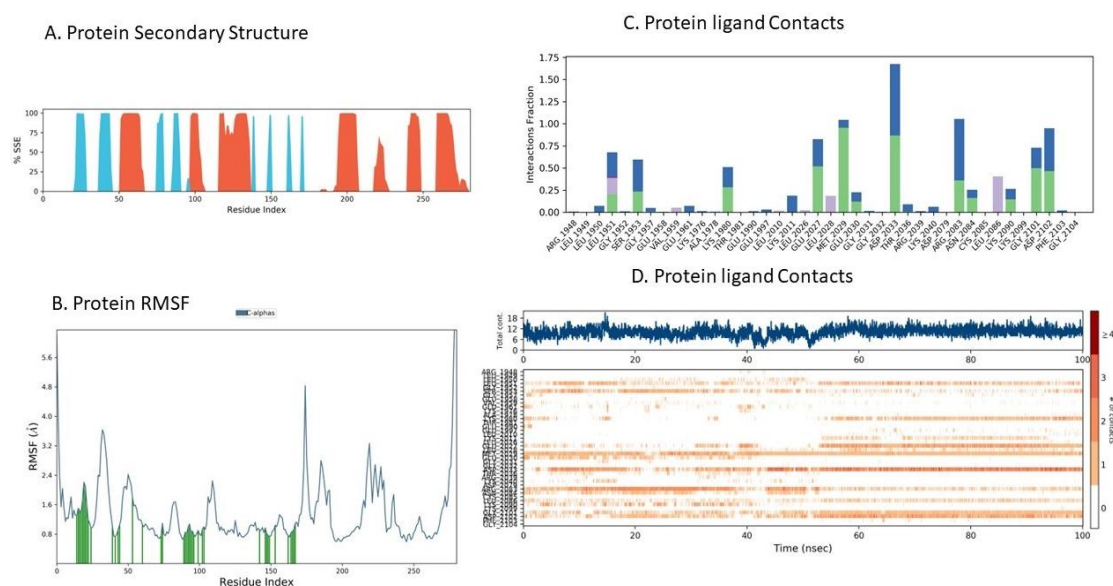


**Figure 4.9 : A. The protein secondary structure. B. Protein RMSF. C & D: Exploring the Diverse Interactions Between ROS1 and Diosmin**

Throughout the simulation, we investigated how the bioactive compounds interacted with the active sites of ROS1 through hydrogen bonds. For ROS1-DIOSMIN, H-bonds were seen in the molecules MET2029, ASP2033, ASP2102, GLU2027, and LYS2090. These molecules are shown in Fig. 8c–d, along with additional interactions created throughout the simulation's 100 ns.

RMSF were assessed for every site in the ligand-protein interactions. RMSF were evaluated for every site in the ligand-protein interactions and shown to represent its degree of flexibility. The protein-ligand complex's RMSF demonstrated the lowest level of volatility for any of the interactions. For all the complexes, the average RMSF values were kept unchanged, as shown in Figures 51. Over the course of the 100 ns simulation period, the RMSF did not vary much.



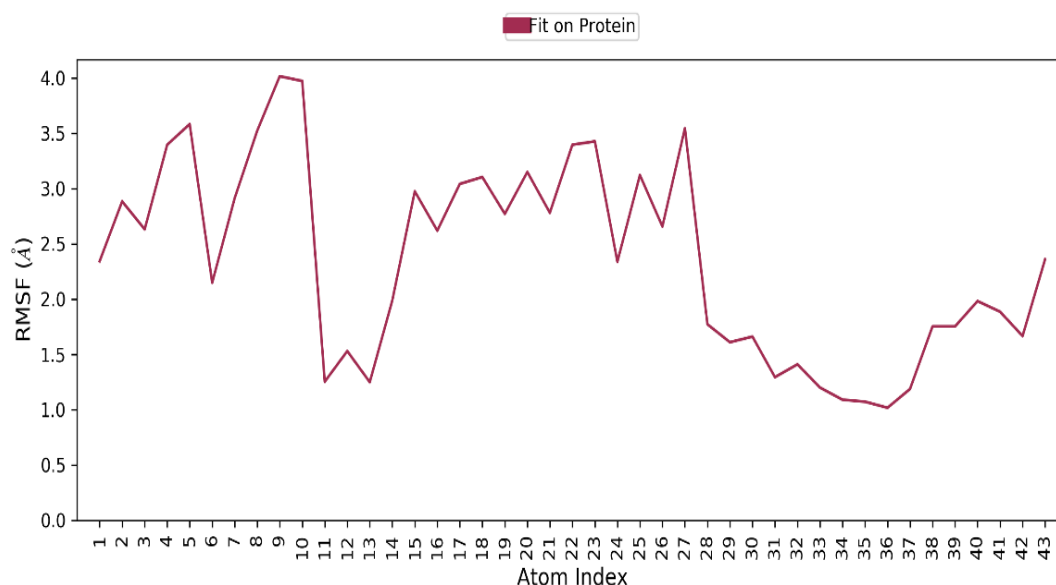


**Figure 4.10 : Root Mean Square Fluctuation (RMSF) analysis, illustrating the 2D structure of the ligand and providing a detailed representation of atomic-level fluctuations within the ligand.**

Figure 4.9 reports the findings of an interaction investigation between DIOSMIN-ROS1 at different stages of the Molecular Simulation. It illustrates the interactions between the complex throughout the simulation. The "Simulation Interactions Diagram " was also used to study each interaction type's more detailed subtypes. The stacked bar charts are standardized throughout the trajectory; for instance, a value of 0.25 indicates that the contact is maintained for half the simulation duration. Values over this are feasible since certain protein residues form several interactions with the ligand of the same subtype. Each of Figure 8c-bottom d's panels provides a timeline picture of the interactions and contacts (H-bonds, Hydrophobic, Ionic, and Water bridges). The interaction study between Ros1 during 100 ns of MDs reveals that DIOSMIN's various atoms have established hydrogen bonds with the amino acids LEU 1951, SER 1953, LYS 1980, GLU 2027, MET 2029, GLU 2030, ASP 2033, ARG 2083, ASN 2084, LYS 2090, GLY2101, and ASP 2102, among others.

#### **4.1.7. Protein Secondary Structure**

During the simulation, beta- and alpha-strands are seen as instances of protein secondary structural components (SSE) (Figure 4.11). The residue index in the



graphic above displays the SSE distribution over the whole protein structure. The graphic below summarizes the SSE component for each trajectory frame throughout the simulation, whereas the bottom figure tracks the SSE assignment of each residue over time.

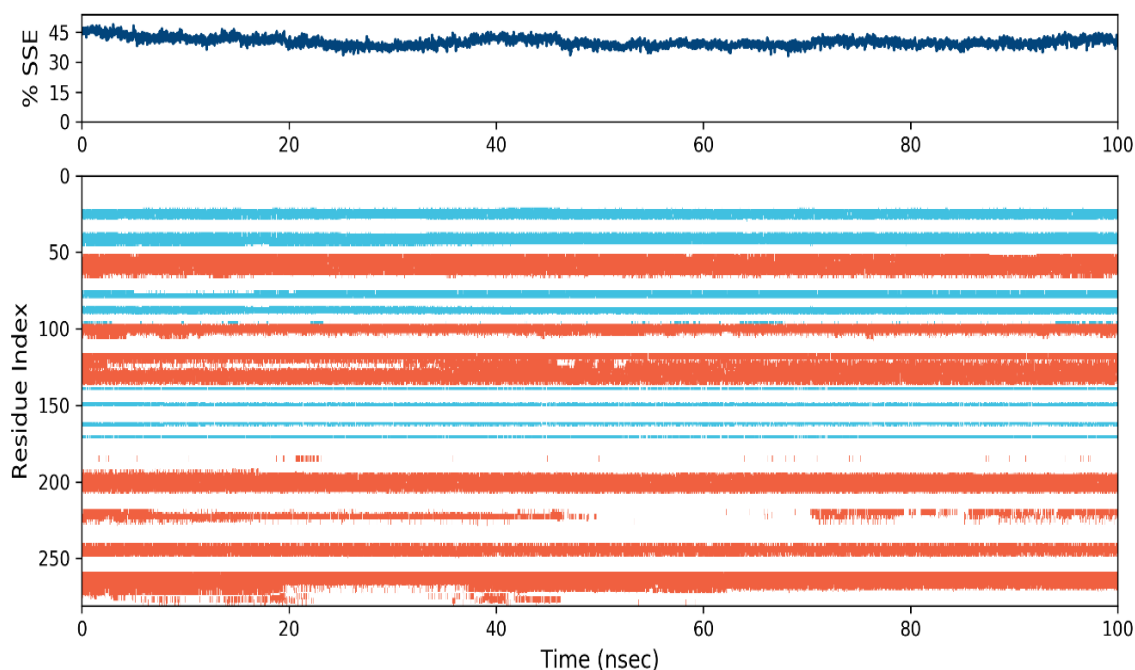


**Figure 4.11 : Secondary structure analysis of proteins, summarizing the composition of secondary structural elements (SSE) observed across each trajectory frame throughout the simulation.**

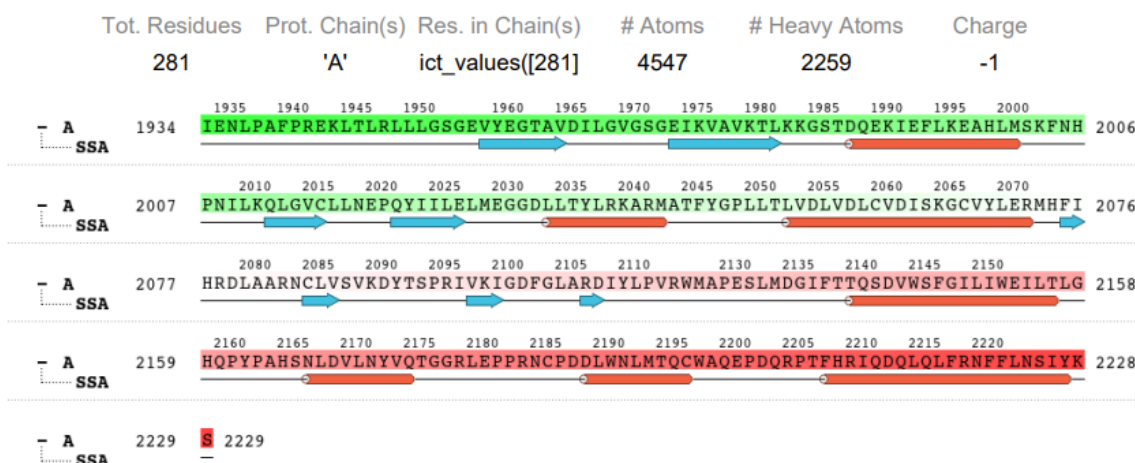


**Figure 4.12 : Chain A of the protein has 281 residues, 2259 total atoms, 2300 heavy atoms, and a charge of -1.**

#### 4.1.8. Virtual Screening and Molecular Docking Analysis (EGFR)

Hesperidin exhibits a significantly higher GOLD score of 60.98 with EGFR (PDB ID: 6DUK), which depicts that it may possess better anti-cancer properties and could be an efficient candidate for treating LC. (Figure 4.13). Hesperidin has H-bonds with LYS:745, ARG:841 and ALA:743 of EGFR. The docking results provide a platform for further pre-clinical evaluation. *Table 1* shows the top 10 compounds with Gold Score. To further validate the GOLD score, we utilized Glide (Schrodinger,) and it shows an Xp Score of -9.433 kcal/mol and a Glide energy of -70.911 kcal/mol (figure 4.14). Figure 3B describes the hydrogen bond interactions maintained throughout the 100 ns simulation. This finding suggests that Hesperidin possesses a higher binding affinity towards the target protein EGFR. The higher binding affinity towards the EGFR may have potential anti-cancer activity and could emerge as a promising agent for curing LC.

**Table 4.2 : Demonstrates the top 10 compounds with EGFR GOLD Score.**

S.no.	Compound Name	GOLD Score (Kcal/mol)
1.	Hesperidin	60.98
2.	Icariin	58.32
3.	Rutin	58.09
4.	Isoliquiritin apioside	57.83
5.	Silymarin	57.52
6.	Pectolinarin	55.16
7.	Myricitrin	53.53
8.	Lichochalcone	53.35
9.	Formononetin	52.97
10.	Epicatchin gallate	52.42

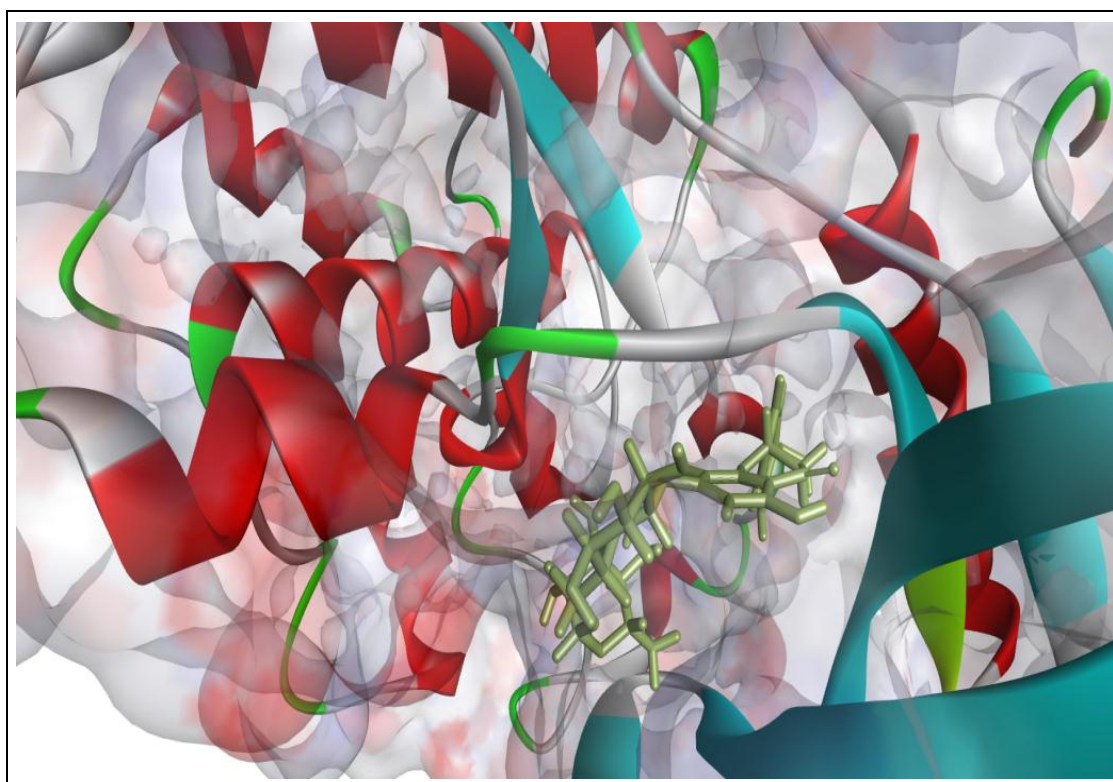
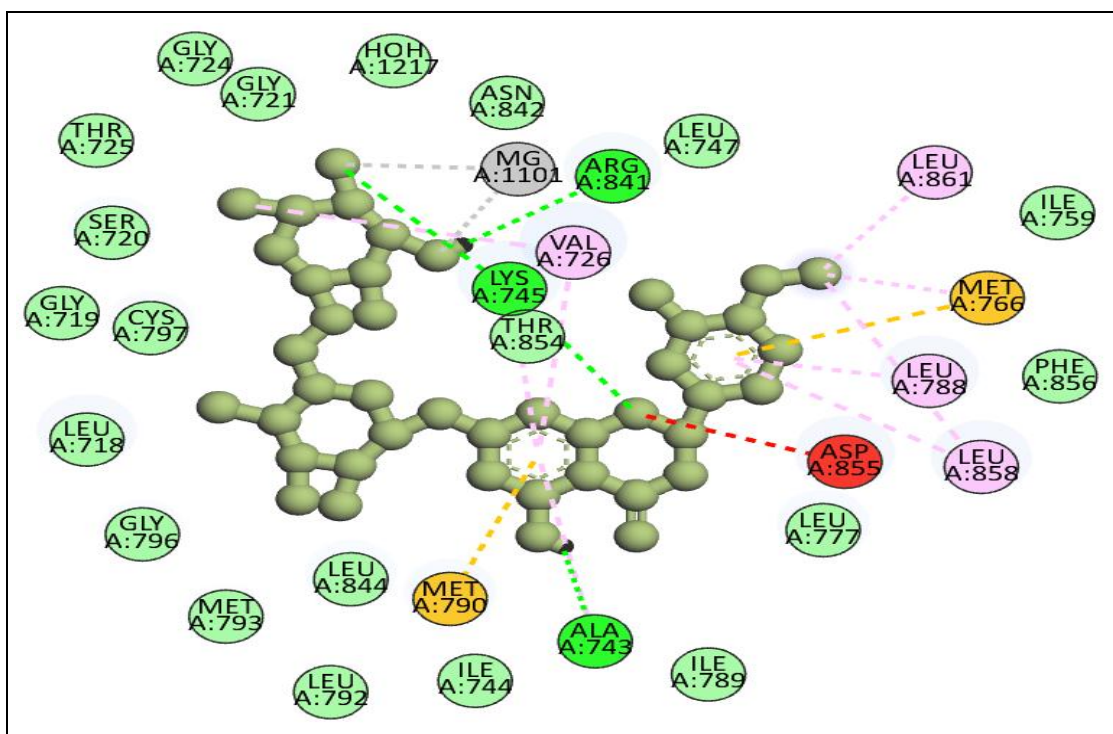


**Figure 4.13 : The 2D and 3D interaction with *EGFR*-Hesperidin was displayed in green, showing hydrogen bonding. It shows that positions A: 745-LYS, A:841-ARG, and A: 743-ALA have hydrogen bonds and positions.**

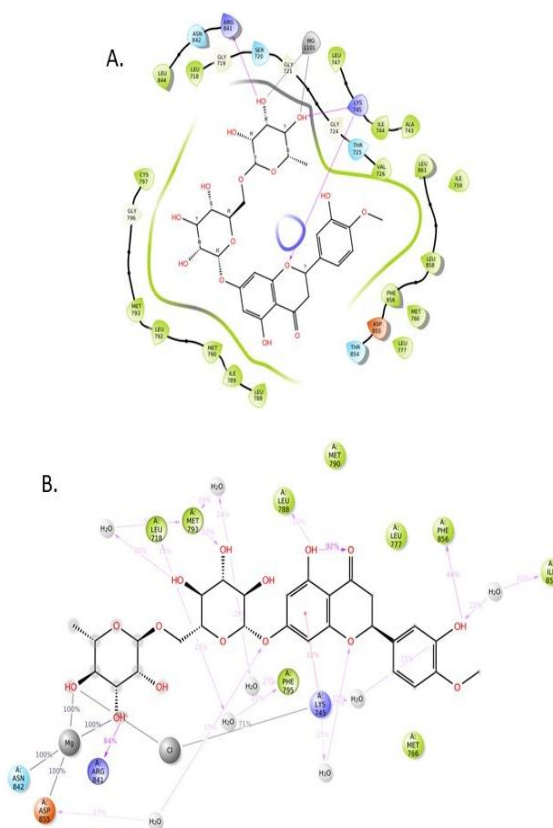


**Figure 4.14 : Docking complex having a Glide XP score of -9.433 kcal/mol and a Glide energy of -70.911 kcal/mol. pink color arrows are the H bonds between Hesperidin and *EGFR*.**

**B.** Demonstrating the precise connections between all atoms of Hesperidin and protein sites. Relationships that last more than 10.0% of the simulation period are shown in the viewable pathway (0.00 to 100.01 nsec). Because individual residues may have several contacts of the same sort utilizing the same ligand atom, engaging with >100% is conceivable.

#### 4.1.9 DFT Analysis

The characteristics of the Hesperidin in donating and receiving electrons were investigated. Furthermore, the significant energy difference between HOMO and LUMO causes an unfavorable condition of electron transfer and reduces reactivity with protein. The present research found a low energy gap (HOMO-LUMO) for the Hesperidin compound, which indicates that the Hesperidin is more reactive (Figure 4.15).

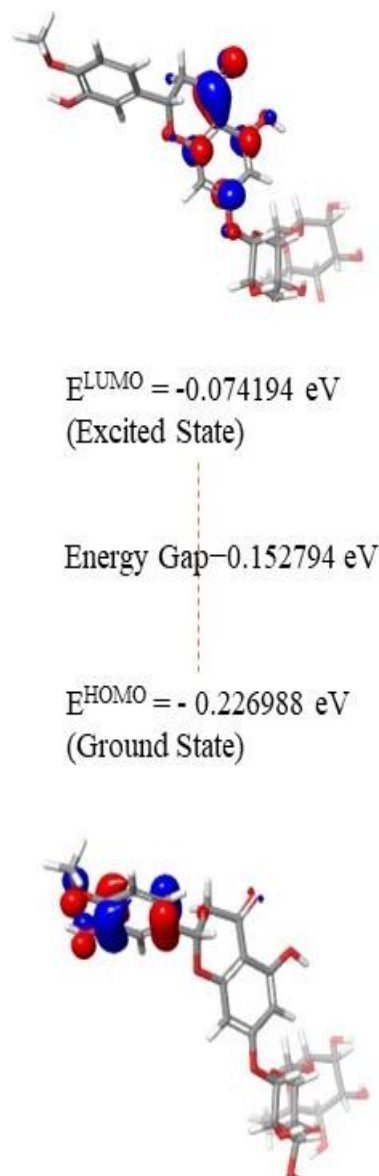


**Figure 4.15 : Hesperidin border chemical energy levels (HOMO-LUMO) and the associated transitional Strength of Hesperidin.**

#### **4.1.10. ADME Evaluation**

ADME prediction is critical in finding and developing new drugs and attempting to forecast the pharmacokinetics of compounds [13]. Tables 1 and 2 present the pharmacological characteristics of the compounds under investigation. These characteristics provide valuable information regarding the compounds' absorption, distribution, metabolism, and excretion properties, critical determinants of their pharmacological profiles. By considering ADME predictions alongside other

evaluations, researchers can make informed decisions regarding the suitability and potential of these compounds as drug candidates.

**Table 4.3 : ADME Characteristics of the Hesperidin and Diosmin Compound.**

S.No.	Compound Name	CYP_2C9 inhibition	CYP_2C19 inhibition	CYP_2D6 inhibition	Pgp inhibition	CYP_3A4 inhibition	CYP_2D6 substrate	CYP_3A4 substrate
1	Hesperidin	No	No	No	Inhibitor	No	No	No
2	Diosmin	No	No	No	Inhibitor	No	No	No

The study exhibits values within an acceptable range, indicating their favorable pharmacological characteristics. Notably, Hesperidin falls within this range, suggesting its inherent permeability. Specifically, Hesperidin, as a chemical entity, demonstrates excellent pharmacokinetic properties. Consequently, this Hesperidin compound possesses good bioavailability and is a naive agent with significant potential. These findings highlight the promising nature of Hesperidin as a candidate for further exploration and development in the future.

This computational analysis offers a crucial foundation for pharmaceutical research, offering valuable insights for in-vitro and in-vivo studies. By exploring the multifaceted functions of Hesperidin, researchers can gain a comprehensive understanding of its potential as a bioactive compound against LC. This knowledge serves as a stepping-stone for devising informed strategies in utilizing Hesperidin for therapeutic purposes.

**Table 4.4 . Drug-like properties of Hesperidin and Diosmin.**

S.No.	Name of compound	MW	Log p	HB donor	HB acceptor	No. of rotatable bond
1.	Hesperidin	610.56	0.85	8	15	7
2.	Diosmin	608.54	2.66	8	15	7

#### 4.1.11. BOILED Egg Plot Analysis

In addition to ADME prediction, the efficacy and safety of the compound can be compromised by unfavorable pharmacokinetic characteristics. However, Figure 4.16 demonstrates the two favorable pharmacokinetic properties of the Hesperidin compound, as indicated by the Boiled Egg plot [13]. This plot illustrates the ability absorbed in the gastrointestinal tract and its permeability across the Blood-Brain Barrier.

Notably, the Hesperidin molecule doesn't exhibit a moderate gastrointestinal absorption rate, & brain permeability depicts its positioning within the boiled egg in Figure 4.16. Consequently, it can be inferred that Hesperidin demonstrates limited permeability in the brain and gastrointestinal tract. These observations suggest potential limitations regarding the compound's distribution and absorption in these regions.

Despite these considerations, Hesperidin has shown outstanding anti-cancer efficacy in our research. However, further investigation of this native molecule is required to confirm and elaborate the results of this study. Continued exploration will help ascertain the full potential of Hesperidin as a therapeutic agent and provide a more comprehensive understanding of its pharmacological properties.

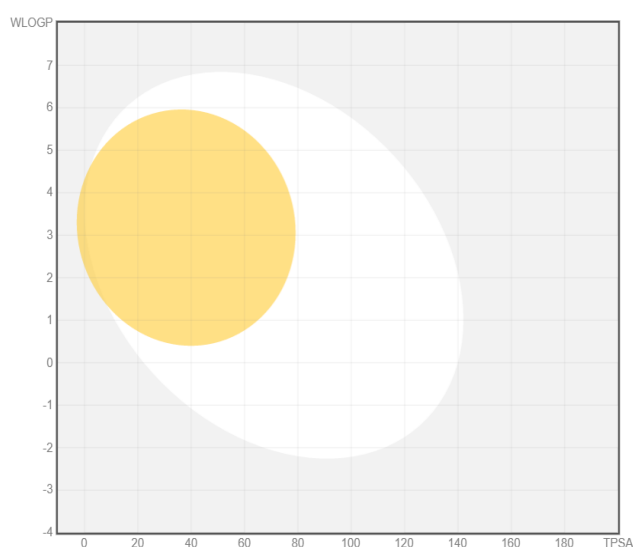


**Figure 4.16 : Boiled egg plot of Hesperidin. It showed that Hesperidin does not have BBB and gastrointestinal absorption.**



#### 4.1.12. Evaluation of Molecular Dynamics Simulation

RMSD, RMSF, and hydrogen bonds are just a few of the metrics that were looked at to gauge the stability of the Hesperidin-EGFR protein complex and comprehend the nature of their interactions. The RMSD profile of the Hesperidin-EGFR complex during a 100-ns molecular dynamics simulation in a solvent environment is shown in Figure 4.17. Throughout the simulation, the RMSD values for the Hesperidin-EGFR complex remained relatively constant, ranging between 1.2 and 2.6 Å. Notably, in the initial and end phases of the simulation (15-20 & 90 ns), fluctuations in the RMSD were observed, which can be attributed to the movements of the activation loop in the EGFR protein [11]. However, minimal changes were observed beyond this early stage, indicating a stable configuration of the Hesperidin-EGFR interaction. The consistent and averaged RMSD values throughout the 100-nanosecond simulation suggest that the Hesperidin-EGFR complex maintained its structural integrity, and Hesperidin remained bound to the protein without dissociation.

Further analyses, such as RMSF and hydrogen bond assessments, can provide additional insights into the flexibility of the complex and the specific interactions involved in stabilizing the Hesperidin-EGFR binding. These findings contribute to our understanding of the molecular dynamics of the complex and provide valuable information for further investigations and potential drug development efforts.

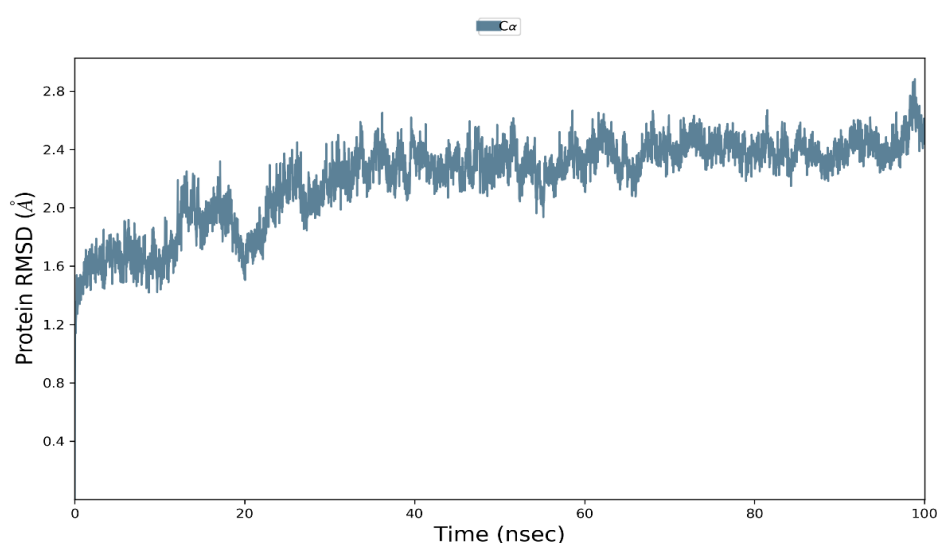


**Figure 4.17 : RMSD performed using Desmond. It is stable throughout 100ns between 1.6-2.6Å and, after 20ns, very stable on 2.2Å.**



In the present study, the RMSD analysis was employed to assess the stability of the protein backbone and the protein-ligand complex. To determine any alterations between the initial and final conformations, the RMSD was calculated, providing insights into the system's overall stability. The computed values of the RMSD indicated a consistent and steady profile for complex, with minimal fluctuations observed throughout the simulation. Figure 4.17 illustrates the structural stability of the protein-ligand complex, as revealed by the RMSD analysis. The trajectory analysis demonstrated that the initial and final structures maintained a stable conformation throughout the simulation, indicating an equilibrium state at 100 ns. This observation supports that the protein-ligand complex remains structurally intact and exhibits promising dynamics throughout the simulation. These findings contribute to the overall understanding of the stability and potential activity of the protein-ligand complex. The steady and stable behaviour observed in the RMSD analysis suggests a favourable interaction between the protein and the ligand, highlighting the potential of the complex as an active entity. Further investigations and studies can build upon these results to elucidate the protein-ligand complex's specific interactions and functional implications.

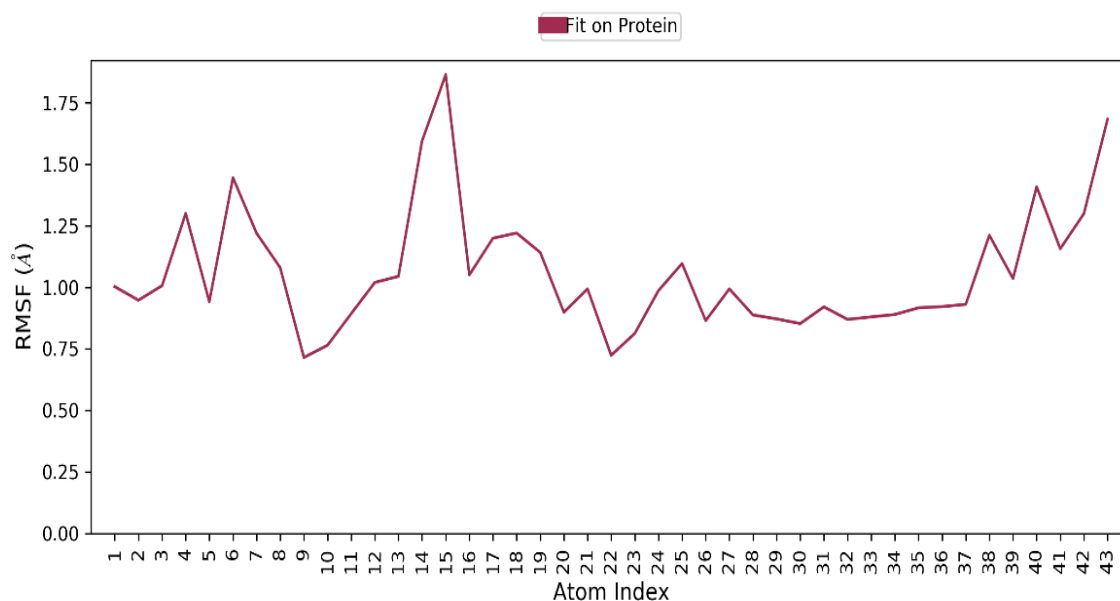


**Figure 4.18 : Ligand RMSF, which is stable throughout the 100ns at above 1.0Å.  
Some components are below 1.0Å, which may not participate in docking interactions.**

The flexibility of the protein's activation loop was further investigated using RMSF analysis, as depicted in Figure 4.19. Calculating the RMSF values for each residue along the simulation trajectory can identify protein regions with higher flexibility and variation. These variations reflect the dynamic behavior of specific amino acid residues, particularly in loop and disorder regions of the protein. In the case of the protein-ligand complex, the RMSF of the ligand diagram (Figure 4.18) reveals that specific residues exhibit significant fluctuations below 1Å. However, it is essential to note that these residues are not involved in the binding process as identified in the docking studies. Hence, the observed fluctuations do not adversely affect the stability of the protein-Hesperidin complex. Most residues exhibit lower changes, with RMSF values exceeding 1Å indicating stable behavior throughout the simulation. Another crucial aspect of the protein-ligand complex is the formation of hydrogen bonds. The hydrogen bond interaction analysis between Hesperidin and the EGFR protein is shown in Figure 61C. During the simulation, five hydrogen bonds were formed between specific amino acid residues and the OH group of the Hesperidin molecule. These hydrogen bonds contribute to the stabilization of Hesperidin in its binding site, validating the findings from the docking studies.

These additional analyses enhance the robustness of the findings and provide a comprehensive understanding of the protein-ligand interactions. The RMSF analysis and hydrogen bond examination collectively contribute valuable insights into the flexibility and stability of the protein-ligand complex. The results demonstrate the compatibility of the observed fluctuations and hydrogen bonding patterns with the docking studies, supporting the overall reliability of the simulation and suggesting the favorable binding and stability of Hesperidin in its interaction with the EGFR protein.

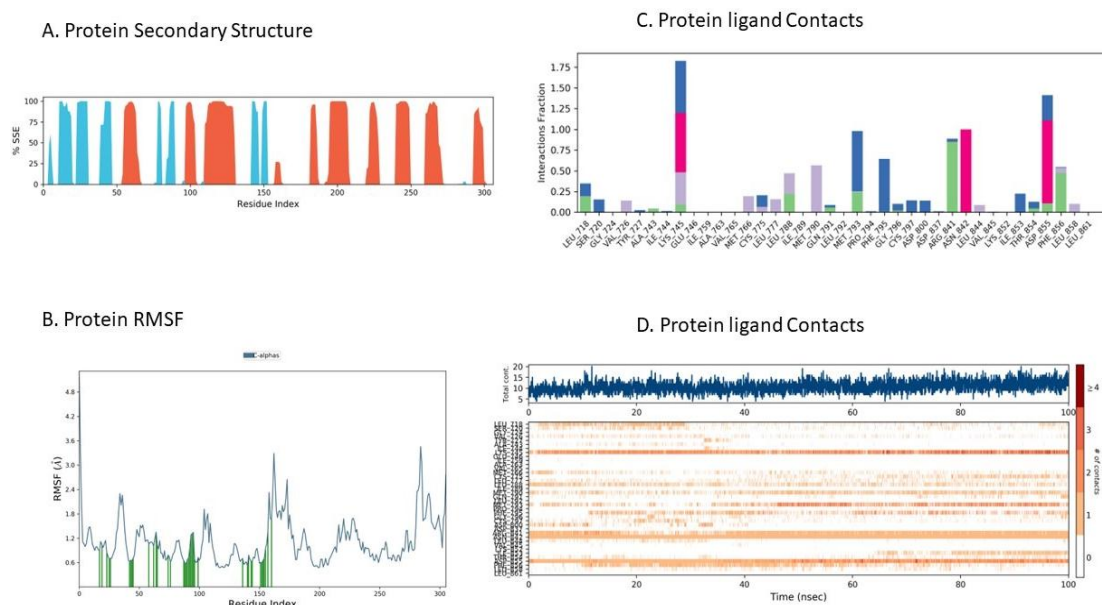


**Figure 4.19.A : Visualization of the protein's secondary structure dynamics throughout the simulation. B. Root Mean Square Fluctuation (RMSF) analysis illustrating atom-by-atom ligand-protein interactions. C & D. Comprehensive timeline of protein-ligand interactions, highlighting key connections such as hydrogen bonds, hydrophobic interactions, ionic interactions, and water bridges. The top panel depicts the total number of distinct interactions between the protein and the ligand during the simulation. The bottom panel maps the specific residues involved in ligand interactions across each trajectory frame, with dark orange residues indicating versatile interaction modes.**

#### 4.1.13. Ligand Torsion Profile and Properties

During the simulation trajectory spanning from 0.00 to 100.01 nanoseconds [15], [20], each rotatable bond (RB) in the ligand [23] experienced conformational modifications are evident from the ligand torsions chart and other relevant features (Figures 4.20 and 4.21). The top panel (Figure 61A) of the figures presents a two-dimensional representation of the compound, highlighting the rotatable bonds with different colors. Each rotatable bond's torsion is illustrated using a dial plot and a corresponding color-coded bar plot. The dial plots visually display the changes in torsion angles throughout the simulation, with the temporal progression radiating outward from the starting point at the center of the radial map. On the other hand, the

bar plots summaries the torsion data by showing the probability density of each torsion angle.

Additionally, the figure showcases the potential energy associated with each rotatable bond by incorporating the possible torsional information. The likely energy values are depicted on the chart's left Y-axis and measured in kcal/mol. By examining the histogram and torsion potential correlations, one can gain insights into the structural variations and anomalies experienced by the ligand to maintain a conformation suitable for binding to the protein. These comprehensive visual representations of the ligand's stable bonds and their conformational changes provide valuable information about its flexibility and how it adapts to the protein-binding environment throughout the simulation.

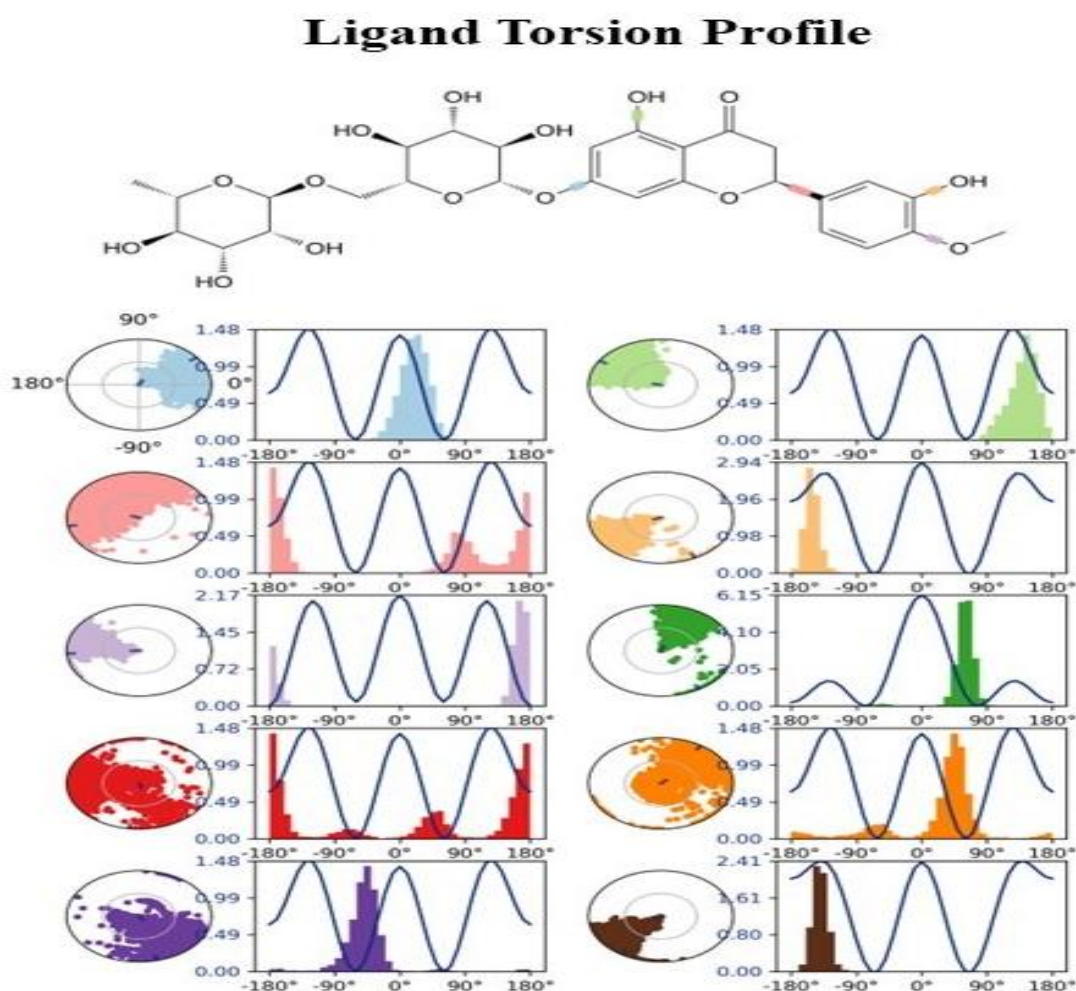


**Figure 4.20 : 2D & 3D compound torsional patterns.**

## Ligand Properties

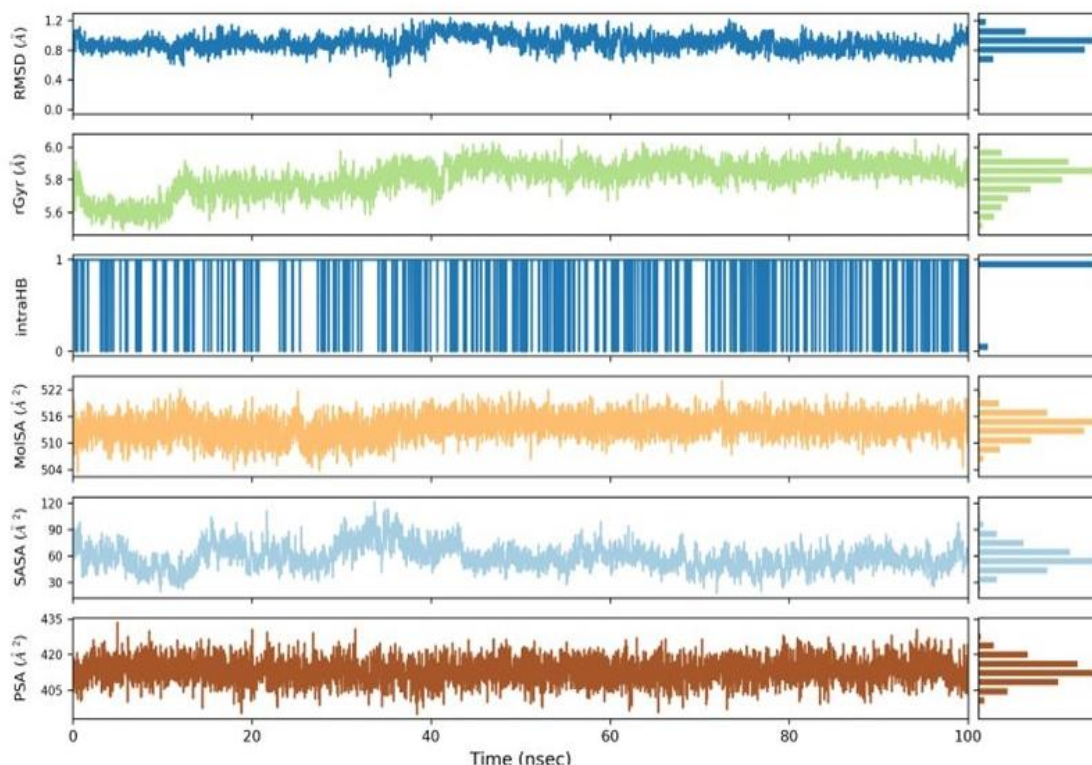


**Figure 4.21 : RMSD, RGYR, IntraHB, MolSA, SASA and PSA.**

### 4.1.14. Protein Secondary Structure

The simulation analysis includes monitoring the presence of beta- and alpha-strands as representative examples of protein secondary structural elements (SSE). The distribution of these SSEs across the protein structure is visualized in the plot above, with the residue index indicating their positions. The bottom plot provides a dynamic view of the SSE assignment for each residue over time, allowing for the observation of fluctuations in SSEs during the simulation. On the other hand, the plot below summarises the SSE composition for each trajectory frame throughout the simulation. These visualizations can be seen in Figures 4.22 and 4.23. By tracking the SSEs, we gain insights into the stability and structural changes of the protein during the simulation. The analysis helps us understand how the protein's secondary structure evolves and how it may interact with the ligand or other components within the system.

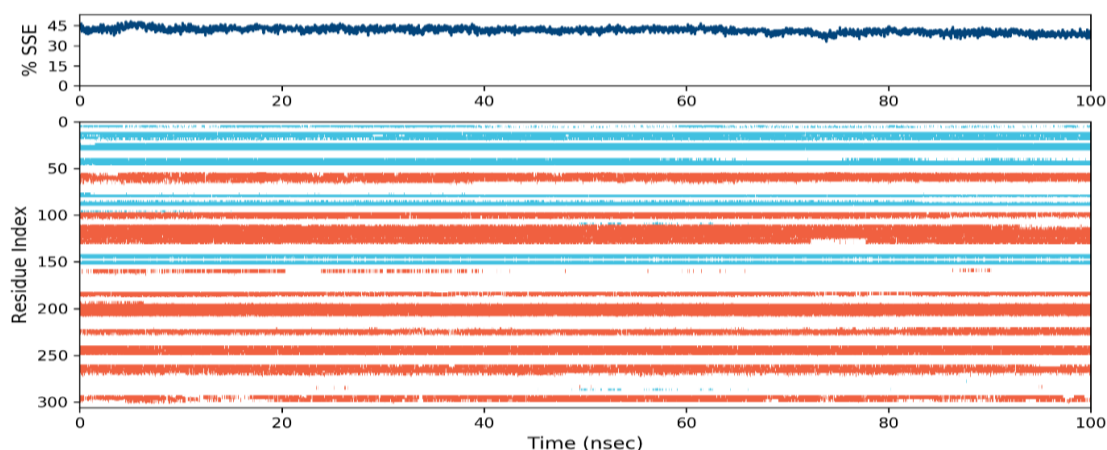


**Figure 4.22 : Secondary protein structures of EGFR. The plot above represents the SSE, while the figure below highlights the SSE content for every trajectory step during the experiment.**

#### Protein Information

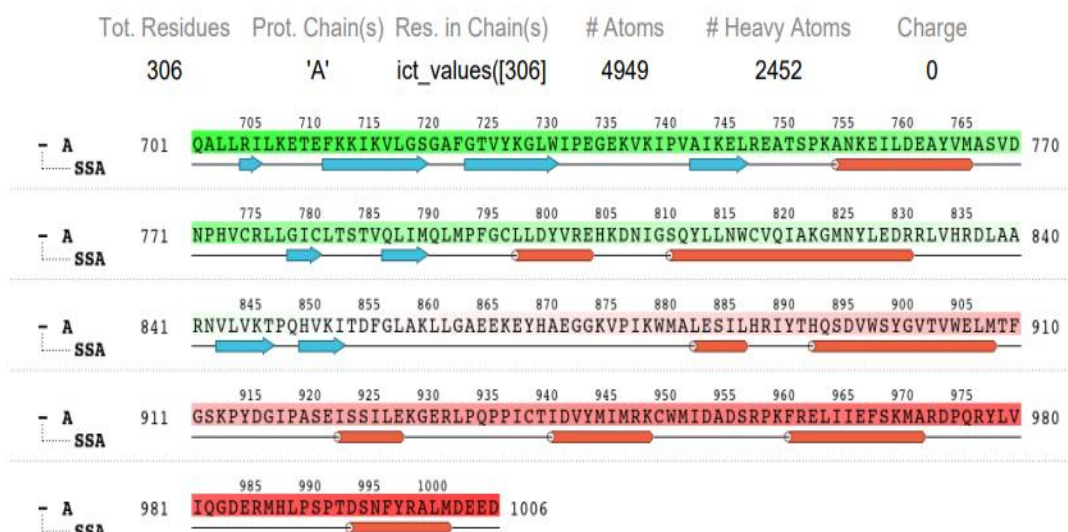


**Figure 4.23 : The protein report contains 288 residues in chain A of EGFR, 4653 total atoms, 2300 heavy atoms, and +5 charges.**

**Objective 2:** To Evaluate the selected molecules based nano formulations against LC

We procure Diosmin and Hesperidin from Otto Kemi Pvt. Ltd. Mumbai having +98 purity.



## **4.2 CHARACTERIZATION OF DIOSMIN**

We employ several approaches for evaluating Diosmin, including FTIR, XRD and DSC.

### **4.2.1 FTIR (Fourier Transform Infrared)**

By analysing the peaks detected in the IR radiation band, the FTIR (Fourier Transform Infrared) technique was used to determine the organic & inorganic parts of the materials. When exposed to FTIR analysis, each ingredient of the sample compounds was identified based on its own peak frequency.

FTIR was used to establish the presence of many organic and inorganic elements inside the sample. Figures 4.24 show the FTIR analysis findings, which provide vital information on the chemical composition and structural properties of the material.

It is crucial to remember, however, that FTIR has several limits. One of these disadvantages is that it cannot expose the metallic features of any chemical. An alternate approach for analysing metallic components or compounds is NMR (Nuclear Magnetic Resonance) spectroscopy. NMR spectroscopy is very valuable for studying the characteristics and structures of metal-containing compounds, as it provides extensive information on their coordination, oxidation state, and ligand interactions. A thorough knowledge of the sample's chemical composition and characteristics may be attained by using the capabilities of FTIR for detecting inorganic and organic components and supplementing it with NMR for metallic details.



**Figure 4.24 : FTIR analysis of Diosmin (DM). The Fourier Transform Infrared (FTIR) spectrum provides a detailed molecular fingerprint, highlighting characteristic absorption bands that reveal the chemical bonds and functional groups present in the molecule. This analysis facilitates the identification and screening of key structural components within Diosmin.**

#### 4.2.2 NMR

NMR (Nuclear Magnetic Resonance) spectroscopy is a powerful source for analysing the structure of substances by monitoring & measuring nuclear spin interactions in a strong magnetic field. As shown in Figure 4.25, this analytical approach gives useful insights into the physical, chemical, and biological properties of materials.

NMR spectroscopy is widely used in pharmacology for detecting and characterising compounds. By evaluating the distinctive NMR spectra of substances, pharmacologists may establish their identification and makeup. By analysing the chemical shifts, coupling patterns, and relaxation periods in the NMR spectrum, useful information on the analysed substances' molecular structure, connectivity, and conformation may be gleaned.



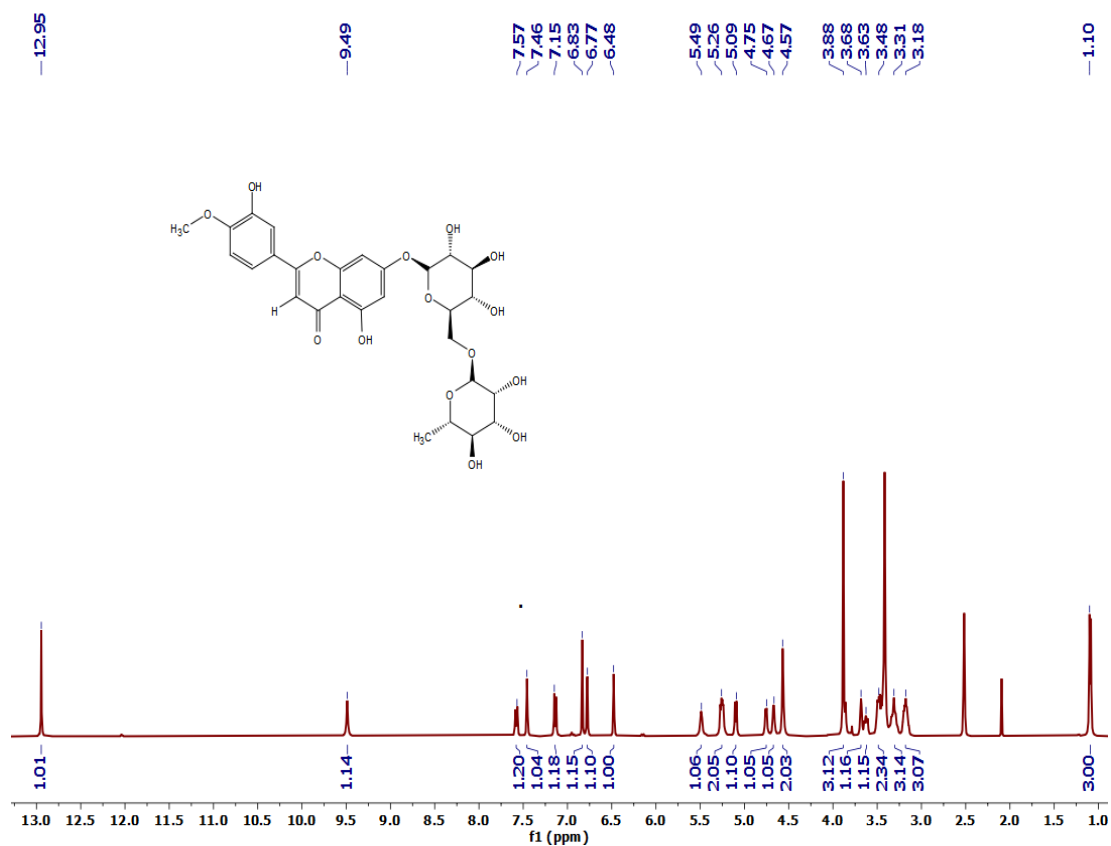


**Figure 4.25 : NMR result of Diosmin**

### 4.2.3 DSC

A DSC (Differential Scanning Calorimetry) device with thermal expansion capability was used to determine DM (Diosmin). To guarantee precise readings, the device was calibrated before to the study using a standard reference material.

A 1.90 mg sample was carefully measured and placed in an aluminium testing crucible for analysis. The crucible was then firmly sealed, and the sample was heated in an atmosphere of nitrogen (N<sub>2</sub>). The temperature was raised by 10°C every minute until it reached 300°C.

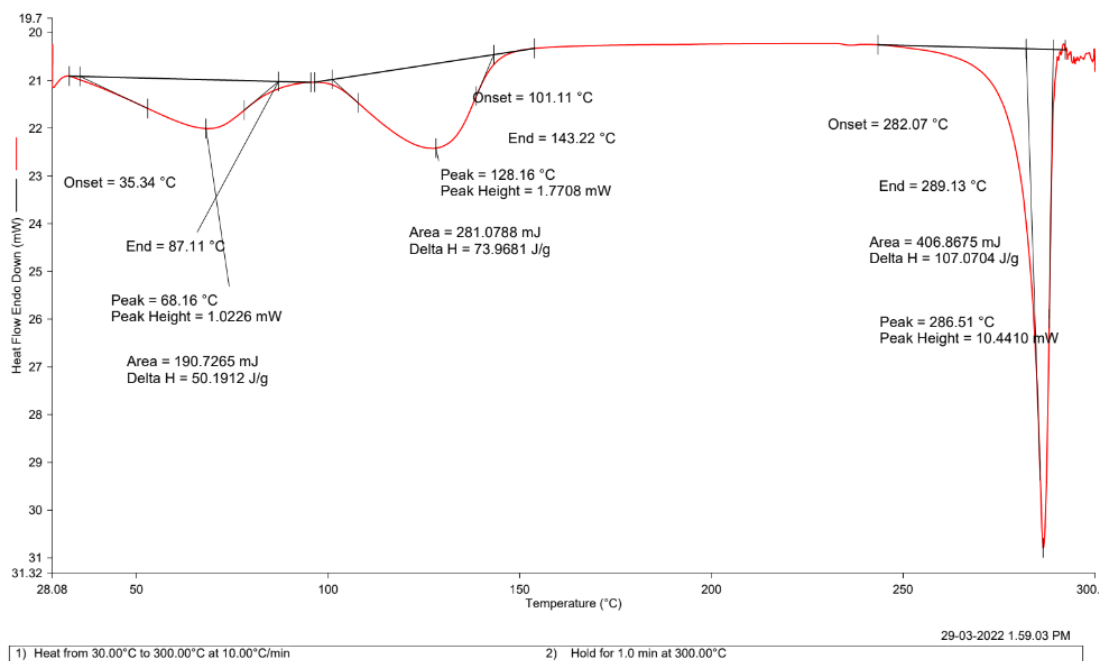


**Figure 4.26 : DSC analysis of Diosmin. These diagrams depict the thermal behaviour of the compounds, including the typical melting ranges and accompanying thermal events.**

These findings add to a thorough understanding of the physical properties of the compounds and can help in a variety of applications, including pharmaceutical formulation and process optimisation.

Figure 68 depicts the DSC Trend of DM. The curve of the DSC reveals an exothermic peak about 128°C, demonstrating that the formation of crystals is causing a process that is exothermic. The peak of endothermic activity noticed at roughly 286°C is due to an endothermic because it is known as "melting."

#### 4.2.4 XRD

To analyse the form or type of the specimens, the XRD (X-ray Diffraction) technique was used, which distinguished between crystalline and amorphous structures. The XRD pattern can provide vital information about the sample's structural features.

If the resultant XRD chart shows crisp and clear peaks, it suggests that the material is crystalline in nature. These peaks represent the regular arrangement of atoms in a

crystal lattice, and their locations and intensities reveal information about the crystal structure.

If, on the other hand, the XRD graph shows a generally featureless or flat profile, the sample is amorphous. The lack of sharp peaks in the XRD pattern suggests a lack of long-range order in the atomic arrangement, which is typical of amorphous materials.

The XRD data for Diosmin is shown in Figures 4.27. The diffraction peaks in figure 13 at 12°, 16°, 20°, and 23° could be indexed to (1200), (1550), (1549), and (1050) planes and figure 4.27 at 11°, 19.9°, 23.2°, and 25.1° could be indexed to (2600), (2800), (1900), and (1400) planes. These images depict the XRD patterns, which reflect the crystallinity of the materials.

This information is crucial to grasp the atomic structure of the molecules and has implications, including medicinal investigation, materials science, as well as quality assurance.

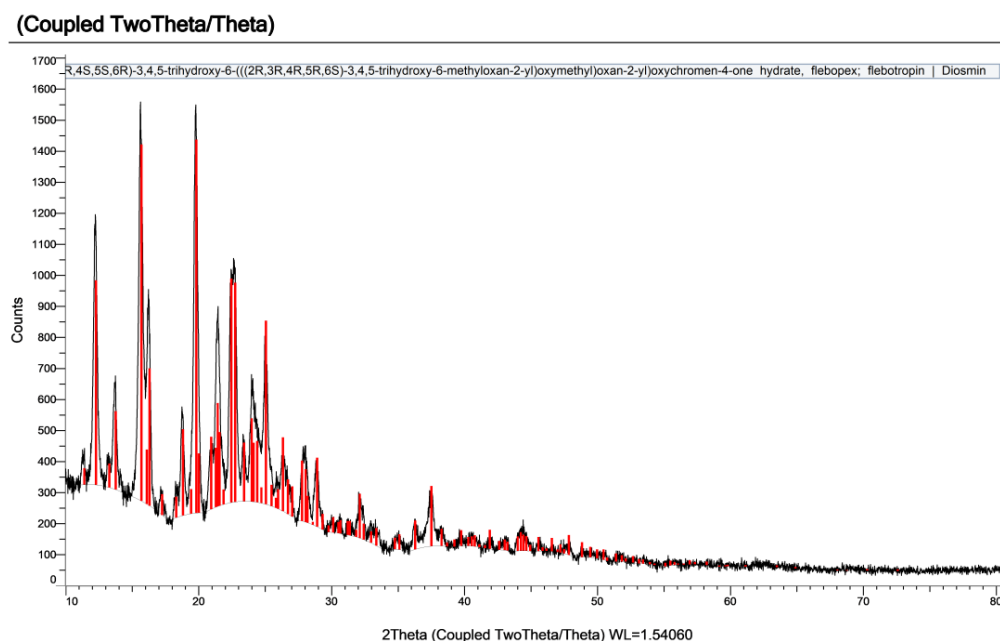


**Figure 4.27 : DM XRD discovery. An XRD chart is employed to determine the material type. The material can be classified as crystalline if it has sharp peaks. The diffraction peaks at 12°, 16°, 20°, and 23° could be indexed to (1200), (1550), (1549), and (1050) planes.**

#### 4.2.5 Characterization of Hesperidin

We employ several approaches for evaluating Hesperidin, including FTIR, XRD and DSC.

**4.2.5.1. FTIR (Fourier Transform Infrared) :** By analysing the peaks detected in the IR radiation band, the FTIR (Fourier Transform Infrared) technique was used to determine the organic & inorganic parts of the materials. When exposed to FTIR analysis, each ingredient of the sample compounds was identified based on its own peak frequency.

FTIR was used to establish the presence of many organic and inorganic elements inside the sample. Figure 4.28 shows the FTIR analysis findings, which provide vital information on the chemical composition and structural properties of the material.

It is crucial to remember, however, that FTIR has several limits. One of these disadvantages is that it cannot expose the metallic features of any chemical. An alternate approach for analysing metallic components is NMR (Nuclear Magnetic Resonance) spectroscopy. NMR spectroscopy is very valuable for studying the characteristics and structures of metal-containing compounds, as it provides extensive information on their coordination, oxidation state, and ligand interactions. A thorough knowledge of the sample's chemical composition and characteristics may be attained by using the capabilities of FTIR for detecting inorganic and organic components and supplementing it with NMR for metallic details.

Several notable peaks were discovered after analysing the FTIR graph. The existence of C=C aromatic bonds was indicated by a peak at  $1565\text{ cm}^{-1}$ , whereas the presence of C=O bonds was indicated by a peak at  $1657\text{ cm}^{-1}$ . A peak at  $1064\text{ cm}^{-1}$  showed C-O stretching, whereas a peak at  $1065\text{ cm}^{-1}$  represented C-H bending. Notably, there were two different peaks associated with C=C aromatic bonds, one of which appeared at  $1515\text{ cm}^{-1}$ . Similarly, two peaks linked with C=O bonds were discovered, one of which appeared at  $1644\text{ cm}^{-1}$ .

FTIR examination also showed other peaks, including one at  $2361\text{ cm}^{-1}$ , indicating the presence of carbon dioxide (CO<sub>2</sub>). The existence of an OH group was revealed by a peak at  $3675\text{ cm}^{-1}$ , which correlated to C-H stretching.

The chemical structure of the molecule under inquiry shared identical components, according to detailed analysis of the FTIR spectrum. The observed peaks matched the predicted molecular properties of Hesperidin, indicating the existence of particular functional groups and providing vital information about its composition.

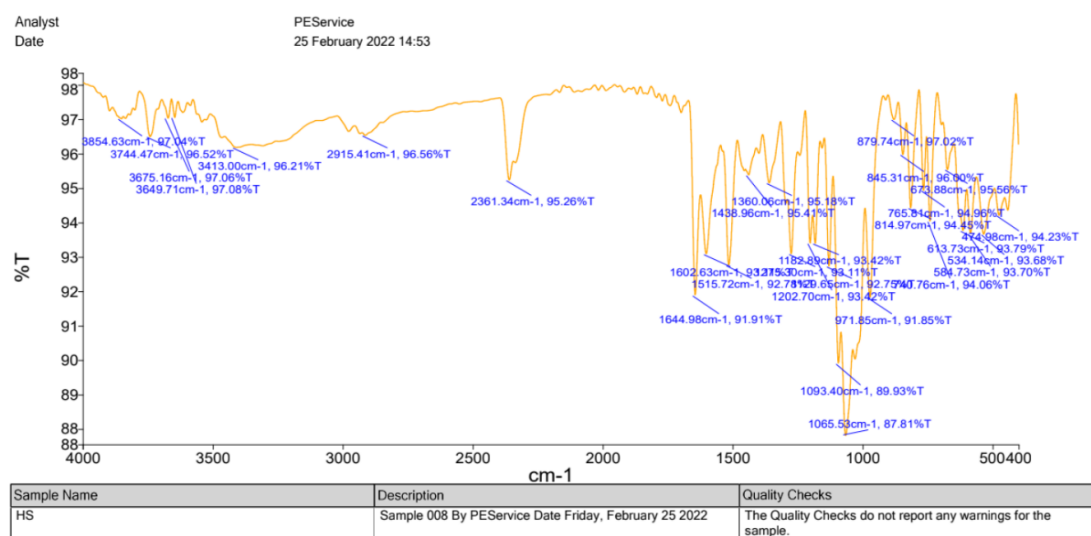


**Figure 4.28 : FTIR result of Hesperidin. After analysis of the graph, we found different peaks, i.e., C-H Bending peak at 1065, C=C Aromatic peak at 1515, C=O peak at 1644, 2361 peak due to carbon dioxide, 2915 peak due to C-H stretching, 3675 peak is due OH group. However, after analysis, we found that our compound has the same components in its structure.**

**4.2.5.2. NMR :** NMR (Nuclear Magnetic Resonance) spectroscopy is a powerful source for analysing the structure of substances by monitoring & measuring nuclear spin interactions in a strong magnetic field. As shown in Figure 4.29, this analytical approach gives useful insights into the physical, chemical, and biological properties of materials.

NMR spectroscopy is widely used in pharmacology for detecting and characterising compounds. By evaluating the distinctive NMR spectra of substances, pharmacologists may establish their identification and makeup. By analysing the chemical shifts, coupling patterns, and relaxation periods in the NMR spectrum, useful information on the analysed substances' molecular structure, connectivity, and conformation may be gleaned.

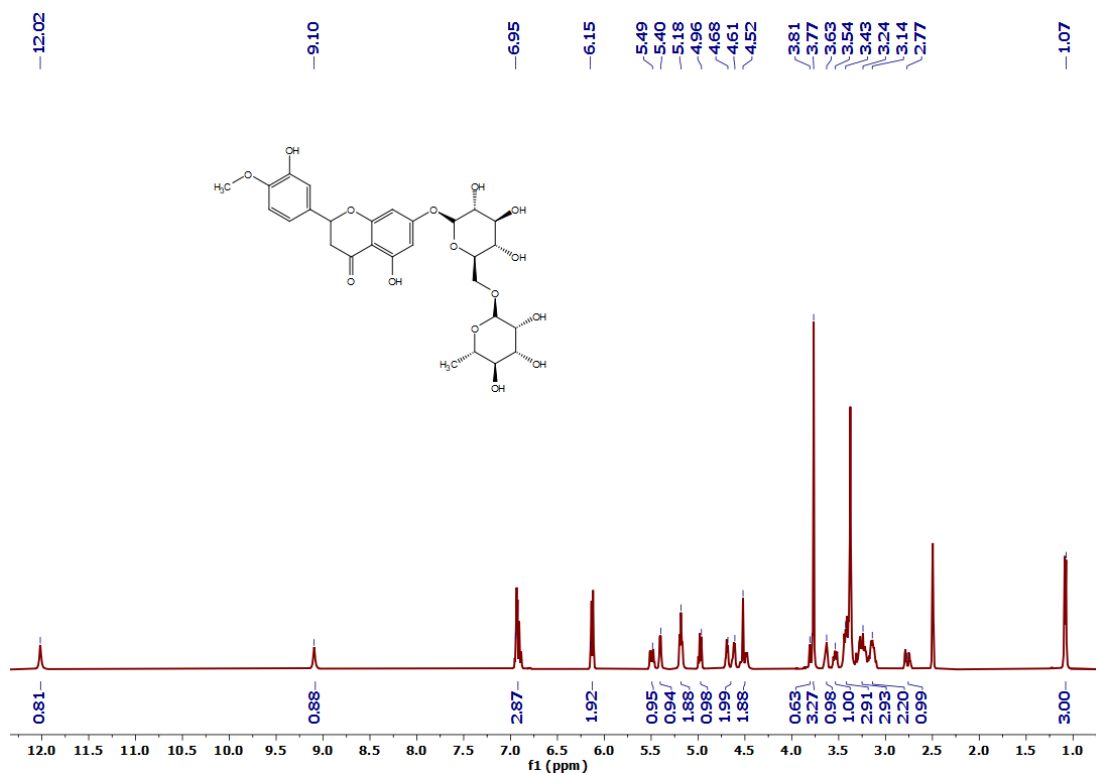


Figure 4.29 : NMR of Hesperidin.

**5-hydroxy-2-(3-hydroxy-4-methoxyphenyl)-7-(((2R,3R,4S,5S,6R)-3,4,5-trihydroxy-6-(((2S,3R,4R,5R,6S)-3,4,5-trihydroxy-6-methyltetrahydro-2H-pyran-2-yl)oxy)methyl)tetrahydro-2H-pyran-2-yl)oxy)chroman-4-one (HESPERIDIN).**

$^1\text{H}$  NMR (400 MHz,  $\text{DMSO}-d_6$ )  $\delta$  12.02 (s, 1H), 9.10 (s, 1H), 6.95 (s, 3H), 6.15 (s, 2H), 5.49 (s, 1H), 5.40 (s, 1H), 5.18 (s, 2H), 4.96 (s, 1H), 4.64 (d,  $J = 29.7$  Hz, 2H), 4.52 (s, 2H), 3.81 (s, 1H), 3.77 (s, 3H), 3.63 (s, 1H), 3.54 (s, 1H), 3.43 (s, 3H), 3.24 (s, 3H), 3.14 (s, 2H), 2.77 (s, 1H), 1.07 (s, 3H);  $^{13}\text{C}$  NMR (100 MHz,  $\text{DMSO}-d_6$ )  $\delta$  197.49, 165.59, 163.46, 163.00, 131.34, 118.42, 114.61, 103.77, 101.06, 99.84, 96.84, 96.00, 78.84, 76.73, 75.97, 73.44, 72.53, 71.16, 70.73, 70.05, 68.78, 56.13, 18.30

**4.2.5.3. DSC:** A DSC (Differential Scanning Calorimetry) device with thermal expansion capability was used to determine Hesperidin. To guarantee precise readings, the device was calibrated before the study using a standard reference material.

A 1.90 mg sample was carefully measured and placed in an aluminium testing crucible for analysis. The crucible was then firmly sealed, and the sample was heated in an atmosphere of nitrogen (N<sub>2</sub>). The temperature was raised by 10°C every minute until it reached 300°C.

Figure 4.30 shows the findings of the DSC analysis of Hesperidin. These diagrams depict the thermal behaviour of the compounds, including the typical melting ranges and accompanying thermal events.

These findings add to a thorough understanding of the physical properties of the compounds and can help in a variety of applications, including pharmaceutical formulation and process optimisation.

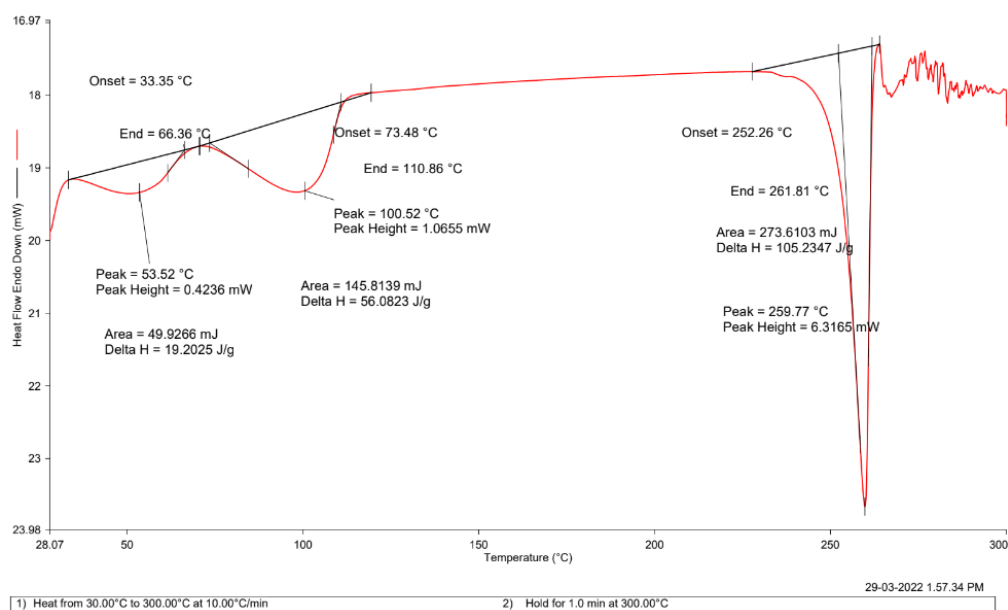


**Figure 4.30. Hesperidin DSC waveform. The DSC data has an exothermic process at 100°C, demonstrating a process that is exothermic triggered by crystallization. The peak of endothermic activity detected at roughly 259°C is due to an endothermic event known as "melting."**

**4.2.5.4. XRD :** To analyse the form or type of the specimens, the XRD (X-ray Diffraction) technique was used, which distinguished between crystalline and amorphous structures. The XRD pattern can provide vital information about the sample's structural features.

If the resultant XRD chart shows crisp and clear peaks, it suggests that the material is crystalline in nature. These peaks represent the regular arrangement of atoms in a crystal lattice, and their locations and intensities reveal information about the crystal structure.

If, on the other hand, the XRD graph shows a generally featureless or flat profile, the sample is amorphous. The lack of sharp peaks in the XRD pattern suggests a lack of long-range order in the atomic arrangement, which is typical of amorphous materials.

The XRD data for Hesperidin are shown in Figure 4.31, respectively. The diffraction peaks at  $11^\circ$ ,  $19.9^\circ$ ,  $23.2^\circ$ , and  $25.1^\circ$  could be indexed to (2600), (2800), (1900), and (1400) planes. These images depict the XRD patterns, which reflect the crystallinity of the materials.

This information is crucial to grasp the atomic structure of the molecules and has implications, including medicinal investigation, materials science, as well as quality assurance.

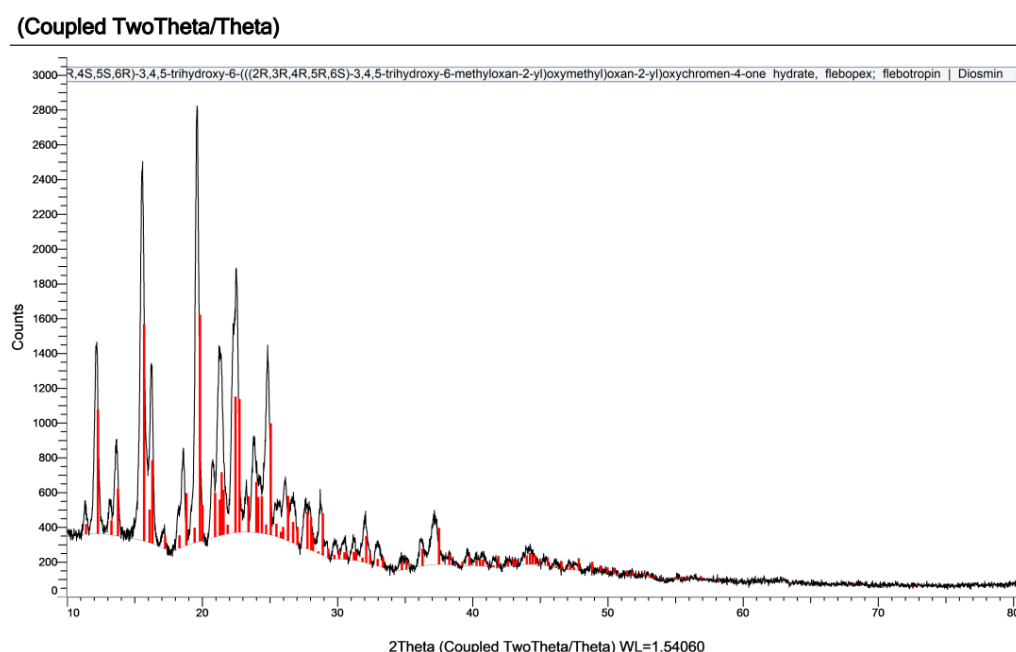


**Figure 4.31 : Hesperidin XRD results. The nature of the substance is determined using an XRD graph. The material is crystalline if it has sharp peaks. It is a Polycrystalline material that shows larger peaks, the diffraction peaks at  $11^\circ$ ,  $19.9^\circ$ ,  $23.2^\circ$ , and  $25.1^\circ$  could be indexed to (2600), (2800), (1900), and (1400) planes.**



#### 4.2.6 Pre-Nano Formulations

To develop a nano-formulation, firstly we performed some pre-formulation studies for Diosmin and Hesperidin i.e., Solubility studies, Lambda max, and straight-line graph.

**Table 4.5 : Solubility of Diosmin.**

Chemical	Quantity of Compound Soluble (In mg)
Chloroform	20
Ethanol	15
Methanol	10
DMSO	20
Acetone	15
N-hexane	10
Ethyl acetate	15
Acetonitrile	10
N-octanol	10

After this study, we found that our compound is soluble in No. of samples, but we take DMSO 0.5% as a solvent for further studies because it is non-toxic for the body.

After this analysis, we dissolve Diosmin in ethanol and take the lambda max.

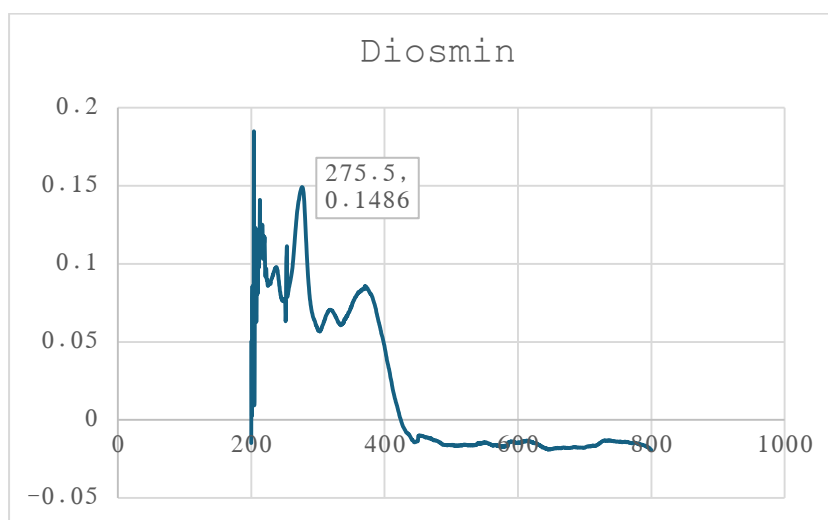


**Figure. 4.32 : UV lambda max. Graph for Diosmin**

After analyse the lambda max, we take OD on the specific wavelength and draw the below graph.

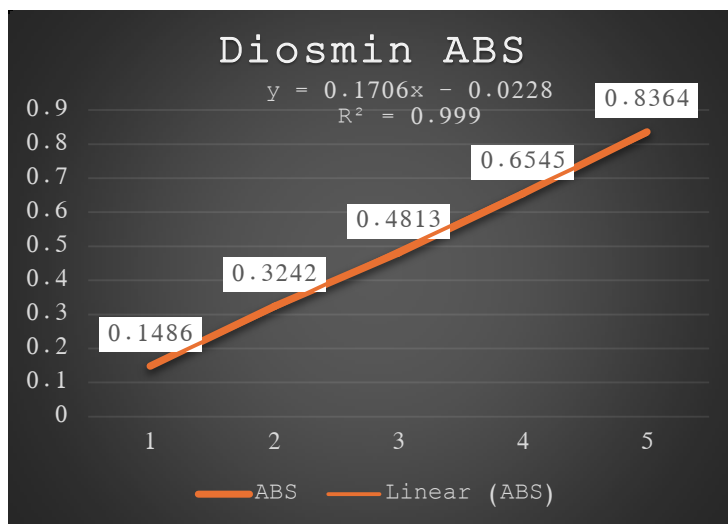


**Figure 4.33 : Straight line graph for Diosmin.**

**Table 4.6 : Solubility of Hesperidin.**

Chemical	Quantity of Compound Soluble (In mg)
Chloroform	20
Ethanol	10
Methanol	25
DMSO	20
Acetone	15
N-hexane	15
Ethyl acetate	15
Acetonitrile	5
N-octanol	10

After this study, we found that our compound is soluble in No. of samples, but we take DMSO 0.5% as a solvent for further studies because it is non-toxic for the body.

After this analysis, we dissolve Hesperidin in ethanol and take the lambda max.

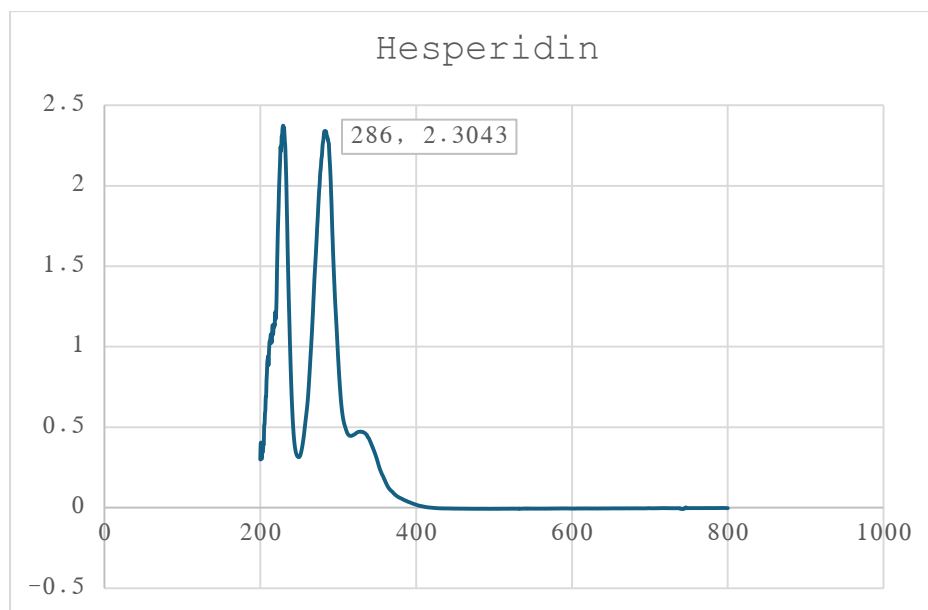


**Figure. 4.34 : UV lambda max. Graph for Hesperidin**

After analyse the lambda max, we take OD on the specific wavelength and draw the below graph.

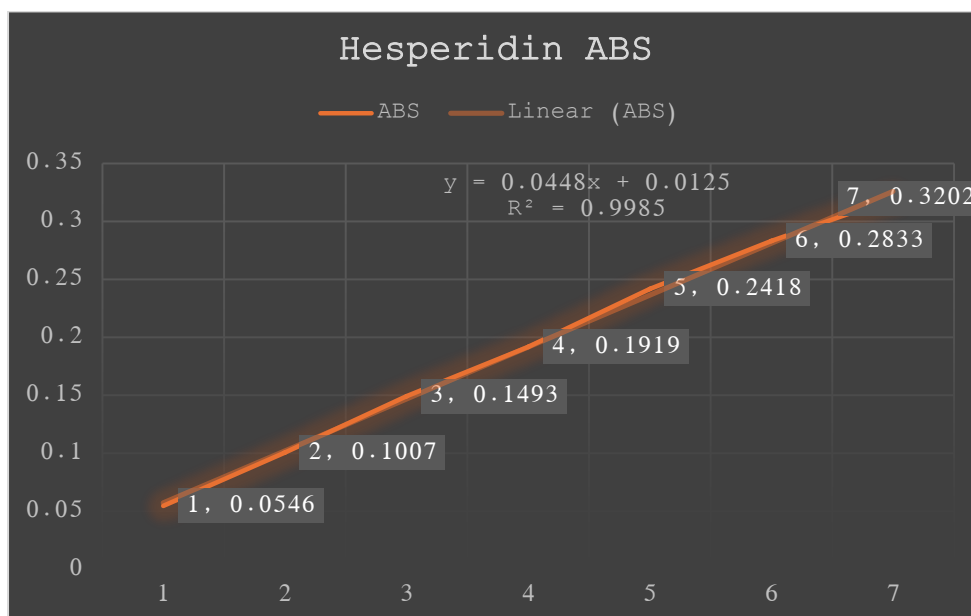


**Figure 4.35 : Straight line graph for Hesperidin.**

#### 4.2.6.1. Nano-formulations

We formulated Go, Ag, Zn nanoparticles in racemic mix and in pure form.

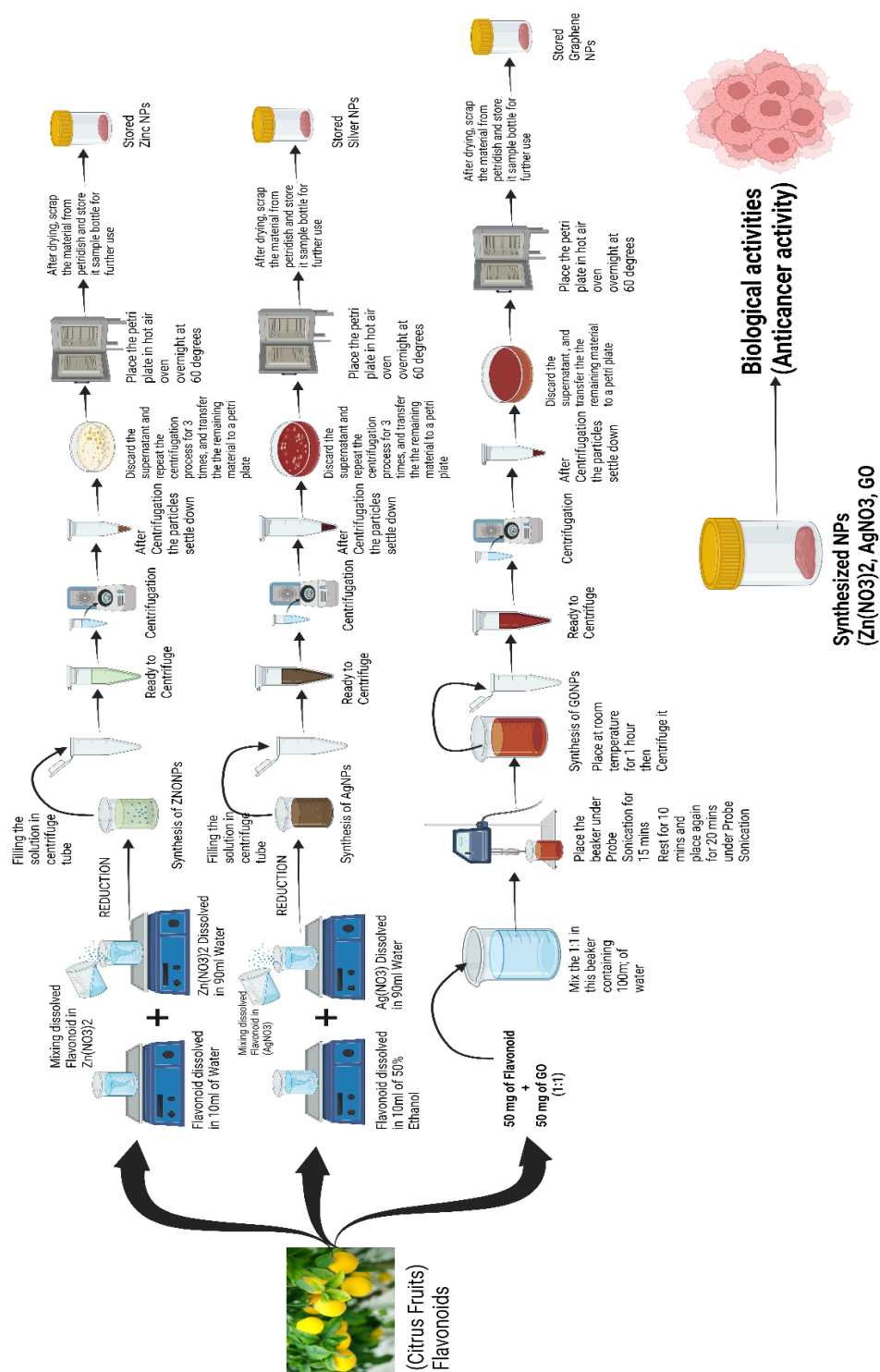


Figure 4.36 : Workflow of nano-formulation.

#### 4.2.6.2. Characterization of Nano-formulations

For characterization, we employed FTIR, Zeta potential and FESEM.

#### 4.2.6.2.1. FTIR

**4.2.6.2.1.1. Graphene Hesperidin nano-formulation:** The FTIR spectrum of Graphene Hesperidin np, exhibits distinct absorption bands corresponding to specific molecular vibrations. Notably, these bands include the O-H stretch, the C=O stretch associated with the methylene groups of the protein, and various other vibrational modes of functional groups, observed at frequencies of 3350.35, 1728.22, 1641.42 and 1604.77.

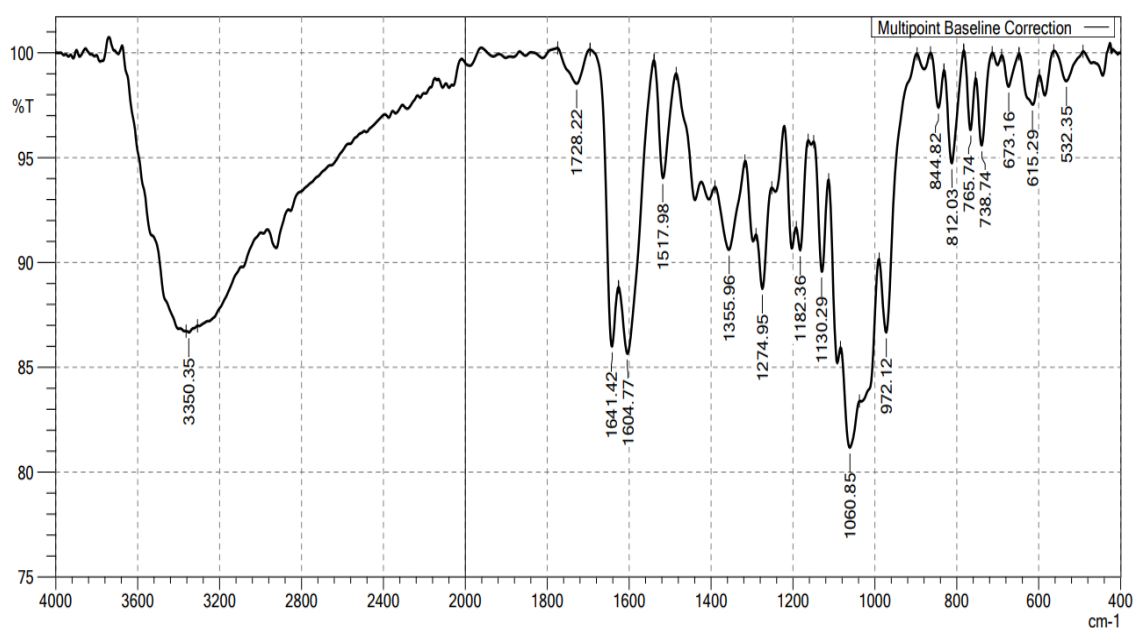


**Figure 4.37 : FTIR graph of Graphene Hesperidin nano-formulation.**

**4.2.6.2.1.2. Graphene Diosmin nano-formulation :** The FTIR spectrum analysis reveals characteristic peaks corresponding to specific functional groups. The peak around 1600 cm<sup>-1</sup> is attributed to C=O stretching, indicating the presence of carbonyl groups in both graphene oxide and diosmin. A peak near 1500 cm<sup>-1</sup> corresponds to aromatic C=C stretching, which is characteristic of diosmin. The broad peak around 3300 cm<sup>-1</sup> is associated with O-H stretching vibrations, arising from diosmin and adsorbed water molecules. Additionally, the region between 1200 and 1000 cm<sup>-1</sup> signifies C-O stretching vibrations, representing various functional groups present in the sample.

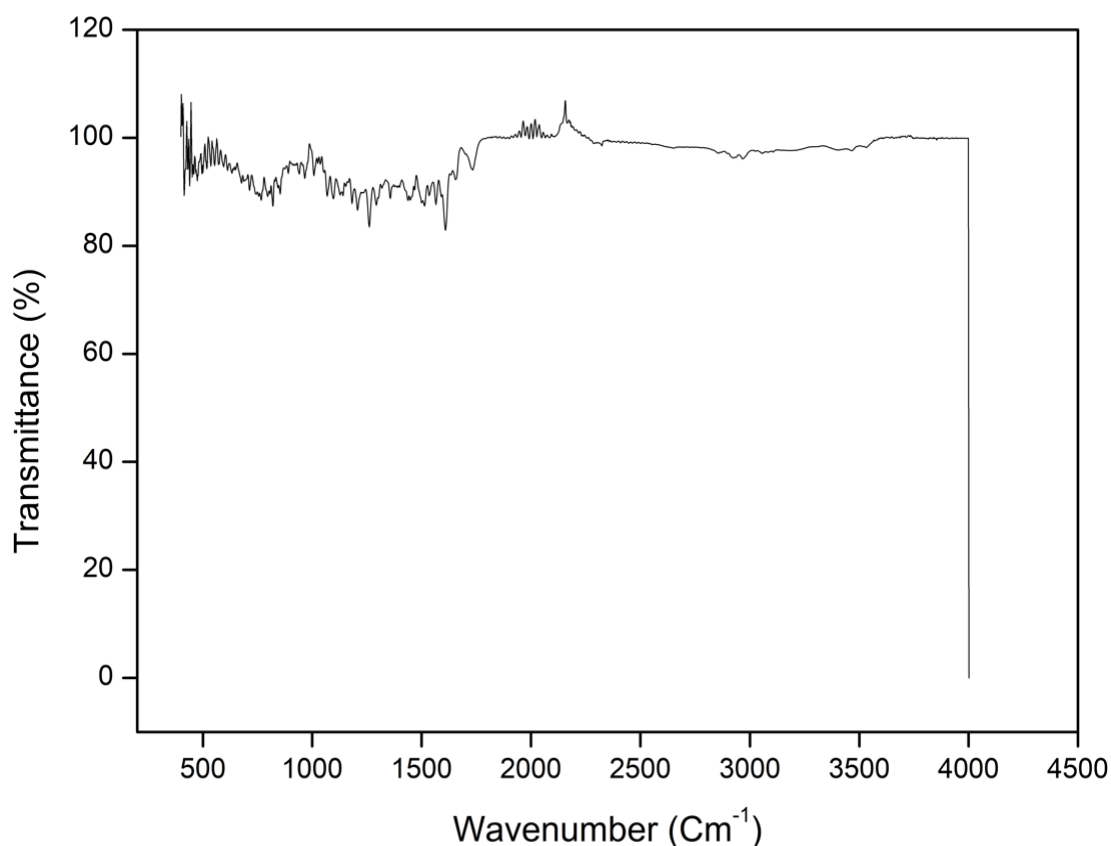


**Figure 4.38 : FTIR graph of Graphene Diosmin nano-formulation.**

#### ***4.2.6.2.1.3. Conjugates of Graphene nano-formulations***

We developed graphene-based nanoconjugates, including formulations combining graphene with diosmin and hesperidin.

The FTIR spectral analysis of the graphene conjugates formulations highlights key vibrational bands representing distinct functional groups. The broad peak observed around  $3300\text{ cm}^{-1}$  corresponds to O-H stretching vibrations, indicative of the presence of diosmin, hesperidin, and adsorbed water. A prominent peak near  $1600\text{ cm}^{-1}$  is associated with C=O stretching, attributed to carbonyl groups in graphene oxide, diosmin, and hesperidin. Aromatic C=C stretching is evident between  $1500$  and  $1400\text{ cm}^{-1}$ , primarily arising from the diosmin and hesperidin molecules. Additionally, the region between  $1200$  and  $1000\text{ cm}^{-1}$  reveals C-O stretching vibrations, representing contributions from various functional groups within the formulations.

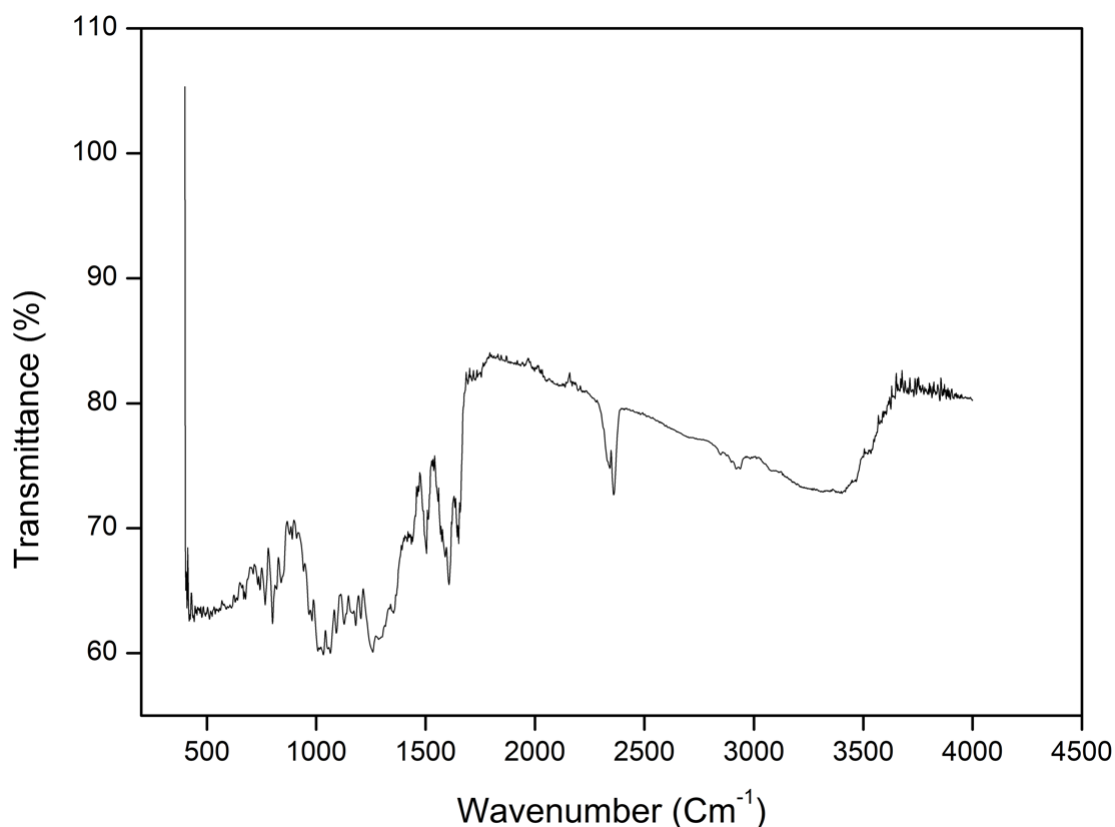


**Figure 4.39 : FTIR graphs of graphene (HD) conjugates nano-formulations**

**4.2.6.2.1.4. Silver Hesperidin nano-formulations :** The FTIR spectrum of the silver-hesperidin nano-formulation demonstrates characteristic peaks corresponding to functional groups associated with both the silver nanoparticle and hesperidin capping/stabilizing agents. The broad absorption peak near  $3410\text{ cm}^{-1}$  indicates O-H stretching, suggesting the presence of hydroxyl groups. Peaks around  $1610\text{ cm}^{-1}$  and  $1265\text{ cm}^{-1}$  correspond to C=C aromatic stretching and C-O stretching vibrations, respectively, confirming the flavonoid structure of hesperidin. The sharp peak at  $798\text{ cm}^{-1}$  is indicative of aromatic bending, while the small peaks near  $720\text{ cm}^{-1}$  and below reflect vibrational modes associated with metal-ligand interactions, specifically Ag-O bonds. These features confirm successful conjugation and stabilization of silver nanoparticles by hesperidin. The spectrum validates the role of bioactive molecules in capping and reducing agents during nanoparticle synthesis.

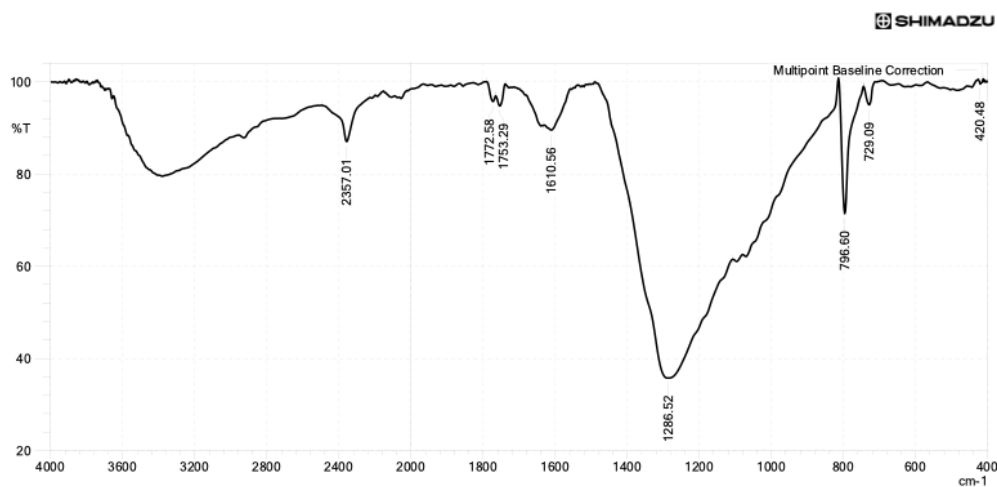


**Figure 4.40 : FTIR graph of Ag Hesperidin nano-formulation.**

**4.2.6.2.1.5. Silver Diosmin nano-formulations :** FTIR spectrum of the Ag Diosmin NP shows absorption bands associated with the O H stretch, the C O stretch of the methylene groups of the protein, and the other vibration of groups at 3462.22, 3396.64, 2927 and 2353.16, respectively. So, based on the FTIR results we can say that nano-formulation is formed and is pure.

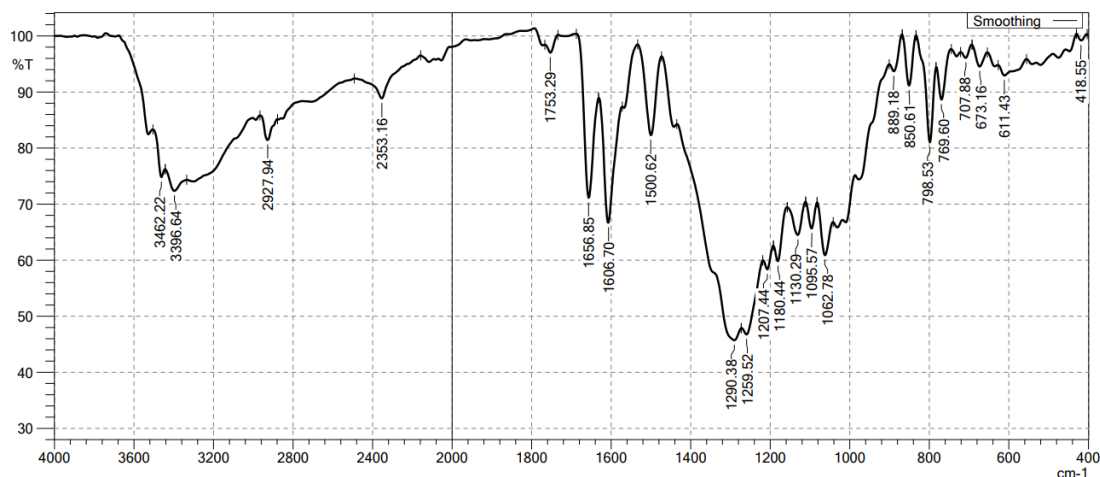


**Figure 4.41 : FTIR graph of Ag Diosmin nano-formulation.**

**4.2.6.2.1.6. Conjugates of silver nano-formulations :**

We developed silver-based nanoconjugates, including formulations combining silver with diosmin and hesperidin.



The FTIR spectrum reveals characteristic peaks corresponding to functional groups present in the sample. A strong peak at  $3350\text{ cm}^{-1}$  signifies O-H stretching vibrations, indicative of hydroxyl groups commonly found in alcohols or phenols, which are abundant in both diosmin and hesperidin. The peak at  $1653\text{ cm}^{-1}$  corresponds to C=O stretching vibrations, likely originating from carbonyl groups in ketones, esters, or carboxylic acids, with diosmin's conjugated carbonyl group contributing prominently in this region. Peaks at  $1510\text{ cm}^{-1}$  and  $1455\text{ cm}^{-1}$  represent aromatic C=C stretching vibrations, characteristic of the phenyl rings present in both diosmin and hesperidin. Additionally, the broad region between  $1260\text{--}1000\text{ cm}^{-1}$  reflects C-O stretching vibrations from functional groups such as alcohols, phenols, and ethers, with glycosidic linkages in diosmin and hesperidin making significant contributions. This analysis confirms the structural integrity and presence of these functional groups in the sample.

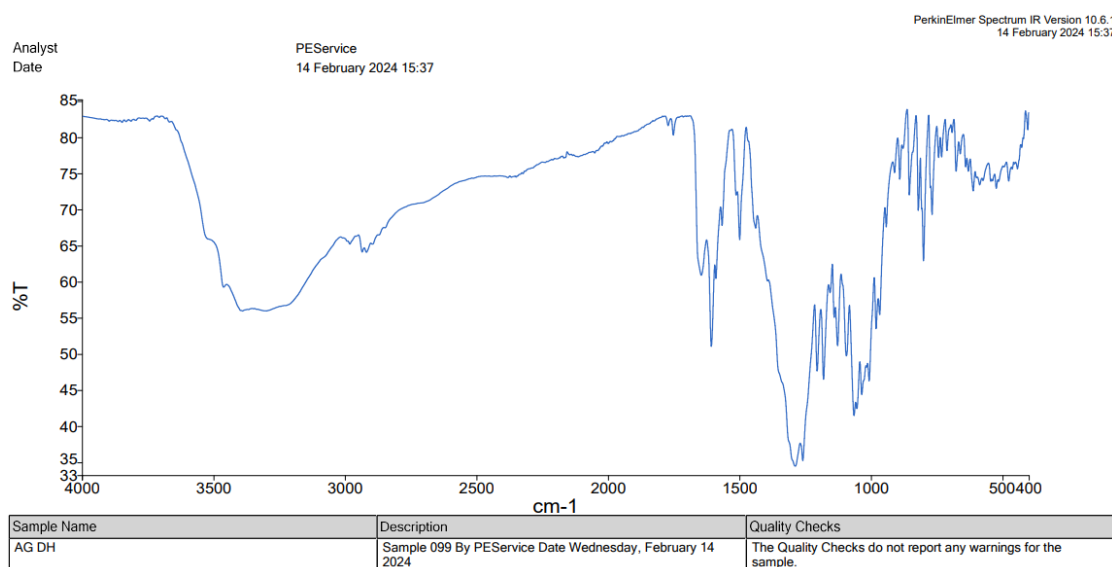


**Figure 4.42 : FTIR graphs of Ag conjugates nano-formulations.**

**4.2.6.2.1.7. Zinc Hesperidin Nano-formulations :** The FTIR spectrum of zinc hesperidin nanoparticles reveals key functional groups involved in their structure and interactions. A broad peak observed around  $3200\text{--}3500\text{ cm}^{-1}$  indicates O-H stretching vibrations, suggesting the presence of hydroxyl groups from hesperidin or hydrogen-bonded water molecules. The peak near  $2900\text{ cm}^{-1}$  corresponds to C-H stretching vibrations, characteristic of aliphatic or aromatic groups within the hesperidin

structure. A sharp absorption band around  $1600\text{--}1700\text{ cm}^{-1}$  is attributed to  $\text{C}=\text{O}$  stretching vibrations from carbonyl groups, indicative of the flavonoid structure of hesperidin, with potential shifts suggesting interaction with zinc ions. The region around  $1400\text{--}1500\text{ cm}^{-1}$  shows aromatic  $\text{C}=\text{C}$  stretching, confirming the aromatic backbone of hesperidin. Broad absorptions in the  $1000\text{--}1300\text{ cm}^{-1}$  range correspond to  $\text{C}-\text{O}$  stretching vibrations from ether or phenolic groups. Additionally, peaks below  $1000\text{ cm}^{-1}$ , part of the fingerprint region, highlight structural specificity and further confirm the functionalization of zinc nanoparticles with hesperidin. These spectral features collectively suggest successful synthesis of zinc hesperidin nanoparticles, with evidence of functional group involvement in chelation and stabilization of the nanoparticle structure.

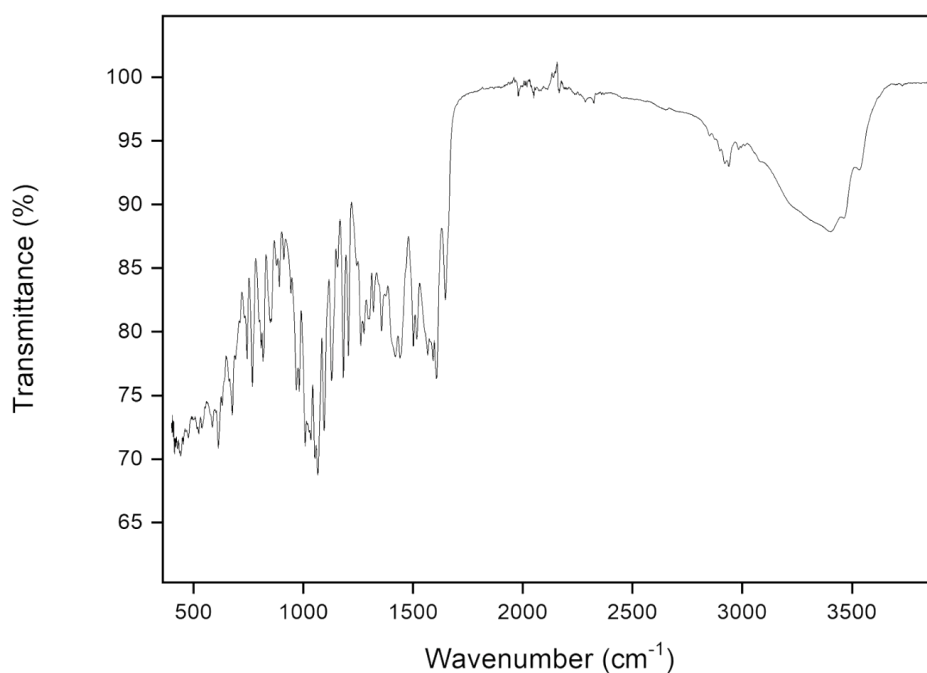


**Figure 4.43 : FTIR graphs of zinc Hesperidin nano-formulations.**

**4.2.6.2.1.8. Zinc Diosmin Nano-formulations :** The FTIR spectrum of the zinc nanoparticles, synthesized through the utilization of Diosmin, Hesperidin, exhibited distinctive absorption bands corresponding to specific molecular vibrations. Notably, these included the  $\text{O}-\text{H}$  stretch at  $3253.91\text{ cm}^{-1}$ , the  $\text{C}=\text{O}$  stretch of the methylene groups within the protein at  $1631.78\text{ cm}^{-1}$ , and other characteristic vibrational modes at  $1504.48\text{ cm}^{-1}$ .

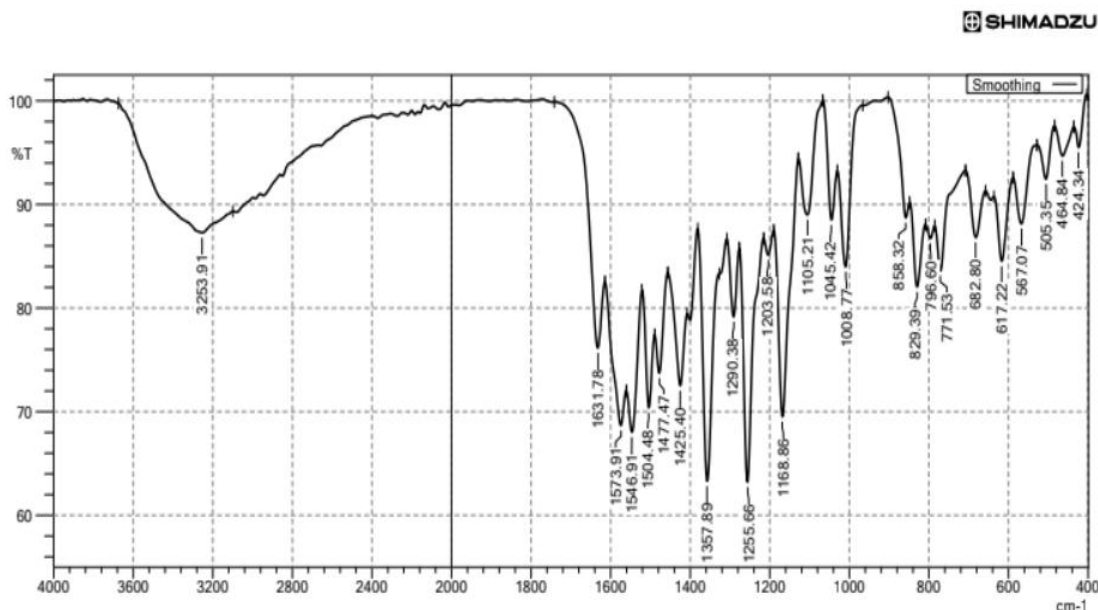


**Figure. 4.44 : FTIR graph of Zinc Diosmin nano-formulation.**

#### **4.2.6.2.1.9. Conjugates of zinc nano-formulations**

We developed zinc-based nanoconjugates, including formulations combining zinc with diosmin and hesperidin.

The FTIR spectrum exhibits characteristic peaks that provide insights into the functional groups present in the sample. The broad peak around 3300 cm<sup>-1</sup> corresponds to O-H stretching vibrations, attributed to the hydroxyl groups in diosmin, hesperidin, and possibly adsorbed water. A distinct peak at 1600 cm<sup>-1</sup> indicates C=O stretching, arising from carbonyl groups present in all three components, with potential peak shifts caused by intermolecular interactions. The region between 1500–1400 cm<sup>-1</sup> shows peaks characteristic of aromatic C=C stretching, attributed to the phenyl rings in diosmin and hesperidin. Additionally, the range from 1200–1000 cm<sup>-1</sup> represents C-O stretching vibrations, contributed by various functional groups present in all components. This analysis highlights the key structural features of the sample and suggests interactions between the constituents.

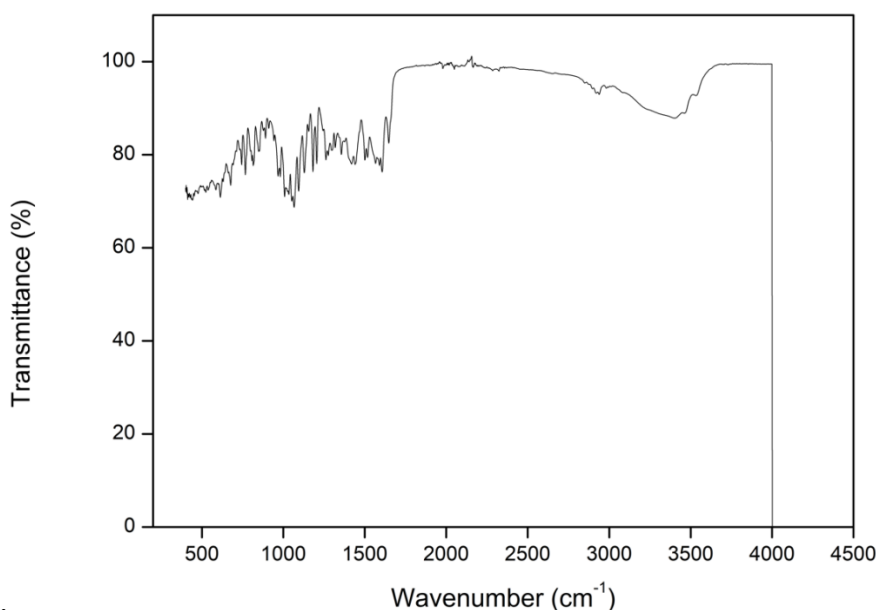


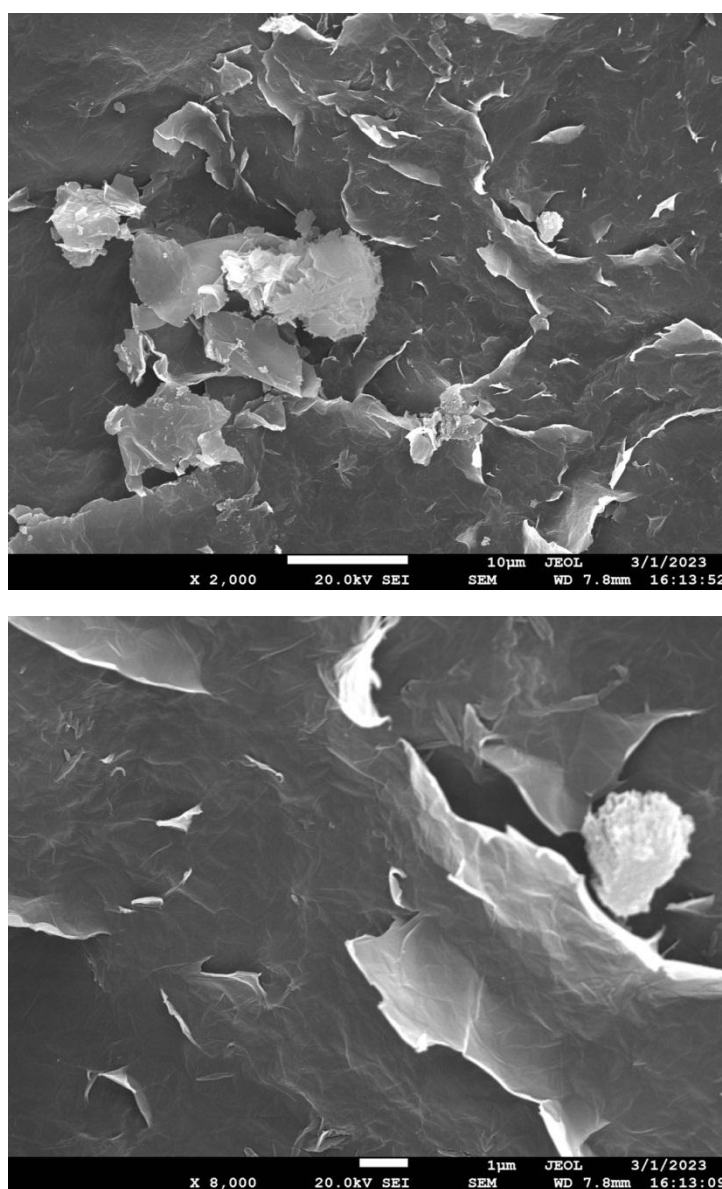
**Figure 4.45 : FTIR graphs of Zinc conjugates nano-formulations**

#### **4.2.6.2.2. FESEM**

**4.2.6.2.2.1. Graphene Hesperidin nano-formulations :** The FESEM image of the graphene-hesperidin composite reveals a layered morphology characteristic of graphene sheets with visible crumpling and folds. These structures indicate high surface area, crucial for enhanced interaction with hesperidin molecules. The observed agglomerations suggest successful incorporation and adsorption of hesperidin onto the graphene surface, likely facilitated by  $\pi$ - $\pi$  interactions between the aromatic rings of hesperidin and the graphene sheets. The irregular yet well-distributed layers imply uniform functionalization, which can enhance the composite's mechanical and chemical properties for potential biomedical or nanotechnological applications. The microstructure supports effective surface modifications and stability of the composite material.

The FESEM image of the graphene-hesperidin composite, taken at a finer scale of 1  $\mu$ m, provides detailed insight into the nanoscale interactions within the material. The image highlights the crumpled and layered structure of the graphene sheets, which ensures a high surface area for hesperidin adsorption. The smooth and thin layers exhibit clear edges and folds, indicative of good structural integrity and minimal aggregation at the nanoscale. The incorporation of hesperidin is evident, with smaller

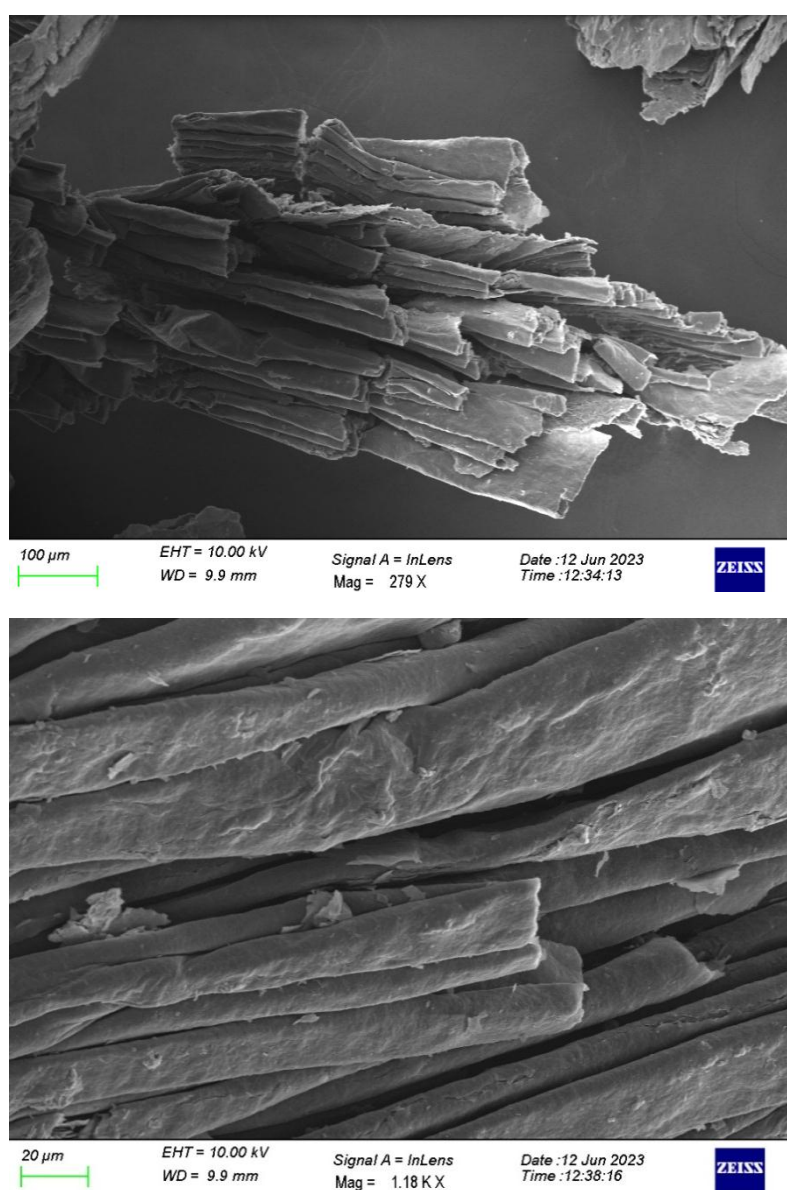
agglomerations and surface features suggesting uniform functionalization. This nanoscale morphology complements the 10  $\mu\text{m}$  image analysis, confirming the effective integration of hesperidin within the graphene framework, making the composite suitable for biomedical or nanotechnology applications.



**Figure 4.46 : FESEM graphs of graphene Hesperidin nano-formulations**  
**A. 10 $\mu\text{m}$  and B. 1 $\mu\text{m}$ .**

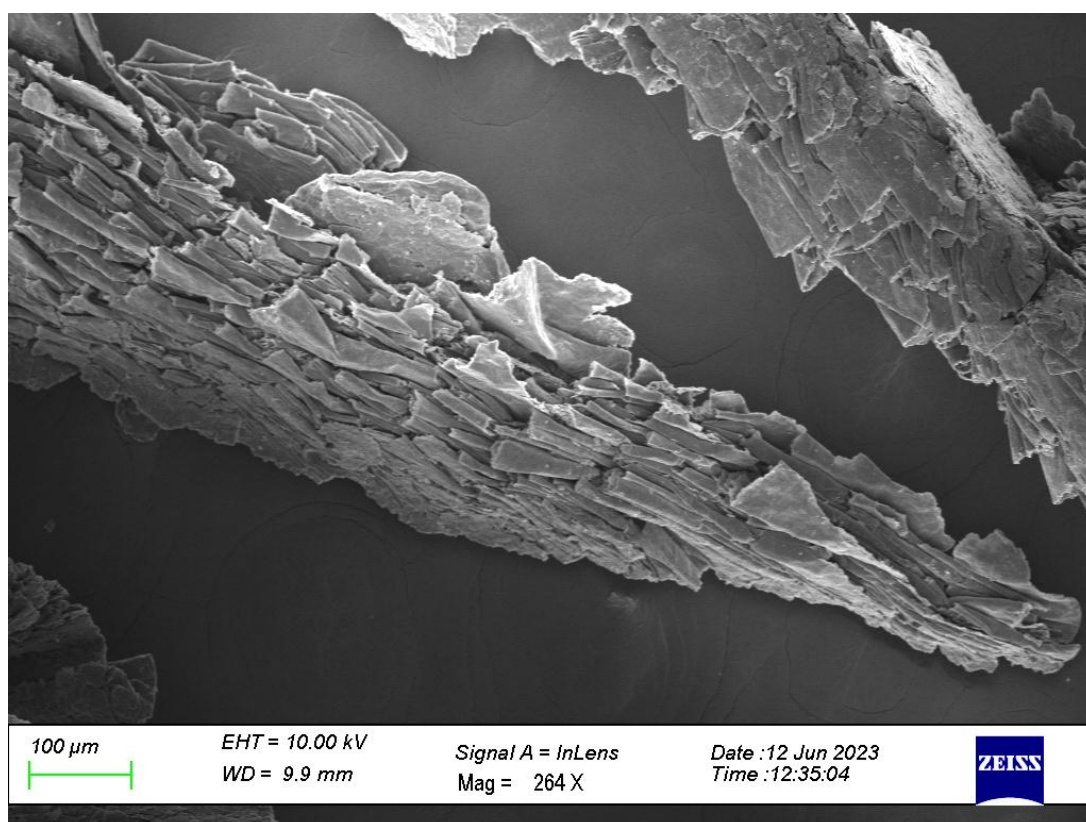
**4.2.6.2.2.2. Graphene Diosmin nano-formulations:** The provided FESEM images depict the surface morphology of graphene Diosmin at two magnifications: 20  $\mu\text{m}$  (1.18 KX) and 100  $\mu\text{m}$  (279X). The image at 20  $\mu\text{m}$  reveals a layered, sheet-like

structure with tightly stacked and smooth edges, characteristic of graphene-based materials. The layers appear continuous, indicating a degree of structural integrity and uniformity. At 100  $\mu\text{m}$ , the broader morphology shows loosely aggregated, stacked sheets with varying thicknesses, creating a more three-dimensional architecture. This hierarchical structure is favourable for applications like drug delivery or catalysis, as it enhances surface area and interaction sites. The detailed morphology suggests that graphene Diosmin maintains a hybrid structure combining the high surface area of graphene with Diosmin's inherent properties.



**Figure 4.47 : FESEM graphs of graphene Diosmin nano-formulations**  
**A. 100 $\mu\text{m}$  and B. 20 $\mu\text{m}$ .**

**4.2.6.2.2.3. Conjugates of Graphene nano-formulations :** The FESEM images depict the surface morphology of graphene Diosmin Hesperidin at two magnifications: 20  $\mu\text{m}$  (558X) and 100  $\mu\text{m}$  (264X). At 20  $\mu\text{m}$ , the structure displays a flake-like morphology with irregular, overlapping layers, indicating a heterogeneous surface with potential nanoscale roughness. The surface appears compact and interconnected, suggesting good structural integrity, which may enhance its functional properties. At 100  $\mu\text{m}$ , a stacked and layered arrangement is observed, where the sheets are more dispersed, forming a porous, three-dimensional network. This hierarchical structure is advantageous for applications such as adsorption, drug delivery, or catalysis, as it combines a high surface area with structural stability. The composite material demonstrates promising morphological characteristics suitable for synergistic interactions between graphene and the bioflavonoid components Diosmin and Hesperidin.





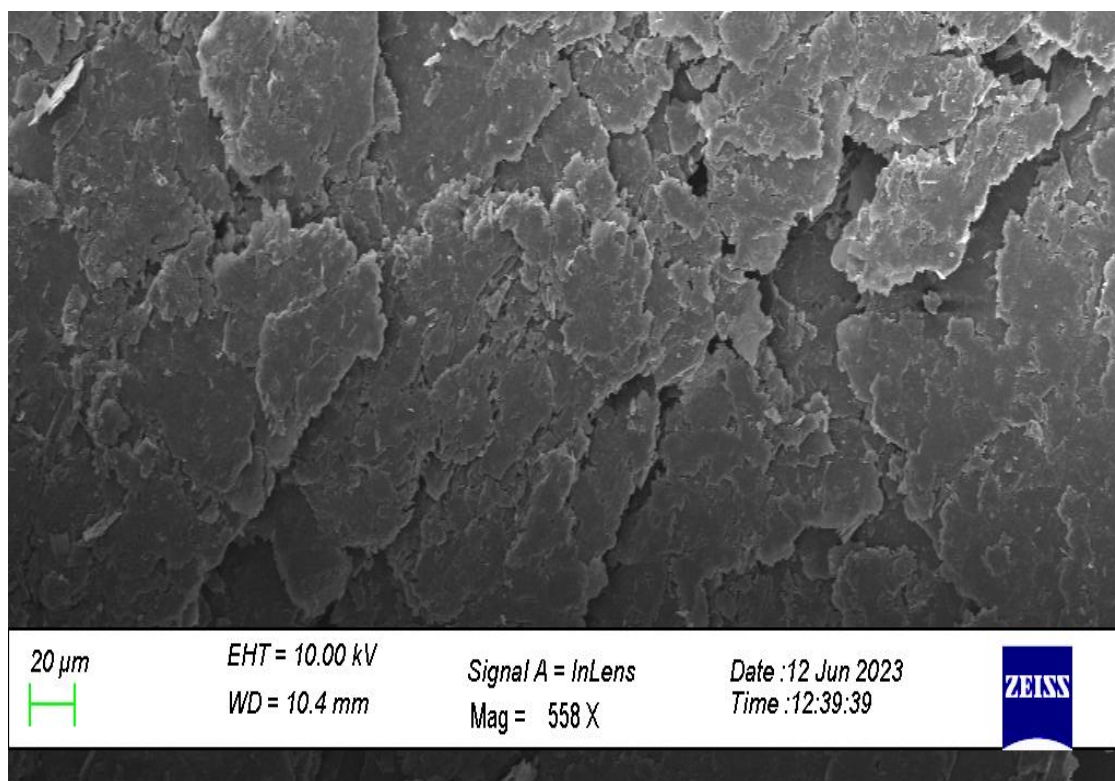


**Figure 4.48 : FESEM graphs of graphene conjugates nano-formulations  
A. 100μm and B. 20μm.**

**4.2.6.2.2.4. Silver Hesperidin nano-formulations :** The FESEM images illustrate the surface morphology of silver Hesperidin at two magnifications: 1 μm (16,000X) and 100 nm (65,000X). At the 1 μm scale, the sample reveals a dense aggregation of nanoparticles with spherical to irregular shapes, forming a compact cluster. The distribution appears heterogeneous, with some larger particles or agglomerates interspersed among smaller ones. At the higher magnification of 100 nm, individual nanoparticles are more distinctly visible, showcasing smooth surfaces and a relatively uniform morphology. The nanoscale observations suggest effective stabilization of silver nanoparticles within the matrix of Hesperidin, which may enhance the material's bioactivity and functional properties, such as antimicrobial or antioxidant capabilities. The combination of nanoscale features and aggregated clusters indicates the potential for synergistic interactions between the silver nanoparticles and Hesperidin molecules.



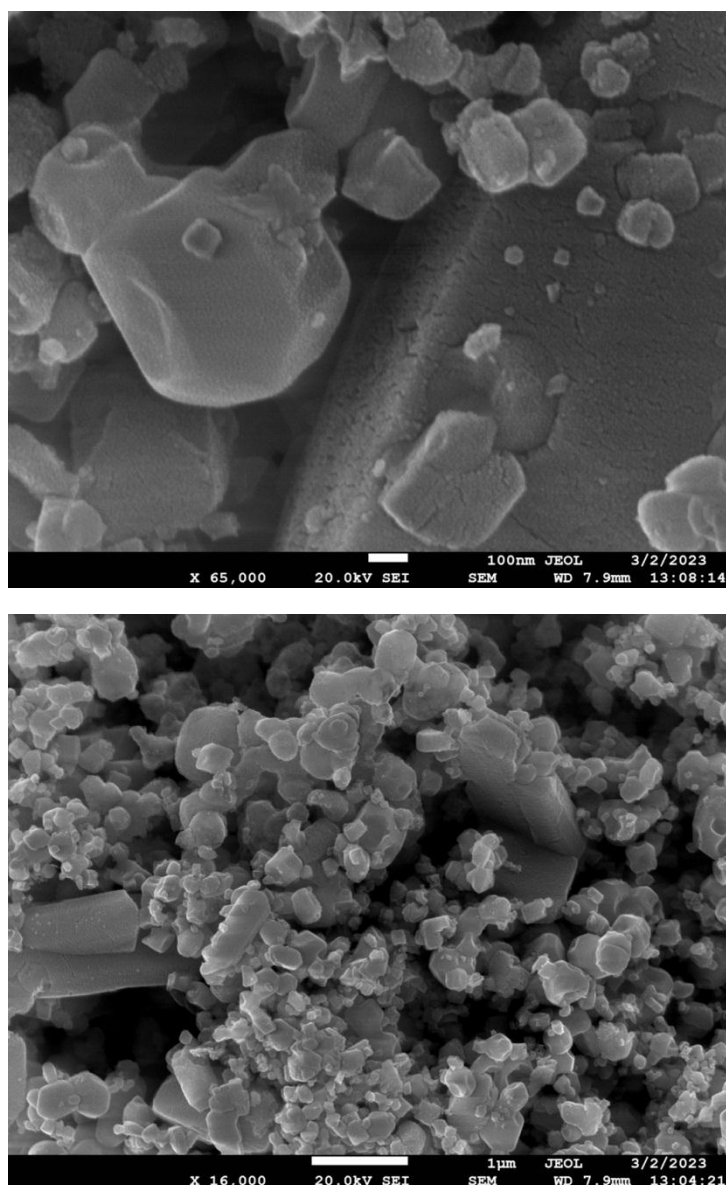


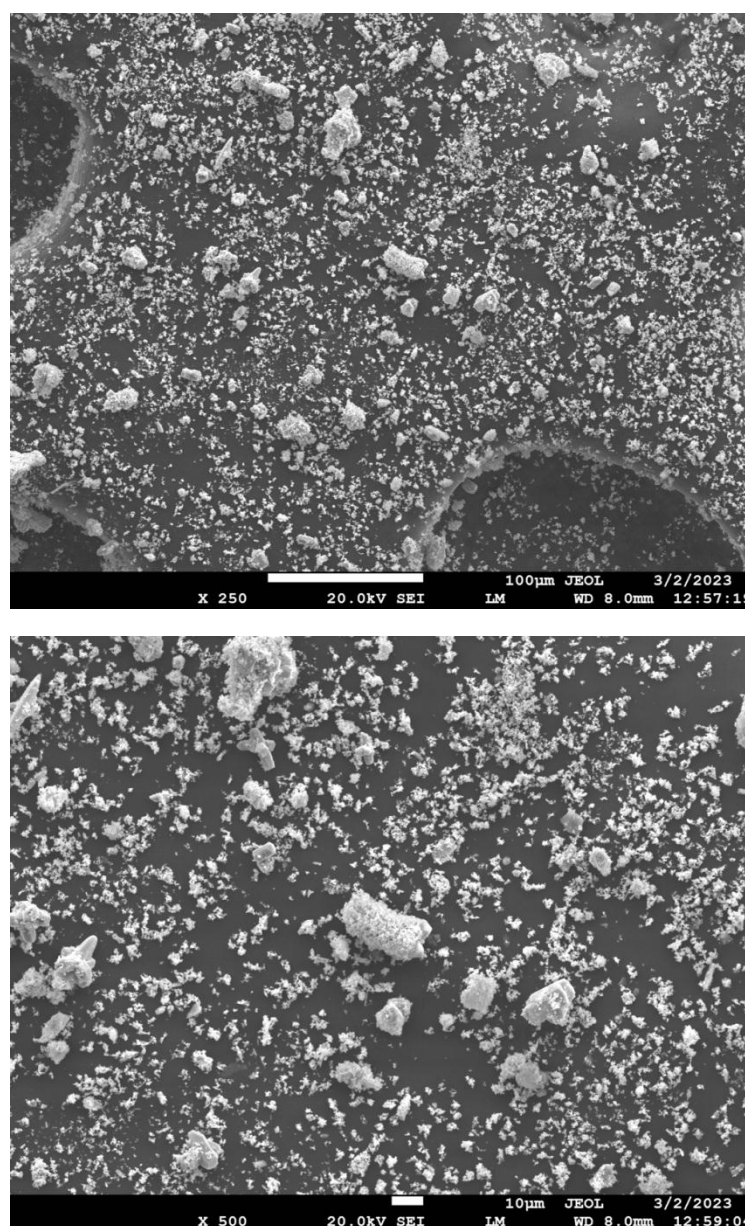
**Figure 4.49. FESEM graphs of silver Hesperidin nano-formulations**

**A. 100µm and B. 1µm.**

#### **4.2.6.2.2.5. Silver Diosmin nano-formulations**

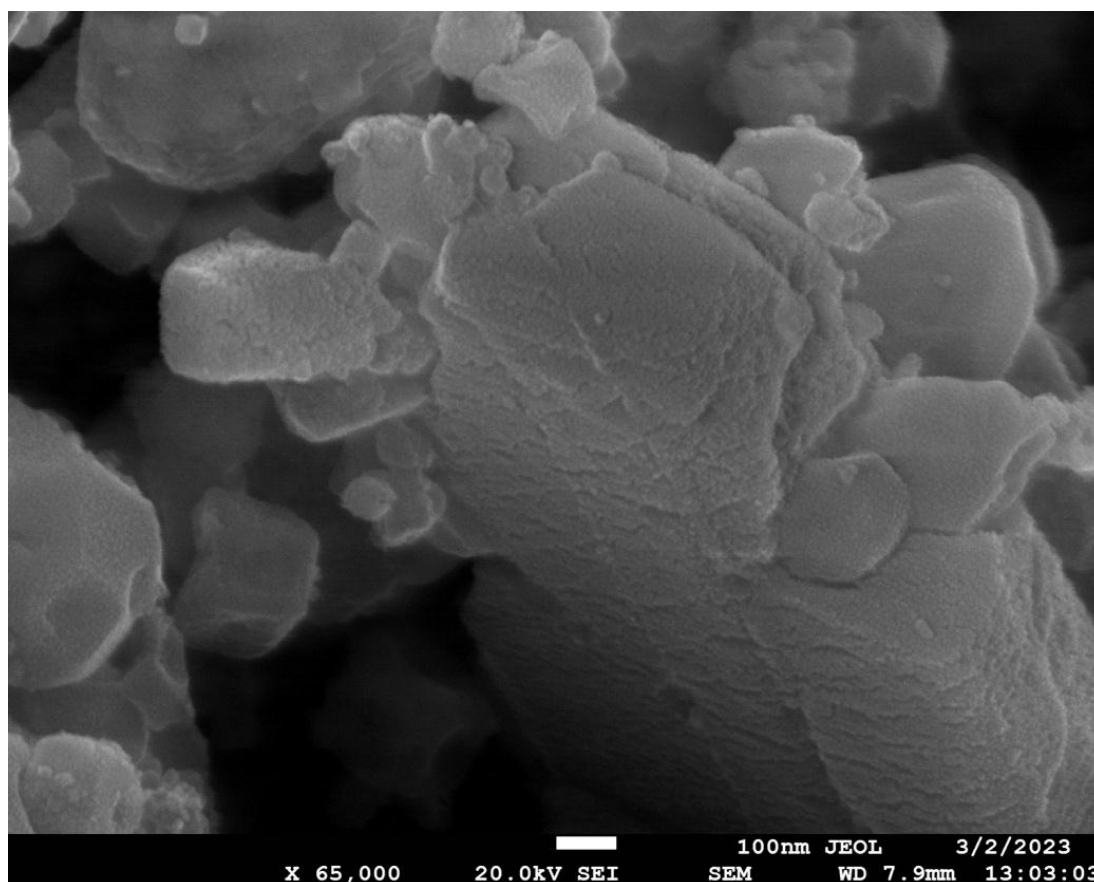
The field emission scanning electron microscopy (FESEM) images presented depict the surface morphology of silver Diosmin at magnifications of 10 µm and 100 µm. The 10 µm image, captured at 500x magnification, reveals a high-density distribution of irregularly shaped silver Diosmin particles, exhibiting various sizes and a rough, aggregated texture. These smaller structures suggest a heterogeneous distribution, possibly indicating a crystalline or semi-crystalline nature, with a propensity for

agglomeration. In contrast, the 100  $\mu\text{m}$  image at 250x magnification provides a broader view of the sample, demonstrating the larger-scale dispersion of the particles. This lower magnification highlights the overall uniformity and surface coverage, with some larger clusters distinctly visible, surrounded by smaller particulates. The comparative analysis suggests that the silver Diosmin nanoparticles possess both micro- and sub-microscale features, likely contributing to enhanced surface reactivity and potential applications in nanomedicine or material science.



**Figure 4.50 : FESEM graphs of silver Diosmin nano-formulations**  
**A. 100 $\mu\text{m}$  and B. 10 $\mu\text{m}$ .**

**4.2.6.2.2.6. Conjugates of Silver nano-formulations :** The provided FESEM images illustrate the surface morphology of silver Diosmin-Hesperidin at magnifications of 1  $\mu\text{m}$  and 100  $\mu\text{m}$ . At 1  $\mu\text{m}$  (4000x magnification), a highly agglomerated structure is observed, indicating the presence of clustered micro-particles with rough surfaces, suggesting potential crystalline or semi-crystalline formations. This aggregation may be due to strong interparticle interactions between silver, Diosmin, and Hesperidin, forming a composite material. In the 100  $\mu\text{m}$  image (65,000x magnification), the higher-resolution view reveals distinct, plate-like nanoparticles with smooth surfaces, highlighting their nanoscale features. These smaller structures likely contribute to the overall stability and surface reactivity of the composite, potentially enhancing its functional properties in biomedical or pharmaceutical applications. The combination of micro- and nanostructures suggests a complex morphology that could play a significant role in the material's therapeutic efficacy and performance.



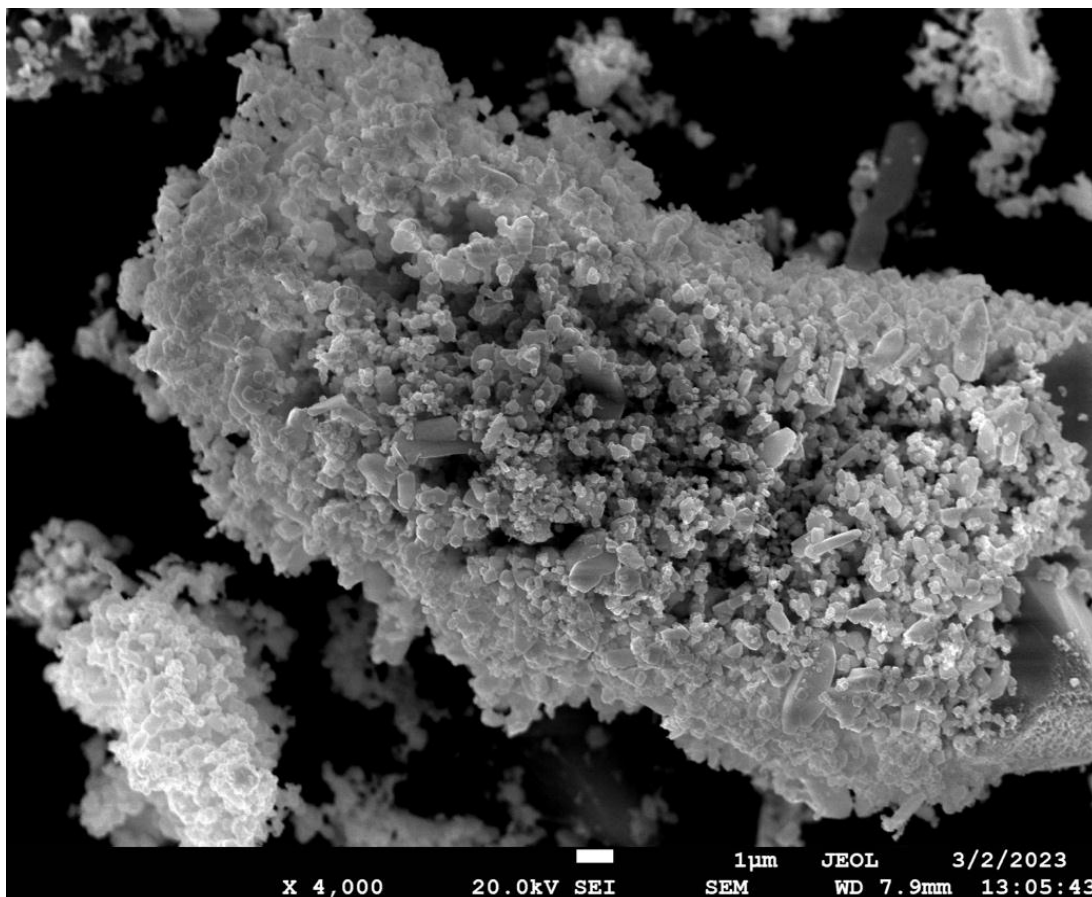
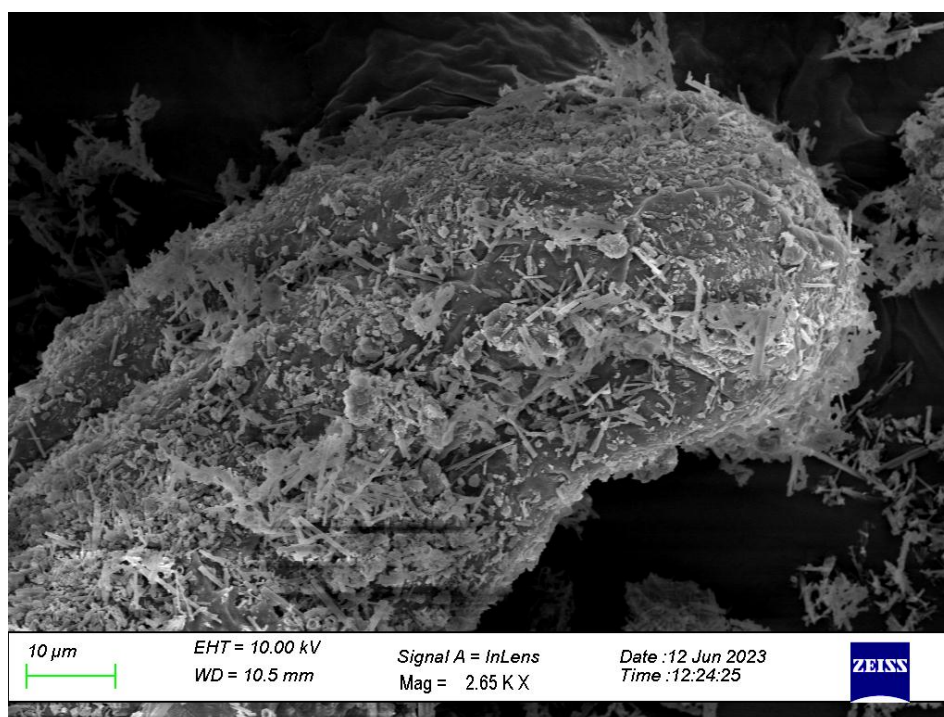
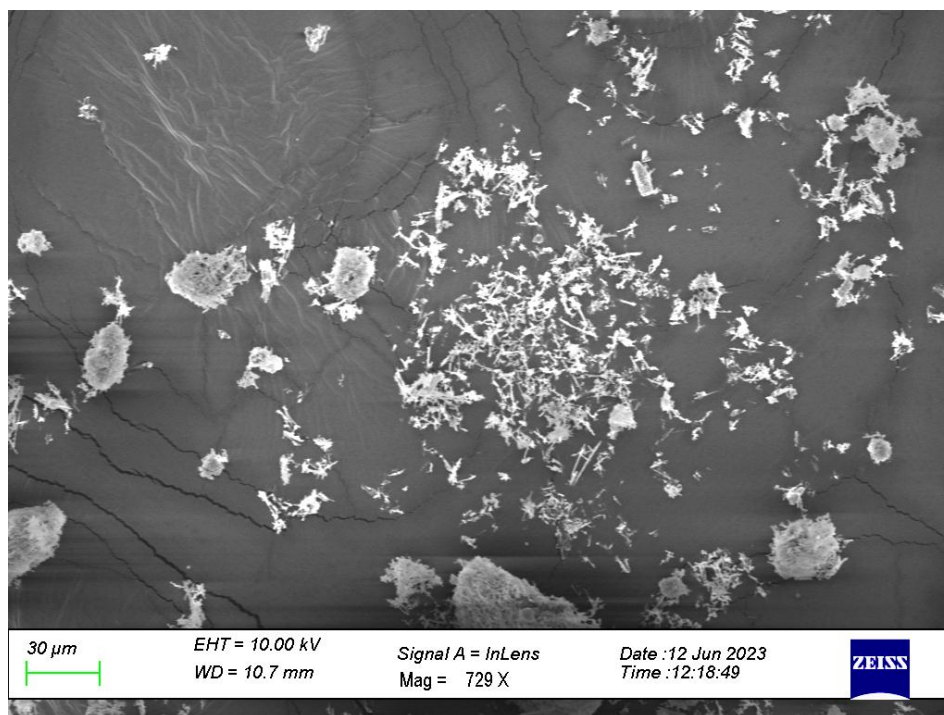


**Figure 4.51 : FESEM graphs of silver conjugates nano-formulations**

**A. 100µm and B. 1µm.**

**4.2.6.2.2.7. Zinc Hesperidin nano-formulations :** The FESEM images of Zinc-Hesperidin at magnifications of 30 µm and 10 µm provide insight into the composite's surface morphology. At 30 µm (729x magnification), the surface appears heterogeneous, with dispersed clusters of Zinc-Hesperidin particles of varying sizes, showing a scattered distribution. The rough surface texture and the presence of micro-cracks suggest that the material might exhibit crystalline or semi-crystalline behavior, with potential stress-induced features or drying artifacts. The 10 µm image (2.65kx magnification) reveals a higher density of microstructures, displaying aggregated formations with a more pronounced rough, porous surface. These structures include needle-like protrusions, indicative of the crystallization pattern of Zinc-Hesperidin. The presence of these micro and sub-micro structures suggests a complex, hierarchical morphology that may enhance the composite's surface area

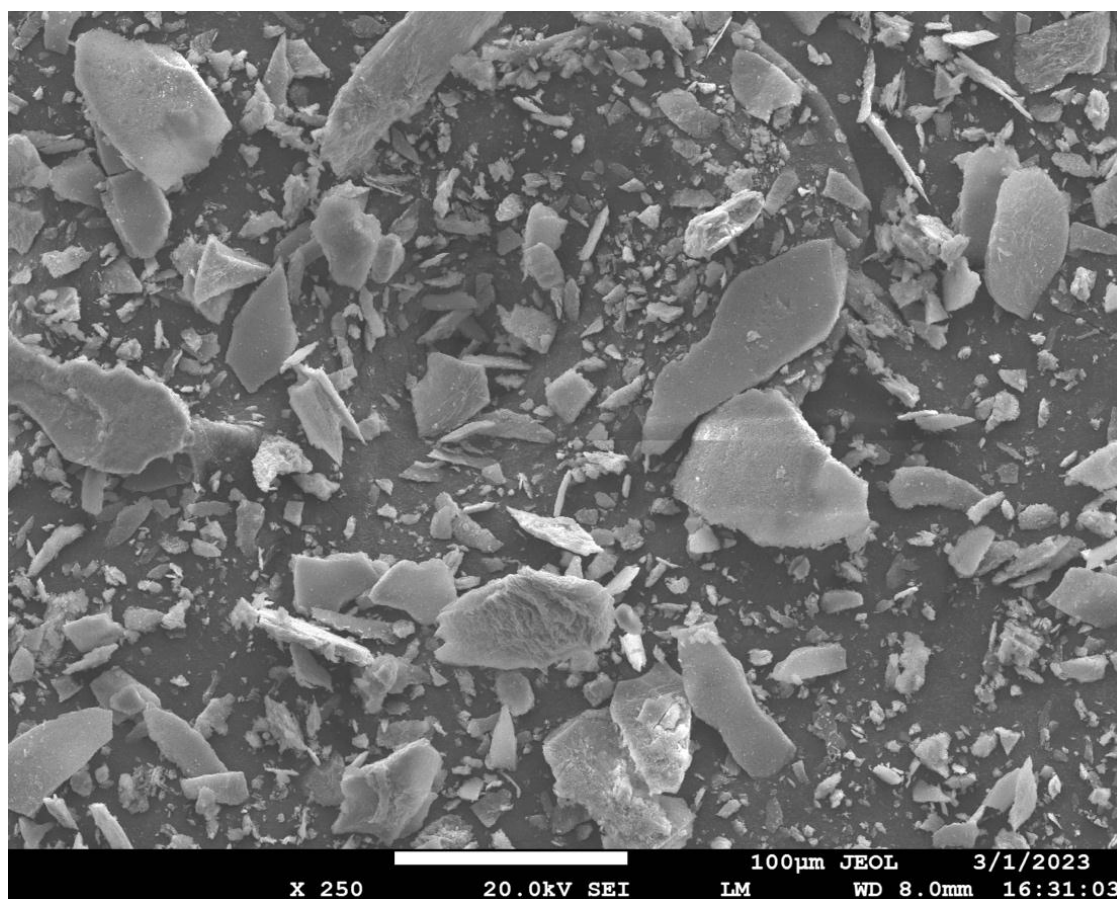
and, consequently, its functional performance, particularly for biomedical or material science applications.



**Figure 4.52 : FESEM graphs of zinc hesperidin nano-formulations  
A. 30μm and B. 10μm.**



**4.2.6.2.2.8. Zinc Diosmin nano-formulations :** At 100 microns , the particles appear as irregularly shaped aggregates with a range of sizes and rough surfaces, indicating a heterogeneous morphology. The particle edges are sharp, and there are notable variations in thickness, suggesting a crystalline or layered structure. At 10 microns, a closer view reveals fine, plate-like fragments with clear stratification and surface irregularities. These features suggest that Zinc Diosmin has a lamellar structure with possible microcracks or fractures on the particle surfaces. The observed morphology could influence its surface area and dissolution properties, which are critical for its pharmaceutical applications. This structural analysis highlights the importance of particle size and morphology in determining the material's behavior in different formulations.



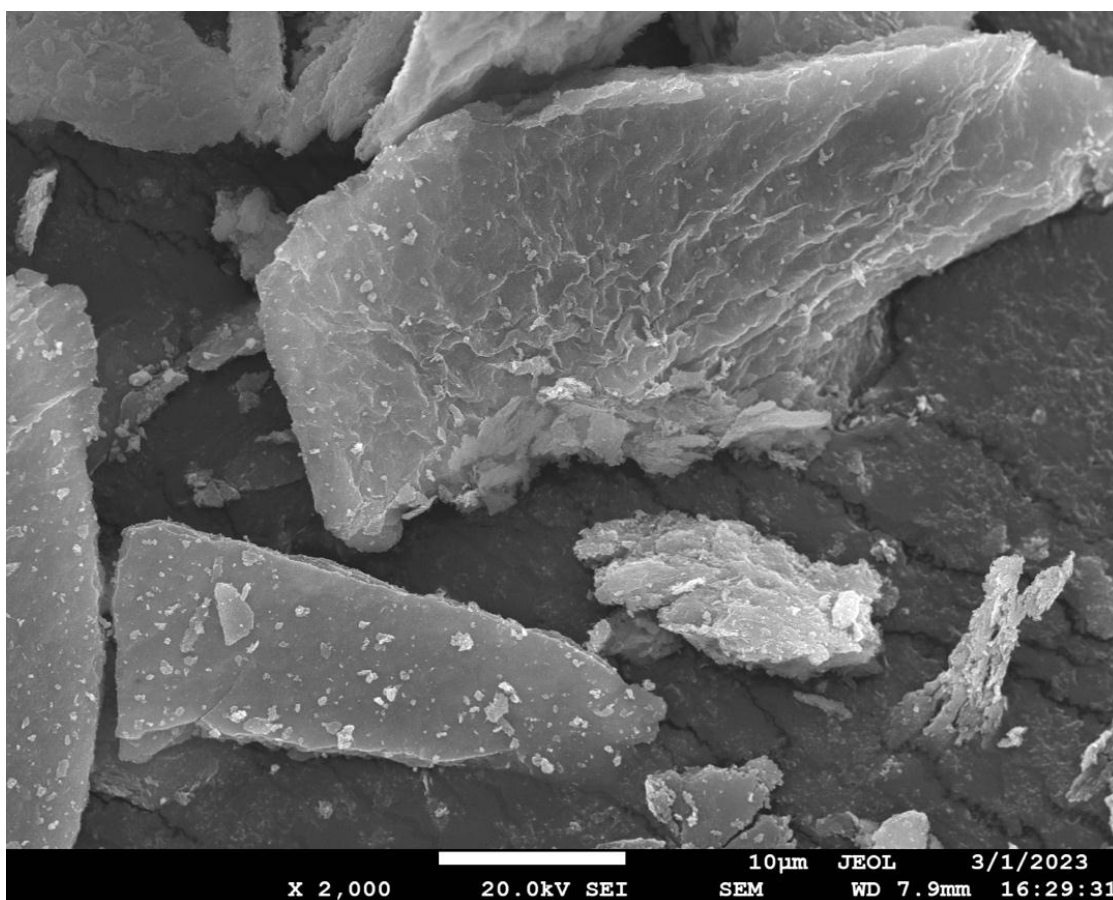


**Figure 4.53. : FESEM graphs of zinc Diosmin nano-formulations**

**A. 100µm and B. 10µm.**

**4.2.6.2.2.9. Conjugates of Zinc nano-formulations :** The FESEM images of Zinc Diosmin Hesperidin at 100 microns and 30 microns illustrate a detailed view of its microstructure. At 100 microns, the material shows a dispersed arrangement of irregularly shaped particles with varying sizes, suggesting a heterogeneous mixture. The surface of the particles appears rough, with edges that are jagged and fragmented. The distribution of smaller particulates around larger fragments could indicate potential breakage or separation of finer particles. At 30 microns, the magnified view reveals elongated, plate-like structures with a layered or stratified appearance. The surface shows significant textural complexity, with roughness and ridges likely contributing to the material's surface area. These morphological features imply that the material's physical structure may enhance its dissolution and interaction properties, which are essential for its effectiveness in pharmaceutical

applications. The presence of cracks or fissures might also affect its mechanical properties and processing.

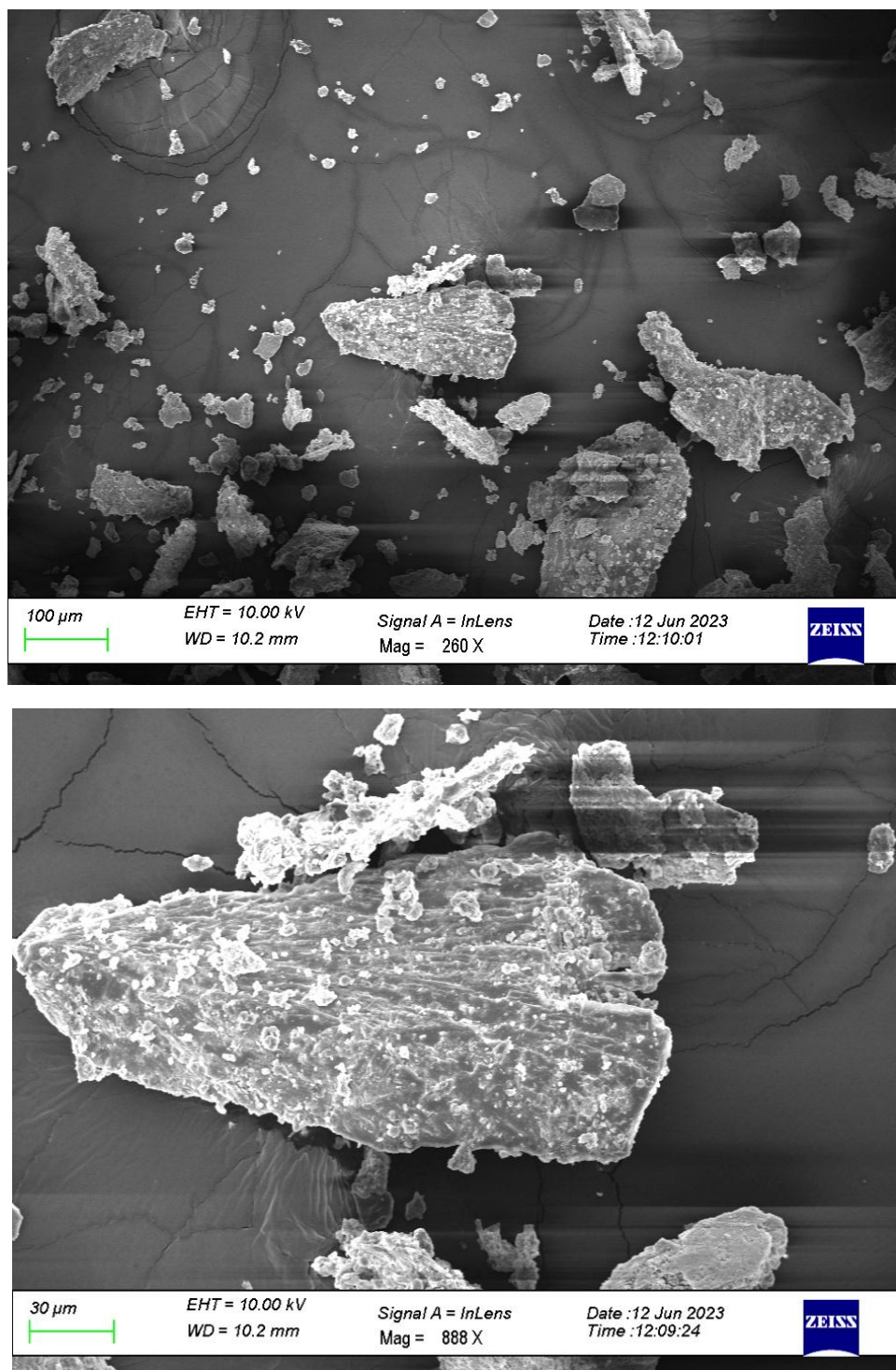


**Figure 4.54 : FESEM graphs of zinc conjugates nano-formulations  
A. 100 $\mu\text{m}$  and B. 30 $\mu\text{m}$ .**



FESEM analysis was used to ascertain the morphology and particle size of the graphene nanoparticle samples that were synthesized. In general, it has a rectangular morphology and measures an average of  $50 \pm 10$  nm in diameter.

**4.2.6.2.3. Zeta particle size analyzer :** The analysis of Zeta particle size yields crucial insights into the physical properties and behaviour of nano-formulations. By determining the size distribution of particles suspended in a solution, we can elucidate various phenomena such as stability, aggregation, and interaction forces within the system. The Zeta particle size results provide quantitative data regarding the average size and distribution of particles, offering valuable information for industries ranging from pharmaceuticals to cosmetics and beyond. Understanding the Zeta particle size allows us to tailor formulations, optimize processes, and enhance product performance, ultimately advancing innovation and efficiency in diverse applications.

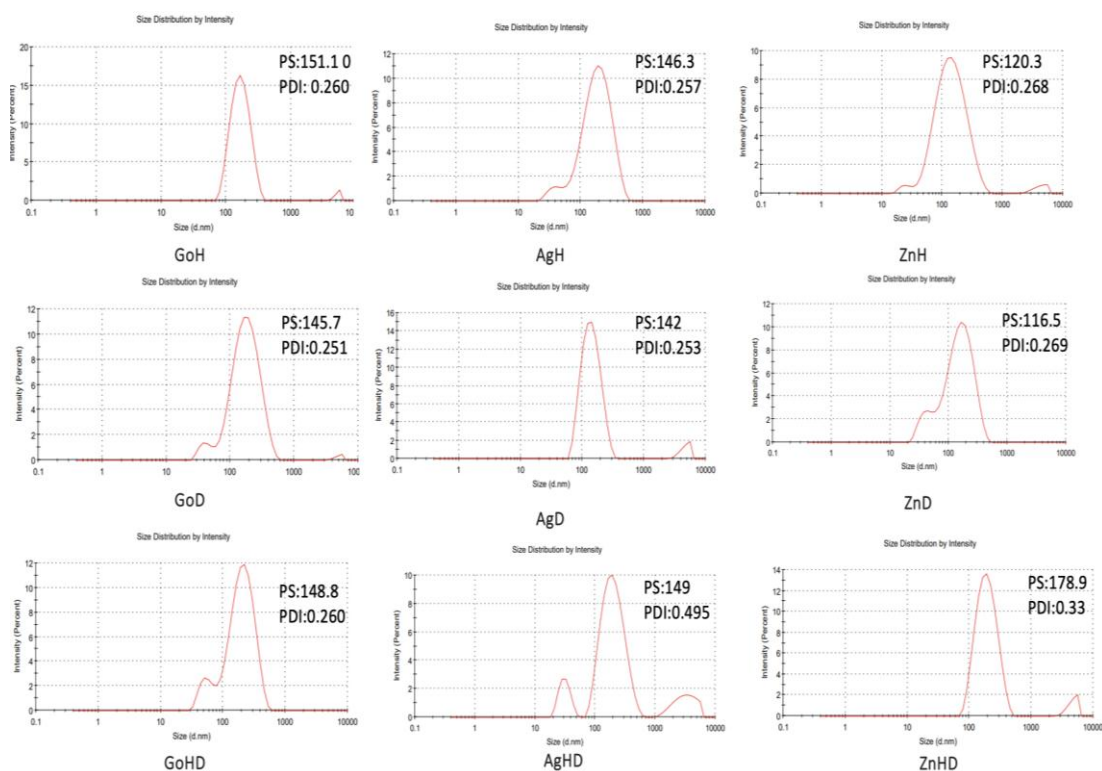


**Figure 4.55 : Zeta potential images of all the conjugates of various nano-formulations**

**Table 4.7: Nano-encapsulation of drug:**

S. No	Nanoparticle	Encapsulation efficiency
1.	GoH	74%
2.	GoD	72%
3.	GoHD	69%
4.	AgD	69%
5.	AgH	72%
6.	AgHD	79%
7.	ZnH	69%
8.	ZnD	64%
9.	ZnHD	76%

**Objective 3:** To examine the qualitative and quantitative assessment of altered proteins through system biology-based approaches.

### 4.3 BIOLOGICAL ASSAY OF (PURE) DIOSMIN

In this work, we employed the MTT cell viability test to assess the cytotoxic activity potential of Diosmin compounds at various concentrations. We discovered that Diosmin significantly reduced cell viability in a dose-dependent approach. A549 cells were particularly responsive to Diosmin (26.62  $\mu\text{g/ml}$ ). Based on this analysis, we conclude that diosmin is cytotoxic in nature.

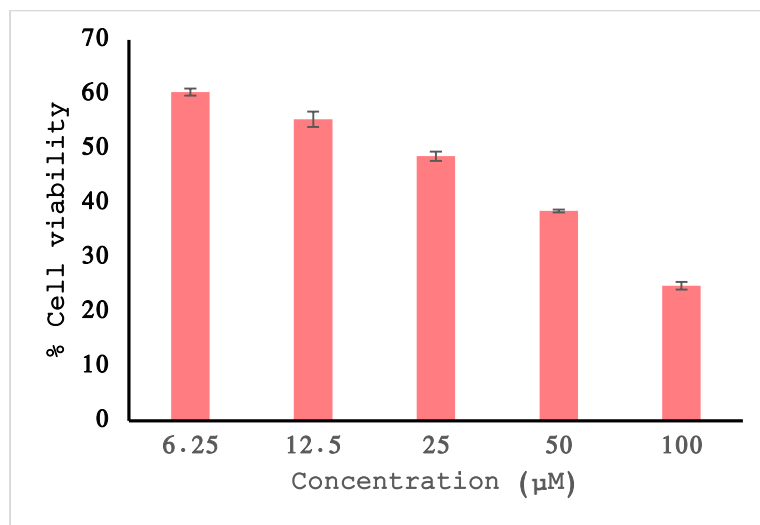


**Figure. 4.56. IC50 graph of Diosmin on A549 cell line.**

#### 4.4 BIOLOGICAL ASSAY OF (PURE) HESPERIDIN

In this work, we employed the MTT cell viability test to assess the cytotoxic activity potential of hesperidin compounds at various concentrations. We discovered that hesperidin significantly reduced cell viability in a dose-dependent approach (Figure 4.43). A549 cells were particularly responsive to hesperidin (34.25  $\mu\text{g/ml}$ ). Based on this analysis, we conclude that hesperidin is cytotoxic in nature.

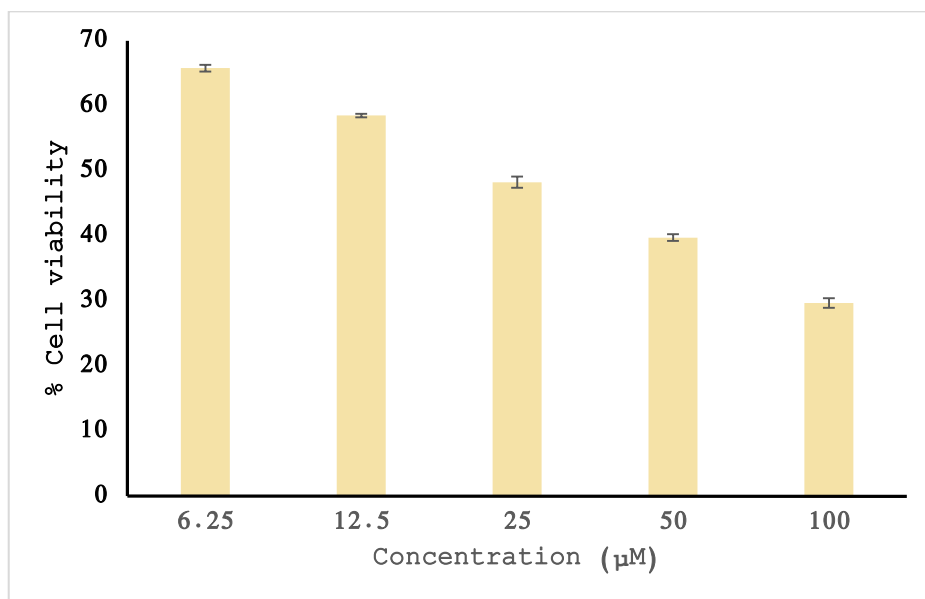


Figure 4.57 : Cytotoxicity of Hesperidin.

#### 4.5 BIOLOGICAL ASSAY OF NANO-FORMULATIONS

##### 4.5.1 Biological Assay for Graphene Conjugate nano-formulations

The graph represents the dose-response curves for cell death in the A549 cell line treated with different graphene nano-formulations: Graphene-Hesperidin (GoH), Graphene-Diosmin (GoD), and Graphene-Hesperidin-Diosmin (GoHD). The blue curve (GoH) shows a sharp decline in cell viability with increasing concentration, indicating a highly potent effect on inducing cell death, with an  $\text{IC}_{50}$  value of **25.4178  $\mu\text{g/mL}$** , making it the most effective formulation. The orange curve (GoD) exhibits a gradual and linear reduction in cell viability, reflecting moderate cytotoxic activity with an  $\text{IC}_{50}$  value of **73.8095  $\mu\text{g/mL}$** , the least effective among the formulations. The green curve (GoHD) shows a relatively flat response with

minimal reduction in cell viability compared to GoH but demonstrates moderate potency with an IC<sub>50</sub> value of **39.6331  $\mu\text{g/mL}$** . In summary, GoH shows the strongest cytotoxic activity, followed by GoHD and GoD, highlighting GoH as the most effective nano-formulation for inducing cell death in A549 cells.

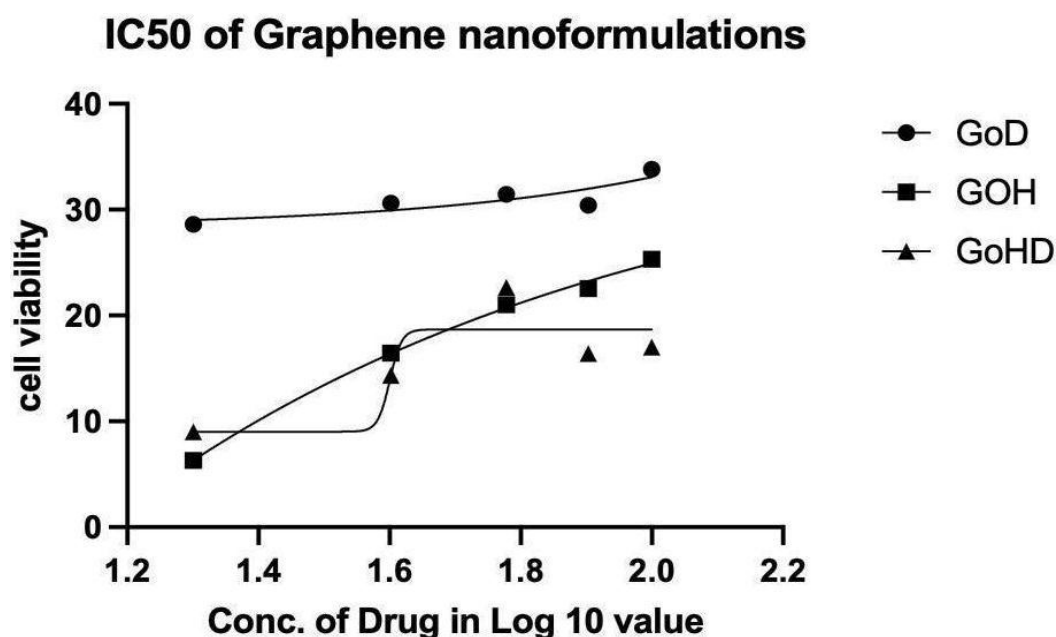


**Figure 4.58 : Cytotoxicity of Graphene nano-formulations**

#### **4.5.2 Biological Assay for Silver Conjugate nano-formulations**

The graph represents the dose-response curves for cell death in the A549 cell line treated with different silver nano-formulations: Silver-Hesperidin (AgH), Silver-Diosmin (AgD), and Silver-Hesperidin-Diosmin (AgHD). The pink curve (AgH) shows a noticeable decline in cell viability with increasing concentration, indicating significant cytotoxic activity with an IC<sub>50</sub> value of **25.4178  $\mu\text{g/mL}$** . The purple curve (AgD) also demonstrates effective cytotoxic activity with an IC<sub>50</sub> value of **28.1421  $\mu\text{g/mL}$** , slightly less potent than AgH. In contrast, the blue curve (AgHD) exhibits the steepest decline and achieves the lowest IC<sub>50</sub> value of **8.8148  $\mu\text{g/mL}$** , highlighting it as the most potent formulation among the three. In summary, the data reveal that AgHD has the strongest cytotoxic effect on A549 cells, followed by AgH and AgD, with respective IC<sub>50</sub> values confirming the superior efficacy of the silver nano-formulations incorporating both hesperidin and diosmin.

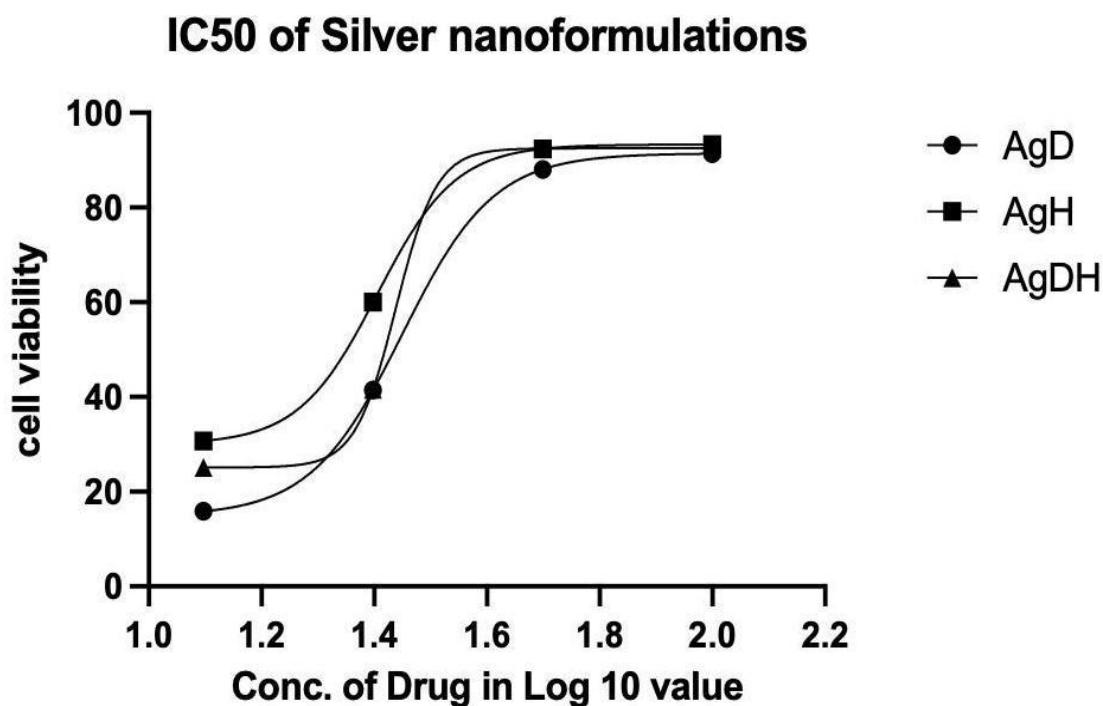
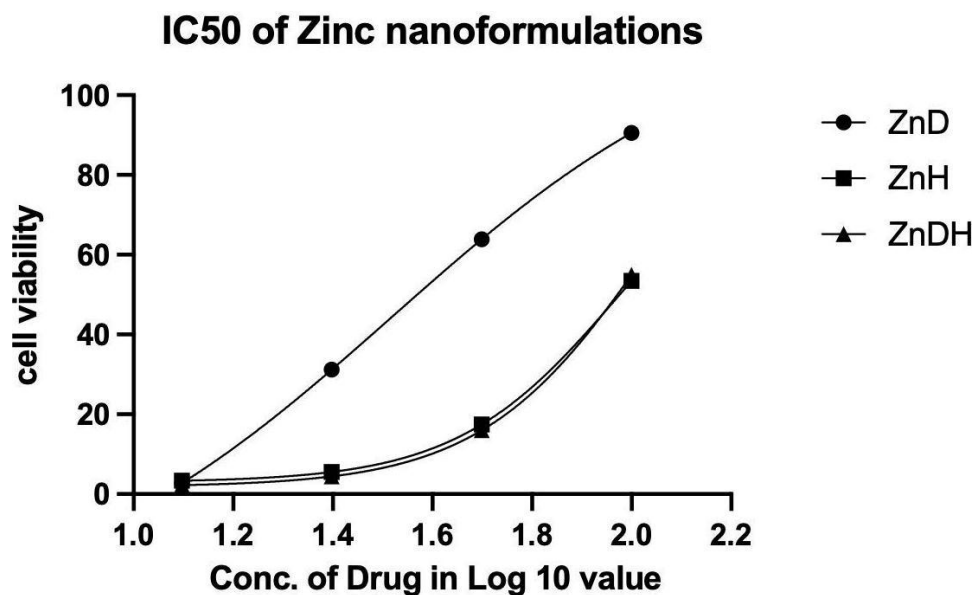


Figure 4.59 : Cytotoxicity of Silver nano-formulations

#### 4.5.3 Biological Assay for Zinc Conjugate nano-formulations

The graph illustrates the dose-response curves for cell death in the A549 cell line treated with different zinc nano-formulations: Zinc-Hesperidin (ZnH), Zinc-Diosmin (ZnD), and Zinc-Hesperidin-Diosmin (ZnHD). The green curve (ZnH) shows a minimal decline in cell viability with increasing concentration, indicating relatively low cytotoxic activity with an IC<sub>50</sub> value of **64.0929 µg/mL**. The orange curve (ZnD) exhibits a steeper decline, demonstrating moderate cytotoxic activity with an IC<sub>50</sub> value of **86.6801 µg/mL**, which is less potent than ZnH. The brown curve (ZnHD), however, has the highest IC<sub>50</sub> value of **29.49431 µg/mL**, indicating the weakest cytotoxic effect among the formulations and requiring a significantly higher concentration to induce cell death. In conclusion, the data indicate that ZnH is the most effective formulation in inducing cytotoxicity in A549 cells, followed by ZnD and ZnHD, as evidenced by their respective IC<sub>50</sub> values.



**Figure 4.60 : Cytotoxicity of Zinc nano-formulations**

#### 4.6 SCRATCH ASSAY

Scratch Assay of Sample A549 cell line:

The results of the wound healing scratch assay highlight the antiproliferative effects exerted by the prepared nanosuspension on A549 cell lines. Cells treated with nanoparticles demonstrated migration rates of 35.25% for A549, while treatment with 20  $\mu\text{g/mL}$  resulted in reduced migration rates of 21.35% for A549 after 24 hours. In comparison, Untreated A549 cells (controls) exhibited the highest migration rates of approximately 78.42%. The migration data, analysed using wimasis software and ImageJ, clearly demonstrate a significant reduction in cell migration in response to NPs treatment.

These findings suggest that nanoparticles effectively inhibits cell invasion and migration in the proliferating cancer cell lines studied. This observation aligns with previous studies that reported similar effects of biosynthesized ZnO and Ag NPs in other cancer cell lines. The antiproliferative effects of NPs are primarily attributed to their ability to selectively target tumor cells through the enhanced permeability and retention (EPR) effect.

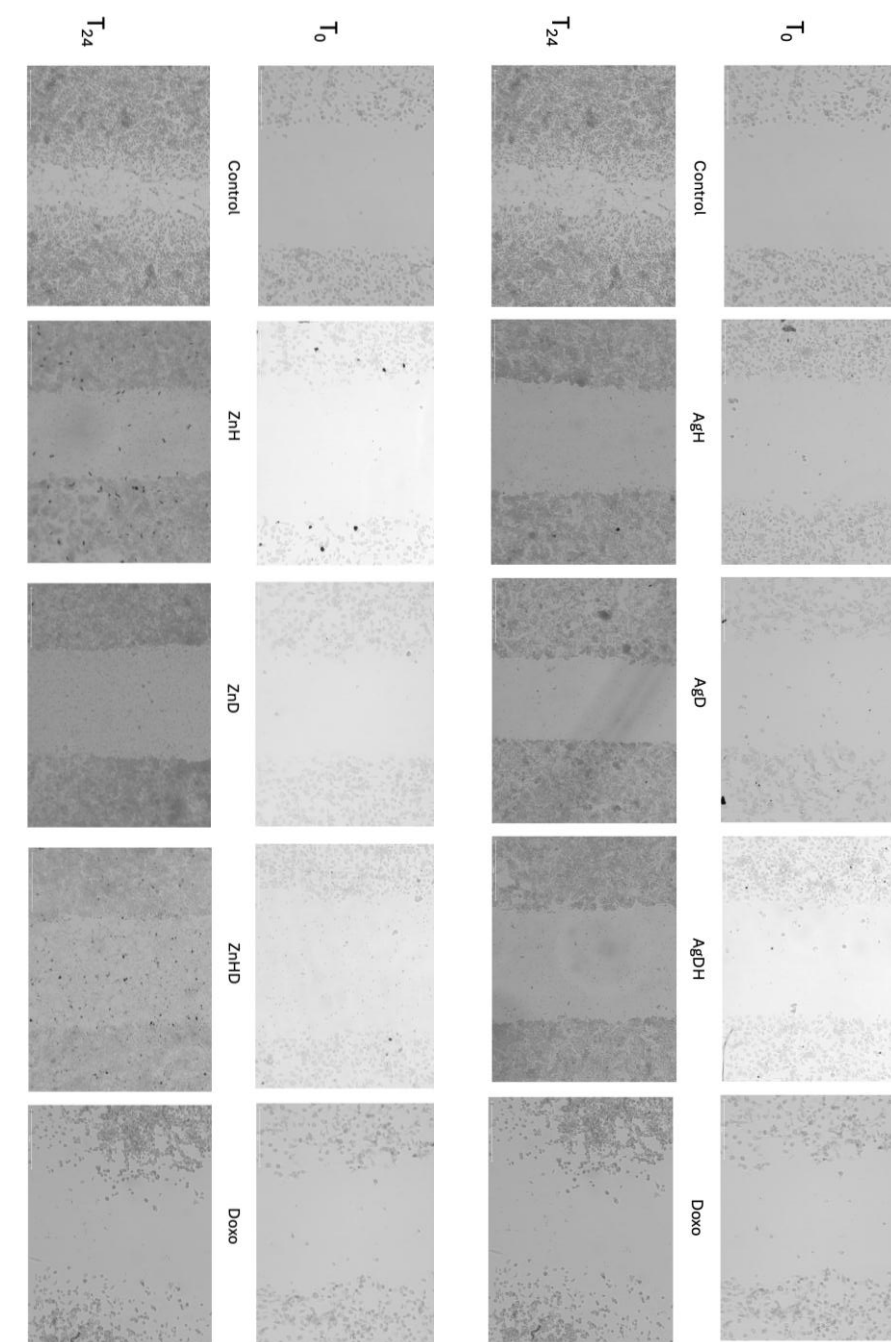


**Figure 4.61 : Scratch assay images of standard drug Doxo. at zero time and 24 hours.**

#### **4.7 LCMS ANALYSIS**

The protein from the cell Lysate was extracted and confirmed SDS-PAGE Analysis. The extracted protein were then digested and injected into Mass Spectroscopy. The mass spectroscopy data was analysed against the Human Lung Cancer protein

Database retrieved from Uniport using PLGS Software. Identified list of protein is listed in table below.

## MSTIC

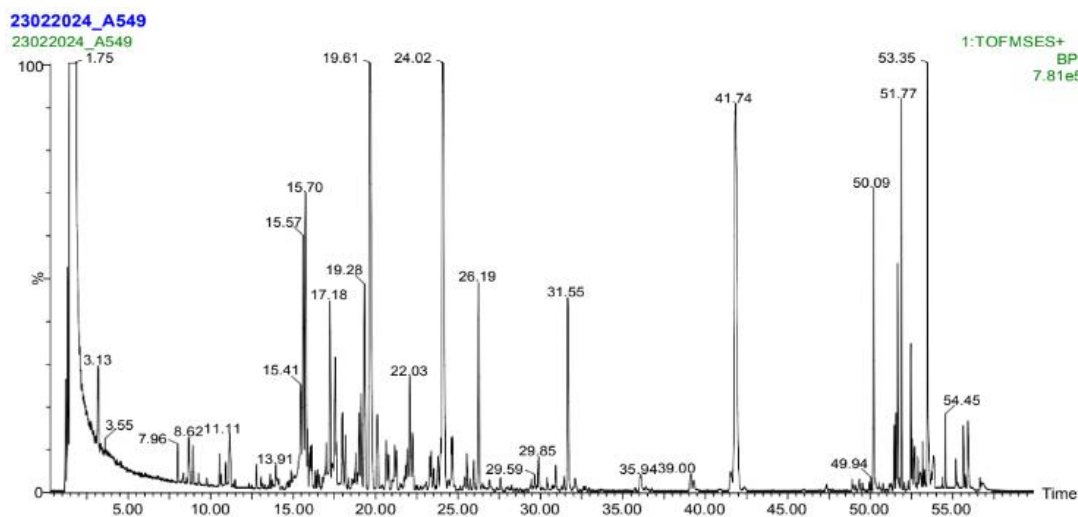


Figure 4.62 : MSTIC graph of LCMS analysis.

## MS spectrum

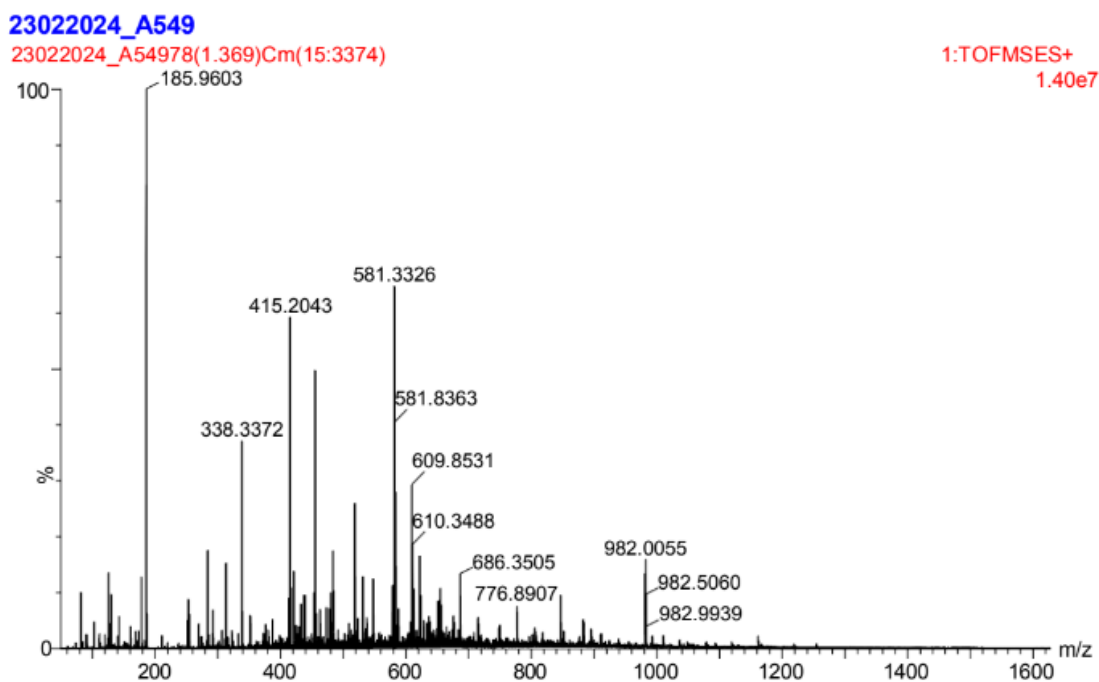


Figure 4.63 : MS spectrum graph of LCMS analysis



**Table 4.8 : The Identified Proteins from LCMS Analysis**

<b>Accession no</b>	<b>Gene</b>	<b>Evidence level</b>	<b>Sequence version</b>	<b>mW (Da)</b>	<b>PI (pH)</b>	<b>PLGS Score</b>	<b>Coverage (%)</b>	<b>Modified peptides</b>
M1VPF4	TPM3-ROS1	2	1	82367	4.708	1735.379	27.8621	4
P63261	ACTG1	1	1	41765	5.1606	1024.535	61.6	8
Q13356	PPIL2	1	1	58786	8.9839	530.2833	25.3846	0
P04075	ALDOA	1	2	39395	8.0654	519.3104	19.7802	0
P18615	NELFE	1	3	43213	9.7251	402.4473	42.8947	0
C1PHA2	KIF5B-ALK	2	1	167799	6.1904	374.9897	23.3985	5
Q96AZ6	ISG20	1	2	20350	9.2271	379.8324	27.0718	0
Q9UJZ1	STOML2	1	1	38510	7.2642	368.8327	27.809	2
P20810	CAST	1	4	76526	4.7798	342.644	28.1073	1
B3XZL9	-	2	1	86346	8.647	325.1569	24.0764	2
Q9UM73	ALK	1	3	176328	6.6504	314.0672	18.0864	1
G5EKE5	PPFIBP1-ALK	2	1	90683	5.4302	310.9492	23.1813	3
Q9UET6	FTSJ1	1	2	36056	5.2896	291.569	11.2462	0

Accession no	Gene	Evidence level	Sequence version	mW (Da)	PI (pH)	PLGS Score	Coverage (%)	Modified peptides
P26196	DDX6	1	2	54382	8.8359	284.6222	26.7081	2
Q6IQ55	TTBK2	1	2	137327	6.5449	279.1321	27.9743	5
Q9HC52	CBX8	1	3	43369	10.3169	286.14	23.9075	1
Q16384	SSX1	1	2	21917	9.8628	273.8456	54.2553	3
O60356	NUPR1	1	1	8867	10.3975	271.0223	70.7317	0
Q9H1E3	NUCKS1	1	1	27280	4.79	268.0811	27.9835	0
Q2TAM9	TUSC1	1	4	23090	11.5811	263.4199	26.3158	0
Q9NXR8	ING3	1	2	46713	5.8301	212.3033	32.0574	7
B4DNT1	SMARCA2	1	1	31715	5.6982	260.8049	24.2754	1
Q6ZMR5	TMPRSS11A	1	3	47196	9.3794	260.1033	14.5933	0
Q13886	KLF9	1	1	27217	8.5356	256.2356	25.8197	1
Q8WXI9	GATAD2B	1	1	65220	10.1279	238.4032	25.801	2
Q16181	SEPTIN7	1	2	50648	8.8887	251.2517	24.9428	6
Q9Y2J2	EPB41L3	1	2	120603	4.9131	220.5498	17.5713	2

<b>Accession no</b>	<b>Gene</b>	<b>Evidence level</b>	<b>Sequence version</b>	<b>mW (Da)</b>	<b>PI (pH)</b>	<b>PLGS Score</b>	<b>Coverage (%)</b>	<b>Modified peptides</b>
P20042	EIF2S2	1	2	38364	5.4521	232.7796	20.1201	1
Q9Y265	RUVBL1	1	1	50196	5.9868	232.132	36.4035	4
Q86VW1	SLC22A16	1	1	64572	8.0815	231.6724	10.3986	0
Q9NRW7	VPS45	1	1	65035	8.2866	222.293	26.6667	3
P08151	GLI1	1	1	117830	6.9434	216.6294	17.9928	2
P55957	BID	1	1	21981	5.0991	215.8693	14.8718	1
Q9BYG3	NIFK	1	1	34201	10.2935	215.5587	32.4232	0
P16989	YBX3	1	4	40066	10.021	184.9107	25	0
Q9Y606	PUS1	1	3	47439	8.4185	207.226	23.4192	1
P50542	PEX5	1	3	70820	4.2393	215.0963	23.1612	1
P15531	NME1	1	1	17137	5.7671	204.3967	34.2105	2
Q13322	GRB10	1	2	67188	7.7153	203.0346	27.7778	2
P53365	ARFIP2	1	1	37832	5.6455	201.8924	36.9501	1
P17544	ATF7	1	3	51724	7.9512	195.8589	19.0476	0

Accession no	Gene	Evidence level	Sequence version	mW (Da)	PI (pH)	PLGS Score	Coverage (%)	Modified peptides
Q6IBS0	TWF2	1	2	39523	6.3882	190.5861	15.7593	0
P14550	AKR1A1	1	3	36549	6.3384	187.4874	35.3846	0
Q13554	CAMK2B	1	3	72632	6.8818	185.273	25.5255	2
O75832	PSMD10	1	1	24412	5.6689	184.5384	30.0885	1
O75638	CTAG2	1	3	21076	10.4634	184.5287	58.5714	1
O76080	ZFAND5	1	1	23117	8.5122	184.5146	22.0657	1
Q8WXF1	PSPC1	1	1	58706	6.2344	184.3183	28.6807	4
Q9UBE0	SAE1	1	1	38425	4.9951	182.3027	24.8555	0
Q12849	GRSF1	1	3	53092	5.7744	182.0489	27.2917	0
Q96DA6	DNAJC19	1	3	12490	10.5029	181.4129	25	0
Q9UIM3	FKBPL	1	1	38152	5.2324	179.3553	2.8653	0
Q86VQ1	GLCCI1	1	1	57987	9.7632	179.0193	18.83	0
Q9HD26	GOPC	1	1	50488	5.5151	178.8029	21.645	1
Q9H334	FOXP1	1	1	75269	6.1978	175.6377	35.7459	3

Accession no	Gene	Evidence level	Sequence version	mW (Da)	PI (pH)	PLGS Score	Coverage (%)	Modified peptides
P17029	ZKSCAN1	1	3	63590	6.6021	175.471	24.3339	0
P62877	RBX1	1	1	12265	6.5552	171.3619	31.4815	2
Q96L93	KIF16B	1	2	151916	5.7788	166.9648	18.1473	4
Q13123	IK	1	3	65561	6.2197	166.5892	20.2873	0
Q96N77	ZNF641	1	2	49496	5.7451	166.024	11.1872	0
P35221	CTNNA1	1	1	100008	5.8755	165.2285	23.5099	5
Q7L5Y9	MAEA	1	1	45258	8.7598	163.6847	17.9293	3
I3WA68	EGFR	4	1	21222	8.2427	160.75	28.2723	0
Q16842	ST3GAL2	1	1	40146	8.3584	160.1676	23.1429	0
Q6J9G0	STYK1	1	4	47546	7.147	159.8792	13.7441	1
Q5W041	ARMC3	1	2	96344	5.811	159.3952	35.6651	5
P26038	MSN	1	3	67777	6.0103	158.1366	26.3432	5
Q5T6S3	PHF19	1	1	65549	8.8857	157.9559	29.8276	0
P57078	RIPK4	1	1	91553	6.709	157.6743	14.6635	1

Accession no	Gene	Evidence level	Sequence version	mW (Da)	PI (pH)	PLGS Score	Coverage (%)	Modified peptides
Q14978	NOLC1	1	2	73559	9.9507	157.3655	20.7439	0
P51523	ZNF84	1	2	85402	8.7803	156.482	21.5447	0
Q5SQI0	ATAT1	1	1	46781	10.3213	156.1593	19.4774	0
O43182	ARHGAP6	1	3	105882	7.0166	155.015	28.5421	4
O75113	N4BP1	1	4	100315	5.0757	154.9586	22.0982	3
Q9UMX0	UBQLN1	1	2	62479	4.8413	154.7057	26.4856	2
Q96S59	RANBP9	1	1	77798	6.3208	154.261	24.417	2
Q8IWA4	MFN1	1	3	84106	5.8887	153.7126	24.1565	2
Q5T0W9	FAM83B	1	1	114728	9.2168	153.041	22.453	0
Q9NX63	CHCHD31	1	1	26136	8.3745	152.4346	22.467	0
Q9BZ95	NSD3	1	1	161509	8.0874	151.3004	23.4516	7
O00481	BTN3A1	1	3	57640	7.9937	150.0453	22.807	1
O15146	MUSK	1	1	96993	6.8936	148.958	18.8723	4
Q92575	UBXN4	1	2	56742	6.0234	148.0121	19.0945	0

Accession no	Gene	Evidence level	Sequence version	mW (Da)	PI (pH)	PLGS Score	Coverage (%)	Modified peptides
A9YLN4	CD74/ROS fusion	2	1	79488	5.8608	147.7119	17.6387	3
P00533	EGFR	1	2	134190	6.2344	147.2963	17.438	3
Q9BQA1	WDR77	1	1	36701	4.8384	146.0274	17.5439	0
P42166	TMPO	1	2	75445	7.5132	145.8168	17.2911	2
Q9NRR5	UBQLN4	1	2	63812	4.96	145.557	31.614	4
Q8TEW8	PARD3B	1	2	132412	8.4185	144.8977	22.6556	1
Q5T5Y3	CAMSAP1	1	2	177860	6.2651	143.0573	20.8489	2
Q9Y619	SLC25A15	1	1	32714	9.3325	142.9352	26.2458	2
P30530	AXL	1	4	98274	5.0801	142.2663	21.7002	1
Q05932	FPGS	1	3	64568	7.8062	140.8903	21.4651	3
U6FSN9	Mprip-Ntrk1 fusion	2	1	150386	5.8682	139.8288	22.0887	5
Q15654	TRIP6	1	3	50255	7.0723	139.4738	14.2857	0
O15372	EIF3H	1	1	39905	6.0835	138.7346	26.9886	1
Q9NWQ4	GPATCH2L	1	3	54225	8.3979	138.1738	13.278	1

Accession no	Gene	Evidence level	Sequence version	mW (Da)	PI (pH)	PLGS Score	Coverage (%)	Modified peptides
P51813	BMX	1	1	77961	8.5444	137.9827	30.0741	2
Q9GZT9	EGLN1	1	1	45991	8.5298	136.7699	17.6056	2
O00425	IGF2BP3	1	2	63665	9.1846	136.534	19.5164	0
Q8N371	KDM8	1	1	47240	5.4126	136.1777	17.7885	2
Q8IVH2	FOXP4	1	1	73442	5.9502	134.8965	15.5882	0
Q8N6T7	SIRT6	1	2	39094	9.5391	133.8846	31.2676	1
P22570	FDXR	1	3	53803	8.4609	133.0129	26.6802	2
Q687X5	STEAP4	1	1	51947	9.4907	131.952	25.7081	2
Q8TES7	FBF1	1	2	125369	6.6255	131.1223	30.0088	4
Q5XKK7	FAM219B	1	1	21089	8.2808	130.0421	12.6263	0
O43852	CALU	1	2	37083	4.2773	130.0122	11.746	0
Q00325	SLC25A3	1	2	40068	9.6387	128.375	11.8785	1
Q96JB2	COG3	1	3	94036	5.2456	128.2342	25.7246	2
Q9NVH1	DNAJC11	1	2	63238	8.5166	128.1134	21.4669	1



Accession no	Gene	Evidence level	Sequence version	mW (Da)	PI (pH)	PLGS Score	Coverage (%)	Modified peptides
Q9NZJ0	DTL	1	3	79417	8.9517	127.8514	15.0685	0
Q9Y5S2	CDC42BPB	1	2	194191	5.9268	125.2766	17.2414	2
P78332	RBM6	1	5	128565	5.8696	125.0632	23.3304	1
O94986	CEP152	1	4	195502	5.3057	123.4454	18.3041	2
Q9H4G0	EPB41L1	1	2	98442	5.2866	122.5512	28.3768	2
Q9H6R7	WDCP	1	1	79085	6.23	122.3388	15.6727	1
Q9UPN4	CEP131	1	3	122074	8.9604	122.255	22.0683	5
A0A0F6MY87	ANKRD18B	2	1	161793	7.2744	121.6208	22.9836	7
Q16584	MAP3K11	1	1	92630	8.0669	121.5524	13.9315	0
P46379	BAG6	1	2	119334	5.2778	121.2125	21.7314	4
P29692	EEF1D	1	5	31102	4.708	120.8803	39.8577	2
Q15303	ERBB4	1	1	146712	5.9458	120.5156	15.2905	0
P28340	POLD1	1	2	123552	6.6182	120.0638	14.1825	1
Q9P2M7	CGN	1	3	136973	5.2705	119.7537	20.6983	3

Accession no	Gene	Evidence level	Sequence version	mW (Da)	PI (pH)	PLGS Score	Coverage (%)	Modified peptides
Q14687	GSE1	1	3	136080	7.4429	118.9882	20.378	3
O14827	RASGRF2	1	2	140674	7.2437	118.7446	22.6354	7
P43361	MAGEA8	1	2	35192	4.5161	118.506	30.1887	1
Q16539	MAPK14	1	3	41267	5.3862	117.9276	8.6111	0
Q15027	ACAP1	1	1	81484	7.4355	117.8315	17.5676	0
Q9BUQ8	DDX23	1	3	95524	9.9668	117.5031	18.7805	1
J7M2B1	EZR-ROS1	2	1	98885	5.7231	117.0934	20.6294	4
P29508	SERPINB3	1	2	44536	6.3662	117.0931	28.4615	2
O14522	PTPRT	1	6	162030	6.4365	117.0693	18.8064	3
Q00987	MDM2	1	1	55198	4.4019	117.0363	11.609	0
O60711	LPXN	1	1	43303	5.5752	117.0309	25.6477	0
P35240	NF2	1	1	69646	6.0601	116.8803	24.0336	1
Q9NRF8	CTPS2	1	1	65635	6.4629	116.8725	17.9181	1
Q6UWY5	OLFML1	1	2	45921	8.0581	115.9335	12.6866	0

Accession no	Gene	Evidence level	Sequence version	mW (Da)	PI (pH)	PLGS Score	Coverage (%)	Modified peptides
F6MDI4	BARD1	2	1	39711	7.9688	115.6156	28.5714	1
Q13796	SHROOM2	1	1	176301	6.6372	115.0599	18.9975	2
O60271	SPAG9	1	4	146114	4.8633	114.7029	32.5511	4
Q8TDF6	RASGRP4	1	2	74834	7.8765	114.0278	15.6018	0
P07992	ERCC1	1	1	32541	5.8374	113.9938	25.5892	1
O00203	AP3B1	1	3	121244	5.6572	113.8783	19.4698	1
Q9UJX4	ANAPC5	1	2	85022	6.4014	113.8014	19.6026	0
Q8WUJ0	STYX	1	1	25475	5.8564	113.7651	23.7668	2
Q56UN5	MAP3K19	2	1	150441	6.6094	113.2218	23.5693	6
Q5T1V6	DDX59	1	1	68766	7.1909	113.0537	13.5703	3
Q9UBK8	MTRR	1	4	77625	6.0308	112.8512	15.1862	1
Q0VD83	APOBR	1	3	115564	4.1807	112.477	21.7867	1
Q9HB71	CACYBP	1	2	26193	8.5825	112.4564	14.0351	0
Q7Z4V0	ZNF438	1	2	91777	9.7632	112.3381	16.3043	1

Accession no	Gene	Evidence level	Sequence version	mW (Da)	PI (pH)	PLGS Score	Coverage (%)	Modified peptides
Q9H4H8	FAM83D	1	3	64384	6.0806	112.3313	14.8718	1
Q9H3D4	TP63	1	1	76736	6.1025	112.1859	12.5	1
Q9H792	PEAK1	1	4	192985	6.4409	111.0889	19.3585	7
Q4LE39	ARID4B	1	2	147718	4.8545	110.9997	20.0457	6
Q38SD2	LRRK1	1	3	225247	6.2314	110.295	23.5732	3
O00755	WNT7A	1	2	38979	8.6587	110.0301	18.6246	0
O00629	KPNA4	1	1	57850	4.6128	109.9186	23.6084	2
Q8TF76	HASPIN	1	3	88439	9.4028	109.6112	14.6617	0
Q15067	ACOX1	1	3	74376	8.1489	108.8077	23.0303	3
Q6WKZ4	RAB11FIP1	1	3	137082	5.1357	108.638	21.2003	7
O75387	SLC43A1	1	1	61436	7.5483	108.632	14.3113	1
Q13873	BMPR2	1	2	115128	5.7729	108.3852	34.104	8
M1VE91	KIF5B-RET(NM_020630)_K24;R11	2	1	155717	6.104	108.3044	19.3997	4

Accession no	Gene	Evidence level	Sequence version	mW (Da)	PI (pH)	PLGS Score	Coverage (%)	Modified peptides
P10809	HSPD1	1	2	61016	5.5503	108.2195	15.3578	0
Q6XZF7	DNMBP	1	1	177235	5.0962	108.1259	17.8186	2
Q8NFY9	KBTBD8	1	2	68778	5.8389	107.8224	18.1364	0
Q13882	PTK6	1	1	51801	6.5786	107.0486	9.5344	0
Q96PZ2	FAM111A	1	2	70151	8.5737	107.0273	22.2586	0
Q14153	FAM53B	1	2	45738	6.3179	106.851	21.564	1
P54259	ATN1	1	3	125337	9.2109	106.8361	8.3193	0
Q9H307	PNN	1	5	81579	6.7456	106.7978	25.9414	4
P55327	TPD52	1	2	24312	4.5908	106.5136	21.875	0
O94885	SASH1	1	3	136567	5.6924	106.5082	23.8974	7
Q9NWT1	PAK1IP1	1	2	43935	9.1978	106.4625	11.4796	1
Q9BXJ9	NAA15	1	1	101207	7.1396	106.3859	26.3279	4
O14513	NCKAP5	1	2	208407	7.979	106.307	23.7821	3
Q92870	APBB2	1	3	83321	5.6719	105.817	23.0871	1

Accession no	Gene	Evidence level	Sequence version	mW (Da)	PI (pH)	PLGS Score	Coverage (%)	Modified peptides
P00519	ABL1	1	4	122796	8.8052	105.8004	14.7788	2
Q14241	ELOA	1	3	87176	9.9712	105.6118	20.5959	2
Q8IUF8	RIOX2	1	1	52767	6.23	104.8238	15.0538	1
Q9HC21	SLC25A19	1	1	35488	9.8306	104.7055	15.3125	0
Q9BVI0	PHF20	1	2	115313	6.5449	104.6489	16.2055	0
Q9UBU9	NXF1	1	1	70138	8.5928	104.0749	19.8708	1
Q92922	SMARCC1	1	3	122790	5.4023	103.9383	20.362	2
Q9Y4W2	LAS1L	1	2	83012	4.4487	103.7634	15.5313	0
Q6AWC2	WWC2	1	2	133808	5.2383	103.2181	20.8893	1
P36776	LONP1	1	2	106422	5.9619	103.1366	27.8415	6
Q15111	PLCL1	1	3	122649	5.3042	102.9353	30.8676	4
Q99683	MAP3K5	1	1	154439	5.4126	102.9084	24.0902	9
P40199	CEACAM6	1	4	37213	5.4609	102.7477	17.4419	0
Q5UW39	-	2	1	73647	5.4507	102.606	16.1491	1

Accession no	Gene	Evidence level	Sequence version	mW (Da)	PI (pH)	PLGS Score	Coverage (%)	Modified peptides
Q5TCQ9	MAGI3	1	3	162847	8.0566	102.3544	18.9737	2
Q9P287	BCCIP	1	1	35956	4.311	101.7228	25.1592	1
O60259	KLK8	1	1	28029	7.3887	101.6852	26.9231	0
Q96KR1	ZFR	1	2	116938	9.2314	101.5377	20.5773	2
P98082	DAB2	1	3	82397	5.1738	101.4222	14.8052	1
Q16254	E2F4	1	2	43933	4.4619	101.1925	15.2542	0
Q9Y463	DYRK1B	1	1	69154	9.3179	100.983	27.027	2
O43572	AKAP10	1	2	73771	5.9312	100.6228	14.5015	3
Q8N344	MIER2	1	2	59906	4.3345	100.6058	20.9174	4
P49589	CARS1	1	3	85419	6.2988	100.4731	15.107	1
Q9NQW6	ANLN	1	2	124121	8.0039	100.0789	29.1815	4
Q9BPU6	DPYSL5	1	1	61382	6.7559	99.6958	27.4823	5
Q9Y2Y9	KLF13	1	1	31160	9.8628	99.631	11.8056	1
Q16644	MAPKAPK3	1	1	42959	6.9229	99.4658	19.1099	1

Accession no	Gene	Evidence level	Sequence version	mW (Da)	PI (pH)	PLGS Score	Coverage (%)	Modified peptides
P68104	EEF1A1	1	1	50109	9.3428	99.3663	15.1515	1
Q96T51	RUFY1	1	2	79767	5.4243	99.1537	23.3051	3
Q9Y4E8	USP15	1	3	112347	4.8838	99.0829	33.945	2
P12956	XRCC6	1	2	69799	6.2036	99.0667	17.8982	1
Q9NZ20	PLA2G3	1	2	57130	9.1245	98.9818	18.0747	0
Q9HCS4	TCF7L1	1	1	62591	9.2329	98.9406	19.898	1
Q0JRZ9	FCHO2	1	2	88869	6.4175	98.0377	25.4321	1
M1VE83	SDC4-ROS1_S4;R34	2	1	71612	4.5059	97.9461	14.4635	1
Q9BZ29	DOCK9	1	2	236293	7.1543	97.8749	25.5196	14
Q9C0C2	TNKS1BP1	1	4	181683	4.5776	97.5633	30.48	5
O00329	PIK3CD	1	2	119402	6.7676	97.4115	11.3985	3
P37173	TGFBR2	1	2	64526	5.5093	97.3185	18.3422	3
Q14240	EIF4A2	1	2	46372	5.1636	97.1725	14.9877	2
Q75N03	CBLL1	1	1	54484	8.2266	96.8998	14.2566	1



Accession no	Gene	Evidence level	Sequence version	mW (Da)	PI (pH)	PLGS Score	Coverage (%)	Modified peptides
P54753	EPHB3	1	2	110259	5.8901	96.8155	23.5471	5
P08240	SRPRA	1	2	69767	9.29	96.8091	23.3542	2
Q16658	FSCN1	1	3	54496	6.876	96.7773	15.0101	0
Q5THK1	PRR14L	1	1	237148	5.8916	96.5394	14.4119	2
Q9NQB0	TCF7L2	1	2	67876	8.5986	96.5019	11.3086	0
Q6IQ49	SDE2	1	1	49710	5.6836	96.451	22.8381	2
P42680	TEC	1	2	73533	8.4507	96.3188	26.6244	2
Q9Y4E1	WASHC2C	1	5	147064	4.4927	96.1902	18.6428	3
Q9UPZ3	HPS5	1	2	127368	5.2119	96.0134	14.7919	2
M1VE86	LRIG3(NM_001136051)-ROS1	2	1	145089	5.3921	96.0079	15.249	4
Q8IZJ1	UNC5B	1	2	103571	5.6045	95.8719	17.3545	3
O60536	N/A	2	1	38834	9.4834	95.7744	19.1257	1
P42336	PIK3CA	1	2	124202	6.8408	95.751	14.6067	3
Q7Z4F1	LRP10	1	2	76144	5.1606	95.6711	14.7265	0

Accession no	Gene	Evidence level	Sequence version	mW (Da)	PI (pH)	PLGS Score	Coverage (%)	Modified peptides
P34947	GRK5	1	1	67743	8.0347	95.1457	16.4407	1
Q92769	HDAC2	1	2	55328	5.5078	95.0713	20.9016	0
Q9UJA3	MCM8	1	2	93637	7.5952	94.9643	17.8571	1
Q9BX84	TRPM6	1	2	231558	7.5615	94.4273	21.6617	5
Q8WVB6	CHTF18	1	1	107316	6.7881	94.2425	35.8974	5
Q63ZY3	KANK2	1	1	91117	5.2983	94.2074	30.9048	4
Q53QZ3	ARHGAP15	1	2	54510	9.8086	94.054	22.1053	2
Q9H270	VPS11	1	1	107768	6.5991	94.0306	18.8098	2
P55285	CDH6	1	1	88254	4.5747	93.9687	20.6329	0
P48729	CSNK1A1	1	2	38889	9.8555	93.8799	15.727	2
Q6PML9	SLC30A9	1	1	63474	8.3218	93.6348	16.5493	3
P05556	ITGB1	1	2	88356	5.0977	93.2954	13.9098	0
Q659C4	LARP1B	1	2	105257	7.3638	93.0454	18.1619	1
Q6UUV9	CRTC1	1	2	67258	5.5986	92.8684	19.4006	1

Accession no	Gene	Evidence level	Sequence version	mW (Da)	PI (pH)	PLGS Score	Coverage (%)	Modified peptides
P21757	MSR1	1	1	49730	5.5298	92.8621	21.9512	2
Q9Y6K1	DNMT3A	1	4	101793	6.1421	92.6285	22.1491	5
Q9ULX3	NOB1	1	1	46645	6.7632	92.4049	10.4369	0
Q8TDM6	DLG5	1	4	213733	7.0547	92.3485	14.5909	4
Q8N5Y2	MSL3	1	1	59786	8.2324	92.2797	21.3052	0
O43353	RIPK2	1	2	61156	6.6504	92.2629	21.1111	0
Q9NXZ1	SAGE1	1	2	99162	6.0117	92.2428	34.4027	9
Q05516	ZBTB16	1	2	74225	6.0044	91.8549	26.003	3
Q5TCY1	TTBK1	1	2	142649	5.313	91.8528	20.5905	2
Q86UP2	KTN1	1	1	156178	5.3657	91.5069	21.8865	7
O95243	MBD4	1	1	66009	9.022	90.6948	22.4138	2
P21802	FGFR2	1	1	91965	5.5034	90.509	21.9245	2
P50613	CDK7	1	1	39013	8.6133	90.4937	19.3642	0
P02771	AFP	1	1	68633	5.3569	90.4168	27.422	1

Accession no	Gene	Evidence level	Sequence version	mW (Da)	PI (pH)	PLGS Score	Coverage (%)	Modified peptides
Q86SQ7	SDCCAG8	1	1	82630	5.4814	90.3357	20.3366	1
Q8IW35	CEP97	1	1	96920	4.7314	90.2387	14.2197	1
Q9HA77	CARS2	1	1	62184	8.3335	89.3456	16.4894	2
P53990	IST1	1	1	39725	5.0376	89.2855	15.6593	1
Q13308	PTK7	1	2	118316	6.6606	89.1077	16.3551	3
Q8N9T8	KRI1	1	3	82547	4.8721	88.9243	21.1949	0
Q8IXJ9	ASXL1	1	4	165328	5.7861	88.8944	16.8722	3
Q8NG66	NEK11	1	2	74144	4.8105	88.6328	12.8682	3
Q9P2R3	ANKFY1	1	2	128318	5.6572	88.5054	15.9966	2
Q16322	KCNA10	1	2	57748	4.6538	88.3249	22.3092	1
Q16566	CAMK4	1	1	51892	5.4829	88.2507	23.8901	3
Q8NFU7	TET1	1	2	235159	8.1401	88.181	20.1311	0
Q12860	CNTN1	1	1	113249	5.5137	88.1695	11.4931	1
P31513	FMO3	1	5	59994	7.6919	88.1047	20.3008	2

Accession no	Gene	Evidence level	Sequence version	mW (Da)	PI (pH)	PLGS Score	Coverage (%)	Modified peptides
Q13200	PSMD2	1	3	100135	4.9014	87.8968	15.0881	2
Q92539	LPIN2	1	1	99337	5.0112	87.7142	21.0938	3
Q7Z6E9	RBBP6	1	1	201440	10.0269	87.6618	20.3125	3
Q13164	MAPK7	1	2	88331	5.502	87.2177	8.2108	1
Q96JH7	VCPIP1	1	2	134235	6.7632	87.0855	22.6678	3
P42356	PI4KA	1	4	236675	6.624	87.085	17.2217	9
Q15007	WTAP	1	2	44216	4.9321	86.3349	13.3838	2
Q92574	TSC1	1	2	129685	6.0015	86.117	20.3608	3
Q86UG4	SLCO6A1	1	2	79180	8.54	86.1037	9.1794	2
Q9Y3S1	WNK2	1	4	242522	5.7158	86.1008	14.8019	9
P28838	LAP3	1	3	56130	7.9072	85.8162	26.3969	1
P29376	LTK	1	3	91622	6.0425	85.6682	17.5926	1
Q969X0	RILP2	1	1	23971	4.752	85.6243	17.5355	0
Q9ULI3	HEG1	1	3	147368	5.7495	85.4348	17.4511	3

Accession no	Gene	Evidence level	Sequence version	mW (Da)	PI (pH)	PLGS Score	Coverage (%)	Modified peptides
Q9H4A4	RNPEP	1	2	72549	5.395	85.3819	15.2308	1
Q96DC8	ECHDC3	1	3	32612	8.7759	85.2111	13.8614	1
Q13237	PRKG2	1	1	87377	8.5371	85.1718	10.3675	1
P52756	RBM5	1	2	92096	5.8667	84.9737	18.8957	5
P39060	COL18A1	1	5	178076	5.5957	84.595	15.9635	0
P35222	CTNNBI	1	1	85442	5.4478	84.2516	14.7247	2
Q7L2J0	MEPCE	1	1	74309	9.8408	84.23	6.8215	0
Q9UPQ7	PDZRN3	1	2	119521	5.6104	83.8429	25.8912	3
P63010	AP2B1	1	1	104486	5.0552	83.7023	16.5422	4
Q86U38	NOP9	1	1	69394	6.8818	83.6352	10.5346	2
Q2HXI4	PTPRD	2	1	214649	6.1157	83.5474	22.3326	4
P42575	CASP2	1	2	50652	6.3501	83.5045	12.8319	1
Q9UHB6	LIMA1	1	1	85173	6.4043	83.2161	20.2899	2
Q9NXG2	THUMPD1	1	2	39290	7.8911	82.9256	27.4788	3

Accession no	Gene	Evidence level	Sequence version	mW (Da)	PI (pH)	PLGS Score	Coverage (%)	Modified peptides
Q96PY6	NEK1	1	2	142739	5.5723	82.7403	13.1955	1
Q7L7V1	DHX32	1	1	84363	4.6978	82.7129	26.1104	3
Q9UPY3	DICER1	1	3	218541	5.335	82.6429	18.9906	7
P30041	PRDX6	1	3	25019	5.9575	82.1063	16.5179	2
P33527	ABCC1	1	3	171480	6.6958	81.7905	26.6492	8
Q9Y6D6	ARFGEF1	1	2	208633	5.4756	81.6114	13.2504	5
Q9H2K2	TNKS2	1	2	126838	6.7573	81.5997	22.9846	3
Q9BRS2	RIOK1	1	2	65541	5.7686	81.4463	29.4014	2
O94988	FAM13A	1	2	116859	6.0352	81.3613	21.5054	2
Q9H1R3	MYLK2	1	3	64643	6.6182	81.1688	20.302	4
Q02880	TOP2B	1	3	183151	7.9834	81.115	18.5732	8
Q6PJI9	WDR59	1	2	109723	7.7593	81.034	10.7803	1
Q659A1	ICE2	1	2	109941	6.687	81.0072	14.8676	5
Q9UGU0	TCF20	1	3	211639	9.2593	80.9406	19.0816	4

Accession no	Gene	Evidence level	Sequence version	mW (Da)	PI (pH)	PLGS Score	Coverage (%)	Modified peptides
Q86X10	RALGAPB	1	1	166691	6.3223	80.5457	13.3869	2
Q12768	WASHC5	1	1	134200	6.5347	80.5415	16.9111	2
Q9H7N4	SCAF1	1	3	139186	9.624	80.4043	15.7012	1
P08631	HCK	1	5	59561	6.2607	80.3256	22.0532	1
Q9UHW9	SLC12A6	1	2	127534	6.6387	80.276	16.5217	4
Q9UK32	RPS6KA6	1	1	83818	5.8901	80.2571	18.255	1
Q13363	CTBP1	1	2	47505	6.293	80.1855	6.3636	0
Q02297	NRG1	1	3	70347	8.9531	79.6975	13.125	0
Q14498	RBM39	1	2	59342	10.4956	79.6747	14.5283	3
P49736	MCM2	1	4	101832	5.1943	79.6692	23.2301	3
Q6DN90	IQSEC1	1	1	108247	6.4893	79.6411	18.2762	1
Q96N16	JAKMIP1	1	1	73164	5.7451	79.3457	13.099	2
O14929	HAT1	1	2	49508	5.3716	79.0335	10.5012	0
Q5VT25	CDC42BPA	1	1	197181	6.1333	79.0071	19.515	5



Accession no	Gene	Evidence level	Sequence version	mW (Da)	PI (pH)	PLGS Score	Coverage (%)	Modified peptides
Q14527	HLTF	1	2	113856	8.6982	78.9832	16.9475	2
O75143	ATG13	1	1	56536	4.8032	78.631	24.9516	1
Q96T92	INSM2	1	3	59454	9.5171	78.5612	11.8375	0
Q96PC5	MIA2	1	4	159735	4.418	78.5396	14.8017	3
Q96Q89	KIF20B	1	3	210498	5.3906	78.433	22.8571	3
Q13470	TNK1	1	3	72421	9.7764	78.4307	8.7087	0
P16234	PDGFRA	1	1	122591	4.8779	78.2531	24.5179	3
P17980	PSMC3	1	3	49172	4.9409	78.2464	23.4624	3
P49815	TSC2	1	2	200480	6.9302	78.1362	18.7604	4
Q7Z406	MYH14	1	2	227730	5.3584	78.1136	19.4486	3
Q6AHZ1	ZNF518A	1	2	166675	9.6094	78.1109	22.1173	4
Q8TEU7	RAPGEF6	1	2	179309	5.9502	77.8389	19.8001	5
Q86VX9	MON1A	1	3	72849	8.1167	77.8304	13.0368	1
Q8NI08	NCOA7	1	2	106095	5.2749	77.3996	9.6603	1

Accession no	Gene	Evidence level	Sequence version	mW (Da)	PI (pH)	PLGS Score	Coverage (%)	Modified peptides
Q8NFG4	FLCN	1	1	64432	5.7876	77.3646	12.6079	2
Q8N6Y1	PCDH20	2	2	104853	4.7271	77.2845	10.3049	1
Q9NX02	NLRP2	1	1	120437	5.6675	77.171	8.3804	0
Q9H1H9	KIF13A	1	2	202181	5.291	77.0296	20.4432	10
P11388	TOP2A	1	3	174275	8.9897	76.3048	24.6244	10
O14645	DNALI1	1	2	29643	8.6704	76.2981	17.8295	3
Q13464	ROCK1	1	1	158074	5.5488	76.097	25.4062	5
Q8NC51	SERBP1	1	2	44938	9.1304	75.7064	17.402	1
Q15833	STXBP2	1	2	66410	6.0908	75.5149	26.4755	2
Q5U5Z8	AGBL2	1	2	104127	9.1758	75.4888	19.4013	3
Q5T6F0	DCAF12	1	1	50485	9.3018	75.3102	24.0618	1
P51168	SCNN1B	1	2	72611	5.8564	75.2133	13.2813	1
P29322	EPHA8	1	2	110931	7.9336	74.748	18.9055	4
P51784	USP11	1	3	109747	5.1313	74.7475	23.053	3

Accession no	Gene	Evidence level	Sequence version	mW (Da)	PI (pH)	PLGS Score	Coverage (%)	Modified peptides
Q13129	RLF	1	2	217812	6.3076	74.2323	19.0178	8
P78310	CXADR	1	1	40004	7.4355	74.0766	18.9041	0
O94993	SOX30	1	1	81803	6.9741	73.9393	17.3971	0
Q9UNF1	MAGED2	1	2	64914	9.7148	73.9392	18.3168	4
Q8WU20	FRS2	1	4	56994	5.5605	73.9183	15.5512	0
Q96T88	UHRF1	1	1	89756	7.3579	73.8877	25.599	4
Q16643	DBN1	1	4	71385	4.2026	73.8755	18.0277	0
P13497	BMP1	1	2	111177	6.457	73.8433	17.7485	2
Q9UHB7	AFF4	1	1	127381	9.6855	73.8297	26.7412	5
P51617	IRAK1	1	2	76488	6.1685	73.785	15.4494	3
Q08378	GOLGA3	1	2	167251	5.1724	73.6366	24.2991	9
Q92932	PTPRN2	1	2	111202	5.4478	73.6156	22.4631	1
Q96QB1	DLC1	1	4	170484	5.9458	73.4268	17.6702	4
Q92499	DDX1	1	2	82379	6.813	73.4256	16.3514	2

<b>Accession no</b>	<b>Gene</b>	<b>Evidence level</b>	<b>Sequence version</b>	<b>mW (Da)</b>	<b>PI (pH)</b>	<b>PLGS Score</b>	<b>Coverage (%)</b>	<b>Modified peptides</b>
O75132	ZBED4	1	2	130238	6.3691	73.4009	17.848	2
A8MWY0	ELAPOR2	1	2	113767	5.6748	73.2265	12.828	2
O14511	NRG2	1	1	91621	9.5933	73.2158	11.6471	0
Q9UN79	SOX13	1	3	69184	6.2505	73.1384	30.0643	2
A2A2Y4	FRMD3	1	1	68728	5.9429	72.9831	24.9581	3
Q8WUJ3	CEMIP	1	2	152900	7.6699	72.7419	13.7399	3
Q6ZN16	MAP3K15	1	2	147344	5.291	72.5141	16.9078	3
P42679	MATK	1	1	56433	8.9634	72.4643	13.8067	1
Q8TD06	AGR3	1	1	19158	8.1855	72.1549	24.0964	0
Q9BYT3	STK33	1	1	57794	6.6226	72.091	20.2335	2
Q14296	FASTK	1	1	61065	10.1323	71.8454	8.561	0
Q13547	HDAC	1	1	55067	5.1636	71.7727	20.9544	3
P21675	TAF1	1	3	214577	4.7637	71.7177	13.7348	6
P28799	GRN	1	2	63499	6.394	71.2697	14.8398	1

Accession no	Gene	Evidence level	Sequence version	mW (Da)	PI (pH)	PLGS Score	Coverage (%)	Modified peptides
Q9UBC3	DNMT3B	1	1	95690	8.3672	71.1975	21.5709	7
Q6ZN28	MACC1	1	2	96577	6.4365	71.1013	21.1268	5
Q16620	NTRK2	1	1	91939	6	70.8246	28.5888	4
O75923	DYSF	1	1	237142	5.3042	70.672	16.8269	6
Q7L1V2	MON1B	1	1	59180	5.8447	70.6059	11.883	0
Q16696	CYP2A13	1	3	56651	9.6138	70.2214	14.5749	1
O60237	PPP1R12B	1	2	110336	5.3833	70.2163	16.0896	2
P98174	FGD1	1	2	106494	6.123	70.1909	10.0937	0
Q8WW38	ZFPM2	1	3	128077	6.0088	69.7057	18.3319	3
Q13459	MYO9B	1	3	243247	8.8989	69.6954	15.9481	6
P01127	PDGFB	1	1	27266	9.4131	69.5747	18.2573	0
F8WD03	HYDIN	4	1	81515	5.8916	69.5517	21.2414	4
P12645	BMP3	1	2	53338	9.9185	69.3779	28.6017	2
Q8WYB5	KAT6B	1	3	231231	5.5913	69.326	12.9281	3

Accession no	Gene	Evidence level	Sequence version	mW (Da)	PI (pH)	PLGS Score	Coverage (%)	Modified peptides
O15164	TRIM24	1	3	116757	6.7017	69.2323	19.1429	3
Q96JG6	YPS50	1	3	111103	5.7847	69.1635	20.7469	2
P51532	SMARCA4	1	2	184529	7.7856	69.1407	14.5719	4
P0DMS8	ADORA3	1	1	36160	8.9634	69.0583	9.7484	0
Q149M9	NWD1	1	3	174440	6.2725	69.0296	28.0691	3
Q9NZM1	MYOF	1	1	234558	5.7642	68.1271	15.5264	4
Q8IXI2	RHOT1	1	2	70739	5.8271	68.0672	14.7249	0
P35916	FLT4	1	3	152660	5.8623	67.7283	28.4666	3
Q92834	RPGR	1	2	113315	4.5952	67.636	20.7843	6
O15055	PER2	1	2	136493	6.0146	67.6306	12.4303	3
Q8IX12	CCAR1	1	2	132738	5.4272	67.439	12.7826	1
Q69YN4	VIRMA	1	2	201897	4.7124	67.4177	17.7152	3
Q13705	ACVR2B	1	3	57686	5.3511	67.2413	24.0234	4
A0A097ZMP4	CUX1-RETc	2	1	74228	5.7964	66.831	14.2195	2

Accession no	Gene	Evidence level	Sequence version	mW (Da)	PI (pH)	PLGS Score	Coverage (%)	Modified peptides
Q8IX15	HOMEZ	1	2	61202	4.6685	66.7939	9.6364	1
Q9NWM0	SMOX	1	1	61780	5.1475	66.7614	17.1171	2
P06213	INSR	1	4	156232	5.7744	66.5861	24.7467	6
Q8N163	CCAR2	1	2	102837	4.9673	66.5186	9.5341	0
Q8NEC7	GSTCD	1	2	71032	7.6274	66.008	15.7978	0
Q8N5R6	CCDC33	1	3	107149	6.3105	65.9196	22.1294	2
Q76I76	SSH2	1	1	158115	5.1123	65.865	20.2389	5
Q5T0N5	FNBP1L	1	3	70021	6.1787	65.7513	26.281	3
Q9BQS8	FYCO1	1	3	166878	4.6685	65.4889	25.8457	7
P19474	TRIM21	1	1	54135	5.9429	65.2934	17.8947	1
Q92597	NDRG1	1	1	42807	5.4111	64.9374	10.1523	0
Q6R2W3	SCAND3	1	1	151569	6.2725	64.9287	22.6415	4
Q9BY21	GPR87	2	1	41408	9.6636	64.8825	14.5251	1
Q96S15	WDR24	1	2	88150	6.0439	64.8664	16.962	3

Accession no	Gene	Evidence level	Sequence version	mW (Da)	PI (pH)	PLGS Score	Coverage (%)	Modified peptides
Q9Y6D5	ARFGEF2	1	3	201908	5.8916	64.8288	15.8543	5
O15091	PRORP	1	2	67272	8.9033	64.6878	14.7513	0
P49746	THBS3	1	1	104134	4.2363	64.551	11.6109	1
A0A0A8K8C2	URLC7	2	1	13241	12.1333	64.4751	28.4553	0
Q96R06	SPAG5	1	2	134337	4.7476	64.2606	13.1601	3
P46940	IQGAP1	1	1	189132	6.041	64.2427	14.6651	6
Q15643	TRIP11	1	3	227445	5.0112	64.1944	22.5872	7
Q8TD19	NEK9	1	2	107100	5.3906	63.9612	23.3912	6
P12757	SKIL	1	2	76926	6.709	63.8732	29.386	4
Q86U86	PBRM1	1	1	192823	6.4424	63.777	19.4198	11
Q16659	MAPK6	1	1	82628	4.73	63.7154	19.1401	3
Q14160	SCRIB	1	5	174807	4.8164	63.6211	9.9387	1
B7Z7E5	FLJ58703	2	1	60672	9.4673	63.5718	33.2724	4
P00749	PLAU	1	3	48491	8.3291	63.5604	17.4014	1



Accession no	Gene	Evidence level	Sequence version	mW (Da)	PI (pH)	PLGS Score	Coverage (%)	Modified peptides
Q7Z2Z1	TICRR	1	2	210723	8.8828	63.5181	18.8482	4
Q13619	CUL4A	1	3	87624	8.146	63.4503	19.2358	3
Q9BPY3	FAM118B	1	1	39474	5.5723	63.3311	26.7806	1
Q9NRM7	LATS2	1	2	120060	8.1563	63.3165	14.614	1
Q13191	CBLB	1	2	109380	7.7388	63.2524	11.0998	0
Q8N1T3	MYO1H	1	2	118961	9.3032	63.1317	15.6977	1
Q14145	KEAP1	1	2	69620	5.981	63.1262	26.2821	3
O60524	NEMF	1	4	122877	5.9194	63.0561	17.1933	4
P35968	KDR	1	2	151430	5.4902	62.9106	22.5664	8
Q07912	TNK2	1	3	114496	6.8452	62.903	17.052	3
Q96PK6	RBM	1	4	69448	9.8042	62.7118	9.417	0
Q9Y6Q9	NCOA3	1	1	155194	7.1455	62.6569	24.7191	5
Q96S52	PIGS	1	3	61617	6.0308	62.4311	9.9099	1
Q52LW3	ARHGAP29	1	2	141973	6.3003	62.3342	23.5527	5

Accession no	Gene	Evidence level	Sequence version	mW (Da)	PI (pH)	PLGS Score	Coverage (%)	Modified peptides
Q9H7Z7	PTGES2	1	2	41916	9.4072	62.2539	27.0557	2
Q6UXH8	CCBE1	1	1	44074	7.4106	62.0978	12.069	1
P40227	CCT6A	1	3	57987	6.2241	61.9469	20.904	3
Q9H4B4	PLK3	1	2	71584	9.3589	61.4301	20.1238	4
Q12931	TRAP1	1	3	80059	8.2852	61.3725	19.0341	3
Q96L96	ALPK3	1	3	180558	6.1274	61.3472	17.478	2
Q53GL7	PARP10	1	2	109930	4.7168	61.2608	17.1707	5
Q5VV67	PPRC1	1	1	177433	6.0718	61.1381	11.6587	0
P18074	ERCC2	1	1	86854	6.7324	61.0118	16.4474	1
A7KAX9	ARHGAP32	1	1	230383	6.2666	60.3869	18.8788	7
Q96SN8	CDK5RAP2	1	5	214903	5.2954	60.3519	15.1083	5
O60477	BRINP1	1	2	88703	8.9575	60.3397	25.7556	2
Q02763	TEK	1	2	125749	6.4468	60.3324	15.2135	2
O95835	LATS1	1	1	126789	8.8726	60.1441	15.3097	5

Accession no	Gene	Evidence level	Sequence version	mW (Da)	PI (pH)	PLGS Score	Coverage (%)	Modified peptides
Q9BZF3	OSBPL6	1	1	106238	6.4775	59.8919	23.8758	3
Q86V15	CASZ1	1	4	189947	6.5815	59.7671	18.249	5
Q8IWX8	CHERP	1	3	103637	9.2593	59.7431	11.2445	2
P35228	NOS2	1	2	131033	7.8091	59.6576	14.3105	2
O43303	CCP110	1	3	113352	8.7935	59.6359	20.8498	4
P07333	CSF1R	1	2	107915	5.9063	59.5431	10.5967	3
Q8IZA0	KIAA0319L	1	2	115585	5.6353	59.5288	15.3479	1
Q8TAT5	NEIL3	1	3	67725	9.126	59.3997	20.1653	3
P16615	ATP2A2	1	1	114682	5.0522	59.3595	12.572	2
Q58F21	BRDT	1	4	107886	9.2842	59.2595	19.3242	3
Q9ULW0	TPX2	1	2	85600	9.6387	59.2207	11.3788	0
Q96KR6	FAM210B	1	2	20411	10.8442	59.1766	11.4583	1
Q6T4R5	NHS	1	2	179024	6.394	59.1487	11.6899	0
P27708	CAD	1	3	242827	5.9927	58.9152	15.5955	6

Accession no	Gene	Evidence level	Sequence version	mW (Da)	PI (pH)	PLGS Score	Coverage (%)	Modified peptides
Q09013	DMPK	1	3	69341	4.7329	58.8585	18.7599	2
Q9Y219	JAG2	1	3	133277	5.4316	58.7748	8.7237	0
Q9NS56	TOPORS	1	1	119124	9.7969	58.73	10.1435	1
O95803	NDST3	1	1	100837	7.9907	58.6112	4.2383	0
Q8TE59	ADAMTS19	1	2	133960	7.3462	58.4964	13.5046	3
G5EA03	LIMCH1	1	1	164336	5.9312	52.9718	13.6333	2
W0S1J7	Pe7Fe14	2	1	96217	4.3857	48.9289	15.035	3
Q9Y238	DLEC1	1	2	195558	5.8872	43.4596	11.0541	6
F8VUA7	OSBPL8	1	8	79003	6.3311	41.4498	13.5447	1
P16591	FER	1	2	94577	6.731	29.2282	18.6131	7

This table summarizes key peptide properties, demonstrating the molecular weight, isoelectric point, sequence coverage, and any post-translational modifications identified in the LC-MS analysis.

## Chapter – 5

### SIGNIFICANCE OF STUDY

The exploration embarked upon in this study ventures into the very heart of one of humanity's most formidable adversaries: lung cancer. As the second most prevalent affliction worldwide, trailing only behind cardiovascular disease, lung cancer exacts a staggering toll on global health. Conventional therapeutic modalities, though valiant in their efforts, grapple with formidable limitations. These incumbents, fraught with adverse effects and prone to engendering remission and resistance, underscore the pressing imperative for pioneering treatments.

In response to this clarion call for innovation, this research unveils the potential of two novel agents, Diosmin and Hesperidin, as heralds of a transformative era in lung cancer therapy. Positioned as ROS1 and EGFR inhibitors, their emergence onto the stage of medical intervention heralds a paradigm shift of monumental proportions. Leveraging a tapestry of advanced computational methodologies, spanning from in-silico molecular docking to rigorous in-vitro investigations, this inquiry orchestrates a symphony of analysis elucidating the therapeutic prowess of Diosmin and Hesperidin.

Central to this endeavour is the intricate choreography of molecular docking, a ballet of molecular interaction wherein ligands pirouette into the receptive embrace of target receptors. Through the auspices of esteemed algorithms such as GOLD and GLIDE, this ballet attains an unparalleled precision and fidelity, furnishing a scaffold upon which future therapeutic innovations may ascend.

Yet, the tapestry of discovery is interwoven with the threads of pharmacokinetic exigency, wherein the symphony of drug development finds its rhythm. Factors as profound as the role of Pgp in hepatic metabolism and the adherence to Lipinski's rule for pharmacokinetic favourability are meticulously honoured, ensuring that the journey from bench to bedside remains steadfast and efficacious.

In the crucible of molecular dynamics simulations, the ligand-receptor complex emerges not as static entities, but as dynamic landscapes sculpted by the tempestuous

winds of solvent dynamics. Here, the essence of molecular interaction unfurls in all its complexity, bestowing upon the investigator a vista of insight into the fluid dynamics that govern therapeutic efficacy.

Yet, it is not solely within the ethereal realms of computational analysis that the significance of this study is rendered manifest. In the crucible of the laboratory, amidst the clatter of glassware and the hum of instrumentation, Diosmin and Hesperidin emerge as stalwart sentinels, wielding their potency against the insidious machinations of lung cancer.

In this synthesis of computational ingenuity and experimental validation, this research bequeaths not mere theoretical conjecture, but tangible hope to those confronting the harrowing spectre of lung cancer. It stands as a beacon, illuminating the path towards a future wherein targeted therapies usher in a new era of efficacy and compassion in the battle against this formidable foe.

In its totality, this study transcends the realm of mere scientific inquiry; it is a testament to human resilience, ingenuity, and unwavering determination in the face of adversity. It heralds a future wherein the shadows of lung cancer are dispersed by the radiant light of discovery, beckoning forth a new dawn of healing and hope.

From a societal perspective, this research addresses a pressing global health challenge, offering a pathway to more affordable, accessible, and effective treatments for LC. By leveraging naturally occurring compounds with proven health benefits, this study aligns with the growing demand for safer, nature-inspired therapeutics, making it a valuable addition to cancer research and treatment paradigms.

## REFERENCES

- Acquaviva, J., Wong, R., & Charest, A. (2009). The multifaceted roles of the receptor tyrosine kinase ROS in development and cancer. *Biochimica et Biophysica Acta*, 1795(1), 37–52. <https://doi.org/10.1016/j.bbcan.2008.07.006>
- Aggarwal, V., Tuli, H. S., Thakral, F., Singhal, P., Aggarwal, D., Srivastava, S., Pandey, A., Sak, K., Varol, M., Khan, M. A., & Sethi, G. (2020). Molecular mechanisms of action of hesperidin in cancer: Recent trends and advancements. *Experimental Biology and Medicine (Maywood, N.J.)*, 245(5), 486–497. <https://doi.org/10.1177/1535370220903671>
- Ali, M. A., Vuree, S., Goud, H., Hussain, T., Nayariseri, A., & Singh, S. K. (2019). Identification of high-affinity small molecules targeting Gamma secretase for the treatment of Alzheimer's disease. *Current Topics in Medicinal Chemistry*, 19(13). <https://doi.org/10.2174/1568026619666190617155326>
- Assoian, R. K., & Zhu, X. (1997). Cell anchorage and the cytoskeleton as partners in growth factor dependent cell cycle progression. *Current Opinion in Cell Biology*, 9(1), 93–98. [https://doi.org/10.1016/s0955-0674\(97\)80157-3](https://doi.org/10.1016/s0955-0674(97)80157-3)
- Barta, J. A., Powell, C. A., & Wisnivesky, J. P. (2019). Global epidemiology of lung cancer. *Annals of Global Health*, 85(1), 1–16. <https://doi.org/10.5334/aogh.2419>
- Batra, P., & Sharma, A. K. (2013). Anti-cancer potential of flavonoids: recent trends and future perspectives. *3 Biotech*, 3(6), 439–459. <https://doi.org/10.1007/s13205-013-0117-5>
- Baylin, S. B., & Jones, P. A. (2016). Epigenetic determinants of cancer. *Cold Spring Harbor Perspectives in Biology*, 8(9). <https://doi.org/10.1101/cshperspect.a019505>
- Berk, Ş., Kaya, S., Akkol, E. K., & Bardakçı, H. (2022). A comprehensive and current review on the role of flavonoids in lung cancer—Experimental and

- theoretical approaches. *Phytomedicine*, 98, 153938.  
<https://doi.org/https://doi.org/10.1016/j.phymed.2022.153938>
- Bosetti, C., Bravi, F., Talamini, R., Parpinel, M., Gnagnarella, P., Negri, E., Montella, M., Lagiou, P., Franceschi, S., & La Vecchia, C. (2006). Flavonoids and prostate cancer risk: a study in Italy. *Nutrition and Cancer*, 56(2), 123–127. [https://doi.org/10.1207/s15327914nc5602\\_1](https://doi.org/10.1207/s15327914nc5602_1)
- Braicu, C., Mehterov, N., Vladimirov, B., Sarafian, V., Nabavi, S. M., Atanasov, A. G., & Berindan-Neagoe, I. (2017). Nutrigenomics in cancer: Revisiting the effects of natural compounds. *Seminars in Cancer Biology*, 46, 84–106. <https://doi.org/10.1016/j.semcancer.2017.06.011>
- Bray, F., Ferlay, J., Soerjomataram, I., Siegel, R. L., Torre, L. A., & Jemal, A. (2018). Global cancer statistics 2018: GLOBOCAN estimates of incidence and mortality worldwide for 36 cancers in 185 countries. *CA: A Cancer Journal for Clinicians*, 68(6), 394–424.
- Budisan, L., Gulei, D., Zanoaga, O. M., Irimie, A. I., Sergiu, C., Braicu, C., Gherman, C. D., & Berindan-Neagoe, I. (2017). Dietary Intervention by Phytochemicals and Their Role in Modulating Coding and Non-Coding Genes in Cancer. *International Journal of Molecular Sciences*, 18(6). <https://doi.org/10.3390/ijms18061178>
- Chen, H., Zhu, J., Le, Y., Pan, J., Liu, Y., Liu, Z., Wang, C., Dou, X., & Lu, D. (2022). Salidroside inhibits doxorubicin-induced cardiomyopathy by modulating a ferroptosis-dependent pathway. *Phytomedicine: International Journal of Phytotherapy and Phytopharmacology*, 99, 153964. <https://doi.org/10.1016/j.phymed.2022.153964>
- Chen, J. (2016). The Cell-Cycle Arrest and Apoptotic Functions of p53 in Tumor Initiation and Progression. *Cold Spring Harbor Perspectives in Medicine*, 6(3), a026104. <https://doi.org/10.1101/cshperspect.a026104>
- Choong, N. W., Dietrich, S., Seiwert, T. Y., Tretiakova, M. S., Nallasura, V., Davies, G. C., Lipkowitz, S., Husain, A. N., Salgia, R., & Ma, P. C. (2006). Gefitinib



- response of erlotinib-refractory lung cancer involving meninges--role of EGFR mutation. *Nature Clinical Practice. Oncology*, 3(1), 50–57; quiz 1 p following 57. <https://doi.org/10.1038/ncponc0400>
- Comprehensive genomic characterization of squamous cell lung cancers. (2012). *Nature*, 489(7417), 519–525. <https://doi.org/10.1038/nature11404>
- Cui, M., Han, Y., Li, P., Zhang, J., Ou, Q., Tong, X., Zhao, R., Dong, N., Wu, X., Li, W., & Jiang, G. (2020). Molecular and clinicopathological characteristics of ROS1-rearranged non-small-cell lung cancers identified by next-generation sequencing. *Molecular Oncology*, 14(11), 2787–2795. <https://doi.org/10.1002/1878-0261.12789>
- Daina, A., Michielin, O., & Zoete, V. (2017). SwissADME: a free web tool to evaluate pharmacokinetics, drug-likeness and medicinal chemistry friendliness of small molecules. *Scientific Reports*, 7(1), 42717. <https://doi.org/10.1038/srep42717>
- Davies, K. D., & Doebele, R. C. (2013). Molecular pathways: ROS1 fusion proteins in cancer. *Clinical Cancer Research: An Official Journal of the American Association for Cancer Research*, 19(15), 4040–4045. <https://doi.org/10.1158/1078-0432.CCR-12-2851>
- Denisenko, T. V., Budkevich, I. N., & Zhivotovsky, B. (2018). Cell death-based treatment of lung adenocarcinoma. *Cell Death & Disease*, 9(2), 117. <https://doi.org/10.1038/s41419-017-0063-y>
- Dias, M. C., Pinto, D. C. G. A., & Silva, A. M. S. (2021). Plant Flavonoids: Chemical Characteristics and Biological Activity. *Molecules (Basel, Switzerland)*, 26(17). <https://doi.org/10.3390/molecules26175377>
- Ding, L., Getz, G., Wheeler, D. A., Mardis, E. R., McLellan, M. D., Cibulskis, K., Sougnez, C., Greulich, H., Muzny, D. M., Morgan, M. B., Fulton, L., Fulton, R. S., Zhang, Q., Wendl, M. C., Lawrence, M. S., Larson, D. E., Chen, K., Dooling, D. J., Sabo, A., ... Wilson, R. K. (2008). Somatic mutations affect

key pathways in lung adenocarcinoma. *Nature*, 455(7216), 1069–1075.  
<https://doi.org/10.1038/nature07423>

Falcone Ferreyra, M. L., Rius, S. P., & Casati, P. (2012). Flavonoids: biosynthesis, biological functions, and biotechnological applications. *Frontiers in Plant Science*, 3, 222. <https://doi.org/10.3389/fpls.2012.00222>

Ferlay, J., Soerjomataram, I., Dikshit, R., Eser, S., Mathers, C., Rebelo, M., Parkin, D. M., Forman, D., & Bray, F. (2015). Cancer incidence and mortality worldwide: sources, methods and major patterns in GLOBOCAN 2012. *International Journal of Cancer*, 136(5), E359–E386.

Fidler, I. J. (2003). The pathogenesis of cancer metastasis: the “seed and soil” hypothesis revisited. *Nature Reviews. Cancer*, 3(6), 453–458.  
<https://doi.org/10.1038/nrc1098>

Fitzmaurice, C., Abate, D., Abbasi, N., Abbastabar, H., Abd-Allah, F., Abdel-Rahman, O., Abdelalim, A., Abdoli, A., Abdollahpour, I., Abdulle, A. S. M., Abebe, N. D., Abraha, H. N., Abu-Raddad, L. J., Abualhasan, A., Adedeji, I. A., Advani, S. M., Afarideh, M., Afshari, M., Aghaali, M., ... Murray, C. J. L. (2019). Global, Regional, and National Cancer Incidence, Mortality, Years of Life Lost, Years Lived With Disability, and Disability-Adjusted Life-Years for 29 Cancer Groups, 1990 to 2017: A Systematic Analysis for the Global Burden of Disease Study. *JAMA Oncology*, 5(12), 1749–1768.  
<https://doi.org/10.1001/jamaoncol.2019.2996>

Gazdar, A. F., Shigematsu, H., Herz, J., & Minna, J. D. (2004). Mutations and addiction to EGFR: the Achilles “heal” of lung cancers? *Trends in Molecular Medicine*, 10(10), 481–486. <https://doi.org/10.1016/j.molmed.2004.08.008>

Global burden of 87 risk factors in 204 countries and territories, 1990-2019: a systematic analysis for the Global Burden of Disease Study 2019. (2020). *Lancet (London, England)*, 396(10258), 1223–1249.  
[https://doi.org/10.1016/S0140-6736\(20\)30752-2](https://doi.org/10.1016/S0140-6736(20)30752-2)

- Govindan, R., Ding, L., Griffith, M., Subramanian, J., Dees, N. D., Kanchi, K. L., Maher, C. A., Fulton, R., Fulton, L., Wallis, J., Chen, K., Walker, J., McDonald, S., Bose, R., Ornitz, D., Xiong, D., You, M., Dooling, D. J., Watson, M., ... Wilson, R. K. (2012). Genomic landscape of non-small cell lung cancer in smokers and never-smokers. *Cell*, 150(6), 1121–1134. <https://doi.org/10.1016/j.cell.2012.08.024>
- Greulich, H., Chen, T.-H., Feng, W., Jänne, P. A., Alvarez, J. V., Zappaterra, M., Bulmer, S. E., Frank, D. A., Hahn, W. C., Sellers, W. R., & Meyerson, M. (2005). Oncogenic transformation by inhibitor-sensitive and -resistant EGFR mutants. *PLoS Medicine*, 2(11), e313. <https://doi.org/10.1371/journal.pmed.0020313>
- Hamilton-Reeves, J. M., Banerjee, S., Banerjee, S. K., Holzbeierlein, J. M., Thrasher, J. B., Kambhampati, S., Keighley, J., & Van Veldhuizen, P. (2013). Short-term soy isoflavone intervention in patients with localized prostate cancer: a randomized, double-blind, placebo-controlled trial. *PloS One*, 8(7), e68331. <https://doi.org/10.1371/journal.pone.0068331>
- Hitomi, M., Shu, J., Agarwal, M., Agarwal, A., & Stacey, D. W. (1998). p21Waf1 inhibits the activity of cyclin dependent kinase 2 by preventing its activating phosphorylation. *Oncogene*, 17(8), 959–969. <https://doi.org/10.1038/sj.onc.1202005>
- Hollman, P. C., Van Het Hof, K. H., Tijburg, L. B., & Katan, M. B. (2001). Addition of milk does not affect the absorption of flavonols from tea in man. *Free Radical Research*, 34(3), 297–300. <https://doi.org/10.1080/10715760100300261>
- Huang, R. S. P., Haberberger, J., Sokol, E., Schrock, A. B., Danziger, N., Madison, R., Trabucco, S., Jin, D., Pavlick, D., Ramanan, V., Hole, K., McGregor, K., Venstrom, J., & Ross, J. S. (2021). Clinicopathologic, genomic and protein expression characterization of 356 ROS1 fusion driven solid tumors cases. *International Journal of Cancer*, 148(7), 1778–1788. <https://doi.org/10.1002/ijc.33447>

- Ide, R., Fujino, Y., Hoshiyama, Y., Mizoue, T., Kubo, T., Pham, T.-M., Shirane, K., Tokui, N., Sakata, K., Tamakoshi, A., & Yoshimura, T. (2007). A prospective study of green tea consumption and oral cancer incidence in Japan. *Annals of Epidemiology*, 17(10), 821–826. <https://doi.org/10.1016/j.annepidem.2007.04.003>
- Isbrucker, R. A., Bausch, J., Edwards, J. A., & Wolz, E. (2006). Safety studies on epigallocatechin gallate (EGCG) preparations. Part 1: genotoxicity. *Food and Chemical Toxicology: An International Journal Published for the British Industrial Biological Research Association*, 44(5), 626–635. <https://doi.org/10.1016/j.fct.2005.07.005>
- Janisch, K. M., Williamson, G., Needs, P., & Plumb, G. W. (2004). Properties of quercetin conjugates: modulation of LDL oxidation and binding to human serum albumin. *Free Radical Research*, 38(8), 877–884. <https://doi.org/10.1080/10715760410001728415>
- Ju, Y. S., Lee, W.-C., Shin, J.-Y., Lee, S., Bleazard, T., Won, J.-K., Kim, Y. T., Kim, J.-I., Kang, J.-H., & Seo, J.-S. (2012). A transforming KIF5B and RET gene fusion in lung adenocarcinoma revealed from whole-genome and transcriptome sequencing. *Genome Research*, 22(3), 436–445. <https://doi.org/10.1101/gr.133645.111>
- Kermi, C., Aze, A., & Maiorano, D. (2019). Preserving Genome Integrity During the Early Embryonic DNA Replication Cycles. *Genes*, 10(5). <https://doi.org/10.3390/genes10050398>
- Khan, N., & Mukhtar, H. (2013). Tea and health: studies in humans. *Current Pharmaceutical Design*, 19(34), 6141–6147. <https://doi.org/10.2174/1381612811319340008>
- Kim, E. S. (2016). Chemotherapy Resistance in Lung Cancer. *Advances in Experimental Medicine and Biology*, 893, 189–209. [https://doi.org/10.1007/978-3-319-24223-1\\_10](https://doi.org/10.1007/978-3-319-24223-1_10)

- Kohno, T., Ichikawa, H., Totoki, Y., Yasuda, K., Hiramoto, M., Nammo, T., Sakamoto, H., Tsuta, K., Furuta, K., Shimada, Y., Iwakawa, R., Ogiwara, H., Oike, T., Enari, M., Schetter, A. J., Okayama, H., Haugen, A., Skaug, V., Chiku, S., ... Shibata, T. (2012). KIF5B-RET fusions in lung adenocarcinoma. *Nature Medicine*, 18(3), 375–377. <https://doi.org/10.1038/nm.2644>
- Kolodziej, M., Hoverman, J. R., Garey, J. S., Espirito, J., Sheth, S., Ginsburg, A., Neubauer, M. A., Patt, D., Brooks, B., White, C., Sitarik, M., Anderson, R., & Beveridge, R. (2011). Benchmarks for value in cancer care: an analysis of a large commercial population. *Journal of Oncology Practice*, 7(5), 301–306. <https://doi.org/10.1200/JOP.2011.000394>
- Kopustinskiene, D. M., Jakstas, V., Savickas, A., & Bernatoniene, J. (2020). Flavonoids as anticancer agents. *Nutrients*, 12(2), 1–25. <https://doi.org/10.3390/nu12020457>
- Kreeger, P. K., & Lauffenburger, D. A. (2010). Cancer systems biology: a network modeling perspective. *Carcinogenesis*, 31(1), 2–8. <https://doi.org/10.1093/carcin/bgp261>
- Kumar, S., & Pandey, A. K. (2013). Chemistry and Biological Activities of Flavonoids: An Overview. *The Scientific World Journal*, 2013, 162750. <https://doi.org/10.1155/2013/162750>
- Kurahashi, N., Sasazuki, S., Iwasaki, M., Inoue, M., & Tsugane, S. (2008). Green tea consumption and prostate cancer risk in Japanese men: a prospective study. *American Journal of Epidemiology*, 167(1), 71–77. <https://doi.org/10.1093/aje/kwm249>
- Li, Z., Ma, W., Ali, I., Zhao, H., Wang, D., & Qiu, J. (2020). Green and Facile Synthesis and Antioxidant and Antibacterial Evaluation of Dietary Myricetin-Mediated Silver Nanoparticles. *ACS Omega*, 5(50), 32632–32640. <https://doi.org/10.1021/acsomega.0c05002>

- Lipson, D., Capelletti, M., Yelensky, R., Otto, G., Parker, A., Jarosz, M., Curran, J. A., Balasubramanian, S., Bloom, T., Brennan, K. W., Donahue, A., Downing, S. R., Frampton, G. M., Garcia, L., Juhn, F., Mitchell, K. C., White, E., White, J., Zwirko, Z., ... Stephens, P. J. (2012). Identification of new ALK and RET gene fusions from colorectal and lung cancer biopsies. *Nature Medicine*, 18(3), 382–384. <https://doi.org/10.1038/nm.2673>
- Liskova, A., Koklesova, L., Samec, M., Smejkal, K., Samuel, S. M., Varghese, E., Abotaleb, M., Biringer, K., Kudela, E., Danko, J., Shakibaei, M., Kwon, T. K., Büsselberg, D., & Kubatka, P. (2020). Flavonoids in Cancer Metastasis. In *Cancers* (Vol. 12, Issue 6). <https://doi.org/10.3390/cancers12061498>
- Liu, J., Ren, H., Liu, B., Zhang, Q., Li, M., & Zhu, R. (2016). Diosmetin inhibits cell proliferation and induces apoptosis by regulating autophagy via the mammalian target of rapamycin pathway in hepatocellular carcinoma HepG2 cells. *Oncology Letters*, 12(6), 4385–4392.
- Liu, P., Morrison, C., Wang, L., Xiong, D., Vedell, P., Cui, P., Hua, X., Ding, F., Lu, Y., James, M., Ebben, J. D., Xu, H., Adjei, A. A., Head, K., Andrae, J. W., Tschannen, M. R., Jacob, H., Pan, J., Zhang, Q., ... You, M. (2012). Identification of somatic mutations in non-small cell lung carcinomas using whole-exome sequencing. *Carcinogenesis*, 33(7), 1270–1276. <https://doi.org/10.1093/carcin/bgs148>
- Lounnas, V., Ritschel, T., Kelder, J., McGuire, R., Bywater, R. P., & Foloppe, N. (2013). Current progress in structure-based rational drug design marks a new mindset in drug discovery. *Computational and Structural Biotechnology Journal*, 5(6), e201302011. <https://doi.org/10.5936/csbj.201302011>
- Lynch, T. J., Bell, D. W., Sordella, R., Gurubhagavatula, S., Okimoto, R. A., Brannigan, B. W., Harris, P. L., Haserlat, S. M., Supko, J. G., Haluska, F. G., Louis, D. N., Christiani, D. C., Settleman, J., & Haber, D. A. (2004). Activating mutations in the epidermal growth factor receptor underlying responsiveness of non-small-cell lung cancer to gefitinib. *The New England*

- Journal of Medicine*, 350(21), 2129–2139.  
<https://doi.org/10.1056/NEJMoa040938>
- Manach, C., Scalbert, A., Morand, C., Rémésy, C., & Jiménez, L. (2004). Polyphenols: food sources and bioavailability. *The American Journal of Clinical Nutrition*, 79(5), 727–747. <https://doi.org/10.1093/ajcn/79.5.727>
- McGuire, S. (2016). World Cancer Report 2014. Geneva, Switzerland: World Health Organization, International Agency for Research on Cancer, WHO Press, 2015. *Advances in Nutrition (Bethesda, Md.)*, 7(2), 418–419. <https://doi.org/10.3945/an.116.012211>
- Michael McClain, R., Wolz, E., Davidovich, A., & Bausch, J. (2006). Genetic toxicity studies with genistein. *Food and Chemical Toxicology: An International Journal Published for the British Industrial Biological Research Association*, 44(1), 42–55. <https://doi.org/10.1016/j.fct.2005.06.004>
- Muthumanickam, S., Indhumathi, T., Boomi, P., Balajee, R., Jeyakanthan, J., Anand, K., Ravikumar, S., Kumar, P., Sudha, A., & Jiang, Z. (2020). In silico approach of naringin as potent phosphatase and tensin homolog (PTEN) protein agonist against prostate cancer. *Journal of Biomolecular Structure and Dynamics*, 0(0), 1–10. <https://doi.org/10.1080/07391102.2020.1830855>
- Nemeth, K., & Piskula, M. K. (2007). Food content, processing, absorption and metabolism of onion flavonoids. *Critical Reviews in Food Science and Nutrition*, 47(4), 397–409. <https://doi.org/10.1080/10408390600846291>
- Newman, D. J., & Cragg, G. M. (2020). Natural products as sources of new drugs over the nearly four decades from 01/1981 to 09/2019. *Journal of Natural Products*, 83(3), 770–803.
- Obaya, A. J., & Sedivy, J. M. (2002). Regulation of cyclin-Cdk activity in mammalian cells. *Cellular and Molecular Life Sciences : CMLS*, 59(1), 126–142. <https://doi.org/10.1007/s00018-002-8410-1>

- Odle, B., Dennison, N., Al-Nakkash, L., Broderick, T. L., & Plochocki, J. H. (2017). Genistein treatment improves fracture resistance in obese diabetic mice. *BMC Endocrine Disorders*, 17(1), 1. <https://doi.org/10.1186/s12902-016-0144-4>
- Organization, W. H. (2019). *International agency for research on cancer*.
- Paez, J. G., Jänne, P. A., Lee, J. C., Tracy, S., Greulich, H., Gabriel, S., Herman, P., Kaye, F. J., Lindeman, N., Boggon, T. J., Naoki, K., Sasaki, H., Fujii, Y., Eck, M. J., Sellers, W. R., Johnson, B. E., & Meyerson, M. (2004). EGFR mutations in lung cancer: correlation with clinical response to gefitinib therapy. *Science (New York, N.Y.)*, 304(5676), 1497–1500. <https://doi.org/10.1126/science.1099314>
- Pao, W., Miller, V., Zakowski, M., Doherty, J., Politi, K., Sarkaria, I., Singh, B., Heelan, R., Rusch, V., Fulton, L., Mardis, E., Kupfer, D., Wilson, R., Kris, M., & Varmus, H. (2004). EGF receptor gene mutations are common in lung cancers from “never smokers” and are associated with sensitivity of tumors to gefitinib and erlotinib. *Proceedings of the National Academy of Sciences of the United States of America*, 101(36), 13306–13311. <https://doi.org/10.1073/pnas.0405220101>
- Patel, K., Gadewar, M., Tahilyani, V., & Patel, D. K. (2013). A review on pharmacological and analytical aspects of diosmetin: A concise report. In *Chinese Journal of Integrative Medicine* (Vol. 19, Issue 10, pp. 792–800). <https://doi.org/10.1007/s11655-013-1595-3>
- Patidar, K., Panwar, U., Vuree, S., Sweta, J., Sandhu, M. K., Nayariseri, A., & Singh, S. K. (2019). An in silico approach to identify high affinity small molecule targeting m-TOR inhibitors for the clinical treatment of breast cancer. *Asian Pacific Journal of Cancer Prevention*, 20(4). <https://doi.org/10.31557/APJCP.2019.20.4.1229>
- Pietanza, M. C., Byers, L. A., Minna, J. D., & Rudin, C. M. (2015). Small cell lung cancer: will recent progress lead to improved outcomes? *Clinical Cancer Research*, 21(10), 2244–2255.



- Pistritto, G., Trisciuglio, D., Ceci, C., Garufi, A., & D'Orazi, G. (2016). Apoptosis as anticancer mechanism: function and dysfunction of its modulators and targeted therapeutic strategies. *Aging*, 8(4), 603–619. <https://doi.org/10.18632/aging.100934>
- Ponte, L. G., Pavan, I. C., Mancini, M. C., da Silva, L. G., Morelli, A. P., Severino, M. B., Bezerra, R. M., & Simabuco, F. M. (2021). The Hallmarks of Flavonoids in Cancer. In *Molecules* (Vol. 26, Issue 7). <https://doi.org/10.3390/molecules26072029>
- Prasain, J. K., & Barnes, S. (2007). Metabolism and Bioavailability of Flavonoids in Chemoprevention: Current Analytical Strategies and Future Prospectus. *Molecular Pharmaceutics*, 4(6), 846–864. <https://doi.org/10.1021/mp700116u>
- Qiu, M., Wei, W., Zhang, J., Wang, H., Bai, Y., & Guo, D. (2023). A Scientometric Study to a Critical Review on Promising Anticancer and Neuroprotective Compounds: Citrus Flavonoids. In *Antioxidants* (Vol. 12, Issue 3). <https://doi.org/10.3390/antiox12030669>
- Rahmani, A. H., Babiker, A. Y., & Anwar, S. (2023). Hesperidin, a Bioflavonoid in Cancer Therapy: A Review for a Mechanism of Action through the Modulation of Cell Signaling Pathways. In *Molecules* (Vol. 28, Issue 13). <https://doi.org/10.3390/molecules28135152>
- Rahmanian, N., Hamishehkar, H., Dolatabadi, J. E. N., & Arsalani, N. (2014). Nano graphene oxide: A novel carrier for oral delivery of flavonoids. *Colloids and Surfaces B: Biointerfaces*, 123, 331–338. <https://doi.org/https://doi.org/10.1016/j.colsurfb.2014.09.036>
- Riaz, N., Havel, J. J., Makarov, V., Desrichard, A., Urba, W. J., Sims, J. S., Hodi, F. S., Martín-Algarra, S., Mandal, R., Sharfman, W. H., Bhatia, S., Hwu, W.-J., Gajewski, T. F., Slingsluff, C. L. J., Chowell, D., Kendall, S. M., Chang, H., Shah, R., Kuo, F., ... Chan, T. A. (2017). Tumor and Microenvironment Evolution during Immunotherapy with Nivolumab. *Cell*, 171(4), 934–949.e16. <https://doi.org/10.1016/j.cell.2017.09.028>

- Rikova, K., Guo, A., Zeng, Q., Possemato, A., Yu, J., Haack, H., Nardone, J., Lee, K., Reeves, C., Li, Y., Hu, Y., Tan, Z., Stokes, M., Sullivan, L., Mitchell, J., Wetzel, R., Macneill, J., Ren, J. M., Yuan, J., ... Comb, M. J. (2007). Global survey of phosphotyrosine signaling identifies oncogenic kinases in lung cancer. *Cell*, 131(6), 1190–1203. <https://doi.org/10.1016/j.cell.2007.11.025>
- Roskoski, R. J. (2017). ROS1 protein-tyrosine kinase inhibitors in the treatment of ROS1 fusion protein-driven non-small cell lung cancers. *Pharmacological Research*, 121, 202–212. <https://doi.org/10.1016/j.phrs.2017.04.022>
- Ruiz-Casado, A., Martín-Ruiz, A., Pérez, L. M., Provencio, M., Fiuza-Luces, C., & Lucia, A. (2017). Exercise and the Hallmarks of Cancer. *Trends in Cancer*, 3(6), 423–441. <https://doi.org/10.1016/j.trecan.2017.04.007>
- Saleemi, M. A., Alallam, B., Yong, Y. K., & Lim, V. (2022). Synthesis of Zinc Oxide Nanoparticles with Bioflavonoid Rutin: Characterisation, Antioxidant and Antimicrobial Activities and In Vivo Cytotoxic Effects on Artemia Nauplii. In *Antioxidants* (Vol. 11, Issue 10). <https://doi.org/10.3390/antiox11101853>
- Schiliro, C., & Firestein, B. L. (2021). Mechanisms of Metabolic Reprogramming in Cancer Cells Supporting Enhanced Growth and Proliferation. In *Cells* (Vol. 10, Issue 5). <https://doi.org/10.3390/cells10051056>
- seer. (n.d.). *No Title*. <https://seer.cancer.gov/statfacts/html/prost.html>
- Seyedi, S. S., Shukri, M., Hassandarvish, P., Oo, A., Shankar, E. M., Abubakar, S., & Zandi, K. (2016). Computational Approach Towards Exploring Potential Anti-Chikungunya Activity of Selected Flavonoids. *Scientific Reports*, 6, 24027. <https://doi.org/10.1038/srep24027>
- Shanmugam, S., Thangaraj, P., Lima, B. D. S., Chandran, R., de Souza Araújo, A. A., Narain, N., Serafini, M. R., & Júnior, L. J. Q. (2016). Effects of luteolin and quercetin 3-β-d-glucoside identified from Passiflora subpeltata leaves against acetaminophen induced hepatotoxicity in rats. *Biomedicine &*

- Pharmacotherapy = Biomedecine & Pharmacotherapie*, 83, 1278–1285.  
<https://doi.org/10.1016/j.biopha.2016.08.044>
- Sharp, A., Bhosle, J., Abdelraouf, F., Popat, S., O'Brien, M., & Yap, T. A. (2016). Development of molecularly targeted agents and immunotherapies in small cell lung cancer. *European Journal of Cancer*, 60, 26–39.
- Sheoran, S., Arora, S., Singh, H., Kumar, A., & Vuree, S. (2023). Characterisation, development and validation of UV spectrophotometric technique for the determination of Diosmetin in bulk and nanoformulations. *Results in Chemistry*, 100972.  
<https://doi.org/https://doi.org/10.1016/j.rechem.2023.100972>
- Siddiqui, M., & Rajkumar, S. V. (2012). The high cost of cancer drugs and what we can do about it. *Mayo Clinic Proceedings*, 87(10), 935–943.  
<https://doi.org/10.1016/j.mayocp.2012.07.007>
- Skoulidis, F., & Heymach, J. V. (2019). Co-occurring genomic alterations in non-small-cell lung cancer biology and therapy. *Nature Reviews Cancer*, 19(9), 495–509. <https://doi.org/10.1038/s41568-019-0179-8>
- Sordella, R., Bell, D. W., Haber, D. A., & Settleman, J. (2004). Gefitinib-sensitizing EGFR mutations in lung cancer activate anti-apoptotic pathways. *Science (New York, N.Y.)*, 305(5687), 1163–1167.  
<https://doi.org/10.1126/science.1101637>
- Spagnuolo, C., Russo, G. L., Orhan, I. E., Habtemariam, S., Daglia, M., Sureda, A., Nabavi, S. F., Devi, K. P., Loizzo, M. R., Tundis, R., & Nabavi, S. M. (2015). Genistein and Cancer: Current Status, Challenges, and Future Directions. *Advances in Nutrition*, 6(4), 408–419. <https://doi.org/10.3945/an.114.008052>
- Spencer, J. P. E., Abd-el-Mohsen, M. M., & Rice-Evans, C. (2004). Cellular uptake and metabolism of flavonoids and their metabolites: implications for their bioactivity. *Archives of Biochemistry and Biophysics*, 423(1), 148–161.  
<https://doi.org/10.1016/j.abb.2003.11.010>

- Sweta, J., Khandelwal, R., Srinitha, S., Pancholi, R., Adhikary, R., Ali, M. A., Nayarisseri, A., Vuree, S., & Singh, S. K. (2019). Identification of high-affinity small molecule targeting IDH2 for the clinical treatment of acute myeloid leukemia. *Asian Pacific Journal of Cancer Prevention*, 20(8). <https://doi.org/10.31557/APJCP.2019.20.8.2287>
- Takahashi, A., & Ohnishi, T. (2004). The significance of the study about the biological effects of solar ultraviolet radiation using the Exposed Facility on the International Space Station. *Uchu Seibutsu Kagaku*, 18(4), 255–260. <https://doi.org/10.2187/bss.18.255>
- Takeuchi, K., Soda, M., Togashi, Y., Suzuki, R., Sakata, S., Hatano, S., Asaka, R., Hamanaka, W., Ninomiya, H., Uehara, H., Lim Choi, Y., Satoh, Y., Okumura, S., Nakagawa, K., Mano, H., & Ishikawa, Y. (2012). RET, ROS1 and ALK fusions in lung cancer. *Nature Medicine*, 18(3), 378–381. <https://doi.org/10.1038/nm.2658>
- Tang, Z., Jiang, S., Du, R., Petri, E. T., El-Telbany, A., Chan, P. S. O., Kijima, T., Dietrich, S., Matsui, K., Kobayashi, M., Sasada, S., Okamoto, N., Suzuki, H., Kawahara, K., Iwasaki, T., Nakagawa, K., Kawase, I., Christensen, J. G., Hirashima, T., ... Ma, P. C. (2009). Disruption of the EGFR E884-R958 ion pair conserved in the human kinome differentially alters signaling and inhibitor sensitivity. *Oncogene*, 28(4), 518–533. <https://doi.org/10.1038/onc.2008.411>
- Testa, I., Salvatori, C., Di Cara, G., Latini, A., Frati, F., Troiani, S., Principi, N., & Esposito, S. (2018). Soy-Based Infant Formula: Are Phyto-Oestrogens Still in Doubt? . In *Frontiers in Nutrition* (Vol. 5). <https://www.frontiersin.org/articles/10.3389/fnut.2018.00110>
- Thandra, K. C., Barsouk, A., Saginala, K., Aluru, J. S., & Barsouk, A. (2021). Epidemiology of lung cancer. *Contemporary Oncology (Poznan, Poland)*, 25(1), 45–52. <https://doi.org/10.5114/wo.2021.103829>

- Torgovnick, A., & Schumacher, B. (2015). DNA repair mechanisms in cancer development and therapy. *Frontiers in Genetics*, 6, 157. <https://doi.org/10.3389/fgene.2015.00157>
- Travis, W. D., Brambilla, E., Nicholson, A. G., Yatabe, Y., Austin, J. H. M., Beasley, M. B., Chirieac, L. R., Dacic, S., Duhig, E., Flieder, D. B., Geisinger, K., Hirsch, F. R., Ishikawa, Y., Kerr, K. M., Noguchi, M., Pelosi, G., Powell, C. A., Tsao, M. S., & Wistuba, I. (2015). The 2015 World Health Organization Classification of Lung Tumors: Impact of Genetic, Clinical and Radiologic Advances Since the 2004 Classification. In *Journal of thoracic oncology : official publication of the International Association for the Study of Lung Cancer* (Vol. 10, Issue 9, pp. 1243–1260). <https://doi.org/10.1097/JTO.0000000000000630>
- Tröger, W., Zdrle, Z., Tišma, N., & Matijašević, M. (2014). Additional Therapy with a Mistletoe Product during Adjuvant Chemotherapy of Breast Cancer Patients Improves Quality of Life: An Open Randomized Clinical Pilot Trial. *Evidence-Based Complementary and Alternative Medicine : ECAM*, 2014, 430518. <https://doi.org/10.1155/2014/430518>
- Walker, E. H., Pacold, M. E., Perisic, O., Stephens, L., Hawkins, P. T., Wymann, M. P., & Williams, R. L. (2000). Structural determinants of phosphoinositide 3-kinase inhibition by wortmannin, LY294002, quercetin, myricetin, and staurosporine. *Molecular Cell*, 6(4), 909–919. [https://doi.org/10.1016/s1097-2765\(05\)00089-4](https://doi.org/10.1016/s1097-2765(05)00089-4)
- Walle, T. (2007). Methoxylated flavones, a superior cancer chemopreventive flavonoid subclass? *Seminars in Cancer Biology*, 17(5), 354–362. <https://doi.org/10.1016/j.semcancer.2007.05.002>
- Walle, T., Browning, A. M., Steed, L. L., Reed, S. G., & Walle, U. K. (2005). Flavonoid glucosides are hydrolyzed and thus activated in the oral cavity in humans. *The Journal of Nutrition*, 135(1), 48–52. <https://doi.org/10.1093/jn/135.1.48>

- Waqar, S. N., & Morgensztern, D. (2017). Treatment advances in small cell lung cancer (SCLC). *Pharmacology & Therapeutics*, 180, 16–23.
- Yadav, M., Khandelwal, R., Mudgal, U., Srinitha, S., Khandekar, N., Nayariseri, A., Vuree, S., & Singh, S. K. (2019). Identification of potent VEGF inhibitors for the clinical treatment of glioblastoma, a virtual screening approach. *Asian Pacific Journal of Cancer Prevention*, 20(9). <https://doi.org/10.31557/APJCP.2019.20.9.2681>
- Yamakoshi, J., Saito, M., Kataoka, S., & Kikuchi, M. (2002). Safety evaluation of proanthocyanidin-rich extract from grape seeds. *Food and Chemical Toxicology*, 40(5), 599–607. [https://doi.org/https://doi.org/10.1016/S0278-6915\(02\)00006-6](https://doi.org/10.1016/S0278-6915(02)00006-6)
- Yarden, Y., & Sliwkowski, M. X. (2001). Untangling the ErbB signalling network. *Nature Reviews. Molecular Cell Biology*, 2(2), 127–137. <https://doi.org/10.1038/35052073>
- Zeng, W., Rong, M., Hu, X., Xiao, W., Qi, F., Huang, J., & Luo, Z. (2014). Incorporation of chitosan microspheres into collagen-chitosan scaffolds for the controlled release of nerve growth factor. *PloS One*, 9(7), e101300.
- Zhang, H., Wang, Y., Bai, M., Wang, J., Zhu, K., Liu, R., Ge, S., Li, J., Ning, T., Deng, T., Fan, Q., Li, H., Sun, W., Ying, G., & Ba, Y. (2018). Exosomes serve as nanoparticles to suppress tumor growth and angiogenesis in gastric cancer by delivering hepatocyte growth factor siRNA. *Cancer Science*, 109(3), 629–641. <https://doi.org/10.1111/cas.13488>
- Zhang, Y., & He, J. (2013). The development of targeted therapy in small cell lung cancer. *Journal of Thoracic Disease*, 5(4), 538.

## LIST OF PUBLICATIONS

- Sumit Sheoran, **Swati Arora**, R. Samson, Pilli Govindaiah, Sugunakar Vuree, **“Lipid-based nanoparticles for treatment of cancer”** Heliyon cell press, Impact Factor 3.776 Volume 8, Issue 5, May 2022, e09403, DOI: <https://doi.org/10.1016/j.heliyon.2022.e09403>
- Sumit Sheoran, **Swati Arora**, Himanshu Singh, Anupam Kumar, Sugunakar Vuree, Harish Vancha and Smita C Pawar, **“Characterisation, development and validation of UV Spectrophotometric technique for determining Diosmetin in bulk and nanoformulations”** Results in Chemistry, Impact Factor 2.3, Volume 5, 2023, 100972, DOI: <https://doi.org/10.1016/j.rechem.2023.100972>
- Satbir Kour, Indrani Biswas, Sumit Sheoran, **Swati Arora**, Prasanna Sheela, Santosh Kumari Duppala, Dwarkanath K. Murthy, Smita C. Pawar, Himanshu Singh, Deepak Kumar, Dhamodharan Prabhu, Sugunakar Vuree, Raj Kumar **“Artificial Intelligence and Nanotechnology for cervical cancer treatment: Current Status and future perspectives”** JDDST, Elsevier, Impact Factor 5.062. Volume 83, May 2023, 104392 DOI: <https://doi.org/10.1016/j.jddst.2023.104392>
- Sumit Sheoran, **Swati Arora**, Tanmayee Basu, Swati Negi, Naidu Subbarao, Anupam Kumar, Himanshu Singh, Dhamodharan Prabhu, Atul Kumar Upadhyay, Neeraj Kumar & Sugunakar Vuree **“In silico analysis of Diosmetin as an effective chemopreventive agent against prostate cancer: molecular docking, validation, dynamic simulation and pharmacokinetic prediction-based studies”** Journal of Biomolecular Structure and Dynamics, Taylor & Francis, Impact Factor: 5.20, <https://doi.org/10.1080/07391102.2023.2250451>
- **Swati Arora**, Sumit Sheoran, Bhuvanesh Baniya, Naidu Subbarao, Himanshu Singh, Dhamodharan Prabhu, Neeraj Kumar, Smita C. Pawar, and Sugunakar Vuree, **“Hesperidin’s Role in the Treatment of Lung Cancer: In-silico and**

**In-vitro Findings,”** *In Silico Pharmacology*, 2024, **10.1007/s40203-024-00265-6**

- Satbir Kour, Indrani Biswas, Sumit Sheoran, **Swati Arora**, Anjuvan Singh, Dhamodharan Prabhu, Smita C. Pawar, Shyam Perugu, Sugunakar Vuree, **“Betulin: a novel triterpenoid anti-cancerous agent targeting cervical cancer through epigenetic proteins”** *Molecular Diversity*, 2024, <https://doi.org/10.1007/s11030-024-10930-9>
- Sumit Sheoran, **Swati Arora**, Tanmayee Basu, Naidu Subbarao, Atul Kumar Upadhyay, Sugunakar Vuree, **“Assessment of polyphenolic secondary metabolites and small molecules against the xenobiotic metabolic and cell cycle regulatory proteins in prostate cancer”** *Cancer Research*, Impact Factor 13.312 page no: 5342, 4,2023, DOI: <https://doi.org/10.1158/1538-7445.AM2023-5342>
- **Swati Arora**, Sumit Sheoran, Tanmayee Basu, Naidu Subbarao, Atul Kumar Upadhyay, Sugunakar Vuree, **“Evaluating the screened polyphenolics molecules as potential chemosensitizers against the oncogenic signaling proteins in Lung Cancer”** *Cancer Research*, Impact Factor 13.312, page no. 5343, 4,2023, DOI: <https://doi.org/10.1158/1538-7445.AM2023-5342>

#### **BOOK CHAPTER:**

- **Swati Arora**, Shefali Srivastava, Utkarsh Verma, Sumit Sheoran, Neeraj Kumar, **"Flavonoids as an Alternative Option to Treat Cancer,"** *Interdisciplinary Cancer Research*, Springer Nature Switzerland AG, 2024. DOI: [10.1007/16833\\_2024\\_482](https://doi.org/10.1007/16833_2024_482).
- Sumit Sheoran, **Swati Arora**, Aayushi Velingkar, Smita C Pawar, Sugunakar Vuree, **“Empowering treatment strategies for pancreatic cancer by employing lipid nanoparticle-driven drug delivery”**, 2024, *Recent Advances in Nanocarriers for Pancreatic Cancer Therapy*.



**COPYRIGHTS:**

- “Nano-formulated diosmin and hesperidin: A synergistic approach for lung cancer therapy-an integrated analysis”, Patent Number [L-151932/2024].
- “Enhanced prostate cancer therapy with nano-diosmetin: An in silico and in-vitro exploration of therapeutic potential”, Patent Number [L-152959/2024].

## LIST OF CONFERENCES, WORKSHOPS AND WEBINARS

- **Two-Day International Conference** on "Recent Advances for Quality Enhancement in Science and Technology," HMV, Jalandhar, India (16-17 January 2017).
- **Indian Conference on Bioinformatics (INBIX'17)** organized by Birla Institute of Scientific Research, Jaipur, India (2017).
- **Indian Conference on Bioinformatics (INBIX'19)** organized by Hans Raj Mahila Maha Vidyalaya, Jalandhar, India (22-23 February 2019).
- **International Conference on Recent Trends in Biotechnology and Bioinformatics (ICBAB-2019)** organized by the Department of Biotechnology and Bioinformatics, Jaypee University of Information Technology, Solan, India (1-3 August 2019).
- **International Symposium on Bioinformatics** organized by Hans Raj Mahila Maha Vidyalaya, Jalandhar, India (21-22 December 2019).
- **International Conference on Integrative Biology and Applied Genetics (ICIBAG-2022)** organized by the Department of Genetics & Biotechnology, Osmania University, Hyderabad, India (20-22 July 2022).
- **International Conference on Frontiers in Nutrition, Medical Genomics and Drug Discovery (INBIX'22)** organized by Vignan University, Guntur, India (31 October-2 November 2022).

### WORKSHOPS:

- **Workshop on Big Data Analytics for Whole Exome Sequencing**, Birla Institute of Scientific Research, Jaipur, India (22-28 June 2017).
- **National Conference Cum Workshop on Recent Advancements in Science and Technology**, DAV Chandigarh, India (12-13 March 2018).
- **DBT-Sponsored Workshop on Machine Learning Algorithms for Biological Data Analysis**, HMV, Jalandhar, India (31 March-1 April 2018).
- **National Workshop on Bioinformatics and Biomedical Image Analysis (NBBIA-2019)**, Jaypee University of Information Technology, Solan, India (29-31 May 2019).

- **DBT-Sponsored One-Week Faculty Development Program on Capacity Building and Enhancement in Higher Education**, Kanya Maha Vidyalaya, Jalandhar, India (16-21 December 2019).

#### **POSTER PRESENTATIONS:**

- Screening and Identification of Phytochemicals as Potential Inhibitors of Lung Cancer Using Structure-Based Molecular Docking and Simulation Analysis, **ICIBAG-2022**, Osmania University, Hyderabad, India (20-22 July 2022).
- Structure-based Docking Studies Explore the Anti-Cancerous Activity of Diosmin against Selected Targets in Lung Cancer, **INBIX'22**, Vignan University, Guntur, India (31 October-2 November 2022).
- Structure-based In-Silico Analysis of Selected Flavonoids against Target Protein in Prostate Cancer, **INBIX'22**, Vignan University, Guntur, India (31 October-2 November 2022).



## Review article

Lipid-based nanoparticles for treatment of cancer<sup>☆</sup>

Sumit Sheoran<sup>a,h,\*</sup>, Swati Arora<sup>b,h,1</sup>, R. Samsonraj<sup>c,d</sup>, Pilli Govindaiah<sup>e,f</sup>,  
Sugunakar vuree<sup>g,h,\*\*</sup>

<sup>a</sup> Dept. of Biochemistry, School of Biosciences and Bioengineering, Lovely Professional University, Jalandhar

<sup>b</sup> Dept. of Biotechnology and Bioinformatics, School of Biosciences and Bioengineering, Lovely Professional University, Jalandhar

<sup>c</sup> Dept. of Molecular Biology, School of Biosciences and Bioengineering, Lovely Professional University, Jalandhar

<sup>d</sup> Research and Development, Biocon Research Limited, Bengaluru

<sup>e</sup> Dept. of Pharmaceutical Chemistry, School of Pharmacy, Lovely Professional University, Jalandhar

<sup>f</sup> School of Medicine, Wayne State University, Detroit, Michigan, USA

<sup>g</sup> Department of Biotechnology, School of Bioengineering and Biosciences, Lovely Professional University, 144111 Punjab, India

<sup>h</sup> Bioclues.org, Hyderabad, India



## ARTICLE INFO

## Keywords:

Lipid based Nanoparticles

Tumour

Clinical trials

Liposomes

Solid lipid nanoparticles

## ABSTRACT

Investigators were continuously creating novel nanotechnologies to address unmet requirements throughout the administration of therapeutic medicines & imaging agents for cancer treatment & diagnostics, appropriately. LNPs (Lipid nanoparticles) are legitimate particulates (approx. 100 nm in size) gathered from various lipid as well as other biochemical compounds which overall functionality to resolve biological barriers (biobarriers), allowing LNPs to selectively collect somewhere outside of disease-target cells again for responsive therapeutics. Most pharmaceutically important compounds were insoluble throughout water solutions, were chemical & physiologically unstable, or have toxicities. Among the most potential drug carrier for bioactive organic compounds is LBNPs (Lipid based nanoparticles) technologies. Its present use in chemotherapy have transformed treatment for cancer by increasing the antitumor effect of a number of chemotherapeutics. Because they may be created using naturally occurring sources, LBNPs have great temporal and thermal stability, maximum load potential, simplicity of preparations, cheap manufacturing costs, & big manufacturing output. Furthermore, combining chemotherapeutic drugs with LNPs reduces active therapeutic dosage and toxicities, lowers treatment resistance, & raises drug concentration in tumour cells while reducing concentrations in normal tissue. LBNPs were widely studied in cancer treatment, both in vitro and in vivo, with encouraging outcomes in certain clinical trials. This study provides an overview of the many types of LBNPs which have been created in latest years and their applications and contributions in different types of cancers.

## 1. Introduction

Tumour is a category of illness that are explained as irregular cell development with ability to spread toward other cells or areas of the body. It is among the biggest killers, of over 100 distinct forms of cancer [1]. Inside the undeveloped nation, diseases like H. pylori, hbv, hep C, hpv infection, Epstein-Barr viruses, and HIV cause 15% of malignancies [2]. Those variables function, at least in part, through altering a cell's genes. Many genetic alterations are often necessary before cancer starts [3]. Cancers are caused by inherited genetic

abnormalities in 5–10% of cases [4]. Various indications & indicators, as well as medical tests, can help identify malignancy. It would then be generally explored forward with diagnostic imaging & verified with a biopsy [5]. During 2015, around 90.5 million individuals were diagnosed with cancer [6]. Annually, nearly 18 million new cases are recorded in 2019 [7]. It was blamed for almost 8.8 million deaths each and every year [8]. Lung cancer, prostate cancer, colorectal cancer, and stomach cancer are the most prevalent kinds of cancer in men [9]. Breast cancer, colorectal cancer, lung cancer, and cervical cancer are the most prevalent kinds of cancer in women [10]. Skin cancers other

<sup>☆</sup> This article is a part of the “Lipid-Based Nanoparticles in Diagnosis and Treatment” Special issue.

\* Corresponding author.

\*\* Corresponding author.

E-mail addresses: [sheoran080897@gmail.com](mailto:sheoran080897@gmail.com) (S. Sheoran), [sugunakar.24344@lpu.co.in](mailto:sugunakar.24344@lpu.co.in) (S. vuree).

<sup>1</sup> First equal contributing authors: Sumit Sheoran, and Swati Arora.

than melanoma would account for around 40percent of new cases of cancer per year if total new cancer cases had been included [11, 12]. Acute lymphoblastic & brain cancer seem to be the most frequent in youngsters, other than in African, wherein non-Hodgkin cancer is more frequent [13].

"Fat" seems to be another term for "lipid." The lipids seem to be a material which is unable to dissolve insoluble in h<sub>2</sub>o but having ability to dissolve in alcoholic, (C<sub>2</sub>H<sub>5</sub>)<sub>2</sub>O, & chcl<sub>3</sub> [14]. Lipids were essential components of human cells. Lipids, along with Cx (H<sub>2</sub>O)y & proteins, were its primary components of plant and animal cells. Triglycerides and cholesterol are both lipids. Lipids are rapidly achieved and retained within system. It serves as an energy reference and is an important component of cell composition. Lipids include fatty acids, neutral fats, waxes, and steroids (like cortisone). Compound lipids include lipoproteins, glycolipids, and phospholipids (lipids complexed with another type of chemical molecule). Lipids are sometimes defined as aquaphobic or amphipathic small molecules; the amphiphilic characteristic of certain lipids enables us to build formations in an aqueous environment like vesicle, large unilamellar liposomes, or membrane. Biological lipid is made up of two types of biochemical subunits or "building blocks": ketoacyl and isoprene groups. Structure of SLN, Liposomes and Lipid Emulsion are shown in Figure 1.

Because of their biocompatibility as transporters, lipids have gotten a lot of attention since the beginning of the pharmacological era. They have little oral absorption due to their highly hydrophobic nature

[15]. As a consequence, the desire to extend the range of applications for such carriers was unsatisfactory, and they're not employed in propulsion systems till 1900, while they were encased into colloidal delivery systems [16, 17, 18, 19]. Lipid nanoparticles (LNPs) were seen to be better beneficial than polymeric nanoparticles in the creation of nanoparticle-based delivery systems, and they've been widely employed for drug delivery [20]. Because LNPs are made from physiologic and/or biodegradable lipids, these lipid-based carrier systems are also referred to as "Nano safe" carriers [21]. The very well LNP synthesis is solid lipid nanoparticles (SLNs), that were created in the early 1990s [22]. Because of the various benefits of prior carriers like emulsifiers, liposomes, & polymeric nanoparticles, that delivering method was introduced [23]. The feasibility of the production procedures and levelling-up process, the GRAS (generally recognised as safe) quality of all formulations, and the lack of polar compounds are the characteristics that distinguish SLNs from liposomes [24].

Tumor nanotechnology has now been created as a potential cancer therapeutic method for antitumor drug delivery [25]. Nanoparticles have diameters ranging from 1 to 1000 nm and boost therapeutic bioavailability as well as anticancer drug specificity [26]. Numerous nanoparticles (NPs) and nanotech methods to cancer treatment have recently been presented shown in Figure 2. Because of their distinctive optical characteristics, broad excitation spectrum, and overly limited symmetric intensity distribution, semiconductor quantum dots (QDs) may now be used as a flexible material system with tremendous promise for biological applications. Semiconductor QDs are an exciting new class of

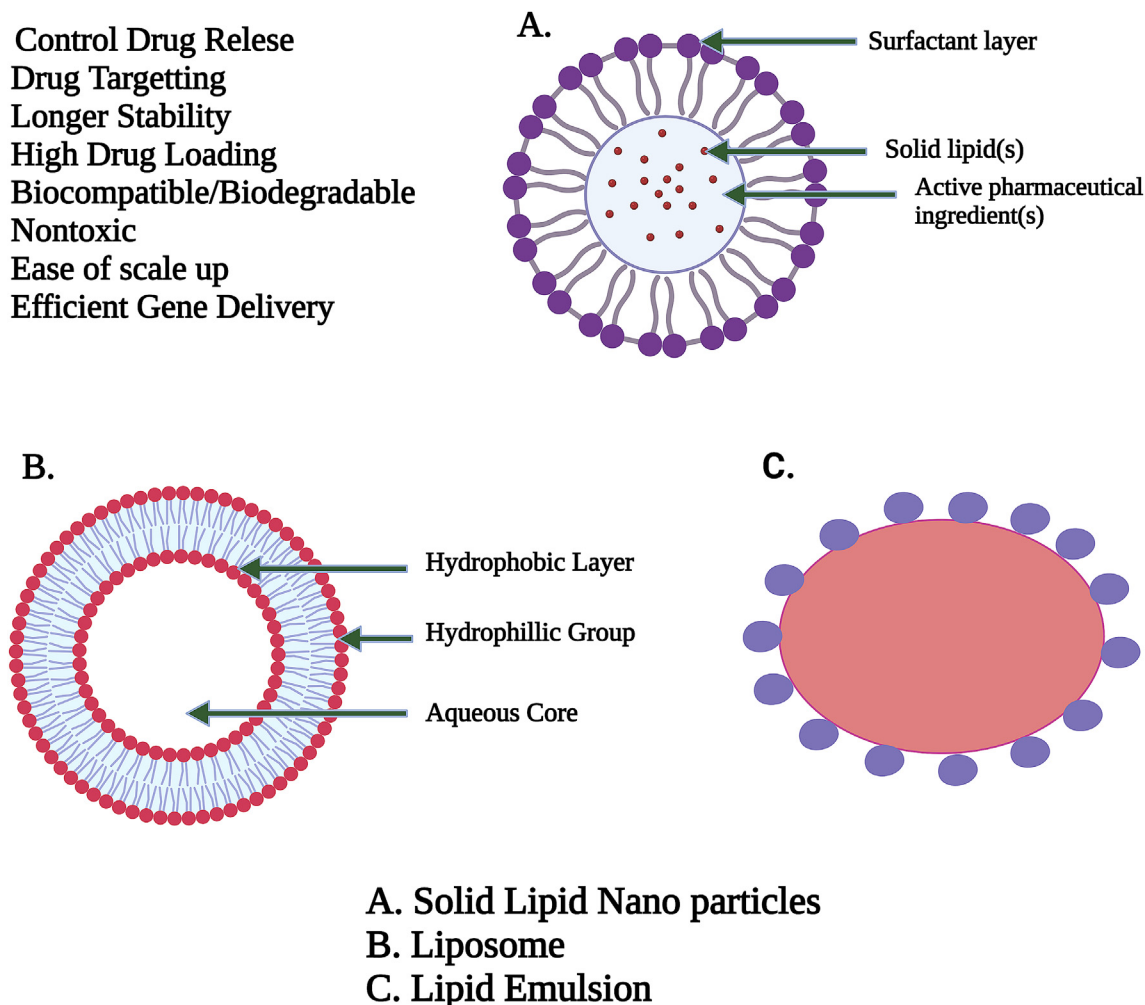


**Figure 1.** The overall arrangement of solid lipid nanoparticles, which have benefits over liposomes and lipid emulsions, is represented schematically. Adopted from [80].

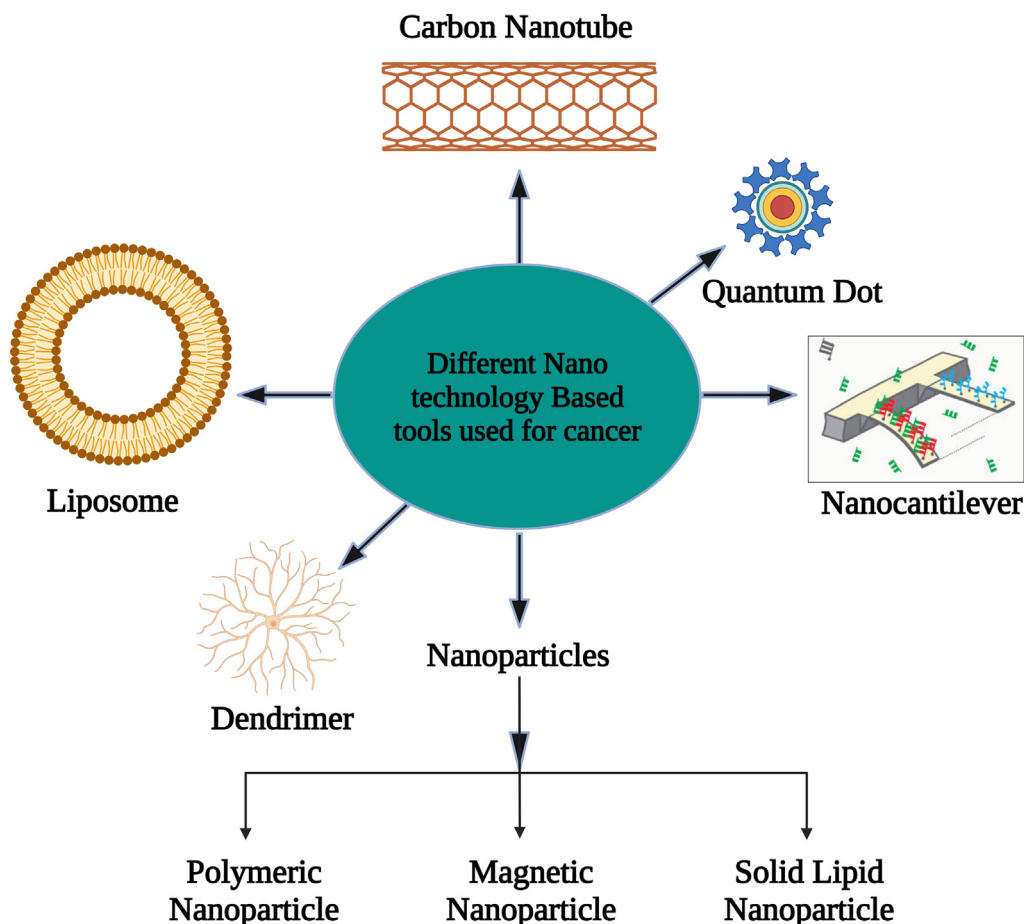


Figure 2. Various Nanotechnology based tools utilized in treatment of cancer. Adopted from [81].

fluorescence components. They are employed in bioimaging, biolabeling, and biosensing applications. QDs have a greater impact than ordinary fluorophores. They are brighter, have more fluorescence intensity controllability, and are less photobleached. Different colored QDs may be excited by a single source of light and have broad absorption and narrow emission spectra. The aforementioned QDs appear to be the best alternative for screening cell receptors. To generate effective fluorescence probes, the surface of QDs must be changed utilising various biological substances [27].

Among the various nano formulations utilised in cancer shown in Figure 2., we emphasize those based on lipid formulations since substantial breakthroughs in preparation and alternative compositions have been realised in recent decades. Chemical changes to lipid nano systems can be used to evade immune system detection or to increase medication availability. These could also be manufactured in pH-sensitive compositions to increase release of the drug in an acidic condition, and they can be coupled along antibodies those detect tumour cells & their receptor like (FoA) folic acid [28]. Nano drugs can potentially be utilised in conjunction with other treatment approaches to increase patient 's response.

Numerous antitumour drugs, including cisplatin, irinotecan (IRI), paclitaxel (PTX), doxorubicin (DOX), oxaliplatin, daunorubicin, cytarabine, and vincristine, have already been analysed in nano formulations, and some were investigated in clinical studies and/or are commercially present for their clinical utilization [29]. In fact, first commercially utilised anticancer drug NanoSystems was Doxil®, a liposome formulation containing DOX. provides an overview of the many types of LBPs (Figure 3) which have been created in latest years and their applications and contributions in different types of cancers.

## 2. Solid lipid nanoparticles

These are hard sized ranged between 1-1000nanometer. The size of particles mostly between 150-300nanometer. SLNs are solid, sub-micronic colloidal nanocarriers with a size range of 1e1000 nm. The particle size is mainly between 150 and 300 nm. Such delivery of drugs methods, like polymeric nanoparticles, provide a framework for regulated releases [30]. Their solid matrix of SLNs allows them to restrict medication motility & offer better stabilization, allowing them to combine the benefits of polymeric nanoparticles, liposomes, and micronized emulsifiers [31]. Moreover, tests show that SLNs were highly advantageous in a variety of aspects (Figure 4), such as the prevention of utilising organic solvent while manufacturing, possible scaling [32], as well as the inclusion both of lipophilic and hydrophilic medicines in significant quantities [33]. SLNs are created by replacing a solid lipid or even a combination of solid lipids for the liquid lipid (oil) in the structure of an oil in water emulsion. One important feature of SLNs is that they have been solid at both room as well as temperature of body [34]. Such drug transport systems are composed of 0.1–30% (w/w) solid lipid dispersed in an aqueous medium. SLNs are typically composed of solid form lipid such as higher purity of triglycerides, free fatty acids, free fatty alcohols, complex glyceride blends, and even wax (typically well-known physiologic lipids) [35]. It is also feasible to use more complicated structures [36].

### 2.1. Limitations of SLN and way to overcome

Although SLNs are most often made up of solid lipid, degradation and instability may become a concern. Factors that must be considered are

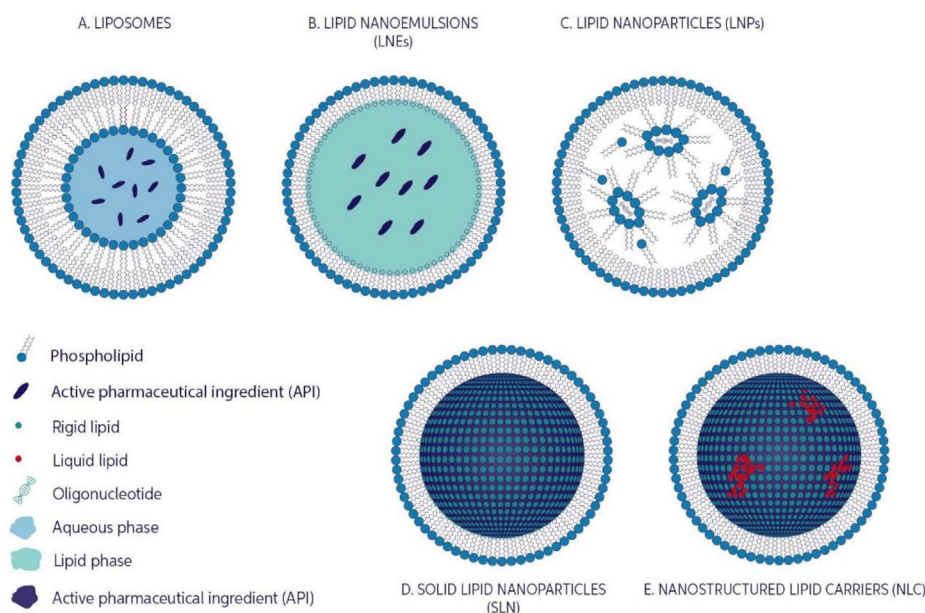


**Figure 3.** Lipid based nanoparticles showing A) LIPOSOMES, B) LIPID NANOEMULSIONS C) LIPID NANOPARTICLES, D) SOLID LIPID NANOPARTICLES, E) NANOSTRUCTURED LIPID CARRIERS. Adopted from [83].

including high pressure-induced drug degradation, the coexistence of different lipid modifications and colloidal species, the minimal drug-loading potential, and the kinetics of delivery process.

## 2.2. High pressure-induced drug degradation

Molecular size & structure are the primary causes of drug degradation, and high pressure homogeneity has also been shown to reduce polymeric molecular weight. High molecular weight composites or chain length elements are much more vulnerable than low molecular compounds with a spherical form, despite the fact that several studies show that high-pressure homogenization-induced drug degradation is not a concern for the overwhelming bulk of bioactive metabolites. Nevertheless, large molecular weight chemicals such as DNA, albumin, and dextrose are particularly vulnerable to breakage; hence, a separate approach must be used to integrate these elements into SLNs.

## 2.3. Lipid crystallization and drug incorporation

A further critical factor to take into account is lipid crystallisation. For past decade, researchers have been studying the relationship among lipid alteration and medication administration. The study of lipid changes is well known. The majority of the methods rely on X-ray and differential scanning calorimetric measurements. Nevertheless, the majority of the information has come from studies on huge quantities lipids. Due to the obvious nanosize of the carrier and the huge number of interface active participants needed to maintain the colloidal lipid dispersal, the effectiveness of SLNs may vary significantly. As a result, lipid crystallisation and drug inclusion have an impact on lipid particle properties. The following important considerations must be taken into consideration while discussing drugs capture within SLNs: (1) the occurrence of super-cooled melts; (2) the occurrence of multiple lipid alterations; (3) the morphology of lipid nanodispersions; and (4) gelation processes.

## 2.4. Several colloidal species coexist

The cohabitation of numerous nanoparticles within SLNs has received little attention from researchers, despite the fact that it is a crucial aspect to address. Surfactants are incorporated on both the lipid surface and the

interior. In glycocholate/lecithin stabilised and related systems, heterogeneous micelles must be acknowledged. Because micelles, combined micelles, and liposomes are known to dissolve pharmaceuticals, they can be used as alternative therapeutic inclusion targets. The presence of various heterogeneous entities alone is insufficient to characterize the structure of colloidal lipid phase separation, because dynamic processes are critical for drug stabilization and releasing. As a result, the kinetics of distribution processes must be taken into account. For illustrate, hydrolytic medications will degrade quicker in water dissolved & interface localised compounds than in lipid compounds.

The rates of breakdown will be regulated by: (1) the medication's chemical nature, and (2) the drug concentration in the aqueous phase or at the lipid/water boundary. Volatile medications will undergo hydrolysis quickly when they come into touch with liquid, causing the drug's dispersion balance between various habitats to be disrupted. Carriers are only beneficial if they prohibit the medication from being redistributed. Naturally, enhancing the matrix thickness reduces the diffusion coefficient of the medication inside the transporter, hence SLNs are projected to outperform lipid nanoemulsions. To create an effective delivery mechanism, comprehensive transparency about bits' in vitro and in vivo destiny must be provided.

## 3. Nanostructured carriers of lipid (SLN & NLC)

Although their protection and effectiveness, SLNs have many major disadvantages, including higher moisture concentration (70–99.9%), poor drug content owing to crystalline form, drug ejection while preservation, and potential polymorphism transitions and particles development while storing. As a result, changes to the Solid Lipid Nanoparticles organization are necessary to reach these constraints. Ongoing research led to development of a "2nd gen" of LNPs at the millennium's turn: the NLCs [37]. Following that, Dr. Rimpler's (Wedemark, Germany) developed the very first NLC concepts: Nano repair Q10 cream, Nano repair Q10 serum, and Chemisches Laboratorium's Nano lipid CLR Restore (Berlin, Germany). With numerous possible applications as well as a brief period among discovery & commercial launch, Solid Lipid Nanoparticles will be at the leading edge of nanotechnology innovation [38]. The existing information suggests that SLNs & NLCs were ideal for the integration of lipophilic substances, despite the fact that drug loading with aquaphilic molecules is rather modest [39]. Early research on the



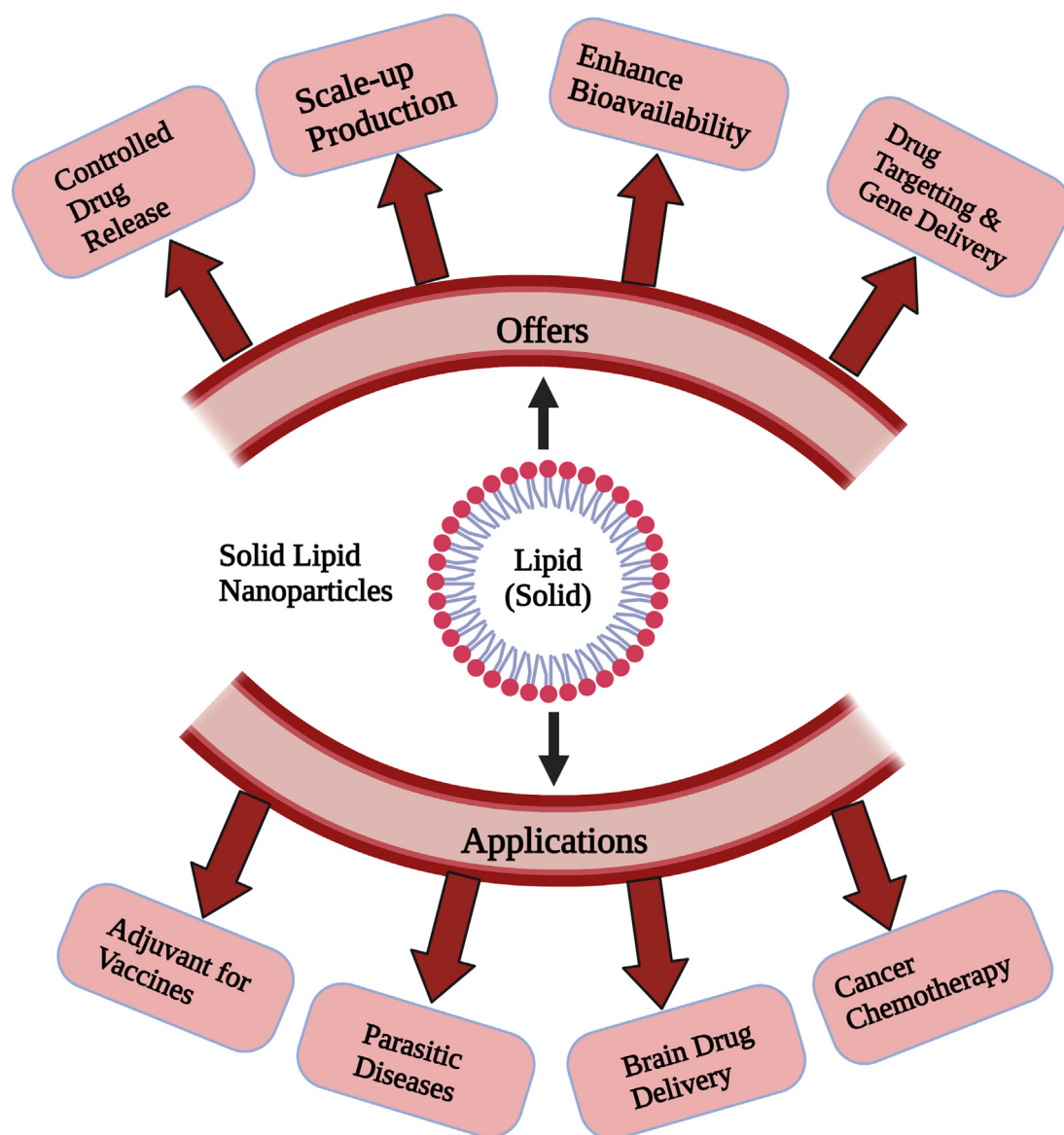


Figure 4. The Benefits and uses of SLN are depicted schematically. Adopted from [82].

topic shows that only very powerful aquaphilic medicines with modest quantities of efficacy could be fully incorporated throughout the solid lipid matrix [40].

#### 4. Medical applications of SLN

##### 4.1. Cancer chemoimmunotherapy

Tumour chemoimmunotherapy would be a medication which combines all beneficial effects of chemotherapeutic with immunotherapeutic. Chemo usually entails use of such traditional cytotoxic medicines as well as new molecularly targeted treatments. Immunotherapy, on the other hand, is a relatively new kind of cancer treatment which employs the sufferer's native immune system to fight cancer cells. It includes the Immune checkpoint inhibitors, adoptive cell therapy, cancer vaccinations, & cytokine therapies are all being used.

##### 4.2. Nanoparticles based on lipids in cancer immunotherapy

Due to specific benefits, nanotech has received a lot of interest in cancer therapy [41]. Nanoparticle, in illustration, such as Polymeric

micelles, lipid-based nanoparticles, gold nanoparticles, and inorganic nanoparticles are all examples of nanoparticles, are frequently employed to transport therapeutics including small molecules (either hydrophilic or hydrophobic), protein, & heredity materials for chemotherapeutic agents. Those nanomaterials can transport therapeutic drugs to certain cells via passively focusing techniques like the EPR impact or active targeting techniques like specific ligand [42].

Lipid-based nanoparticles, in particular, have appealing pharmacological & multifunctional properties, such as bio-compatibility, bio-degradability, as well as the potential to intimidate both aquaphilic and aquaphobic therapies [43, 44, 45]. Furthermore, the surface characteristics of lipid-based nanoparticles may be readily changed by changing the lipid components or altering the surface. Presently some of that are under preclinical trails such as hybrid lipid-based nanoparticles, nano discs, & liposomes, some of these are given in Table 1.

##### 4.3. Liposomes

Liposomes are nanosized particles composed largely of cholesterol and phospholipids that have proven improvements in bio-compatibility and increased directed payloads distribution with little harm. With its



**Table 1.** Lipid based nanoparticles in clinical trials.

Composition	Chemotherapy	Immunotherapy	Type of Cancer	Mode of Operations	References
<b>Liposomes</b>					
PEGylated liposomes	Doxorubicin	Alendronate	Breast cancer	i.v.	[46]
Charge-reversal cell penetrating peptide-modified liposomes	Paclitaxel	PD-L1 antibody	Melanoma	i.v.	[47]
pH-responsive liposomes	Mitoxantrone	Indoximod	Breast cancer and renal cancer	i.v.	[48]
Enzyme/pH dual-sensitive micelle-liposomes	Paclitaxel	HY19991	Metastatic breast cancer	i.v.	[49]
<b>Hybrid lipid-based nanoparticles</b>					
Thermo-sensitive exosome-liposome hybrid nanoparticles	Docetaxel	GM-CSF	Metastatic peritoneal carcinoma	i.v.	[50]
Lipid-coated calcium nanoparticles	Zoledronate	Zoledronate	Lung cancer	i.v.	[51]
Liposome-coated mesoporous silica nanoparticles	All-trans retinoic acid + doxorubicin	IL-2	Melanoma	i.v.	[52]
<b>Nano discs</b>					
HDL-Nano disc	Doxorubicin	$\alpha$ PD-1	Colorectal cancer	i.v.	[53]
	Docetaxel Colon	Cholesterol modified CpG	carcinomas	Intra-tumoral	[54]

lipid soluble ends, amphiphilic phospholipids self-assemble it into circular lipid bilayer form, allowing water insoluble medicines to be enclosed. Water - soluble head of phospholipids, but at the other hand, form an external surface as well as a watery centre which can contain aquaphilic substances. Numerous medicinal compounds can be encapsulated into liposomes via charge-charge interactions or interactions with chemical linkers on the liposomal surface. Liposomes, which allow for the administering drugs including both lipid and water-soluble therapeutic drugs while maintaining effectiveness, are one of the most effective nanotech medications in cancer treatment. Although PEGylated liposomal DOX (Doxil<sup>®</sup>) has become the first Food and drug administration approved nano-drug in 1995, the FDA has authorised more than six liposomal medicines to be used in cancer treatment. Liposomes were used as among the most appealing targeted delivery in chemo-immunotherapy, building on the success of liposomes in chemo. Liposomes are the first and mostly explored nanocarriers for cancer drug delivery, which have shown great promise in clinical applications, but their limited accumulation and penetration into the tumor interstitial space, significantly reduce the therapeutic efficacy [55].

#### 4.4. Nano disc

Nano discs are a synthetic model membrane system comprised of a phospholipid bilayer with the hydrophobic edge filtered by two amphipathic proteins are known as membranes scaffolding proteins (MSP). The MSP in certain nano discs is enhanced apolipoprotein A1 (apoA1), which would be the primary component of high-density lipoproteins (HDL). Nano discs have a shape comparable to discoidal HDL, which simulates a more natural environment than liposomes and micelles. In immunotherapy, this biomimicking delivery method appears to be more successful. Schwendeman's group completed extensive research on nano disc-based chemoimmunotherapy. Originally, they created an HDL-mimicking nano-disc that was attached to draining lymph nodes with a neoantigen (Ag peptide) and adjuvant (CpG). The nano-disc evoked upwards to 47-fold more neoantigen specific CTLs than solubilized vaccines and 31-fold more than the clinical trial adjunct. Those findings reinforced a novel potent strategy to cancer immunotherapy [56].

#### 4.5. Nanoparticles based on a hybrid of lipids

Lipid-based hybrid nanoparticles with flexible configurations are appealing for chemoimmunotherapy. Towards effective therapeutic dosage, several inorganic nanoparticles with a lipids coating are being created. Kong et al., created lipid-coated bio-degradable hollow

mesoporous silica nanoparticles (dHMLB) with all-trans retinoic acid (ATRA) co-encapsulation for chemoimmunotherapy [57]. A lipid component of hybrid nanoparticles is also being utilised as dosage form during chemoimmunotherapy. Zhang et al. created TCNs for synchronized bio-distribution & selective administration of SF & IMD-0354 to cancerous cells & TAMs, accordingly, to improve cancer-localized chemoimmunotherapy [58].

### 5. Applications in cancer therapy

Lipid-Based NPs (LBNPs) are a vast and diversified class of nanoparticles that are especially important in BreC therapy [59]. But besides their diversity, liposomes are widely employed because of their great biocompatibility and ability to encapsulate a wide range of cargos. LBNPs are now being employed in a number of studies, and a few of them (for example, Doxil<sup>®</sup> or Abraxane<sup>®</sup>) have previously been licenced for BreC therapy [6, 38]. This part presents the most recent major breakthroughs in the use of LBNPs in the treatment of the most common kinds of cancer.

#### 5.1. Bowel cancer

Bowel cancer is a major health concern because of its high death rate (it is the second leading cause of death) and the recent increase in its incidence [60, 61]. LBNPs provide a possible method for improving existing treatments, particularly in advanced colorectal cancer where chemotherapy (5-FU alone or in combination with other medicines) or monoclonal antibodies (bevacizumab, trastuzumab, cetuximab) are ineffective. In comparison to a 5-FU thermosensitive gel-mediated microemulsion (ME), a thermosensitive gel-mediated 5-FU microemulsion (ME) was able to enhance Caco-2 permeability and cell uptake, as well as its accumulation in rectal tissue in vivo.

Low et al. [62] created a sophisticated device based on Pickering emulsions (PE) that consists of a magnetic cellulose nanocrystal loaded with CUR and is capable of regulated drug release when exposed to an external magnetic field. In both monolayer and multicellular spheroids, this approach inhibited the development of HCT116 cells. Furthermore, Ektate et al. [63] activated macrophages in the tumour environment using lipopolysaccharide (LPS) from attenuated Salmonella bacteria coated with DOX-thermosensitive liposomes and high-intensity focused ultrasonic waves.

Through changes in membrane fluidity, this approach was able to enhance DOX internalisation and reduce tumour development in vivo. Liposome characterisation is also being utilised to enhance CRC therapy. As a result, Moghimipour et al. [64] utilised FoA to enhance 5-FU uptake

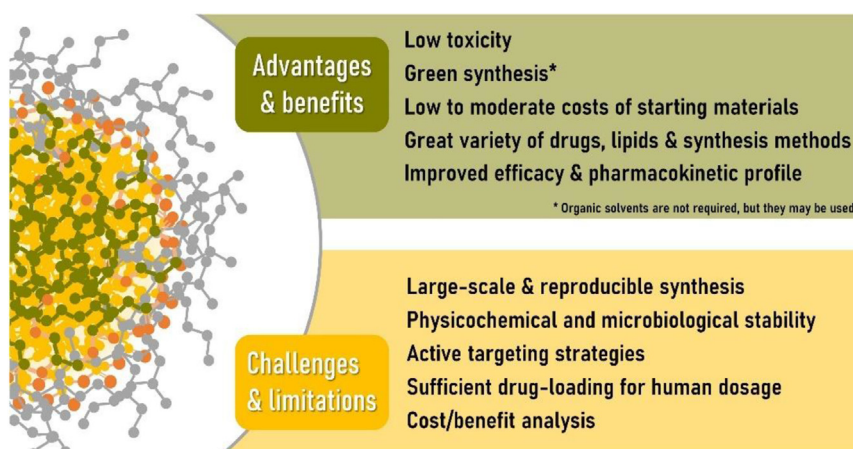


Figure 5. Studying with solid lipid nanoparticles for drug carriers: benefits, present obstacles, and limits. Adopted from [84].

in CT-26 cells, lowering its IC<sub>50</sub> & reducing tumour volume. Kaseem et al. [65] created niosomes containing imatinib mesylate (IM), which bring down the IC<sub>50</sub> of the free drug (16-fold) in HCT-116 cells.

### 5.2. Stomach cancer

It is the globe's 5th another very frequent malignancy as well as the major cause of malignancy mortality [60,61]. Only stomach malignancy that has not spread to the lymph nodes could be managed via surgical removal only. Severe stomach carcinoma, should be managed with combination chemotherapy, which have significant adverse impacts. New treatments relying upon nano formulation are currently being explored to enhance patient responses. Liposomes were broadly applied in GC therapy, either alone or in combination with compounds including the Arg-Gly-Asp peptides [66], SATB1 siRNA/CD44 antibodies [67], or in the formation of DNA complexes [68]. Their use enhanced drug deposition in cancerous cells of any animals grafted with SGC7901 cells expressing high levels of integrin 51 [66]. Liposomes also exhibited increased targeting accuracy and were able to suppress SATB1 gene expression by about 80% in CD44 + GC starting cells [67]. Furthermore, liposomes recognised peritoneally dispersed GC MKN-45P cells, decreasing their accumulation in the liver. Initial studies using SLNs in GC [69] revealed that etoposide (VP16) had increased action in SGC-7901 cell, increasing inhibition of growth, causing cell arrests in the G2/M stage (17.13 percent), & triggering mitochondria-involved apoptotic. Li et al. [70] created an SLN for use in conjunction with in ATRA and sorafenib as well as miR-542-3p. This method improved the absorption of both anticancer medicines and had a synergistic activity on MGC-803 cells.

### 5.3. Breast tumour

It is the leading cause of mortality in women [60] and is experiencing significant shifts as a result of the development of NPs, notably in the treatment of metastatic cancer. Throughout the tolerant MCF-7/ADR cancer cell, NEs preloaded wit DOX & bromo tetra trandrine (W198, P-glycoprotein (P-gp) inhibitor) have been examined. That increased cellular absorption and deposition of DOX in cancer cells. DOX, on the other hand, reduced stomach & cardiac damage [71]. In contrast, DOX-liposome-based compositions were evaluated in clinical studies.

PLD in conjunction to lapatinib have been recently utilised in HER2-positive BreC sufferers (stage Ib) to find the best conjunction including both therapies at the highest acceptable dosage [72]. Furthermore, a phase 3 trials of Myocet in combination with cyclophosphamide (CM) or vinorelbine (MV) in cancer patients BreC has also been established [73].

SLNs are another type of LBNP employed in BreC investigations. Yu et al. [74] suggested a method for combining PTX & derivatized DNA delivery with such a pH-sensitive ligand. In vivo, this approach is responsible for reducing tumour volume while also lowering PTX deposition in all further organs. Furthermore, Garg et al. [75] created a fucose-methotrexate SLN that accumulated preferentially in tumour tissue just 2 h after treatment, as opposed to free methotrexate, that accumulates throughout the kidney, liver, & spleen.

### 5.4. Glandular carcinoma

Presently, the primary LBNPs under investigated as potential treatment methods in prostate cancer include NEs, liposomes, and solid-lipid NPs (SLNs) (PrC). Ahmad et al. [76] recently created an oil-in-water NE containing a toxoid therapeutic agent linked to an omega-3 fatty acid. That NE is effective to lessen the toxoid IC<sub>50</sub> of PPT2 cell types 12-fold, enabling for a larger tumour size decrease in tumour-bearing rats than Abraxane<sup>TM</sup>. In PC-3 cells, similar antitumor effects were seen when NE was loaded with catechin extract (flavanols having anticancer activities) [77]. Regarding liposomes, 22Rv1 PrC cells were treated with PEG-folate-targeted-oleuropein-liposomes.

In in vivo models, these nanoplatfroms enhanced 22Rv1 cell apoptosis, oleuropein bioavailability, and survival [78]. Hua et al. [79] also created NPs that contains diversified liposome burdened with docetaxel and a gold nanorod, demonstrating 100 percent suppression of PrC cell growing by merge the mode with the use of a radiation.

And there are lots of application in all other types of cancer including lung cancer, nervous system cancer, liver cancer, pancreatic cancer etc. In recent years there are lot of modification and newly synthesized nanoparticles are introduced in cancer treatment.

## 6. Conclusion and future challenges

Lipid Based Nanoparticles are a varied and comprehensive category of compounds that have been utilised to treat various diseases, most notably malignancy. Liposomes are now the most often utilised Lipid Based Nanoparticles because to its excellent biocompatibility & flexibility; although, SLNs as well as NLCs have lately gained popularity.

Nonetheless, studies are just not focused primarily on such Nanoparticles, and there are several papers focusing on novel techniques for utilising Lipid Based Nanoparticles to heal other kinds of cancer. Some of it has already progressed towards the next stage & began new careers in clinical studies.

SLNs and nanostructured lipid carriers have received a lot of interest in the recent decade as prospective delivery of drugs (nano)systems. One 's main benefit may be the utilisation of biomaterial, environmentally

safe ingredients and techniques of production (Figure 5). It really should be stressed, however, that prior to mass producible & distribution of these schemes, rigorous clinical and environmental safety analysis must be done. The establishment of standardised processes for assessing possible dangers of nano - materials consumption, as well as the corresponding regulatory environment, is considered necessary. As with other nanosized drug carriers, melanoma therapy is an important research area in which SLNs can be used, which might also represent both large level of funding in the field as well as the appropriateness of nanostructures for such delivering of cytotoxic drugs, owing to the direct and indirect attacking prompted by malignant cellular level. Nonetheless, there are numerous clinical sectors which derive value from using lipid nanoparticles. Regrettably, more research, extra effort & working capital facilities should be provided for SLN/NLC to be shown therapeutically effective in real-world circumstances. For said time being, the rarity of SLNs which have advanced to medical studies suggests that it would be at least a few years before such innovations approach the national or international drug market.

## Declarations

### Author contribution statement

All authors listed have significantly contributed to the development and the writing of this article.

### Funding statement

This research did not receive any specific grant from funding agencies in the public, commercial, or not-for-profit sectors.

### Data availability statement

Data included in article/supplementary material/referenced in article.

### Declaration of interests statement

The authors declare no conflict of interest.

### Additional information

No additional information is available for this paper.

## Acknowledgments

We deeply acknowledge Dr. Aparna Banerjee, Chile for her support providing the Biorender tool for image drawing.

## References

- J.C. Underwood, S.S. Cross, General and Systematic Pathology, Elsevier health science, Amsterdam, Netherlands, 2009.
- Cancer, World Health Organization, 12 September 2018.
- World Cancer Report 2014, World Health Organization, 2014. Chapter 1.1.
- H. Rehder, Family cancer syndromes, *Hered. Tumors* (2009) 41–86.
- How Is Cancer Diagnosed?, American Cancer Society, 29 January 2013.
- GBD 2015 Disease and Injury Incidence and Prevalence, Collaborators, Global, regional, and national incidence, prevalence, and years lived with disability for 310 diseases and injuries, 1990–2015: a systematic analysis for the Global Burden of Disease Study 2015, *Lancet* 388 (10053) (8 October 2016) 1545–1602.
- Marco Sciacovelli, Christina Schmidt, Eamonn R. Maher, Christian Frezza, Metabolic drivers in hereditary cancer syndromes, *Annu. Rev. Cell Biol.* 4 (2020) 77–97.
- GBD 2015 Mortality and Causes of Death, Collaborators, Global, regional, and national life expectancy, all-cause mortality, and cause-specific mortality for 249 causes of death, 1980–2015: a systematic analysis for the Global Burden of Disease Study 2015, *Lancet* 388 (10053) (8 October 2016) 1459–1544.
- World Cancer Report 2014, World Health Organization, 2014. Chapter 1.1.
- World Cancer Report 2014, World Health Organization, 2014. Chapter 1.1. Archived from the original on 12 July 2017.
- L.E. Dubas, A. Ingrassia, Nonmelanoma skin cancer, *Fac. Plastic Surg. Clin. North Am.* 21 (1) (February 2013) 43–53.
- B.Ö. Cakir, P. Adamson, C. Cingi, Epidemiology and economic burden of nonmelanoma skin cancer, *Fac. Plastic Surg. Clin. North Am.* 20 (4) (November 2012) 419–422.
- World Cancer Report, World Health Organization 2014, 2014 pp. Chapter 1.3. Archived from the original on 12 July 2017.
- IUPAC, Compendium of Chemical Terminology, second ed., The "Gold Book", 1997. Online corrected version: (2006–) "lipids".
- J.S. Jingling Tang, Self-emulsifying drug delivery systems: strategy for improving oral delivery of poorly soluble drugs, *Curr. Drug Ther.* 2 (2007), 85e93.
- A.J. Humberstone, W.N. Charman, Lipid-based vehicles for the oral delivery of poorly water-soluble drugs, *Adv. Drug Deliv. Rev.* 25 (1997), 103e28.
- M. Kuentz, Lipid-based formulations for oral delivery of lipophilic drugs, *Drug Discov. Today Technol.* 9 (2012), 97e104.
- A.R. Patel, K.P. Velikov, Colloidal delivery systems in foods: a general comparison with oral drug delivery, *Food Sci. Technol.* 44 (2011), 1958e64.
- C.W. Pouton, C.J. Porter, Formulation of lipid-based delivery systems for oral administration: materials, methods and strategies, *Adv. Drug Deliv. Rev.* 60 (2008), 625e37.
- R.H. Müller, K. Karsten, S.G. Mäder, Solid lipid nanoparticles (SLN) for controlled drug delivery e a review of the state of the art, *Eur. J. Pharm. Biopharm.* 50 (1) (2000), 161e77, 66 CHAPTER 3 Lipid-Based Nanoparticles for Drug Delivery Systems.
- J. Pardeike, A. Hommoss, R.H. Müller, Lipid Nanoparticles (SLN, NLC) in Cosmetic and Pharmaceutical Dermal Products 366, 2009, pp. 170–184.
- M.R. Gasco, Method for producing solid lipid microspheres having a narrow size distribution, U.S. Patent No. 5 250 (1993) 236.
- R.H. Müller, J.S. Lucks, Medication Vehicles Made of Solid Lipid Particles (Solid Lipid Nanospheres SLN), 1996.
- S. Doktorovova, E.B. Souto, A.M. Silva, Nanotoxicology applied to solid lipid nanoparticles and nanostructured lipid carriers e a systematic review of in vitro data, *Eur. J. Pharm. Biopharm.* 87 (2014) 1–18.
- G. Bor, I.D. Mat Azmi, A. Yaghmur, Nanomedicines for cancer therapy: current status, challenges and future prospects, *Ther. Deliv.* 10 (2019) 113–132.
- E. Miele, G.P. Spinelli, E. Miele, E. Di Fabrizio, E. Ferretti, S. Tomao, A. Gulino, Nanoparticle-based delivery of small interfering RNA: challenges for cancer therapy, *Int. J. Nanomed.* 7 (2012) 3637–3657.
- I. Fatima, A. Rahdar, S. Sargazi, M. Barani, M. Hassanisaadi, V.K. Thakur, Quantum dots: synthesis, antibody conjugation, and HER2-receptor targeting for breast cancer therapy, *J. Funct. Biomater.* 12 (2021) 75.
- A.R. Rama, J. Jimenez-Lopez, L. Cabeza, C. Jimenez-Luna, M.C. Leiva, G. Perazzoli, R. Hernandez, I. Zafra, R. Ortiz, C. Melguizo, et al., Last advances in nanocarriers-based drug delivery systems for colorectal cancer, *Curr. Drug Deliv.* 13 (2016) 830–838.
- M. Alavi, M. Hamidi, Passive and active targeting in cancer therapy by liposomes and lipid nanoparticles, *Drug Metab. Pers. Ther.* 34 (2019).
- R.H. Muller, R. Shegokar, C.M. Keck, 20 years of lipid nanoparticles (SLN and NLC): present state of development and industrial applications, *Curr. Drug Discov. Technol.* 8 (3) (2011) 207–227.
- N. Kathe, B. Henriksen, H. Chauhan, Physicochemical Characterization Techniques for Solid Lipid Nanoparticles: Principles and Limitations 9045, 2014, pp. 1–11.
- V. Teeranachaiadekul, R.H. Muller, V. Junyaprasert, Encapsulation of ascorbyl palmitate in nanostructured lipid carriers (NLC) e effects of formulation parameters on physicochemical stability, *Int. J. Pharm.* 340 (2007) 198–206.
- P. Jaiswal, B. Gidwani, A. Vyas, Nanostructured lipid carriers and their current application in targeted drug delivery, *Artif. Cell Nanomed. Biotechnol.* (2014) 1–14.
- A.M. Lima, C.D. Pizzol, F.B. Monteiro, T.B. Creczynski-Pasa, G.P. Andrade, A.O. Ribeiro, et al., Hypericin encapsulated in solid lipid nanoparticles: phototoxicity and photodynamic efficiency, *J. Photochem. Photobiol., B* 125 (2013) 146–154.
- S.A. Wissing, O. Kayser, R.H. Mu, Solid Lipid Nanoparticles for Parenteral Drug Delivery 56, 2004, pp. 1257–1272.
- H. Svilenov, C. Tzachev, Solid lipid nanoparticles - a promising drug delivery, *Nanomedicine* (2009) 187–237.
- R.H. Muller, R. Shegokar, C.M. Keck, 20 years of lipid nanoparticles (SLN and NLC): present state of development and industrial applications, *Curr. Drug Discov. Technol.* 8 (3) (2011) 207–227.
- M.A. Iqbal, Md S, J.K. Sahni, S. Baboota, S. Dang, J. Ali, Nanostructured lipid carriers system: recent advances in drug delivery, *J. Drug Target.* 20 (10) (2012) 813–830.
- A.J. Almeida, E. Souto, Solid Lipid Nanoparticles as a Drug Delivery System for Peptides and Proteins 59, 2007, pp. 478–490.
- A.J. Almeida, S. Runge, R. Muller, Peptide-loaded solid lipid nanoparticles (SLN): influence of production parameters, *Int. J. Pharm.* 149 (1997) 255–265.
- D. Peer, J.M. Karp, S. Hong, O.C. Farokhzad, R. Margalit, R. Langer, Nanocarriers as an emerging platform for cancer therapy, *Nat. Nanotechnol.* 2 (2007) 751–760.
- A. Zafar, N.K. Alruwaili, S.S. Imam, K.S. Alharbi, M. Afzal, N.H. Alotaibi, M. Yasir, M. Elmowafy, S. Alshehri, Novel nanotechnology approaches for diagnosis and therapy of breast, ovarian and cervical cancer in female: a review, *J. Drug Deliv. Sci. Technol.* 61 (2020) 102198.
- S. Ramishetti, R. Kedmi, M. Goldsmith, F. Leonard, A.G. Sprague, B. Godin, M. Gozin, P.R. Cullis, D.M. Dykxhoorn, D. Peer, Systemic gene silencing in

- primary T lymphocytes using targeted lipid nanoparticles, *ACS Nano* 9 (2015) 6706–6716.
- [44] A. Khan, S.S. Imam, M. Aqil, A. Ahad, Y. Sultana, A. Ali, K. Khan, Brain targeting of temozolomide via the intranasal route using lipid-based nanoparticles: brain pharmacokinetic and scintigraphic analyses, *Mol. Pharm.* 13 (2016) 3773–3782.
- [45] A. Khan, M. Aqil, S.S. Imam, A. Ahad, Y. Sultana, A. Ali, K. Khan, Temozolomide loaded nano lipid based chitosan hydrogel for nose to brain delivery: characterization, nasal absorption, histopathology and cell line study, *Int. J. Biol. Macromol.* 116 (2018) 1260–1267.
- [46] H. Shmeeda, Y. Amitay, J. Gorin, D. Tzemach, L. Mak, S.T. Stern, Y. Barenholz, A. Gabizon, Coencapsulation of alendronate and doxorubicin in pegylated liposomes: a novel formulation for chemoimmunotherapy of cancer, *J. Drug Target.* 24 (2016) 878–889.
- [47] M. Li, Y. Yang, C. Xu, J. Wei, Y. Liu, X. Cun, Q. Yu, X. Tang, S. Yin, Z. Zhang, et al., Tumor-targeted chemoimmunotherapy with immune-checkpoint blockade for enhanced anti-melanoma efficacy, *AAPS J.* 21 (2019) 18.
- [48] K.C. Mei, Y.P. Liao, J. Jiang, M. Chiang, M. Khazaei, X. Liu, X. Wang, Q. Liu, C.H. Chang, X. Zhang, et al., Liposomal delivery of mitoxantrone and a cholesterol indoximide prodrug provides effective chemo-immunotherapy in multiple solid tumors, *ACS Nano* 14 (2020) 13343–13366.
- [49] T. Lang, Y. Liu, Z. Zheng, W. Ran, Y. Zhai, Q. Yin, P. Zhang, Y. Li, Cocktail strategy based on spatio-temporally controlled nano device improves therapy of breast cancer, *Adv. Mater.* 31 (2019), e1806202.
- [50] G. Wang, B. Wu, Q. Li, S. Chen, X. Jin, Y. Liu, Z. Zhou, Y. Shen, P. Huang, Active transportation of liposome enhances tumor accumulation, penetration, and therapeutic efficacy, *Small* 16 (2020) 2004172.
- [51] Q. Lv, L. Cheng, Y. Lu, X. Zhang, Y. Wang, J. Deng, J. Zhou, B. Liu, J. Liu, Thermosensitive exosome-liposome hybrid nanoparticle-mediated chemoimmunotherapy for improved treatment of metastatic peritoneal cancer, *Adv. Sci.* 7 (2020) 2000515.
- [52] relay drug delivery for amplifying antitumor efficiency. *Biomaterials* 2018, 185, 205–218. [CrossRef] 138 X. Zang, J. Zhou, X. Zhang, D. Chen, Y. Han, X. Chen, Dual-targeting tumor cells and tumor associated macrophages with lipid coated calcium zoledronate for enhanced lung cancer chemoimmunotherapy, *Int. J. Pharm.* 594 (2021) 120174.
- [53] M. Kong, J. Tang, Q. Qiao, T. Wu, Y. Qi, S. Tan, X. Gao, Z. Zhang, Biodegradable hollow mesoporous silica nanoparticles for regulating tumor microenvironment and enhancing antitumor efficiency, *Theranostics* 7 (2017) 3276–3292.
- [54] R. Kuai, W. Yuan, S. Son, J. Nam, Y. Xu, Y. Fan, A. Schwendeman, J.J. Moon, Elimination of established tumors with nanodisc-based combination chemoimmunotherapy, *Sci. Adv.* 4 (2018), eaao1736.
- [55] L.M. Scheetz, M. Yu, D. Li, M.G. Castro, J.J. Moon, A. Schwendeman, Synthetic HDL nanoparticles delivering docetaxel and CpG for chemoimmunotherapy of colon adenocarcinoma, *Int. J. Mol. Sci.* 21 (2020) 1777.
- [56] R. Kuai, L.J. Ochyl, K.S. Bahjat, A. Schwendeman, J.J. Moon, Designer vaccine nanodiscs for personalized cancer immunotherapy, *Nat. Mater.* 16 (2017) 489–496.
- [57] M. Kong, J. Tang, Q. Qiao, T. Wu, Y. Qi, S. Tan, X. Gao, Z. Zhang, Biodegradable hollow mesoporous silica nanoparticles for regulating tumor microenvironment and enhancing antitumor efficiency, *Theranostics* 7 (2017) 3276–3292.
- [58] T. Wang, J. Zhang, T. Hou, X. Yin, N. Zhang, Selective targeting of tumor cells and tumor associated macrophages separately by twin-like core-shell nanoparticles for enhanced tumor-localized chemoimmunotherapy, *Nanoscale* 11 (2019) 13934–13946.
- [59] B. García-Pinel, C. Porras-Alcalá, A. Ortega-Rodríguez, F. Sarabia, J. Prados, C. Melguizo, J.M. López-Romero, Lipid-based nanoparticles: application and recent advances in cancer treatment, *Nanomaterials* 9 (4) (2019) 638.
- [60] F. Bray, J. Ferlay, I. Soerjomataram, R.L. Siegel, L.A. Torre, A. Jemal, Global cancer statistics 2018: GLOBOCAN estimates of incidence and mortality worldwide for 36 cancers in 185 countries, *CA Cancer J. Clin.* 68 (2018) 394–424.
- [61] J. Ferlay, M. Colombet, I. Soerjomataram, C. Mathers, D.M. Parkin, M. Piñeros, A. Znaor, F. Bray, Estimating the global cancer incidence and mortality in 2018: GLOBOCAN sources and methods, *Int. J. Cancer* 144 (2019) 1941–1953.
- [62] L.E. Low, L.T.-H. Tan, B.-H. Goh, B.T. Tey, B.H. Ong, S.Y. Tang, Magnetic cellulose nanocrystal stabilized Pickering emulsions for enhanced bioactive release and human colon cancer therapy, *Int. J. Biol. Macromol.* 127 (2019) 76–84.
- [63] K. Ektate, M.C. Munteanu, H. Ashar, J. Malayer, A. Ranjan, Chemo-immunotherapy of colon cancer with focused ultrasound and Salmonella-laden temperature sensitive liposomes (thermobots), *Sci. Rep.* 8 (2018) 13062.
- [64] E. Moghimipour, M. Rezaei, Z. Ramezani, M. Kouchak, M. Amini, K.A. Angali, F.A. Dorkoosh, S. Handali, Folic acid-modified liposomal drug delivery strategy for tumor targeting of 5-fluorouracil, *Eur. J. Pharmaceut. Sci.* 114 (2018) 166–174.
- [65] M.A. Kassem, H.S. El-Sawy, F.I. Abd-Allah, T.M. Abdelghany, K.M. El-Say, Maximizing the therapeutic efficacy of imatinib mesylate-loaded niosomes on human colon adenocarcinoma using box-behnken design, *J. Pharm. Sci.* 106 (2017) 111–122.
- [66] J. Ding, M. Feng, F. Wang, H. Wang, W. Guan, Targeting effect of PEGylated liposomes modified with the Arg-Gly-Asp sequence on gastric cancer, *Oncol. Rep.* 34 (2015) 1825–1834.
- [67] F. Yang, Z. Zheng, L. Zheng, J. Qin, H. Li, X. Xue, J. Gao, G. Fang, SATB1 siRNA-encapsulated immunoliposomes conjugated with CD44 antibodies target and eliminate gastric cancer-initiating cells, *OncoTargets Ther.* 11 (2018) 6811–6825.
- [68] E. Wonder, L. Simón-Gracia, P. Scodeller, R.N. Majzoub, V.R. Kotamraju, K.K. Ewert, T. Teesalu, C.R. Safinya, Competition of charge-mediated and specific binding by peptide-tagged cationic liposome-DNA nanoparticles in vitro and in vivo, *Biomaterials* 166 (2018) 52–63.
- [69] J. Wang, R. Zhu, X. Sun, Y. Zhu, H. Liu, S.-L. Wang, Intracellular uptake of etoposide-loaded solid lipid nanoparticles induces an enhancing inhibitory effect on gastric cancer through mitochondria-mediated apoptosis pathway, *Int. J. Nanomed.* 9 (2014) 3987–3998.
- [70] T. Li, Y. Zhang, Y.-P. Meng, L.-S. Bo, W.-B. Ke, miR-542-3p appended sorafenib/all-trans retinoic acid (ATRA)-loaded lipid nanoparticles to enhance the anticancer efficacy in gastric cancers, *Pharm. Res. (N. Y.)* 34 (2017) 2710–2719.
- [71] X. Cao, J. Luo, T. Gong, Z.-R. Zhang, X. Sun, Y. Fu, Coencapsulated doxorubicin and bromotetrandrine lipid nanoemulsions in reversing multidrug resistance in breast cancer in vitro and in vivo, *Mol. Pharm.* 12 (2015) 274–286.
- [72] A. Rocca, L. Ceconetto, A. Passardi, E. Melegari, D. Andreis, M. Monti, R. Maltoni, S. Sarti, E. Pietri, A. Schirone, et al., Phase Ib dose-finding trial of lapatinib plus pegylated liposomal doxorubicin in advanced HER2-positive breast cancer, *Cancer Chemother. Pharmacol.* 79 (2017) 863–871.
- [73] V. Lorusso, F. Giotta, R. Bordonaro, E. Maiello, S. Del Prete, V. Gebbia, G. Filippelli, S. Piscanti, S. Cinieri, S. Romito, et al., Non-pegylated liposome-encapsulated doxorubicin citrate plus cyclophosphamide or vinorelbine in metastatic breast cancer not previously treated with chemotherapy: a multicenter phase III study, *Int. J. Oncol.* 45 (2014) 2137–2142.
- [74] D. Yu, W. Li, Y. Zhang, B. Zhang, Anti-tumor efficiency of paclitaxel and DNA when co-delivered by pH responsive ligand modified nanocarriers for breast cancer treatment, *Biomed. Pharmacother.* 83 (2016) 1428–1435.
- [75] N.K. Garg, B. Singh, A. Jain, P. Nirbhavane, R. Sharma, R.K. Tyagi, V. Kushwah, S. Jain, O.P. Katare, Fucose decorated solid-lipid nanocarriers mediate efficient delivery of methotrexate in breast cancer therapeutics, *Colloids Surf. B Biointerfaces* 146 (2016) 114–126.
- [76] G. Ahmad, R. El Sadda, G. Botchkina, I. Ojima, J. Egan, M. Amiji, Nanoemulsion formulation of a novel taxoid DHA-SBT-1214 inhibits prostate cancer stem cell-induced tumor growth, *Cancer Lett.* 406 (2017) 71–80.
- [77] B.-H. Chen, Y.J. Tsai, Preparation of catechin extracts and nanoemulsions from green tea leaf waste and their inhibition effect on prostate cancer cell PC-3, *Int. J. Nanomed.* 11 (2016) 1907.
- [78] A.M. Nassir, I.A.A. Ibrahim, S. Md, M. Waris, M.R. Ain, I. Ahmad, N. Shahzad, Surface functionalized folate targeted oleuropein nano-liposomes for prostate tumor targeting: invitro and invivo activity, *Life Sci.* 220 (2019) 136–146.
- [79] H. Hua, N. Zhang, D. Liu, L. Song, T. Liu, S. Li, Y. Zhao, Multifunctional gold nanorods and docetaxel-encapsulated liposomes for combined thermo- and chemotherapy, *Int. J. Nanomed.* 12 (2017) 7869–7884.
- [80] Rakesh K. Tekade, Rahul Maheshwari, Muktika Tekade, Mahavir B. Chougule, Solid lipid nanoparticles for targeting and delivery of drugs and genes, Academic Press, 2017, pp. 256–286.
- [81] Chandana. Mohanty, Improvement of cancer therapy by nanotechnology, *Viro. Immunol. J.* 1 (2017).
- [82] Rakesh K. Tekade, Rahul Maheshwari, Muktika Tekade, Mahavir B. Chougule, Chapter 8 - solid lipid nanoparticles for targeting and delivery of drugs and genes, nanotechnology-based approaches for targeting and delivery of drugs and genes, Academic Press, 2017, pp. 256–286.
- [83] InProcess-LSP, Lipid-based nanoparticles: manufacturing and inline size characterization, *AzoNano*, 2021, September 30. Retrieved on May 19, 2022 from, <https://www.azonano.com/article.aspx?ArticleID=5646>.
- [84] Scioli Montoto Sebastián, Muraca Giuliana, María Ruiz, Esperanza, Solid lipid nanoparticles for drug delivery: pharmacological and biopharmaceutical aspects, *Front. Mol. Biosci.* 7 (2020).





# Characterisation, development and validation of UV Spectrophotometric technique for determining Diosmetin in bulk and nanoformulations

Sumit Sheoran<sup>a,c</sup>, Swati Arora<sup>a,c</sup>, Himanshu Singh<sup>a</sup>, Anupam Kumar<sup>a</sup>, Sugunakar Vuree<sup>b,c,\*</sup>, Harish Vancha<sup>d</sup>, Smita C Pawar<sup>e</sup>

<sup>a</sup> School of Bioengineering and Biosciences, Lovely Professional University, Jalandhar, India

<sup>b</sup> MNR Foundation for Research & Innovation (MNR-FRI), MNR Medical College and Hospital, MNR University, Fasalwadi Village, Sangareddy (District), Telangana 502294, India

<sup>c</sup> Unite Lifescience, Hyderabad, Telangana, India

<sup>d</sup> School of Pharmaceutical Sciences, Lovely Professional University, Phagwara, Jalandhar, Punjab, India

<sup>e</sup> Department of Genetics and Biotechnology, Osmania University, Hyderabad, Telangana 506002, India

## ARTICLE INFO

### Keywords:

Diosmetin  
UV Method  
Characterization  
DSC  
XRD  
FTIR  
NMR

## ABSTRACT

**Background:** From ancient times, India and many other countries have utilised natural products to manage various illnesses. Because they are abundantly available and have fewer adverse effects than synthetic medications, flavonoids are secondary metabolites with diverse biological activities. But till now, no formulations are developed by utilizing Diosmetin and no technique was formulated by utilizing self-biosynthesized Diosmetin (pure). It is a flavone (subclass of flavonoids) isolated from multiple medicinal plants but, in large amounts, is found in citrus plants. They have a variety of biological and pharmacological properties. They also improve lymphatic drainage by raising the duration and severity of lymphatic compression and the exact number of fully operational lymphatic capillaries.

**Methodology:** We have procured Diosmetin from Otto Kemi Pvt. Ltd. and other chemicals from SIGMA chemicals. Furthermore, the characterisation of selected flavone has been performed through solubility studies and method development for development and validation by the UV method for nano-formulation.

**Result:** Diosmetin is pure and soluble in various solvents and has a melting point between 259.14 and 261.84°Celsius, and is more soluble in Acetone, Chloroform, and DMSO, but we have utilised Diosmetin for Cancer studies, so we have taken it in 5% DMSO for further studies. Diosmetin is stable in DMSO till 20 mg/ml at room temperature.

## Introduction

Since long ago, nature has given us food and herbal medicines for primary healthcare. However, until around two to three decades ago, most therapies were entirely based on plant medications. Because herbal drugs are more readily available and have fewer adverse effects than synthetic pharmaceuticals, they are more prevalent in today's medical system [1,2]. In addition, various plant materials cure multiple illnesses [3–6]. Natural sources provide approximately 25% of the medications used in the current healthcare profession. Ancient remedies were utilised for primary healthcare throughout Africa, Asia, and India; a large segment of the population depends on traditional herbal treatments to

address various health issues. They have different biological and pharmacological activities and are already found in multiple published data Fields [7–10]. Approximately 7000 flavonoids are identified, and still, the numbers are increasing.

Diosmetin (DM) is a naturally occurring methylated flavone (Fig. 7). It has the chemical formula  $C_{16}H_{12}O_6$  with a molecular size of 300 g/mol [11]. Further, it contains three hydroxyl groups in regions 5, 7, and 3' with a double bond at C2-C3 and 4-carbonyl unit but no C3 hydroxyl group at ring C. In addition to the 4'-methoxy band in DMT and the 4'-hydroxyl group in luteolin, the DM molecule is highly comparable to luteolin. DM is a Diosmin aglycone or DM 7-O-rutinoside [12]. It has been isolated from a wide range of plant species (Fig. 2) [10,13].

\* Corresponding author.

E-mail addresses: [sheoran080897@gmail.com](mailto:sheoran080897@gmail.com) (S. Sheoran), [swati.bioinfo95@gmail.com](mailto:swati.bioinfo95@gmail.com) (S. Arora), [sugunakarvuree@gmail.com](mailto:sugunakarvuree@gmail.com) (S. Vuree), [harish.24838@lpu.co.in](mailto:harish.24838@lpu.co.in) (H. Vancha), [smita.prof@gmail.com](mailto:smita.prof@gmail.com) (S.C. Pawar).

<https://doi.org/10.1016/j.rechem.2023.100972>

Received 27 April 2023; Accepted 21 May 2023

Available online 24 May 2023

2211-7156/© 2023 The Authors. Published by Elsevier B.V. This is an open access article under the CC BY license (<http://creativecommons.org/licenses/by/4.0/>).

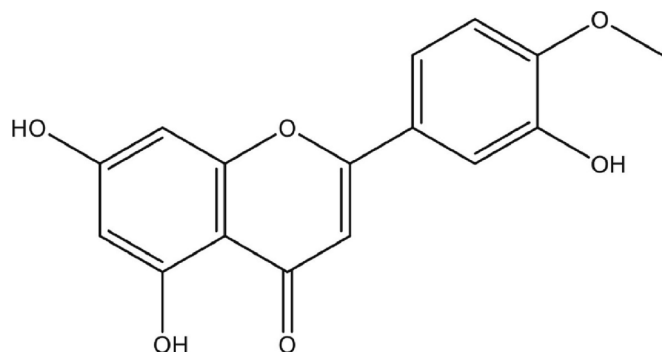


Fig. 1. Depicts the structure of DM.

As per the existing data, no analytical methods for DM were disclosed. So, here in this research paper, we characterise DM and develop their UV methodology for utilisation in various nano-formulations.

## Results and discussion

The analytical technique's uniformity, accuracy, truthfulness, detection limits (LOD), quantification limits (LOQ), & ruggedness were all evaluated.

### Linearity

Based on the regression analysis model, the calibration curves (Fig. 2) were straight across the 2–1000 g/ml range of DM concentrations.

Absorbances versus concentrations were displayed, and linear regression analysis was carried out on the resultant graphs; correlation coefficients for DM were estimated to be 0.999, Regression equation:  $y = 0.0565x + 0.138$ , Linearity ( $\mu\text{g/mL}$ ): 2–1000.

### Precision

A statistical test was done to assess the procedure's repetition. Three individuals examined the quantity of DM five times on the same day at one-hour intervals and three times on separate days for intra- and inter-

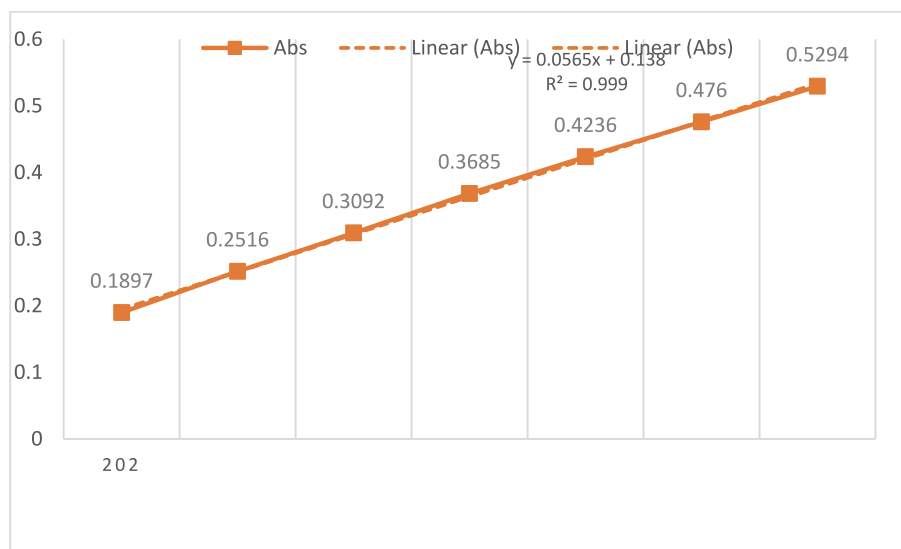


Fig. 2. Calibration curve of DM. It is a way to identify the concentration of an unknown substance. These curves use data points of known substances at varying concentrations, and researchers or developers can use these curves to find where an unknown substance plots.

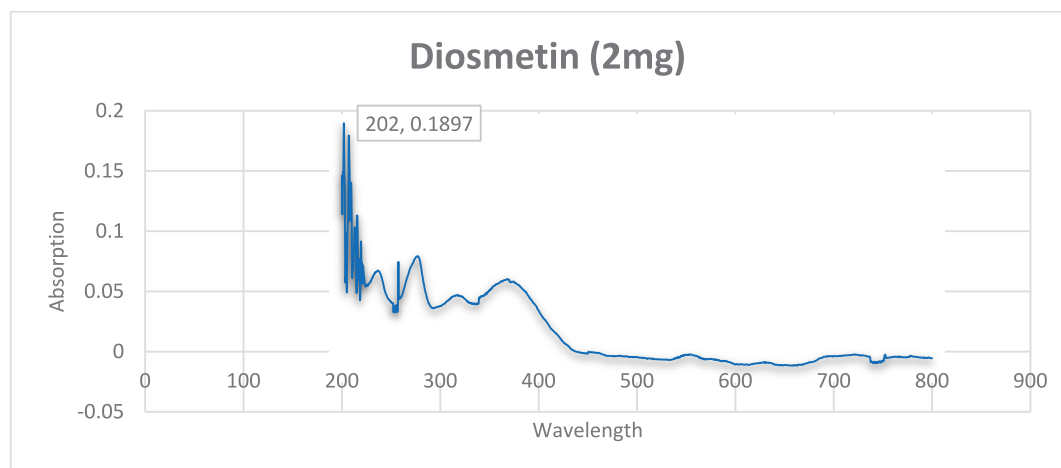
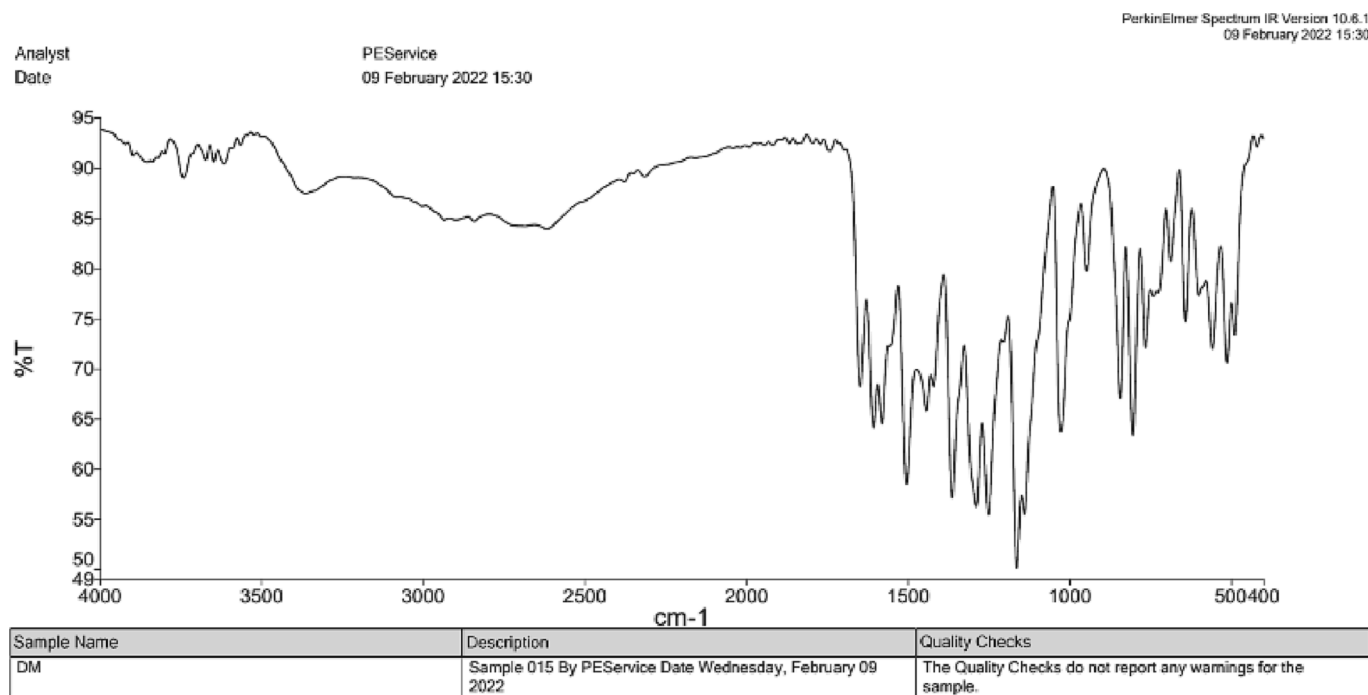
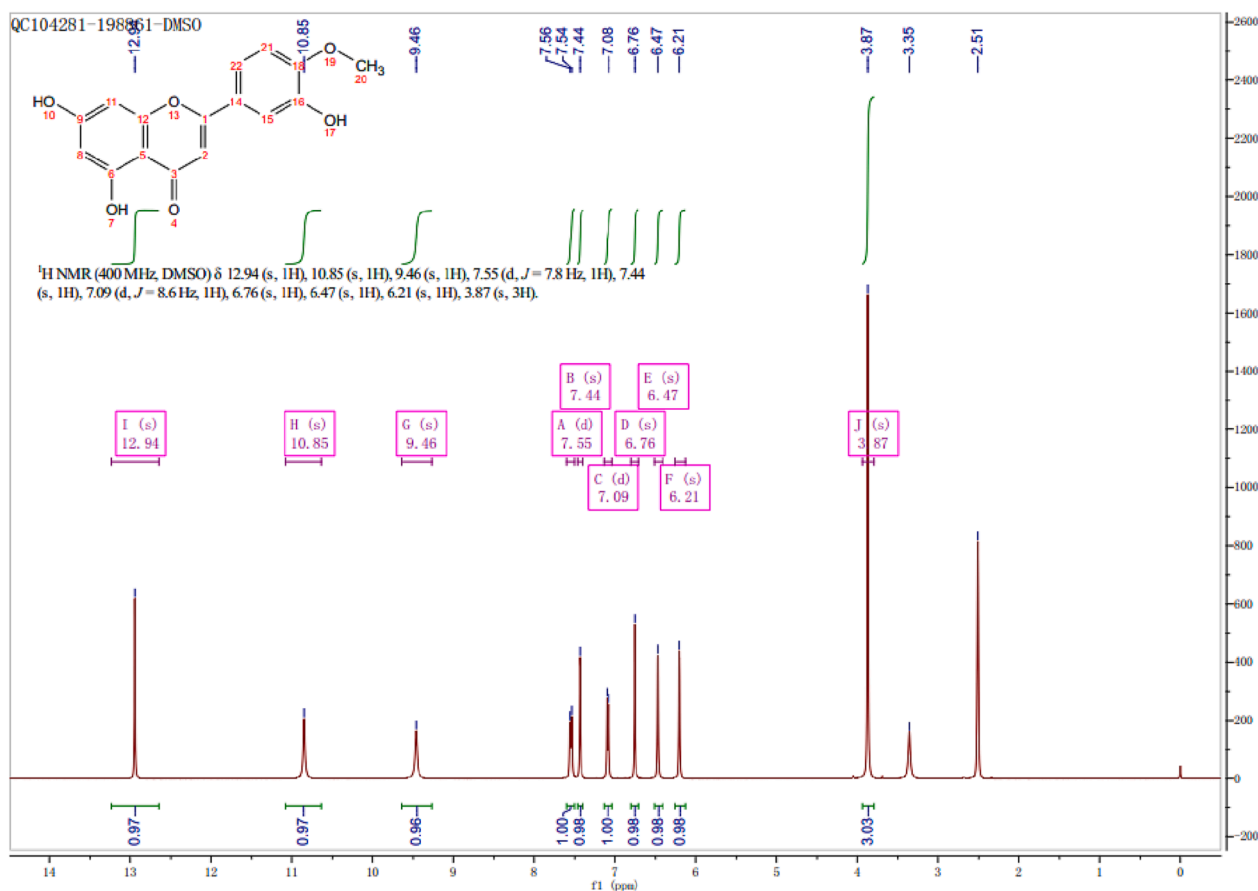


Fig. 3. Showing Lambda max of DM. Lambda max ( $\lambda_{\text{max}}$ ): The wavelength at which a substance has its strongest photon absorption (highest point along the spectrum's y-axis). This ultraviolet–visible spectrum for DM has  $\lambda_{\text{max}} = 202 \text{ nm}$ .



**Fig. 4.** FTIR Result of DM. Fourier Transform Infrared Spectroscopy (FTIR) identifies chemical bonds in a molecule by producing an infrared absorption spectrum. The spectra produce a profile of the sample, a distinctive molecular fingerprint that can be used to screen and scan samples for many different components. Here C-H Bending at 1065, the OH group peak at 3675, C-O stretching peak at 1027 and C = O peak at 1742, the C = C peak at 1580 and OH stretching peak at 3618.



**Fig. 5.** Shows the NMR result of DM.

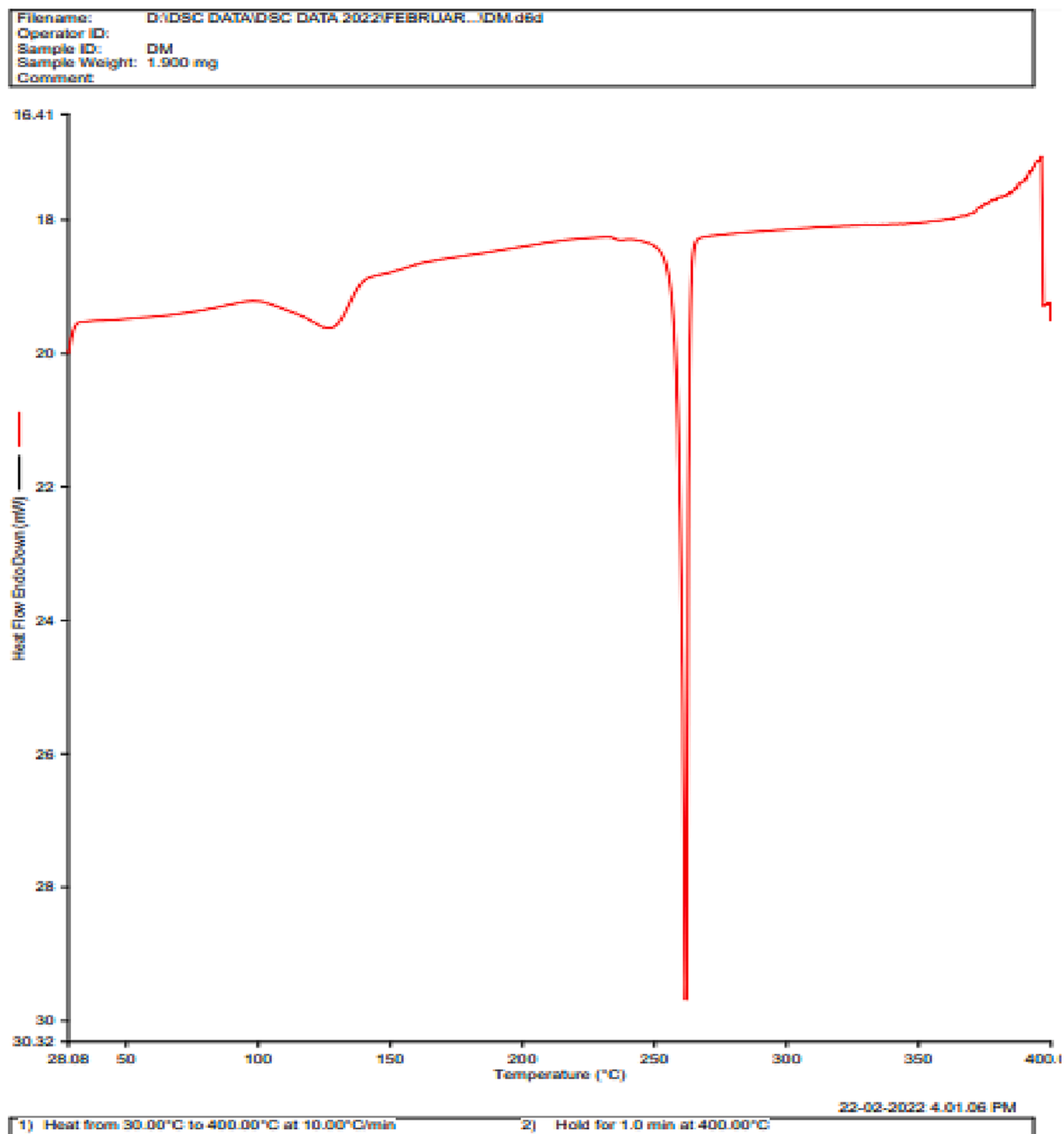


**Fig. 6.** Showing the DSC Graph of DM. The DSC curve shows an exothermic peak around 130 °C, indicating an exothermic reaction caused by crystallisation. The endothermic peak observed at around 260 °C refers to an endothermic reaction by “melting”.

day tests. The standard deviation (SD) and mean were calculated at Conc. 10 (µg/mL), inter-day(%RSD) 0.45 and intra-day (%RSD): 0.11.

#### Accuracy

The approach was used to a drug content containing a known reference volume to execute recuperation experiments. Diosmetin have been added to match labelling assertions 50, 100, and 150. Through

each step of the quantity, three determinations were performed.

#### LOD and LOQ

The LOD for DM was 6.4 g/mL, while the LOQ was 9.6 g/mL, respectively.



## (Coupled TwoTheta/Theta)

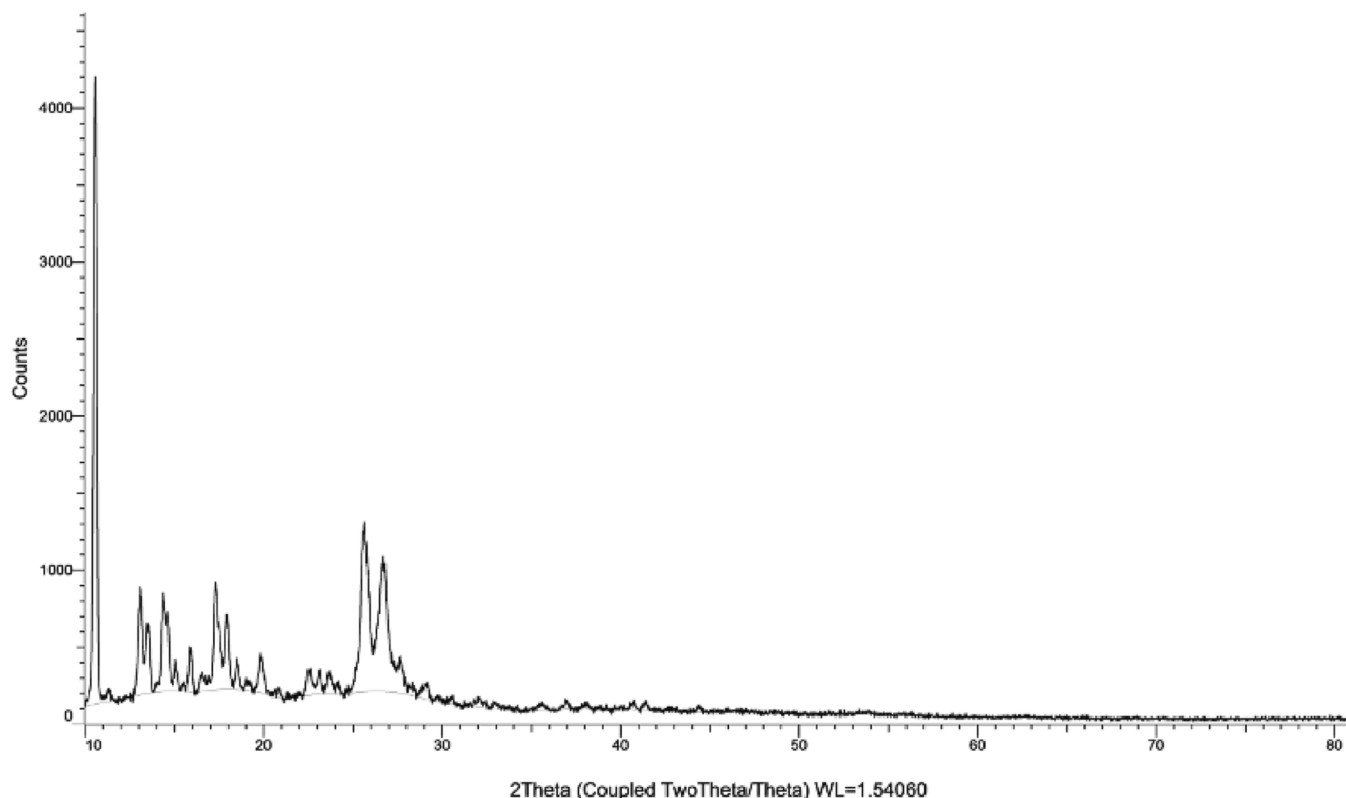


**Fig. 7.** XRD result of DM. An XRD graph (Intensity vs two thetas) is used to find the nature of the material. For sharp peaks, the material may be taken as crystalline. For a broader peak, it may be polycrystalline, while in case of no peak but with some noisy pattern, the materials are said to have amorphous nature. In our case, Sharp peaks are there; then it shows that the nature of the sample is crystalline.

**Table 1**  
Solubility of DM in Different Solvents.

Chemical	Quantity of Compound Soluble (In mg)
Chloroform	20
Ethanol	15
Methanol	10
DMSO	20
Acetone	25
N-hexane	10
Ethyl acetate	10
Acetonitrile	10
N-octanol	20

#### Characterisation of compounds

To characterise Desired compound, i.e., DM, we use various methods such as DSC, FTIR, and XRD.

#### FTIR

The FTIR method was employed to identify the materials' inorganic and organic components based on the readings of several peaks in the IR radiation area. Whenever the sample of chemicals was put through the FTIR, the constituents were distinguished based on their peak frequency. The existence of several inorganic and organic components of the substance was verified by FTIR analysis (Fig. 4). However, it has significant drawbacks, such as not displaying the metallic details of any chemical, for which we can use NMR.

#### NMR

It is a technique for assessing the chemical structure of a substance by viewing and quantifying the interconnection of nuclear spins in an intense magnetic field. It investigates the material's physical, chemical, and biological characteristics (Fig. 5). Pharmacologists employ it to detect the identity and composition of molecules. In addition, MRI, a multidimensional NMR imaging technology, is used by doctors for medical diagnostics.

5, 7-dihydroxy-2-(3-hydroxy-4-methoxyphenyl)-4H-chromen-4-one (SSD).

<sup>1</sup>H NMR (400 MHz, DMSO-d<sub>6</sub>)  $\delta$  12.96 (s, 1H), 10.88 (s, 1H), 9.50 (s, 1H), 7.54 (s, 1H), 7.44 (s, 1H), 7.10 (s, 1H), 6.76 (s, 1H), 6.48 (s, 1H), 6.21 (s, 1H), 3.88 (s, 3H). <sup>13</sup>C NMR (100 MHz, DMSO-d<sub>6</sub>)  $\delta$  182.16, 164.65, 163.96, 161.93, 157.77, 151.57, 147.23, 119.16, 113.39, 112.54, 104.21, 103.96, 99.32, 94.36, 56.19.

#### DSC

DM was determined using DSC apparatus with thermal expansion. Standardization was formerly conducted using a calibrating reagent. After that, 1.90 mg of the specimen was weighed and stored in an aluminium testing crucible, capped, and then warmed to 300 °C in N<sub>2</sub> atmosphere at a frequency of 10 °C minute<sup>-1</sup>. This method is employed to determine the melting range of a material (Fig. 6).

#### XRD

This method is employed to identify the shape or type of the specimens, such as crystalline or amorphous. For example, if the chart has a

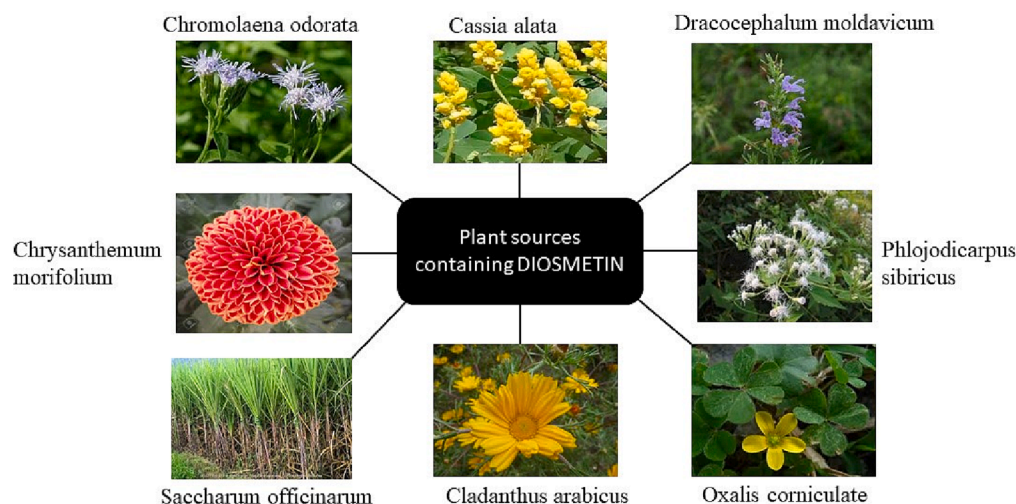


Fig. 8. Different plant sources of DM.

sharp peak, the sample is crystallised; the model is amorphous if the graph has a flat mount (Fig. 7).

## Methodology

### Chemicals and instruments

The DM was synthesised in the laboratory, Dept. of Biochemistry, School of Biosciences and Bioengineering, Lovely Professional University, Jalandhar. Methanol, acetonitrile, ethanol, chloroform, DMSO, acetone, N-hexane, ethyl acetate, and N-octanol were provided by SIGMA Chemicals. The Distilled water was prepared using water purification equipment. The characterisation used a Shimadzu Model 1800 UV-Visible dual beam spectrophotometer, DSC, FTIR, and XRD.

### Method

First, we synthesise the DM (Fig. 1) in our laboratory; after that, we characterise the obtained compounds using various approaches, including FTIR, NMR, XRD, and DSC, and then we examine the solubility of both flavonoids in Solvents such as methanol, ethanol, Acetonitrile, Chloroform, DMSO, Acetone, N-hexane, Ethyl acetate, distilled water, and N-octanol. After solubility studies, DM is stable in all solvents in different conc. As shown in Table 1 Following the solubility test, we determine the partition co-efficient and their lambda max (Fig. 3). After that, we use UV spectroscopy to determine absorbency. The UV spectra of Diosmetin were obtained in ethanol at various concentrations. (Result shown in Fig. 2).

### Synthesis procedure of DM

Several investigators presently employ that approach for DM production, which involves Hesperidin biochemical transformation [14,15]. According to Victor et al. 2021, we fixed a method for retrieving hesperidin using the Citrus plant *Sinesis L. osbeck*. We utilise their peel waste for extraction by separating it with methanol and afterwards crystallising in aqua by adding dichloroethane, lowering the solvent amount, & transferring it to hot retrieval for fresh citrus albedo with methanol, which was intended to generate better yields. In addition, chemical oxidising and hydrolysed were used to convert purified hesperidin to diosmetin, which increased its therapeutic potential [14]. DM can be obtained from different plant sources shown in Fig. 8.

DM (2–1000 µg/mL) were made and examined in various concentrations. The two highest absorbances were observed at the two wavelengths used for the investigation. At all wavelengths, the absorbance of

DM was measured, and absorptivity ratios E (1 per cent 1 cm) were calculated. The following equations can be used to compute the concentration of medicines in a mixture:

$$C^{DM} = (A1\alpha_2 - A2\alpha_1)\alpha_2\alpha_1 - \alpha_1\alpha_2 \quad (1)$$

where  $C^{DM}$  is the concentration of DM, respectively, in sample solutions. A1 and A2 are the absorbances of the DM sample at 202 nm.  $\alpha_1$  and  $\alpha_2$  are the absorptivities of DM at given wavelengths, respectively.

## Conclusion

This method is uncomplicated, reliable, as well as effective offering exact outcomes having a reduced limit of detection and a quicker reaction. The excellent results obtained in all instances, as well as the regular consistency with the published process, illustrate the capability of this method for measuring Diosmetin supplied orally with excellent precision. In addition, the reduced Diosmetin processing time suggests that this technology is appropriate for systematic study in pharmaceutical formulations or nano-formulations.

## CRediT authorship contribution statement

**Sumit Sheoran:** Data curation, Formal analysis, Investigation, Writing – original draft, Project administration. **Swati Arora:** Formal analysis, Data curation, Investigation. **Himanshu Singh:** Writing – review & editing. **Anupam Kumar:** Writing – review & editing. **Sugunakar Vuree:** Supervision, Conceptualization, Writing – review & editing, Methodology.

## Declaration of Competing Interest

The authors declare that they have no known competing financial interests or personal relationships that could have appeared to influence the work reported in this paper.

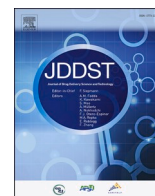
## Data availability

No data was used for the research described in the article.

## References

- [1] D.K. Patel, D. Laloo, R. Kumar, S. Hemalatha, *Pedaliu murex* Linn.: an overview of its phytopharmacological aspects, *Asian Pac. J. Trop. Med.* 4 (9) (Sep. 2011) 748–755, [https://doi.org/10.1016/S1995-7645\(11\)60186-7](https://doi.org/10.1016/S1995-7645(11)60186-7).

- [2] K. Patel, M. Gadewar, R. Tripathi, S.K. Prasad, D.K. Patel, A review on medicinal importance, pharmacological activity and bioanalytical aspects of beta-carboline alkaloid "Harmine", *Asian Pac. J. Trop. Biomed.* 2 (8) (Aug. 2012) 660–664, [https://doi.org/10.1016/S2221-1691\(12\)60116-6](https://doi.org/10.1016/S2221-1691(12)60116-6).
- [3] D.K. Patel, R. Kumar, D. Laloo, S. Hemalatha, Diabetes mellitus: an overview on its pharmacological aspects and reported medicinal plants having antidiabetic activity, *Asian Pac. J. Trop. Biomed.* 2 (5) (May 2012) 411–420, [https://doi.org/10.1016/S2221-1691\(12\)60067-7](https://doi.org/10.1016/S2221-1691(12)60067-7).
- [4] D.K. Patel, S.K. Prasad, R. Kumar, S. Hemalatha, An overview on antidiabetic medicinal plants having insulin mimetic property, *Asian Pac. J. Trop. Biomed.* 2 (4) (Apr. 2012) 320–330, [https://doi.org/10.1016/S2221-1691\(12\)60032-X](https://doi.org/10.1016/S2221-1691(12)60032-X).
- [5] D.K. Patel, R. Kumar, S.K. Prasad, S. Hemalatha, "Pharmacologically screened aphrodisiac plant-A review of current scientific literature, *Asian Pac. J. Trop. Biomed.* vol. 1 (no. 1(Supplement)) (2011) S131–S138, [https://doi.org/10.1016/S2221-1691\(11\)60140-8](https://doi.org/10.1016/S2221-1691(11)60140-8).
- [6] D.K. Patel, S.K. Prasad, R. Kumar, S. Hemalatha, Cataract: A major secondary complication of diabetes, its epidemiology and an overview on major medicinal plants screened for anticataract activity, *Asian Pacific J. Trop. Dis.* 1 (4) (2011) 323–329, [https://doi.org/10.1016/S2222-1808\(11\)60075-3](https://doi.org/10.1016/S2222-1808(11)60075-3).
- [7] S. Gao, M. Hu, Bioavailability challenges associated with development of anti-cancer phenolics, *Mini Rev. Med. Chem.* 10 (6) (Jun. 2010) 550–567, <https://doi.org/10.2174/138955710791384081>.
- [8] O. Zanoaga, C. Braicu, A. Jurj, A. Rusu, R. Buiga, I. Berindan-Neagoe, Progress in research on the role of flavonoids in lung cancer, *Int. J. Mol. Sci.* 20 (17) (2019) 4291.
- [9] E.W.C. Chan, Y.K. Ng, C.Y. Tan, L. Alessandro, S.K. Wong, H.T. Chan, Diosmetin and tamarixetin (methylated flavonoids): a review on their chemistry, sources, pharmacology, and anticancer properties, *J. Appl. Pharm. Sci.* 11 (3) (2021) 022–028, <https://doi.org/10.7324/JAPS.2021.110302>.
- [10] M. Garg, S.K. Chaudhary, A. Goyal, P. Sarup, S. Kumari, N. Garg, L. Vaid, B. Shiveena, Comprehensive review on therapeutic and phytochemical exploration of diosmetin: a promising moiety, *Phytomedicine Plus* 2 (1) (2022) 100179.
- [11] K. Patel, M. Gadewar, V. Tahilyani, D.K. Patel, A review on pharmacological and analytical aspects of diosmetin: a concise report, *Chin. J. Integr. Med.* 19 (10) (Oct. 2013) 792–800, <https://doi.org/10.1007/s11655-013-1595-3>.
- [12] X. Chen, L. Xu, S. Guo, Z. Wang, L. Jiang, F. Wang, J. Zhang, B. Liu, Profiling and comparison of the metabolites of diosmetin and diosmin in rat urine, plasma and feces using UHPLC-LTQ-Orbitrap MSn, *J. Chromatogr. B* 1124 (2019) 58–71.
- [13] S.R. Numonov, M.N. Qureshi, H.A. Aisa, Development of HPLC protocol and simultaneous quantification of four free flavonoids from dracocephalum heterophyllum benth, *Int. J. Analyt. Chem.* 2015 (2015) 1–5.
- [14] M.M. Victor, J.M. David, M.V.M. Cortez, J.L. Leite, G.S.B. da Silva, A high-yield process for extraction of hesperidin from orange (citrus sinensis L. osbeck) peels waste, and its transformation to diosmetin, A valuable and bioactive flavonoid, *Waste and Biomass Valorization* 12 (1) (2021) 313–320.
- [15] C. Shuanglian, W. Zheng, W. Jing, W. Qian, S. Yang, Synthesis and biological activities of natural flavonoid diosmetin and its derivatives, *Chinese J. Org. Chem.* 32 (3) (2012) 560–566.



## Review article

# Artificial intelligence and nanotechnology for cervical cancer treatment: Current status and future perspectives

Satbir Kour<sup>a,1</sup>, Indrani Biswas<sup>b,1</sup>, Sumit Sheoran<sup>a,1</sup>, Swati Arora<sup>a,1</sup>, Prasanna Sheela<sup>c</sup>, Santosh Kumari Duppala<sup>a</sup>, Dwarkanath K. Murthy<sup>d</sup>, Smita C. Pawar<sup>d</sup>, Himanshu Singh<sup>a</sup>, Deepak Kumar<sup>e</sup>, Dhamodharan Prabhu<sup>f</sup>, Sugunakar Vuree<sup>g,\*\*</sup>, Raj Kumar<sup>h,\*</sup>

<sup>a</sup> School of Bioengineering and Biosciences, Lovely Professional University, Punjab, 144111, India

<sup>b</sup> Mahatma Gandhi Medical Advanced Research Institute (MGMRI), Sri Balaji Vidyapeeth (Deemed to be University), Puducherry, 607402, India

<sup>c</sup> Department of Biotechnology, Telangana University, Dichpally, Nizamabad, 503322, Telangana, India

<sup>d</sup> Department of Genetics, Osmania University, Hyderabad, Telangana, 500007, India

<sup>e</sup> School of Chemical Engineering and Physical Sciences, Lovely Professional University, Punjab, 144111, India

<sup>f</sup> Centre for Drug Discovery, Department of Biotechnology, Karpagam Academy of Higher Education, Coimbatore - 641021, India

<sup>g</sup> MNR Foundation for Research & Innovation, MNR Medical College & Hospital, MNR University, Fasalwadi Village, Sangareddy (District), Telangana, 502294, India

<sup>h</sup> Department of Pharmaceutical Sciences, University of Nebraska Medical Center, Omaha, NE, 68105, USA

## ARTICLE INFO

## Keywords:

Phytochemicals  
Epigenetics  
DNA Methylation  
Histone deacetylation  
Artificial intelligence  
Nanoscience

## ABSTRACT

Cancer epigenetics has become increasingly popular due to the reversible nature of epigenetic changes that tend to take place during carcinogenesis. Cervical tumorigenesis is influenced by epigenetic changes such as DNA methylation and acetylation. Several epigenetically active inhibitors targeting DNA methyltransferase (DNMTs) and histone deacetylases (HDACs) are either approved or under clinical trials to treat cervical cancer. However, most synthetic inhibitors have shown adverse side effects, off-target specificity, and are expensive. Hence, bioactive phytochemicals, widely available with lesser toxicity impacts, have been evaluated for their role in the modulation of epigenetic traits involved in gene regulation for cervical cancer prevention and therapy. Most of these phytochemicals potentially altered the expression of oncogenes and key tumor suppressor genes through modulation of DNA methylation and chromatin modification in different forms of cancer including cervical cancer. Even though these compounds exerted potential anti-tumor activity, there is a paucity of studies reported on their targeted delivery with desirable effects. In this scenario, nano-encapsulated drugs exhibited multi-parametric anti-tumor activity, yet there are some crucial factors such as the tumor-microenvironment (TME) and toxicological effects of these nano-formulated therapeutics may pose a difficult task from its clinical use. However, computational pharmaceuticals employing artificial intelligence (AI) tools and nano-formulations might elevate the present therapeutic strategy compared to the conventional route. This review also supports significant future research for developing AI and nanotechnology based therapeutics that are needed for advanced, precise, and personalized healthcare systems.

## 1. Introduction

Cervical cancer is the fourth most frequent female cancer worldwide and poses a significant planetary health concern [1]. Annually, more than 500,000 women are diagnosed with cervical cancer, and the illness kills over 300,000 people globally. The therapeutic potential of conventional therapies is limited against cervical cancer. Unlike other

cancers, despite tremendous efforts to combat cervical cancer, most therapeutic strategies are minimally successful; thereby, the integration of multiple disciplinary routes has emerged as a necessary pre-requisite to treat it. In addition, most of the synthetic compounds used for treatment provoke a typical drug resistance amongst these tumors, driving the process of drug design a complicated and challenging task [2].

Considering cancer stem cells (CSCs) segregate away from the

\* Corresponding author.

\*\* Corresponding author.

E-mail addresses: [sugunakarvure@gmail.com](mailto:sugunakarvure@gmail.com) (S. Vuree), [rk7410@gmail.com](mailto:rk7410@gmail.com) (R. Kumar).

<sup>1</sup> Authors contributed equally.

treatment in the tumor microenvironment, the risk of recurrence of cervical cancer is approximately 35%. This is most likely due to medication retention or outflow. Cytotoxicity, impairment to other non-targeted tissues, loss of hair, neurotoxic, multidrug resistance, nausea, anaemia, and neutropenia are all common side effects in cancer patients undergoing chemotherapy or radiation [3,4]. These adverse effects restrict and/or potentially ruin the efficacy of treatment methods. As a result, there will be an immediate need for further discovery of novel antitumor medicines that are more effective for cancer treatment while having fewer negative impacts on the rest of the healthy tissue. Based on these findings, flavones were investigated, and it was discovered that flavone analogues had the possibility to be antitumor medications [5]. Zutphen discovered that flavonoids reduced the chance of death from respiratory tract malignancies. Since 1930, phytochemicals have been employed as potential bioactive anti-cancer compounds/pharmacological leads, attributed to their low toxicity, bioavailability, and less off-target side effects [6]. From 1967 to 1991, a wide scientific community studied the effect of flavonoids in the prevention of lung cancer, malignant neoplasms, and ovarian cancer. Furthermore, phytochemicals in combination with synthetic drugs to treat cervical cancer with a focus on epigenetic markers have been less explored. Epigenetics, known as the state of extra-genetic elements, plays a key role in regulating gene expression patterns involved in cellular-biochemical-physiological processes [7,8]. Histone deacetylases (HDAC) and DNA methyltransferases (DNMTs), the prudent ailments of epigenetics, modulate the activity of the genotypic-phenotypic representation of a cell, and alteration of these molecules provoke the process of tumorigenesis [9,10].

On the contrary, *in silico* tools and techniques, the rising red queen race of artificial intelligence (AI) and virtual screening has emerged as crucial players in drug designing to combat several cancers including cervical [11]. AI can be categorized broadly as supervised and unsupervised machine learning methods, which facilitate random screening of several compounds, prediction of bioactivities of known and unknown pharmaceuticals, drug screening, and toxicological screening, that put off the enormous time and resources expenditure required otherwise performed using *in vitro* experimental set-up [12,13]. Furthermore, this tool facilitates the stabilization and development of appropriate formulations of drugs exposed to the least error-prone. In this perception, the present review discusses the plausible pharmacological activities of phytochemicals focusing on epigenetic markers and the concurrent implementation of AI assisted nano-formulations in the field of anti-tumor therapeutics, which can enrich the platform for framing targeted anti-cervical therapeutics.

## 2. Phytochemicals regulating epigenetic modulators

Plant-derived phytochemicals are bioactive non-nutrient substances that have been linked to a reduction in the incidence of several medical problems. The biochemical and pharmacological action of the anti-cancer compounds derived from natural resources exhibits divergent bioactivities such as anti-inflammation, antioxidant, and immunomodulatory accompanying different pathogenic signaling pathways [14,15]. Most of the anti-tumor compounds exert apoptosis in tumor cells, with a concurrent reduction in the expression of growth and proliferation-associated genes, attributed to the 'go/grow' traits irrespective of any cancer type [16,17]. One of the significant pathways in regulating tumor genesis includes epigenetic molecular alterations, that trigger tumor promotion and progression [18,19].

Regulation of epigenetic factors modulated by phytochemicals are summarised in Table 1. Amongst the phytochemicals listed in Table 1, curcumin was administered in phase I/II clinical trials of cervical cancer patients as a potent chemosensitizer for paclitaxel therapy [20]. One potent phytochemical Carboplatin (Paclitaxel) "Old-Gold Rider," has been approved by the Food and Drug Administration (FDA) in combination with Taxol and implemented in most cancer types, including

**Table 1**  
Regulation of epigenetic factors modulated by Phytochemicals.

Phytochemical/ Dietary agent (source)	Epigenetic modification(s)	Mechanism(s)	Reference
Green tea polyphenol— epigallocatechin-3- gallate (EGCG) (green tea)	DNA methylation Histone modifications Differential miRNA modulations	DNMT inhibitor Promoter methylation ↓ SAM, 5 mC ↓ HDAC activity ↓ HAT exp ↑ Ac-H3, H3K9Ac, Ac- H4 ↑ HMT inhibitor BMI-1, SUZ12, EZH2, EED, H3K27me3 ↓	[32–42].
Curcumin (turmeric)	DNA methylation Histone modifications Differential miRNA modulations	DNMT inhibitor Promoter methylation ↓ 5 mC ↓ MeCP2 binding ↑ H3K27me3 ↑ HDAC1, HDAC-3, HDAC-8 ↓ p300 (HAT) ↓ Ac-H3, Ac- H4 ↓ miR-22 ↑, miR- 186 ↓ miR-15a ↑, miR16	[43–54]
Sulforaphane	DNA methylation Histone modifications	DNMT expression ↓ Promoter methylation ↓ HDAC inhibitor Ac-H3 and Ac-H4 ↑	[54–57]
Genistein	DNA methylation Histone modifications Differential miRNA modulations	DNMT inhibitor Promoter methylation ↓ HDAC exp ↓ HAT exp ↑ Ac- H3, Ac-H4, Ac-H3K9 ↑ H3K9me2 ↑ miR- 200 ↓, miR1296 ↑, miR-27a ↓	[58–67]
Resveratrol (Grapes)	DNA methylation Histone modifications	DNMT inhibitor MBD2 recruitment ↓ Promoter methylation ↓ MTA1/NuRD corepressor complex ↓	[68]
Lycopene	DNA methylation	Promoter methylation ↓	[69]
Quercetin	DNA methylation Histone modifications	DNMT inhibitor Promoter methylation ↓ Ac- H3 ↑ HDAC-1 ↓ miR-let-7e, miR- 370, miR-373* and miR-526b ↑ let-7a, let-7c, let-7d ↓	[70]
Ellagitannins	Differential miRNA modulations		[71]

cervical cancer [21]. Polyphenolic compounds have been ubiquitous in nature and are an integral part of the diet, acting to enhance chemopreventive and chemosensitizer properties in nutritional supplements [22]. Furthermore, several cohort studies showed an increase in life span and reduction of invasive cervical cancer propagation is directly associated with the intake of pigmented fruits and vegetables [23]. Another randomized, double-blind, multi-centre clinical trial assessed the efficacy of 3, 3'- diindolylmethane (DIM, a stable form of Indole-3-carbinol), a sulfur-containing glucosinolate obtained from cruciferous vegetables, whereby more than 90.5% of patients had histological regression in cervical cancer patients [24]. One of the potent phytochemicals, berberine (Ber), an isoquinoline alkaloid derivative, has been evaluated for its cervical cancer preclinical efficacy [25]. Phytochemicals exhibit their anti-tumor effects by alteration of signaling molecules which involved in growth, proliferation, survival, invasion, metastasis, angiogenesis, and major hallmarks of any malignancy [26]. Of specific note, one of the key features interplayed in



deregulating tumor cells by these natural products is mediated by the epigenetic modulation [27]. Studies reported that green tea polyphenolic component (EGCG) leads to inhibition of DNMT activity (Table 1) elucidated using molecular modelling studies, where hydrogen-bonds are formed within the catalytic pocket of DNMT against the residues- Pro (1223) and Glu (1265), Cys (1225), Ser (1229), and Arg (1309), unraveling a new dimension in the perspective of *in silico*-based epigenetic phytochemical modulator [28]. GSTP1, a gene observed in many cancers, undergoes a similar inhibition pattern in prostate cancer cell line LNCaP treated with a very narrow range of Guanosine Tri-phosphate (GTP) [29]. Interestingly, in the same study, it was noticed that treatment with GTP does not lead to alteration in levels of hypomethylation but assures to sustain genomic integrity. Likewise, Resveratrol, a widely known polyphenolic compound found in grapes, known to exert profound anticancer effects, is also a DNMT inhibitor, which facilitates cancer prevention and treatment [30]. A rarely known polyphenolic compound hesperidin inhibits both DNMT1 and HDAC which has been shown to exert anticancer effects in several cancer cell lines, including cervical, mediated by different signaling molecules such as GSTP1, AKT, MAPK1, RAS, MAPK3, affecting proliferation and reactive oxygen species (ROS) production with concurrent induction of apoptosis [31].

Some of the other polyphenolic compounds, like kaempferol, displayed anti-tumor effects in different cancer cell lines (Breast cancer-MCF-7, Lung cancer- A549, Liver cancer-SK-HEP1, Colorectal cancer-HT-29, Cervical- KB-V1, and SiHa and other cancer cells) by inhibiting expression of DNMT3a, DNMT3b, and HDAC1 and in xenograft mice model. Another polyphenolic compound, pterostilbene, is a DNMT inhibitor that reduces expression of SIRT1 activity and was evaluated in MDA-MB-231 cells (breast cancer cell line) and mice model [72]. Naringenin, a potent polyphenolic compound, is DNMT1, DNMT3a, DNMT3b, and HDAC1 inhibitor molecule, exhibits anticancer effects in different cancer lines (Lung cancer-A549, Esophageal cancer-KYSE-510, Liver cancer-HepG2, Huh-7, HA22T, Colorectal cancer-HCT116, SW480, Lovo, and HT-29 cells) as well as in resected rat model [73]. Provided the vast strides of phytochemicals in modulating anti-tumor responses in different cancer cell lines and animal models, these pharmacological leads are considered potent chemopreventive agents [74], but the individual administration of these items may pose a challenging fact and they have been rarely investigated as nano-formulated conjugated compounds, which might come across the hurdles faced across conventional therapeutic strategies.

Nonetheless, very few of them have been approved by FDA to combat this typical oncogenic process in the cervix. There is a lacuna in an exploration of the underlying molecular mechanism of their anti-cancer efficacy in a clinical/pre-clinical setup. Thereby, there is a dire requirement to reframe novel therapeutic strategies that might overcome this battle. Since the 1990s, the implementation of AI has been initiated in the biomedical field; nevertheless, there exist loopholes concerning its appropriate usage in this field, and hence it is warranted.

## 2.1. Novel era for treatment in cancer: Nanoscience & nanotechnology

Drug circulation and multidrug resistance (MDR) are the major challenges faced while treating most cancers [75]. In the past few years, nano-medicine and nanoscience have gained increasing importance from the perception of targeted delivery of anti-cancer therapeutics [76]. Implementing nano-medicines has effectively enriched the route of targeted drug delivery and therapy [77]. Nano-formulations, a typical category of nanomedicines, are broadly classified as metallic nanoparticles [78], inorganic and organic nano-particles [79], nano-composites [80], natural nano-carriers [81], and several other nano-medicines [82]. Studies have reported the effectiveness of drug loading and release through nano-formulated phytochemicals for treating several cancers [83]. Physical and chemical methods can prepare MNPs; however, green synthesis can also be implemented.

Al-Sheddi et al. [84] achieved the biosynthesis of silver nanoparticles using *Nepeta deflersianaplant* extract. The biosynthesized silver nanoparticles demonstrated the concentration dependent anticancer potential against human cervical cancer (HeLa) cells [84].

Gold (Au) and Silver (Ag) nano-particles exhibited potent anticancer activity in different cervical cancer cell lines [85]. Polyphenols derived from tea-synthesized nano-particles and copper (II) (LQM402) was reported to inhibit proliferation in different cervical cancer cell lines [85]. Among the diverse variety of inorganic nano-particles [86], magnetic nano-particles, and quantum dots [87] are well-known players in terms of anticancer diagnostics and therapeutics, which has not been explored much so far. Organic nano-particles comprise liposomes [88], phytosomes, chitosan/gelatin, and poly-DL-lactide-co-glycolic acid (PLGA) [89] conjugated phytochemicals that exhibited drug delivery at targeted sites efficiently [70]. In 1995, the FDA recognized the very first nano-drug, PEGylated liposomal DOX (Doxil®). Till date, the FDA has approved more than six liposome based nanomedicine for cancer treatment. Following the success of liposomes in chemotherapy, liposomes were employed as one of the most compelling targeted drug carriers in chemoimmunotherapy [90]. Cationic chitosan-conjugated nano-particles served as effective drug carriers and delivery agents in several *in vivo* and *in vitro* tumor models [91] as well as in pre-clinical studies [92]. Artificial DNA nano-carriers are composed of artificially synthesized DNA hybrid structures, which can conjugate with other metallic nanoparticles or liposomes and might prove as effective drug delivery agents due to their high retentivity in cancer cells compared to free drugs [93]. Most of these nano-formulations are resistant to enzymatic degradation. Cell-pH-based drug release determines the nature of the release of the drug, which is a determining factor in most drug delivery systems [94]. However, the clinical efficacy of these nano-formulations as potential therapeutics remains limited [95]. Aptamers, a special class of nano-formulation of very low molecular weight, are basic RNA oligonucleotides that efficiently bind to the target molecule. These features enable more efficient drug delivery because of their ability to reach the core of cancer cells through the endosomal pathway. Alternatively, these are termed as 'Theranostics' [93]. Photo-ablation and photo-dynamic therapy utilize this nano-formulations to aggravate the temperature surrounding the tumor microenvironment, while the nano-bio interactions remain poorly understood [96]. According to Yadav et al. [97] PLGA nanoparticles have more functional groups and surface area than other types of particles, which helps them survive longer in bodily fluids. Additionally, HepG2 liver cancer cell growth was inhibited by quercetin/PLGA-lipid nanoparticles both *in vitro* and *in vivo* models by reducing the expression of histone deacetylases [97]. Likewise, quercetin-loaded mesoporous silica augmented the chemotherapeutic activity of paclitaxel. This combination reduced CD44 (receptor-mediated) expression of MCF-7/ADR cells, which induced apoptosis by G2/M cell cycle arrest [98]. Similarly, fabricated chitosan as well as co-delivery of quercetin and paclitaxel enunciated the cytotoxicity in A549 lung cancer cells [99]. A similar study reported that docetaxel and thymoquinone coated in chitosan and lipid nano-particles enhanced cytotoxicity in breast cancer cells MCF7 and MDA-MDB231 cells [100]. Glioblastoma (GB) or Glioblastoma multiforme (GBM), also coined as the butterfly tumor, develops extensive infiltration and chemo-resistance against the standard drug Temozolomide (TMZ). In a recently reported study, nano-micelles-coated curcumin was reported to induce the highest cytotoxicity in U87 GB cells by modulation of the Wnt-signaling cascade [101].

Likewise, another study demonstrated that curcumin and siRNA were successfully co-delivered with the dint of functional dendrimers in Hela cervical cancer cell line. This demonstrated improved cytotoxicity with subsequent reduction of Bcl2 expression in Hela cells in a synergistic manner [102]. Zaman et al. formulated the curcumin loaded PLGA nanoparticles which showed potential to inhibit cell growth with concurrent up-regulation of apoptosis which is mediated by cell cycle arrest in the cervical cancer cell line. To an extent of the same study,

interestingly, it was reported that its sub-sided expression of miR-21 (oncogenic miRNA, responsible for tumorigenesis in most cancers including cervical) with a concurrent reduction in expression of  $\beta$ -catenin, thereby arresting cervical tumor genesis. So far, nano-formulations targeting epigenetic modulators in cervical cancer remain to be explored.

Nevertheless, nano-formulated chemotherapeutics may arise disputes in pharmacokinetics and pharmacodynamics along with better retention and enhanced binding specificities of the drug moieties within a tumor microenvironment (TME) [102]. However, the harsh conditions of tumor microenvironment affect the potential of small molecule inhibitors such as Taxol and carboplatin. Therefore, screening and preparation in an *in silico* experimental set-up using AI has become a mandatory prerequisite to determine the extent of the behavioral response of the drug and other associated pharmaceutical disparities.

## 2.2. AI assisted surface characterization of nano-carriers

Given the rationale of using nano-carriers as anti-cancer agents, it is also important to know their physicochemical properties such as shape, size, permeability or presence of functional groups, key ingredients to its appropriate bioactivity. With the dint of automation, nano-carriers will attain a dynamic DDS model. Several AI algorithms such as the Light GBM model demonstrated a sufficient standard response against the development of nano-crystals, which was amended by high-pressure homogenization and wet billing methods field [103]. Additionally, cost-effective theoretical computational tools can be implemented in place of experiments. Molecular dynamics and Monte Carlo Simulations are among them, which have been implemented in lieu of experiments, as they provide accurate quantitative measurements. Similarly, for targeted self-emulsifying DDS (SEDDS) AI based algorithms play a critical role in the accurate development of these SEDDS. Seven different types of algorithms were developed based on the different datasets that defined the composition of SEDDS, comprising oil surfactants and co-surfactants. Interestingly, random forest-based formation of SEDDS was more sensitive, specific and accurate in comparison to other methods [104].

## 2.3. AI accompanying nanotechnology for anti-cancer activity

Even though extensive applications of nano-carriers exist, nano-formulated drugs or therapeutics have demonstrated potent anti-tumor activity against different cancer cells (section 2.1). However, there are some unmet challenges in this field such as robust characterization methods and optimizable approaches following regulatory and safety guidelines with a rising concern about toxicity and other associated side effects. Besides, inadequate *in vitro* and *in vivo* models substantiate their toxicological and other accompanying effects. Moreover, biodistribution and pharmacokinetics profiles may serve as the additive factor that might interfere during targeted or nano-formulated drug delivery system (DDS) process. In this scenario, AI assisted rather “computational pharmaceuticals” have improvised the process of multiscale-based pharmaceutical development by considering physical and chemical properties, pharmacokinetics and *in vitro/in vivo* correlated models. Within the past two years, studies have employed AI based algorithms such as random forest or other machine learning methods (possessed 85% approximation) that depicted accurate stability and time-dependent release activity with several folds of validation and the least errors. One of the crucial points addressed by nano-carriers is binding to multiple targeted receptors; it possesses different shapes, sizes and other pharmacokinetic/pharmacodynamics properties [103]. Therefore, an optimal nano-formulated DDs is essential prior to its effective pharmaceutical response. In this context, the optimization of nano-carriers assisted with AI tools has elevated the platform for drug loading, retention and formulation of stability. For example, nano-robots have been designed as micro-atomic, cellular and molecular

structures that attempt to diagnose and treat lethal diseases. One of the major hotspot functions of nano-robots is in the field of anti-cancer therapy. Interestingly, nano-robots function as micro-nano- electromechanical device or the biosensor needs assistance from automation tools such as AI. This has necessitated the integration of both of these techniques that serve multi-parametric assessment to produce the desired effect in the targeted site [105]. Besides, integration of artificial neural networks (ANN), nano-robots have been designed to serve both as biosensor and transducers, which enables tumor cell detection and targeted drug delivery and hence plays an important role not only as apt anti-cancer theranostics but also pulls down the associated side effects [106]. Thereby, there is a mandatory need for detailed exploratory studies to elucidate the AI assisted nano-techniques which exert potent anti-tumor activities.

## 2.4. AI in drug screening and physicochemical properties

In the past few years, the widespread adoption of AI has enabled computer-aided drug design (CADD) to surpass the difficulties faced across conventional anti-cancer drugs [107]. AI is increasingly utilized in numerous community sections, including the pharmacy sector. In this review, we emphasize the application of AI in several areas of pharmaceutical business, such as drug repurposing, medicine development & research, increasing biopharmaceutical output, and clinical trials.

AI uses programming that enables tasks skillfully with sub-field machine learning (ML) tools like Gaussian process, support vector machine, k-nearest neighbor, random forest, naïve Bayes classifier, and regression tree, which sheds noticeable insights into pharmaceuticals [108], including optimization of gradient conditions in chromatography, designing the pre-formulations using new drugs/leads, analyzing the multivariate nonlinear relationships, predicting the behavior of drugs. The amount of drug loaded and released in a system is a determining factor in analyzing the pharmacokinetics-pharmacodynamics of a drug [49]. Thus, optimizing conditions of DDSs should be found in an appropriate manner [109]. More precise interpretation, management, and analysis of complex functions or data should be implemented using AI algorithms. This intervention, if paved in a clinical setup, can enhance the rate of prediction of drug-target interactions along with fixation of drug dosages, Quantitative Structure-Activity Relationship (QSAR) or Quantitative Structure-Property Relationship (QSPR), *in vivo* responses, ability to cross the blood-brain barrier (BBB) permeability and other pharmaceutical profiles, in contrast to performed in a conventional route of pre-clinical experimental set up [110].

## 2.5. AI assisted drug delivery system and pharmacokinetics

Drug delivery systems play an important role in the treatment of various diseases, including cancer. The drug release mechanism involves nano-carrier binding and linking with the drug and the receptor. The targeted drug delivery can occur through a linker mechanism or encapsulation. The steps involved in pharmacokinetics as the drug is administered are absorption, distribution, metabolism, and elimination [103]. Nano-materials can furnish controlled drug dosing by fixing the drug release rate to the patient's specific pharmacokinetics and pharmacodynamic profiles. The use of AI in nano-theranostics formulations have significant impacts in therapeutics and diagnostics. In this case, the imaging agents and the drug need to be loaded into the particle prediction machine-learning algorithms can be applied to predict their encapsulation efficiency [108].

## 2.6. AI in prediction of bioactivity

The bioactivity of a drug is measured in terms of the nature of interaction/affinity between the drug, and the target receptor, a prime factor, before entitling them as “therapeutic drugs” [111]. Drug-target binding affinity (DTBA) is a vital prerequisite to determining

drug-target interactions. One of the AI methods is feature-based selection, which utilizes the drug target's features and properties to decide the appropriate drug target [111]. In contrast, similarity-based interaction utilizes the similarity features among the drugs, and a common assumption is made that similar medications interact with the same targets. Interestingly, several web-based application software like Chem-Mapper and similarity-based ensemble approach (SEA) are accessible to predict drug-target interactions in an online platform [107]. Likewise, SIMBOOST and other software (Paul et al., 2021) avail both similarity and feature-based selection to predict drug-target interactions. In addition, SMILES provides the structure of drug molecules in a 1-Dimension (1D) representation, which helps in toxicity prediction analysis [107,111–113].

Similarly, WideDTA uses a Convolutional Neural Network (CNN) based deep learning approach that implements ligand SMILES, amino acid sequences, and protein domain and motifs information that assist in finding the appropriate binding affinity of the drug molecule against the drug target, precisely [114]. Deep Learning (DL) is an independent interpretable software that considers SMILES of drugs and protein structures to estimate physicochemical properties [115]. On the other side, Unsupervised Machine Learning implements MANTRA and PRE-DICT software, which predicts the bioactivities of drugs (for known and unknown pharmaceutical moieties) against the target protein of interest, a cutting-edge approach in the drug discovery process.

In computational chemistry, AI technology is becoming a precious asset. A slew of machine learning models for activity estimation has evolved, making it an essential method for mining chemical knowledge from big complex databases. These techniques allow compound revelation to be automated to locate physiologically active compounds with crucial features. ML is a branch of AI in which computers learn from data, recognize trends, and decide without even being pattern recognition. Even though ML algorithms were developed in the 1950s, ML began to flourish in the 1990s and is now the greatest prominent sub-field of the AI [116]. There are two types of machine learning methodologies: supervised learning and unsupervised. In the latter, given input-output pairings, the system learns a feature to patch the inputs to the outcome to predict situations accurately. Trends are learned explicitly from unsupervised learning in the latter. Supervised algorithms are commonly used to estimate bioactivity.

ML is widely implemented in numerous domains, including computational chemistry, owing to its good precision and low expense. Recent computational improvements, and the creation of repositories for storing molecular structures and attributes, have expedited the field's evolution [117]. Investigators employed a variety of classic ML algorithms and advanced deep learning (DL) structures. The need for these approaches is to improve quantitative structure-activity relationship (QSAR) models; enhancing the bioactivity estimation of numerous substances, which are primarily studied topics in computational chemistry. Using AI bioactivity estimation is crucial in order to identify and characterize vast strides of biomolecules/pharmacological leads with desirable features. The goal is to select molecules by all those under investigation that seem more likely to become bioactive than a randomly selected one. Accessibility to vast databases is critical for the effectiveness of ML in domain estimation. Several huge databases are accessible from open-source archives suitable for activity forecasting (Table 2).

## 2.7. AI based models for the prediction of drug loading

AI predicts the factors that are essential tools for a successful therapeutic outcome. Nevertheless, encapsulated formulated drugs require targeted delivery; mostly, there is a failure due to the mechanistic fluidity traversing across our entire body system. Thereby, there is a need for an alternative stratagem which might facilitate entangling this unresolved twist. Liu et al. reported the specific loading of ibuprofen-based metal-organic framers (MOFs), which encodes for several

**Table 2**

A collection of current research in which AI employs anticipate bioactivity.

ML Method	Study Description	References
SVMs, KNN, RFs, NB, DNNs	Comparison of DL methods on a large-scale drug discovery dataset and other ML and target prediction methods	[118]
RF, KNN, NB, DNN	Predicting kinase activities for around 200 different kinases using multiple ML methods	[119]
NB, SVMs, LgR, RFs, DNN	Different ML methods were compared using a standardized dataset from ChEMBL and standardized metrics	[120,121]
NB, LgR, DTs, RFs, SVMs, DNNs	Comparison between DNNs and other ML algorithms for diverse endpoints (bioactivity, solubility, and ADME properties)	[122]
Multitask DNNs	Use of multitask DNNs as an improvement over single learning	[123]
DNNs, SVMs, RFs, NB, KNN	Shows that, when optimized, DNNs are capable of outperforming shallow methods across diverse activity classes	[124]
DNNs, SVMs, and RFs	Results from the Tox21 competition. DNNs show good predictivity on 12 different toxic endpoints	[125]
Multitask DNNs	Multitask learning provided benefits over single-task models. Smaller datasets tend to benefit more than larger datasets	[126]
Multitask DNNs	Performance analysis of multitasking DNNs (DeepChem implementation) and related DL models on pharmaceutical datasets	[127]

applications. Machine learning models such as support vector regression (SVR), random forest (RF), and adaptive boostin (AdaBoost) Catboost algorithms are quite effective and potential tools to develop powerful tools for drug loading. However, in the same study, they reported that Catboost algorithm employs categorical features and Gradient boosting which resolves the conditional bias, randomly assorts the categorical features and avoids the problem of overfitting datasets in a particular frame, in comparison to the other algorithm tools. Further, this algorithm helps to quantify the errors in terms of  $R^2$  and root mean squared error (RMSE), which enhanced the assurance of prediction-based drug loading capacity of ibuprofen. This study has enunciated the application of machine learning algorithms specific to the application of drug loading [128]. However, there is a need for exploratory investigation focused on AI implemented drug-loading capacities and their extensive biomedical applications.

## 2.8. AI in toxicity analysis

It is projected that just 10% of novel chemical compounds that undergo the initial phase as potential medications will get eventual FDA clearance, owing mostly to safety risks, which account for 35% of preliminary rejections and 28% of phase 2 failings. Most setbacks in introducing new medications are due to safety concerns resulting from inadequate preclinical toxicity [129]. However, it has been demonstrated that toxicity estimations based on *in vivo* methods concur once extended to humans in 43 and 63% of the cases respectively in experimental animals and non-experimental animals, as well as fewer than 30% when it comes to knowing adverse drug reactions (ADRs) in target organs. As a result, the rejection of potentially innovative medications due to toxicology studies on safety generally using laboratory animals is debatable [130].

Drug safety is rising in its attempts to enhance *in silico* models, taking advantage of the huge quantities of previously existing evidence which reflect a huge opportunity in the field of anti-tumor pharmaceuticals, using AI, DL & ANN [131]. AI tools can analyse toxicity using ML and DL. ML method possesses low orders of complexity, which predicts drug toxicity, mechanism of action, trial design, and drug development of random forest and logistic regression are implemented majorly to predict the toxicity of drugs (Fig. 1). By contrast, DL, a sub-method of ML, has also gained increasing importance since the 1990s due to its wide



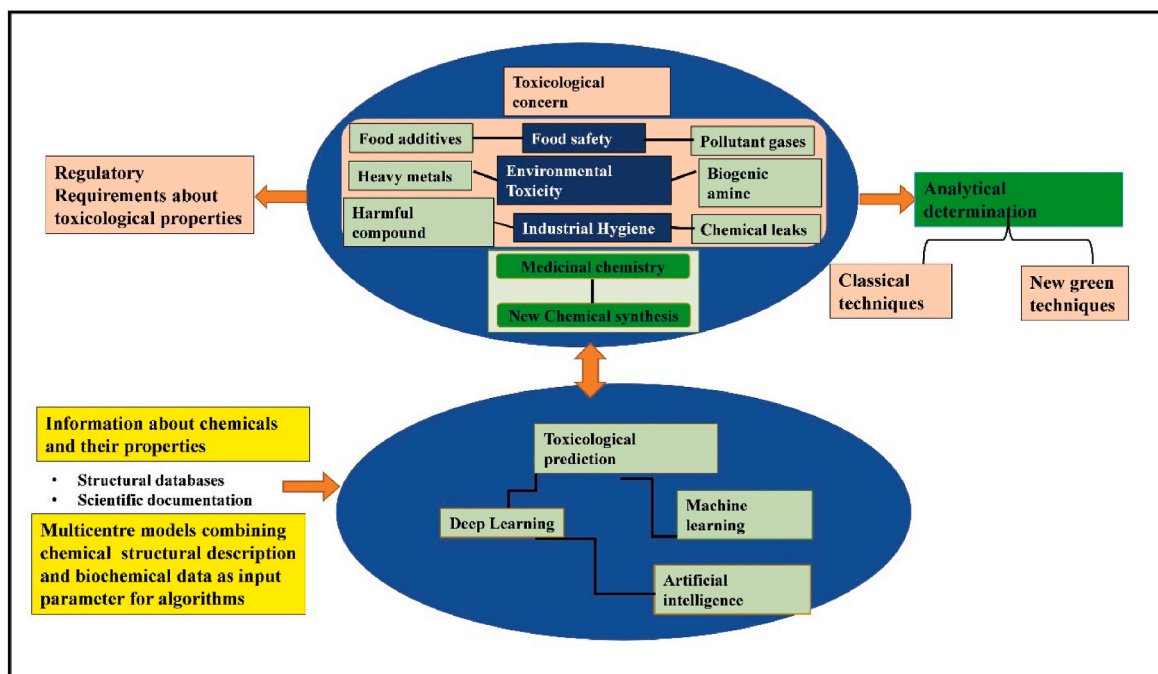


Fig. 1. Showing AI for estimation of toxicological Predictions adopted from Efrén Pérez Santín et al., 2021, Wires Computational Molecular Science. Reproduced with permission from ref. 68. Copyright 2021 Wiley.

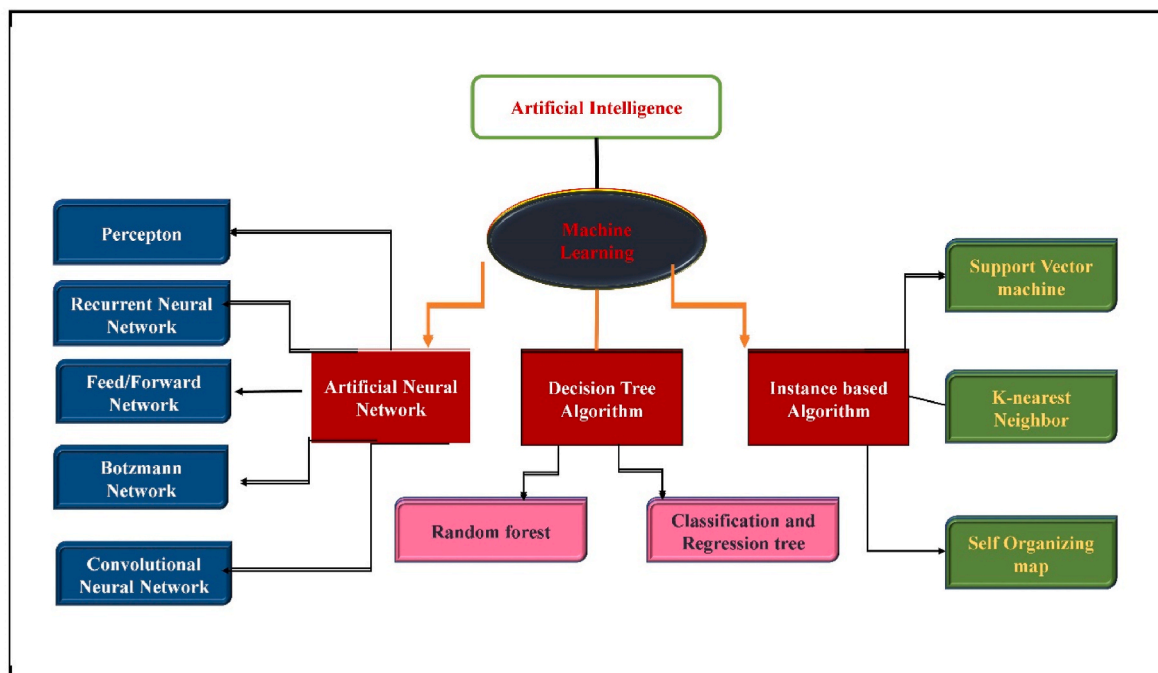


Fig. 2. AI and its different methodology widely implemented in the field of drug design, adopted from Debleena Paul et al., 2021, Drug Discovery Today. Reproduced with permission from ref. 53. Copyright 2021 Elsevier.

applications in medical and data sciences, arriving at clinical decisions, and adhering to regulatory affairs concerned with drug design and discovery [132]. As schematically represented (Figs. 1 and 3) with respect to the divergent applications of AI, it has a predominant role in analysing mutation's that enroute to develop the malignancies. We also summaries the literature of AI based toxicity analysis (Table 3) (see Fig. 2).

## 2.9. Mutagenesis and malignancy

Because of its catastrophic effects on human health, chemical tumorigenesis is becoming increasingly essential in medicinal investigation [149]. Chemical tumorigenesis is predominantly caused due to adverse exposure to carcinogens, which damage DNA or affect normal cell metabolic activities, most likely causing cancer, increasing its incidence, or shortening its time [150].

Carcinogenicity testing in animals is costly, time-demanding, and

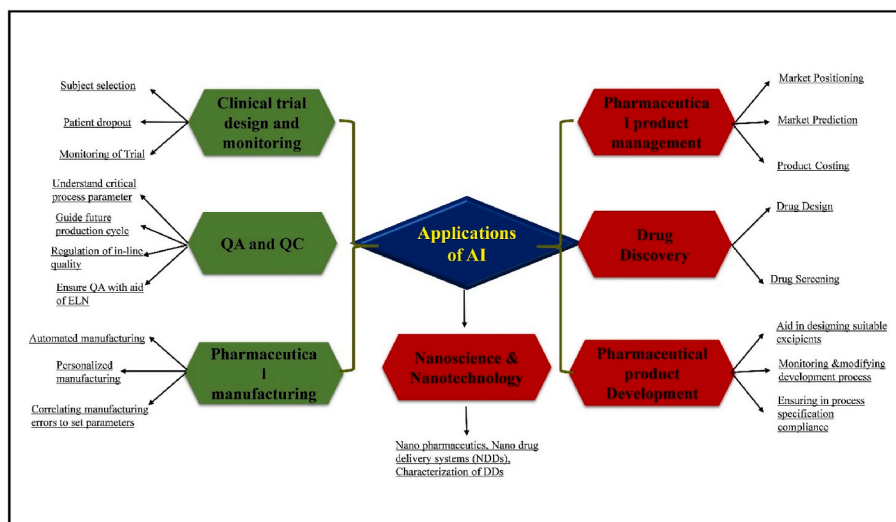


**Fig. 3.** Showing Application for AI, which depicts various AI approach domains and their sub - fields which can be used in pharmaceutical research, adopted from Debleena Paul et al., 2021, Drug Discovery Today. Reproduced with permission from ref. 53. Copyright 2021 Elsevier.

unethical [151]. Thereby, *in silico* approaches for carcinogenicity prediction have recently become a subject of attention. QSAR approaches were the most extensively researched of the bunch. Fjodorova et al. [152] used the ANN model to classify carcinogenicity potency by employing 27 2D descriptors, achieving validity for the initial dataset and the test data set is 92 and 68%, respectively [152]. Zhong and his colleagues developed an SVM estimation system utilizing 24 chemical remarks that outperformed the test set by 80% [153]. Singh et al. created a probabilistic neural network (PNN) estimation system with five observations using over 800 pieces of structural information, with a categorization precision of 92% [154]. The drawbacks of this investigation focus on the model's cynical applicability, whereby the barriers when acquired estimated results can be certainly assured, i.e., the restricted applicability domain (AD) as per the scope of chosen descriptors used by the authors, but not the feasibility of implementing the data achieved beyond rats, mice, or hamsters. Wang and their team created Caps-Carcino, a novel DL architecture that distinguishes between carcinogens and noncarcinogens with an efficiency of 85% on an external validation set [155,156]. Guan et al. created and merged QSAR models using a range of ML algorithms to estimate carcinogenic qualities. Their model predicts rat carcinogenicity with 79% efficiency and 70% AUC. One of the major cardinal features of AI is prediction analysis of the impacts caused due to chemotherapies, which otherwise can't be demonstrated using the conventional route for treatment.

## 2.10. Mutagenesis and mode of action of phytochemicals

Mutagenicity is commonly described as the start of specific alterations in an individual's DNA, or genetic information, that may be persistent and inborn [157]. Point mutations, frameshift mutations, and other types of mutations are possible. Point mutations affect just a particular nucleotide and a few nucleotides inside a gene and are classified into three types: base pair replacement, where one base pair is replaced with another; deletion, where one or more base pairs are deleted; and insertion, where an extra base pair is introduced [158]. Some substances known as antimutagens may regulate, reduce, or eliminate the harmful mutagenic effects generated by mutagens [159]. Phytoconstituents are the primary source of a wide range of active substances with pharmaceutical as well as antimutagenic characteristics. Earlier studies have reported the anti-mutagenic properties of these phytoconstituents [160]. Furthermore, detailed investigations for experimental validation of traditional medicinal herbs employed for their antimutagenic properties are warranted.

The inclusion of Phyto phenolic catechin, tannin, flavanones, and isoflavones is primarily essential to induce genotoxicity in tumor cells. This seems to be due to flavonoids' inhibition of topoisomerase I and II enzymes, which alter replication and transcription processes, culminating in cleavable DNA-enzyme aggregates which induce mutations [161]. Phytoconstituents' anti-genotoxic properties might be caused by stimulating or suppressing specific catalysts such as GSH or CYP1A1 in conjunction with polyphenol' antioxidant and scavenging activities [162]. Hunting free radicals seem to be the most important reason that allows anti-mutagenesis. Secondary metabolites found in plants exhibit radical scavenging function, oxidase suppression, metals chelate, as well as the ability to influence huge alterations in the expression of genes [163,164]. The antioxidant activities of phytonutrients including flavonoids, particularly kaempferol, quercetin, & proanthocyanin, have explicit DNA repair activity in response to damage caused by hydrogen peroxide [165]. The phenolic compound contents of the extract are primarily responsible for its powerful antioxidants and radical scavenging activities. The effectiveness of an extract is determined by the polyphenol sub-classes present in nutritional supplements and medicines [166,167].

Acacia salicina extracts were shown to defend against the DNA strand breakage caused by LA and 4-nitro-o-phenylenediamine. Curcumin, a major component of turmeric, shows antimutagenic action against NaN<sub>3</sub> and methyl methane sulfonate [168]. Natural anti-mutagens can limit the activation potential of mutagens by inhibiting the enzymes involved in bioconversion [68]. Methanolic extract of lichens with antimutagenic properties against NaN<sub>3</sub> inhibited the formation of the NaN<sub>3</sub> metabolite L-azido alanine [159]. Likewise, phytoconstituents of Terminalia arjuna were shown to reduce mutagenic effects through the aromatic amine 2-aminofluorene (2-AF) metabolic suppression [159].

## 3. Artificial intelligence in drug screening

Drug design and development could take another decade and cost \$2.8 billion. 9 out of 10 medicinal compounds fail Phase II clinical studies and are not approved by regulatory authorities [130]. Methods such as Nearest-Neighbor classifiers, RF, extreme learning machines, SVMs, and deep neural networks (DNNs) can be used for VS depending on synthesizing capability [107]. They may also forecast *in vivo* behaviour and cytotoxicity. Numerous pharmaceutical companies, including Bayer, Roche, and Pfizer, have collaborated with IT firms to create a framework for developing medicines for cardiovascular diseases

**Table 3**

Current data, investigations on the subject of AI implemented in toxicology have been conducted.

The main subject	Significant deviations from the available literature	Major Highlights	References
AI. Drug toxicity and safety.	Not simply toxicological issues, but the entire drug discovery process in general.	Systematically explanation of present AI-based approaches used in drug toxicology	[12]
Computer models. Estimation of molecular characteristics, considering toxicological considerations	Computational approaches are covered in context since they are used for challenges like docking, ranking, ligand binding estimation, etc. However, toxicological properties were not extensively examined.	Concerns itself with the constraints of computational prediction methodologies and ML algorithms specifically, including predictive performance and overfitting.	[133]
Estimation of drug metabolism for effectiveness and safety. Approaches are used in computational, <i>in vitro</i> , and <i>in vivo</i> .	They are focused particularly on drug metabolism, a critical yet specialized element of drug toxicity.	Provides a complete overview of the software applications used throughout drug metabolism estimation and the extent and limits of computational methodologies and relevant data.	[134]
Toxicology <i>in silico</i> . A thorough examination of the merits and drawbacks of present modelling methodologies and algorithms for toxicity estimation.	Not concerned with actual regulatory obligations.	A clear understanding of computational toxicity testing technologies, prediction model generation processes, & prediction model classifications.	[135]
Millions of molecules and their characteristics are described via publicly available data.	Databases and molecular descriptors are two examples of particular aspects of the numerous steps.	A useful compilation of freely accessible small molecule resources. A view of the fingerprints used to create chemical gaps.	[136]
AI-powered drug discovery computational models Drug options' safety and effectiveness are assessed.	Not particularly on toxicology, but across the AI computational development & discovery of the drug.	A concise summary of the progress of AI tools in discovering a drug, with a crystal clear image of the present state of affairs.	[137]
Drug discovery computational approaches. DL methodology	A look into Deep learning in drug development. Define the fundamental ideas or underlying principles of Deep learning frameworks. Give a current real example.	We are not primarily concerned with toxic effects but with DL techniques used in drug development.	[138]
Computational approaches for predicting toxic effects. Medication creation. Database	It deals with <i>in silico</i> approaches generally, focusing on ML methodology at times. Though still	Toxicity-specific A comprehensive view of programs, databases, and cloud services. Covers	[139]

**Table 3 (continued)**

The main subject	Significant deviations from the available literature	Major Highlights	References
and server software.	not comprehensive, it is linked to several subjects.	many forms of toxicity.	
Connections between drugs in the case of drug quality Serious adverse reactions Data analysis. Artificial intelligence and computational approaches	The focus is on data mining approaches for discovering novel DDIs, with just a hazy idea of how that data may be used in the future.	A concise review of research detailing sources for mining pharmacovigilance data to find DDIs.	[140]
Negative occurrences occur throughout the drug development process <i>in silico</i> . Metabolism of cytochrome P450 (CYP) was predicted computationally.	Nothing relevant to the toxicity of the drug, but just too diverse factors connected to the metabolism of the drug	A comprehensive review of the potential, problems, and hazards of drug metabolism estimation, includes toxification—a short review of diverse computational methods incorporating ML.	[141]
DL is being used in pharmaceuticals.	Concerned about DL approaches in bioinformatics, which are not explicitly hazardous but is included. It doesn't cover all aspects of AI but rather focuses on deep learning approaches.	A comprehensive overview of DL approaches and comparisons to other methodologies.	[142]
Computational strategies are evolving Machine Learning and Deep Learning in drug discovery	Relevant to sensible drug development and discovery, not only toxicology.	Detailed view regarding current advancements in ML methods employed to develop drugs includes elements relevant to toxicity.	[143]
Estimation of toxicity Distinguishes among organ toxicity. Several characteristics (multiparametric approach)	This doesn't include complicated technicalities of computational techniques. Not interested in AI-based approaches.	Methodical approach A comprehensive examination of the present computational methodologies. In silico methods, such as cytotoxicity tests utilized <i>in vivo</i> toxicity testing, are thoroughly summarised—an informative analysis of potential organ-specific toxicity candidates.	[50]
ADRs. Practical or computational approaches, particularly AI-based approaches linked to toxicity prediction, including DILI.	Hepatotoxicity was explicitly mentioned.	Study of <i>in vivo</i> (animal) and computational methodologies designed to recognize DILI models. A comprehensive summary of artificial intelligence approaches used in the toxicological study.	[144]
Big data and machine learning for	Paper provides a comprehensive	A thorough examination of the	[129]

(continued on next page)

Table 3 (continued)

The main subject	Significant deviations from the available literature	Major Highlights	References
medication toxicity evaluation	survey encompassing methodologies, data sets, and computational toxicology estimation techniques but still doesn't highlight the many domains these developments may be used widely.	most often used ML approaches for toxicity evaluation. A detailed survey of various data sets and toxicity tools presents to create computational mephitic estimation techniques. A thorough analysis of methods and resources for extracting molecular information and toxicity and freely released toxicology prognosis programs.	
REACH legislation Information about the toxicity of the chemical. ANNs.	QSAR & ANN approaches were particularly emphasized. Numerous characteristics are investigated, and a more recent & appealing approach to computational toxicity prediction.	Demonstrates the potential outcomes of ANN utilized to QSAR approaches for meeting specific components of the REACH legislation. Enumerates the requirements that must be satisfied for computational methods to be used rather than testing on animals and how such approaches could be used to execute REACH, with an intriguing selection of case stories.	[145]
Artificial neural networks in drug discovery: Benefits and downsides. Quantitative structure-activity relationship. Issues with interpretability issues & testing	Examine the vast range of applications of ANNs in drug development, including but not restricted to toxicology.	A detailed overview of the characteristics that make ANNs viable and appealing instruments for QSAR. Such models' current limits and problems are evaluated. Summarizes the many forms of ANNs that are commonly utilized in drug discovery. Encompasses a set of frequently employed ANN software, whether freeware or not.	[146]
Toxicology estimation using computational methods. Machine learning techniques Common chemical descriptions Estimation using cellular transcriptomic data.	They concentrate on fundamental technical features of various techniques rather than extensively analysing their practical relevance in multiple domains.	Investigate ML approaches used to estimate toxicity, such as DL, Random Forests, k-nearest Neighbours, & SVM. Address the input variables to the Machine Learning algorithm, notably transition by utilizing merely chemical structure descriptions mostly to current techniques merging with the data of	[55]

Table 3 (continued)

The main subject	Significant deviations from the available literature	Major Highlights	References
Estimation of skin sensitization toxicity. Non-animal testing methods ANNs, support vector machine models, Bayesian networks, and judgment trees are all examples of artificial neural networks. Open-source software applications.	They are assigned to a particular feature of chemical compound toxicity, such as skin sensitivity. Although AI-based approaches account for most of the evaluation, they are not the only ones available.	human transcriptome inspection. The primary categories of chemical-based characteristics and traditional information sources of toxicity compounds. Analyses the concert of varying configurations of chemical descriptors and machine learning models. Methodologies able to represent non-animal skin sensitization test methods, presented to the OECD as "definite strategies," are qualitative as well as quantitative evaluated, illustrating a quantity of <i>in silico</i> predictions that is now, in most instances equitable or greater to current animal studies, effectively estimating human skin sensitization consequences both for dangers and effectiveness, recognizing specified methodologies that might serve as important substitutions for analysing humans	[147]
Acute toxicity evaluation. In-silico methodologies incorporate methods that rely on QSAR/QSTR.	The acute toxicity of chemical substances was the emphasis. Not re-based methods.	Strengths and downsides of the numerous QSAR/QSTR technologies. It's the first multiplexing QSTR approach for predicting acute toxicity simultaneously.	[148]

and cancer [169]. Estimating the medication's physical and chemical characteristics, such as fluidity, partition coefficient (logP), degree of ionization, and intrinsic permeability, impact its pharmacokinetics qualities and target receptor class indirectly and should thus be addressed when creating a novel medicine [170]. Physical and chemical qualities may be predicted using a variety of AI-based methods. For example, ML trains the software using massive data sets generated from earlier compound optimization. Drug discovery and development algorithms use molecular descriptors in 3D to construct viable compounds and forecast their attributes using DNN [171]. In Table 4 we have summarised the AI tool used in drug discovery.

Models that rely on ANNs, graphing kernels, or kernel ridges have been proposed to estimate the constant dissociation constants of substances [138]. Likewise, to collect evidence, cell lines, including Madin-Darby canine kidney cells and human colon adenocarcinoma (Caco-2) cells, were employed, which were then put into AI-assisted



**Table 4**

Some AI tools are responsible for drug discovery.

Tool	Features	Website	Ref.
DeepChem	MLP model that searches for a suitable candidate in drug discovery using a programming language AI system.	<a href="https://github.com/deepchem/deepchem">https://github.com/deepchem/deepchem</a>	[50]
Deep Tox	A program that forecasts the cytotoxicity of over a thousand medications.	<a href="http://www.bioinf.jku.at/research/DeepTox">http://www.bioinf.jku.at/research/DeepTox</a>	[49]
Deep Neural Net QSAR	Python-based system powered by analytical techniques for detecting compounds' chemical stability.	<a href="https://github.com/Merck/DeepNeuralNet-QSAR">https://github.com/Merck/DeepNeuralNet-QSAR</a>	[51]
ORGANIC	A molecular synthesis software that aids in creating compounds with desired attributes.	<a href="https://github.com/aspuru-guzik-group/ORGANIC">https://github.com/aspuru-guzik-group/ORGANIC</a>	[52]
Potential Net	NNs are utilized to estimate drug binding ability.	<a href="https://pubs.acs.org/doi/full/10.1021/acscentsci.8b00507">https://pubs.acs.org/doi/full/10.1021/acscentsci.8b00507</a>	[53]

classifiers. Bioactivity predicts the affinities of bioactive compounds against receptors or target proteins, determining their effectiveness. Large molecules that do not bind with or have relationships with the protein target wouldn't respond to therapy. Artificial intelligence relies on approaches that can calculate a medication's binding affinity by considering the traits or commonalities among the drug and its target [107]. To identify the feature vectors, feature-based interaction recognizes the molecular moiety of medication and receptors.

### 3.1. The use of AI technology in drug research & development

The enormous chemical domain, consisting of around 1060 molecules, promotes the formulation of many pharmacological compounds [172]. Nevertheless, the absence of modern technology constrains the medication development cycle, making it a time-consuming and costly endeavour that may be solved by utilizing AI [173]. AI can identify top synthetic analogues, provide faster drug candidates' confirmation, and optimize the therapeutic structural system [174].

Despite these benefits [107], AI has substantial data difficulties, including volume of data, development, variety, and unpredictability. Classical ML algorithms may be unable to cope with the data sets accessible for drug discovery in pharmaceutical organizations, including millions of molecules. A computer program that relies on the quantitative structure-activity relationship (QSAR) may quickly anticipate physical and chemical properties of the small molecules, polymers and formulations [175]. Unfortunately, these models fall short of predicting complicated genetic components such as chemical activity and side effects. To add on, models that rely on QSAR encounter issues that include a shortage of scientific confirmations, restricted training data, and experimentally inaccuracies in the testing set [176]. To meet these obstacles, quickly developing AI methods, like DL and relevant modelling studies, could be employed to survey the efficacy and safety of pharmaceutical drugs (Fig. 3) through big data investigation and design [137]. Merck funded a QSAR ML project in 2012 to examine the potential of DL in the field of medical medication discovery and development [107]. For 15 pharmaceutical candidates absorbing, dispersion, metabolic activity, expulsion, and toxicology (ADMET) data sources, models outperformed classic ML techniques in terms of predictability.

The digital biochemical space resembles a geographical map of molecules by depicting various concentrations of atoms and associated attributes. The goal of biochemical space visualization is to gather positioning information regarding chemicals inside the space to explore bioactive components; hence, virtual screening aids in the selection of relevant molecules for subsequent testing [177]. Numerous chemical sites are available, including PubChem, ChemBank, DrugBank, and ChemDB which are serve as repositories for leads that connect to the

virtual screening process.

Several *in silico* techniques for virtual screening chemicals using virtual molecular spaces and structural and ligand-based methodologies allow superior-profile analysis, quicker removal of non-lead compounds, and therapeutic molecule selection at a lower cost [178,179]. To pick a lead ingredient, drug design techniques such as coulomb matrices and molecular fingerprint recognition examine the physical, pharmacological, and toxicology characteristics [180].

QSAR modelling techniques were used to identify prospective drug targets and also have developed into Intelligence QSAR methods such as linear discriminant analysis (LDA), support vector machines (SVMs), random forest (RF), and decisions trees that may be used to accelerate QSAR study [181].

### 3.2. AI in pharmaceutical products

AI can be envisioned as being involved in the creation of drug products first from the work surface to the point of care because it can support medicinal chemistry, assist in making decisions, and identify the correct treatment for a service user, such as personalized tablets or drugs, and clinical data management recorded and utilized for upcoming medication development [182]. Eularis' E-VAI is an analysis and course of action AI platform that uses Machine learning and easy-to-use user interaction to develop predictive frameworks relying on opponents, and interested parties, including existing market presence, to forecast important sales and marketing variables, allowing marketing people to allocate resources most efficiently share of the market gain, trying to reverse poor sales, and anticipating where and how to invest [107]. The following diagram describes the various implementations of AI in drug development and investigation (Fig. 3).

## 4. Pitfalls and future directions

Nanoscience tools have gone far to improvise the therapeutic approach in several cancers. Yet there are some hindrances faced in combating cancer; one of them is tumor microenvironment (TME), which influences not only the pathogenesis but also impose a barrier to most of the conventional therapeutics. In this context, remarkable progress has been perceived in the AI based drug discovery process. The successful prediction of biological activity and pharmacokinetic properties such as absorption, distribution, metabolism, excretion, and toxicity (ADMET) along with pharmacokinetic profiles have generated sufficient evidence to demonstrate their powerful computational intelligence in the field of targeted therapeutics. Additionally, there have been extensive applications in developing a structure or ligand-based drug-like molecules for the development of the Quantitative-structure activity-based relationship (QSAR/QSPR) model, or drug screening with appropriate doses, pharmaceutical products formulation or targeted inhibition of mutations by phytochemicals by the dint of AI tools. However, there are some limitations faced with AI based tools for feature attribute techniques undertaken by DL methods. There is a need to bridge the gap between drug discovery specialists and developers of DL models. Also, there is a mandatory requirement for technical support and a user-friendly approach, which is a huge setback for researchers with a non-computational background. A brief overview of the improvised therapeutic strategy is shown in Fig. 4.

## 5. Conclusion

One of the critical factors that have got to regulate cellular growth, proliferation, and differentiation is epigenetic modulation, which serves to methylate or demethylate; acetylate or deacetylate DNA and histones or histone-modifying enzymes; alteration of these components can promote tumorigenesis. Several studies reported the improved of therapeutic potential of nanoparticles based drug delivery system against cervical cancer compared to conventional chemotherapy. This is due to

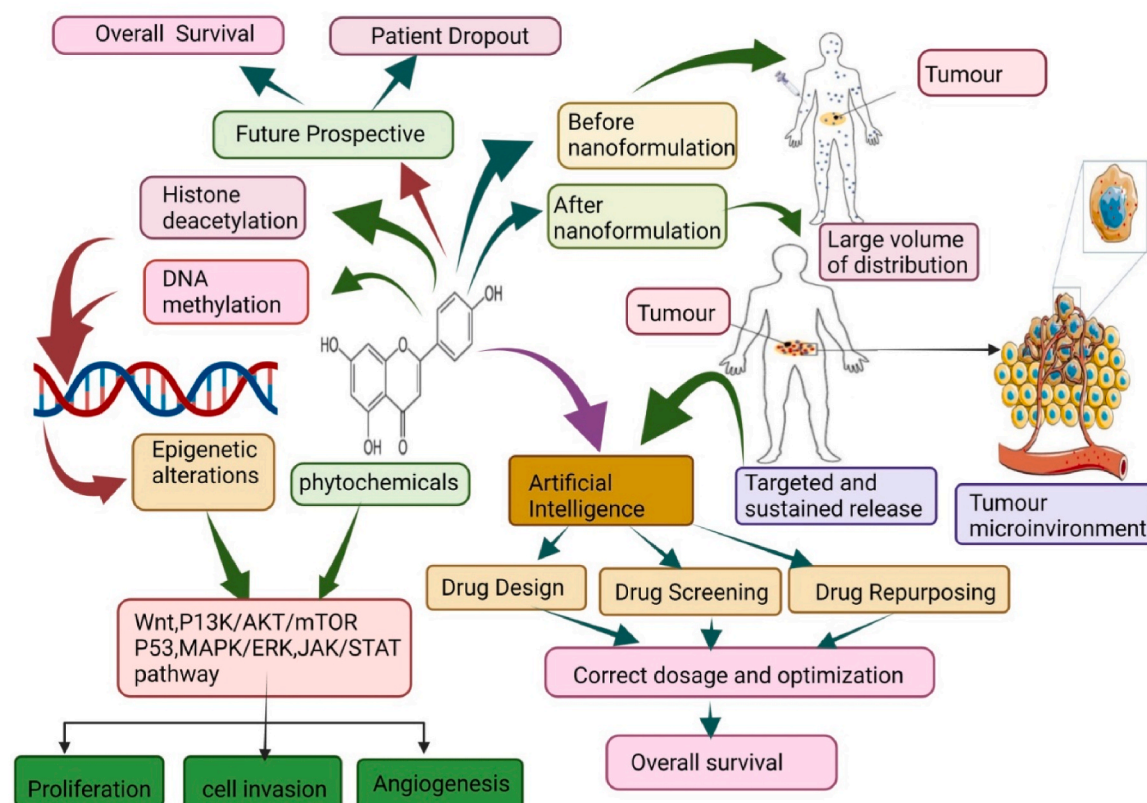


Fig. 4. Schematic orientation of the present study with respect to nanoscience and AI tools and its implications in cervical cancer.

biocompatibility, targeting site of disease and cells and controlled release of drugs. Targeted delivery can be achieved through targeting the specific surface markers expressed on cancer cells that are rarely expressed on healthy cells would be ideal. Thus, employing nano-formulated therapeutics might enhance the efficacy of targeted drug delivery, but on the same hand, it might vary depending on the physical status of patients and their cancer stage. Formulation of natural drugs with nano-carriers may have the least side effects, and these natural nano-drugs might be effective. On the same note, nano-carriers formulated drugs might impose several challenges, one of them being approval from regulatory affairs to encompass clinical trials and hence AI accompanying these nano-carriers or nano-DDs might provoke the current platform for this kind of novel interventional therapies. AI based algorithms have emerged as an innovative tool for diagnosing and treating most cancers. AI tools provide a rational platform to screen a wide variety of compounds using models, which cut off the resources and time expenditure, unlike wet-lab approaches. The preliminary screening using AI can fasten the rate for the drug discovery process, following which *in vitro* and *in vivo* experimental validation is a prerequisite for precise anti-tumor or anticancer drugs development. Besides, AI also has been implemented to predict drug toxicity, drug loading and characterization at the surface level in addition to other factors such as bioactivity, drug-target identification, de-novo drug design, prediction of physicochemical properties, and QSAR-based drug development. Additionally, AI based development of nano-formulated drugs and their druggable target can be one of the crucial applications to enrich the platform for designing novel anticancer therapeutics. Given the rapid growth and emerging applications of “computer pharmaceuticals development” in developing drugs efforts should be put across to enrich the platform for rapid implementation of these novel techniques and the associated concerning regulatory affairs. Above all, the unveiled route of discovering and employing AI accompanied nano-formulations might plausibly overcome the bumpy journey of treating

cervical cancer.

#### Declaration of competing interest

All author declared there is no conflict of interest.

#### Data availability

Data will be made available on request.

#### References

- [1] F. Bray, J. Ferlay, I. Soerjomataram, R.L. Siegel, L.A. Torre, A. Jemal, Global cancer statistics 2018: GLOBOCAN estimates of incidence and mortality worldwide for 36 cancers in 185 countries, *CA A Cancer J. Clin.* 68 (6) (2018) 394–424.
- [2] S. Vinogradov, X. Wei, Cancer stem cells and drug resistance: the potential of nano-medicine, *Nano-medicine* 7 (4) (2012 Apr 1) 597–615.
- [3] P. Srivastava, A. Srivastava, In vitro anti-cancer activity of ethanolic extract of curcumin longa (turmeric) in HEP-2 cell lines, *Int. J. Eng. Res. Gen. Sci.* 3 (5) (2015) 495–508.
- [4] G. Gutheil W, G. Reed, A. Ray, S. Anant, A. Dhar, Crocetin: an agent derived from saffron for prevention and therapy for cancer, *Curr. Pharmaceut. Biotechnol.* 13 (1) (2012) 173–179.
- [5] M.K. Nicholas, S.J. Linton, P.J. Watson, Main CJ, Group “Decade of the Flags” Working. Early identification and management of psychological risk factors (“yellow flags”) in patients with low back pain: a reappraisal, *Phys. Ther.* 91 (5) (2011) 737–753.
- [6] D.J. Newman, G.M. Cragg, Natural products as sources of new drugs over the nearly four decades from 01/1981 to 09/2019, *J. Nat. Prod.* 83 (3) (2020) 770–803.
- [7] S. Kumar, V. Chinnusamy, T. Mohapatra, Epigenetics of modified DNA bases: 5-methylcytosine and beyond, *Front. Genet.* 9 (2018).
- [8] D.E. Handy, R. Castro, J. Loscalzo, Epigenetic modifications: basic mechanisms and role in cardiovascular disease, *Circulation* 123 (19) (2011 May 17) 2145–2156.
- [9] S. Ropero, M. Esteller, The role of histone deacetylases (HDACs) in human cancer, *Mol. Oncol.* 1 (1) (2007) 19–25.
- [10] G. Li, Y. Tian, W.G. Zhu, The roles of histone deacetylases and their inhibitors in cancer therapy, *Front. Cell Dev. Biol.* 8 (2020) 1004.

- [11] R. Gupta, D. Srivastava, M. Sahu, S. Tiwari, R.K. Ambasta, P. Kumar, Artificial intelligence to deep learning: machine intelligence approach for drug discovery, *Mol. Divers.* 25 (3) (2021 Aug) 1315–1360.
- [12] A.O. Basile, A. Yahi, N.P. Tatonetti, Artificial intelligence for drug toxicity and safety, *Trends Pharmacol. Sci.* 40 (9) (2019) 624–635.
- [13] J. Vamathevan, D. Clark, P. Czodrowski, I. Dunham, E. Ferran, G. Lee, et al., Applications of machine learning in drug discovery and development, *Nat. Rev. Drug Discov.* 18 (6) (2019) 463–477.
- [14] N. Yahfoufi, N. Alsadi, M. Jambi, C. Matar, The Immunomodulatory and Anti-inflammatory Role of Polyphenols, vol. 10, *Nutrients*, 2018.
- [15] V. Gangwar, A. Garg, K. Lomore, K. Korla, S.S. Bhat, R.P. Rao, et al., Immunomodulatory Effects of a Concoction of Natural Bioactive Compounds—Mechanistic Insights, vol. 9, *Biomedicines*, 2021.
- [16] G. Pistritto, D. Trisciuglio, C. Ceci, A. Garufi, G. D'Orazi, Apoptosis as anticancer mechanism: function and dysfunction of its modulators and targeted therapeutic strategies, *Aging* 8 (4) (2016 Apr) 603–619.
- [17] R.S.Y. Wong, Apoptosis in cancer: from pathogenesis to treatment, *J. Exp. Clin. Cancer Res.* 30 (1) (2011) 87.
- [18] R. Kanwal, S. Gupta, Epigenetic modifications in cancer, *Clin. Genet.* 81 (4) (2012) 303–311.
- [19] S.B. Baylin, P.A. Jones, Epigenetic determinants of cancer, *Cold Spring Harbor Perspect. Biol.* 8 (9) (2016).
- [20] A.K. Panda, D. Chakraborty, I. Sarkar, T. Khan, G. Sa, New insights into therapeutic activity and anticancer properties of curcumin, *J. Exp. Pharmacol.* 9 (2017) 31.
- [21] M. Foote, Using nano-technology to improve the characteristics of antineoplastic drugs: improved characteristics of nab-paclitaxel compared with solvent-based paclitaxel, *Biotechnol. Annu. Rev.* 13 (2007) 345–357.
- [22] S. Dai, C. Xu, Y. Tian, W. Cheng, B. Li, In vitro stimulation of calcium overload and apoptosis by sonodynamic therapy combined with hematoporphyrin monomethyl ether in C6 glioma cells, *Oncol. Lett.* 8 (4) (2014) 1675–1681.
- [23] S.D. Mittelman, The role of diet in cancer prevention and chemotherapy efficacy, *Annu. Rev. Nutr.* 40 (2020 Sep) 273–297.
- [24] M. Woźniak, R. Krajewski, S. Makuch, S. Agrawal, Phytochemicals in gynecological cancer prevention, *Int. J. Mol. Sci.* 22 (3) (2021) 1219.
- [25] A.S. Choudhary, P.C. Mandave, M. Deshpande, P. Ranjekar, O. Prakash, Phytochemicals in cancer treatment: from preclinical studies to clinical practice, *Front. Pharmacol.* (2020) 1614.
- [26] D.H. Kim, Y.J. Surh, Chemopreventive and therapeutic potential of phytochemicals targeting cancer stem cells, *Curr. Pharmacol. Rep.* 1 (5) (2015) 302–311.
- [27] C. Pinel, B. Prainsack, C. McKevitt, Markers as mediators: a review and synthesis of epigenetics literature, *BioSocieties* 13 (1) (2018) 276–303.
- [28] M.Z. Fang, D. Chen, Y. Sun, Z. Jin, J.K. Christman, C.S. Yang, Reversal of hypermethylation and reactivation of p16INK4a, RAR $\beta$ , and MGMT genes by genistein and other isoflavones from soy, *Clin. Cancer Res.* 11 (19) (2005) 7033–7041.
- [29] J.H. Lee, T.O. Khor, L. Shu, Z.Y. Su, F. Fuentes, A.N.T. Kong, Dietary phytochemicals, and cancer prevention: Nrf2 signaling, epigenetics, and cell death mechanisms in blocking cancer initiation and progression, *Pharmacol. Ther.* 137 (2) (2013) 153–171.
- [30] D. Sinha, N. Sarkar, J. Biswas, A. Bishayee, Resveratrol for breast cancer prevention and therapy: preclinical evidence and molecular mechanisms, in: *Seminars in Cancer Biology*, Elsevier, 2016, pp. 209–232.
- [31] S.H. Tuli, V. Aggarwal, G. Parashar, D. Aggarwal, C.N. Parashar, J.M. Tuorkey, et al., Xanthohumol: a metabolite with promising anti-Neoplastic potential, *Anti Cancer Agents Med. Chem.* 22 (2022) 418–432.
- [32] B. Stefanska, K. Rudnicka, A. Bednarek, K. Fabianowska-Majewska, Hypomethylation and induction of retinoic acid receptor beta 2 by concurrent action of adenosine analogues and natural compounds in breast cancer cells, *Eur. J. Pharmacol.* 638 (1) (2010) 47–53.
- [33] E. Tili, J.J. Michaille, H. Alder, S. Volinia, D. Delmas, N. Latruffe, et al., Resveratrol modulates the levels of microRNAs targeting genes encoding tumor-suppressors and effectors of TGF $\beta$  signaling pathway in SW480 cells, *Biochem. Pharmacol.* 80 (12) (2010) 2057–2065.
- [34] W.J. Lee, J.Y. Shim, B.T. Zhu, Mechanisms for the inhibition of DNA methyltransferases by tea catechins and bioflavonoids, *Mol. Pharmacol.* 68 (4) (2005 Oct 1) 1018. LP – 1030.
- [35] M. Pandey, S. Shukla, S. Gupta, Promoter demethylation and chromatin remodeling by green tea polyphenols leads to re-expression of GSTP1 in human prostate cancer cells, *Int. J. Cancer* 126 (11) (2010) 2520–2533.
- [36] J.B. Berletch, C. Liu, W.K. Love, L.G. Andrews, S.K. Katiyar, T.O. Tollefsbol, Epigenetic and genetic mechanisms contribute to telomerase inhibition by EGCG, *J. Cell. Biochem.* 103 (2) (2008) 509–519.
- [37] S.M. Meeran, S.N. Patel, T.H. Chan, T.O. Tollefsbol, A novel prodrug of epigallocatechin-3-gallate: differential epigenetic hTERT repression in human breast cancer cells, *Cancer Prev. Res.* 4 (8) (2011 Aug) 1243–1254 (Philadelphia, Pa). 2011/03/16.
- [38] S.R. Volate, S.J. Muga, A.Y. Issa, D. Nitcheva, T. Smith, M.J. Wargovich, Epigenetic modulation of the retinoid X receptor  $\alpha$  by green tea in the azoxymethane-ApcMin/+ mouse model of intestinal cancer, *Mol. Carcinog.* Published in cooperation with the University of Texas MD Anderson Cancer Center 48 (10) (2009) 920–933.
- [39] S. Balasubramanian, T.M. Scharadin, B. Han, W. Xu, R.L. Eckert, The Bmi-1 helix–turn and ring finger domains are required for Bmi-1 antagonism of (–) epigallocatechin-3-gallate suppression of skin cancer cell survival, *Cell. Signal.* 27 (7) (2015) 1336–1344.
- [40] V.S. Thakur, K. Gupta, S. Gupta, Green tea polyphenols causes cell cycle arrest and apoptosis in prostate cancer cells by suppressing class I histone deacetylases, *Carcinogenesis* 33 (2) (2012) 377–384.
- [41] W.P. Tsang, T.T. Kwok, Epigallocatechin gallate up-regulation of miR-16 and induction of apoptosis in human cancer cells, *J. Nutr. Biochem.* 21 (2) (2010) 140–146.
- [42] L.N. Fix, M. Shah, T. Efferth, M.A. Farwell, B. Zhang, MicroRNA expression profile of MCF-7 human breast cancer cells and the effect of green tea polyphenol-60, *Cancer Genomics Proteomics* 7 (5) (2010) 261–277.
- [43] Z. Liu, Z. Xie, W. Jones, R.E. Pavlovicz, S. Liu, J. Yu, et al., Curcumin is a potent DNA hypomethylation agent, *Bioorg. Med. Chem. Lett.* 19 (3) (2009) 706–709.
- [44] T.O. Khor, Y. Huang, T.Y. Wu, L. Shu, J. Lee, A.N.T. Kong, Pharmacodynamics of curcumin as DNA hypomethylation agent in restoring the expression of Nrf2 via promoter CpGs demethylation, *Biochem. Pharmacol.* 82 (9) (2011) 1073–1078.
- [45] M.G. Marcu, Y.J. Jung, S. Lee, E.J. Chung, M.J. Lee, J. Trepel, et al., Curcumin is an inhibitor of p300 histone acetyltransferase, *Med. Chem.* 2 (2) (2006) 169–174.
- [46] K. Balasubramanyam, R.A. Varier, M. Altaf, V. Swaminathan, N.B. Siddappa, U. Ranga, et al., Curcumin, a novel p300/CREB-binding protein-specific inhibitor of acetyltransferase, represses the acetylation of histone/nonhistone proteins and histone acetyltransferase-dependent chromatin transcription, *J. Biol. Chem.* 279 (49) (2004) 51163–51171.
- [47] J. Kang, J. Chen, Y. Shi, J. Jia, Y. Zhang, Curcumin-induced histone hypoacetylation: the role of reactive oxygen species, *Biochem. Pharmacol.* 69 (8) (2005) 1205–1213.
- [48] Y. Chen, W. Shu, W. Chen, Q. Wu, H. Liu, G. Cui, Curcumin, both histone deacetylase and p300/CBP-specific inhibitor, represses the activity of nuclear factor kappa B and Notch 1 in Raji cells, *Basic Clin. Pharmacol. Toxicol.* 101 (6) (2007) 427–433.
- [49] W.F. Hua, Y.S. Fu, Y.J. Liao, W.J. Xia, Y.C. Chen, Y.X. Zeng, et al., Curcumin induces down-regulation of EZH2 expression through the MAPK pathway in MDA-MB-435 human breast cancer cells, *Eur. J. Pharmacol.* 637 (1–3) (2010) 16–21.
- [50] H. Li, Y. Chen, Cui G. hui, J. feng Zhou, Curcumin, a potent anti-tumor reagent, is a novel histone deacetylase inhibitor regulating B-NHL cell line Raji proliferation, *Acta Pharmacol. Sin.* 26 (5) (2005) 603–609.
- [51] S. Reuter, S.C. Gupta, B. Park, A. Goel, B.B. Aggarwal, Epigenetic changes induced by curcumin and other natural compounds, *Genes & Nutrition* 6 (2) (2011) 93–108.
- [52] M. Sun, Z. Estrov, Y. Ji, K.R. Coombes, D.H. Harris, R. Kurzrock, Curcumin (diferuloylmethane) alters the expression profiles of microRNAs in human pancreatic cancer cells, *Mol. Cancer Therapeut.* 7 (3) (2008 Mar) 464–473.
- [53] J. Yang, Y. Cao, J. Sun, Y. Zhang, Curcumin reduces the expression of Bcl-2 by upregulating miR-15a and miR-16 in MCF-7 cells, *Med. Oncol.* 27 (4) (2010) 1114–1118.
- [54] M. Traka, A.V. Gasper, J.A. Smith, C.J. Hawkey, Y. Bao, R.F. Mithen, Transcriptome analysis of human colon Caco-2 cells exposed to sulforaphane, *J. Nutr.* 135 (8) (2005) 1865–1872.
- [55] S.M. Meeran, S.N. Patel, T.O. Tollefsbol, Sulforaphane causes epigenetic repression of hTERT expression in human breast cancer cell lines, *PLoS One* 5 (7) (2010), e11457.
- [56] M.C. Myzak, P.A. Karplus, F.L. Chung, R.H. Dashwood, A novel mechanism of chemoprotection by sulforaphane: inhibition of histone deacetylase, *Cancer Res.* 64 (16) (2004) 5767–5774.
- [57] M.C. Myzak, K. Hardin, R. Wang, R.H. Dashwood, E. Ho, Sulforaphane inhibits histone deacetylase activity in BPH-1, LnCaP and PC-3 prostate epithelial cells, *Carcinogenesis* 27 (4) (2006) 811–819.
- [58] Y. Li, T.G. VandenBoom, D. Kong, Z. Wang, S. Ali, P.A. Philip, et al., Up-regulation of miR-200 and let-7 by natural agents leads to the reversal of epithelial-to-mesenchymal transition in gemcitabine-resistant pancreatic cancer cells, *Cancer Res.* 69 (16) (2009) 6704–6712.
- [59] A. King-Batoon, J.M. Leszczynska, C.B. Klein, Modulation of gene methylation by genistein or lycopene in breast cancer cells, *Environ. Mol. Mutagen.* 49 (1) (2008) 36–45.
- [60] A. Vardi, R. Bosviel, N. Rabiau, M. Adjakly, S. Satih, P. Dechelotte, et al., Soy phytoestrogens modify DNA methylation of <em>GSTP1</em>, <em>RASSF1A</em>, <em>EPH2</em> and <em>BRCA1</em> promoter in prostate cancer cells, *In Vivo* 24 (4) (2010 Jul 1) 393. LP – 400.
- [61] M. Adjakly, R. Bosviel, N. Rabiau, J.P. Boiteux, Y.J. Bignon, L. Guy, et al., DNA methylation and soy phytoestrogens: quantitative study in DU-145 and PC-3 human prostate cancer cell lines, *Epigenomics* 3 (6) (2011 Dec) 795–803.
- [62] Z. Wang, H. Chen, Genistein increases gene expression by demethylation of WNT5a promoter in colon cancer cell line SW1116, *Anticancer Res.* 30 (11) (2010) 4537–4545.
- [63] S. Majid, N. Kikuno, J. Nelles, E. Noonan, Y. Tanaka, K. Kawamoto, et al., Genistein induces the p21WAF1/CIP1 and p16INK4a tumor suppressor genes in prostate cancer cells by epigenetic mechanisms involving active chromatin modification, *Cancer Res.* 68 (8) (2008) 2736–2744.
- [64] A. Andres, S.M. Donovan, T.B. Kuhlenschmidt, M.S. Kuhlenschmidt, Isoflavones at concentrations present in soy infant formula inhibit rotavirus infection in vitro, *J. Nutr.* 137 (9) (2007 Sep 1) 2068–2073.
- [65] S. Basak, D. Pookot, E.J. Noonan, R. Dahiya, Genistein down-regulates androgen receptor by modulating HDAC6-Hsp90 chaperone function, *Mol. Cancer Therapeut.* 7 (10) (2008) 3195–3202.



- [66] S. Majid, A.A. Dar, S. Saini, Y. Chen, V. Shahyari, J. Liu, et al., Regulation of minichromosome maintenance gene family by microRNA-1296 and genistein in prostate cancer, *Cancer Res.* 70 (7) (2010) 2809–2818.
- [67] L.G. Wang, A. Beklemisheva, X.M. Liu, A.C. Ferrari, J. Feng, J.W. Chiao, Dual action on promoter demethylation and chromatin by an isothiocyanate restored GSTP1 silenced in prostate cancer, *Mol. Carcinog.*: Published in cooperation with the University of Texas MD Anderson Cancer Center 46 (1) (2007) 24–31.
- [68] V.S. Thakur, G. Deb, M.A. Babcook, S. Gupta, Plant phytochemicals as epigenetic modulators: role in cancer chemoprevention, *AAPS J.* 16 (1) (2014) 151–163.
- [69] L.J. Fu, Y.B. Ding, L.X. Wu, C.J. Wen, Q. Qu, X. Zhang, et al., The effects of lycopene on the methylation of the GSTP1 promoter and global methylation in prostatic cancer cell lines PC3 and LNCaP, *Int. J. Endocrinol.* 2014 (2014).
- [70] A. Majchrzak-Celińska, A. Warych, M. Szoszkiewicz, Novel approaches to epigenetic therapies: from drug combinations to epigenetic editing, *Genes* 12 (2) (2021) 208.
- [71] X. Wen, S. Wu, Z. Li, Z. Liu, J. Zhang, G. Wang, et al., Ellagitannin (BJA3121), an anti-proliferative natural polyphenol compound, can regulate the expression of MiRNAs in HepG2 cancer cells, *Phytother. Res.: Int. J. Devoted Pharmacol. Toxicol. Eval. N. Prod. Deriv.* 23 (6) (2009) 778–784.
- [72] J. Paluszczak, V. Krajka-Kuźniak, W. Baer-Dubowska, The effect of dietary polyphenols on the epigenetic regulation of gene expression in MCF7 breast cancer cells, *Toxicol. Lett.* 192 (2) (2010) 119–125.
- [73] M. Bhia, M. Motallebi, B. Abadi, A. Zarepour, M. Pereira-Silva, F. Saremnejad, et al., Naringenin nano-delivery systems and their therapeutic applications, *Pharmaceutics* 13 (2) (2021) 291.
- [74] M. Dhupal, D. Chowdhury, Phytochemical-based nano-medicine for advanced cancer theranostics: perspectives on clinical trials to clinical use, *Int. J. Nanomed.* 15 (2020) 9125.
- [75] X. Yang, C. Yi, N. Luo, C. Gong, Nano-medicine to overcome cancer multidrug resistance, *Curr. Drug Metabol.* 15 (6) (2014) 632–649.
- [76] R. Kumar, S.V. Dalvi, P.F. Siril, Nanoparticle-based drugs and formulations: current status and emerging applications, *ACS Appl. Nano Mater.* 3 (6) (2020) 4944–4961.
- [77] D. Khiev, Z.A. Mohamed, R. Vichare, R. Paulson, S. Bhatia, S. Mohapatra, et al., Emerging Nano-Formulations and Nano-Medicines Applications for Ocular Drug Delivery, vol. 11, *Nano-materials*, 2021.
- [78] A. Tiwari, R. Kumar, O. Shefi, J.K. Randhawa, Fluorescent mantle carbon coated core-shell SPIONS for neuroengineering applications, *ACS Appl. Bio Mater.* 3 (7) (2020) 4665–4673.
- [79] R. Kumar, K. Mondal, P.K. Panda, A. Kaushik, R. Abolhassani, R. Ahuja, H. G. Rubahn, Y.K. Mishra, Core-shell nanostructures: perspectives towards drug delivery applications, *J. Mater. Chem. B.* 8 (2020) 8992–9027.
- [80] A. Mohan, M. Girdhar, R. Kumar, H.S. Chaturvedi, A. Vadhel, P.R. Solanki, A. Kumar, D. Kumar, N. Mamidi, Polyhydroxybutyrate-based nanocomposites for bone tissue engineering 14 (11) (2021) 1163.
- [81] J. Machhi, F. Shahjin, S. Das, M. Patel, M.M. Abdelmoaty, J.D. Cohen, P.A. Singh, A. Baldi, N. Bajwa, R. Kumar, L.K. Vora, A. Patel, M.D. Oleynikov, D. Soni, P. Yeapuri, I. Mukadam, R. Chakraborty, C.G. Saksena, J. Herskovitz, M. Hasan, D. Oupicky, S. Das, R.F. Donnelly, K.S. Hettie, L. Chang, H.E. Gendelman, B. D. Kevadiya, Nanocarrier vaccines for SARS-CoV-2, *Adv. Drug Deliv. Rev.* 171 (2021) 215–239.
- [82] R. Kumar, K.R. Aadil, K. Mondal, Y.K. Mishra, D. Oupicky, S. Ramakrishna, A. Kaushik, Neurodegenerative disorders management: state-of-art and prospects of nano-biotechnology, *Crit. Rev. Biotechnol.* 42 (8) (2022) 1180–1212.
- [83] E.S. Al-Sheddi, N.N. Farshori, M.M. Al-Oqail, S.M. Al-Massarani, Q. Saquib, R. Wahab, et al., Anticancer potential of green synthesized silver nano-particles using extract of *Nepeta deflexiana* against human cervical cancer cells (HeLa), *Bioinorgan. Chem. Appl.* 2018 (2018), 9390784.
- [84] K.K. Bharadwaj, B. Rabha, S. Pati, T. Sarkar, B.K. Choudhury, A. Barman, et al., Green synthesis of gold nano-particles using plant extracts as beneficial prospect for cancer theranostics, *Molecules* 26 (21) (2021) 6389.
- [85] F. Ordikhani, M. Erdem Arslan, R. Marcelo, I. Sahin, P. Grigsby, J.K. Schwarz, et al., Drug delivery approaches for the treatment of cervical cancer, *Pharmaceutics* 8 (3) (2016) 23.
- [86] R. Kumar, R. Rauti, D. Scaini, M. Antman-Passig, O. Meshulam, D. Naveh, L. Ballerini, O. Shefi, Graphene-based nanomaterials for neuroengineering: recent advances and future prospective, *Adv. Funct. Mater.* 31 (46) (2021) 2104887.
- [87] V.B. Kumar, R. Kumar, A. Gedanken, O. Shefi, Fluorescent metal-doped carbon dots for neuronal manipulations, *Ultrason. Sonochem.* 52 (2019) 205–213.
- [88] R. Kumar, A. Singh, N. Garg, P.F. Siril, Solid lipid nanoparticles for the controlled delivery of poorly water soluble non-steroidal anti-inflammatory drugs, *Ultrason. Sonochem.* 40 (2018) 686–696.
- [89] J. Walker, J. Albert, D. Liang, J. Sun, R. Schutzman, R. Kumar, C. White, M. Beck-Broichsitter, S.P. Schwendeman, In vitro degradation and erosion behavior of commercial PLGAs used for controlled drug delivery, *Drug Deliv. Transl. Res.* 13 (1) (2023) 237–251.
- [90] S. Sheoran, S. Arora, G. Pilli, Lipid based nano-particles for treatment of cancer, *Heliyon* (2022), e09403.
- [91] J. Li, C. Cai, J. Li, J. Li, T. Sun, et al., Chitosan-based nano-materials for drug delivery, *Molecules* 23 (10) (2018) 2661.
- [92] R.X. Zhang, J. Li, T. Zhang, M.A. Amini, C. He, B. Lu, et al., Importance of integrating nano-technology with pharmacology and physiology for innovative drug delivery and therapy—an illustration with firsthand examples, *Acta Pharmacol. Sin.* 39 (5) (2018) 825–844.
- [93] S. Rawal, M. Patel, Bio-Nano-carriers for lung cancer management: befriending the barriers, *Nano-Micro Lett.* 13 (1) (2021) 1–54.
- [94] R. Singh, J.W. Lillard, Nano-particle-based targeted drug delivery, *Exp. Mol. Pathol.* 86 (3) (2009) 215–223.
- [95] D. Vetricka, L. Sivak, C.M. Jogdeo, R. Kumar, R. Khan, Y. Hang, D. Oupický, Gene silencing delivery systems for the treatment of pancreatic cancer: where and what to target next? *J. Control. Release* 331 (2021) 246–259.
- [96] L.E. Low, J. Wu, J. Lee, B.T. Tey, B.H. Goh, J. Gao, et al., Tumor-responsive dynamic nano-assemblies for targeted imaging, therapy, and microenvironment manipulation, *J. Contr. Release : Off. J. Control. Release Soc.* 324 (2020 Aug) 69–103.
- [97] N. Yadav, S. Parveen, M. Banerjee, Potential of nano-phytochemicals in cervical cancer therapy, *Clin. Chim. Acta* 505 (2020) 60–72.
- [98] M. Liu, M. Fu, X. Yang, G. Jia, X. Shi, J. Ji, et al., Paclitaxel and quercetin co-loaded functional mesoporous silica nano-particles overcoming multidrug resistance in breast cancer, *Colloids Surf. B Biointerfaces* 196 (2020), 111284.
- [99] Y. Wang, H. Yu, S. Wang, C. Gai, X. Cui, Z. Xu, et al., Targeted delivery of quercetin by nano-particles based on chitosan sensitizing paclitaxel-resistant lung cancer cells to paclitaxel, *Mater. Sci. Eng. C* 119 (2021), 111442.
- [100] S. Zafar, S. Akhter, I. Ahmad, Z. Hafeez, M.M. Alam Rizvi, G.K. Jain, et al., Improved chemotherapeutic efficacy against resistant human breast cancer cells with co-delivery of Docetaxel and Thymoquinone by Chitosan grafted lipid nano-capsules: formulation optimization, in vitro and in vivo studies, *Colloids Surf. B Biointerfaces* 186 (2020), 110603.
- [101] A. Bagherian, R. Mardani, B. Roudi, M. Taghizadeh, H.R. Banfshe, A. Ghaderi, et al., Combination therapy with nano-micellar-curcumin and Temozolomide for in vitro therapy of glioblastoma multiforme via Wnt signaling pathways, *J. Mol. Neurosci. : MN* 70 (10) (2020 Oct) 1471–1483.
- [102] C. Fernandes, D. Soares, M.C. Yergeri, Tumor microenvironment targeted nano-therapy, *Front. Pharmacol.* 9 (2018).
- [103] S. Khamis, Nano-carrier drug delivery systems: characterization, limitations, future perspectives, and implementation of artificial intelligence, *Pharmaceutics* (2022 Apr 15) 14.
- [104] W. Wang, Z. Ye, H. Gao, D. Ouyang, Computational pharmaceutics - a new paradigm of drug delivery, *J. Contr. Release* 338 (2021 Oct) 119–136.
- [105] P.K. Prabhakar, N. Khurana, M. Vyas, V. Sharma, G. E-S. Batiha, H. Kaur, J. Singh, D. Kumar, N. Sharma, A. Kaushik, R. Kumar, Aspects of nanotechnology for COVID-19 vaccine development and its delivery applications, *Pharmaceutics* 15 (2) (2023) 451.
- [106] M. Soltani, F. Moradi Kashkooli, M. Souri, S. Zare Harofte, T. Harati, A. Khadem, et al., Enhancing clinical translation of cancer using nano-informatics, *Cancers* 13 (10) (2021 May 19) 2481.
- [107] D. Paul, G. Sanap, S. Shenoy, D. Kalyane, K. Kalia, R.K. Tekade, Artificial intelligence in drug discovery and development, *Drug Discov. Today* 26 (1) (2021) 80.
- [108] A. Zhavoronkov, Artificial Intelligence for Drug Discovery, Biomarker Development, and Generation of Novel Chemistry, vol. 15, *Molecular Pharmaceutics*. ACS Publications, 2018, pp. 431–4313.
- [109] T.O.B. Olusanya, R.R. Haj Ahmad, D.M. Ibegbu, J.R. Smith, A.A. Elkordy, Liposomal drug delivery systems and anticancer drugs, *Molecules* 23 (4) (2018 Apr).
- [110] S. Hua, Physiological and pharmaceutical considerations for rectal drug formulations, *Front. Pharmacol.* (2019) 1196.
- [111] J. Shim, Z.Y. Hong, I. Sohn, C. Hwang, Prediction of drug–target binding affinity using similarity-based convolutional neural network, *Sci. Rep.* 11 (1) (2021) 1–9.
- [112] X. An, X. Chen, D. Yi, H. Li, Y. Guan, Representation of molecules for drug response prediction, *Briefings Bioinf.* 23 (1) (2022 Jan 1) bbab393.
- [113] S. Raschka, B. Kaufman, Machine learning and AI-based approaches for bioactive ligand discovery and GPCR-ligand recognition, *Methods* 180 (2020) 89–110.
- [114] C. Wang, J. Liu, F. Luo, Y. Tan, Z. Deng, Q.N. Hu, Pairwise input neural network for target-ligand interaction prediction, in: 2014 IEEE International Conference on Bioinformatics and Biomedicine (BIBM), IEEE, 2014, pp. 67–70.
- [115] S. Lim, Y. Lu, C.Y. Cho, I. Sung, J. Kim, Y. Kim, et al., A review on compound-protein interaction prediction methods: data, format, representation, and model, *Comput. Struct. Biotechnol. J.* 19 (2021) 1541–1556.
- [116] A.S. Lundervold, A. Lundervold, An overview of deep learning in medical imaging focusing on MRI, *Z. Med. Phys.* 29 (2) (2019) 102–127.
- [117] J. Schmidt, M.R.G. Marques, S. Botti, M.A.L. Marques, Recent advances and applications of machine learning in solid-state materials science, *npj Comput. Mater.* 5 (1) (2019) 83.
- [118] A. Mayr, G. Klambauer, T. Unterthiner, M. Steijaert, J.K. Wegner, H. Ceulemans, et al., Large-scale comparison of machine learning methods for drug target prediction on ChEMBL, *Chem. Sci.* 9 (24) (2018) 5441–5451.
- [119] B. Merget, S. Turk, S. Eid, F. Rippmann, S. Fulle, Profiling prediction of kinase inhibitors: toward the virtual assay, *J. Med. Chem.* 60 (1) (2017 Jan 12) 474–485.
- [120] A. Gaulton, A. Hersey, M. Nowotka, A.P. Bento, J. Chambers, D. Mendez, et al., The ChEMBL database in 2017, *Nucleic Acids Res.* 45 (D1) (2017 Jan 4) D945–D954.
- [121] E.B. Lenselink, N. Ten Dijke, B. Bongers, G. Papadatos, H.W.T. Van Vlijmen, W. Kowalczyk, et al., Beyond the hype: deep neural networks outperform established methods using a ChEMBL bioactivity benchmark set, *J. Cheminf.* 9 (1) (2017) 1–14.
- [122] A. Korotcov, V. Tkachenko, D.P. Russo, S. Ekins, Comparison of deep learning with multiple machine learning methods and metrics using diverse drug discovery data sets, *Mol. Pharm.* 14 (12) (2017 Dec 4) 4462–4475.
- [123] Y. Xu, J. Ma, A. Liaw, R.P. Sheridan, V. Svetnik, Demystifying multitask deep neural networks for quantitative structure–activity relationships, *J. Chem. Inf. Model.* 57 (10) (2017 Oct 23) 2490–2504.



- [124] A. Koutsoukas, K.J. Monaghan, X. Li, J. Huan, Deep-learning: investigating deep neural networks hyper-parameters and comparison of performance to shallow methods for modeling bioactivity data, *J. Cheminf.* 9 (1) (2017) 42.
- [125] A. Mayr, G. Klambauer, T. Unterthiner, S. Hochreiter, DeepTox: toxicity prediction using deep learning, *Front. Environ. Sci.* 3 (2016).
- [126] S. Kearnes, B. Goldman, V. Pande, Modeling Industrial ADMET Data with Multitask Networks, 2016.
- [127] B. Ramsundar, B. Liu, Z. Wu, A. Verras, M. Tudor, R.P. Sheridan, et al., Is multitask deep learning practical for pharma? *J. Chem. Inf. Model.* 57 (8) (2017 Aug 28) 2068–2076.
- [128] X. Liu, Y. Wang, J. Yuan, X. Li, S. Wu, Y. Bao, et al., Prediction of the ibuprofen loading capacity of MOFs by machine learning, *Bioengineering* 9 (10) (2022 Oct) 517.
- [129] A.H. Vo, T.R. Van Vleet, R.R. Gupta, M.J. Liguori, M.S. Rao, An overview of machine learning and big data for drug toxicity evaluation, *Chem. Res. Toxicol.* 33 (1) (2020 Jan 21) 20–37.
- [130] G.A. Van Norman, Phase II trials in drug development and adaptive trial design, *JACC: Basic to Translational Science* 4 (3) (2019) 428–437.
- [131] R.S.K. Vijayan, J. Kihlberg, J.B. Cross, V. Poongavanam, Enhancing preclinical drug discovery with artificial intelligence, *Drug Discov. Today* 27 (4) (2022) 967–984.
- [132] E. Pérez Santín, R. Rodríguez Solana, M. González García, M.D.M. García Suárez, G.D. Blanco Díaz, M.D. Cima Cabal, et al., Toxicity prediction based on artificial intelligence: a multidisciplinary overview, *WIREs Computational Molecular Science* 11 (5) (2021 Sep 1) e1516.
- [133] C.F. Matta, M.C. Hutter, Foreword: computational special focus issue, *Future Med. Chem.* 10 (13) (2018 Jul 1) 1517–1519.
- [134] J. Kirchmair, A.H. Göller, D. Lang, J. Kunze, B. Testa, I.D. Wilson, et al., Predicting drug metabolism: experiment and/or computation? *Nat. Rev. Drug Discov.* 14 (6) (2015) 387–404.
- [135] A.B. Raies, V.B. Bajic, In Silico Toxicology: Computational Methods for the Prediction of Chemical Toxicity, *Wiley Interdisciplinary Reviews: Computational Molecular Science*, 2016;6(April), pp. 147–172.
- [136] M. Awale, R. Visini, D. Probst, J. Arús-Pous, J.L. Reymond, Chemical space: big data challenge for molecular diversity, *CHIMIA.Int. J.Chem.* 71 (10) (2017) 661–666.
- [137] H. Zhu, Big data and artificial intelligence modeling for drug discovery, *Annu. Rev. Pharmacol. Toxicol.* 60 (2020) 573–589.
- [138] A. Lavecchia, Deep learning in drug discovery: opportunities, challenges, and future prospects, *Drug Discov. Today* 24 (10) (2019) 2017–2032.
- [139] H. Yang, L. Sun, W. Li, G. Liu, Y. Tang, In silico prediction of chemical toxicity for drug design using machine learning methods and structural alerts, *Front. Chem.* 6 (2018).
- [140] S. Vilar, C. Friedman, G. Hripsak, Detection of drug–drug interactions through data mining studies using clinical sources, scientific literature and social media, *Briefings Bioinf.* 19 (5) (2018 Sep 28) 863–877.
- [141] J.D. Tyzack, J. Kirchmair, Computational methods and tools to predict cytochrome P450 metabolism for drug discovery, *Chem. Biol. Drug Des.* 93 (4) (2019 Apr 1) 377–386.
- [142] S. Ekins, The Next era: deep learning in pharmaceutical research, *Pharmaceut. Res.* 33 (11) (2016) 2594–2603.
- [143] L. Zhang, J. Tan, D. Han, H. Zhu, From machine learning to deep learning: progress in machine intelligence for rational drug discovery, *Drug Discov. Today* 22 (11) (2017) 1680–1685.
- [144] K. Fraser, D.M. Bruckner, J.S. Dordick, Advancing predictive hepatotoxicity at the intersection of experimental, in silico, and artificial intelligence technologies, *Chem. Res. Toxicol.* 31 (6) (2018) 412–430.
- [145] J.C. Dearden, P.H. Rowe, Use of artificial neural networks in the QSAR prediction of physicochemical properties and toxicities for REACH legislation, in: *Artificial Neural Networks*, Springer, 2015, pp. 65–88.
- [146] D. Dobchev, M. Karelson, Have artificial neural networks met expectations in drug discovery as implemented in QSAR framework? *Expet Opin. Drug Discov.* 11 (7) (2016) 627–639.
- [147] S. Hoffmann, N. Kleinstreuer, N. Alépée, D. Allen, A.M. Api, T. Ashikaga, et al., Non-animal methods to predict skin sensitization (I): the Cosmetics Europe database, *Crit. Rev. Toxicol.* 48 (5) (2018) 344–358.
- [148] V. V. Kleandrova, F. Luan, A. Speck-Planche, N.D.S. Cordeiro, In silico assessment of the acute toxicity of chemicals: recent advances and new model for multitasking prediction of toxic effect, *Mini Rev. Med. Chem.* 15 (8) (2015) 677–686.
- [149] S.C. Casey, M. Vaccari, F. Al-Mulla, R. Al-Temaimi, A. Amedei, M.H. Barcellos-Hoff, et al., The effect of environmental chemicals on the tumor microenvironment, *Carcinogenesis* 36 (Suppl\_1) (2015) S160–S183.
- [150] N. Parsa, Environmental factors inducing human cancers, *Iran. J. Public Health* 41 (11) (2012) 1.
- [151] R.L. Melnick, K.A. Thayer, J.R. Bucher, Research| mini-monograph, *Environ. Health Perspect.* 116 (2008) 130–135.
- [152] N. Fjodorova, M. Vracko, M. Tušar, A. Jezierska, M. Novič, R. Kühne, et al., Quantitative and qualitative models for carcinogenicity prediction for non-congeneric chemicals using CP ANN method for regulatory uses, *Mol. Divers.* 14 (3) (2010) 581–594.
- [153] M. Zhong, X. Nie, A. Yan, Q. Yuan, Carcinogenicity prediction of noncongeneric chemicals by a support vector machine, *Chem. Res. Toxicol.* 26 (5) (2013) 741–749.
- [154] K.P. Singh, S. Gupta, P. Rai, Predicting carcinogenicity of diverse chemicals using probabilistic neural network modeling approaches, *Toxicol. Appl. Pharmacol.* 272 (2) (2013) 465–475.
- [155] D. Guan, K. Fan, I. Spence, S. Matthews, Combining machine learning models of in vitro and in vivo bioassays improves rat carcinogenicity prediction, *Regul. Toxicol. Pharmacol.* 94 (2018) 8–15.
- [156] Y.W. Wang, L. Huang, S.W. Jiang, K. Li, J. Zou, S.Y. Yang, CapsCarcino: a novel sparse data deep learning tool for predicting carcinogens, *Food Chem. Toxicol.* 135 (2020), 110921.
- [157] V. Tiwari, D.M. Wilson III, DNA damage and associated DNA repair defects in disease and premature aging, *Am. J. Hum. Genet.* 105 (2) (2019) 237–257.
- [158] T.A. Brown, Mutation, repair, and recombination, in: *Genomes*, second ed., Wiley-Liss, 2002.
- [159] K. Sloczyńska, B. Powroźnik, E. Pékala, A.M. Waszkielewicz, Antimutagenic compounds and their possible mechanisms of action, *J. Appl. Genet.* 55 (2) (2014) 273–285.
- [160] D. Tungmunthum, A. Thongboonyou, A. Pholboon, A. Yangsabai, Flavonoids, and other phenolic compounds from medicinal plants for pharmaceutical and medical aspects: an overview, *Medicines* 5 (3) (2018) 93.
- [161] M.R. Webb, S.E. Ebeler, Comparative analysis of topoisomerase IB inhibition and DNA intercalation by flavonoids and similar compounds: structural determinates of activity, *Biochem. J.* 384 (3) (2004) 527–541.
- [162] L. Koklesova, A. Liskova, M. Samec, T. Qaradakh, A. Zulli, K. Smejkal, et al., Genoprotective activities of plant natural substances in cancer and chemopreventive strategies in the context of 3P medicine, *EPMA J.* 11 (2) (2020) 261–287.
- [163] V. Lobo, A. Patil, A. Phatak, N. Chandra, Free radicals, antioxidants, and functional foods: impact on human health, *Phcog. Rev.* 4 (8) (2010) 118.
- [164] E. Andresen, E. Peiter, H. Küpper, Trace metal metabolism in plants, *J. Exp. Bot.* 69 (5) (2018) 909–954.
- [165] M. Simunkova, Z. Barbierikova, K. Jomova, L. Hudecova, P. Lauro, S.H. Alwasel, et al., Antioxidant vs. prooxidant properties of the flavonoid, kaempferol, in the presence of Cu(II) ions: a ROS-scavenging activity, fenton reaction and DNA damage study, *Int. J. Mol. Sci.* 22 (4) (2021) 1619.
- [166] K.B. Pandey, S.I. Rizvi, Plant polyphenols as dietary antioxidants in human health and disease, *Oxid. Med. Cell. Longev.* 2 (5) (2009) 270–278.
- [167] N. Kumar, N. Goel, Phenolic acids: natural versatile molecules with promising therapeutic applications, *Biotechnol. Rep.* 24 (2019), e00370.
- [168] I. Ragunathan, N. Panneerselvam, Antimutagenic potential of curcumin on chromosomal aberrations in *Allium cepa*, *J. Zhejiang Univ. - Sci. B* 8 (7) (2007) 470–475.
- [169] L.P. Parker, D.D. Taylor, J. Kesterson, D.S. Metzinger, C. Gercel-Taylor, Modulation of microRNA associated with ovarian cancer cells by genistein, *Eur. J. Gynaecol. Oncol.* 30 (6) (2009) 616–621.
- [170] X. Yang, Y. Wang, R. Byrne, G. Schneider, S. Yang, Concepts of artificial intelligence for computer-assisted drug discovery, *Chem. Rev.* 119 (18) (2019) 10520–10594.
- [171] S. Dara, S. Dhamercherla, S.S. Jada, C.H. Babu, M.J. Ahsan, Machine learning in drug discovery: a review, *Artif. Intell. Rev.* 1–53 (2021).
- [172] M.H.S. Segler, T. Kogej, C. Tyrchan, M.P. Waller, Generating focused molecule libraries for drug discovery with recurrent neural networks, *ACS Cent. Sci.* 4 (1) (2018) 120–131.
- [173] D. Taylor, The Pharmaceutical Industry and the Future of Drug Development, 2015.
- [174] S. Nag, A.T.K. Baidya, A. Mandal, A.T. Mathew, B. Das, B. Devi, et al., Deep learning tools for advancing drug discovery and development, *3 Biotech* 12 (5) (2022) 1–21.
- [175] J. Mao, J. Akhtar, X. Zhang, L. Sun, S. Guan, X. Li, et al., Comprehensive strategies of machine-learning-based quantitative structure-activity relationship models, *iScience* 24 (9) (2021), 103052.
- [176] L.K. Tsou, S.H. Yeh, S.H. Ueng, C.P. Chang, J.S. Song, M.H. Wu, et al., Comparative study between deep learning and QSAR classifications for TNBC inhibitors and novel GPCR agonist discovery, *Sci. Rep.* 10 (1) (2020) 1–11.
- [177] A. Klenner, V. Hähnke, T. Geppert, P. Schneider, H. Zettl, S. Haller, et al., From virtual screening to bioactive compounds by visualizing and clustering of chemical space, *Molecular informatics* 31 (1) (2012) 21–26.
- [178] E. Lionta, G. Spyrou, D.K. Vassiliatis, Z. Cournia, Send orders for reprints to reprints@benthamscience. Net structure-based virtual screening for drug discovery: principles, applications and recent advances, *Curr. Top. Med. Chem.* 14 (2014) 1923–1938.
- [179] S. Ekins, J. Mestres, B. Testa, In silico pharmacology for drug discovery: methods for virtual ligand screening and profiling, *Br. J. Pharmacol.* 152 (1) (2007) 9–20.
- [180] G. Sliwoski, S. Kothiwale, J. Meiler, E.W. Lowe, Computational methods in drug discovery, *Pharmacol. Rev.* 66 (1) (2014) 334–395.
- [181] P. Ambure, A.K. Halder, H. Gonzalez Diaz, M.N.D.S. Cordeiro, QSAR-Co: an open source software for developing robust multitasking or multitarget classification-based QSAR models, *J. Chem. Inf. Model.* 59 (6) (2019) 2538–2544.
- [182] N.J. Schork, Artificial intelligence and personalized medicine, in: *Precision Medicine in Cancer Therapy*, Springer, 2019, pp. 265–283.



## *In silico* analysis of Diosmetin as an effective chemopreventive agent against prostate cancer: molecular docking, validation, dynamic simulation and pharmacokinetic prediction-based studies

Sumit Sheoran, Swati Arora, Tanmayee Basu, Swati Negi, Naidu Subbarao, Anupam Kumar, Himanshu Singh, Dhamodharan Prabhu, Atul Kumar Upadhyay, Neeraj Kumar & Sugunakar Vuree

**To cite this article:** Sumit Sheoran, Swati Arora, Tanmayee Basu, Swati Negi, Naidu Subbarao, Anupam Kumar, Himanshu Singh, Dhamodharan Prabhu, Atul Kumar Upadhyay, Neeraj Kumar & Sugunakar Vuree (24 Aug 2023): *In silico* analysis of Diosmetin as an effective chemopreventive agent against prostate cancer: molecular docking, validation, dynamic simulation and pharmacokinetic prediction-based studies, Journal of Biomolecular Structure and Dynamics, DOI: [10.1080/07391102.2023.2250451](https://doi.org/10.1080/07391102.2023.2250451)

**To link to this article:** <https://doi.org/10.1080/07391102.2023.2250451>



Published online: 24 Aug 2023.



Submit your article to this journal [↗](#)



Article views: 249



View related articles [↗](#)




View Crossmark data [↗](#)



Citing articles: 1 View citing articles [↗](#)



## *In silico* analysis of Diosmetin as an effective chemopreventive agent against prostate cancer: molecular docking, validation, dynamic simulation and pharmacokinetic prediction-based studies

Sumit Sheoran<sup>a</sup>, Swati Arora<sup>a</sup>, Tanmayee Basu<sup>b</sup>, Swati Negi<sup>c</sup>, Naidu Subbarao<sup>d</sup>, Anupam Kumar<sup>a</sup>, Himanshu Singh<sup>a</sup>, Dhamodharan Prabhu<sup>e</sup>, Atul Kumar Upadhyay<sup>b</sup>, Neeraj Kumar<sup>f</sup>  and Sugunakar Vuree<sup>a,g</sup>

<sup>a</sup>School of Bioengineering & Biosciences, Lovely Professional University, Jalandhar, India; <sup>b</sup>Department of Biotechnology, Thapar Institute of Engineering and Technology, Patiala, India; <sup>c</sup>Department of Chemistry, Delhi University, New Delhi, India; <sup>d</sup>School of Computational & Integrative Sciences, Jawaharlal Nehru University, New Delhi, India; <sup>e</sup>Centre for Drug Discovery, Department of Biotechnology, Karpagam Academy of Higher Education, Coimbatore, India; <sup>f</sup>Geetanjali Institute of Pharmacy, Udaipur, India; <sup>g</sup>MNR Foundation for Research and Innovation (MNR-FRI), MNR Medical College and Hospital, Fasalwadi Village, Hyderabad, India

Communicated by Ramaswamy H. Sarma

### ABSTRACT

Prostate cancer is the second most dangerous cancer type worldwide. While various treatment options are present i.e. agonists and antagonists, their utilization leads to adverse effects and due to this resistance developing, ultimately the outcome is remission. So, to overcome this issue, we have undertaken an *in-silico* investigation to identify promising and unique flavonoid candidates for combating prostate cancer. Using GOLD software, the study assessed the effectiveness of 560 natural secondary polyphenols against CDKN2. Protein Data Bank was used to retrieve the 3D crystal structure of CDKN2 (PDB Id: 4EK3) and we retrieved the structure of selected secondary polyphenols from the PubChem database. The compound Diosmetin shows the highest GOLD score with the selected Protein i.e. CDKN2 which is 58.72. To better understand the 2-dimensional and 3-dimensional interactions, the interacting amino acid residues were visualised using Discovery Studio 3.5 and Maestro 13.5. Using Schrodinger-Glide, the Diosmetin and CDKN2 were re-docked, and decoy ligands were docked to CDKN2, which was used to further ascertain the study. The ligands with the highest Gold score were forecasted for pharmacokinetics characteristics, and the results were tabulated and analysed. Utilising the Gromacs software and Desmond packages, 100 ns of Diosmetin molecular dynamics simulations were run to evaluate the structural persistence and variations of protein-ligand complexes. Additionally, our investigation revealed that Diosmetin had a better binding affinity with CDKN2 measuring 58.72, and it also showed remarkable stability across a 100-ns simulation. Thus, following *in-vitro* and *in-vivo* clinical studies, diosmetin might lead to the Prostate regimen.

**Abbreviations:** RMSD: Root mean square deviation; RGYR: Radius of Gyration; IntraHB: Intramolecular hydrogen bonds; MolSA: Molecular surface area; SASA: Solvent-accessible surface area; PSA: Polar Surface area; SSE: Secondary structural elements

### ARTICLE HISTORY

Received 23 May 2023  
Accepted 12 August 2023

### KEYWORDS

*In silico*; CDKN2; molecular docking; diosmetin; molecular simulation

## 1. Introduction

In Western nations, prostate cancer (PCa) has evolved as one of the men's most often detected tumors (Siegel et al., 2016). As of the most recent cancer data, the overall number of other incidences and mortality from PCa in the statistics for U. S. 2021 are 248530 and 34130, respectively, and the five-year survival rate is 97.5% (<https://seer.cancer.gov/stat-facts/html/prost.html>). Further, the GLOBOCAN 2020 report shows that, 34540 cases were recorded for prostate cancer in a year, which includes 16783 cases leading to death. Moreover, the prevalence rate is 9.47 in 100000 individuals (International Agency for Research on Cancer, 2020). Androgen hormones or their executioner AR are known to play vital roles in the genesis and development of PCa (Dehm & Tindall, 2006; Suzuki et al., 2003; Tan et al., 2015).

According to studies, AR promotes prostate epithelial cells' proliferation and differentiation throughout the Prostate cancer Field's progression (Singh et al., 2014). One of the most widely given AR blockers comprises steroidal medicines such as Cyproterone acetate (Gao et al., 2006; Goldenberg & Bruchovsky, 1991). Even though a variety of GnRH blockers and anti-androgens have evolved as one of the most common chemotherapeutic medications treating PCa, the dilemma of developing cancer after a brief time of resistance and enhanced toxicity owing to drug intake remains a significant barrier to efficient therapy. In this regard, the excellent correlation between flavonoid consumption and lower incidence of PCa has piqued researchers' curiosity, directing their emphasis on flavonoids as chemotherapy drugs in PCa (Bommareddy et al., 2013). Natural chemicals with a solid

affinity for prostate cells/androgen sensors may result in efficient PCa therapy.

Flavonoids have health-beneficial characteristics that can be used for nutritional, pharmacological and cosmetic purposes (Panche et al., 2016). Antioxidants, antibacterial, anti-allergic, anti-inflammatory, antitumor, and pharmacological actions are among the pharmaceutical characteristics (Di Leo et al., 2017; Guven et al., 2019). Flavonoids would treat cancer and other illnesses like cardiac, rheumatism, obesity, high blood cholesterol, hypertension, and neurological disorders (Ballard & Maróstica, 2018). The antitumor activity of Flavonoids is more active during the tumorigenesis, beginning, promotional, and advancement phases of cancer. Flavonoids could suppress tumor growth throughout the initiating; promotional stages (Abotaleb et al., 2018). In addition, flavonoids can suppress Pro angiogenesis, manage metastases, cause cytotoxic and apoptotic, cause cell cycle arrest and revert multi-drug resistance (MDR) at various stages of development and combining approaches (Chahar et al., 2011). Numerous research has presented empirical proof of flavonoids; cytotoxic activity *in vivo* and *in vitro* (Chan et al., 2021). Diosmetin is a natural compound abundantly present in legumes and olive leaves and has been shown to have the potential for use as an anticancer agent (Xu et al., 2017). Diosmetin selectively induces apoptosis and inhibits cancer cell growth without affecting normal cells (Xu et al., 2017). It has been suggested that diosmetin exerts growth-inhibitory effects through various signal transduction pathways, which have relevance in the cancer (Liu et al., 2016).

The subcellular environment halts cell growth, cause apoptotic, impair mitotic spindle development, and block angiogenesis, making them especially useful anti-cancer agents (Batra & Sharma, 2013). There, a molecular basis, flavonoids have been identified to control many kinases (Hou & Kumamoto, 2010) Furthermore, researchers have already found flavonoids to arrest cell growth in a dosage and time-dependent way. Based on their structural and tumor formation, they could stop the cell cycle at either the G0/G1 or G2/M stage (Kobayashi et al., 2002; Woo et al., 2005). Furthermore, Flavonols, a flavonoid subclass, were shown to have a molecular resemblance to testosterone, implying a high probability of cohesive forces with AR or many anti-androgenic activities in the PCa (Boam, 2015). Thus, examining the interaction of such diverse flavonoid classes i.e. flavonols also having anticancer properties (Sheoran et al., 2022) might provide perspective into their possible use in PCa therapy. Along with its capacity to estimate the conformational of simple ligands within the best target binding pocket with high precision, molecular docking is among the most often utilized approaches in structure-based drug discovery and development. As a result, it may be used to investigate the interactions among flavonoids and selected targets.

CDKs are well-known cell cycle stage mediators. Therefore, they are important therapeutic candidates, and unanticipated CDK stimulation might promote tumour growth (Malumbres & Barbacid, 2009). One of its most

essential CDKs is *CDKN2*. It links up with cyclin E to create a cluster. The cyclin E/CDK2 combination phosphorylates the domain RB<sup>1</sup> and accelerates the cell cycle transformation from G1 to S, resulting in cancer. Furthermore, *CDKN2* has already been identified as a critical mediator in the induction of apoptosis following DNA damage (Bačević et al., 2017). Moreover, the finding demonstrates that inhibiting *CDKN2* lowers tumour growth, and *CDKN2* inhibitors are already being tested in clinical studies (Rizzolio et al., 2010). Molecular docking is a two-step approach that begins with ligand conformational changes in the active region of the receptors. Afterwards, it ranks these based on respective interaction conformational energy for every interaction conformation (Seyedi et al., 2016). In addition, to determine the docking interaction affinity of different ligand-receptor conformations, widely accessible tools such as Auto Dock, Swiss dock, click docking, and GOLD are broadly applied (Lounnas et al., 2013). Therefore, we utilize GOLD for molecular docking because of its performance, accuracy, flexibility, and comprehensive analysis. Our virtual screening experiments are predicated on the notion that flavonoids may conflict with goals, inhibiting PCa genesis and development. In the process, we utilize flavonoids against selected targets such as *CDKN2*. In our present paper, we describe the selected target *CDKN2* (Figure 1 shows the genes associated with *CDKN2* by employing *GeneMania* (Warde-Farley et al., 2010) interaction with a specific flavonoid Diosmetin through *in-silico* studies such as molecular docking, drug-like properties, and pharmacokinetic properties and Molecular Simulation).

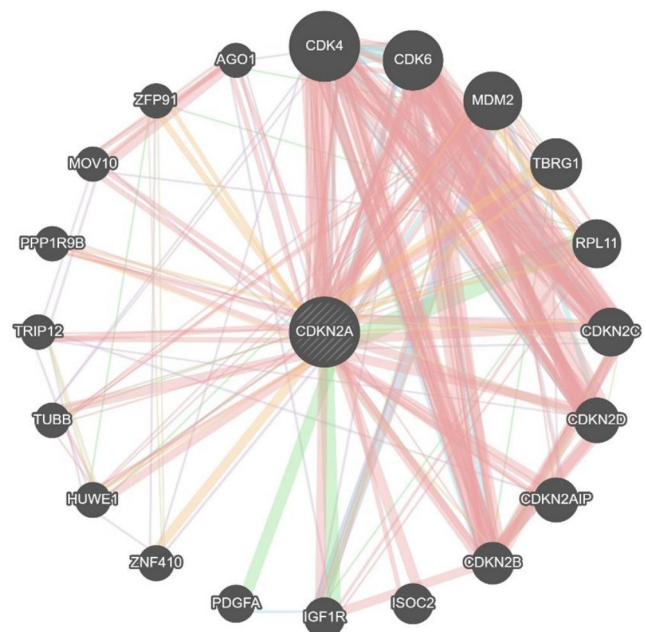


**Figure 1.** Showing the genes associated with the selected target *CDKN2*. *CDKN2* has Physical interaction (77.64%) with all the proteins except *PDGFA* and *ZNF410*. And co-expression (8.01%) with *CDK6*, *AGO1*, *MOV10*, *PPP1R9B*, *ZNF410* and *CDKN2C*. having PREDICTED (5.37%) with *ZFP91*, *PPP1R9B*, *HUWE1*, *ZNF410*, *CDKN2C*, *RPL11*, and *TBRG1*. Further genetic interaction (2.87%) with *PDGFA*, *IGF1R* and *RPL11*. Further pathway (1.88%) with *CDK4*, *CDK6* and *MDM2*. And shared protein domain with *CDKN2C*, *CDKN2D* and *CDKN2B*.



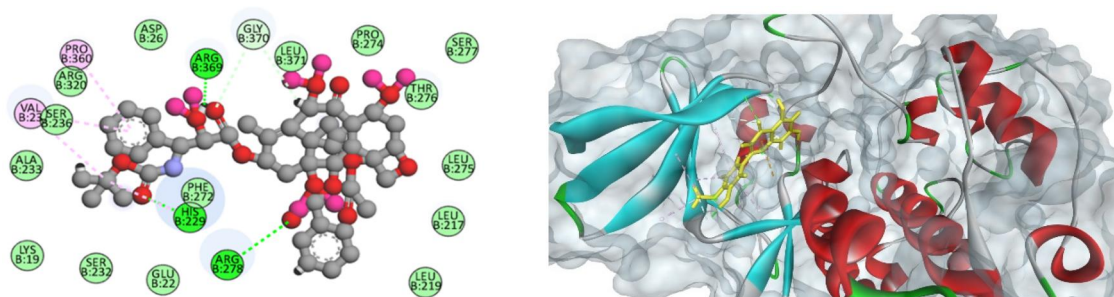


**Figure 2.** Showing 2D and 3D interaction with *CDKN2* and Diosmetin (Green colour line denotes the hydrogen bonding). the positions B:229-HIS, B: 278-ARG, B: 369-ARG have formed hydrogen bonds and the positions B: 22-GLU, B:19-LYS, B: 26-ASP, B: 232-SER, B:233-ALA, B:236-SER, B:320-ARG, B: 371-LEU, B:274-PRO, B: 276-THR, B:277-SER, B:275-LEU, B:217-LEU, & B:219-LEU formed H-C bonds. The residues B:23-VAL and B:360-PRO established pi bonding. Due to all these interactions, the diosmetin has produced a high GOLD score.

**Table 1.** The docking results of the top 10 compounds obtained from Gold.

Compound Name	GOLD Score
Baicalein	47.93
Chrysin	47.00
Diosmin	57.50
Diosmetin	58.72
Hesperidin	57.20
Kaempferol	51.99
Myricetin	53.73
Naringenin	47.66
Rutin	56.44
Tamarixetin	49.19

## 2. Methodology

### 2.1. Preparation of ligand for docking study

The structure of 560 selected polyphenol secondary metabolite molecules under the class of flavonoids on the basis of the literature review was obtained from PubChem in SDF file format (Ali et al., 2019; Patidar et al., 2019; Sweta et al., 2019; Yadav et al., 2019). The energy was then minimised using the Avogadro program (Maicas et al., 2021) and the MMF force field (Park et al., 2021). The steepest descent technique with a range of 200 rounds at RMS gradients of 0.1. was used to achieve the optimisation. Finally, minimised ligands were subjected to docking studies.

### 2.2. Protein preparation for docking study

The 3-D structure of the selected prostate cancer protein target, i.e. *CDKN2* (PDB ID: 4EK3), has been downloaded from the PDB database (Pranweerapaiboon et al., 2022) & prepared for future investigation (Information on protein secondary structure is in Figure 12). Employing Chimera, all unnecessary water molecules are eliminated & polar hydrogens are introduced to the molecule (Shivanika et al., 2022). To eliminate poor connections, the building must be energy efficient. Localized strain can occur because of minor flaws in the initial structure, such as poor Van der Waals connections. To relieve the strain, the structures were optimized by performing energy reduction under a vacuum hypothesis. Chimera was used to minimize energy. The optimized protein compounds having partial atomic charges were employed in a subsequent docking analysis to estimate the optimal orientations of the complexes within the receptors'

active center and determine the essential residues engaged in interaction with the ligand molecules. By using prank web <https://prankweb.cz/> we identified the active sites.

### 2.3. Molecular docking protocol by employing GOLD

GOLD software was used to study (Adeniyi & Ajibade, 2013) the binding mode and selectivity of the selected compounds with target proteins. Further, as reported in the literature, it was used to allocate hydrogens and active peptides torsions, which were docked further into binding pockets. The binding site area was developed within a 5-Å distance range. Water molecules and unwanted ligands were deleted after selecting binding sites or atoms ligands. Further, we have selected a scoring function for calculating binding energy, and a default generic algorithm was employed during the molecular docking process. The scoring function was used to group & evaluate the resulting structures. Finally, the docking results were compared with good conformation posture, and the best groups with the highest docked value were chosen for examination.

#### 2.3.1. Molecular docking protocol by employing glide

Docking was accomplished using the Schrodinger-Glide module (Olubode et al., 2022) The crystal structure of *CDKN2* was prepared suitably prior to dock with Diosmetin. The Extra Precision (XP) docking mode was performed to predict Diosmetin's binding energy and glide score with *CDKN2*. The semi-flexible docking research was conducted by allowing the Diosmetin to generate various conformations within the defined rigid active site of the *CDKN2* structure.

### 2.4. Drug-like & pharmacokinetic properties

To be effective as a drug, a potent molecule must reach its target in the body in sufficient concentration and also must remain there in a bioactive form long enough for the expected biological events to occur. Drug development involves the assessment of absorption, distribution, metabolism and excretion (ADME). To develop novel drug molecules, pharmacokinetic parameters are one of the essential properties. Any medicinal compound to evolve as a drug candidate should have optimum biological activity and

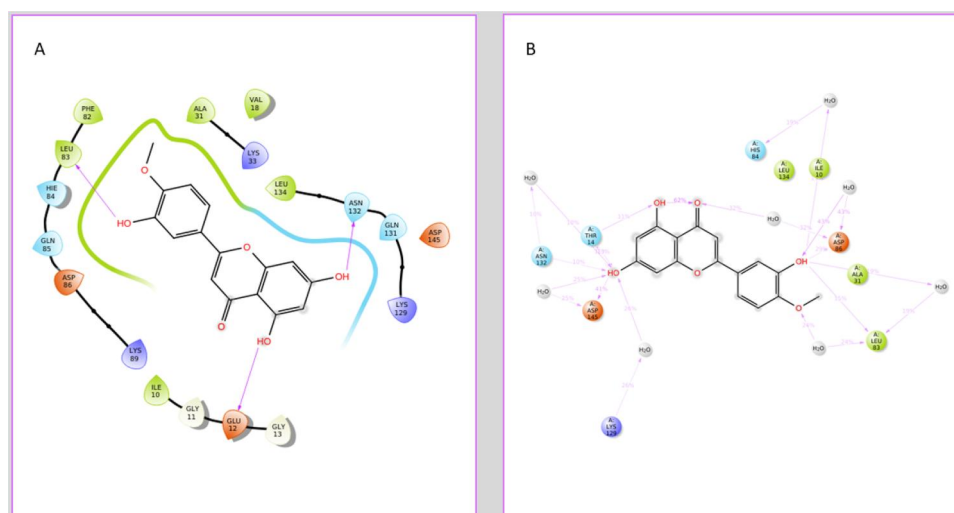


**Figure 3.** (A) The 2D interaction of Diosmetin with *CDKN2* was derived from Schrödinger-Glide, which has shown an Xp score of -7.529 and a Glide energy of -46.719. The pink colour arrow depicts the hydrogen bonding between Diosmetin and the active site residue of selected target *CDKN2*. (B) demonstrates the exact interactions among the atoms of the drug and protein residues. Interactions that last more than 10.0% of the simulation duration are shown in the selected path (0.00 to 100.01 nsec). It is possible to interact with >100% because certain residues might have multiple interactions of the same kind using the same ligand atom.

pharmacokinetic properties. To analyse the pharmacokinetic properties, we employed SwissADME (Daina et al., 2017) and ADMELab 2.0 (Xiong et al., 2021). In pharmacokinetic properties, Pgp (p-glycoprotein), which plays a vital role in drug discovery and development and presents in the liver, works as an efflux pump (Muthumanickam et al., 2022). If the drug molecule inhibits the Pgp, it is a good candidate and vice versa.

## 2.5. Drug-like properties

In 2007, Lipinski proposed the 'Rule of Five' (Di Leo et al., 2017), an essential drug-likeness filter commonly used for all drug candidates, which provides four rules to determine whether a molecule has good oral absorption or not. A compound may not be orally active if it violates two or more rules. To predict Lipinski's rule of drug-like properties such as Molecular weight (MW), Partition coefficient (Log p), hydrogen bond donors (HBD), hydrogen bond acceptors (HBA) and the number of rotatable bonds, we have used the zinc online server & SwissADME.

## 2.6. Molecular simulation using Gromacs

Gromacs is a widely used molecular dynamics simulation package (Abraham et al., 2015) known for its efficiency and scalability, making it suitable for handling large and complex systems. By employing Gromacs, the study benefits from its robust algorithms and optimized force fields, allowing for extensive exploration of conformational space and accurate representation of protein-ligand interactions. MD simulation of the protein-ligand complex was performed using the GROMACS 2020.1 software package. The simulation was accomplished by operating the CHARMM36-July 2021 force field for a runtime of 100 ns. The external CGenFF webserver was utilised to construct the ligand topology. The default water model (CHARMM modified TIP3P) was adopted to

solvate the system in a manner like the protein-ligand conjugate; by maintaining a triclinic solvation box and positioning it at least 1.0 nm from its border in the centre  $\text{Cl}^-$  ions were introduced for neutralisation. The system with the 1 bar pressure was used after the 300 K of 100 ns was equilibrated using the Parrinello-Rahman barostat method. The GROMACS utilities RMSD, RMSF, and hBond were examined following the MD simulation. The average displacement change of the frame is measured using the RMSD. For each frame in the trajectory, it is computed. The RMSD for frame  $x$  is:

$$\text{RMSD}_x = \frac{1}{N} \sum_{i=1}^N (r'_i(t_x) - r_i(t_{\text{ref}}))^2$$

The local alterations of protein chain can be defined using the RMSF. The RMSF for residue  $i$  is:

$$\text{RMSF} = \frac{1}{T} \sum_{t=1}^T < (r'_i(t) - r_i(t_{\text{ref}}))^2 >$$

The protein regions that fluctuate the most during the simulation are indicated by peaks on this map.

Contacts with Ligand: The protein residues that make interactions with the ligand are indicated in Figure 8C by vertical bars that are green in colour.

### 2.6.1. Molecular simulation using Desmond (Schrodinger)

Schrödinger's Desmond is a molecular dynamics simulation software that offers specialized tools and features for analyzing protein-ligand interactions and binding free energies (Ivanova et al., 2018). Desmond 2021-4 simulated molecular dynamics on an Acer workstation running Ubuntu 22.04. In order to generate the topology for the Complex, the force field for OPLS-2005 was processed. The complex was created using the system builder platform by solving the straightforward point-charge clear water models within an orthorhombic simulation box. The solvated complex system was neutralised with sufficient  $\text{Na}^+/\text{Cl}^-$  counter ions and a

concentration of salt of 0.15 M to mimic physiological conditions. The receptor-ligand complex system was located using the OPLS-2005 force field, and a clear fluid model containing

SPC water atoms was used in this framework in an orthorhombic box. Desmond At 300 K and 1.0325 bar of pressure, simulations were run for 100 ns after system minimization for 100 ps and relaxation of the systems using the default technique.

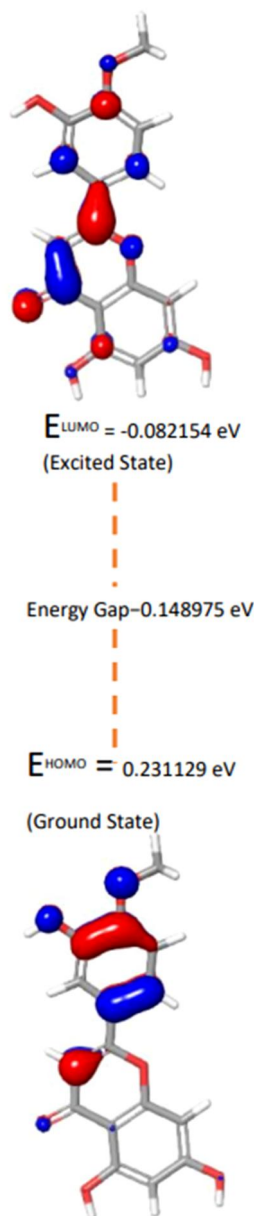


**Figure 4.** Depicts diosmetin's boundary chemical orbitals (HOMO-LUMO) and the accompanying transitioning energies.

## 2.7. BOILED EGG plot analysis

The Estimate D permeation method (BOILED- Egg) in the brain or intestinal tract is a reliable prediction model for determining ligand lipophilicity and polarity. It offers a distinctive statistical image for examining the ligand molecules' bioavailability characteristics. By looking at cooked eggs, physicochemical characteristics, including blood-brain barrier & gastrointestinal absorption permeability, are anticipated. BOILED plots, which are necessary for drug development and discovery, are created using the Swiss ADME online service (Daina et al., 2017).

## 3. Result and discussion

### 3.1. Molecular docking evaluation

Diosmetin has a higher gold score (58.72) with *CDKN2* (4EK3) (Figures 2 and International Agency for Research on Cancer, 2020), thus, it could have anti-cancerous activity and promising agent for treating prostate cancer. It also has drug-like & pharmacokinetic properties, and the top 10 compounds docking results are in Table 1. Diosmetin has three hydrogen bonding interactions with the residues HIS, and ARG of *CDKN2*. Also, Diosmetin has hydrogen-carbon bonding with the residues GLU, LYS, ASP, SER, ALA, ARG, LEU, PRO and THR of *CDKN2*. These in-silico studies may provide a significant platform for further evaluations in *in-vitro* and *in-vivo* experiments to explore their biological activity in order to consider the bioactive compound against tumour sickness. We are in the process of *in-vitro* evaluation on this compound in our lab (CGTR & DD and Unite Life Science labs).

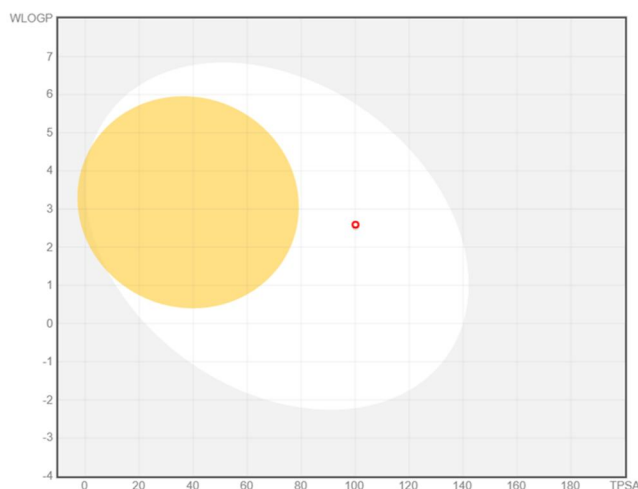
Further, to validate the result of GOLD docking, the molecular docking of Diosmetin with *CDKN2* in Schrodinger-Glide has shown an Xp score of  $-7.529$  and a Glide energy of  $-46.719$  (Figure 3A). The Figure 3B depicts the bonding interactions in percentages throughout the 100 ns simulation.

**Table 2.** ADME properties of selected top 10 flavonoids.

S.No.	COMPOUND NAME	CYP_2C19 inhibition	CYP_2C9 inhibition	CYP_2D6 inhibition	CYP_2D6 substrate	CYP_3A4 inhibition	CYP_3A4 substrate	Pgp inhibition
1	Baicalein	No	Inhibitor	Inhibitor	No	Inhibitor	No	No
2	Chrysin	No	No	Inhibitor	No	Inhibitor	No	No
3	Diosmin	No	No	No	No	No	No	Inhibitor
4	Diosmetin	No	Inhibitor	Inhibitor	No	No	No	No
5	Hesperidin	No	No	No	No	No	No	Inhibitor
6	Kaempferol	No	No	Inhibitor	No	Inhibitor	No	No
7	Myricetin	No	No	No	No	Inhibitor	No	No
8	Naringenin	No	No	No	No	Inhibitor	No	Inhibitor
9	Rutin	No	No	No	No	No	No	Inhibitor
10	Tamarixetin	No	Inhibitor	Inhibitor	No	Inhibitor	No	no

**Table 3.** Drug-like properties of selected top 10 flavonoids.

S.No.	Name of compound	MW	Log p	HB donor	HB acceptor	No. of rotatable bond
1.	Baicalein	270.24	2.43	3	5	1
2.	Chrysin	254.24	2.27	2	4	1
3.	Diosmin	608.54	2.66	8	15	7
4.	Diosmetin	300.26	2.47	3	6	2
5.	Hesperidin	610.56	0.85	8	15	7
6.	Kaempferol	286.84	1.7	4	6	1
7.	Myricetin	318.24	1.08	6	8	1
8.	Naringenin	272.25	1.75	3	5	1
9.	Rutin	610.52	0.46	10	16	6
10.	Tamarixetin	316.26	2.24	4	7	2

**Figure 5.** Shows the Boiled egg graph. As shown in the graph Diosmetin (red dot) is present in the white centre not in the yellow centre, so it has a high gastrointestinal absorption rate. It has a high blood-brain permeability if it is present in the yellow centre.

### 3.2. DFT analysis

DFT calculations were done by using Schrodinger- Jaguar to examine the molecular geometry and the electron distribution in the solid (Figure 4). The DFT method is a crucial and valuable tool for examining the connection between chemical compounds' geometry and electronic characteristics. We, therefore, present DFT calculations that take into account vibrational frequency analysis, electronic spectra, HOMO-LUMO energy with a range of chemical reactivity parameters, the Mulliken population analysis, the molecular electrostatic potential, the HOMA index, the natural population analysis and an investigation of the Schiff base's natural bond orbital (NBO).

The LUMO has no electron but can accept electron, indicating the molecule's susceptibility to nucleophilic attack which makes them electrophilic in nature while HOMO is the highest energy molecular orbitals with an electron and has the potential to donate an electron, it is used to describe the ability of molecules to resist electrophilic attack that is they are nucleophilic (Muthu et al., 2015). Furthermore, the interaction between a filled HOMO and an empty LUMO on one or more molecules can explain chemical processes and resonance. In FMO analysis, a small energy difference between HOMO and LUMO indicates that they are more reactive, chemically soft and less stable. In contrast, a high energy gap indicates that they are less reactive, chemically harder

and more stable (Benjamin et al., 2022). From the DFT results, it is evident that the Diosmetin is observed to be more reactive.

### 3.3. ADME analysis

ADME prediction plays an important part in drug discovery and development, with the ultimate objective of predicting the *in vivo* pharmacokinetics of a potential therapeutic molecule. Along with molecular docking research, ADME evaluations are performed to categorise the safety and effectiveness of a pharmacological molecule (Seyedi et al., 2016). Tables 2 and 3 provide pharmacological characteristics.

The values of the tested compounds in this investigation are within an acceptable range. The natural molecule Diosmetin falls in the acceptable values, indicating that it is readily permeable. The results showed that, compared to the screened compounds from the PubChem, and Zinc database, the natural chemical Diosmetin followed Lipinski's RO5. The Diosmetin chemical has excellent oral absorption in humans and has desirable pharmacokinetic characteristics. As a result, this Diosmetin compound is expected to have high bioavailability and to function as an active therapeutic molecule.

Cytochrome P450s is an important enzyme system for drug metabolism in the liver. The two main subtypes of cytochrome P450 are CYP2D6 and CYP3A4. The results showed that Diosmetin were not a substrate for the two subtypes. Further, it was also not predicted to be a CYP2C19 inhibitor and predicted to inhibit CYP2C9 inhibitor and CYP2D6 inhibitors. This suggested that it may be metabolized in the liver.

P-gp acts as a drug-extracting pump that needs energy in the process. The efflux occurs through a pore in the cell membrane that consists of 12  $\alpha$ -helices. High expression levels of P-gp are found in normal tissues such as the liver, pancreas, kidneys (renal tubules), colon, and adrenal cortex (Ruiz Gómez et al., 2002). These findings suggest that P-gp could have a physiological role in secretion. In tumor tissues, there is a correlation between the increase of P-gp expression. Binding to P-gp prediction was calculated with SwissADME.

### 3.4. BOILED egg plot analysis

Aside from ADME prediction, minor molecule toxicity and effectiveness are failures owing to adverse pharmacokinetic characteristics. As demonstrated in Figure 5, the Diosmetin Boiled Egg plot exhibits two favourable pharmacokinetic



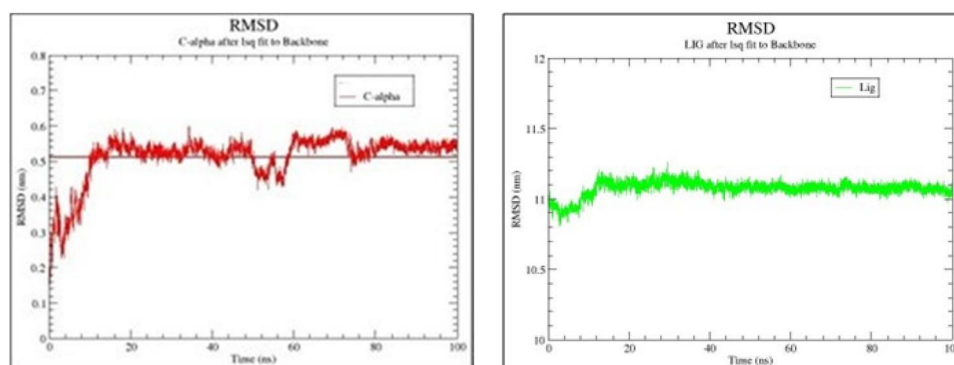


**Figure 6.** The RMSD quickly reaches 0.1 nm (1 Å), but the average protein during the simulation is  $\sim 0.5$  nm (5 Å) and is quite unstable throughout the 100 ns.

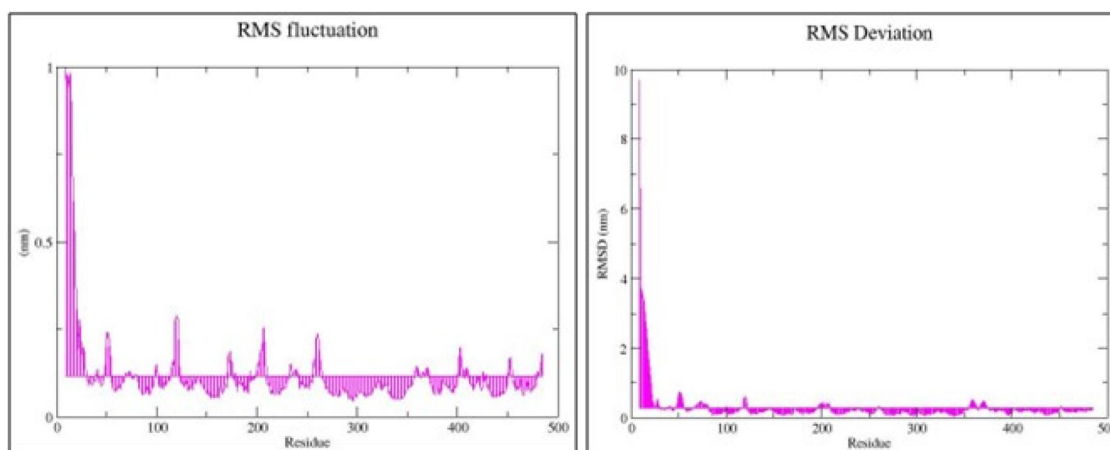


**Figure 7.** The regions of high flexibility are the protein residues- 0–25, 50–53, 112–125, 160–175, 200–214, 260–270, and 400–410. RMSD vs the residue plot shows that the initial residues fluctuating most are responsible for the high RMSD in the simulation.

properties: gastrointestinal absorption and Blood Brain Barrier (Ali et al., 2019). This chemical has a high gastrointestinal absorption rate, which is visible in the white zone of the egg (Figure 5). As a result, this Diosmetin molecule is brain impermeable. Overall, Diosmetin was shown to be the most effective anti-cancer drug in our investigation. However, more *in vitro* and *in vivo* research on the natural ligand is needed to confirm the findings of this work.

### 3.5. Molecular simulation evaluation

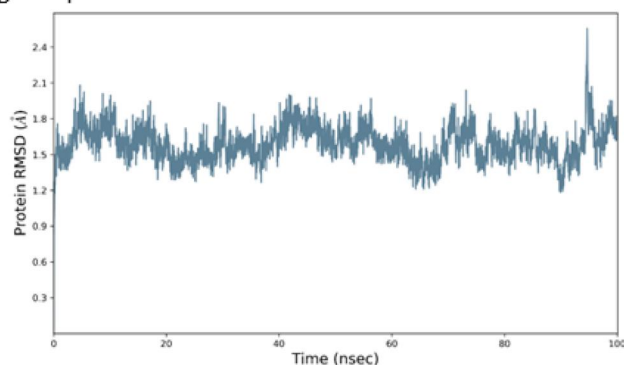
To explore the stability of Diosmetin with CDKN2 protein, the types of interactions involved in the binding process, RMSD, RMSF, and Hbonds are determined. Figure 6 depicts the RMSD of the Diosmetin-CDKN2 complex after a 100-ns molecular dynamics simulation in the solvent environment. Throughout the simulation, the RMSD of the Diosmetin-CDKN2 protein combination was between 0.1 and 0.5 nm. The movements of the CDKN2 protein's activation loop may be responsible for the early simulation stage between 0 and 15 ns (Bačević et al., 2017). Minimal fluctuations are seen beyond the initial steps. As a result, the RMSD averaged constant snaps demonstrated that the arrangement of the CDKN2-Diosmetin interaction remained steady throughout the 100-nanosecond simulation, and Diosmetin did not dissolve from the protein.

The RMSD computes the variations in the protein's backbone between the initial and final conformations and, as a result, evaluates the protein's stability. The protein backbone RMSD (backbone) and protein-ligand complex RMSD (complex) were assessed in the current investigation. According to the findings, computed values have indicated a steady RMSD with any variances. Despite both exhibiting stability throughout the simulation run, the backbone RMSD has consistently shown lower RMSD than the complex.

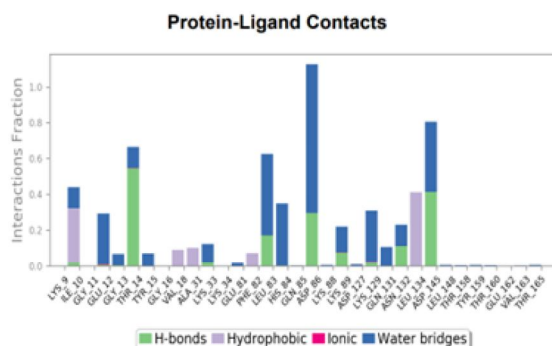
Furthermore, Figure 6 depicts the structural steadiness of the protein-ligand complex, which is studied using the RMSD result (Rizzolio et al., 2010). As a consequence of the equilibrium state at 100 ns, it was discovered that both the original simulated structure and the end structure had stable confirmation throughout the period. According to the trajectory study, the complex looks prospective and active.

RMSF also investigates the flexibility of the activation loop, as demonstrated in Figure 7. Calculating the RMSF of all residues along the simulation trajectory identifies the region with greater flexibility in the protein. The data reflects the variation of specific amino acid residues due to the protein's loop and disorder regions. Using the complex's RMSF diagram (Figure 7), it is discovered that the primary peaks of variation between residues are more than 0.1 nm. These residues are not detected in docking studies. Hence the fluctuation does not affect the protein-Diosmetin chemical

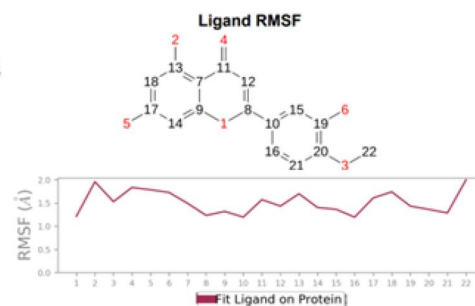
## A Ligand-protein RMSD



## C



## B



## D

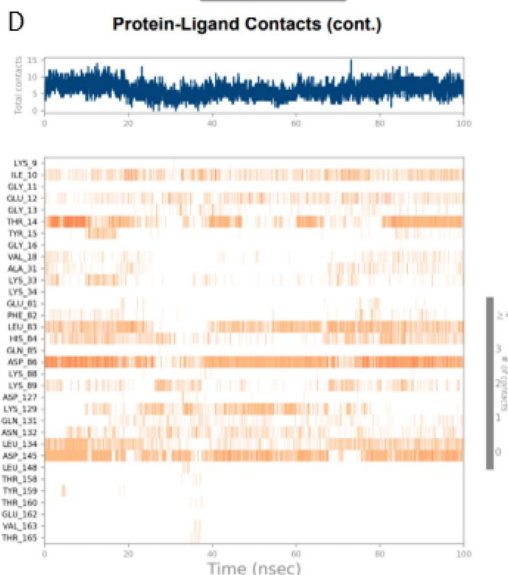


**Figure 8.** (A) Shows the MD simulation performed using Schrodinger-Desmond. The complex is stable between 1.5 and 1.8 Å throughout the 100 ns simulation except at 90 ns. (B) Ligand RMSF, which corresponds to the 2D structure in the top panel, displays the ligand's fluctuations broken down by atom. (C) Displayed interactions between proteins and their ligands, including hydrogen bonds, hydrophobic interactions, ionic interactions, and water bridges. (D) Timeline depicting connections and linkages (H-bonds, hydrophobic, ionic, and water bridges). The top panel shows the total number of unique interactions the protein makes with the ligand during the journey. The bottom panel shows which residues in each trajectory frame interact with the ligand. Dark orange represents residues that interact with the ligand in multiple ways.

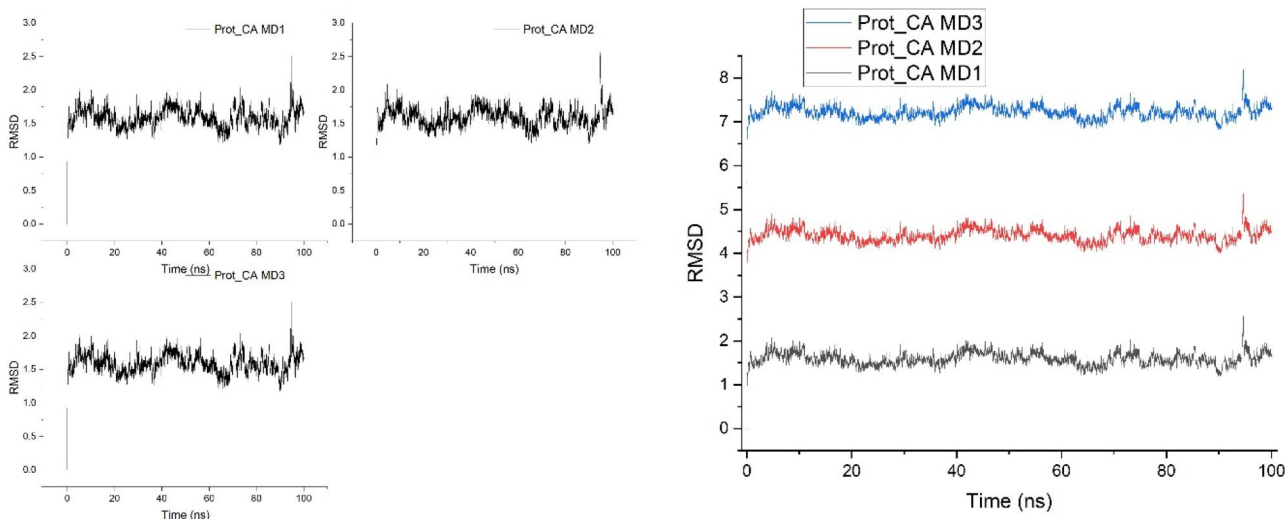


**Figure 9.** Depicts the triplicates results of RMSD by employing Desmond (Schrodinger), and throughout the triplicates, no significant difference is found, and results are identical and similar.

binding. The rest of the residues are stable at less than 1 nm. The hydrogen bond is one of the most critical factors in the protein-ligand complex. The Gromacs package is used to identify the hydrogen bond between Diosmetin and the

CDKN2 protein. Throughout the simulation, three hydrogen bonds remain stable in the binding process. Hydrogen bonds form all amino acid residues, including HIS and ARG (278,369). Through contact, each amino acid has contributed

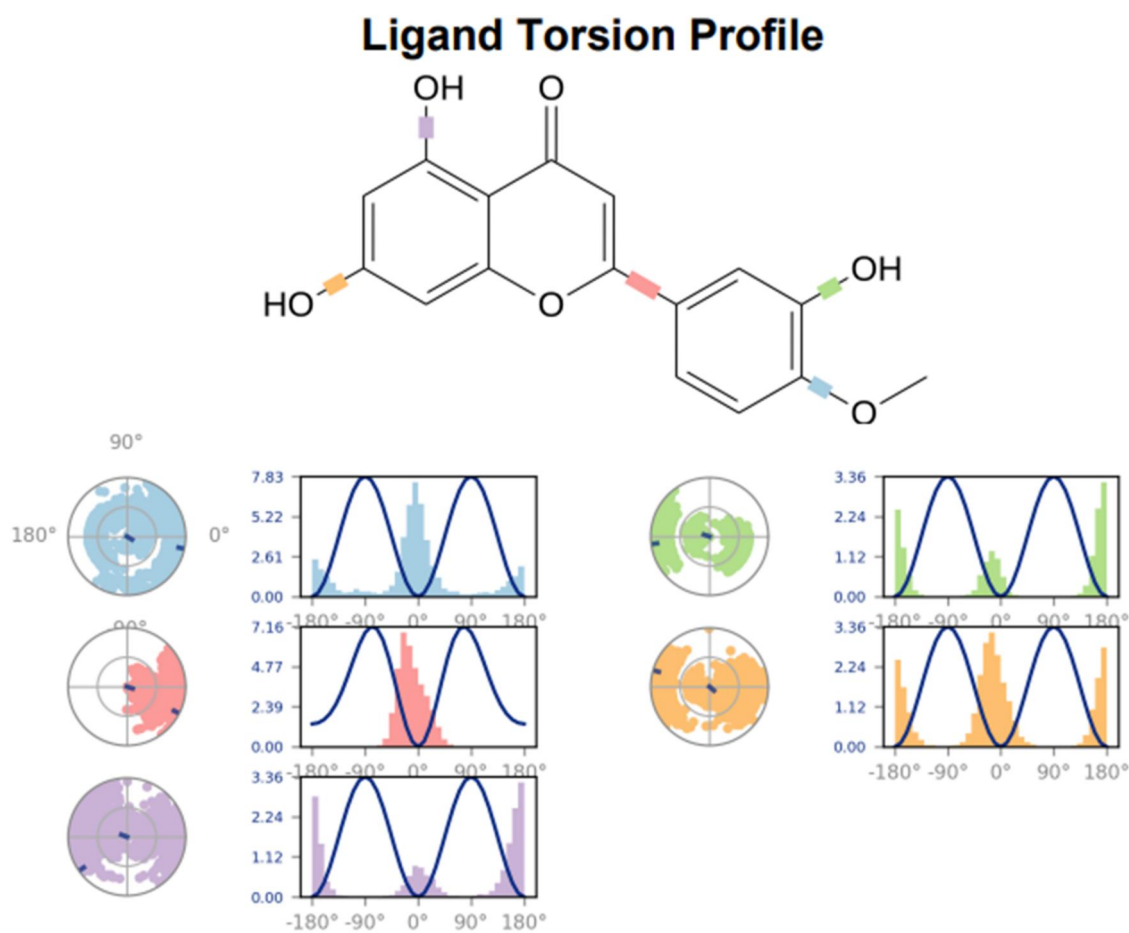


**Figure 10.** Depicts the 2D and 3D ligand torsion profiles it describes the torsions of ligands at different points. Each color defines the one point of torsion.

### Ligand Properties

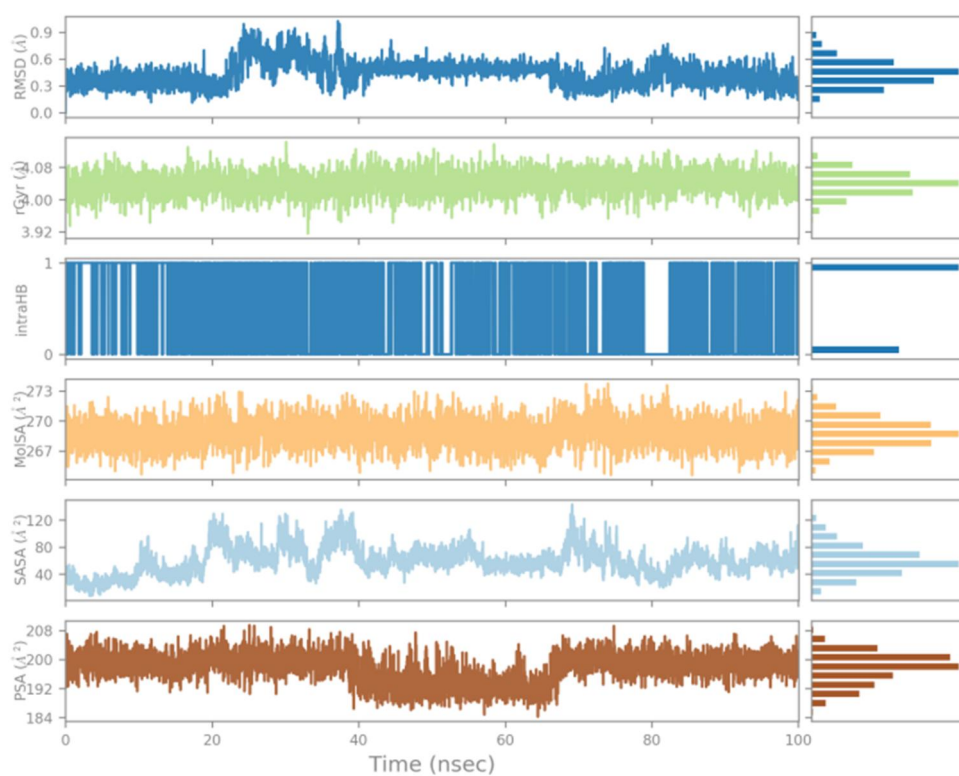


**Figure 11.** Shows the RMSD, RGYR, IntraHB, MolSA, SASA and PSA.

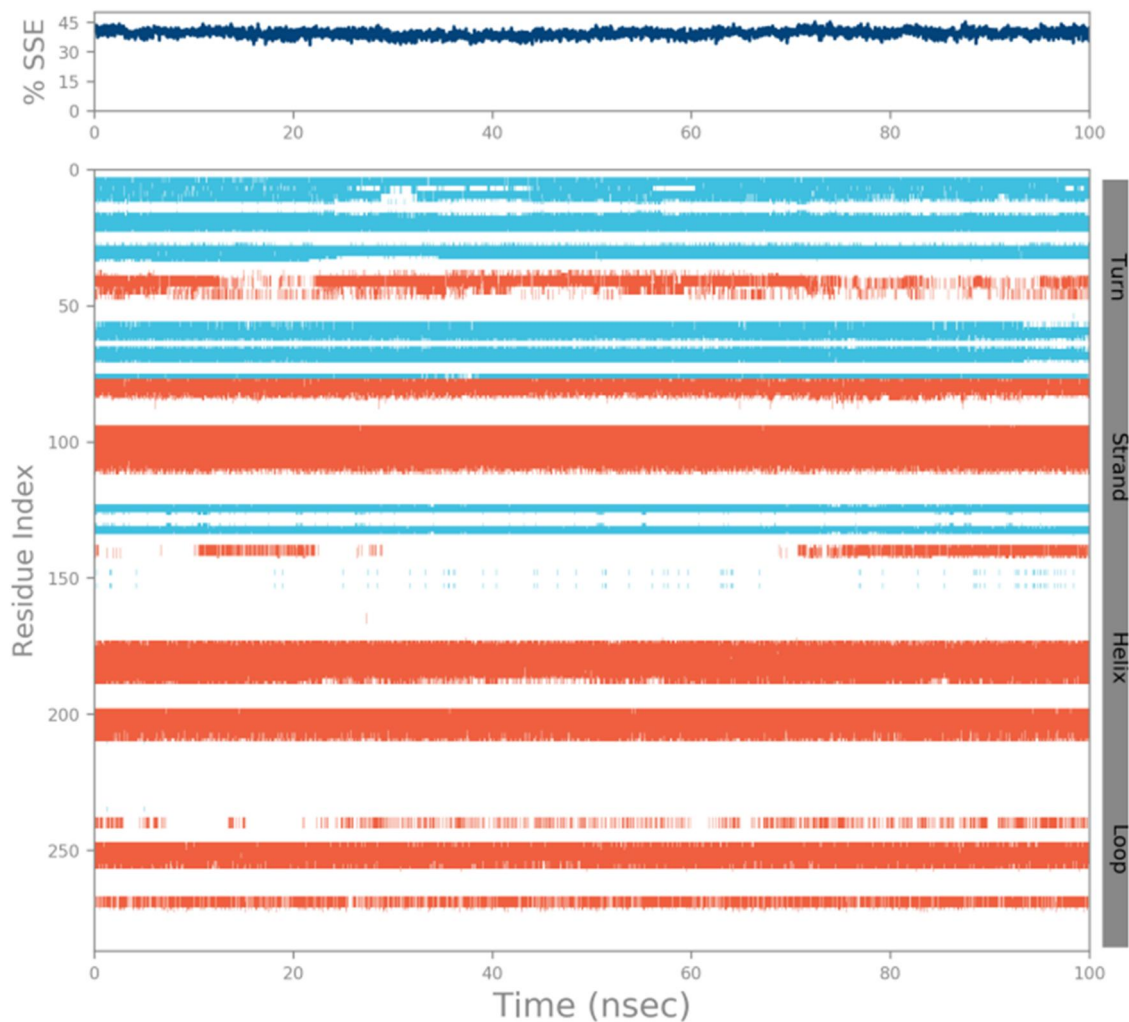


Figure 12. Depicts protein secondary structures. The above plot represents the SSE, and the below plot summarizes the SSE composition for each trajectory frame over the course of the simulation.

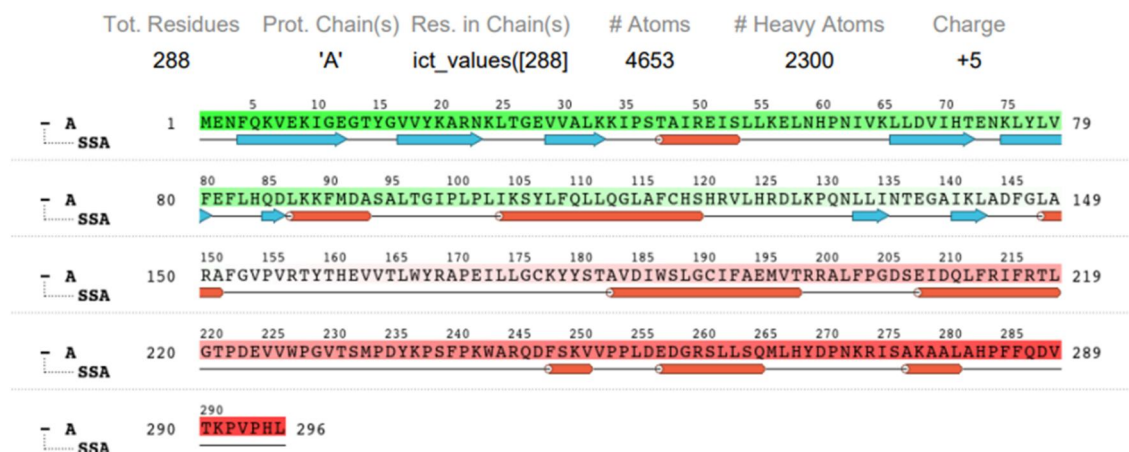


Figure 13. Protein information has total residues 288 chain a and total atoms 4653 with heavy atoms 2300 and charges +5.

to the OH group of the Diosmetin molecule. This interaction has the potential to stabilise Diosmetin in its interaction location. Consequently, the presence of a hydrogen bonding association between the Diosmetin and the *CDKN2* protein is in good accord with the docking research results.

Further, to validate and robust the study, we utilize Desmond to simulate the Diosmetin docked with *CDKN2* complex for 100 ns in triplicate. We observed that in Gromacs, the complex is quite fluctuating throughout 100 ns. However, in Desmond, the complex is stable throughout the



100 ns. In triplicate, we found no significant difference in RMSD (Figures 8 and 9).

### 3.5.1. Ligand torsion profile and properties

Each rotatable bond (RB) in the ligand (Zaki et al., 2023) underwent a conformational change during the simulation trajectory (0.00 to 100.01 nsec) (Sangai et al., 2018), which is depicted in the ligand torsions chart and other properties (Figures 10 and 11). The top panel displays a two-dimensional representation of a ligand with coloured rotatable bonds. Each rotatable bond torsion includes a dial plot and matching-colour bar plots. Dial (or radial) charts show how the torsion has changed over the duration of the simulation. The temporal development appears radially outwards from the simulation's starting point, which is in the centre of the radial map. By displaying the probability density of the torsion, the bar plots provide a summary of the data on the dial plots. The figure also displays the potential of the rotatable bond (by adding the potential of the associated torsions) if torsional potential information is available. The potential values are shown on the chart's left Y-axis and are given in kcal/mol. The structural strain the ligand experiences to retain a protein-bound shape can be understood by examining the correlations between the histogram and torsion potential.

In the present study, during the dynamic simulation process, the radius of gyration (Rg) and RMSD values were used to calculate structure deviation that determines whether the protein suffered any distortion or maintained its conformation during the 100-ns duration. The Rg that measures protein compactness was found to be 4.08 Å<sup>2</sup> (Figure 11). The trajectory RMSD values were found to be 0.3 to 0.9 Å<sup>2</sup> (Figure 11) during the 100-ns period.

### 3.3. Protein secondary structure

Beta- and alpha-strands are monitored throughout the simulation as protein secondary structural elements (SSE) examples. The SSE distribution across the protein structure is shown in the plot above by residue index. The bottom plot tracks each residue's SSE assignment through time, whereas the plot below summarises the SSE component for every trajectory frame throughout the simulation (shown in Figures 12 and 13).

Further, we are in the process of *In-vitro* and *In-vivo* studies because Computational studies have some limitations. To overcome these limitations, *in vitro* and *in vivo* investigations are crucial.

## 4. Conclusion

In the current study, we utilize *in-silico* analyses to find promising novel small compounds as viable candidates for Prostate cancer regimens. Further, we investigated *in silico* a series of compounds from the PubChem and the natural substance Diosmetin docked with CDKN2. Based on the Gold score, ten top-ranked compounds from virtual screening and molecular docking studies were chosen as the most effective

leading molecules. Diosmetin shows the best ranking based on the Gold score i.e. 58.72. The overall pharmacokinetic profile and ADME analyses assessed the molecule's characteristics. The Diosmetin molecule was shown to obey Lipinski RO5 and all other drug-like rules in an ADME analysis, and egg plot investigations demonstrate that it has a high gastrointestinal absorption rate and is brain impermeable. Consequently, MD simulations at 100 ns using the Diosmetin-CDKN2 complex were performed using Gromacs, and the findings revealed high binding stability. To further validate, we also perform Docking and simulation by Schrodinger. In addition, the results of *in silico* experiments provided better support for future *in vitro* & *in vivo* investigations. These findings showed that Diosmetin might be investigated as a potential lead molecule to cure Prostate cancer. As per Christine Oak and team (Oak et al., 2018), Diosmetin inhibits the growth of Prostate cells in the PC3 cell line by employing cell cycle arrest and apoptosis further, it is also a promising candidate for liver cancer (Ma & Zhang, 2020). Further investigation and the generation of scientific evidence are necessary to determine whether the therapeutic effects of newly identified and synthetically produced flavones benefit patients. Diosmetin was discovered to have a greater affinity with CDKN2 than tested compounds based on *In silico* experiments. *In vitro* & *In vivo* studies will be conducted at CGTR & DD and Unite Life Science labs. Overall, this study's implications lie in advancing our understanding of prostate cancer biology, identifying potential therapeutic targets, and exploring novel treatment options. It contributes to the broader field of prostate cancer research by shedding light on the molecular interactions involved in the disease and providing a foundation for further investigation and development of targeted therapies.

## Acknowledgements

We acknowledge the School of Bioengineering and Biosciences, Lovely Professional University, Jalandhar, MNR-Foundation for Research and Innovation (FRI), MNR University, SangaReddy and Unite Life Sciences, Hyderabad, for their continued support and encouragement.

## Disclosure statement

No potential conflict of interest was reported by the authors.

## Funding

The author(s) reported there is no funding associated with the work featured in this article.

## ORCID

Neeraj Kumar  <http://orcid.org/0000-0001-5508-0616>

## Authorship statement

Sugunakar Vuree (SV) Conceptualize the idea and formulate the methodology, proofreading and editing the complete manuscript. Sumit Sheoran (SS) writes the first draft of the manuscript. SS and Swati Arora (SA)

performed Molecular Docking, ADME, Drug-like properties, and Boiled Egg plots. *Tanmayee Basu (TB)*, *Atul Upadhyay (AU)* in performing Gromacs and *Neeraj Kumar (NK)* in performing Desmond (Schrodinger) Molecular simulation. *Naidu Subbarao (NS)* in providing Gold software for docking. *Dhamodharan Prabhu (DP)* performed molecular docking in Glide and DFT calculations. *Himanshu Singh (HS)* and *Anupam Kumar (AK)*, and *Swati Negi (SN)* with proofreading.

## References

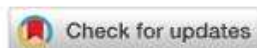
- Abotaleb, M., Samuel, S. M., Varghese, E., Varghese, S., Kubatka, P., Liskova, A., & Büsselberg, D. (2018). Flavonoids in cancer and apoptosis. *Cancers*, 11(1), 28. <https://doi.org/10.3390/cancers11010028>
- Abraham, M. J., Murtola, T., Schulz, R., Páll, S., Smith, J. C., Hess, B., & Lindahl, E. (2015). GROMACS: High performance molecular simulations through multi-level parallelism from laptops to supercomputers. *SoftwareX*, 1–2, 19–25. <https://doi.org/10.1016/j.softx.2015.06.001>
- Adeniyi, A. A., & Ajibade, P. A. (2013). Comparing the suitability of auto-dock, gold and glide for the docking and predicting the possible targets of Ru(II)-based complexes as anticancer agents. *Molecules (Basel, Switzerland)*, 18(4), 3760–3778. <https://doi.org/10.3390/molecules18043760>
- Ali, M. A., Vuree, S., Goud, H., Hussain, T., Nayariseri, A., & Singh, S. K. (2019). Identification of high-affinity small molecules targeting Gamma secretase for the treatment of Alzheimer's disease. *Current Topics in Medicinal Chemistry*, 19(13), 1173–1187. <https://doi.org/10.2174/1568026619666190617155326>
- Bačević, K., Lössaint, G., Achour, T. N., Georget, V., Fisher, D., & Dulić, V. (2017). Cdk2 strengthens the intra-S checkpoint and counteracts cell cycle exit induced by DNA damage. *Scientific Reports*, 7(1), 13429. <https://doi.org/10.1038/s41598-017-12868-5>
- Ballard, C. R., & Maróstica, M. R. (2018). *Health benefits of flavonoids*. Elsevier Inc.
- Batra, P., & Sharma, A. K. (2013). Anti-cancer potential of flavonoids: Recent trends and future perspectives. 3 *Biotech*, 3, 439–459. <https://doi.org/10.1007/s13205-013-0117-5>
- Benjamin, I., Udoikono, A. D., Louis, H., Agwamba, E. C., Unimuke, T. O., Owen, A. E., & Adeyinka, A. S. (2022). Antimalarial potential of naphthalene-sulfonic acid derivatives: Molecular electronic properties, vibrational assignments, and in-silico molecular docking studies. *Journal of Molecular Structure*, 1264, 133298. <https://doi.org/10.1016/j.molstruc.2022.133298>
- Boam, T. (2015). Anti-androgenic effects of flavonols in prostate cancer. *Ecancermedicalscience*, 9, 585. <https://doi.org/10.3332/ecancer.2015.585>
- Bommareddy, A., Eggleston, W., Prelewicz, S., Antal, A., Witczak, Z., Mccune, D. F., & Vanwert, A. L. (2013). Chemoprevention of prostate cancer by major dietary phytochemicals. *Anticancer Research*, 33(10), 4163–4174. <http://ar.iiarjournals.org/content/33/10/4163.abstract>
- Chahar, M. K., Sharma, N., Dobhal, M. P., & Joshi, Y. C. (2011, January). Flavonoids: A versatile source of anticancer drugs. *Pharmacognosy Reviews*, 5(9), 1–12. <https://doi.org/10.4103/0973-7847.79093>
- Chan, E. W. C., Ng, Y. K., Tan, C. Y., Alessandro, L., Wong, S. K., & Chan, H. T. (2021). Diosmetin and tamarixetin (methylated flavonoids): A review on their chemistry, sources, pharmacology, and anticancer properties. *Journal of Applied Pharmaceutical Science*, 11(3), 22–28.
- Daina, A., Michielin, O., & Zoete, V. (2017). SwissADME: A free web tool to evaluate pharmacokinetics, drug-likeness and medicinal chemistry friendliness of small molecules. *Scientific Reports*, 7(1), 42717. <https://doi.org/10.1038/srep42717>
- Dehm, S. M., & Tindall, D. J. (2006). Molecular regulation of androgen action in prostate cancer. *Journal of Cellular Biochemistry*, 99(2), 333–344. <https://doi.org/10.1002/jcb.20794>
- Di Leo, N., Battaglini, M., Berger, L., Giannaccini, M., Dente, L., Hampel, S., Vittorio, O., Cirillo, G., & Raffa, V. (2017, May). A catechin nanoformulation inhibits WM266 melanoma cell proliferation, migration and associated neo-angiogenesis. *European Journal of Pharmaceutics and Biopharmaceutics*, 114, 1–10. <https://doi.org/10.1016/j.ejpb.2016.12.024>
- Gao, W., Kim, J., & Dalton, J. T. (2006). Pharmacokinetics and pharmacodynamics of nonsteroidal androgen receptor ligands. *Pharmaceutical Research*, 23(8), 1641–1658. <https://doi.org/10.1007/s11095-006-9024-3>
- Goldenberg, S. L., & Bruchovsky, N. (1991). Use of cyproterone acetate in prostate cancer. *Urologic Clinics of North America*, 18(1), 111–122. [https://doi.org/10.1016/S0094-0143\(21\)01398-7](https://doi.org/10.1016/S0094-0143(21)01398-7)
- Guven, H., Arici, A., & Simsek, O. (2019). Flavonoids in our foods: A short review. *Journal of Basic and Clinical Health Sciences*, 3, 96–106. <https://doi.org/10.30621/jbachs.2019.555>
- Hou, D. X., & Kumamoto, T. (2010). Flavonoids as protein kinase inhibitors for cancer chemoprevention: Direct binding and molecular modeling. *Antioxidants & Redox Signaling*, 13(5), 691–719. <https://doi.org/10.1089/ars.2009.2816>
- International Agency for Research on Cancer. (2020). Time trend in breast and cervix cancer of women in India.pdf. *Globocan*, 361, 2. <https://gco.iarc.fr/today/data/factsheets/populations/356-india-factsheets.pdf>
- Ivanova, L., Tammiku-Taul, J., García-Sosa, A. T., Sidorova, Y., Saarma, M., & Karelson, M. (2018). Molecular dynamics simulations of the interactions between glial cell line-derived neurotrophic factor family receptor GFR $\alpha$ 1 and small-molecule ligands. *ACS Omega*, 3(9), 11407–11414. <https://doi.org/10.1021/acsomega.8b01524>
- Kobayashi, T., Nakata, T., & Kuzumaki, T. (2002). Effect of flavonoids on cell cycle progression in prostate cancer cells. *Cancer Letters*, 176(1), 17–23. [https://doi.org/10.1016/S0304-3835\(01\)00738-8](https://doi.org/10.1016/S0304-3835(01)00738-8)
- Liu, J., Ren, H., Liu, B., Zhang, Q., Li, M., & Zhu, R. (2016). Diosmetin inhibits cell proliferation and induces apoptosis by regulating autophagy via the mammalian target of rapamycin pathway in hepatocellular carcinoma HepG2 cells. *Oncology Letters*, 12(6), 4385–4392. <https://doi.org/10.3892/ol.2016.5301>
- Lounnas, V., Ritschel, T., Kelder, J., McGuire, R., Bywater, R. P., & Foloppe, N. (2013). Current progress in structure-based rational drug design marks a new mindset in drug discovery. *Computational and Structural Biotechnology Journal*, 5(6), e201302011. <https://doi.org/10.5936/csbj.201302011>
- Ma, A., & Zhang, R. (2020). Diosmetin inhibits cell proliferation, induces cell apoptosis and cell cycle arrest in liver cancer. *Cancer Management and Research*, 12, 3537–3546. <https://doi.org/10.2147/CMAR.S240064>
- Maicas, R., Yungerman, I., Weber, Y. B., & Srebnik, S. (2021). United-atom molecular dynamics study of the mechanical and thermomechanical properties of an industrial epoxy. *Polymers*, 13(19), 3443. <https://doi.org/10.3390/polym13193443>
- Malumbres, M., & Barbacid, M. (2009). Cell cycle, CDKs and cancer: A changing paradigm. *Nature Reviews. Cancer*, 9(3), 153–166. <https://doi.org/10.1038/nrc2602>
- Muthu, S., Elamurugu Porchelvi, E., Karabacak, M., Asiri, A. M., & Swathi, S. S. (2015). Synthesis, structure, spectroscopic studies (FT-IR, FT-Raman and UV), normal coordinate, NBO and NLO analysis of salicylaldehyde p-chlorophenylthiosemicarbazone. *Journal of Molecular Structure*, 1081, 400–412. <https://doi.org/10.1016/j.molstruc.2014.10.024>
- Muthumanickam, S., Indhumathi, T., Boomi, P., Balajee, R., Jeyakanthan, J., Anand, K., Ravikumar, S., Kumar, P., Sudha, A., & Jiang, Z. (2022). In silico approach of naringin as potent phosphatase and tensin homolog (PTEN) protein agonist against prostate cancer. *Journal of Biomolecular Structure & Dynamics*, 40(4), 1629–1638. <https://doi.org/10.1080/07391102.2020.1830855>
- Oak, C., Khalifa, A. O., Isali, I., Bhaskaran, N., Walker, E., & Shukla, S. (2018). Diosmetin suppresses human prostate cancer cell proliferation through the induction of apoptosis and cell cycle arrest. *International Journal of Oncology*, 53(2), 835–843. <https://doi.org/10.3892/ijo.2018.4407>
- Olubode, S. O., Bankole, M. O., Akinnusi, P. A., Adanlawo, O. S., Ojubola, K. I., Nwankwo, D. O., Edjebah, O. E., Adebesein, A. O., & Ayodele, A. O. (2022). Molecular modeling studies of natural inhibitors of androgen signaling in prostate cancer. *Cancer Informatics*, 21, 11769351221118556. <https://doi.org/10.1177/11769351221118556>
- Panche, A. N., Diwan, A. D., & Chandra, S. R. (2016). Flavonoids: An overview. *Journal of Nutritional Science*, 5, e47. <https://doi.org/10.1017/jns.2016.41>

- Park, H., Zhou, G., Baek, M., Baker, D., & DiMaio, F. (2021). Force field optimization guided by small molecule crystal lattice data enables consistent sub-angstrom protein–ligand docking. *Journal of Chemical Theory and Computation*, 17(3), 2000–2010. <https://doi.org/10.1021/acs.jctc.0c01184>
- Patidar, K., Panwar, U., Vuree, S., Sweta, J., Sandhu, M. K., Nayariseri, A., & Singh, S. K. (2019). An in silico approach to identify high affinity small molecule targeting m-TOR inhibitors for the clinical treatment of breast cancer. *Asian Pacific Journal of Cancer Prevention*, 20(4), 1229–1241. <https://doi.org/10.31557/APJCP.2019.20.4.1229>
- Pranweerapaiboon, K., Garon, A., Seidel, T., Janta, S., Plubrukarn, A., Chaithirayanon, K., & Langer, T. (2022). In vitro and in silico studies of holothurin A on androgen receptor in prostate cancer. *Journal of Biomolecular Structure & Dynamics*, 40(23), 12674–12682. <https://doi.org/10.1080/07391102.2021.1975562>
- Rizzolio, F., Tuccinardi, T., Caligiuri, I., Lucchetti, C., & Giordano, A. (2010). CDK inhibitors: From the bench to clinical trials. *Current Drug Targets*, 11(3), 279–290. <https://doi.org/10.2174/138945010790711978>
- Ruiz Gómez, M. J., Souviron Rodríguez, A., & Martínez Morillo, M. (2002). La glicoproteína-P una bomba de membrana que representa una barrera a la quimioterapia de los pacientes con cáncer. *Anales de Medicina Interna*, 19(9), 49–57. <https://doi.org/10.4321/S0212-71992002000900011>
- Sangai, N. P., Patel, C. N., & Pandya, H. A. (2018). Ameliorative effects of quercetin against bisphenol A-caused oxidative stress in human erythrocytes: An in vitro and in silico study. *Toxicology Research*, 7(6), 1091–1099. <https://doi.org/10.1039/c8tx00105g>
- Seyedi, S. S., Shukri, M., Hassandarvish, P., Oo, A., Shankar, E. M., Abubakar, S., & Zandi, K. (2016). Corrigendum: Computational approach towards exploring potential anti-chikungunya activity of selected flavonoids. *Scientific Reports*, 6(1), 24027. <https://doi.org/10.1038/srep26368>
- Sheoran, S., Arora, S., Samsonraj, R., Govindaiah, P., & Vuree, S. (2022). Lipid based nanoparticles for treatment of cancer. *Heliyon*, 8(5), e09403. <https://doi.org/10.1016/j.heliyon.2022.e09403>
- Shivanika, C., Kumar, D., Ragunathan, V., Tiwari, P., & Sumitha, A. (2022). Molecular docking, validation, dynamics simulations, and pharmacokinetic prediction of natural compounds against the SARS-CoV-2 main-protease. *Journal of Biomolecular Structure & Dynamics*, 40(2), 585–611. <https://doi.org/10.1080/07391102.2020.1815584>
- Siegel, R. L., Miller, K. D., & Jemal, A. (2016). Cancer statistics, 2016. *CA: A Cancer Journal for Clinicians*, 66(1), 7–30. <https://doi.org/10.3322/caac.21332>
- Singh, M., Jha, R., Melamed, J., Shapiro, E., Hayward, S. W., & Lee, P. (2014). Stromal androgen receptor in prostate development and cancer. *The American Journal of Pathology*, 184(10), 2598–2607. <https://doi.org/10.1016/j.ajpath.2014.06.022>
- Suzuki, H., Ueda, T., Ichikawa, T., & Ito, H. (2003). Androgen receptor involvement in the progression of prostate cancer. *Endocrine-Related Cancer*, 10(2), 209–216. <https://doi.org/10.1677/erc.0.0100209>
- Sweta, J., Khandelwal, R., Srinitha, S., Pancholi, R., Adhikary, R., Ali, M. A., Nayariseri, A., Vuree, S., & Singh, S. K. (2019). Identification of high-affinity small molecule targeting IDH2 for the clinical treatment of acute myeloid leukemia. *Asian Pacific Journal of Cancer Prevention*, 20(8), 2287–2297. <https://doi.org/10.31557/APJCP.2019.20.8.2287>
- Tan, M. H. E., Li, J., Xu, H. E., Melcher, K., & Yong, E-I (2015). Androgen receptor: Structure, role in prostate cancer and drug discovery. *Acta Pharmacologica Sinica*, 36(1), 3–23. <https://doi.org/10.1038/aps.2014.18>
- Warde-Farley, D., Donaldson, S. L., Comes, O., Zuberi, K., Badrawi, R., Chao, P., Franz, M., Grouios, C., Kazi, F., Lopes, C. T., Maitland, A., Mostafavi, S., Montojo, J., Shao, Q., Wright, G., Bader, G. D., & Morris, Q. (2010). The GeneMANIA prediction server: Biological network integration for gene prioritization and predicting gene function. *Nucleic Acids Research*, 38, W214–W220. <https://doi.org/10.1093/nar/gkq537>
- Woo, H.-H., Ryong Jeong, B., & Hawes, M. C. (2005). Flavonoids: From cell cycle regulation to biotechnology. *Biotechnology Letters*, 27, 365–374. <https://doi.org/10.1007/s10529-005-1521-7>
- Xiong, G., Wu, Z., Yi, J., Fu, L., Yang, Z., Hsieh, C., Yin, M., Zeng, X., Wu, C., Lu, A., Chen, X., Hou, T., & Cao, D. (2021). ADMETlab 2.0: An integrated online platform for accurate and comprehensive predictions of ADMET properties. *Nucleic Acids Research*, 49(W1), W5–W14. <https://doi.org/10.1093/nar/gkab255>
- Xu, Z., Yan, Y., Xiao, L., Dai, S., Zeng, S., Qian, L., Wang, L., Yang, X., Xiao, Y., & Gong, Z. (2017). Radiosensitizing effect of diosmetin on radioresistant lung cancer cells via Akt signaling pathway. *PLoS One*, 12(4), e0175977. <https://doi.org/10.1371/JOURNAL.PONE.0175977>
- Yadav, M., Khandelwal, R., Mudgal, U., Srinitha, S., Khandekar, N., Nayariseri, A., Vuree, S., & Singh, S. K. (2019). Identification of potent VEGF inhibitors for the clinical treatment of glioblastoma, a virtual screening approach. *Asian Pacific Journal of Cancer Prevention*, 20(9), 2681–2692. <https://doi.org/10.31557/APJCP.2019.20.9.2681>
- Zaki, M. E. A., Al-Hussain, S. A., Al-Mutairi, A. A., Samad, A., Ghosh, A., Chaudhari, S., Khatale, P. N., Ajmire, P., & Jawarkar, R. D. (2023). In-silico studies to recognize repurposing therapeutics toward arginase-I inhibitors as a potential onco-immunomodulators. *Frontiers in Pharmacology*, 14, 1129997. <https://doi.org/10.3389/fphar.2023.1129997>



# Abstract 5342: Assessment of polyphenolic secondary metabolites and small molecules against the xenobiotic metabolic and cell cycle regulatory proteins in prostate cancer FREE

Sumit Sheoran; Swati Arora; Tanmay Basu; Naidu Subbarao; Atul Kumar Upadhyay; Sugunakar Vuree



[+ Author & Article Information](#)

*Cancer Res* (2023) 83 (7\_Supplement): 5342.

<https://doi.org/10.1158/1538-7445.AM2023-5342>

Split-Screen

Share

Tools

Versions

## Abstract

**Background:** Prostate cancer (PCa) is the second most frequent kind of cancer in males globally after Lung Cancer. In clinical practice, medicines that act as antagonists/partial agonists of hormone receptors against prostate tissue are employed in PCa treatment. Cyproterone acetate, Flutamide, and Bicalutamide are prominent medications that induce acute and long-term toxicity and create drug resistance in patients and remission. We concentrated on flavonoids since they are non-cytotoxic and have substantial showing inhibitory action.

**Methodology:** We selected 560 flavonoids and small compounds along with 3 targets from the extensive literature review. Three-dimensional (3D) structures of selected proteins were obtained from Protein Data Bank, docked with 560 flavonoids and small molecules 3D structures, obtained from PubChem and ChEMBL database using Gold Docking Software. ADME characteristics were used to determine their bioactivities in the human body and drug-like investigations by using SwissADME and Zinc database, while Lipinski's rule of five was used to evaluate the flavonoids' anti-prostate cancer efficacy. Additionally, we have performed molecular simulation at 100ns and furthermore, we will perform cytotoxicity analysis.

**Results:** Diosmetin (58.72), Lapatinib Ditosylate (121.61), and Estramustine Phosphate Sodium (143.38) has the highest binding affinity for CDKN2 (4EK3), CYP17A1(3RUK), and CYP19A1(3S79), respectively, and are stable throughout 100ns simulation studies. At present, we are working on cytotoxicity studies on PC3 cell lines. As per the literature review by Ansar et al. 2022 quercetin and thymoquinone induce cytotoxicity in breast, lung, and prostate cancer cells effectively; MCF-7 cells were the most sensitive cells to quercetin with an IC50 value of 50  $\mu$ M and PC3 cells were more sensitive to thymoquinone with an IC50 value of 20  $\mu$ M.

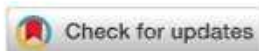
**Conclusion:** As a result of our findings, these four Flavonoids may be viable candidates for additional research into PCa prevention or management. **Keywords:** Diosmetin, Lapatinib Ditosylate, Prostate cancer, In-silico, Simulation

**Citation Format:** Sumit Sheoran, Swati Arora, Tanmay Basu, Naidu Subbarao, Atul Kumar Upadhyay, Sugunakar Vuree. Assessment of polyphenolic secondary metabolites and small molecules against the xenobiotic metabolic and cell cycle regulatory proteins in prostate cancer. [abstract]. In: Proceedings of the American Association for Cancer Research Annual Meeting 2023; Part 1 (Regular and Invited Abstracts); 2023 Apr 14-19; Orlando, FL. Philadelphia (PA): AACR; Cancer Res 2023;83(7\_Suppl):Abstract nr 5342.



# Abstract 5343: Evaluating the screened polyphenolics molecules as potential chemosensitizers against the oncogenic signalling proteins in lung cancer FREE

Swati Arora; Sumit Sheoran; Tanmayee Basu; Naidu Subbarao; Atul Kumar Upadhyay; Sugunakar Vuree



+ Author & Article Information

*Cancer Res* (2023) 83 (7\_Supplement): 5343.

<https://doi.org/10.1158/1538-7445.AM2023-5343>



Split-Screen



Share



Tools



Versions

## Abstract

**Background:** Lung cancer is the most commonly diagnosed cancer globally. There are numerous agonists and antagonistic treatment interventions available for therapy. However, all of them possess different detrimental consequences in addition to resistance and remission in sufferers. Medicinal plants have traditionally been employed to treat a wide range of ailments and problems.

**Methodology:** A total of 550 flavonoids and small molecules retrieved from literature and databases (ChEMBL and PubChem) were analysed for molecular docking, biological activities, ADME, and drug-like properties through SwissADME and PreADMET, Molecular Simulation, and cytotoxicity studies. Simultaneously, review literature is employed to identify the novel protein targets viz. ROS1 (3ZBF) & EGFR (6DUK). Additionally, the crystal structures of the proteins were obtained from PDB and their domains and active sites were predicted using ScanProsite, MOTIF Search, metaPOCKET2, and PrankWeb tools. Finally, the proteins and ligands were energy-minimized using Chimera and open babel tool and subjected to virtual screening and molecular docking using GOLD. Furthermore, the molecular simulation was performed at 100ns by utilizing GROMACS, and cytotoxicity studies were performed by employing the A549 Lung cancer cell line.

**Results:** Diosmin (64.57) and Hesperidin (60.98) had the greatest binding affinity with the identified targets, i.e., ROS1 (3ZBF) and EGFR(6DUK) respectively against Lung Cancer, and remained stable during 100ns of molecular simulation. Furthermore, we have performed cytotoxicity studies on A549 cell lines that show both the compounds have significant anticancer activity and do not affect healthy cells in the range of, i.e., Diosmin (500 µg/ml to 0.024 µg/ml.) and Hesperidin (500 µg/ml to 125 µg/ml).

**Conclusion:** After the analyses, we can conclude that it has the potential to be exploited as a novel therapeutic agent in the treatment of lung cancer. **Keywords:** Diosmin, Hesperidin, In-silico, A549, Lung Cancer, Simulation

**Citation Format:** Swati Arora, Sumit Sheoran, Tanmayee Basu, Naidu Subbarao, Atul Kumar Upadhyay, Sugunakar Vuree. Evaluating the screened polyphenolics molecules as potential chemosensitizers against the oncogenic signalling proteins in lung cancer. [abstract]. In: Proceedings of the American Association for Cancer Research Annual Meeting 2023; Part 1 (Regular and Invited Abstracts); 2023 Apr 14-19; Orlando, FL. Philadelphia (PA): AACR; Cancer Res 2023;83(7\_Suppl):Abstract nr 5343.

## CHAPTER 10

# Empowering treatment strategies for pancreatic cancer by employing lipid nanoparticle-driven drug delivery

Sumit Sheoran<sup>1,2,\*</sup>, Swati Arora<sup>1,2,\*</sup>, Aayushi Velingkar<sup>1</sup>, Smita C. Pawar<sup>3</sup> and Sugunakar Vuree<sup>2,4</sup>

<sup>1</sup>School of Biosciences and Bioengineering, Lovely Professional University, Jalandhar, Punjab, India

<sup>2</sup>Unite Lifescience, Hyderabad, Telangana, India

<sup>3</sup>Department of Genetics, Osmania University, Hyderabad, Telangana, India

<sup>4</sup>MNR Foundation for Research and Innovation (MNR-FRI), MNR Medical College and Hospital, Hyderabad, Telangana, India

### 10.1 Introduction

Solid lipid nanoparticles (LNPs) are being produced as spinel delivery systems for the administration of liquid soluble drugs and effective dynamic treatment adjustment [1]. According to a recent study, SLNs (solid lipid nanoparticles) constitute a flexible, diversified, and adaptable system for delivering drugs. This technology has the capability to improve medication strength as well as regulate drug release from the matrix over time. Furthermore, encapsulating pharmaceuticals in solid LNPs helps them resist enzymatic destruction before they reach their target sites [2]. An agreement has arisen among scientists that lipids are effective good adsorbents for drug administration due to their intrinsic potential to promote stomach solubilization and the immersion of poorly accessible therapeutic ingredients through the lymph system [3,4]. SLNs are one of the innovative prospective dispersion transport systems utilized in lieu of polymers as an alternative to oil-in-water (O/W) emulsifiers for enteral administration, and they are identifiable from O/W emulsions. A solid lipid nanoparticle can replace the fluid lipid in the O/W emulsion [5]. Solid LNPs are created using methodologies such as high-pressure homogenization and solvent evaporation [6,7]. Moreover, the characteristics of SLNs may be modified to increase their efficiency. This is especially beneficial for drugs that are insoluble in water. In order to understand solid LNPs and their prospective uses in the pharmaceutical sector, detailed literature research on the different varieties of SLNs and conventional matrices utilized as drug delivery techniques are required.

For many years, the pharmaceutical industry has used lipid components that really are room-temperature solids to make a range of formulations [8]. Further, Earlier research also

\* First equal authorship.

indicates that SLNs are nontoxic and biodegradable colloidal transporters [9]. It is vital to highlight that SLNs are nanoscale in size, and their strong capability at the intracellular membrane and in the intracellular compartment permits them to successfully infiltrate the cells [10]. Solid LNPs have gotten a lot of interest since they can carry medicines and genes efficiently and can also be utilized for specific therapies [11]. Because of their greater bioactivity, enhanced capacity for drug loading, and scalability, they may have a benefit over other nanoparticle. The lipids employed in the production of the matrix in solid LNPs are consistent with the body's natural defense and also have minimal side effects and acceptable ratings. According to Basha and colleagues, solid LNPs form vibrant, varied, and configurable pharmaceutical carrier systems with enhanced capacity for increasing drug stability and attempting to control drug release from the composite over period, and packaging drugs in solid LNPs aids in trying to resist proteolytic degradation first before drugs reach the desired sites [2]. Additionally, pharmaceutical companies may employ solid LNPs to develop medications for particular human organs depending on their biochemical makeup and kind of responses. Furthermore, the features of the SLNs may be altered to increase their efficiency. This is especially beneficial for medications that are poorly soluble in water. Fig. 10.1 depicts a diagrammatic depiction of SLNs and their targeted particularities from several perspectives.

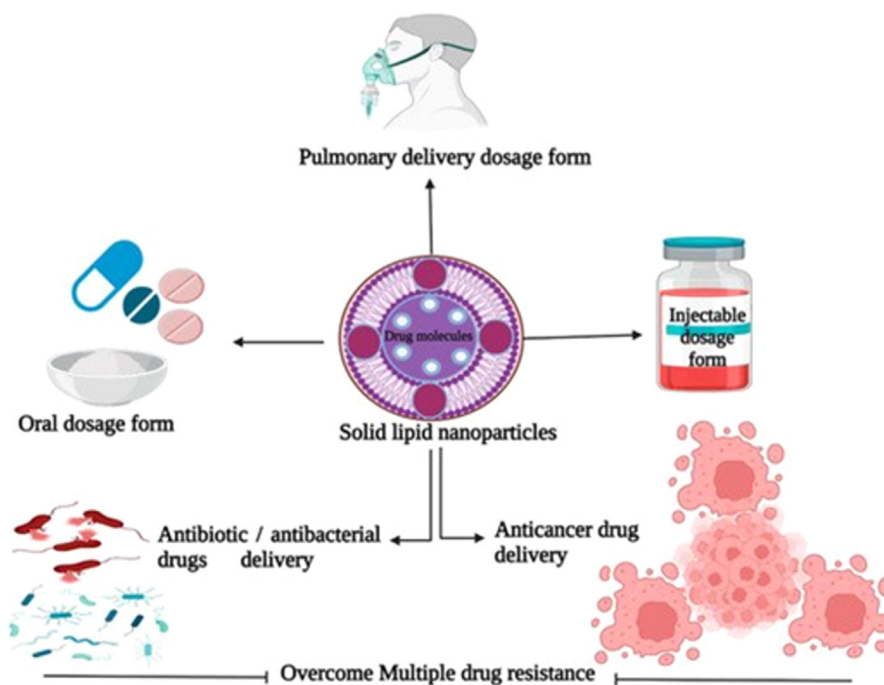


**Figure 10.1** Solid LNPs and their targeted identifications are depicted schematically. *LNPs*, lipid nanoparticles.

The current research concentrates on the various kinds of SLN and conventional matrices used as drug delivery strategies in pancreatic cancer, as well as to understand SLNs and their potential applications.

## 10.2 Symptoms and risk factors of pancreatic cancer

As pancreatic cancer is challenging to detect, it is frequently discovered as an advanced disease. Jaundice and weight loss are symptoms of pancreatic cancer. Diabetes and exposure to certain toxins are a major risk factors. Treatment is based on the size and location of the tumor, in addition to whether or not it really has expanded to other areas of the system.

Pancreatic cancer develops when abnormalities (mutations) in pancreatic cells cause them to grow uncontrollably. A clump of tissue can form as a result. This tumor is often harmless (not cancerous). However, with pancreatic cancer, the mass is malignant (cancerous).

The majority of people do not notice early indications of pancreatic cancer (Fig. 10.2). However, as the condition advances, individuals can observe:

1. Inflammation in the upper abdomen may move to the posterior.
2. Discoloration of the skin and the whites of the eyes (jaundice).
3. Exhaustion.
4. Hunger loss.
5. Light-colored feces.
6. Pitch black poop
7. Malnutrition.
8. The presence of thrombosis in the system.
9. Dry, itching skin.
10. Diabetic, whether new or increasing.
11. Puking and discomfort.

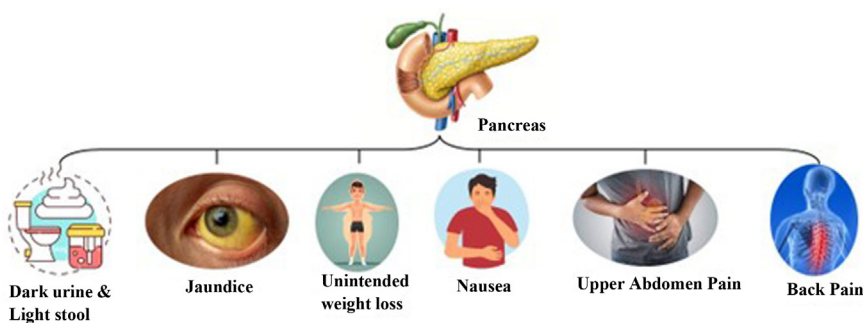


Figure 10.2 Symptoms of pancreatic cancer.

If you experience these signs and have suddenly established diabetes or pancreatitis—a painful condition caused by pancreatic irritation—your healthcare provider may consider pancreatic cancer.

The average lifetime chance of acquiring pancreatic cancer is roughly 1 in 64. A risk factor is anything that increases your chances of getting an illness. There are danger variables (shown in Fig. 10.3) that are a result of behavior and may be modified. Following are some major risk factors for pancreatic:

1. Smoking.
2. Obesity poses a risk factor as well. Having extra weight all around waistline is a danger concern even if you are not obese.
3. Diabetes, particularly type diabetes patients, that is connected to overweight. The emergence of diabetes at an advanced age and in somebody of normal body weight or BMI might be a symptom of pancreatic cancer.
4. Coming in contact with chemicals used by dry cleaners and metal workers.
5. Having chronic pancreatitis.

There are some risk factors that you cannot change, some of which are as follows:

1. Genetic recurrent pancreatitis is caused by gene alterations (mutations) that are handed down from parent to kid.
2. Being a Male.

## RISK FACTORS



Figure 10.3 Risk factors of pancreatic cancer.



3. Being an African American.
4. Being of Ashkenazi Jewish descent.

If you experience certain symptoms or have suddenly established diabetic or pancreatitis, your doctor may suspect pancreatic cancer.

Pancreatic neuroendocrine cancer can vary from classic pancreatic cancer signs, such as losing weight. This is due to the fact that some Pancreatic neuroendocrine tumors (PNETs) increase the production of hormones.

### 10.2.1 The stages of pancreatic cancer?

Pancreatic cancer is divided into five categories (Fig. 10.4). Your prognosis is influenced by the size and location of the tumor, in addition to whether or not really the disease has progressed:

1. Phase 0: Stage 0 cancer, also known as cancer in situ, is distinguished by malignant growth in the pancreatic lining. The cells might develop into cancer and migrate to neighboring tissue.
2. Phase 1: The cancer is in the pancreas.
3. Phase 2: The tumor has migrated to regional lymph nodes, organs, or lymphatic system from the pancreas.
4. Phase 3: The malignancy has progressed to massive blood arteries in the vicinity of the pancreas. It might potentially have migrated to adjacent lymph nodes.
5. Phase 4: The disease has migrated to remote parts of the body in fourth stage of pancreatic cancer. It may have spread to other tissues, organs, or lymph nodes.

## 10.3 Lipid nanoparticles

“Fat” appears to be a synonym for “lipid.” Lipids appear to be a substance that cannot dissolve in water but may dissolve in alcohol,  $(C_2H_5)_2O$ , and  $CHCl_3$  [12]. Individual cells required lipids to thrive. Animal and plant cells were primarily composed of lipids,  $C_x(H_2O)_y$ , and protein. Both triglycerides and cholesterol are lipids. Fats are quickly obtained and maintained inside the system. It is a crucial component of the cell’s structure and acts as an energetic benchmark. Fats sometimes are classified as

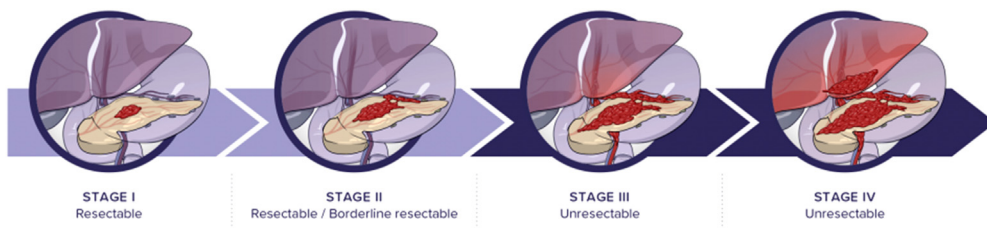


**Figure 10.4** Stages of pancreatic cancer.

Control Drug Release  
Drug Targetting  
Longer Stability  
High Drug Loading  
Biocompatible/Biodegradable  
Nontoxic  
Ease of scale up  
Efficient Gene Delivery

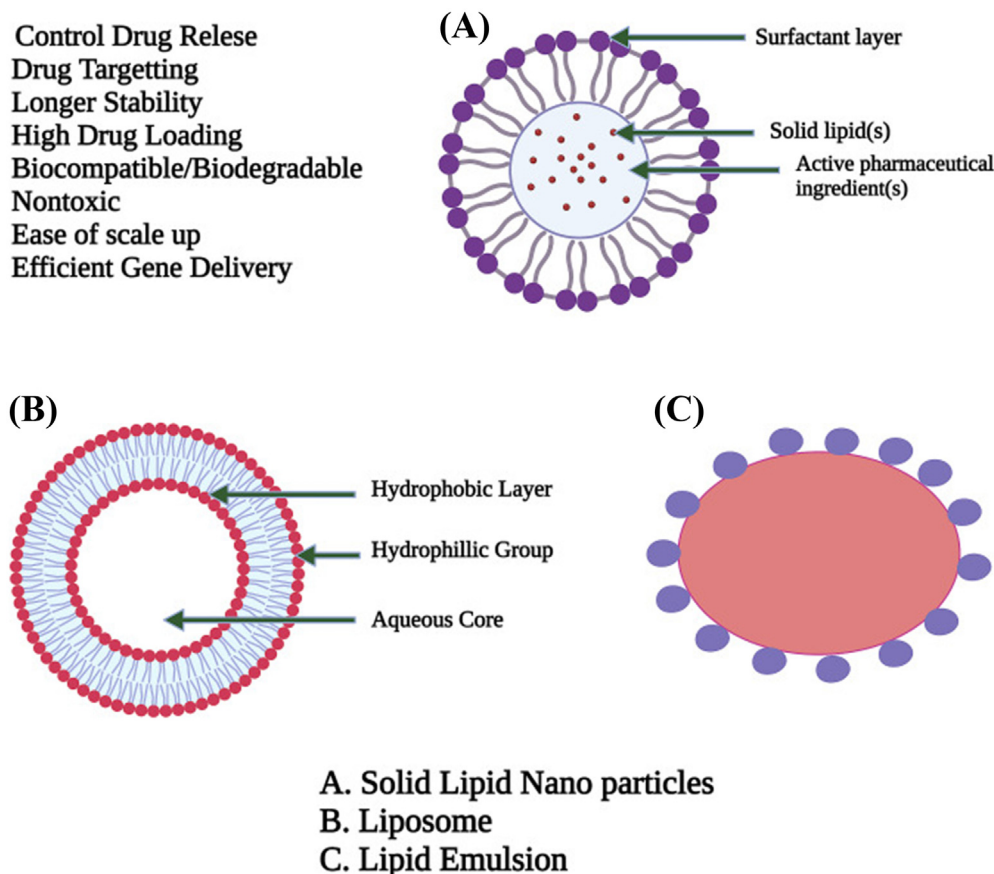


**Figure 10.5** The entire configuration of solid LNPs, which offer advantages over LNPs and lipids emulsions, is graphically represented [13]. A) Solid Lipid Nanoparticles (SLNs), B) Liposomes, C) Lipid Emulsion. *LNPs*, lipid nanoparticles.

aquaphobic or amphoteric low molecular weight compounds; the amphiphilic property of particular lipids allows us to produce watery forms such as vesicles, huge unilamellar liposomes, or membranes. The biochemical constituents or “building blocks” of biological lipids are ketoacyl and isoprene groups. Fig. 10.5 depicts the structures of SLN, liposomes, and lipid emulsion.

Fats have received a nice deal of interest since the commencement of the pharmaceutical era because of their biocompatibility as a transporter. Because they are very repellent, they have low oral absorption [14]. As a result, the ambition to broaden the variety of uses for such transporters fell short, and they were not used in propulsion systems until 1900 after they were enclosed in colloidal delivery methods [15–18]. In the development of nanomaterials delivery systems, LNPs were shown to be more helpful than polymeric NPs [19]. LNPs are considered to as “Nano safe” carriers since they are

constructed of physiologic and/or disposable lipids [20]. Solid LNPs are a well-known LNP synthesis that was created in the early 1990s [21]. Due to the numerous advantages of previous transporters, such as emulsifying agents, lipid membranes, and polymeric nanoparticles (NPs), delivery approach was developed [22]. The practicality of the manufacturing techniques and leveling-up process, the GRAS grade of all formulations, and absence of polar components separate SLNs from liposomes [23].

Tumor nanotechnology is presently being developed as a possible cancer therapy approach for antitumor medication delivery [24]. NPs with sizes ranging from one to 1000 nm improve therapeutic bioavailability and antitumor drug selectivity [25]. Fig. 10.6 depicts a number of NPs and nanotech cancer therapy techniques that have recently been published. Semiconducting quantum dots can really be employed as a versatile composite structure with significant potential for biomedical activities because of its peculiar optical properties, large excitation range, and extremely constrained symmetrical intensity distribution. Semiconductor quantum dots are a novel type of fluorescent element. They are used in cell imaging, biolabeling, and biosensing. Quantum dots have a stronger influence than conventional fluorophores. They are bright, possess better control over emission intensity, and are less photobleached. Different colored quantum dots with wide absorption and narrow emission spectra can be stimulated by a single light source. The previously described quantum dots appear

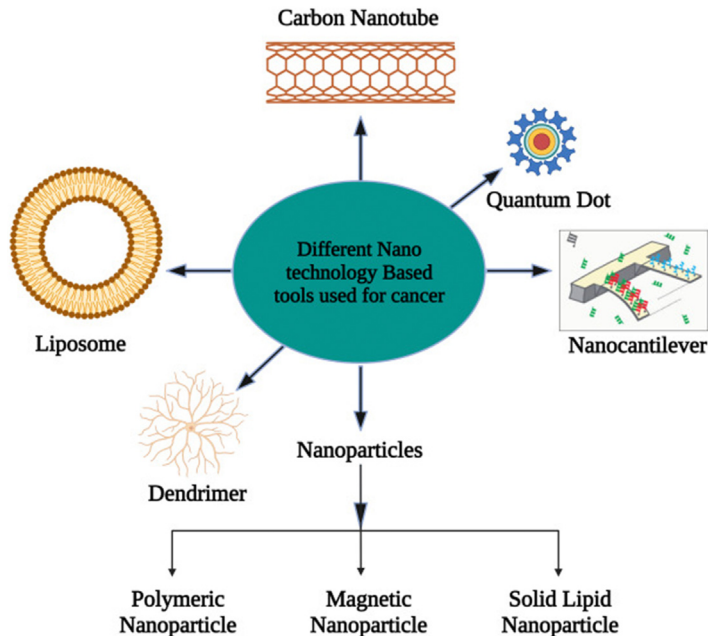


**Figure 10.6** Several nanotechnology-based cancer therapy techniques are in use [13]. Taken from S. Sheoran, S. Arora, and G. Pilli, "Lipid based nanoparticles for treatment of cancer," *Heliyon*, p. e09403, 2022.



to be the most effective option for screening cell receptors. To make good fluorescence probes, the surfaces of quantum dots must be altered using diverse biological molecules [26].

Among the numerous NP formulations used in the treatment of cancer depicted in Fig. 10.6, we highlight ones relying on liquid that flows since significant advances in production and alternative compositions have been made in the last decades. Chemical modifications to lipid nanosystems can be employed to avoid detection by the immune system or to boost pharmaceutical availability. These might also be made in pH-sensitive formulations to boost the release of the drug in acidic conditions, and they could be combined with antibodies that recognize tumor cells and their receptors, such as folic acid (FoA) [27]. Nanomedicines may be used in concert with other therapy techniques to improve patient's response.

Several antitumor drugs, including cisplatin, have already been studied in nanoformulations, and others have been studied in clinical studies and/or are industrially available for medical use [28]. Doxil, a liposome formulation containing DOX, was the first commercially used anticancer medication nanosystem that presents an overview of the many types of LBNPs (Fig. 10.7) that have been developed in recent years, as well as their uses and benefits in various types of malignancies.

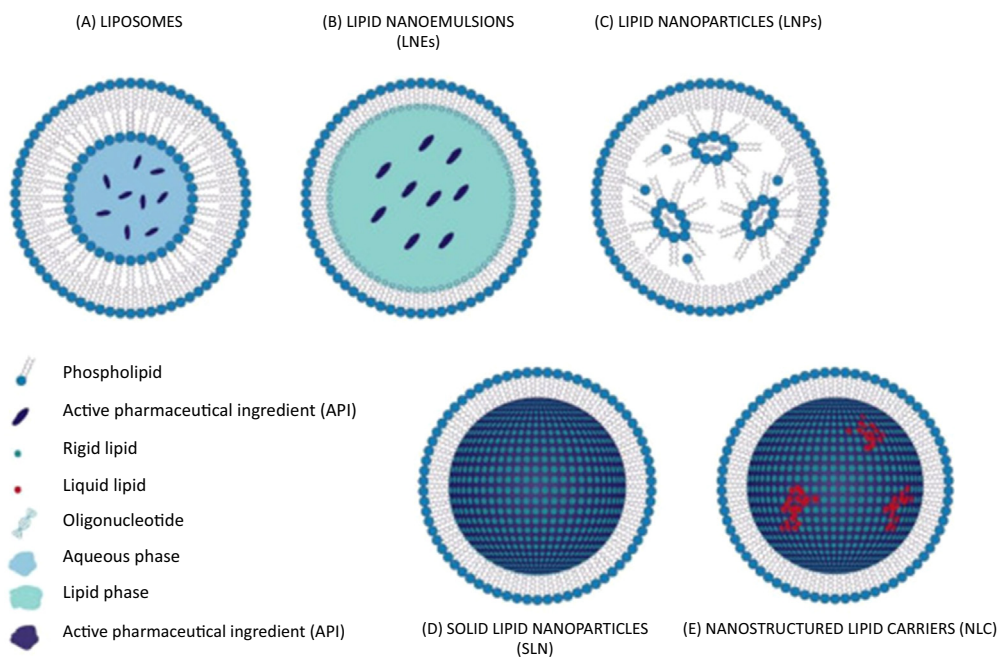


**Figure 10.7** (A) Liposomes, (B) lipid nanoemulsions in lipid-based nanoparticles, (C) solid lipid nanoparticles, (D) and nanostructured lipid carriers. Taken from S. Sheoran, S. Arora, and G. Pilli, "Lipid based nanoparticles for treatment of cancer," *Heliyon*, p. e09403, 2022.

## 10.4 Solid lipid nanoparticles

These really are solid sizes ranging from 1–1000 nm. Nanoparticles range in size between 150 to 300 nm. Solid LNPs are solid, submicronic colloidal nanocarriers with diameters ranging from 1e1000 nm [13]. The granular size ranges from 150 to 300 nm. Nanoparticles, for example, provide a framework for controlled drug release [29]. Their solid SLN method enables them to limit medicine movement and provide greater stability, combining the benefits of polymeric NPs and liposomes and consists of high emulsifiers [30]. Furthermore, experiments reveal that SLNs were particularly beneficial in a variety of ways (Fig. 10.8),

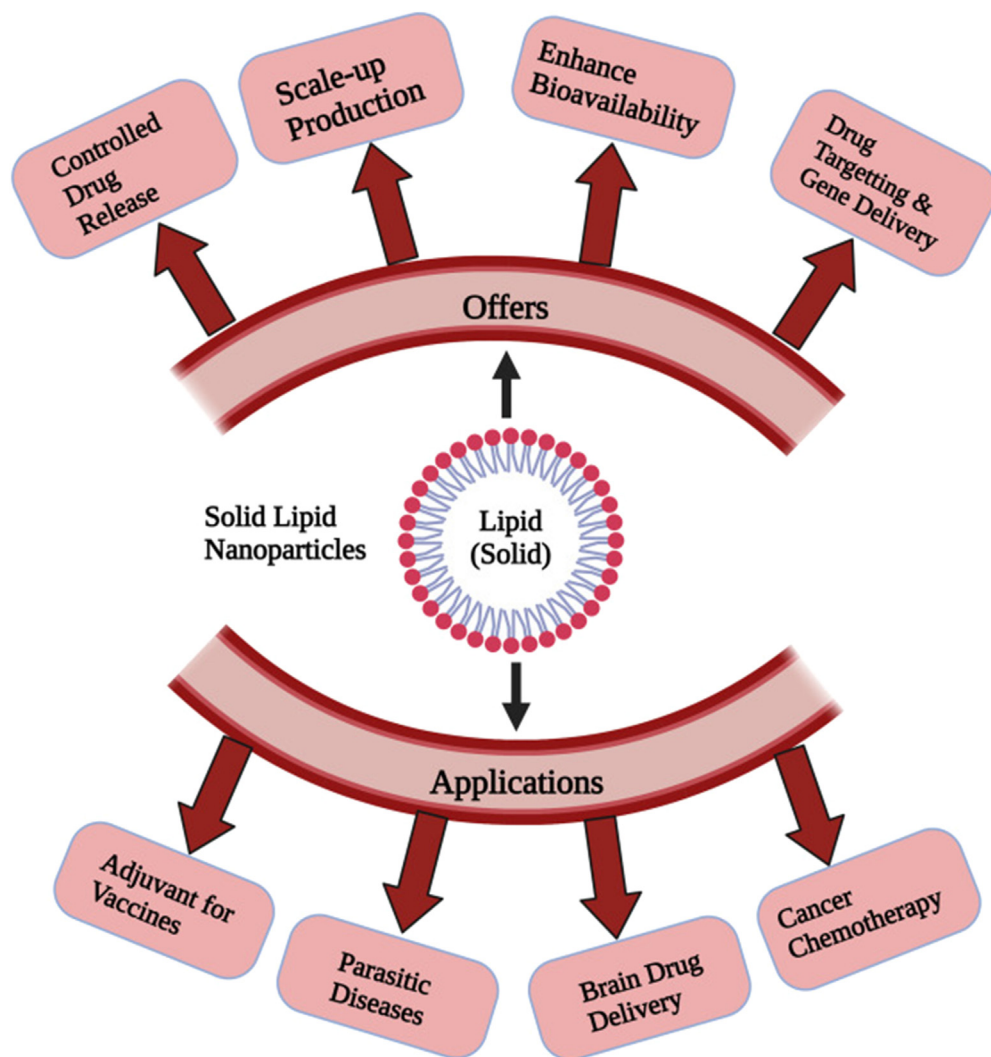


**Figure 10.8** The advantages and applications of SLN are represented graphically [13]. SLN, solid lipid nanoparticles.

including the avoidance of using organic solvents during manufacture, the possibility of scaling [31], and the incorporation of both lipophilic and hydrophilic medications in substantial quantities [32]. SLNs are formed by substituting a solid lipid or a mixture of solid lipids for the liquid lipid (oil) in the formation of an oil and water dispersion. One distinguishing property of SLNs is that they are rigid both at room and body temperatures [33]. These drug delivery systems are composed of 0.1%–30% (w/w) solid lipids distributed in an aqueous media. SLNs are often made up of solid-form lipids such as higher-grade triglycerides, free fatty acids, free fatty alcohols, complex glyceride blends, and even wax (all of which are well-known physiologic lipids) [34]. It is also possible to employ more complex systems [35].

### **10.5 Limitations of solid lipid nanoparticles and way to overcome**

Though SLNs are typically composed of solid lipids, deterioration and unstable may be an issue. Excessive pressure-induced drug disintegration, the coexistence of diverse lipid alterations and colloidal species, the minimum drug-loading potential, and the kinetics of the delivery are all things to consider.

### **10.6 High pressure-induced drug degradation**

The principal reasons for drug disintegration are molecular mass and organization, and high-pressure uniformity has been demonstrated to diminish polymer molecular mass. Regardless of the fact that multiple studies suggest that elevated homogenization-induced drug breakdown is not a problem for the vast majority of bioactive metabolites, high molecular weight composites or chain-length components are significantly more sensitive. However, big molecular weight compounds such as DNA, albumin, and dextrose are more susceptible to breaking; hence, integrating these materials into SLNs requires a unique strategy.

### **10.7 Lipid crystallization and drug incorporation**

Another essential issue to consider is lipids crystallization. Scientists have already been examining the association between lipid changes and medicine-based treatment over the past few years. The investigation of lipid alterations is widely recognized. X-ray and differential scan calorimeter studies are used in the bulk of the approaches. Nonetheless, the majority of the evidence has come from large-scale lipid investigations. The efficiency of SLNs may vary greatly due to the evident nanosize of the carrier, and a large number of interface active participants required to sustain colloidal lipid dissemination. As a result, lipid crystallization and drug inclusion have an effect on the characteristics of lipid particles. When considering medication capture inside solid LNPs, the following important factors must be considered:

(1) the presence of supercooled melts; (2) the presence of various lipid modifications; (3) the shape of lipid nanodispersions; and (4) gelation processes.

### 10.8 Several colloidal species coexist

Researchers have given little consideration to the coexistence of many nanomaterials within solid LNPs, despite the fact that it is an important issue to solve. Surfactants are present on both the lipid surface and the inside of the lipid. Diverse micelles must be recognized in glycocholate/lecithin stabilized and similar systems. Because micelles, mixed micelles, and lipid membranes may dissolve drugs, they can be employed as therapeutic incorporation targets. Because dynamic models are crucial for drug stability and release, the existence of diverse heterogeneous entities alone is inadequate to define the structure of colloidal lipid phase separation. As a result, the kinetics of delivery process must be considered. Enzymatic hydrolysis drugs, for example, breakdown faster in water-soluble and interface-localized chemicals than in lipid molecules.

The rate of disintegration will be governed by two factors: (1) the chemical makeup of the medication and (2) the drug concentration in the aqueous phase or at the lipid/water border. When buoyant drugs come into contact with liquid, they swiftly hydrolyze, disrupting the drug's dispersion balance between diverse habitats. Carriers are only useful if they keep drugs from being redistributed. Increasing the matrix width naturally affects the mass transfer coefficient of the drug within the transporter, hence SLNs are expected to outperform lipid nanoemulsions.

### 10.9 Nanostructured carriers of lipid (solid lipid nanoparticles and nanostructured lipid carriers)

Despite their safety and efficiency, solid LNPs have a number of significant drawbacks, including increased moisture concentrations (70%–99.9%), inadequate drug content due to crystalline shape, drug ejection during preservation, and probable polymorphisms transitions and particle formation during storage. As a consequence, modifications to the Solid LNPs organization are required to meet these limits. At the turn of 2000, further research resulted in the invention of a “second generation” of LNPs: the NLCs [29]. Dr. Rimpler (Wedemark, Germany) then created the first NLC concepts: Nano Repair Q10 cream, Nano Repair Q10 serum, and Chemisches Laboratorium's Nano lipid CLR Restore (Berlin, Germany). Solid LNPs will be at the forefront of nanotechnology innovation, with several potential applications and a short time between discovery and commercialization [36]. Despite the reality that medication loaded with aquaphilic molecules is quite low, previous data shows that SLNs and NLCs were appropriate for the integration of lipophilic drugs [37]. Early research on

the subject indicates that only highly potent aquaphilic medications with low effectiveness might be thoroughly integrated through the solid lipid matrix [38].

### 10.9.1 Solid lipid nanoparticles and nanostructured lipid carriers for drug delivery

Liposomes and different versions have indeed been utilized in lipid-based medicinal compositions since the 1960s and are regarded as the classic forms. Previous research has linked liposomes to inherent failures and poor characteristics in terms of depolymerization, an absence of massive production technology, merging and drug leaking, polymer matrix degradation and cytotoxicity, phospholipid degradation, high production costs, and sterilization issues [20,39–42]. Müller and colleagues coined the words “solid LNPs” and “nanostructured lipid carriers” (NLCs) in 2002. These developed from a natural notion that combined the beneficial properties of NPs with nontoxic and biodegradable lipid components to generate nontoxic and biodegradable parenteral emulsions that could be delivered directly [20].

The nanoparticle is categorized according to its contents, distribution method, and doctors and medical. Depending on their content, a nanoparticle is classified into two types: solid SLNs and NLCs. Since 1990 [42], SLNs have been touted as viable alternatives to liposomes, emulsions, and polymeric nanoparticle carrier systems. They have a spherical shape with an average size of 40–1000 nm and may be studied using transmitted and scanning electron microscopes.

### 10.9.2 Solid lipid nanoparticles as delivery carriers for anticancer agents

Cancer is distinguished by uncontrollable cell proliferation, susceptibility to apoptosis, and the ability to spread to other tissues [43]. Chemotherapeutic, which would be administered through regular medication delivery channels, is the most thorough cancer treatment. However, there are significant disadvantages to this method, including limited solubility, low sensitivity, potential toxicity, and low therapeutic efficacy [44]. Cancer medication resistance is the most challenging obstacle to overcome in cancer treatment. Resistance to chemotherapy medications is common in cancer cells, resulting in treatment failure (Fig. 10.9). Resistance to cancer drugs may be produced by genetic changes that result in parallel changes in signaling pathways. Multidrug treatment with multiple target pathways has been found in studies to be more successful than mono-drug therapy [45].

External factors and obtained resistance to antibiotics, the two leading causes of chemotherapy failure, have a major adverse effect on chemotherapeutics treatment outcomes. Recent advancements in nanotechnology have provided new treatment options for tumors that have grown resistant to traditional treatments [46]. Fig. 10.9 depicts how solid LNPs can bypass medication tolerance by successfully penetrating

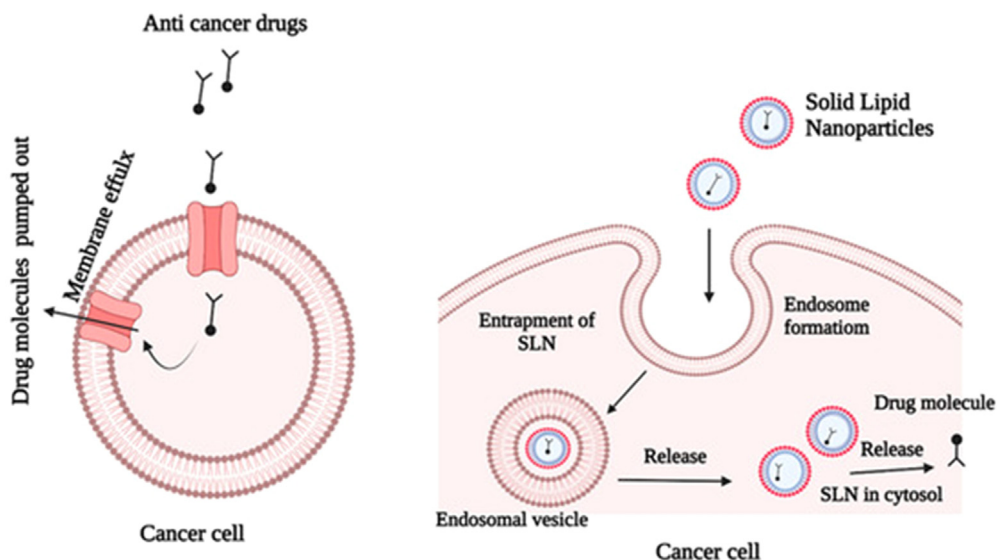


**Figure 10.9** Escape mechanism of solid LNPs that contain anticancer drugs. *LNPs*, lipid nanoparticles.

cancer cells. Based on the nanoparticle composition and manufacturing process, SLNs can hold both hydrophilic and lipophilic anticancer drugs. Drug particles may be included in three ways: (1) they can be spread uniformly in the lipid matrix; (2) they can be incorporated into the nanoparticles; and (3) they can be incorporated into the shell of the nanoparticles. Docetaxel, a natural lipid-soluble molecule, exhibits favorable characteristics for incorporation into Solid Lipid Nanoparticle (SLN) formulations. The inherent properties of docetaxel make it suitable for utilization in SLN systems. Notably, a previous study demonstrated that SLN formulations enhanced the cytotoxicity of docetaxel when tested on MCF-7 breast tumor cells, surpassing the effectiveness of the medication in its conventional form during characterization [47].

In vivo and in vitro research have been conducted to explore the efficacy of SLN absorption in various systems. SLNs have indeed been demonstrated to have less side effects while enhancing the occupancy length and effectiveness of cytotoxic medications. Doxorubicin is a natural drug compound with potent anticancer properties. Its use has a number of negative side effects, including cardiac problems. Doxorubicin may be integrated into SLNs, and when paired with alpha-tocopherol succinate, which also has anticancer potential, it demonstrated excellent cytotoxicity and uptake in drug-resistant MCF-7 human cancer cells [48].

Despite the reality that cancer cells represent for further than 80% points of all malignancies in people, a treatment regimen of solid tumors continues to pose major issues due to poor responses that have been anticipated to be as low as 20% in esophageal cancer, pancreatic cancer, and ovarian cancer [49]. An earlier study indicated that



miRNA-200c might be effectively trapped in SLNs to prevent development of resistance. According to one study, paclitaxel-loaded SLNs might be employed to treat drug-resistant breast cancer cells. This was corroborated by later study findings. Paclitaxel-SLN demonstrated significant effectiveness in both drug-resistant and drug-sensitive MCF-7 cells. According to a recent survey, doxorubicin SLNs have great promise as a beneficial therapeutic method for overcoming multidrug resistance [50].

### 10.9.3 Routes of delivering

The SLN technique has made tremendous progress in the treatment of a variety of ailments. Hydrophilic and lipophilic medicines are encapsulated in SLNs, which decreases their degradation in the body all while allowing for sustained strategic drug release. NPs of various sorts have indeed been developed for the following purposes:

#### 10.9.3.1 Oral delivery

SNLs can be transformed into traditional oral dosage forms. Furthermore, SLN dispersal can be utilized instead of granule fluid in a technique like wet granulation [51]. If the SLN suspensions are powdery, they can be tableted immediately after preparation by lyophilization and spray drying. To enhance expense, crisped SLN powder can be packed in gelatin capsules, generated as liquid polyethylene glycol 600 and packed in soft gel capsules, or turned into a powder form and wrapped in packets following lyophilization [2]. Numerous investigations on bioactive chemicals for SLNs for oral administration have been done. Research effectively proved that SLNs are appropriate delivery systems for oral insulin delivery [52]. Moreover, the solid structure of SLN has been demonstrated to shield insulin from degradation processes in the gastrointestinal system while boosting insulin uptake through the intestinal lining. Recent research revealed that docetaxel-loaded SLNs are potential drug transporters in the prevention and treatment of metastases of breast cancer [53]. In another study, solid LNPs (SLNs) combined with transferrin in the treatment of breast cancer showed a significant ability to transport tamoxifen citrate to tumor cells, resulting in increased therapeutic benefits [54].

#### 10.9.3.2 Parenteral delivery

Administered is the most effective technique for administering bioactive chemotherapeutic drugs with narrow absorption indexes and limited bio-availability, especially for drugs prescribed to patients who have difficulty [55]. Parenteral drug delivery has benefitted from considerable technical advances, which have resulted in the development of complex devices that enable drug targets as well as prolonged or changed outcomes of parenteral drugs [56]. Protein and peptide medicines are more vulnerable to enzymatic breakdown, necessitating regular compensation when administered orally. SLNs with a controlled release mechanism for a route of administration have been

found to be effective treatment techniques for preventing enhanced patient adherence and repeated administration [57]. Parenteral SLN delivery might take various forms, ranging from intravenous to intraarticular. Several studies have been carried out on the pharmacokinetic and distribution of doxorubicin content in SLNs in tissues [2,44]. Just the synaptic connections of rabbits were shown to contain doxorubicin in these experiments. Hidden compounds were incorporated into the SLNs to increase dispersion to the brain. Doxorubicin oral dosing, on the other hand, resulted in lower bio-availability in the heart and liver.

#### **10.9.3.3 Pulmonary delivery**

Respiratory drug delivery is a noninvasive mode of delivery that has many advantages for local treatment of airway illnesses; it immediately enters the epithelium, avoids first metabolizing in the liver, and has minimal toxicity [58]. A study on the pulmonary injection of amikacin-loaded SLNs was conducted with the purpose of increasing its intensity for the treatment of cystic fibrosis-associated lung infections in male rats [59]. Both free medicine and cholesterol-loaded drug administration strategies, such as intravenous and pulmonary delivery routes, were employed. Earlier research found that pulmonary medication release had less negative impacts on the kidneys and a larger drug dosage interval than intravenous administration, leading to higher patient compliance [56,58]. People who do have trouble adhering to SLN drugs or who suffer from renal problems may benefit from pulmonary administration of SLN medications. Other important administration routes for SLN-packaged medications, in addition to oral and parenteral administration, are ocular and rectal delivery, each of which comes with its very own set of benefits.

### **10.10 Applications of solid lipid nanoparticles in pancreatic cancer**

Solid LNPs are one of several kinds of NPs that can be utilized to treat cancer. They are used as potential nanocarriers for the encapsulation of chemotherapeutic medications in addition to enhancing the stability and efficacy of the encapsulated anticancer therapeutics. The high drug loading capacity of solid LNPs is comparable to that of polymeric NPs. Additional benefits of solid LNPs include enhanced pharmacokinetic characteristics and lower in vivo toxicity, which make them an adaptable nanodrug carrier for anticancer medications. delivering these medicines by solid LNPs can considerably reduce the difficulties associated with anticancer drugs, including the assessment of normal tissue toxicity, lower specificity and stability, and the high prevalence of resistance-related problems [60].

Currently, specific cancer cells are killed using magnetic NPs and hyperthermia in the treatment of cancer. A more recent method for treating cancer that involves mixing chemotherapeutic drugs with magnetic NPs has been proven to be effective in



treating a variety of tumors because it offers cancer cells a twofold boost from both hyperthermia and chemotherapy. Chemothermia, a treatment for several types of malignancies, including breast, colon, bladder, and pancreatic cancer, is defined as the combination of hyperthermia with chemotherapy. The results of this study showed how effectively and significantly anticancer medications had improved. The use of NPs can lessen the major adverse effects associated with chemotherapy [61,62].

The total survival time for patients with pancreatic cancer ranges from a few months to five years. Pancreatic cancer is recognized for having a low survival rate. By employing medications, such as curcumin (CUR), sulforaphane (SFN), 5-FU, and GEM, several NPs have been developed to treat pancreatic cancer and have shown encouraging outcomes in preclinical investigations when compared to traditional chemotherapy [61].

According to the study by Inkoom et al., 2022, it is crucial to check the anticancer activity of 4NSG-solid LNPs (4-(N)-stearoyl-gemcitabine) on patient-derived pancreatic cancer cells in vitro using (PPCL-46, PPCL-68) and (PPCL-192, PPCL-135) cell lines obtained from Caucasian (White) and African American (AA) patients, respectively, and to further evaluate the antitumor efficacy in pancreatic cancer PDX mice bearing tumors from both of these populations. It is crucial to note that while several gemcitabine (GEM) analogs have been shown to be successful, in a number of commercially accessible cell lines, there is little evidence available comparing the effectiveness of GEM analogs in patient-derived pancreatic cancer cells from White and AA patients. This study supports the use of patient-derived pancreatic cancer cells to assess the effectiveness of GEM analogs in White and AAs through scientific research investigations [63].

Recent research on nanodrug delivery methods demonstrates enhanced cellular absorption of the solid LNPs formulation in comparison to GEM in numerous organs and cancer types and regulated drug release [64]. To enhance the therapeutic efficacy against pancreatic cancer cells, an unusual solid lipid NP with a substantial payload of GEM was created. To avoid drug dispersion into the aqueous phase, temperature-induced drug degradation, and crystallization modification [65], 4NSG-solid LNPs were prepared using the cold homogenization technique. The selection of surfactants has a significant influence on solid LNPs particle size. Labrasol, tween 80, and lecithin surfactant compositions were kept below 2% in order to create solid LNPs with small particle sizes and to mitigate any potential toxicity concerns brought on by high surfactant amounts [66]. Using TEM for the analysis of 4NSG-solid LNPs formulation revealed spherical NPs with diameters ranging from 63–100 nm, which validated the particle size reduction in 4NSG-solid LNPs. In comparison to the comparable results for GEM-HCL, the IC<sub>50</sub> values of 4NSG-solid LNPs were considerably lower in the PPCL-46, PPCL-68, PPCL-192, and PPCL-135 produced from White and AA individuals, respectively. The IC<sub>50</sub> results indicate that 4NSG-solid LNPs have a strong

antiproliferative effect on the PPCL-46, PPCL-68, PPCL-192, and PPCL-135 cultures. This might be explained by the unique properties of 4NSG-solid LNPs, which are most likely the result of the alteration of the polar nature of GEM-HCL to moderately lipophilic by conjugation of GEM to stearic acid. Additionally, it has been discovered that GEM heavily depends on nucleoside transporters such as hENT1 in order to move between and accumulate inside cancer cells. It has been shown that underexpression of these transporters confers pancreatic cancer resistance [67]. According to earlier published efforts that employ delivery methods for the targeted transport of GEM derivatives [68], the lipophilic nature of 4NSG-solid LNPs implies that it enters pancreatic cancer cells via passive diffusion. Using flow cytometry and confocal imaging, the cellular uptake of 4NSG-solid LNPs was assessed. In their flow cytometry and confocal tests, FITC-solid LNPs displayed a ten-fold increase in geometric fluorescence intensity compared to FITC-exposed cells. This shows that the solid LNPs might capture a larger payload of 4NSG, confirming the FITC-increased solid lipid nanoparticle's intensity above FITC alone. A crucial parameter of cell viability is used in the clonogenic test to assess a cell's capacity for growth and metastasis in colonies of at least 50 cells [69]. According to the results, 4NSG-solid LNPs were more successful than GEM-HCL at preventing cell growth. PPCL-46 and PPCL-192 cells were used in a cell migration experiment to investigate the function of 4NSG-solid LNPs in cell mobility. According to the research, 4NSG-solid LNPs dramatically decreased cell migration in both cells when compared to GEM-HCL. One method for reducing tumor development is thought to be the inhibition of cell cycle progression in cancer cells [70]. The genetic characterization of cell cycle regulators is crucial since the majority of cancer-related disorders are often mutated [71]. The results of the investigation showed that treatment of PPCL-46 and PPCL-192 cells with 4NSG-solid LNPs at a concentration of 5 M significantly stopped the advancement of the cell cycle in the G1 phase. This shows that 4NSG-solid LNPs may have antiproliferative effects that prevent the advancement of the cell cycle. At a concentration of 20, 4NSG-solid LNPs may have caused apoptosis in the PPCL-46 and PPCL-192 cells, confirming that only a small percentage of the cell population had accumulated in the S and G2/M phases. The outcomes of their cell cycle experiments further substantiate our claim that 4NSG-solid LNPs had a more powerful cytotoxic impact than GEM-HCL. The process of cell migration plays a crucial role in promoting tumor spread. In this work, PPCL-192 and PPCL-46 cells' ability to move around was reduced by 4NSG-solid LNPs. Compared to GEM-HCL, the 4NSG-solid LNPs dramatically lowers cellular migration. Very few cells were found in the wound area after administration of the 4NSG-solid LNPs formulation at a dose of 20 mM, demonstrating its superior capacity to inhibit cellular mobility when compared to GEM-HCL. It was demonstrated that the half-life and AUC parameters significantly lengthened the residence duration and increased the proportion of 4NSG-solid LNPs that remained intact

in systemic circulation when the pharmacokinetic profiles of 4NSG-solid LNPs and GEM-HCL were compared.

The prognostic value of EGFR, which is overexpressed in 30%–89% of pancreatic cancer, is still debatable [72,73]. Similar to EGFR, which is overexpressed in between 4% and 50% of pancreatic cancer patients, it is unknown how HER2 affects prognosis [74]. HER2 expression predicts a poorer outcome in certain PDAC patients while showing no correlation in others [75,76]. On the other hand, VEGFR and VEGF overexpression in PDAC is an excellent indicator of advanced stage and recurrence following resection. In this work, they examined the expressions of VEGFR, HER2, and EGFR in pancreatic tumor-bearing PDX mice models treated with GEM-HCL and 4NSG-solid LNPs. Lower expressions of VEGFR, HER2, and EGFR were seen in the tumors of the 4NSG-SLN<sub>AA</sub>T and 4NSG-SLN<sub>WT</sub> treated groups in this particular PDX model made up of members of the White and AA populations. This finding suggests that 4NSG-solid LNPs could be used as an effective VEGFR, HER2, and EGFR-specific therapy [77,78]. In comparison to GEM-HCL treatments, 4NSG-solid LNPs significantly reduced the expression of the VEGFR, HER2, and EGFR receptors in the tumor tissues of the White and AA patients. Clinical evidence suggests that VEGFR, HER2, and EGFR receptor targeting may overcome innate tumor resistance and improve therapy results in pancreatic cancer. This might lead them to hypothesize that 4NSG-capacity solid LNPs to target VEGFR, HER2, and EGFR receptors is what most likely caused the tumor's development to be significantly reduced. In comparison to GEM-HCL, 4NSG-antitumor solid lipid nanoparticle's efficacy demonstrated considerable tumor growth suppression in both White and AA's tumors during a 25-day period. To a significant extent, tumor inhibition was shown in animals carrying White and AA tumors throughout the research period, suggesting that the solid LNPs may play a key role in encapsulating a greater payload of 4NSG that resulted in high build-up in the tumor location. The exceptional tumor effectiveness of 4NSG-solid LNPs might be explained by a number of important aspects, including (1) The 4NSG lacked a free NH<sub>2</sub> group, which prevented the cysteine deaminase enzyme from properly metabolizing GEM. The duration of circulation, greater bioavailability, and enhanced therapeutic effectiveness of 4NSG were most likely made possible by this occurrence. (2) To preserve 4NSG from severe conditions and boost its payload for targeted transport to tumors of interest, it is enclosed in a solid LNP delivery system. (3) The conjugation of GEM to stearic acid may have given 4NSG some degree of lipophilicity, which in turn may help facilitate its delivery to tumor cells.

In this investigation, Inkoom and his team showed that 4NSG improved the permeability and plasma metabolic stability of GEM, which increased its therapeutic effectiveness. The pharmacokinetic properties of GEM were enhanced by chemically converting it to 4NSG and then forming it into 4NSG-solid LNPs, which led to the longer system circulation shown in their study. Comparing the mice with pancreatic

tumors from White and AA patients to the mice treated with GEM, 4NSG-solid LNPs significantly inhibited tumor development in all of the animals [63].

Ferulic acid (FA) is one of the most abundant antioxidants in wheat bran. In cases of breast, skin, colon, and liver cancer, it exhibits anticancer potential [79]. FA has an inferior oral bioavailability due to its weak water solubility. Solid LNPs can compensate for FA's low bioavailability. Glyceryl behenate was used to make solid LNPs that were loaded with FA by Zhang et al. [80]. When compared to aqueous dispersion (10.0 mg/mL and 2.1 hours, respectively), the pharmacokinetic characteristics for solid LNPs exhibited a greater  $C_{max}$  and half-life (18.7 mg/mL and 4.6 hours, respectively), indicating a sustained release from the lipid matrix. Using the *in vivo* imaging technology, it was also shown that solid LNPs retained in the small intestine for a longer period of time than in the free control. For the treatment of pancreatic cancer, Thakkar et al. [81] loaded aspirin (ASP) and FA in chitosan-coated solid LNPs. The lipid core of solid LNPs coated with chitosan demonstrated good durability in an acidic environment thanks to the development of a thick coating around it. The muco-adhesion of solid LNPs was similarly enhanced by this biopolymer covering [82]. Pancreatic cancer cells MIA Panc-1 and PaCa-2 were suppressed by modest dosages of free FA (200  $\mu$ M) and ASP (1  $\mu$ M), respectively, by 45% and 60%. After solid LNPs entrapment, it was shown that FA (40  $\mu$ M) and ASP (25  $\mu$ M) showed equivalent cytotoxicity at 5- and 40-fold lower doses. Oral administration of a combination of FA (75 mg/kg) and ASP (25 mg/kg) in solid LNPs effectively decreased tumor development by 45% when compared to the reference group in the *in vivo* pancreatic cancer xenograft mice research.

Accordingly, the 2015 study by Thakkar et al. looked at the possible chemopreventive effects of a combination of free ASP and FA as well as encapsulated ASP and FA in c-solid LNPs. For the first time, the ASP and FA c-solid LNPs combination inhibiting cell survival in a synergistic manner and causing apoptosis in MIA PaCa-2 and Panc-1 human pancreatic cancer cells was demonstrated. Even while this was not statistically significant, additional *in vivo* experiments showed that the c-solid LNPs combination might decrease tumors. Studies using immunohistochemistry show that the regimen promotes apoptosis due to greatly increased protein expression. The preliminary results from these studies provide a basis for further research to confirm if this combination regimen based on nanotechnology is possibly useful as a chemopreventative therapy for pancreatic cancer [83].

Sutaria et al.'s research has mostly examined the chemopreventive effects of low doses of the ACS (ASP, CUR, and SFN e) combination solid LNPs against pancreatic cancer cells, MIA Panc-1 and PaCa-2 [84]. It was assumed that delivering two or more chemopreventative medications at low concentrations together might have an additive or synergistic effect on the cancer cells because administering a single agent at low concentrations has been demonstrated to be ineffective. This is because carcinogenesis has a

multifaceted nature and cancer arises from a number of cellular modifications over a long period of time. Among the several chemopreventive medications under investigation, ASP, SFN, and CUR have been found to be effective in the chemoprevention of pancreatic cancer [85–87]. Nonsteroidal anti-inflammatory drugs (NSAIDs) such as ASP and celecoxib have been proven in several *in vivo* and *in vitro* studies to aid in the prevention of pancreatic cancer development. Researchers have looked at the chemopreventive effects of CUR and SFN, two substances that are both efficient and nontoxic in nature [88–90]. Therefore using a multidisciplinary approach, this study investigated the synergistic effects of solid LNPs combinations of chemopreventive medicines, especially ASP in combination with CUR and SFN.

However, a number of factors, such as these drugs' limited oral bioavailability after delivery, have greatly impeded their clinical translation. By designing a solid LNPs drug delivery system for these medicines, it is possible to increase their bioavailability in tissues and plasma compared to their free form, thus enhancing their therapeutic efficacy. Additionally, administering medications at lower dosages with a decreased risk of adverse side effects while preserving effectiveness is possible thanks to the drug's encapsulation inside the lipid matrix. Combining drugs with different modes of action makes it easier to achieve the required preventative effect while reducing the dose concentration and its adverse consequences [91]. Both CUR and ASP solid LNPs were discovered to have excellent encapsulation efficiency, good stability at or below room temperature in terms of formulation development, and ideal particle sizes. The use of an organic solvent during the manufacturing procedure may have enhanced the lipid's hygroscopic properties, which might account for the improved stability. The lipophilic properties of both ASP and CUR are responsible for high encapsulation. Additionally, it was discovered that the particles were in the nm range, indicating a higher likelihood of the medications being taken up by cells. The fact that the designed solid LNPs are composed of physiological lipids like stearic acid makes them nontoxic.

In order to establish an additive or synergistic effect on the cancer cells, the effectiveness of these medications was first evaluated by calculating their IC<sub>50</sub> values, and then by combining the ineffective levels to show that they were more effective at lower concentrations. It was compared to how the two drug delivery methods—free form and solid lipid nanoparticle form—performed. When compared to the drug's free form, it was seen that the CUR and ASP solid LNPs IC<sub>50</sub> concentrations had decreased by around 38 and 3 times, respectively. There have been studies showing that drug-loaded solid LNPs had a superior cytotoxicity profile than the free drug [92]. This has mostly been attributed to the NPs' smaller particle size, which improves drug absorption. The surfactant used in the development process determines the inhibitory effect on the cells. Poloxamer 188 was used, which has been shown in the past to target malignant cells, due to differences in the membrane of these cells compared

to the noncancer cells. Poloxamer has been demonstrated to increase proto-apoptotic signalling and reduce antiapoptotic defence in multiple drug-resistant (MDR) cells in addition to inhibiting MDR proteins and other drug efflux transporters on the surface of cancer cells [93]. Three different concentrations of SFN (5 M), ASP (25 M), and CUR (2.5 M) were used in the MTS test on drug-entrapped solid LNPs. The viability of these two cell lines alone exhibited little to no decline, but when the two were mixed, a substantial drop of 60% was seen in MIA Panc1 and PaCa2 cells. Apoptosis assay, which identified the advancement of a cancer cell from four different phases following the addition of the drug—living cell, early apoptotic cell, late apoptotic cell, and necrotic cells—was used to confirm the effectiveness of the combination regimen. These outcomes appear to be in line with what we discovered in the MTS experiment. The suppression of the COX-2 enzyme, control of the P53 suppressor pathway, and manipulation of the Nrf2 pathway are potential processes that might result in a major change for the combination; however, additional research needs to be carried out to verify these findings.

Given that pancreatic cancer cannot be detected at an early stage, it is reasonable to assume that chemoprevention is an effective method of preventing the illness. This study examined the synergistic effects of combining free SFN with ASP and CUR solid LNPs using a multidisciplinary approach. It was observed that the combination of solid LNPs decreased cell viability and induced apoptosis in human pancreatic cancer cell lines for the first time. The effectiveness of this solid LNP combination has to be investigated further *in vivo*, though. The findings from cell-based tests and formulation studies thus amply show the potential for creating drug-encapsulated solid LNPs formulations that combine several drugs to prevent pancreatic cancer [94].

CUR has been shown to be an effective pancreatic cancer chemo-preventive agent among the many chemo-preventive drugs under investigation. However, this agent's limited oral bioavailability following administration has considerably impeded its clinical translation [84]. In contrast to the free form, it is possible to improve the bioavailability in the plasma and tissues of CUR by developing a solid lipid NP drug delivery system, which will boost therapeutic efficacy.

Given the positive outcomes of *in vitro* cytotoxicity tests conducted on CFPAC-1 and PANC-1 cultures, the *in vivo* findings may serve as a good starting point for further research into *in vivo* pancreatic cancer models. According to the study on c-solid LNPs, their findings support the idea of using the created solid LNPs-based delivery systems for entrapping CUR to increase both its chemical stability and water dispersibility, allowing its use in treatment.

Even though the aforementioned results may not meet the ideal standards for *in vivo* delivery, they offer promising insights and a plethora of possibilities for modifying the composition and surface characteristics of SLNs. These findings inspire us to

explore ways to enhance the circulation time of SLNs while simultaneously reducing opsonization, thereby opening avenues for improved drug delivery strategies [93].

With a five-year survival rate of <5%, pancreatic cancer is the fourth most prevalent cancer mortality in the United States. The American Cancer Society estimated that in 2014, 46,420 people would be diagnosed with pancreatic cancer in the United States alone, and 39,590 of them would face death [95]. The poor patient survival rate suggests a greater need for cutting-edge methods of battling this fatal illness. Chemoprevention has lately drawn a lot of interest as a cutting-edge pancreatic cancer treatment method [96,97]. In addition, current research has focused on the use of chemopreventive drugs that have different modes of action and target numerous pathways [84,98]. This strategy offers a low-dose therapeutic method with more efficacy and lesser damage. Studies on combination treatment, especially for the prevention of pancreatic cancer, are still in their early stages.

Numerous epidemiological and animal studies have shown that NSAIDs, such as ASP, that are widely used can lower the incidence and death of many cancer forms [96,97]. Ibuprofen (IBU), an NSAID, has lately been demonstrated to prevent the growth and spread of malignancies in both in vitro and in vivo investigations [99–101]. IBU has a good chemopreventive potential, however, side effects such as increased gastrointestinal ulcers might make it unsuitable for long-term usage [102,103]. According to current literature, encapsulation inside NP formulations may provide the chance to lessen these medications' negative effects while preserving their high efficacy [104,105]. Formulations that may be helpful in chemoprevention include LNPs with a solid matrix, such as solid LNPs and polymeric NPs [96,97,106]. The ability of the drug to reduce renal and hepatic passage, cross mucosal barriers, lower immune recognition, increased stability, enhanced apparent half-lives of the drugs, and increased solubility are just a few of the benefits that these nanosized drug delivery systems have over standard delivery systems [107,108]. The ability of solid LNPs to boost the oral bioavailability of lipophilic drugs, however, is their most significant benefit. The necessity for more study in this field is justified by the rising importance of NPs in cancer treatment and chemoprevention.

SFN is an isothiocyanate that contains sulfur that is naturally occurring and is present in cruciferous vegetables including brussels sprouts, broccoli, cabbage, and cauliflower [109]. In animal models, SFN has been demonstrated to be beneficial in avoiding a variety of chemically generated malignancies and inhibiting the development of preexisting tumors [110–112]. The expression of NF- $\kappa$ B-mediated genes that code for adhesion molecules, inflammatory cytokines, growth factors, and antiapoptotic factors is impacted by SFN, which has been demonstrated to decrease NF- $\kappa$ B activity [95].

In this experiment by Thakkar et al., lipid matrices of stearic acid, Compritol ATO 888, and tripalmitin were combined with either (1) Poloxamer 188 or (2) Tween-80



as the surfactant to improve IBU-loaded solid LNP formulations. The generated IBU-solid LNPs were examined for their entrapment effectiveness, particle size, in vitro drug dissolving rates, and zeta potential. Another group has not yet studied the impact of low-dose free IBU, IBU-solid LNPs, or IBU-solid LNPs coupled with free SFN on pancreatic cancer cells. In order to assess their combined chemopreventive activity in MIA PaCa-2 and Panc-1 human pancreatic cancer cells, they thus adjusted IBU-solid LNPs formulations [113].

## 10.11 Conclusion

Pancreatic cancer therapy is still difficult. Because pancreatic cancer is relatively resistant to traditional therapies, innovative specific target medications have garnered a lot of interest. These focused nanomaterials would have been capable of recognizing cancerous cells, visualizing their spot inside the body, releasing the drug to such cells only, thwarting drug resistance, killing cancer cells without harming normal tissue to minimize adverse effects, and supervising therapeutic efficacy in instantaneously, as well as provide responses about whether sick people react effectively to the treatment options, allowing the diagnosis to be stopped on period. NP materials have demonstrated extremely encouraging outcomes in improving the pharmacological properties of this anticancer medication while also enhancing antitumor activity against experimental solid tumors. In current history, nano-drug means of delivery technology have emerged as a prominent topic. The utilization of nanomaterials as drug-carrier systems is an appealing technique for achieving regulated drug delivery.

## References

- [1] Mehnert W, Mäder K. Solid lipid nanoparticles: production, characterization and applications. *Adv Drug Deliv Rev* 2012;64:83–101.
- [2] Basha SK, Dhandayuthabani R, Muzammil MS, Kumari VS. Solid lipid nanoparticles for oral drug delivery. *Mater Today Proc* 2021;36:313–24.
- [3] Rehman M, et al. Solid lipid nanoparticles for thermoresponsive targeting: evidence from spectrophotometry, electrochemical, and cytotoxicity studies. *Int J Nanomed* 2017;12:8325.
- [4] Mukherjee S, Maity S, Ghosh B, Chakraborty T, Mondal A, Bishayee A. Assessment of the antidiabetic potentiality of glyburide loaded glyceryl monostearate solid lipid nanoparticles. *J Drug Deliv Sci Technol* 2020;55:101451.
- [5] Garud A, Singh D, Garud N. Solid lipid nanoparticles (SLN): method, characterization and applications. *Int Curr Pharm J* 2012;1(11):384–93.
- [6] Dong Z, Xie S, Zhu L, Wang Y, Wang X, Zhou W. Preparation and in vitro, in vivo evaluations of norfloxacin-loaded solid lipid nanoparticles for oral delivery. *Drug Deliv* 2011;18(6):441–50.
- [7] Li H, Zhao X, Ma Y, Zhai G, Li L, Lou H. Enhancement of gastrointestinal absorption of quercetin by solid lipid nanoparticles. *J Control Release* 2009;133(3):238–44.
- [8] De Blaey CJ, Polderman J. Rationales in the design of rectal and vaginal delivery forms of drugs. *Medicinal chemistry*, vol. 9. Elsevier; 1980. p. 237–66.
- [9] Duan Y, et al. A brief review on solid lipid nanoparticles: part and parcel of contemporary drug delivery systems. *RSC Adv* 2020;10(45):26777–91.



- [10] Scioli Montoto S, Muraca G, Ruiz ME. Solid lipid nanoparticles for drug delivery: pharmacological and biopharmaceutical aspects. *Front Mol Biosci* 2020;7:587997.
- [11] Tekade RK, Maheshwari R, Tekade M, Chougule MB. Solid lipid nanoparticles for targeting and delivery of drugs and genes. *Nanotechnology-based approaches for targeting and delivery of drugs and genes*. Elsevier; 2017. p. 256–86.
- [12] IUPAC, Compendium of chemical terminology (Gold Book). Blackwell Scientific Publications, Oxford, 1997.
- [13] Sheoran S, Arora S, Pilli G. Lipid based nanoparticles for treatment of cancer. *Heliyon* 2022; e09403.
- [14] Tang J, Sun J, He Z-G. Self-emulsifying drug delivery systems: strategy for improving oral delivery of poorly soluble drugs. *Curr Drug Ther* 2007;2(1):85–93.
- [15] Humberstone AJ, Charman WN. Lipid-based vehicles for the oral delivery of poorly water soluble drugs. *Adv Drug Deliv Rev* 1997;25(1):103–28.
- [16] Kuentz M. Lipid-based formulations for oral delivery of lipophilic drugs. *Drug Discov Today Technol* 2012;9(2):e97–e104.
- [17] Patel AR, Velikov KP. Colloidal delivery systems in foods: a general comparison with oral drug delivery. *LWT-Food Sci Technol* 2011;44(9):1958–64.
- [18] Pouton CW, Porter CJH. Formulation of lipid-based delivery systems for oral administration: materials, methods and strategies. *Adv Drug Deliv Rev* 2008;60(6):625–37.
- [19] zur Mühlen A, Schwarz C, Mehnert W. Solid lipid nanoparticles (SLN) for controlled drug delivery—drug release and release mechanism. *Eur J Pharm Biopharm* 1998;45(2):149–55.
- [20] Pardeike J, Hommoss A, Müller RH. Lipid nanoparticles (SLN, NLC) in cosmetic and pharmaceutical dermal products. *Int J Pharm* 2009;366(1):170–84. Available from: <https://doi.org/10.1016/j.ijpharm.2008.10.003>.
- [21] Gasco M.R. Method for producing solid lipid microspheres having a narrow size distribution. Google Patents US5250236A, Oct. 05, 1993.
- [22] Geszke-Moritz M, Moritz M. Solid lipid nanoparticles as attractive drug vehicles: composition, properties and therapeutic strategies. *Mater Sci Eng C* 2016;68:982–94. Available from: <https://doi.org/10.1016/j.msec.2016.05.119>.
- [23] Doktorovova S, Souto EB, Silva AM. Nanotoxicology applied to solid lipid nanoparticles and nanostructured lipid carriers—a systematic review of in vitro data. *Eur J Pharm Biopharm* 2014;87(1):1–18.
- [24] Bor G, Mat Azmi ID, Yaghmur A. Nanomedicines for cancer therapy: current status, challenges and future prospects. *Ther Deliv* 2019;10(2):113–32.
- [25] Miele E, et al. Nanoparticle-based delivery of small interfering RNA: challenges for cancer therapy. *Int J Nanomed* 2012;7:3637.
- [26] Fatima I, Rahdar A, Sargazi S, Barani M, Hassanisaadi M, Thakur VK. Quantum dots: synthesis, antibody conjugation, and HER2-receptor targeting for breast cancer therapy. *J Funct Biomater* 2021;12(4):75.
- [27] Rama AR, et al. Last advances in nanocarriers-based drug delivery systems for colorectal cancer. *Curr Drug Deliv* 2016;13(6):830–8.
- [28] Alavi M, Hamidi M. Passive and active targeting in cancer therapy by liposomes and lipid nanoparticles. *Drug Metab Pers Ther* 2019;34(1).
- [29] Muller RH, Shegokar R, Keck CM. 20 years of lipid nanoparticles (SLN and NLC): present state of development and industrial applications. *Curr Drug Discov Technol* 2011;8(3):207–27.
- [30] Kathe N, Henriksen B, Chauhan H. Physicochemical characterization techniques for solid lipid nanoparticles: principles and limitations. *Drug Dev Ind Pharm* 2014;40(12):1565–75.
- [31] Teeranachaideekul V, Müller RH, Junyaprasert VB. Encapsulation of ascorbyl palmitate in nanostructured lipid carriers (NLC)—Effects of formulation parameters on physicochemical stability. *Int J Pharm* 2007;340(1–2):198–206.
- [32] Jaiswal P, Gidwani B, Vyas A. Nanostructured lipid carriers and their current application in targeted drug delivery. *Artif Cells, Nanomed, Biotechnol* 2016;44(1):27–40.

- [33] Lima AM, et al. Hypericin encapsulated in solid lipid nanoparticles: phototoxicity and photodynamic efficiency. *J Photochem Photobiol B Biol* 2013;125:146–54.
- [34] Wissing SA, Kayser O, Müller RH. Solid lipid nanoparticles for parenteral drug delivery. *Adv Drug Deliv Rev* 2004;56(9):1257–72.
- [35] Svilenov H, Tzachev C. Solid lipid nanoparticles—a promising drug delivery system. *Nanomedicine* 2014;2:187–237.
- [36] Iqbal MA, Md S, Sahni JK, Baboota S, Dang S, Ali J. Nanostructured lipid carriers system: recent advances in drug delivery. *J Drug Target* 2012;20(10):813–30.
- [37] Almeida AJ, Souto E. Solid lipid nanoparticles as a drug delivery system for peptides and proteins. *Adv Drug Deliv Rev* 2007;59(6):478–90.
- [38] Almeida AJ, Runge S, Müller RH. Peptide-loaded solid lipid nanoparticles (SLN): influence of production parameters. *Int J Pharm* 1997;149(2):255–65.
- [39] Naseri N, Valizadeh H, Zakeri-Milani P. Solid lipid nanoparticles and nanostructured lipid carriers: structure, preparation and application. *Adv Pharm Bull Sep.* 2015;5(3):305–13. Available from: <https://doi.org/10.15171/apb.2015.043>.
- [40] Mishra V, et al. Solid lipid nanoparticles: emerging colloidal nano drug delivery systems. *Pharmaceutics* 2018;10(4):191.
- [41] Thatipamula RP, Palem CR, Gannu R, Mudragada S, Yamsani MR. Formulation and in vitro characterization of domperidone loaded solid lipid nanoparticles and nanostructured lipid carriers. *Daru* 2011;19(1):23.
- [42] Shazly GA. Ciprofloxacin controlled-solid lipid nanoparticles: characterization, in vitro release, and antibacterial activity assessment. *Biomed Res Int* 2017;2017:2120734.
- [43] ud Din F, et al. Effective use of nanocarriers as drug delivery systems for the treatment of selected tumors. *Int J Nanomed* 2017;12:7291.
- [44] Bayón-Cordero L, Alkorta I, Arana L. Application of solid lipid nanoparticles to improve the efficiency of anticancer drugs. *Nanomaterials* 2019;9(3):474.
- [45] Sivakumar SM. Therapeutic potential of chitosan nanoparticles as antibiotic delivery system: challenges to treat multiple drug resistance. *Asian J Pharm* 2016;10(2).
- [46] Liu J, Wang T, Wang D, Dong A, Li Y, Yu H. Smart nanoparticles improve therapy for drug-resistant tumors by overcoming pathophysiological barriers. *Acta Pharmacol Sin* 2017;38(1):1–8.
- [47] Qureshi OS, et al. Sustained release docetaxel-incorporated lipid nanoparticles with improved pharmacokinetics for oral and parenteral administration. *J Microencapsul* 2017;34(3):250–61.
- [48] Oliveira MS, Aryasomayajula B, Pattni B, Mussi SV, Ferreira LAM, Torchilin VP. Solid lipid nanoparticles co-loaded with doxorubicin and  $\alpha$ -tocopherol succinate are effective against drug-resistant cancer cells in monolayer and 3-D spheroid cancer cell models. *Int J Pharm* 2016;512(1):292–300.
- [49] Nami S, Aghebbati-Maleki A, Aghebbati-Maleki L. Current applications and prospects of nanoparticles for antifungal drug delivery. *EXCLI J* 2021;20:562.
- [50] Kang KW, et al. Doxorubicin-loaded solid lipid nanoparticles to overcome multidrug resistance in cancer therapy. *Nanomed Nanotechnol Biol Med* 2010;6(2):210–13.
- [51] Carvalho PM, Felício MR, Santos NC, Gonçalves S, Domingues MM. Application of light scattering techniques to nanoparticle characterization and development. *Front Chem* 2018;6:237.
- [52] Sarmiento B, Martins S, Ferreira D, Souto EB. Oral insulin delivery by means of solid lipid nanoparticles. *Int J Nanomed* 2007;2(4):743.
- [53] Gulati N, Gupta H. Parenteral drug delivery: a review. *Recent Pat Drug Deliv Formul* 2011;5(2):133–45.
- [54] Bhagwat GS, et al. Formulation and development of transferrin targeted solid lipid nanoparticles for breast cancer therapy. *Front Pharmacol* 2020;11:614290.
- [55] Patel R, Patel KP. Advances in novel parenteral drug delivery systems. *Asian J Pharm* 2010;4(3).
- [56] Deshpande A, Mohamed M, Daftardar SB, Patel M, Boddu SHS, Nesamony J. Solid lipid nanoparticles in drug delivery: opportunities and challenges. *Emerging nanotechnologies for diagnostics, drug delivery and medical devices*. Elsevier; 2017. p. 291–330.
- [57] Weber S, Zimmer A, Pardeike J. Solid lipid nanoparticles (SLN) and nanostructured lipid carriers (NLC) for pulmonary application: a review of the state of the art. *Eur J Pharm Biopharm* 2014;86(1):7–22.

- [58] Badilli U, Gumustas M, Uslu B, Ozkan SA. Lipid-based nanoparticles for dermal drug delivery. *Organic materials as smart nanocarriers for drug delivery*. Elsevier; 2018. p. 369–413.
- [59] Chattopadhyay N, Zastre J, Wong H-L, Wu XY, Bendayan R. Solid lipid nanoparticles enhance the delivery of the HIV protease inhibitor, atazanavir, by a human brain endothelial cell line. *Pharm Res* 2008;25(10):2262–71.
- [60] Newton, AM J, & Kaur, S. Solid lipid nanoparticles for skin and drug delivery. *Nanoarchitectonics bio-medicine*, Elsevier, 295–334, 2019. doi:10.1016/b978-0-12-816200-2.00015-3
- [61] Lu QZ, Yu A, Xi Y, Li H, Song Z, Cui J, et al. Development and evaluation of penciclovir-loaded solid lipid nanoparticles for topical delivery. *Int J Pharm* 2009;372:191–8.
- [62] Paliwal R, Rai S, Vaidya B, Khatri K, Goyal AK, Mishra N, et al. Effect of lipid core material on characteristics of solid lipid nanoparticles designed for oral lymphatic delivery. *Nanomed Nanotechnol Biol Med* 2009;5(2):184–91.
- [63] Inkoom A, Ndemazie N, Smith T, Frimpong E, Bulusu R, Poku R, et al. Application of modified GEMcitabine-loaded solid lipid nanoparticle in the treatment of pancreatic cancer patient-derived xenograft model. Preprint: Research Square, 2022.
- [64] Affram KO, Smith T, Ofori E, Krishnan S, Underwood P, Trevino JG, et al. Cytotoxic effects of gemcitabine-loaded solid lipid nanoparticles in pancreatic cancer cells. *J Drug Deliv Sci Technol* 2020;55:101374. Available from: <https://doi.org/10.1016/j.jddst.2019.101374>.
- [65] Ganesan P, Narayanasamy D. Lipid nanoparticles: different preparation techniques, characterization, hurdles, and strategies for the production of solid lipid nanoparticles and nanostructured lipid carriers for oral drug delivery. *Sustain Chem Pharm* 2017;6:37–56.
- [66] Kalaycioglu GD, Aydogan N. Preparation and investigation of solid lipid nanoparticles for drug delivery. *Colloids Surf A: Physicochem Eng Asp* 2016;510:77–86.
- [67] Wonganan P, Lansakara PD, Zhu S, Holzer M, Sandoval MA, Warthaka M, et al. Just getting into cells is not enough: mechanisms underlying 4-(N)-stearyl gemcitabine solid lipid nanoparticle's ability to overcome gemcitabine resistance caused by RRM1 overexpression. *J Control Release* 2013;169:17–27. Available from: <https://doi.org/10.1016/j.jconrel.2013.03.033>.
- [68] Bildstein L, Dubernet C, Marsaud V, Chacun H, Nicolas V, Gueutin C, et al. Transmembrane diffusion of gemcitabine by a nanoparticulate squalenoyl prodrug: an original drug delivery pathway. *J Control Release* 2010;147:163–70. Available from: <https://doi.org/10.1016/j.jconrel.2010.07.120>.
- [69] Kal H, Barendsen G. Radiosensitivity of surviving cells in tumours pretreated with continuous irradiation. *Br J Radiol* 1973;46:1083.
- [70] Graña X, Reddy EP. Cell cycle control in mammalian cells: role of cyclins, cyclin dependent kinases (CDKs), growth suppressor genes and cyclin-dependent kinase inhibitors (CKIs). *Oncogene* 1995;11:211–20.
- [71] Kastan MB, Canman CE, Leonard CJ. P53, cell cycle control and apoptosis: implications for cancer. *Cancer Metastasis Rev* 1995;14:3–15.
- [72] Tobita K, Kijima H, Dowaki S, Kashiwagi H, Ohtani Y, Oida Y, et al. Epidermal growth factor receptor expression in human pancreatic cancer: significance for liver metastasis. *Int J Mol Med* 2003;11:305–9.
- [73] Bloomston M, Bhardwaj A, Ellison EC, Frankel WL. Epidermal growth factor receptor expression in pancreatic carcinoma using tissue microarray technique. *Dig Surg* 2006;23:74–9.
- [74] Safran H, Steinhoff M, Mangray S, Rathore R, King TC, Chai L, et al. Overexpression of the HER-2/neu oncogene in pancreatic adenocarcinoma. *Am J Clin Oncol* 2001;24:496–9.
- [75] Stoecklein NH, Luecke AM, Erbersdobler A, Knoefel WT, Schraut W, Verde PE, et al. Copy number of chromosome 17 but not HER2 amplification predicts clinical outcome of patients with pancreatic ductal adenocarcinoma. *J Clin Oncol* 2004;22:4737–45.
- [76] Komoto M, Nakata B, Amano R, Yamada N, Yashiro M, Ohira M, et al. HER2 overexpression correlates with survival after curative resection of pancreatic cancer. *Cancer Sci* 2009;100:1243–7.
- [77] Morgan MA, Parsels LA, Kollar LE, Normolle DP, Maybaum J, Lawrence TS. The combination of epidermal growth factor receptor inhibitors with gemcitabine and radiation in pancreatic cancer. *Clin Cancer Res* 2008;14:5142–9. Available from: <https://doi.org/10.1158/1078-0432.CCR-07-4072>.

- [78] Friess H, Berberat P, Schilling M, Kunz J, Korc M, Buchler MW. Pancreatic cancer: the potential clinical relevance of alterations in growth factors and their receptors. *J Mol Med (Berl)* 1996;74:35–42. Available from: <https://doi.org/10.1007/BF00202070>.
- [79] Henderson AJ, Ollila CA, Kumar A, Borresen EC, Raina K, Agarwal R, et al. Chemopreventive properties of dietary rice bran: current status and future prospects. *Adv Nutr* 2012;3:643e53.
- [80] Zhang Y, Li Z, Zhang K, Yang G, Wang Z, Zhao J, et al. Ethyl oleate-containing nanostructured lipid carriers improve oral bioavailability of trans-ferulic acid as compared with conventional solid lipid nanoparticles. *Int J Pharm* 2016;511:57e6.
- [81] Thakkar A, Chenreddy S, Wang J, Prabhu S. Ferulic acid combined with aspirin demonstrates chemopreventive potential towards pancreatic cancer when delivered using chitosan-coated solid-lipid nanoparticles. *Cell Biosci* 2015;5:46.
- [82] Luo Y, Teng Z, Li Y, Wang Q. Solid lipid nanoparticles for oral drug delivery: chitosan coating improves stability, controlled delivery, mucoadhesion and cellular uptake. *Carbohydr Polym* 2015;122:221e9.
- [83] Lin C-H, Chen C-H, Lin Z-C, Fang J-Y. Recent advances in oral delivery of drugs and bioactive natural products using solid lipid nanoparticles as the carriers. *J Food Drug Anal* 2017;25(2):219–34. Available from: <https://doi.org/10.1016/j.jfda.2017.02.001>.
- [84] Sutaria D, Grandhi BK, Thakkar A, Wang J, Prabhu S. Chemoprevention of Pancreatic cancer using solid-lipid nanoparticulate delivery of a novel aspirin, curcumin and sulforaphane drug combination regimen. *Int J Oncol* 2012;41(6):2260–8.
- [85] Fendrich V. Chemoprevention of pancreatic cancer—one step closer. *Langenbecks Arch Surg* 2012;397:495–505. Available from: <https://doi.org/10.1007/s00423-012-0916-x22350613>.
- [86] Logsdon CD, Abbruzzese JL. Chemoprevention of pancreatic cancer: ready for the clinic? *Cancer Prev Res (Phila)* 2010;3:1375–8. Available from: <https://doi.org/10.1158/1940-6207.CAPR-10-021621084259>.
- [87] Husain SS, Szabo IL, Tamawski AS. NSAID inhibition of GI cancer growth: clinical implications and molecular mechanisms of action. *Am J Gastroenterol* 2002;97:542–53. Available from: <https://doi.org/10.1111/j.1572-0241.2002.05528.x11922545>.
- [88] Kuo ML, Huang TS, Lin JK. Curcumin, an antioxidant and anti-tumor promoter, induces apoptosis in human leukemia cells. *Biochim Biophys Acta* 1996;1317(2):95–100. Available from: [https://doi.org/10.1016/S0925-4439\(96\)00032-48950193](https://doi.org/10.1016/S0925-4439(96)00032-48950193).
- [89] Moragoda L, Jaszewski R, Majumdar AP. Curcumin induced modulation of cell cycle and apoptosis in gastric and colon cancer cells. *Anticancer Res* 2001;21(2A):873–8 11396178.
- [90] Lampe JW. Sulforaphane: from chemoprevention to pancreatic cancer treatment? *Gut* 2009;58:900–2. Available from: <https://doi.org/10.1136/gut.2008.16669419520886> 58900902.
- [91] Chaudhary A, Sutaria D, Huang Y, Wang J, Prabhu S. Chemoprevention of colon cancer in a rat carcinogenesis model using a novel nanotechnology-based combined treatment system. *Cancer Prev Res (Phila)* 2011;4:1655–64. Available from: <https://doi.org/10.1158/1940-6207.CAPR-11-0129>.
- [92] Miglietta A, Cavalli R, Bocca C, Gabriel L, Gasco MR. Cellular uptake and cytotoxicity of solid lipid nanospheres (solid lipid nanoparticles) incorporating doxorubicin or paclitaxel. *Int J Pharm* 2000;2:106–67. Available from: [https://doi.org/10.1016/S0378-5173\(00\)00562-711163988](https://doi.org/10.1016/S0378-5173(00)00562-711163988).
- [93] Yan F, Zhang C, Zheng Y. The effect of poloxamer 188 on nanoparticle morphology, size, cancer cell uptake, and cytotoxicity. *Nanomedicine* 2010;6:170–178. Available from: <https://doi.org/10.1016/j.nano.2009.05.00419447200>.
- [94] Chirio D, Peira E, Dianzani C, Muntoni E, Gigliotti CL, Ferrara B, et al. Development of solid lipid nanoparticles by cold dilution of microemulsions: curcumin loading, preliminary in vitro studies, and biodistribution. *Nanomaterials* 2019;9(2):230.
- [95] Kallifatidis G, Rausch V, Baumann B, et al. Sulforaphane targets pancreatic tumour-initiating cells by NF-kappaB-induced anti-apoptotic signalling. *Gut*. 2009;58:949–63.
- [96] Grandhi BK, Thakkar A, Wang J, Prabhu S. A novel combinatorial nanotechnology-based oral chemopreventive regimen demonstrates significant suppression of pancreatic cancer neoplastic lesions. *Cancer Prev Res* 2013;6:1015–25.

- [97] Chaudhary A, Sutaria D, Huang Y, Wang J, Prabhu S. Chemoprevention of colon cancer in a rat carcinogenesis model using a novel nanotechnology-based combined treatment system. *Cancer Prev Res* 2011;4:1655–64.
- [98] Thakkar A, Sutaria D, Grandhi BK, Wang J, Prabhu S. The molecular mechanism of action of aspirin, curcumin and sulforaphane combinations in the chemoprevention of pancreatic cancer. *Oncol Rep* 2013;29:1671–7.
- [99] Palayoor ST, Bump EA, Calderwood SK, Bartol S, Coleman CN. Combined antitumor effect of radiation and ibuprofen in human prostate carcinoma cells. *Clin Cancer Res* 1998;4:763–71.
- [100] Yao M, Zhou W, Sangha S, et al. Effects of nonselective cyclooxygenase inhibition with low-dose ibuprofen on tumor growth, angiogenesis, metastasis, and survival in a mouse model of colorectal cancer. *Clin Cancer Res* 2005;11:1618–28.
- [101] Bonelli P, Tuccillo FM, Federico A, et al. Ibuprofen delivered by poly(lactic-co-glycolic acid) (PLGA) nanoparticles to human gastric cancer cells exerts antiproliferative activity at very low concentrations. *Int J Nanomed* 2012;7:5683–91.
- [102] Lanus A. A review of the gastrointestinal safety data – a gastroenterologist’s perspective. *Rheumatology* 2010;49(Suppl 2):ii3–ii10.
- [103] Mallen SR, Essex MN, Zhang R. Gastrointestinal tolerability of NSAIDs in elderly patients: a pooled analysis of 21 randomized clinical trials with celecoxib and nonselective NSAIDs. *Curr Med Res Opin* 2011;27:1359–66.
- [104] Brigger I, Dubernet C, Couvreur P. Nanoparticles in cancer therapy and diagnosis. *Adv Drug Deliv Rev* 2002;54:631–51.
- [105] Potta SG, Minemi S, Nukala RK, et al. Preparation and characterization of ibuprofen solid lipid nanoparticles with enhanced solubility. *J Microencapsul* 2011;28:74–81.
- [106] Kokawa A, Kondo H, Gotoda T, et al. Increased expression of cyclooxygenase-2 in human pancreatic neoplasms and potential for chemoprevention by cyclooxygenase inhibitors. *Cancer* 2001;91:333–8.
- [107] O’Driscoll CM. Lipid-based formulations for intestinal lymphatic delivery. *Eur J Pharm Sci* 2002;15:405–15.
- [108] Mehnert W, Mäder K. Solid lipid nanoparticles: production, characterization and applications. *Adv Drug Deliv Rev* 2001;47:165–96.
- [109] Matusheski NV, Juvik JA, Jeffery EH. Heating decreases epithiospecifier protein activity and increases sulforaphane formation in broccoli. *Phytochemistry*. 2004;65:1273–81.
- [110] Fahey JW, Haristoy X, Dolan PM, et al. Sulforaphane inhibits extracellular, intracellular, and antibiotic-resistant strains of *Helicobacter pylori* and prevents benzo[a]pyrene-induced stomach tumors. *Proc Natl Acad Sci USA* 2002;99:7610–15.
- [111] Kuroiwa Y, Nishikawa A, Kitamura Y, et al. Protective effects of benzyl isothiocyanate and sulforaphane but not resveratrol against initiation of pancreatic carcinogenesis in hamsters. *Cancer Lett* 2006;241:275–80.
- [112] Chung FL, Conaway CC, Rao CV, Reddy BS. Chemoprevention of colonic aberrant crypt foci in Fischer rats by sulforaphane and phenethyl isothiocyanate. *Carcinogenesis*. 2000;21:2287–91.
- [113] Thakkar A, Chenreddy S, Wang J, Prabhu S. Evaluation of ibuprofen loaded solid lipid nanoparticles and its combination regimens for pancreatic cancer chemoprevention. *Int J Oncol* 2015;46:1827–34. Available from: <https://doi.org/10.3892/ijo.2015.2879>.



# Hesperidin's role in the treatment of lung cancer: *In-silico* and *In-vitro* findings

Swati Arora<sup>1,8,9</sup> · Sumit Sheoran<sup>1,8,9</sup> · Bhuvanesh Baniya<sup>2</sup> · Naidu Subbarao<sup>3</sup> · Himanshu Singh<sup>1</sup> · Dhamodharan Prabhu<sup>4</sup> · Neeraj Kumar<sup>5</sup> · Smita C. Pawar<sup>6</sup> · Sugunakar Vuree<sup>7,9</sup>

Received: 28 July 2024 / Accepted: 23 September 2024

© The Author(s), under exclusive licence to Springer-Verlag GmbH Germany, part of Springer Nature 2024

## Abstract

Lung Cancer remains a significant health concern, necessitating the exploration of novel therapeutic avenues due to the limited efficacy and adverse effects of current treatments. In this study, we utilized a thorough *in-silico* and *in-vitro* methodology to develop prospective drugs for the treatment of lung cancer. The active components of *Citrus latifolia* were identified through the utilization of a variety of pharmacological instruments, such as Gene Ontology, GeneCards, DrugBank, the Chinese Traditional Drug Database, and GeneMANIA. Subsequent molecular docking studies using GOLD software revealed Hesperidin as the most promising candidate, exhibiting a remarkable binding affinity (GOLD score: 60.98 kcal/mol) towards the epidermal growth factor receptor (EGFR), a pivotal target in lung cancer therapy. Further validation through Schrodinger-Glide redocking reaffirmed the robust interaction between Hesperidin and EGFR. Pharmacokinetic profiling of top-scoring ligands indicated favorable drug-like properties, supporting their therapeutic potential. Molecular dynamics simulations employing Desmond software demonstrated the structural stability and persistence of the Hesperidin-EGFR complex over a 100-ns trajectory, corroborating its efficacy. Additionally, cytotoxicity analysis revealed a potent inhibitory effect of Hesperidin with an IC<sub>50</sub> value of 34.25 µg/ml. Collectively, our findings underscore Hesperidin from *Citrus latifolia* as a promising candidate for lung cancer therapy, warranting further investigation through *in-vivo* studies for clinical translation.

---

✉ Sugunakar Vuree  
sugunakarvuree@gmail.com

<sup>1</sup> School of Bioengineering and Biosciences, Lovely Professional University, Jalandhar, Punjab, India

<sup>2</sup> Department of Pharmaceutical Sciences, Mohanlal Sukhadia University, Udaipur, Rajasthan, India

<sup>3</sup> School of Computational and Integrative Sciences, JNU, New Delhi, India

<sup>4</sup> Centre for Drug Discovery, Department of Biotechnology, Karpagam Academy of Higher Education, Coimbatore 641021, India

<sup>5</sup> Department of Pharmaceutical Chemistry, Bhupal Noble's College of Pharmacy Udaipur, Rajasthan 313001, India

<sup>6</sup> Department of Genetics and Biotechnology, Osmania University, Hyderabad, India

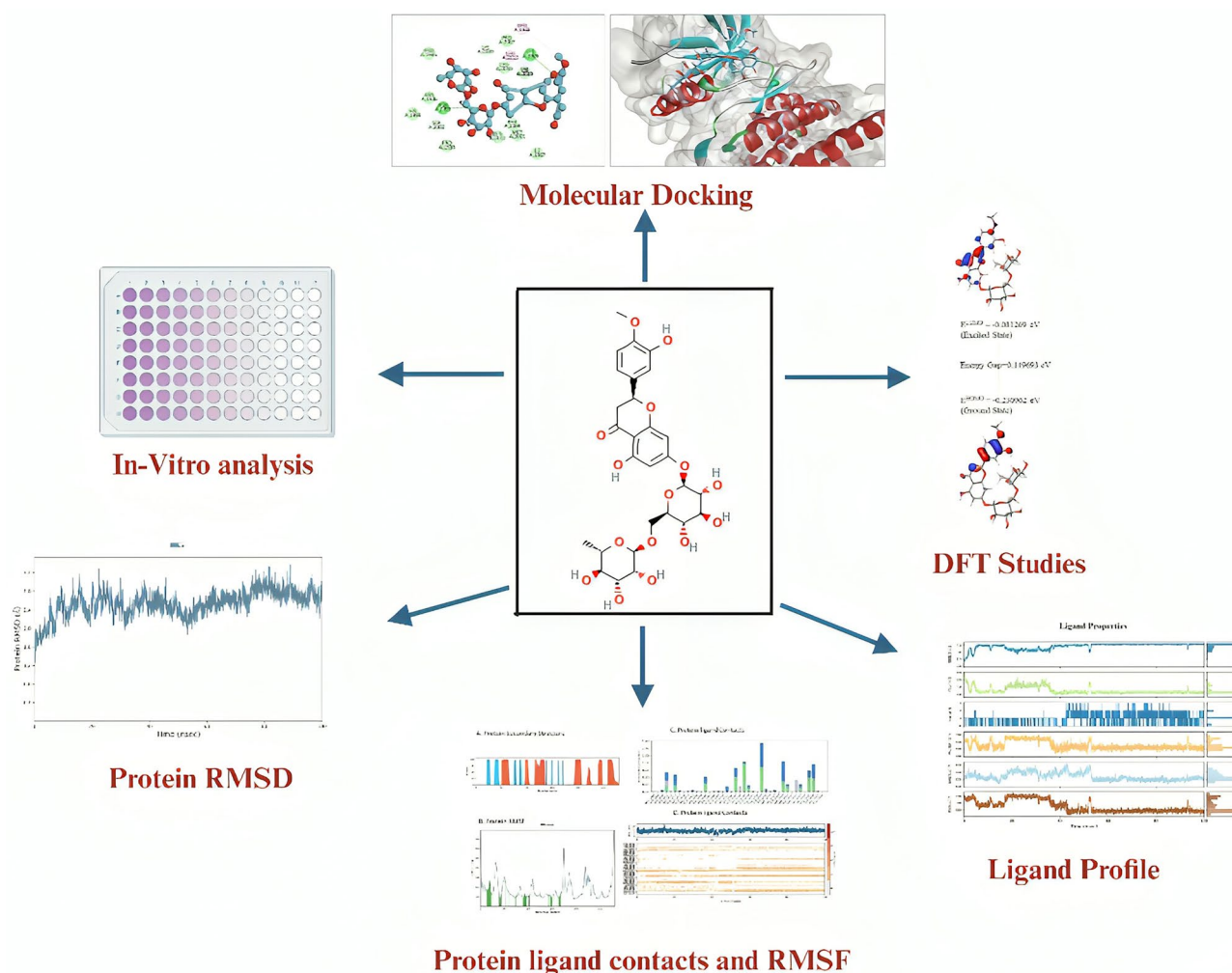
<sup>7</sup> Department of Research and Development, Indo-American Cancer Research Foundation, Basavataarakam Indo-American Cancer Hospital and Research Institute, Hyderabad, Telangana 500034, India

<sup>8</sup> Thyme Phyto BioMed Pvt. Ltd, Hisar, Haryana, India

<sup>9</sup> Bioclues Organization, Hyderabad, Telangana, India



## Graphical Abstract



**Keywords** Lung cancer · *EGFR* · Hesperidin · *In-silico* · *In-vitro*

## Introduction

Lung Cancer remains a significant global health challenge, with non-small cell lung carcinoma (NSCLC) accounting for approximately 85% of cases and exhibiting a high mortality rate (Siegel et al. 2016). Small cell lung carcinomas (SCLC) account for 35% of the population (Seer, xxxx). Adenocarcinoma, squamous cell carcinoma, and large cell carcinoma are subtypes of NSCLC. The management of may be approached with either palliative or curative objectives, contingent upon the disease's stage. Lung cancer is frequently managed with surgical resection, chemotherapy, targeted therapy, radiotherapy, and immunotherapy, among other approaches (Gadgeel et al. 2012). For maximum efficacy, chemotherapeutic drugs are

typically administered in combination with other chemotherapeutic drugs or treatments.

The dysregulated activation of these signalling cascades leads to abnormal cell growth, whereas the inhibition of apoptosis activates oncogenic pathways, thereby exacerbating the severity of the pathological condition (Wee and Wang 2017). Although numerous pharmaceutical agents are available for cancer treatment, their excessive cost, the challenge of developing resistance, and the increased toxicity following drug administration are substantial obstacles to achieving effective therapy. Furthermore, these issues have adverse effects on non-malignant cells. So, there is a significant effort to prioritize the development of novel therapeutic agents that exhibit low cost and high bioavailability to address these challenges in Phyto-based therapeutics.

Flavonoids were used to solve all of the problems because they are widely used in nutrition, medicine, and cosmetics because they have many health-promoting qualities. They possess anti-oxidative, anti-bacterial, anti-allergic, anti-inflammatory, anti-tumor, and other pharmacological properties (Arora et al. 2023; Sheoran et al. 2022, 2023a, 2023b, 2023c). Their antitumor effects, including initiation, promotion, and progression, are particularly pronounced during the distinct phases of tumorigenesis. Consequently, flavonoids can effectively inhibit tumor growth during these stages (Panche et al. 2016). Hesperidin can generate reactive oxygen species (ROS) in cancer cells and activate mitochondrial pathways (by upregulating caspases) and inhibit kinases, which can induce apoptosis. Also, by regulating cell cycle-related proteins, hesperidin can arrest cancer cell cycle in G<sub>0</sub>/G<sub>1</sub> phase and G<sub>2</sub>/M phase (Devi et al. 2015; Aggarwal et al. 2020; Rahmani et al. 2023).

Further, EGFR (Fig. 1) was also chosen as a possible drug target because it plays a key role in the development of lung cancer. Activation of EGFR leads to the initiation of multiple signaling cascades involved in cellular differentiation, proliferation, growth, and survival. One such molecular alteration observed in lung cancer is a rearrangement of the ROS-1 gene, which results in the formation of phosphotyrosine recruitment sites within the terminal tail of the ROS-1 protein, leading to aberrant kinase activity and dysregulated activation of downstream signaling pathways. Abnormal activation of these signaling pathways contributes to the development and progression of lung cancer. The present work utilized pharmacokinetic characteristics, ADME,

molecular docking, modeling, and cytotoxicity studies to investigate the potential of hesperidin in the context of lung cancer.

## Methodology

### Identification, retrieval, and preparation of ligand for docking study

The biologically active component of *Citrus latifolia* was identified through lit. review and acquired from PubChem (<https://pubchem.ncbi.nlm.nih.gov/>) databases in SDF 3D file format (Yadav et al. 2019; Sweta et al. 2019; Patidar et al. 2019). Energy minimization was performed using the Avogadro program and the MMF force field to prepare the ligand for further analysis. The optimization process employed the steepest descent technique with 200 rounds and a threshold of 0.1 for the RMS gradients (Sheoran et al. 2023a). This approach aimed to achieve optimal ligand conformations. After the energy minimization step, the ligands were ready for docking studies, which involved evaluating their interactions with target molecules or proteins.

### Prediction of citrus latifolia and lung cancer targets

Lung Cancer-specific targets of *Citrus latifolia* were extracted from a variety of databases, including genecards (<https://www.genecards.org/>), drugbank (<https://go.drugbank.com/>), Chinese traditional drug database (Ru et al. 2014), and a study of the relevant literature (Yao et al. 2023). To get the established therapeutic targets for lung cancer, the genecards (<https://www.genecards.org/>) and NCBI Gene databases (<https://www.ncbi.nlm.nih.gov/gene>) were used. To enhance the visual depiction of the target network, the researchers used Gephi 0.9.2, (<https://gephi.org/>) a visualization program, to build their network. Additionally, a Venn diagram analysis was conducted to identify the targets shared by *Citrus latifolia* and lung cancer by using the Venny tool.

### Topological analysis and target network development

To establish a network based on the functional relationships of certain target genes, the GeneMANIA (Multiple Association Network Integration Algorithm) Cytoscape (<https://cytoscape3.9.1.org/>) plugin was used to import the genes (Mostafavi et al. 2008). The resulting gene network was then assessed based on their predicted and colocalized protein domains, co-expression, genetic interaction, physical interaction, pathway, and shared protein domains. Additionally, the CytoNCA plugin was used to assess the generated

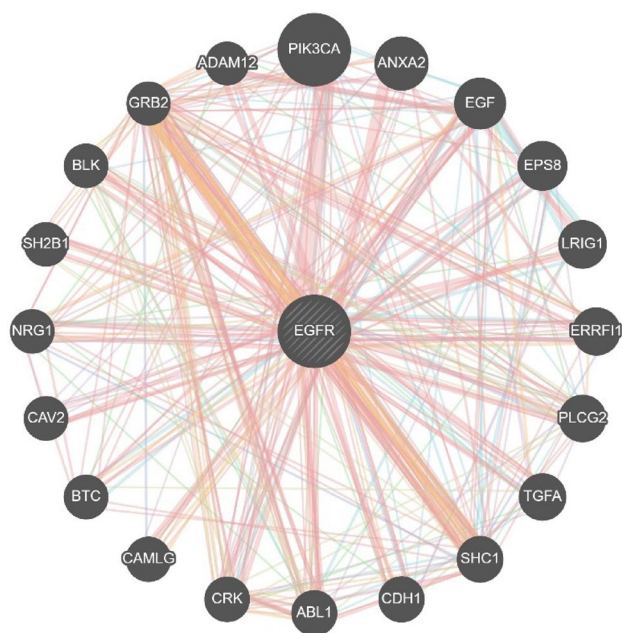


**Fig. 1** Showing the various types of connections of genes with EGFR



network's topological features, including degree centrality (DC), betweenness centrality (BC), and proximity centrality (CC).

### Analysis of target pathway enrichment and gene ontology (GO)

GO is a method for representing in-depth data on the products of genes and their molecular functions (MF), biological processes (BP), and cellular components (The Gene Ontology Consortium 2017). For GO analysis, the PANTHER (<https://www.pantherdb.org/geneListAnalysis.do>) (Protein Analysis Through Evolutionary Relationships) program was used to determine the function of certain target genes in various KEGG pathways.

### Preparation of protein for docking study

The 3-D structure of EGFR (6DUK) was downloaded from the Protein Data Bank (PDB) database and prepared for further investigation (Agu et al. 2023). All non-essential water molecules were removed using Chimera software, and polar hydrogens were added. The protein was energy minimized to ensure an energetically favorable structure to eliminate unfavorable interactions. During the energy minimization process, localized strain arising from minor structural imperfections, such as poor Van der Waals contacts, was alleviated. The energy reduction was performed under the assumption of a vacuum environment. The Chimera software was employed to minimize the energy of the protein structures. The resulting optimized protein structures and their partial atomic charges were utilized in subsequent docking analyses. Docking analysis involves the prediction of optimal orientations of ligand molecules within the active site of the protein and identifying the crucial residues involved in ligand–protein interactions. The aim was to estimate the binding modes and identify the critical interactions between the ligand and the protein receptor.

### Molecular docking protocol by using GOLD

The binding mode and selectivity of target proteins with specific compounds were investigated using the GOLD software. Additionally, the software was utilized to assign hydrogens and define torsional angles for active peptides, which were subsequently docked into the protein's binding pocket (Almeida et al. 2023). The search for potential binding sites was conducted within a distance of 5 Å. After identifying binding sites or atoms for the ligands, water molecules and unwanted ligands were removed from the system. A scoring function was employed to the binding energy, and the default genetic algorithm was utilized to conduct the docking. The resulting structures were evaluated

and grouped based on the scoring function, allowing binding affinities. Subsequently, the docking results were compared, focusing on conformations with favorable characteristics. The compounds exhibiting the highest GOLD Score were selected for further analysis.

### Molecular docking protocol by using Schrodinger-Glide

The docking findings were validated using the glide package (Alsaif et al. 2024). It has also been employed in earlier studies to distribute bioactive peptide moieties and hydrogens that were docked into binding pockets. The binding site area was generated within a 5 Å radius. After selecting binding site or atom ligands, water molecules and unwanted ligands were eliminated. In addition, a score is chosen for calculating binding energy and run the default genetic technique (Sheoran et al. 2023a). Further, the complex were categorized and scored using a scoring mechanism. The compound with the highest docked values was chosen for further investigation.

### Density functional theory (DFT)

The most efficient molecule was subjected to DFT. It primarily computes the characteristics of LUMO, HOMO, and electron density to forecast the lead molecule's chemical properties and biological activities (Sheoran et al. 2023a). Composite DFT may be used to acquire precise geometric aspects of a molecule. Schrodinger software determined several molecule electrostatic parameters such as LUMO and HOMO energy. The energy of the electrostatic potential of the compounds of interest was assessed and characterized by colour difference.

### Drug-like & pharmacokinetic properties

Developing novel drug molecules requires a thorough understanding of their pharmacokinetic parameters, which are crucial for their efficacy and safety profiles. An ideal drug candidate should possess optimal biological activity and favorable pharmacokinetic properties. One vital aspect of pharmacokinetics is the interaction with Pgp (p-glycoprotein) in the hepatic as an efflux pump (Sheoran et al. 2023a; Muthumanickam et al. 2020). Inhibiting Pgp can be advantageous for a drug molecule, making it a promising candidate, whereas the opposite scenario indicates a potential limitation. Therefore, assessing the interaction with Pgp is critical in evaluating drug candidates, as it can influence their effectiveness and overall pharmacokinetic profiles. SwissADME was used to predict the compound's drug-like properties and other molecular characteristics.

## Molecular simulation

Molecular Dynamics simulations have been conducted for the docked complexes to study the conformational stability (Sheoran et al. 2023a; Pranweerapaiboon et al. 2022). The study has produced the trajectory of the particle coordinates, velocities, and energies via which the strength of expression of the model system could be analyzed, for which the Molecular Simulation was performed for 100 ns by using the Desmond (version 2021.4-Ubuntu-2022.04) software. The OPLS-2005 force field was utilized to generate the topology. Further, the system builder platform was employed to construct the complex and explicit water models with point charges, creating an orthorhombic box form. The solvated complex system was neutralized by adding Na<sup>+</sup>/Cl<sup>-</sup> ions to achieve a salt concentration of 0.15 M, simulating physiological conditions. Subsequently, the simulations were conducted under conditions of 300 K temperature and 1.0325 bar pressure (Sheoran et al. 2023a). The system was initially minimized to 100 ps, followed by relaxation using the default technique. The simulation was then run for 100 ns to explore the dynamics and behavior of the complex.

## Analysis of the boiled egg plot

The Estimate D permeation method, commonly called BOILED-Egg (Sheoran et al. 2023a; Daina et al. 2017), is a dependable predictive model to assess ligands' lipophilicity and polarity. This method provides a unique statistical framework for evaluating the bioavailability characteristics of ligand molecules. This approach considers the physico-chemical properties associated with blood–brain barrier penetration and gastrointestinal absorption by analogy to a boiled egg. It is generated using the Swiss ADME online server. It enables researchers to visualize and analyze ligand permeability characteristics, aiding in identifying promising candidates with favorable permeation properties in relevant biological systems such as the brain and intestinal tract. By leveraging the BOILED-Egg method and its associated plots, researchers can gain valuable insights into the permeability potential of ligands, contributing to the assessment of their pharmacokinetic properties and ultimately supporting the development of more effective and bioavailable drugs (Sheoran et al. 2023a; Kobayashi et al. 2002).

## Biosynthesis of hesperidin

Many researchers are currently using a method for producing the biochemical transformation of hesperidin. In a recently published 2021 by Victor et al., (Victor et al. 2021) a technique for extracting hesperidin from the *Citrus Sinensis* (L.) Osbeck was formulated to increase yields. The method entailed using the discarded peels of citrus fruit, separated,

and extracted using methanol. Using dichloroethane, the isolated chemical was crystallized in an aqueous solution. The amount of solvent was then lowered, and the mixture was treated to hot retrieval with methanol to achieve fresh citrus albedo. Further, to validate its components and structure, characterization techniques are utilized i.e., NMR, XRD, DSC and FTIR.

## Cytotoxicity by using MTT assay

The MTT test was used to assess active metabolic cells (Czylikowska et al. 2021). The IC<sub>50</sub> (the effective concentration of the tested medication at which a 50% growth decrease in cell growth is detected when compared to the untreated control) approach was employed in this research. An MTT assay was used to assess the *in-vitro* cytotoxicity of the drug against A549 cells acquired from NCCS Pune (Czylikowska et al. 2021; Carmichael et al. 1988). The cells were grown in Dulbecco's Modified Eagle's Medium (GIBCO), 10% FBS (Sigma Aldrich), and MTT (Sigma Aldrich). To finish the studies of the novel compound, the cells were grown overnight at 37 °C with 5% CO<sub>2</sub> in a conventional 96-well flat-bottomed plate containing 10<sup>4</sup> cells/well (Czylikowska et al. 2021). The medium was refilled the next day with 100 µL with medication supplied in varied quantities to the wells. After 24 h of incubation, 100 µL MTT was applied to each well for the next 4 h. A microplate reader was used to quantify the final absorbance at the analytical wavelength Hesperidin (595 nm for blue-violet insoluble formazan). The viability and cell cycle analysis findings were cn. All experiments were in triplicate (Table 4).

## Result and discussion

### Retrieval of active components of *Citrus latifolia*

Following a comprehensive analysis of the literature, 87 active components of *Citrus latifolia* were retrieved and subsequently acquired in the.sdf format. The smiles and molecular weights of the compounds are detailed in Table S1 (Supplementary material).

### Target prediction

In this work, two types of targets (those linked to lung cancer illness and those connected to *C. latifolia*) were gathered from several public databases such as DrugBank, Genecard, the NCBI database, and the literature service. According to literature and databases such as GENecards, DrugBank, and NCBI, there are 131 targets associated with *C. latifolia* and 24,879 targets associated with neurological disorders. Figure citrus shows a network representation of all of these

## Gene-gene interaction

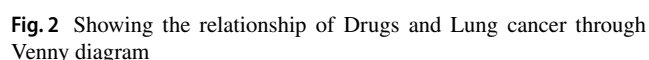


**Fig. 3** The GeneMANIA networks depict the biological interactions between genes of the targets



Protein Kinase D1 (PRKD1), PRKCE protein kinase C epsilon (PRKCE).

### Gene oncology & pathway analysis

A multitude of improved Biological Processes (BP), Molecular Functions (MF), Cellular components (CC), Protein class, and pathways were identified for five primary research objectives. Pathways study of targets were identified to be abundant in 5HT2 type receptor-mediated signaling route, Alpha adrenergic receptor signaling pathway, Alzheimer disease amyloid secretase pathway, Angiogenesis, Apoptosis signaling pathway, CCKR signaling map Cadherin signaling route, EGF receptor signaling pathway, endothelin signaling system, FGF signaling pathway, gonadotropin-releasing hormone receptor pathway, The Gq alpha and Go alpha-mediated route of heterotrimeric G-protein signaling The histamine H1 receptor-mediated signaling pathway Inflammation caused by chemokine and cytokine signaling Interleukin signaling pathway, JAK/STAT signaling pathway, Muscarinic acetylcholine receptor 1 and 3 signaling route, Oxytocin receptor-mediated signaling system, PDGF signaling pathway, Ras pathway, Thyrotropin releasing hormone receptor signaling pathway, VEGF signaling pathway, and Wnt signaling pathway, The EGFR (epidermal growth factor receptor) with the greatest degree (96.0) in the network was chosen for molecular docking. GO and Pathway enrichment studies indicate that EGFR participates in the pathways involved in angiogenesis and apoptotic signaling.

### Docking studies interpretation

Hesperidin exhibits a significantly higher GOLD score of 60.98 with EGFR (PDB ID: 6DUK), which depicts that it may possess better anti-cancer properties and could be an efficient candidate for treating lung cancer. (Fig. 4).

Hesperidin has H-bonds with LYS:745, ARG:841 and ALA:743 of EGFR. The docking results provide a platform for further pre-clinical evaluation. Table 1 shows the top 10 compounds with Gold Score. To further validate the GOLD score, Glide (Schrodinger) was utilized, which revealed an Xp Score of  $-9.433$  kcal/mol and a Glide energy of  $-70.911$  kcal/mol (Fig. 5A). Figure 5B describes the hydrogen bond interactions maintained throughout the 100 ns simulation. This finding suggests that Hesperidin possesses a higher binding affinity towards the target protein EGFR. The higher binding affinity towards the EGFR may have potential anti-cancer activity and be a promising agent for curing lung cancer.

### DFT analysis

The characteristics of the Hesperidin in donating and receiving electrons were investigated. Furthermore, the significant energy difference between HOMO and LUMO causes an unfavorable condition of electron transfer and reduces

**Table 1** Demonstrates the top 10 compounds as per GOLD Score

S.no	Compound name	GOLD score (Kcal/mol)
1	Hesperidin	60.98
2	Icariin	58.32
3	Rutin	58.09
4	Isoliquiritin apioside	57.83
5	Silymarin	57.52
6	Pectolinarin	55.16
7	Myricacitrin	53.53
8	Lichochalcone	53.35
9	Formononetin	52.97
10	Epicatchin gallate	52.42

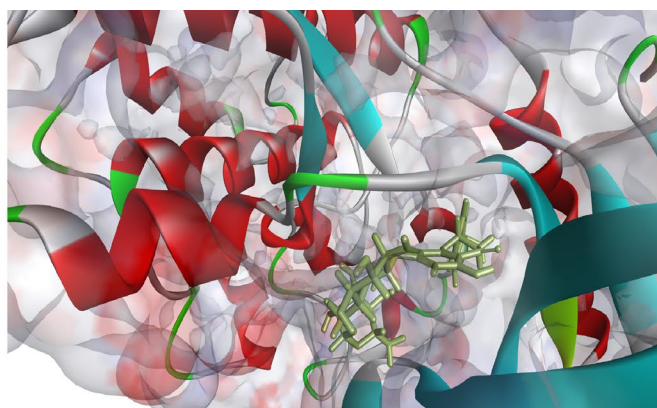
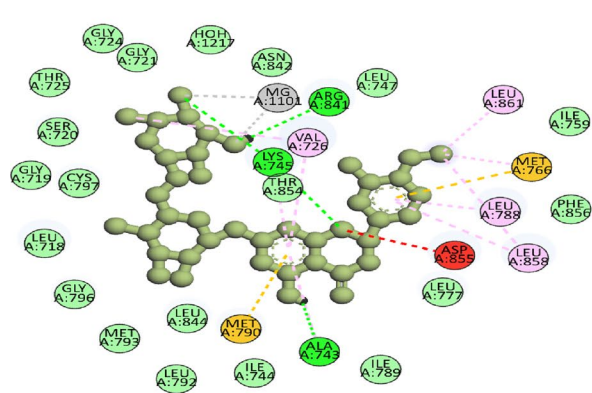


**Fig. 4** The two-dimensional and three-dimensional interactions between EGFR and Hesperidin are shown, with the green hue emphasizing hydrogen bonding. More precisely, there are hydrogen bonds localized at positions A: 745-LYS, A: 841-ARG, and A: 743-ALA

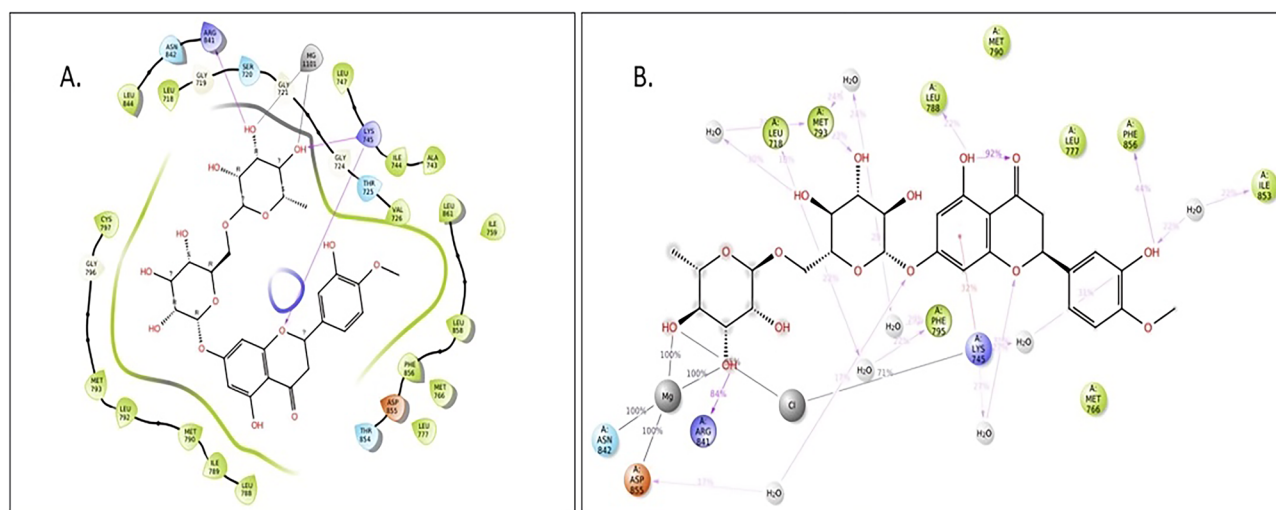


**Fig. 5** **A** Displays the docking complex with a Glide XP score of  $-9.433$  kcal/mol and a Glide energy of  $-70.911$  kcal/mol. The pink arrows represent the hydrogen bonds that exist between Hesperidin and EGFR. **B** Provides a detailed analysis of the specific interactions between every atom of Hesperidin and the protein locations. Con-

nectivity sustained for more than 10.0% of the simulation duration is shown in the visible route (0.00–100.01 ns). Given that individual residues can form several connections of the same kind with the same ligand atom, it is feasible for contact rates to surpass 100%

reactivity with protein. The present research found a low energy gap (HOMO–LUMO) for the Hesperidin compound, which indicates that the Hesperidin is more reactive (Fig. 6).

## ADME evaluation

ADME prediction is critical in finding and developing new drugs and attempting to forecast the pharmacokinetics of compounds (Rahmani et al. 2023). Tables 2 and 3 present the pharmacological characteristics of the compounds under investigation. These characteristics provide valuable information regarding the compounds' absorption, distribution, metabolism, and excretion properties, critical determinants of their pharmacological profiles. By considering ADME predictions alongside other evaluations, researchers can make informed decisions regarding the suitability and potential of these compounds as drug candidates.

The study exhibits values within an acceptable range, indicating their favorable pharmacological characteristics. Notably, Hesperidin falls within this range, suggesting its inherent permeability. Specifically, Hesperidin, as a chemical entity, demonstrates excellent pharmacokinetic properties. Consequently, this Hesperidin compound possesses good bioavailability and is a naive agent with significant potential. These findings highlight the promising nature of Hesperidin as a candidate for further exploration and development in the future.

This computational analysis offers a crucial foundation for pharmaceutical research, offering valuable insights for *in-vitro* and *in-vivo* studies. By exploring the multifaceted functions of Hesperidin, researchers can gain a

comprehensive understanding of its potential as a bioactive compound against lung cancer. This knowledge serves as a stepping-stone for devising informed strategies in utilizing Hesperidin for therapeutic purposes.

## BOILED Egg plot analysis

In addition to ADME prediction, the efficacy and safety of the compound can be compromised by unfavorable pharmacokinetic characteristics. However, Fig. 7 demonstrates the two favorable pharmacokinetic properties of the Hesperidin compound, as indicated by the Boiled Egg plot (Rahmani et al. 2023). This plot illustrates the ability absorbed in the gastrointestinal tract and its permeability across the Blood–Brain Barrier.

Notably, the Hesperidin molecule does not exhibit a moderate gastrointestinal absorption rate, & brain permeability depicts its positioning within the boiled egg in Fig. 7. Consequently, it can be inferred that Hesperidin demonstrates limited permeability in the brain and gastrointestinal tract. These observations suggest potential limitations regarding the compound's distribution and absorption in these regions.

Despite these considerations, Hesperidin has shown outstanding anti-cancer efficacy in our research. However, further investigation of this native molecule is required to confirm and elaborate the results of this study. Continued exploration will help ascertain the full potential of Hesperidin as a therapeutic agent and provide a more comprehensive understanding of its pharmacological properties.

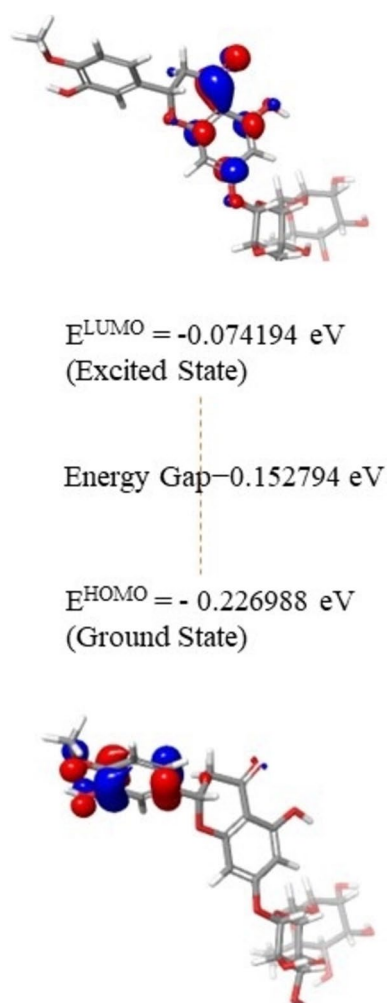


**Fig. 6** Presents the HOMO–LUMO energy levels of Hesperidin together with their corresponding transition strength

### Evaluation of molecular dynamics simulation

RMSD, RMSF, and hydrogen bonds are just a few of the metrics that were looked at to gauge the stability of the Hesperidin-EGFR protein complex and comprehend the nature of their interactions. The RMSD profile of the

Hesperidin-EGFR complex during a 100-ns molecular dynamics simulation in a solvent environment is shown in Fig. 8. Throughout the simulation, the RMSD values for the Hesperidin-EGFR complex remained relatively constant, ranging between 1.2 and 2.6 Å. Notably, in the initial and end phases of the simulation (15–20 & 90 ns), fluctuations in the RMSD were observed, which can be attributed to the movements of the activation loop in the EGFR protein (Devi et al. 2015). However, minimal changes were observed beyond this early stage, indicating a stable configuration of the Hesperidin-EGFR interaction. The consistent and averaged RMSD values throughout the 100-ns simulation suggest that the Hesperidin-EGFR complex maintained its structural integrity, and Hesperidin remained bound to the protein without dissociation.

Further analyses, such as RMSF and hydrogen bond assessments, can provide additional insights into the flexibility of the complex and the specific interactions involved in stabilizing the Hesperidin-EGFR binding. These findings contribute to our understanding of the molecular dynamics of the complex and provide valuable information for further investigations and potential drug development efforts.

In the present study, the RMSD analysis was employed to assess the stability of the protein backbone and the protein–ligand complex. To determine any alterations between the initial and final conformations, the RMSD was calculated, providing insights into the system's overall stability. The computed values of the RMSD indicated a consistent and steady profile for complex, with minimal fluctuations observed throughout the simulation. Figure 8 illustrates the structural stability of the protein–ligand complex, as revealed by the RMSD analysis. The trajectory analysis demonstrated that the initial and final structures maintained a stable conformation throughout the simulation, indicating an equilibrium state at 100 ns. This observation supports the idea that the protein–ligand complex remains structurally intact and exhibits promising dynamics throughout the simulation. These findings contribute to the overall understanding of the stability and potential activity of the protein–ligand complex. The steady and stable behavior observed in the RMSD analysis

**Table 2** ADME characteristics of the Hesperidin compound

S.No	Compound name	CYP_2C9 inhibition	CYP_2C19 inhibition	CYP_2D6 inhibition	Pgp inhibition	CYP_3A4 inhibition	CYP_2D6 substrate	CYP_3A4 substrate
1	Hesperidin	No	No	No	Inhibitor	No	No	No

**Table 3** Drug-like properties of Hesperidin

S.No	Name of compound	MW	Log p	HB donor	HB acceptor	No. of rotatable bond
1	Hesperidin	610.56	0.85	8	15	7

**Fig. 7** The boiled egg plot for Hesperidin demonstrates a deficiency in both blood–brain barrier permeability and gastrointestinal absorption processes

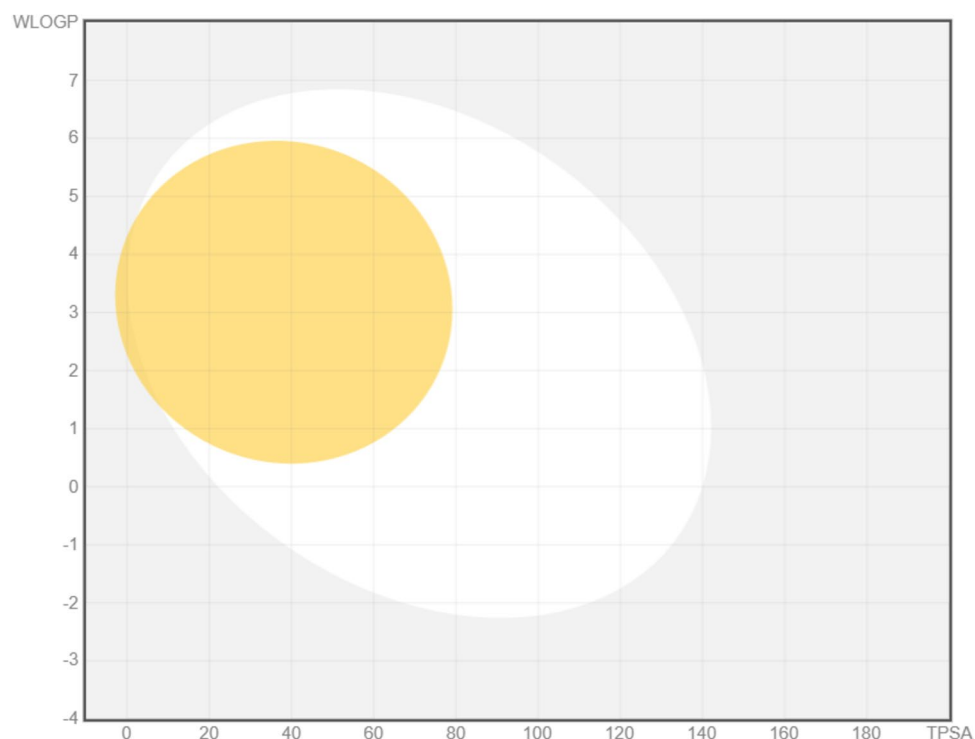
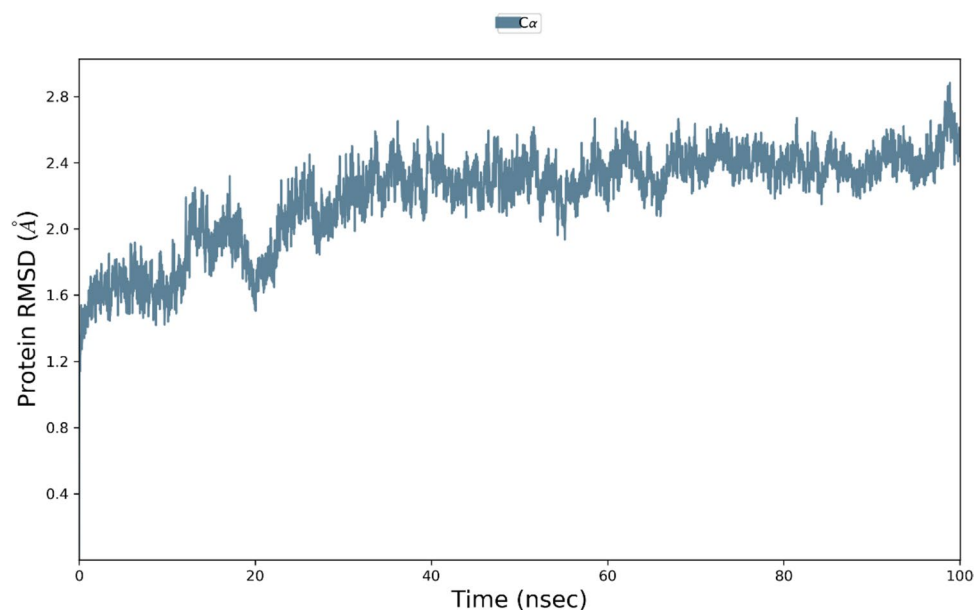


**Fig. 8** The Protein RMSD study conducted with Desmond methodology demonstrates consistent stability across the 100 ns simulation, with fluctuations ranging from 1.6 to 2.6 Å. The RMSD stabilizes at roughly 2.2 Å after 20 ns



suggests a favorable interaction between the protein and the ligand, highlighting the potential of the complex as an active entity. Further investigations and studies can build upon these results to elucidate the protein–ligand complex's specific interactions and functional implications.

The flexibility of the protein's activation loop was further investigated using RMSF analysis, as depicted in Fig. 9. Calculating the RMSF values for each residue along the simulation trajectory can identify protein regions with

higher flexibility and variation. These variations reflect the dynamic behavior of specific amino acid residues, particularly in loop and disorder regions of the protein. In the case of the protein–ligand complex, the RMSF of the ligand diagram (Fig. 9) reveals that specific residues exhibit significant fluctuations below 1 Å. However, it is essential to note that these residues are not involved in the binding process as identified in the docking studies. Hence, the observed fluctuations do not adversely affect

the stability of the protein-Hesperidin complex. Most residues exhibit lower changes, with RMSF values exceeding 1 Å, indicating stable behavior throughout the simulation. These additional analyses enhance the robustness of the findings and provide a comprehensive understanding of the protein–ligand interactions. The protein secondary structure (Fig. 10A) and Protein RMSF analysis (Fig. 10B) and hydrogen bond examination (Fig. 10C) collectively contribute valuable insights into the flexibility and stability of the protein–ligand contacts (Fig. 10D). The protein–ligand complex is the formation of hydrogen bonds. The hydrogen bond interaction analysis between Hesperidin and the EGFR protein is shown in Fig. 10C and D. During the simulation, five hydrogen bonds were formed between specific amino acid residues and the OH group of the Hesperidin molecule. These hydrogen bonds contribute to the stabilization of Hesperidin in its binding site, validating the findings from the docking studies.

The results demonstrate the compatibility of the observed fluctuations and hydrogen bonding patterns with the docking studies, supporting the overall reliability of the simulation and suggesting the favorable binding and stability of Hesperidin in its interaction with the EGFR protein.

### Ligand torsion profile and properties

The top panel (Fig. 10D) of the figures presents a two-dimensional representation of the compound, highlighting the rotatable bonds with assorted colors. During the simulation trajectory spanning from 0.00 to 100.01 ns (Sweta et al. 2019; The Gene Ontology Consortium 2017), each rotatable bond (RB) in the ligand (Alsaif et al. 2024) experienced conformational modifications are evident from the ligand torsions chart and other relevant features (Figs. 11 and 12). Each rotatable bond's torsion is illustrated using a dial plot and a corresponding color-coded bar plot. The dial plots visually display the changes in torsion angles throughout the

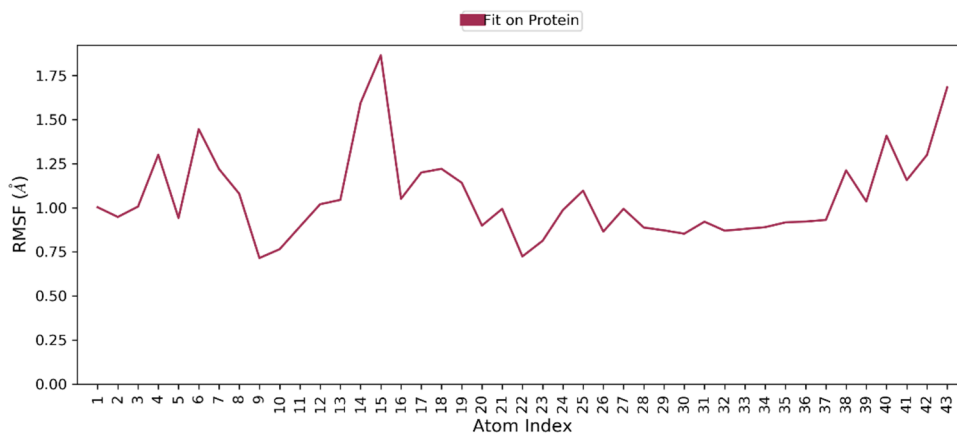
simulation, with the temporal progression radiating outward from the starting point at the Centre of the radial map. On the other hand, the bar plots summarize the torsion data by showing the probability density of each torsion angle.

Additionally, the figure showcases the potential energy associated with each rotatable bond by incorporating possible torsional information. The likely energy values are depicted on the chart's left Y-axis and measured in kcal/mol. By examining the histogram and torsion potential correlations, one can gain insights into the structural variations and anomalies experienced by the ligand to maintain a conformation suitable for binding to the protein. These comprehensive visual representations of the ligand's stable bonds and their conformational changes provide valuable information about its flexibility and how it adapts to the protein-binding environment throughout the simulation.

### Protein secondary structure

The simulation analysis includes monitoring the presence of beta- and alpha-strands as representative examples of protein secondary structural elements (SSE). The distribution of these SSEs across the protein structure is visualized in the plot above, with the residue index indicating their positions. The bottom plot provides a dynamic view of the SSE assignment for each residue over time, allowing for the observation of fluctuations in SSEs during the simulation. On the other hand, the plot below summarizes the SSE composition for each trajectory frame throughout the simulation. These visualizations can be seen in Figs. 13 and 14. By tracking the SSEs, we gain insights into the stability and structural changes of the protein during the simulation. The analysis helps us understand how the protein's secondary structure evolves and how it may interact with the ligand or other components within the system (Fig. 14).

**Fig. 9** Presents the Ligand Root Mean Square Fluctuation (RMSF), which maintains a constant value above 1.0 Å for the 100 ns simulation. Certain components have values below 1.0 Å, indicating their potential lack of involvement in docking interactions





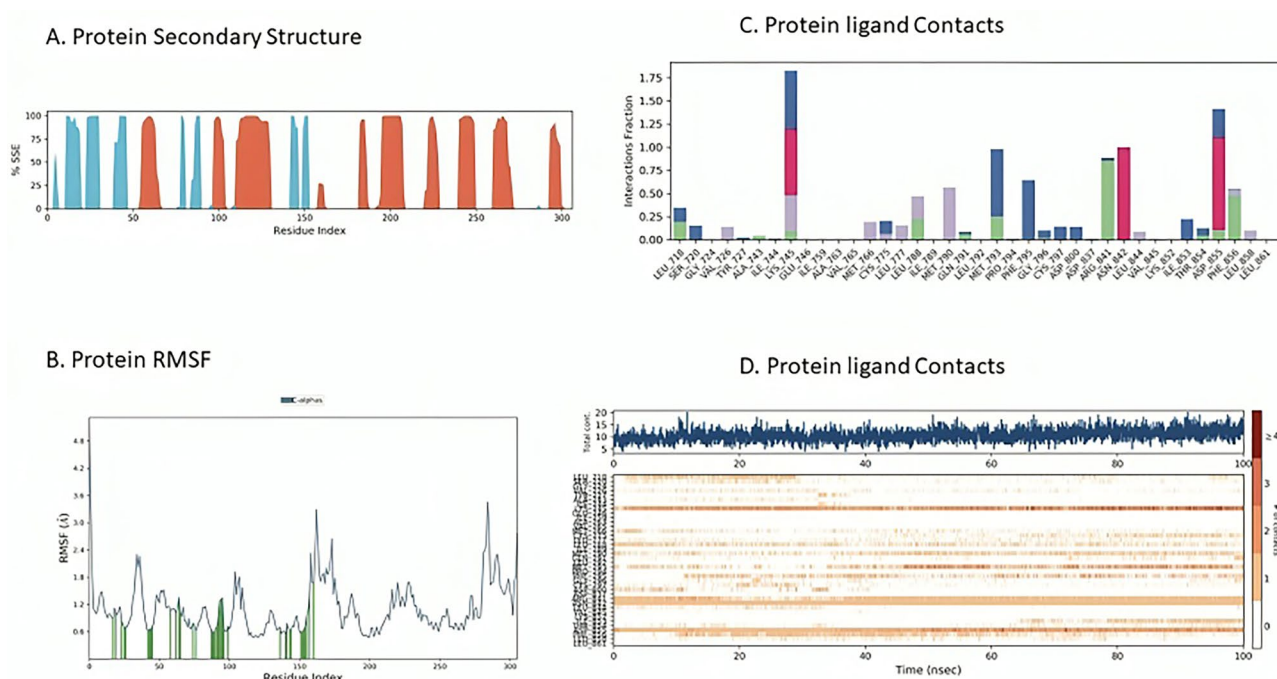


**Fig. 10** **A** Illustrates the secondary structure of the protein during the simulation. **B** displays the protein RMSF, providing a comprehensive analysis of the ligand–protein interactions at an atom-by-atom level. **C** and **D** Illustrating the chronological sequence of interactions between proteins and their ligands, encompassing several types of connections such as hydrogen bonds, hydrophobic interactions, ionic

bonds, and water bridges. The uppermost panel exhibits the temporal distribution of unique contacts between the protein and ligand, whilst the lower panel discloses the specific residues that engage with the ligand in each trajectory frame. The presence of dark orange residues indicates different sorts of interactions with the ligand. (“Identification of agonists specific to allatostatin type-C receptors”)

### Characterization of biosynthesized hesperidin

FTIR, NMR, XRD and DSC was employed to find the purity and structural analysis of hesperidin.

#### FTIR (Fourier transform infrared spectroscopy) analysis of hesperidin

By analyzing the peaks detected in the IR radiation band, the FTIR technique was used to determine the organic & inorganic parts of the materials. When exposed to FTIR analysis, each ingredient of the sample compounds was identified based on its peak frequency.

FTIR was used to establish the presence of many organic and inorganic elements inside the sample. Figure 15 shows the FTIR analysis findings, which provide vital information on the material’s chemical composition and structural properties.

It is crucial to remember, however, that FTIR has several limits. One of these disadvantages is that it cannot expose the metallic features of any chemical. NMR (Nuclear Magnetic Resonance) spectroscopy is an alternate approach for

analyzing metallic components. NMR spectroscopy is unbelievably valuable for studying the characteristics and structures of metal-containing compounds, as it provides extensive information on their coordination, oxidation state, and ligand interactions. A thorough knowledge of the sample’s chemical composition and characteristics may be attained by using the capabilities of FTIR for detecting inorganic and organic components and supplementing it with NMR for metallic details.

Several notable peaks were identified after analyzing the FTIR graph. A peak indicated the existence of C=C aromatic bonds at  $1565\text{ cm}^{-1}$ , whereas a peak characterized the presence of C=O bonds at  $1657\text{ cm}^{-1}$ . A peak at  $1064\text{ cm}^{-1}$  showed C–O stretching, whereas a peak at  $1065\text{ cm}^{-1}$  represented C–H bending. Notably, two heights were associated with C=C aromatic bonds, one of which appeared at  $1515\text{ cm}^{-1}$ . Similarly, two extremes linked with C=O bonds were identified, one of which occurred at  $1644\text{ cm}^{-1}$ .

FTIR examination also showed other peaks, including one at  $2361\text{ cm}^{-1}$ , indicating the presence of carbon dioxide (CO<sub>2</sub>). A rise revealed the existence of an OH group at  $3675\text{ cm}^{-1}$ , which correlated to C–H stretching.

## Ligand Torsion Profile

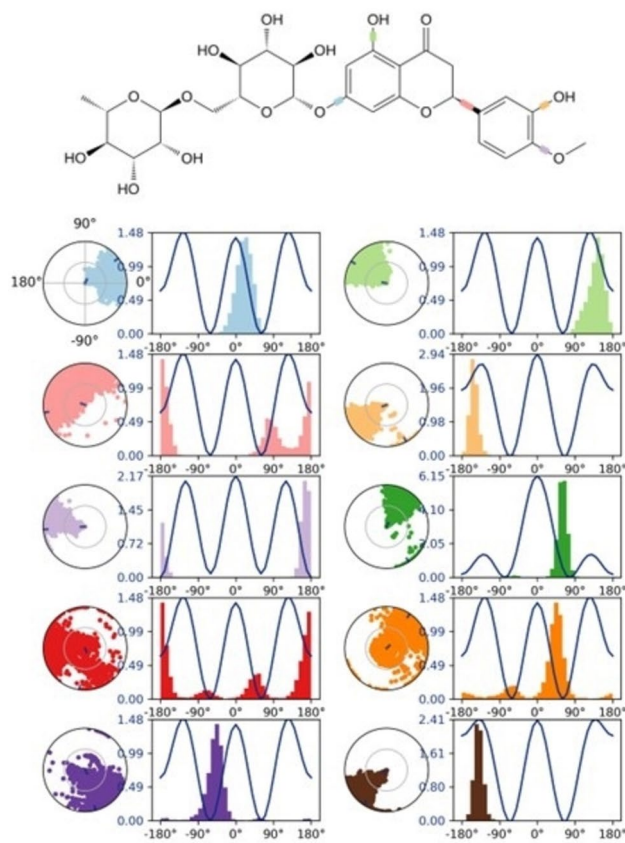


**Fig. 11** Illustrates both the 2-D and 3-D torsional patterns of the complex

The chemical structure of the molecule under inquiry shared identical components, according to a detailed analysis of the FTIR spectrum. The observed peaks matched the predicted molecular properties of Hesperidin, indicating the existence of functional groups and providing vital information about its composition.

### NMR analysis of hesperidin

NMR (Nuclear Magnetic Resonance) spectroscopy is a powerful source for analyzing the structure of substances by monitoring & measuring nuclear spin interactions in a strong magnetic field. As shown in Fig. 16, this analytical approach gives valuable insights into materials' physical, chemical, and biological properties.

By analyzing the chemical shifts, coupling patterns, and relaxation periods in the NMR spectrum, helpful information

on the analyzed substances' molecular structure, connectivity, and conformation may be gleaned.

5-hydroxy-2-(3-hydroxy-4-methoxyphenyl)-7-(((2R,3R,4S,5S,6R)-3,4,5-trihydroxy-6-(((2S,3R,4R,5R,6S)-3,4,5-trihydroxy-6-methyltetrahydro-2H-pyran-2-yl)oxy) methyl)tetrahydro-2H-pyran-2-yl)oxy) chroman-4-one (HESPERIDIN).

$^1\text{H}$  NMR (400 MHz,  $\text{DMSO}-d_6$ )  $\delta$  12.02 (s, 1H), 9.10 (s, 1H), 6.95 (s, 3H), 6.15 (s, 2H), 5.49 (s, 1H), 5.40 (s, 1H), 5.18 (s, 2H), 4.96 (s, 1H), 4.64 (d,  $J=29.7$  Hz, 2H), 4.52 (s, 2H), 3.81 (s, 1H), 3.77 (s, 3H), 3.63 (s, 1H), 3.54 (s, 1H), 3.43 (s, 3H), 3.24 (s, 3H), 3.14 (s, 2H), 2.77 (s, 1H), 1.07 (s, 3H);  $^{13}\text{C}$  NMR (100 MHz,  $\text{DMSO}-d_6$ )  $\delta$  197.49, 165.59, 163.46, 163.00, 131.34, 118.42, 114.61, 103.77, 101.06, 99.84, 96.84, 96.00, 78.84, 76.73, 75.97, 73.44, 72.53, 71.16, 70.73, 70.05, 68.78, 56.13, 18.30.

### DSC analysis of hesperidin

A DSC (Differential Scanning Calorimetry) device with thermal expansion capability was used to determine Hesperidin. The device was calibrated before the study using a standard reference material to guarantee precise readings.

A 1.90 mg sample was carefully measured and placed in an aluminum testing crucible for analysis. The crucible was then firmly sealed, and the sample was heated in an atmosphere of nitrogen ( $\text{N}_2$ ). The temperature was raised by 10  $^\circ\text{C}$  every minute until it reached 300  $^\circ\text{C}$ .

Figure 17 shows the findings of the DSC analysis of Hesperidin. These diagrams depict the thermal behavior of the compounds, including the typical melting ranges and accompanying thermal events.

These findings add to a thorough understanding of the physical properties of the compounds and can help in various applications, including pharmaceutical formulation and process optimization.

### XRD analysis of hesperidin

To analyze the form or type of the specimens, the XRD (X-ray Diffraction) technique was used, which distinguished between crystalline and amorphous structures. The XRD pattern can provide vital information about the sample's structural features.

If the resultant XRD chart shows crisp and clear peaks, it suggests that the material is crystalline. These peaks represent the regular arrangement of atoms in a crystal lattice, and their locations and intensities reveal information about the crystal structure.

## Ligand Properties

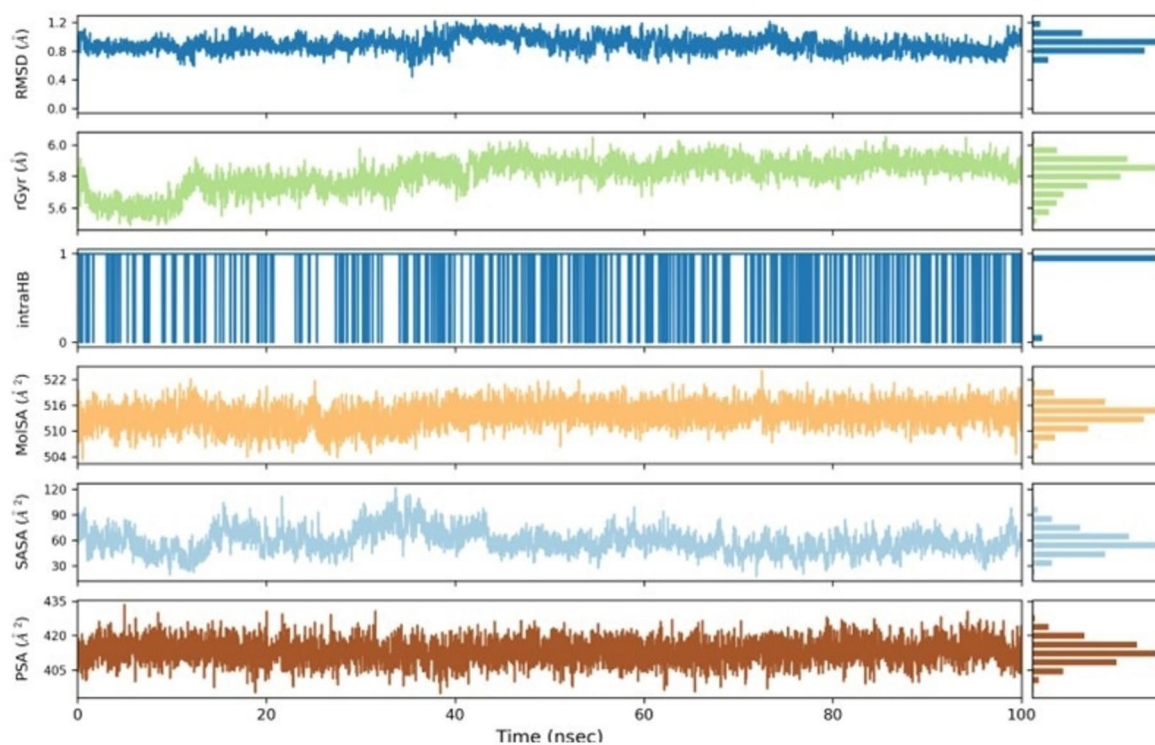


**Fig. 12** Reports the RMSD, RGYR, IntraHB, MolSA, SASA, and PSA measurements

**Fig. 13** Illustrating the secondary protein structures. The graph above illustrates the Standardised Statistical Error (SSE), whereas the picture below emphasizes the SSE content for each trajectory step in the experiment

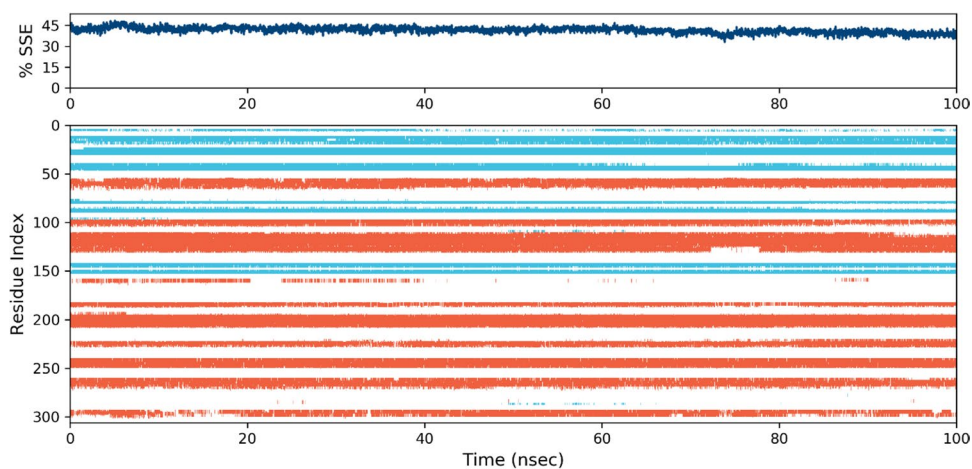




**Fig. 14** Presenting The protein analysis consists of 288 amino acid residues in chain A, 4653 total charged atoms, 2300 heavy atoms, and a net charge of +5

#### Protein Information

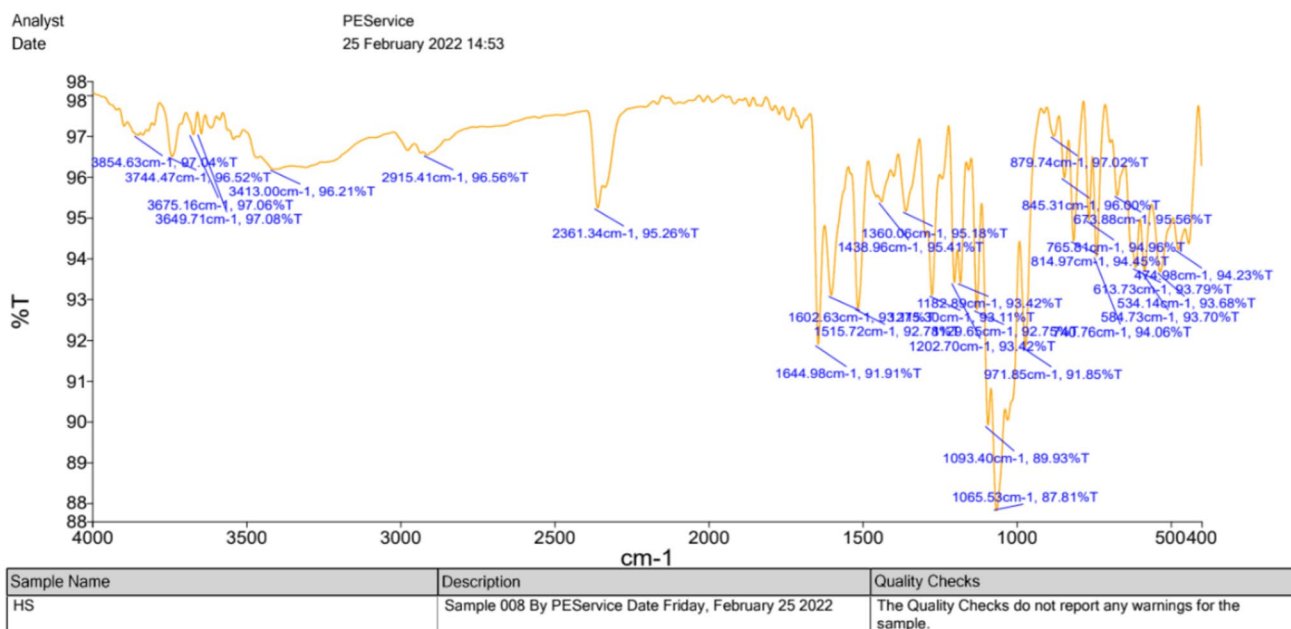
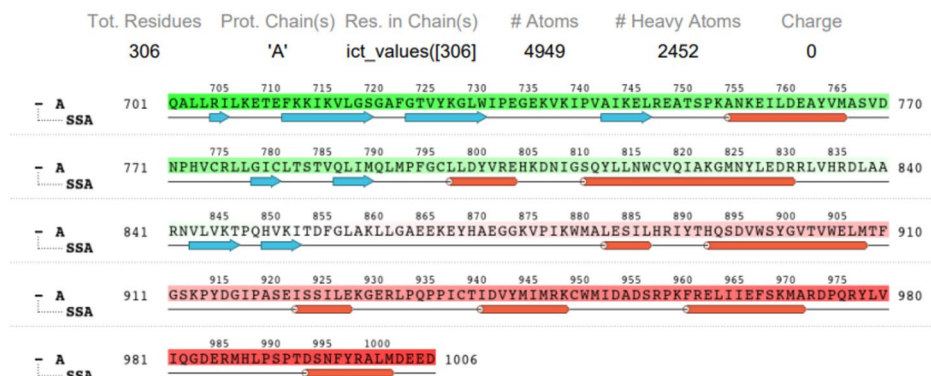


**Fig. 15** Hesperidin was analyzed using FTIR, which showed numerous unique peaks: C-H bending at  $1065\text{ cm}^{-1}$ , C=C aromatic at  $1515\text{ cm}^{-1}$ , C=O at  $1644\text{ cm}^{-1}$ ,  $\text{CO}_2$  at  $2361\text{ cm}^{-1}$ , C-H stretching at

$2915\text{ cm}^{-1}$ , and OH group at  $3675\text{ cm}^{-1}$ . The research verifies that the molecule incorporates these constituents within its molecular framework

Conversely, if the XRD graph shows a featureless or flat profile, the sample is amorphous. The lack of sharp peaks in the XRD pattern suggests a lack of long-range order in the atomic arrangement, which is typical of amorphous materials.

The XRD data for Hesperidin are shown in Fig. 18, respectively. The diffraction peaks at  $11^\circ$ ,  $19.9^\circ$ ,  $23.2^\circ$ , and  $25.1^\circ$  could be indexed to (2600), (2800), (1900), and (1400) planes. These images depict the XRD patterns, which reflect the crystallinity of the materials.

This information is crucial to grasp the atomic structure of the molecules and has implications, including medicinal investigation, materials science, and quality assurance.

#### Biological assay

This work employed the MTT cell viability test to assess the cytotoxic activity potential of hesperidin compounds at various concentrations. Figure 19 shows the dose-dependent reduction in cell viability that was seen while

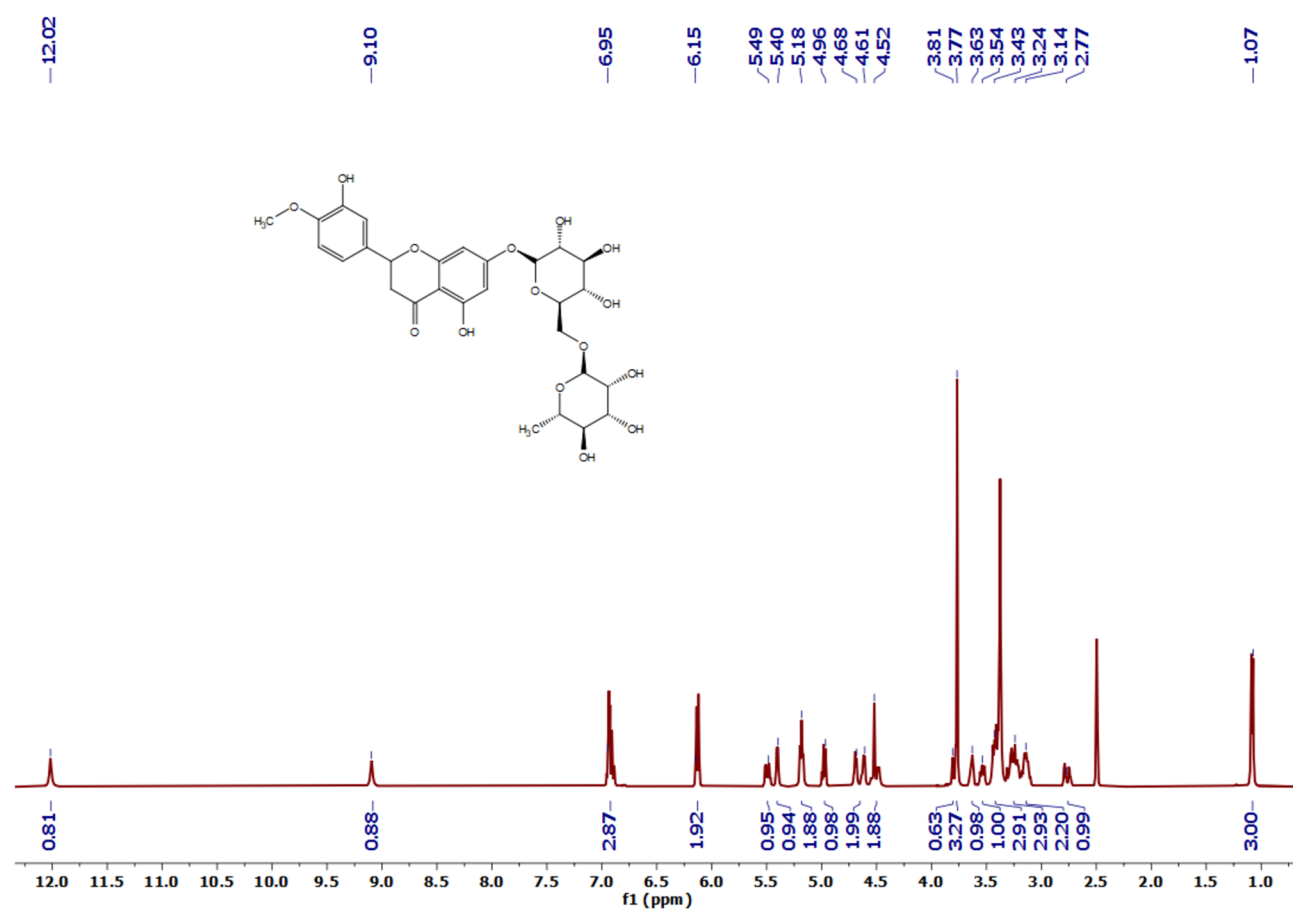
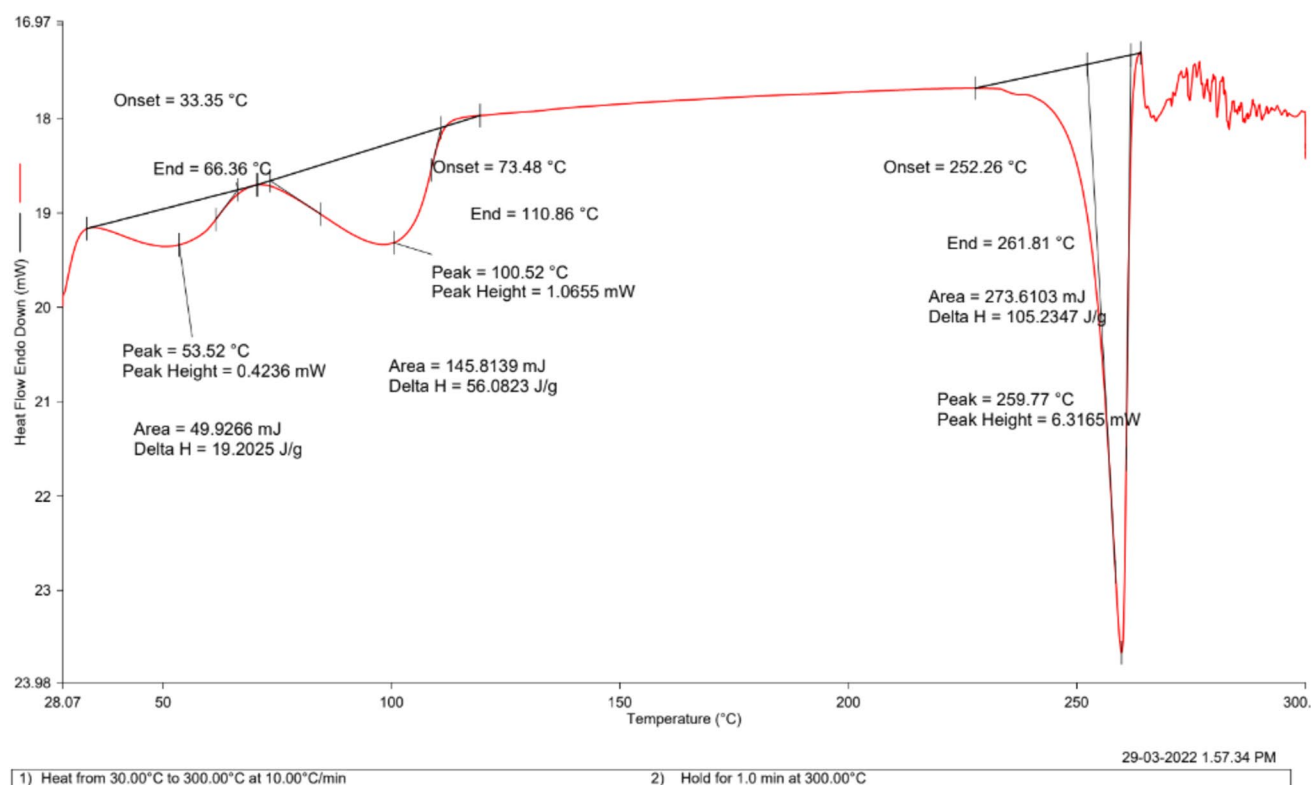


**Fig. 16** Demonstrates Hesperidin's NMR spectra

using hesperidin. The A549 cells showed remarkable sensitivity to hesperidin at a concentration of 34.25  $\mu\text{g}/\text{ml}$ . This research leads us to believe that hesperidin has cytotoxic properties (Table 4).

## Conclusion

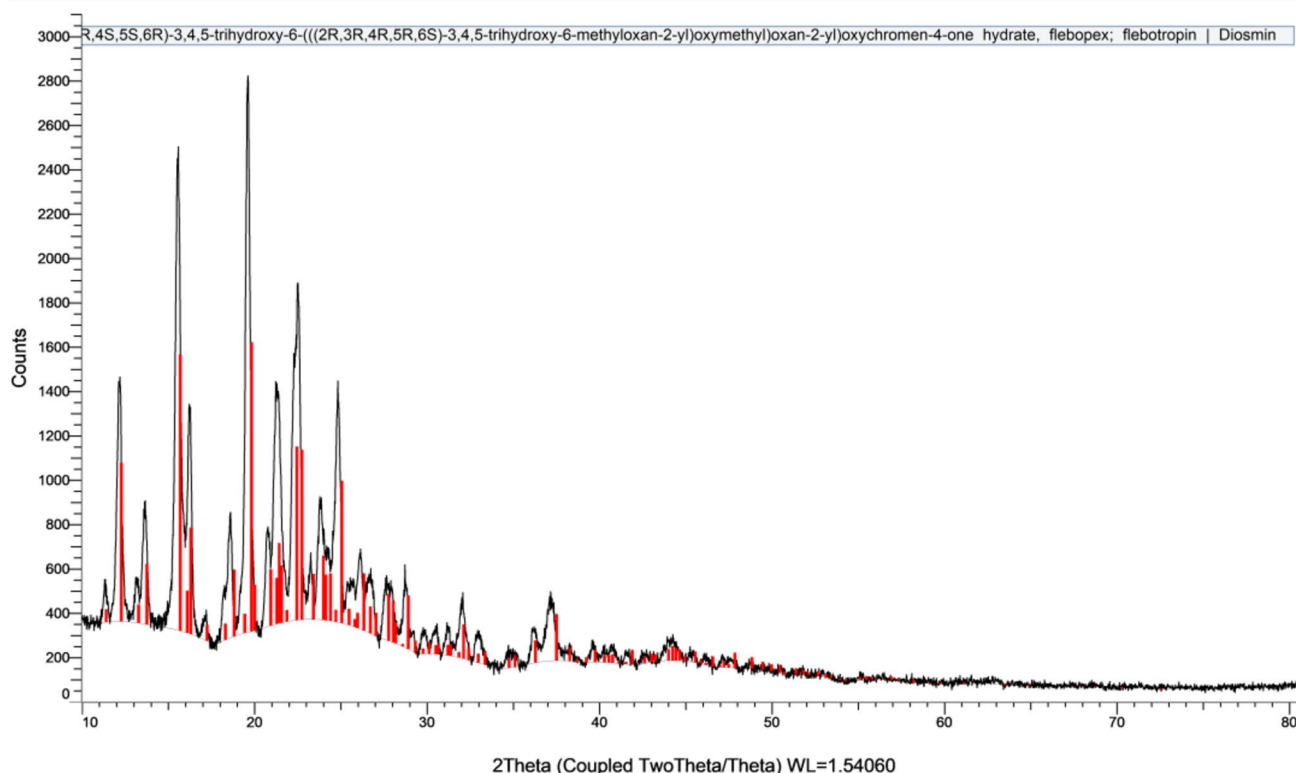
This work employed in-silico and in-vitro methodologies to uncover intriguing small compounds as potential therapeutic modalities for lung cancer. Further, GOLD is utilized for docking, and GLIDE is employed to validate the compound, i.e., Hesperidin docked with EGFR, having the highest score



**Fig. 17** Showing The DSC graph of Hesperidin. The differential scanning calorimetry (DSC) data reveals an exothermic reaction at 100 °C, representing crystallisation. The endothermic peak seen at around 259 °C is indicative of the melting point of Hesperidin

at 60.98 (Gold Score) and Xp Score (− 9.43 kcal/mol) and glide score − 70.911 kcal/mol. Furthermore, ADME, DFT, and Molecular dynamics were used to ensure the stability of protein complex structures. The RMSD, RMSF, and

hydrogen bond interaction results indicate that the complex is highly stable across the simulation time frame (100 ns). Our study included *In-vitro* cytotoxicity investigation, which revealed that Hesperidin had an IC<sub>50</sub> value of 34.25 µg/ml.

**(Coupled TwoTheta/Theta)**

**Fig. 18** Presenting the X-ray diffraction yields of Hesperidin. The composition of the material is classified using an X-ray diffraction (XRD) graph. The substance is classified as crystalline if it has

distinct peaks. The polycrystalline material exhibits distinct peaks, namely at  $11^\circ$ ,  $19.9^\circ$ ,  $23.2^\circ$ , and  $25.1^\circ$ , which can be attributed to the (2600), (2800), (1900), and (1400) planes, respectively

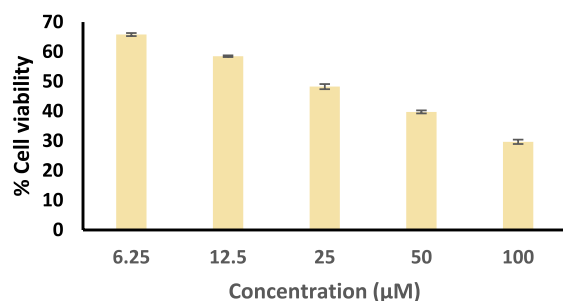


**Fig. 19** Illustrates the cytotoxic effects of Hesperidin on A549 lung cancer cell line

The overall ramification of this work improves our comprehension of lung cancer biology, locating possible therapeutic targets, and investigating innovative therapeutic approaches. By shedding light on the molecular pathways implicated in lung cancer, it paves the way for further investigation on how to increase the bioavailability and target specificity of hesperidin in in vivo environment and the development of tailored treatment.

**Table 4** Statistical analysis of MTT assay

Conc	Control	Treated	Difference	Viability	Average	SD	SEM
6.25	0.192	0.065	0.127	66.14583	65.79861111	0.88524644	0.51109727
	0.192	0.064	0.128	66.66667			
	0.192	0.068	0.124	64.58333			
12.5	0.192	0.079	0.113	58.85417	58.50694444	0.49104638	0.28350576
	0.192	0.081	0.111	57.8125			
	0.192	0.079	0.113	58.85417			
25	0.192	0.099	0.093	48.4375	48.26388889	1.49345925	0.8622491
	0.192	0.103	0.089	46.35417			
	0.192	0.096	0.096	50			
50	0.192	0.115	0.077	40.10417	39.75694444	0.88524644	0.51109727
	0.192	0.118	0.074	38.54167			
	0.192	0.114	0.078	40.625			
100	0.192	0.135	0.057	29.6875	29.6875	1.27577591	0.73656956
	0.192	0.132	0.06	31.25			
	0.192	0.138	0.054	28.125			
Conc	Viability	SEM					
6.25	65.79	0.511097					
12.5	58.5	0.283506		IC <sub>50</sub> = 34.25			
25	48.26	0.862249					
50	39.75	0.511097					
100	29.68	0.73657					

**Acknowledgements** We thank the School of Bioengineering and Biosciences at Lovely Professional University in Jalandhar and Thyme Phyto BioMed Pvt. Ltd. Hisar, Haryana.

**Author contributions** Sugunakar Vuree (SV) conceptualized the idea, developed the methodology flow, and edited and proofread. Swati Arora (SA) is writing the early and final versions of the text. Molecular Docking, ADME, Drug-like characteristics, and Boiled Egg plots were carried out by Sumit Sheoran (SS) and (SA). Desmond (Schrodinger) Molecular simulation was carried out by Neeraj Kumar (NK). Gold docking software is being provided by Naidu Subbarao (NS). Dhamodharan Prabhu (DP) provided Glide docking and DFT. Proofreading: Himanshu Singh (HS), Smita C. Pawar (SCP) and DP.

**Data availability** No datasets were generated or analysed during the current study.

## Declarations

**Conflict of interest** The authors declare no competing interests.

**Ethical approval** None.

## References

- Aggarwal V, Tuli HS, Thakral F, Singhal P, Aggarwal D, Srivastava S, Pandey A, Sak K, Varol M, Khan MA, Sethi G (2020) Molecular mechanisms of action of hesperidin in cancer: recent trends and advancements. *Exp Biol Med* (Maywood) 245:486–497. <https://doi.org/10.1177/1535370220903671>
- Agu PC, Afiukwa CA, Orji OU, Ezech EM, Ofoke IH, Ogbu CO, Ugwuja EI, Aja PM (2023) Molecular docking as a tool for the discovery of molecular targets of nutraceuticals in diseases management. *Sci Rep* 13:13398. <https://doi.org/10.1038/s41598-023-40160-2>
- Almeida CM, Nascimento EC, Martins JB, Mota TH, Oliveira DM, Gatto CC (2023) Crystal Design, antitumor activity and molecular docking of novel palladium(II) and gold(III) complexes with a thiosemicarbazone ligand. *Int J Mol Sci*. <https://doi.org/10.3390/ijms241411442>
- Alsaif G, Tasleem M, Rezgui R, Alshaghda K, Saeed A, Saeed M (2024) Network pharmacology and molecular docking analysis of Catharanthus roseus compounds: implications for non-small cell lung cancer treatment. *J King Saud Univ Sci* 36:103134. <https://doi.org/10.1016/j.jksus.2024.103134>
- Arora S, Sheoran S, Basu T, Subbarao N, Upadhyay AK, Vuree S (2023) Abstract 5343: evaluating the screened polyphenolics molecules as potential chemosensitizers against the oncogenic signaling proteins in lung cancer. *Cancer Res* 83:5343. <https://doi.org/10.1158/1538-7445.AM2023-5343>
- Carmichael J, Mitchell JB, DeGraff WG, Gamson J, Gazdar AF, Johnson BE, Glatstein E, Minna JD (1988) Chemosensitivity testing of human lung cancer cell lines using the MTT assay. *Br J Cancer* 57:540–547. <https://doi.org/10.1038/bjc.1988.125>
- Czylkowska A, Szczesio M, Raducka A, Rogalewicz B, Kręcis P, Czarnecka K, Szymański P, Pitucha M, Pawlak T (2021) Cytotoxic activity against A549 human lung cancer cells and ADMET analysis of new pyrazole derivatives. *Int J Mol Sci*. <https://doi.org/10.3390/ijms22136692>
- Daina A, Michielin O, Zoete V (2017) SwissADME: a free web tool to evaluate pharmacokinetics, drug-likeness and medicinal chemistry friendliness of small molecules. *Sci Rep* 7:42717. <https://doi.org/10.1038/srep42717>



- Devi KP, Rajavel T, Nabavi SF, Setzer WN, Ahmadi A, Mansouri K, Nabavi SM (2015) Hesperidin: a promising anticancer agent from nature. *Ind Crops Prod* 76:582–589. <https://doi.org/10.1016/j.indcrop.2015.07.051>
- Gadgeel SM, Ramalingam SS, Kalemkerian GP (2012) Treatment of lung cancer. *Radiol Clin North Am* 50:961–974. <https://doi.org/10.1016/j.rcl.2012.06.003>
- Kobayashi T, Nakata T, Kuzumaki T (2002) Effect of flavonoids on cell cycle progression in prostate cancer cells. *Cancer Lett* 176:17–23. [https://doi.org/10.1016/S0304-3835\(01\)00738-8](https://doi.org/10.1016/S0304-3835(01)00738-8)
- Mostafavi S, Ray D, Warde-Farley D, Grouios C, Morris Q (2008) GeneMANIA: a real-time multiple association network integration algorithm for predicting gene function. *Genome Biol* 9:S4. <https://doi.org/10.1186/gb-2008-9-s1-s4>
- Muthumanickam S, Indhumathi T, Boomi P, Balajee R, Jeyakanthan J, Anand K, Ravikumar S, Kumar P, Sudha A, Jiang Z (2020) In-silico approach of naringin as potent phosphatase and tensin homolog (PTEN) protein agonist against prostate cancer. *J Biomol Struct Dyn*. <https://doi.org/10.1080/07391102.2020.1830855>
- Panche AN, Diwan AD, Chandra SR (2016) Flavonoids: an overview. *J Nutr Sci*. <https://doi.org/10.1017/jns.2016.41>
- Patidar K, Panwar U, Vuree S, Sweta J, Sandhu MK, Nayariseri A, Singh SK (2019) An in-silico approach to identify high affinity small molecule targeting m-TOR inhibitors for the clinical treatment of breast cancer. *Asian Pacific J Cancer Prev*. <https://doi.org/10.31557/APJCP.2019.20.4.1229>
- Pranweerapaiboon K, Garon A, Seidel T, Janta S, Plubrukarn A, Chaithirayanon K, Langer T (2022) In vitro and in-silico studies of holothurin A on androgen receptor in prostate cancer. *J Biomol Struct Dyn* 40:12674–12682. <https://doi.org/10.1080/07391102.2021.1975562>
- Rahmani AH, Babiker AY, Anwar S (2023) Hesperidin, a bioflavonoid in cancer therapy: a review for a mechanism of action through the modulation of cell signaling pathways. *Molecules*. <https://doi.org/10.3390/molecules28135152>
- Ru J, Li P, Wang J, Zhou W, Li B, Huang C, Li P, Guo Z, Tao W, Yang Y, Xu X, Li Y, Wang Y, Yang L (2014) TCMSP: a database of systems pharmacology for drug discovery from herbal medicines. *J Cheminform* 6:13. <https://doi.org/10.1186/1758-2946-6-13>
- Seer, No title, (n.d.). <https://seer.cancer.gov/statfacts/html/prost.html>
- Sheoran S, Arora S, Pilli G (2022) Lipid based nanoparticles for treatment of cancer. *Heliyon* 8:e09403
- Sheoran S, Arora S, Basu T, Negi S, Subbarao N, Kumar A, Singh H, Prabhu D, Kumar A, Kumar N, Vuree S (2023) In-silico analysis of Diosmetin as an effective chemopreventive agent against prostate cancer : molecular docking, validation, dynamic simulation and pharmacokinetic prediction-based studies. *J Biomol Struct Dyn*. <https://doi.org/10.1080/07391102.2023.2250451>
- Sheoran S, Arora S, Basu T, Subbarao N, Upadhyay AK, Vuree S (2023) Abstract 5342: assessment of polyphenolic secondary metabolites and small molecules against the xenobiotic metabolic and cell cycle regulatory proteins in prostate cancer. *Cancer Res* 83:5342. <https://doi.org/10.1158/1538-7445.AM2023-5342>
- Sheoran S, Arora S, Singh H, Kumar A, Vuree S (2023) Characterisation, development and validation of UV spectrophotometric technique for the determination of Diosmetin in bulk and nano-formulations. *Results Chem*. <https://doi.org/10.1016/j.rechem.2023.100972>
- Siegel RL, Miller KD, Jemal A (2016) Cancer statistics. *CA Cancer J Clin* 66(2016):7–30. <https://doi.org/10.3322/caac.21332>
- Sweta J, Khandelwal R, Srinitha S, Pancholi R, Adhikary R, Ali MA, Nayariseri A, Vuree S, Singh SK (2019) Identification of high-affinity small molecule targeting IDH2 for the clinical treatment of acute myeloid leukemia. *Asian Pacific J Cancer Prev*. <https://doi.org/10.31557/APJCP.2019.20.8.2287>
- The Gene Ontology Consortium (2017) Expansion of the gene ontology knowledgebase and resources. *Nucleic Acids Res* 45:D331–D338. <https://doi.org/10.1093/nar/gkw1108>
- Victor MM, David JM, Cortez MVM, Leite JL, da Silva GSB (2021) A high-yield process for extraction of hesperidin from orange (*Citrus sinensis* L. Osbeck) peels waste, and its transformation to diosmetin, A valuable and bioactive flavonoid. *Waste Biomass Valorization* 12:313–320
- Wee P, Wang Z (2017) Epidermal growth factor receptor cell proliferation signaling pathways. *Cancers (Basel)*. <https://doi.org/10.3390/cancers9050052>
- Yadav M, Khandelwal R, Mudgal U, Srinitha S, Khandekar N, Nayariseri A, Vuree S, Singh SK (2019) Identification of potent VEGF inhibitors for the clinical treatment of glioblastoma, a virtual screening approach. *Asian Pacific J Cancer Prev*. <https://doi.org/10.31557/APJCP.2019.20.9.2681>
- Yao L, Zhang X, Huang C, Cai Y, Wan CC (2023) The effect of citrus aurantium on non-small-cell lung cancer: a research based on network and experimental pharmacology. *Biomed Res Int* 2023:6407588. <https://doi.org/10.1155/2023/6407588>

**Publisher's Note** Springer Nature remains neutral with regard to jurisdictional claims in published maps and institutional affiliations.

Springer Nature or its licensor (e.g. a society or other partner) holds exclusive rights to this article under a publishing agreement with the author(s) or other rightsholder(s); author self-archiving of the accepted manuscript version of this article is solely governed by the terms of such publishing agreement and applicable law.



# Betulin: a novel triterpenoid anti-cancerous agent targeting cervical cancer through epigenetic proteins

Satbir Kour<sup>1</sup> · Indrani Biswas<sup>2</sup> · Sumit Sheoran<sup>1</sup> · Swati Arora<sup>1</sup> · Anjuvan Singh<sup>1</sup> · Dhamodharan Prabhu<sup>3</sup> · Smita C. Pawar<sup>4</sup> · Shyam Perugu<sup>5</sup> · Sugunakar Vuree<sup>6,7</sup>

Received: 1 January 2024 / Accepted: 6 July 2024

© The Author(s), under exclusive licence to Springer Nature Switzerland AG 2024

## Abstract

Worldwide, cervical cancer (CCa) is a major killer of women. As the conventional drugs used to treat cervical cancer are expensive and expose severe side effects, there is a growing demand to search for novel modifications. Therefore, in the current investigation employing a bioinformatic approach, we explored triterpenoids for their anti-cancer efficacy by targeting cervical cancer epigenetic proteins, namely DNMT3A, HDAC4, and KMT2C. The study utilized molecular docking, ADMET assay, Molecular Dynamic simulation, and DFT calculation to unveil Betulin (BE) as the potential lead compound. Comparative analysis with that standard drug indicated that BE has a better glide score with the target protein KM2TC (−9.893 kcal/mol), HDAC4 (−9.720 kcal/mol), and DNMT3A (−7.811 kcal/mol), which depicts that BE could be a potent inhibitor of these three epigenetic proteins and exhibits favorable pharmacokinetic, pharmacodynamics and toxicity properties. Molecular Dynamics simulation revealed noteworthy structural stability and compactness. DFT analysis revealed higher molecular activity of BE and showed the most increased kinetic stability ( $\delta E = 0.254647$  eV). Further, we employed In vitro analysis through MTT assay and found that BE has IC<sub>50</sub> of 15 µg/ml. In conclusion, BE can potentially treat CCa upon further investigations using in vivo models for better understanding.

**Keywords** Triterpenoids · Epigenetic proteins · Molecular docking · MD simulation · DFT calculations · Betulin

## Introduction

Cervical cancer (CCa) is one of the most prevalent forms of gynecological malignancies, accounting for the fourth leading cause of death in women [1]. CCa is categorized in several stages per the International Federation of Obstetricians and Gynecologists classifications, wherein, in stage I, the uterine alongside cervical tissues to the inner layers are affected. Stage II, which is restricted to the pelvis, is also detected in adjacent tissues like the vagina. Stage III: the disease spreads to the pelvic wall and includes tumor cells in the lower vaginal region. At this point, the tumor affects the kidney and results in hydronephrosis. The rectum and bladder are also involved in stage IVA, but the malignancy does not impact other body parts [2].

The deep causal route in cervical malignancy can be traced to the presence of diversified and versatile pathogenic molecules. The pathogenesis of CCa is attributed to one of the most fundamental factors, i.e., human papillomavirus (HPV), which plays a predominant role in its transformation and progression. Viral E6 and E7 are some

✉ Sugunakar Vuree  
sugunakarvuree@gmail.com

<sup>1</sup> School of Bioengineering and Biosciences, Lovely Professional University, Jalandhar, Punjab, India

<sup>2</sup> Mahatma Gandhi Medical Advanced Research Institute, Sri Balaji Vidyapeeth (Deemed-to-Be University), Puducherry, India

<sup>3</sup> Centre for Drug Discovery, Department of Biotechnology, Karpagam Academy of Higher Education, Coimbatore 641021, India

<sup>4</sup> Department of Genetics and Biotechnology, Osmania University, Hyderabad, India

<sup>5</sup> Department of Biotechnology, NIT Warangal, Hyderabad, India

<sup>6</sup> Department of Biotechnology, Vignan's Foundation for Science, Technology & Research, Vadlamudi, Guntur 522213, India

<sup>7</sup> Virchow Biotech Pvt Ltd, Manufacturing and R&D Facilities, Survey No.172 Part, Gagillapur, Hyderabad 500 043, India

of the crucial proteins of HPV, which alter the chromosomal orientation or landscape and promote the tumorigenic phenotype. Additionally, extrachromosomal inheritance, also coined as epigenetics, heuristically changes the fate of cells. In this regard, the existing epigenetic modifications methylation, demethylation, acetylation, or deacetylation are fascinating targets in anti-tumor therapeutics. Among the current epigenetic markers, KM2TC, HDAC4, and DNMT3A are prudent ailments involved in the pathogenesis toward the malignant progression of cervical [3]. These molecules regulate the genotype; hence, an altered fate of phenotypic expression is inevitable [4]. For example, methylation is involved in the propagation of the tumorigenesis process via repression of tumor suppressor genes or elevated expression of proto-oncogenes in most cancers, including cervical [5]. Interestingly, HDAC acetylase inhibitors have gained as intriguing anti-cancer therapeutics since they have exhibited cytotoxic effects against cancer cells without affecting normal cells. Furthermore, epigenetic inhibitory pharmaceuticals arrested cell proliferation via induction of apoptosis mediated by cell cycle arrest or chromosomal fragmentation against cancer cells *in vitro* and *in vivo* models.

Unlike other gynecological cancers, the prime route of treating CCa is chemotherapy, following surgical resection and radiation therapy. As of now, cisplatin, carboplatin, or Paclitaxel (taxol) remain the gold standard chemotherapeutic agent against most cancers, including cervical cancer. Contemporarily synthetic compounds, such as doxorubicin or gemcitabine, have demonstrated potentiating effects against CCa. Nevertheless, severe adverse conditions or side effects have been reported, which have halted their long-ranging cytotoxic potential. On the contrary, natural compounds or derivatives have emerged as one of the prime pharmacological leads in the era of efficacious anti-tumor chemotherapeutic and chemo-sensitive agents, owing to their low toxicological profile and potential efficacy [6]. More than half of all drug types used in clinical settings globally are derived from plants [7]. For instance, Resveratrol, a flavonoid, exhibited effective anti-tumor activities against breast [7], colon [8], liver [9], lungs [10], and cervical cancer cells [11]. Likewise, epigallocatechin gallate (EGCG), a polyphenolic compound available in green tea abundantly, has demonstrated anti-neoplastic solid activities mediated by arrested rate of proliferation by suppressing Ki67, telomerase activity inducing apoptosis in cervical cancer cells, which has materialized as a key anti-tumorigenic agent against most of the cancers, including cervical [12]. Furthermore, silymarin, a natural compound derived from the milk of the thistle plant, has exerted anti-tumor effects via chromatin condensation and nuclear fragmentation, and downregulation of JNK/MAPK pathway with concurrent upregulated expression of p38 led to apoptosis [13].

From the human health standpoint, triterpenoids, a chemically varied class of saponins, have served as vital substances. Among the diverse nature of natural and secondary compounds, terpenoids, a classic source of biologically active components, have exerted as a promising source of anti-tumorigenic agents. Betulin (BE), derived from the bark of botulin, displayed many biologic and pharmacological actions, which include anti-inflammatory, antibacterial, antiviral, anti-diabetic, and anti-tumor capabilities and hence emerged as one of the attractive therapeutic agents [14, 15]. BE is regarded as a potentially effective future anti-tumor phytochemical because of its cytotoxicity against tumor cells [16, 17], and because of its sublimation feature [18, 19], it is simple to identify and isolate.

The conventional route of designing and developing pharmaceuticals employs time and resources under stringent conditions. On the contrary, the era of computational biology and bioinformatics exerts a crucial role in drug organizing regarding adequate time and expenditure. The preliminary screening of drugs against targets deploying computational therapeutics has facilitated the designing effective drug targets. Nevertheless, more studies need to be conducted on the *in silico*-screened drugs against epigenetic markers, specifically against CCa. Considering this, we aimed to explore the anti-tumor potency of BE against epigenetic markers by implementing *in silico* and *in vitro* experimental setups.

## Materials and methods

### Target selection and preparation

The retrieval of targets was carried out for three of the most essential epigenetic proteins, namely (DNA (cytosine-5)-methyltransferase3A (DNMT3A), Histone Deacetylase 4 (HDAC4) and Histone-lysine *N*-methyltransferase 2C (KMT2C). The 3D structures were retrieved from the Protein Data Bank (PDB) (<http://www.rcsb.org/>) using their PDB-ID's 2QRV, 2VQJ, and 5F59, respectively (Table 1) [20]. The protein structures were suitably prepared using default parameters in the Schrodinger-Protein Preparation Wizard for molecular docking (Protein Preparation Wizard, 2021) [21]. Appropriate bond orders were assigned, and missing

**Table 1** List of targets retrieved from RCSB and PDB

S.no	Protein name	PDB-ID	Structure resolution (Å)
1	DNMT3A	2QRV	2.89
2	HDAC4	2VQJ	2.10
3	KMT2C	5F59	2.80

hydrogen bonds were added during preparation. Further, the protein structures were optimized and minimized to attain stable conformation.

### Preparation of ligand molecules

Secondary metabolites were selected from phytochemical constituents of different plants. The 3D structures of ligands were retrieved from PubChem (<https://pubchem.ncbi.nlm.nih.gov/>) [22]. The phytochemical molecules retrieved from the database were suitably prepared in LigPrep by adding hydrogen bonds, assigning appropriate bond order charges, correcting chirality, generating ionization and tautomeric states, minimizing structure for low-energy ring conformation, and geometry optimizations [23].

### Molecular docking of phytochemicals against epigenetic proteins

The co-crystallized ligand molecules in the protein structures were selected to generate a receptor grid to facilitate precise docking. The prepared phytochemical ligand molecules were docked into the respective grid of the target protein using Glide-extra precision mode (GlideXP), and the docking scores were calculated based on the Glide scoring functions. The molecular docking studies employed the flexible method of docking [24].

### Molecular dynamics simulation

Molecular dynamics simulations were executed to determine the stability of the docked complexes. We have used Desmond 2021–2024 to assess the stability of the docked BE complexed with epigenetic proteins DNMT3, HDAC4, and KMT2C [25]. The complexes within the explicit solvent system were solvated using crystallographic water (TIP3P) molecules [26] and subjected to orthorhombic periodic boundary conditions with a buffer zone of 10 Å. The overlapping water molecules were eliminated, and the system was neutralized with Na<sup>+</sup> and Cl<sup>−</sup> as a counterion. To maintain the consistent temperature (300 K) and pressure (1 bar) of the systems, an ensemble (NPT) consisting of nose–hover thermostats [27] and barostats was employed. The study used a hybrid energy minimization approach of 1000 steepest descents and applied conjugate gradient algorithms. The energy reduction process utilized the limited memory Broyden–Fletcher–Goldfarb–Shanno (LBFGS) algorithm, with a convergence threshold gradient set at 1 kcal/mol. The long-range electrostatic interactions, specifically the Van der Waals and Coulomb interactions, were computed using a Smooth Particle Mesh Ewald approach, employing a cut-off radius of 9 Å. The study employed the multiple time-step RESPA

integration method, namely the reference system propagator algorithms, to investigate the dynamics of bonded, near-bonded, and far-bonded interactions. The simulations were conducted for 500 ns, and the data were collected at regular intervals of 100 picoseconds. The resulting trajectory was examined utilizing the Maestro visualization interface.

### Drug-like properties and ADME studies

ADME properties were estimated using the Schrödinger–QikProp package [10]. The ligands that underwent screening were assessed for their drug-like characteristics and ADME. The compounds were evaluated according to the following criteria based on Lipinski's rule of five: (i) The number of hydrogen bond donors should be limited to a maximum of five; (ii) the number of hydrogen bond acceptors should be limited to a maximum of 10; (iii) the molecular weight should be below 500 Daltons; (iv) the partition coefficient, commonly denoted as LogP, is expected to be below 5; and (v) drug candidates adhering to no more than one rule are potential compounds exhibiting improved ADME characteristics. The ligands that met Lipinski's criterion of five were chosen for subsequent study. The ligands were evaluated to determine their drug-like characteristics and important pharmacokinetic parameters as per absorption, Distribution, Metabolism, and Elimination (ADME). P-glycoprotein (Pgp), which plays a crucial role in drug discovery and development and is present in the liver, functions as an efflux pump [28] in estimating pharmacokinetic properties. If the drug molecule inhibits Pgp, based on the criteria mentioned above, the drug candidates were taken forward for further experimental analysis.

### Density functional theory (DFT)

The DFT is a computational method in quantum mechanics used to analyze the electrical properties of atoms, molecules, and compounds [29]. The computational analysis of the electrical and structural characteristics of the BE compound was conducted using the Jaguar software developed by Schrödinger [30]. The calculations employed the Becke3–Lee–Yang–Parr (B3LYP) technique and the 6-31G\*\* basis set. The parameters used in this work encompassed the highest occupied molecular orbitals (HOMOs) and the lowest unoccupied molecular orbitals (LUMOs), together with the energy gaps. These parameters were computed for the BE molecule using the Jaguar software. Furthermore, the reactive chemical sites and promising areas within BE were identified for subsequent enrichment experiments to develop BE as a potent epigenetic therapeutic.

## Cell culture

The work utilized the human cervical cancer (HeLa) cell line obtained from NCS Pune. The cells were cultivated in Dulbecco's modified Eagle's media (DMEM) obtained from. The DMEM was prepared by adding 10% fetal bovine serum (FBS), amphotericin (Sigma, Merck, KgaA), glutamine, and 100× pen-strep (Sigma-Aldrich, Merck, KgaA.). The culture was kept at 37 °C with 5% CO<sub>2</sub> and maintained under high humidity.

## Drug preparation

BE was obtained from OtoChemi PVT Ltd. The main Stock was prepared in DMSO. A 1-mM working concentration using a complete media was prepared from the main stock, and respective dilutions were used for the drug treatment. The concentrations of BE used were 100, 50, 25, and 12.5 µM, respectively.

## Cell viability assay

3-(4,5-dimethyl-2-thiazolyl)-2,5-diphenyl-2-H-tetrazolium bromide (MTT) was employed to estimate the viability of the cells. HeLa cells were seeded at 10<sup>4</sup> cells/well density in a 96-well plate. Post 24 h of incubation, the cells reached 80% confluent, and the corresponding drugs or their combinations were introduced. Following 24 h of treatment, 20 µl of MTT (at a concentration of 5mg/ml) solution was added to 200 µl of PBS without FBS in each well, followed by an incubation period of 2 h. After transferring the media, 100 µL of DMSO was added to each well, and the mixture was incubated for 20 min while agitated.

Absorbance was measured at 570 nm spectrophotometrically (BioTek). Each of the experiments was carried out in triplicates. Cell viability was determined by implementing the following:

$$\% \text{ Cell Viability} = (\text{average OD of the individual test group}) / (\text{average OD of control}) \times 100.$$

## Results

### Molecular docking

Computer-aided drug design (CADD) has emerged as one of the hotspot computational tools in terms of drug design and development. As a preliminary step, the Schrodinger-Glide tool was implemented to determine the binding affinity of triterpenoids against the epigenetic protein molecules HDAC4, DNMT3A, and KMT2C. Typically, all ligands bound with the target proteins through several interactions, which have been decoded through molecular docking studies. The outcomes of the molecular docking process rely entirely on the selection of the binding site residues. We have selected the residues surrounding the co-crystallized molecule in the experimentally determined structures of the epigenetic proteins as the binding site residues (Table 2) for molecular docking. Among the subject triterpenoids, we observed that BE exhibited the highest binding energy with the epigenetic proteins through their active site residues.

Docking studies of triterpenoids against the epigenetic protein DNMT3A (PDB-ID: 2QRV) reported a Glide score ranging from −7.811 to −0.78 kcal/mol as maximum and minimum binding score of these ligands in the present study (Table 3). BE's flexible docking has an energy of −50.305 kcal/mol and a score of −7.811 kcal/mol. At a 2.15 Å bond distance, the ligand molecule has formed a hydrogen bond interaction with Phe636 (Fig. 1a and b). The amine group NH in Val661 has formed a hydrogen bond with the OH atom in BE with a bond length of 2.01 Å. In addition, hydrophobic interactions were observed between the co-crystallized ligand *S*-adenosyl-L-homocysteine and the DNMT3A residues Val661 and Phe636.

Similarly, we observed the typical interaction of BE against KMT2C with the highest binding score of −9.8 kcal/mol, while the triterpenoids produced Glide scores

**Table 2** Active site residues of the target proteins

Sl. no	Epigenetic target	PDB-ID	Residues forming the binding site
1	DNA methyltransferase (DNMT3A)	2qrv	TRP889, ILE-A639, SER -A888, ARG-A887, GLY-A638, GLY-A703, LEU-A726, PRO-A705, VAL-A661, ARG A-684, VAL A-683, ASP A-682, PHE A-636, SER A-659, CYS A-662, GLU A-660
2	Histone deacetylase 4 (HDAC4)	2qvj	LEU156, ASP158, GLY159, ILE167, ASN168, GLU169, ALA196, VAL198, ALA227, TRP290, PHE299, ALA330, GLY331
3	Histone-lysine <i>N</i> -methyltransferase (KMT2C)	5f59	LEU A 4783, TYR A4825, ARG A4845, GLN A 4781, TYR A 4846, GLY A 4782, ASN A 4848, TYR A 4886, CYS A 4899, ILE A 4780, HIS A 4849, MET A 4910, PRO A 4898, ILE A 4897



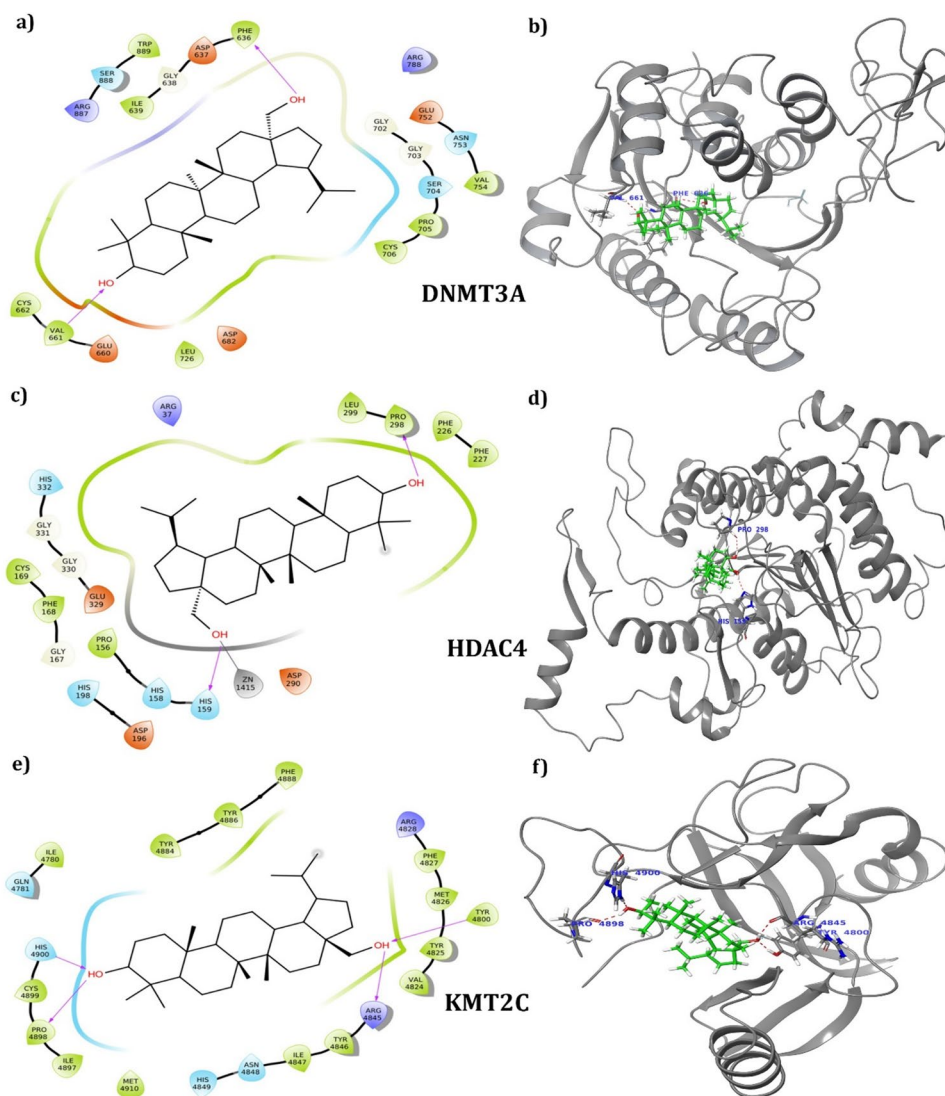
**Table 3** Molecular docking results of triterpenoids with the epigenetic proteins and their interaction profiles

Ligands	Docking score (Kcal/mol)	Binding energy (Kcal/mol)	Type of interaction and its number	Interacting residues
<i>DNA Methyltransferase (DNMT3A), PDB-ID-(2QRV)</i>				
Betulin	− 7.8	− 50.3	Hydrogen bond (2)	PHE636, VAL661
Salsolside C	− 6.4	− 32.0	Hydrogen bond (2)/ salt bridge(1)	CYS662, GLU660/ARG887
2'-O-Acetylsalsolside C	− 5.7	− 34.4	Hydrogen bond (3)	ILE639, PHE636, VAL661
3'-O-Acetylsalsolside C	− 5.0	− 38.5	Hydrogen bond (3)	PRO705, ILE639, CYS662
Shatavarin iv	− 3.3	− 32.0	Hydrogen bond(1)	VAL661
Forskolin	− 2.8	− 21.8	Hydrogen bond(1)	PHE636
Alpha-amyrin	− 2.3	− 20.6	Hydrogen bond(1)	CYS706
Betulnic acid	− 1.4	− 15.5	Hydrogen bond(3)	SER704, PRO705, ILE639
24-Hydroxyolean-12-en-3-one	− 1.3	− 13.7	Hydrogen bond (2)	LEU726, PRO705
Oleanolic acid	− 1.3	− 12.4	Hydrogen bond (3)	TRP889, ARG887, VAL661
Sarsasapogenin	− 0.7	− 17.2	Hydrogen bond (1)	CYS662
<i>Histone deacetylase (HDAC4), (PDB-ID-2QVJ)</i>				
Betulin	− 9.7	− 41.8	Hydrogen bond (2)	HIS159, PRO 298
Salsolside C	− 7.7	− 33.4	Hydrogen bond (3)	HIS158, PRO156, PHE168
2'-O-Acetylsalsolside C	− 6.6	− 53.3	Hydrogen bond (3)	PHE298, PHE226, PHE227
3'-O-Acetylsalsolside C	− 6.4	− 45.0	Hydrogen bond (2)/ Salt bridge (1)	LEU229, PRO298/GLU329
Shatavarin iv	− 5.0	− 30.6	Hydrogen bond(3)	HIS 158, ASP290, PRO156
Forskolin	− 3.7	− 29.0	Hydrogen bond(3)	GLY331, GLY330, PHE226
Alpha-Amyrin	− 3.2	− 26.9	Hydrogen bond(2)	HIS157, HIS198
Betulnic acid	− 2.9	− 23.3	Hydrogen bond(3)	HIS332, PRO156, ASP198
24-Hydroxyolean-12-en-3-one	− 2.8	− 26.0	Hydrogen bond(2)	LEU299, PHE227
Oleanolic acid	− 2.8	− 23.3	Hydrogen bond(4)	ASP290, HIS157, PRO156, PHE168
Sarsasapogenin	− 2.6	− 22.6	Hydrogen bond(2)	PRO156, LEU299
<i>Histone-lysine N-methyltransferase (KMT2C) (PDB-ID-5F59)</i>				
Betulin	− 9.8	− 44.6	Hydrogen bond(4)	HIS4900, PRO4898, TYR4800, ARG4845
Salsolside C	− 7.1	− 33.4	Hydrogen bond(2)	ILE4980, GLN4781
2'-O-Acetylsalsolside C	− 6.6	− 53.3	Hydrogen bond(2)	TRY4886, TRY4884
3'-O-Acetylsalsolside C	− 5.8	− 45.0	Hydrogen bond(2)	ILE4864, GLN4885
Shatavarin iv	− 4.1	− 30.6	Hydrogen bond(4)	ASN4848, VAL4824, ILE4980, TRY4886
Forskolin	− 3.1	− 29.0	Hydrogen bond(2)	PRO4848, HIS4900
Alpha-Amyrin	− 2.7	− 26.9	Hydrogen bond(4)	ARG4845, PRO4898, ILE4980, ASN4848
Betulnic acid	− 2.5	− 23.3	Hydrogen bond(2)	TRY 4800, PRO4898
24-Hydroxyolean-12-en-3-one	− 2.3	− 26.0	Hydrogen bond(3)	GLN4781, VAL4824, HIS4900
Oleanolic acid	− 1.9	− 23.3	Hydrogen bond(2)	PRO4898, ARG4845
Sarsasapogenin	− 1.8	− 22.6	Hydrogen bond(4)	GLN4781, TRY4886, ASN4848, VAL4824

ranging from − 9.83 to − 1.81 kcal/mol (Table 3). The docking of triterpenoids to the crystal structure of the epigenetic protein HDAC4 (PDB ID: 2VQJ) has shown the Glide score from − 9.720 to − 2.698 kcal/mol (Table 3). BE has demonstrated the highest binding affinity with the protein HDAC4 among the triterpenoids (Glide score: − 9.720 kcal/mol and energy: − 41.835), and the HDAC4-BE complex is stabilized by two hydrogen bonds and metal coordination (Fig. 1c and d). The hydroxyl group of the BE molecule has created a hydrogen

bond with His159 at a distance of 2.19 Å (OH–NC). In addition, the hydroxyl group has formed a coordination with the essential catalytic metal ion Zn1415. The His residue in the conserved position formed a hydrogen bond at a distance of 2.92 Å with the co-crystallized inhibitor molecule TFG and a metal coordination with the Zn ion [29]. Thus, the binding of BE to HDAC4 via His159 and metal coordination with Zn ion can inhibit activity comparable to that of the previously reported inhibitor TFG. At a distance of 2.04 Å, the oxygen atom in Pro298

**Fig. 1** BE's 2D and 3D interaction profiles with the three epigenetic targets. Betulin-DNMT3A formed two hydrogen bonds with Val661 and Phe636, BE-HDAC4 complex formed two hydrogen bonds with His159 and Pro28, and BE-KMT2C formed four hydrogen bonds with His4900, Pro4898, Tyr4800, and Arg4845



has formed a hydrogen bond with the hydrogen atom of a hydroxyl group in BE (CN–HO). Likewise, the docking studies of the epigenetic protein KMT2C, BE exhibited the highest Glide score and binding energy of  $-9.893$  and  $-47.06$  kcal/mol, respectively. Four hydrogen bonds were observed between the BE and the protein Histone-KMT2C. The hydroxyl groups at each end of the BE molecule formed two hydrogen bonds with the receptor (Fig. 1e, f). The hydrogen atom in the hydroxyl group of BE formed hydrogen with Pro4898 (OH–OC) at a distance of  $1.87$  Å. With the span of 2 (NH–OH), the hydrogen atom in His4900 has formed a hydrogen bond with an oxygen atom in the same hydroxyl group of BE. A hydroxyl group at the opposite end of the BE molecule has formed hydrogen bonds with Tyr4800 (OH–OH) and Arg4845 (CO–HO) at  $1.69$  and  $1.89$  Å, respectively. His4900 has been observed to form a hydrogen bond with the co-crystallized ligand *S*-adenosyl-L-homocysteine at  $2.86$  Å. In

addition to other residues, the BE-interacting residues Arg4845 and Pro4898 had hydrophobic contacts with the KMT2C, and these interactions were also observed with the co-crystallized ligand *S*-adenosyl-L-homocysteine.

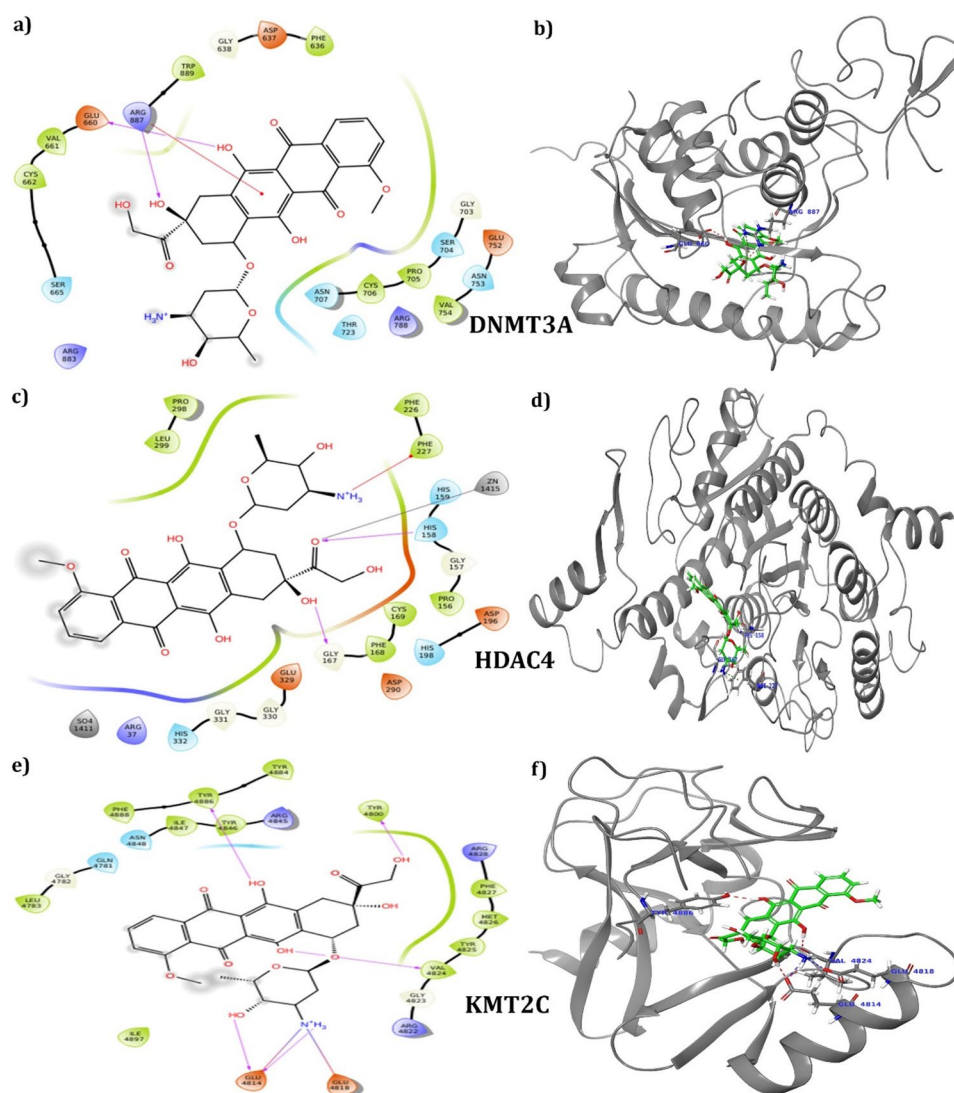
### Comparison with promising cervical cancer drug

To compare our findings to conventional cervical cancer drugs, we downloaded the Doxorubicin (DOX) structure and performed a docking analysis against the epigenetic targets 2QRV, 2QVJ, and 5F59. Table 4 and Fig. 2 represent the docking results of Doxorubicin with the epigenetic targets and their interaction profile. It has been demonstrated that the FDA-approved drug DOX targets the epigenetic proteins [28] with low binding energies in cervical cancer [29]. In contrast, the DOX molecule docked against DNMT3A (2qvj), HDAC4 (2QVJ), and KMT2C (5F59) has produced  $-3.53$ ,  $-8.05$  kcal/mol, and  $-8.43$  kcal/mol.

**Table 4** Molecular docking of standard drug DOX with the three epigenetic proteins

Epigenetic protein	Docking score (kcal/mol)	Binding energy (kcal/mol)	Type of Interaction	Interacting residues
DNMT3A (2QRV)	− 3.5	− 28.8	Hydrogen bond	GLU660, ARG887
HDAC4 (2QVJ)	− 8.5	− 43.9	Hydrogen bond	HIS158, GLY167, PHE227, and
KMT2C (5F59)	− 8.4	− 50.8	Hydrogen bond	GLU4814, GLU4818, VAL4824, TYR4886

**Fig. 2** 2D interaction and 3D interaction profiles of DOX with the three epigenetic targets. DOX-DNMT3A complex formed two hydrogen bonds with GLU660 and ARG 887, DOX-HDAC4 complex formed three hydrogen bonds with HIS158, GLY167, and PHE227, and DOX-KMT2C formed four hydrogen bonds with GLU4814, GLU4818, VAL4824, and TRY4886



Comparatively, Betulin has produced higher docking score than DOX against all three epigenetic proteins DNMT3A (− 7.81 kcal/mol), HDAC4 (− 9.72 kcal/mol), and KMT2C (− 9.89 kcal/mol). Our docking analysis showed that Doxorubicin had high binding energy for all the three epigenetic proteins and thus is not as an active inhibitor of epigenetic proteins against cervical cancer.

### Molecular dynamic simulation

The top-binding cervical cancer inhibitor with the epigenetic protein complexes from molecular docking was further subjected to molecular dynamics simulation to understand its stability and integrity. We performed the MD simulation at 500 ns to validate and confirm the stability of the



indicated protein–ligand complexes. Betulin was chosen as a possible epigenetic inhibitor of DNMT3A, HDAC4, and KMT2C since it has shown the highest docking among the other molecules.

For six different complexes, we calculated the RMSD and RMSF. The RMSD value can predict the stability of the ligand complex in the MD runs. The stability of a protein complex is enhanced when the RMSD value is low. We

compared the MD simulation time to the RMSD of the complexes regarding C $\alpha$  atoms. In general, the RMSD values for all the complexes were relatively low.

The RMSD values for BE-HDAC4 complexes ranged from 2.9 to 4.8 Å. The C atoms exhibited stability in the 350–450 ns range with an RMSD greater than 0.25 Å. Between 200 and 300 ns, the RMSD varied the most, reaching a maximum of 3.6 Å (Fig. 3a). Residue flexibility at

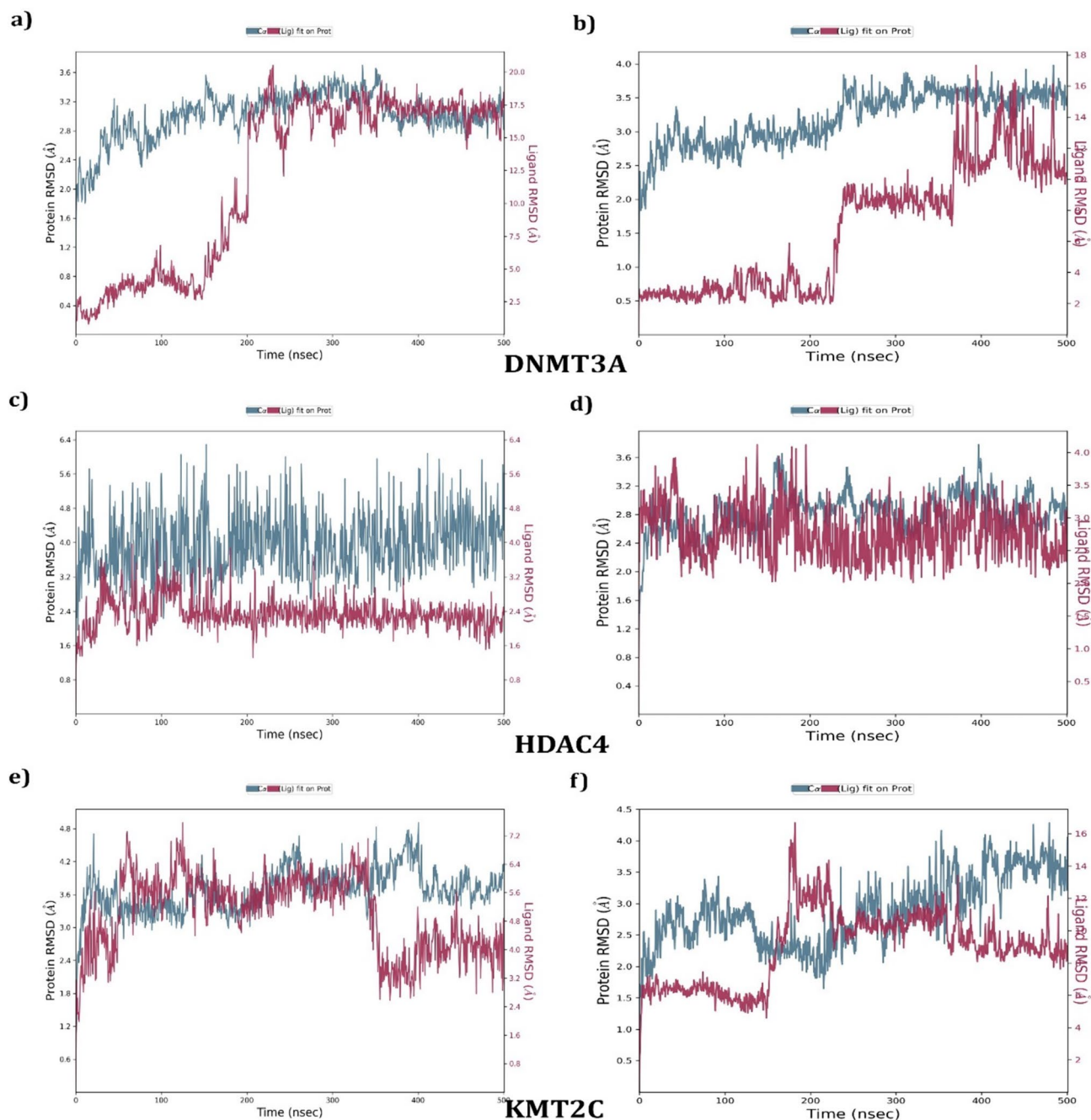


**Fig. 3** RMSD graph of the Protein–ligand complexes during 500-ns MD Simulation. **a** RMSD graph of DNMT3A upon BE binding, **b** RMSD graph of DNMT3A upon DOX binding, **c** RMSD graph of

HDAC4 upon BE binding, **d** RMSD graph of HDAC4 upon DOX binding, **e** RMSD graph of KMT2C upon BE binding, and **f** RMSD graph of KMT2C upon DOX binding

ligand binding sites is investigated using root mean square fluctuations (RMSF) (Fig. 4a). The following amino acids were involved in the 38 ligand interactions with proteins: SER634–ASP663, ILE639, THR641–GLY639, TRY656, GLU660–ASP665, ARG684–SER685, ILE701, PRO705, ASN707, ASP708, LYS717, TYR720–GLY722, ARG725–LEU72, GLU729, PHE751–GLU752, VAL754, ARG786, ASN840, and GLY886–TRP889. The stability

of the ligand is enhanced by hydrophobic interactions with the residues Leu726, Phe751, and Val754, as shown in Fig. 5a. As the simulation progressed from 10 to 65%, it generated hydrogen bonds with Asp637, Asn707, Glu721, Gly722, Arg725, and Arg887. The RMSF of the ligand with the first frame falls between the range of 7.5 and 10.5 Å. Additionally, the additional ligand properties that fall within the range of 4.20–5.05 Å include the polar surface area,

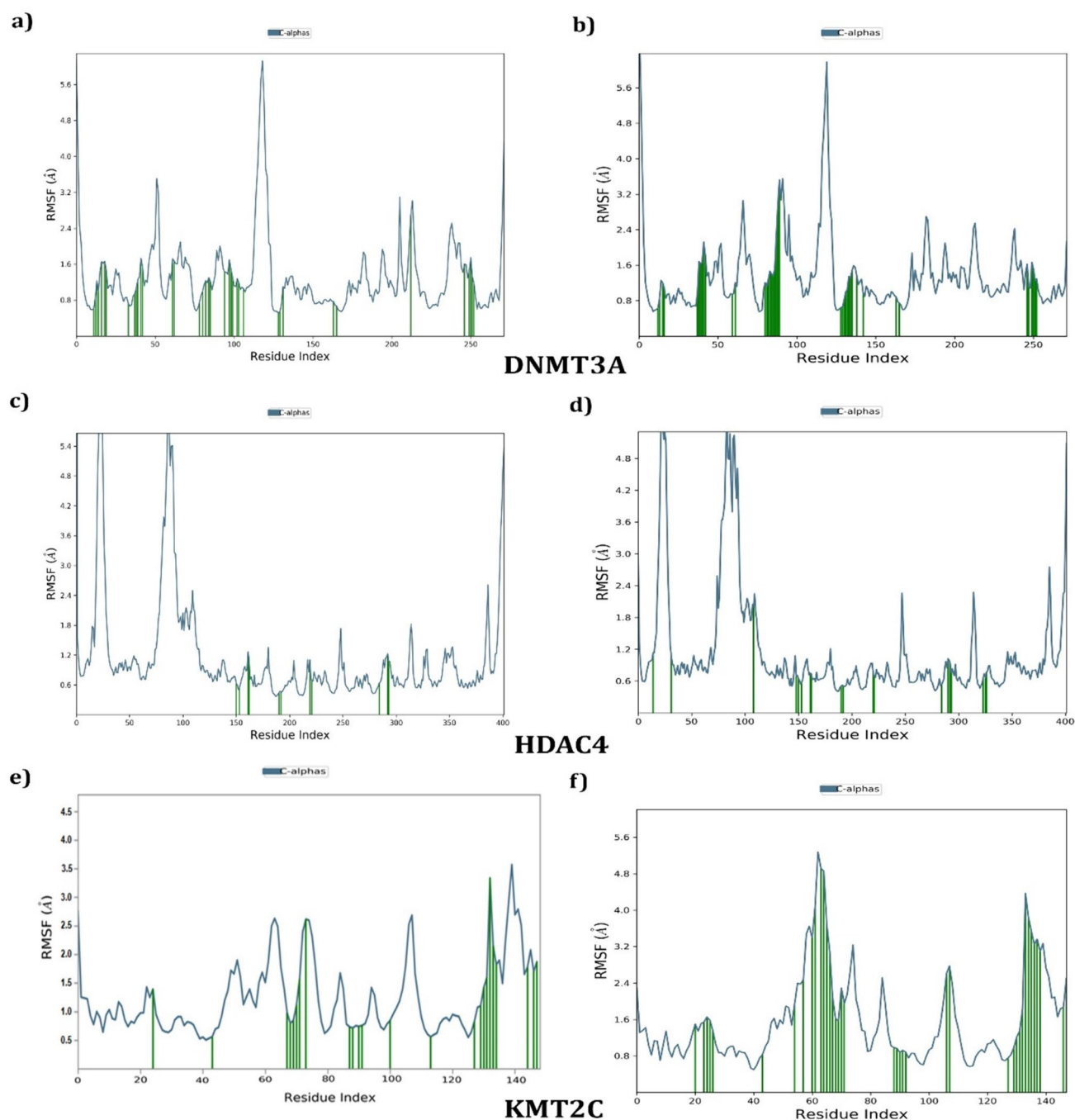


**Fig. 4** RMSF graph of the Protein–ligand during 500-ns MD Simulation. **a** RMSF graph of BE-DNMT3A, **b** RMSF graph of DOX-DNMT3A, **c** RMSF graph of BE-HDAC4, **d** RMSF graph of DOX-HDAC4, **e** RMSF graph of BE- KMT2C, and **f** RMSF graph of DOX-KMT2C

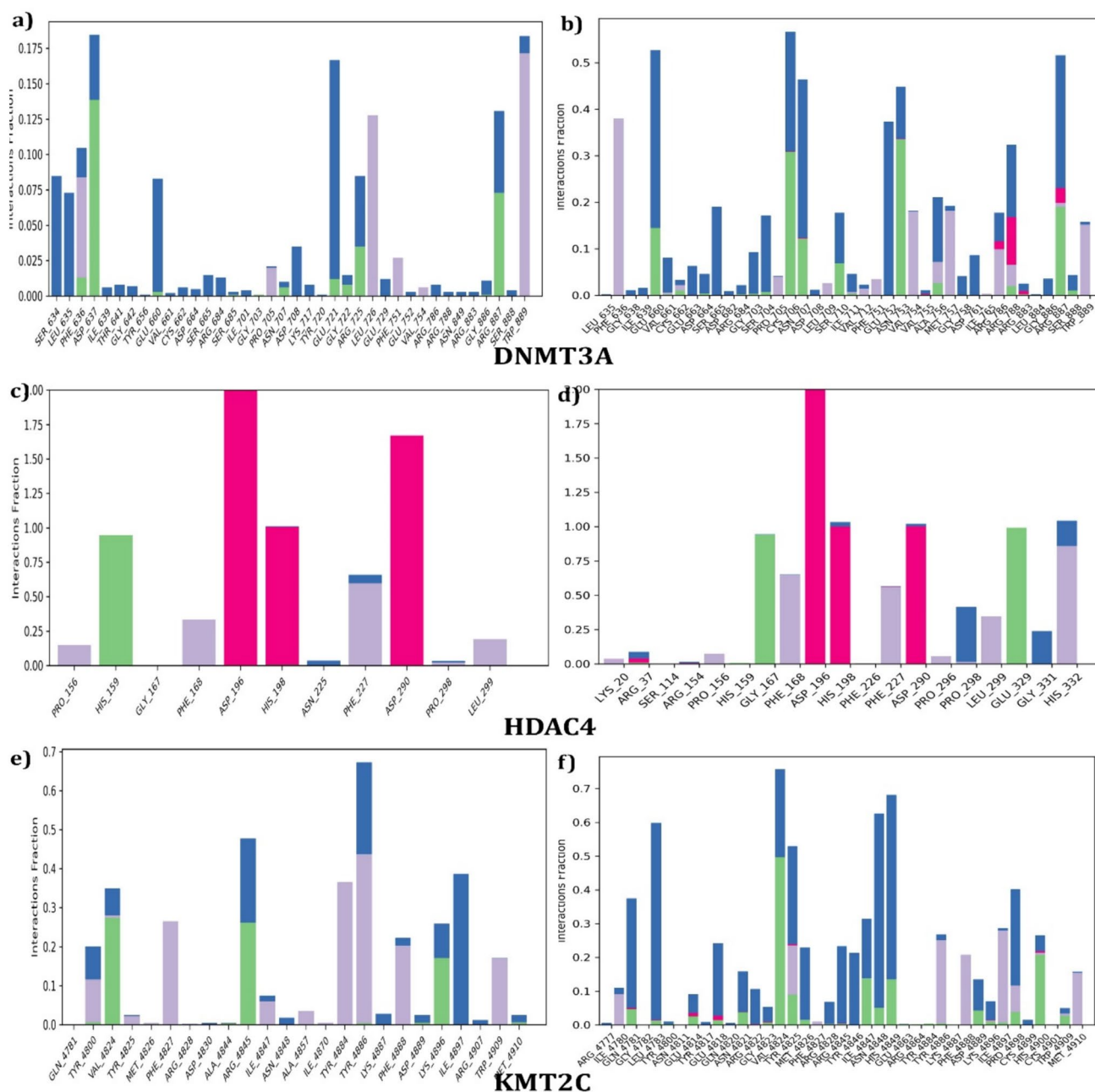


**Fig. 5** The plots represent the intra-molecular interactions of receptors and the ligands. Hydrogen bonds are shown in green, hydrophobic interactions are shown in light purple, water bridges are shown in blue, and salt bridge interaction is shown in pink. **a** Protein–ligand interaction graph of BE-DNMT3A, **b** protein–ligand interaction

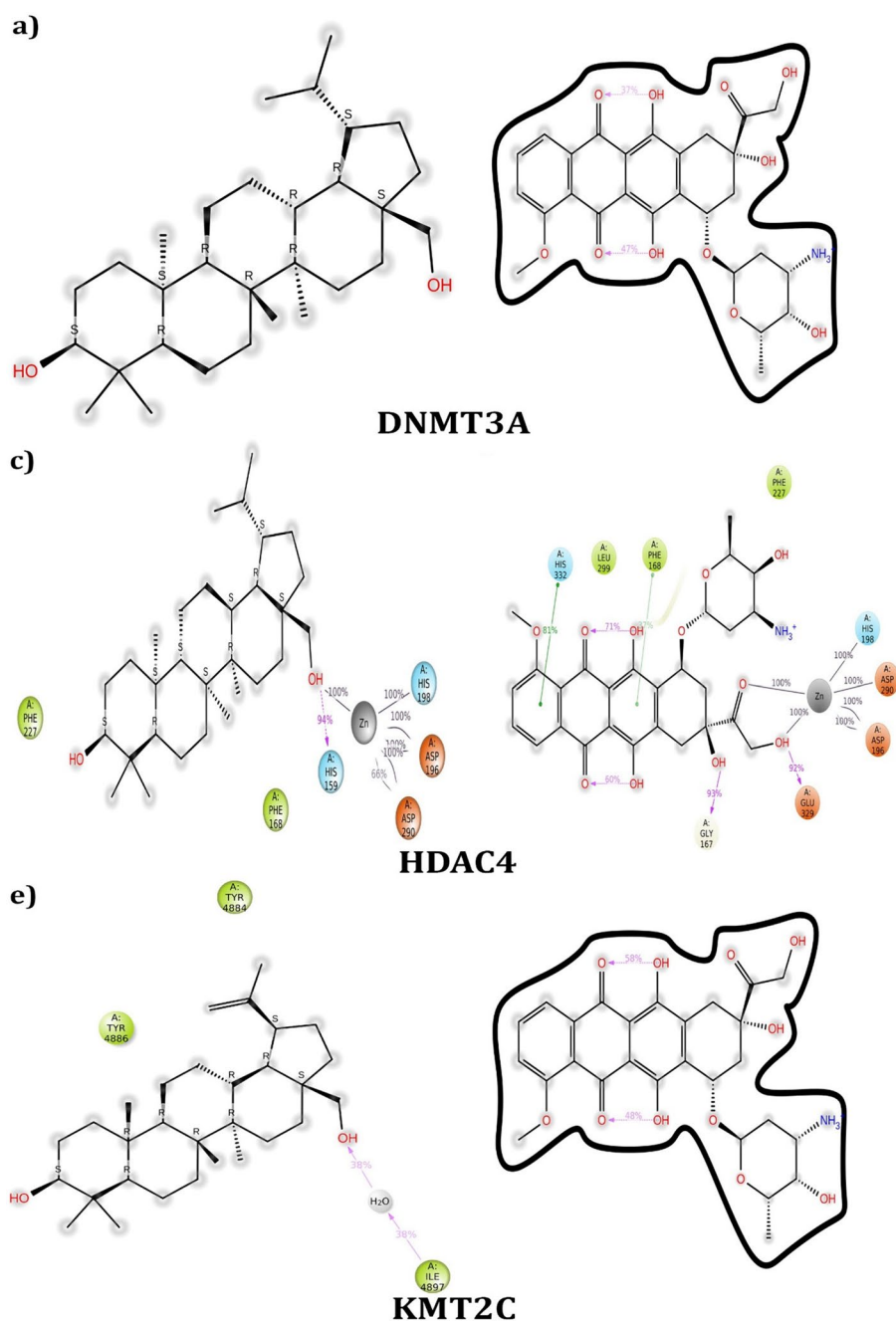
graph of DOX-DNMT3A, **c** Protein–ligand interaction graph of BE-HDAC4, **d** protein–ligand interaction graph of DOX-HDAC4, **e** protein–ligand interaction graph of BE-KMT2C, and **f** protein–ligand interaction graph of DOX-KMT2C

solvent-accessible surface area, molecular surface area, and radius of gyration.

Figure 6a shows a 2D-trajectory interaction diagram showing how docking with Ile4870 creates a hydrophobic connection preserved in the MD trajectory pose. The methanol group in BE supplied a hydrophobic bond to Ile4847, increasing its affinity by 38%. The ligand's RMSF

was between 0.5 and 3.5 Å in the first frame (Fig. 4a). Figure 14a shows that the gyration radius, molecular surface area, solvent-accessible surface area, and polar surface area are additional ligand properties that fall within the range of 4.30–4.45 nm. The complex exhibited higher variations from 50 to 150 and 20 to 400 n, as well as an RMSD

**Fig. 6** 2D diagrams of Betulin and Doxorubicin interaction with the active site residues for 500-ns MD Simulation. **a** 2D interaction diagram of BE-DNMT3A, **b** 2D interaction diagram of DOX-DNMT3A, **c** 2D interaction diagram of BE-HDAC4, **d** 2D interaction diagram of DOX-HDAC4, **e** 2D interaction diagram of BE-KMT2C, and **f** 2D interaction diagram of DOX-KMT2C



ranging from 0.5 to 3.8 Å, over the MD simulations period compared to the DOX-HDAC4 complex.

The graph indicates that the RMSF measurement reveals how flexible the residues are at the ligand binding sites. In addition, heavy atoms, the BE-HDAC4 complex, protein C, and the backbone all had RMSDs ranging from 0.015 to 5.85 Å (Fig. 3c). Between 250 and 480 ns of simulation length, values ranging from 0.01 to 3.98 nm were recorded for the stability of the C atoms with an RMSD of 4.0 Å. The RMSD altered by a maximum of 4.8 Å between 100 and 150 ns, as well as 250 and 300 ns. Residue flexibility at ligand binding

sites is investigated using Root Mean Square Fluctuations (RMSF) (Fig. 4c). They interacted with ligands at positions Pro156, His159, Gly167, Phe168, Asp196, His198, Asn225, Phe227, Asp290, Pro298, and Leu299, among others. The interactions between the ligand and the hydrophobic residues Pro156, Phe227, and Leu299 stabilize it, as seen in Fig. 5c. A 10–65% simulation period saw the formation of more hydrogen bonds with His 159. Figure 5d displays the time-frame of the protein–ligand interaction. The MD trajectory stance maintains the hydrophobic bond established by the docking posture, as shown in the 2D-trajectory interaction



diagram (Fig. 6c). Figure 14b shows that the ligand's relative molecular size (RMSF) ranged from 0.105 to 1.034 nm concerning the beginning frame. The remaining ligand characteristics ranged from 3.943 to 4.402 nm in gyration radius, from 381.112 to 399.601 nm<sup>2</sup> in molecular surface area, from 180.38 to 271.833 nm<sup>2</sup> in solvent-accessible surface area, and from 70.227 to 86.468 nm in polar surface area. When contrasted with the DOX-2qvj complex, for BE-KMT2C, the RMSD values for protein C $\alpha$  varied from 1.35 to 3.0 Å, and for the backbone and heavy atoms, they ranged from 2.9 to 4.8 Å. Throughout the 150–350 ns simulation time, the C $\alpha$  atoms maintained a stable state with values ranging from 1.25 to 2.1 Å with an RMSD of 4.2 Å. The 100–150 ns and 350 ns range showed the largest RMSD fluctuations, reaching up to 4.8 Å. During the simulation, it was discovered that Phe4826 and Tyr4884 establish robust hydrophobic contacts. Residue flexibility at ligand binding sites is investigated using Root Mean Square Fluctuations (RMSF) (Fig. 4e). Arg4907–Met4910 and Gln4781–Lys4897 were the sites of 24 ligand–protein interactions. The hydrophobic residues Tyr4800, Tyr4825, Phe4827, Ile4847, Ala4857, Ile4870, Tyr4884, Tyr4886, Phe4888, and Trp4909 interact with the ligand to keep it in place (Fig. 5e). Hydrogen bonds were generated by Tyr4800, Val4824, Ala4844, Arg4845, Asp4889, Lys4896, and Met4910 during 10–60% of the simulation's duration displays the time-series of interactions between proteins and ligands. Figure 6e shows a 2D-trajectory interaction diagram showing how docking with Ile4870 creates a hydrophobic connection preserved in the MD trajectory pose. The methanol group in BE formed a hydrophobic bond to Ile4847, increasing its affinity by 38%. The ligand's RMSF was 0.5–3.5 Å in the first frame (Fig. 4e). Additional ligand characteristics falling within the 4.30–4.45 nm range were the gyration radius, solvent-accessible surface area, polar surface area, and molecular surface area. For 500 ns, the RMSD varies between 0.5 and 4.4 Å, in contrast to the DOX-5f59 complicated MD simulation. Between 150 and 250 ns simulation time, the RMSD varies the most and reaches a maximum of 4.4 Å (Fig. 3b). Researching the adaptability of residues at ligand binding sites is the purpose of the RMSF measurements. Thirty-nine interactions between ligands and amino acids in proteins were identified (Fig. 5e).

Stability and structural integrity are maintained throughout molecular dynamics simulations of BE-bound complexes of epigenetic protein targets (DNMT3A, HDAC4, KMT2C). The BE molecule was found to be firmly attached within the substrate-binding pocket of the proteins, correlating well with the molecular docking data. Because the bound complex deviates slightly from the native state, the structural integrity of the epigenetic target proteins is preserved in the simulations. The BE-bound epigenetic protein complexes reached equilibrium in the early part of the simulations, even

though modest fluctuations were observed. They stayed at the same level throughout the simulation. The core protein structure is anchored to the ligand and remains bound to the ligand despite residual variations. In epigenetic protein complexes, most amino acid residues show low variability, notably in the central regions of the proteins. Due to their unbound state and loss of packing, the protein's terminal residues are free to move around. Except for a few depositions, all residues across all compounds showed stability with shallow RMSF properties throughout the simulation time.

The system's compactness and equilibrium conformation were verified by measuring the radius of gyration (Rg). Furthermore, the extent to which a protein folds and unfolds is strongly affected by the value of the Rg's. The Rg plots of the BE-bound epigenetic protein complexes show steady values, indicating that the protein complexes have undergone only a mild folding and unfolding process over the simulations. Solvent-accessible surface area (SASA) calculations can be used to detect potential changes in protein solvent accessibility. Changes in a protein's solvent accessibility can be analyzed with SASA. They fluctuated SASA values during the simulation control protein convergence and environment solvent expansion. The BE molecule is shown to suppress the biologic activity of DNMT3A, HDAC4, and KMT2C by MD Modeling, demonstrating that it binds well into the active site of these epigenetic target proteins.

### Physiochemical properties of ligand molecules

ADME prediction aims to predict the pharmacokinetics of a potential therapeutic molecule, making ADME prophecy a vital component of drug discovery and development. ADME evaluations are performed alongside molecular docking research to classify the safety and efficacy of a pharmacological molecule [31]. The quantifiable evaluation of drug-likeness (QED) is determined by integrating desirability functions associated with drug similarity parameters, such as molecular weight, log *P*, the number of hydrogen bond acceptors and donors, aromatic rings, rotatable bonds, polar surface area, and unfavorable functional area warnings. The average QED for attractive compounds is 0.67; molecules with a QED of 0.49 are entertaining and appealing, while those with a QED of 0.34 are exceedingly complex and unattractive. The QED for IE is 0.565. Consider the accessibility score, which evaluates the convenience of synthesizing drug-like compounds by combining fragment contributions and complexity penalty. For phytochemicals, the Synthetic Accessibility Score (SAScore) is 4,936. According to the Lipinski rule, based on physiochemical properties and medicinal chemistry findings, BE is an ideal candidate because it shares similar properties with the substance (Table 5). Under the Pfizer Rule, they demonstrated

**Table 5** ADME properties of triterpenoids

Compounds	Molecular weight <sup>a</sup>	QP logPo/w <sup>b</sup>	QP logS <sup>c</sup>	CIQlogS <sup>d</sup>	QP logHERG <sup>e</sup>	QPP Caco <sup>f</sup>	QLog BB <sup>g</sup>	QPP MDCK <sup>h</sup>	QLogKp <sup>i</sup>	QLog Khsa <sup>j</sup>	Human oral absorption (%) <sup>k</sup>	Pgp Inhibitor
Betulin	444.740	6.022	-7.108	-6.692	-3.818	1762.794	-0.392	912.987	-2.592	1.569	100	Inhibitor
Salsolside C	927.091	-0.146	-4.716	-6.263	-3.86	0.237	-5.492	0.076	-7.642	-1.117	0	Non-inhibitor
2'-O-Acetyl/salsolo-side C	969.128	0.747	-6.135	-7.03	-4.358	0.211	-6.002	0.067	-7.742	-0.883	0	Non-inhibitor
3'-O-Acetyl/salsolo-side C	969.128	0.744	-5.294	-7.03	-3.915	0.368	-5.309	0.122	-7.283	-0.884	0	Non-inhibitor
Shatavarin iv	887.069	-0.038	-4.841	-5.889	-5.652	4.727	-4.664	1.517	-6.342	-0.931	0	Non-inhibitor
Forskolin	410.506	2.288	-3.69	-4.028	-3.469	868.13	-0.676	424.588	-2.976	0.05	93	Inhibitor
Alpha-Amyrin	426.724	6.947	-7.806	-7.261	-3.523	4471.550	0.191	2496.998	-2.041	2.006	100	Inhibitor
Betulinic acid	456.707	6.200	-6.712	-6.823	-1.781	342.203	-0.403	197.425	-2.829	1.331	96	Inhibitor
24-Hydroxyolean-12-en-3-one	440.708	6.558	-7.607	-7.267	-3.778	2193.999	-0.169	1156.608	-2.530	1.830	100	Inhibitor
Oleanolic acid	456.707	6.180	-6.845	-6.947	-1.711	333.602	-0.349	192.068	-2.975	1.373	95	Inhibitor
Sarsasapogenin	416.643	6.033	-7.471	-6.427	-3.999	3440.951	0.054	1881.204	-2.316	1.618	100	Inhibitor

<sup>a</sup>Molecular weight of the molecule (130.0–725.0)<sup>b</sup>Predicted octanol/water partition coefficient (-2.0 to 6.5)<sup>c</sup>Predicted aqueous solubility, logs. S in mol dm<sup>-3</sup> is the concentration of the solute in a saturated solution that is in equilibrium with the crystalline solid (-6.5 to 0.5)<sup>d</sup>CIQlogS: Conformation-independent predicted aqueous solubility, log S in mol dm<sup>-3</sup> is the concentration of the solute in a saturated solution that is in equilibrium with the crystalline solid. (-6.5 to 0.5)<sup>e</sup>Predicted IC50 value for blockage of HERG K<sup>+</sup> channels (concern below -5)<sup>f</sup>QPPCaco: Predicted apparent Caco-2 cell permeability in nm/sec. (>500 great; <25 poor)<sup>g</sup>QLogBB: Predicted brain/blood partition coefficient. (-3.0 to 1.2)<sup>h</sup>QPPMDCK: Predicted apparent MDCK cell permeability in nm/sec. (>500 great; <25 poor)<sup>i</sup>QLogKp: Predicted skin permeability (-8.0 to -1.0)<sup>j</sup>QLogKhsa: Prediction of binding to human serum albumin. (-1.5 to 1.5)<sup>k</sup>HumanOralAbsorption: Predicted human oral absorption on 0–100% scale. (>80% is high; <25% is poor)

excellent absorption and permeability, and the compound is regarded as a mildly toxic candidate due to its high Log  $P$  ( $> 3$ ) and low TPSA ( $> 75$ ) values. Log  $P$  and Log  $D$  values for a molecule with a weight greater than 400 are 5.328 and 5.009, respectively. Additionally, the BE molecule defines the GSK Rule and the Golden Triangle, indicating that it may have an outstanding pharmacological profile. The pharmacokinetic properties of BE suggest that it might be one of the Pgp (*p*-glycoprotein) inhibitors since Pgp functions as an efflux pump in the liver and plays a vital role in drug discovery and development. Therefore, the drug molecule is an excellent candidate if it inhibits the Pgp and vice versa, indicating that it could be a promising drug candidate.

### Minimization and DFT calculations

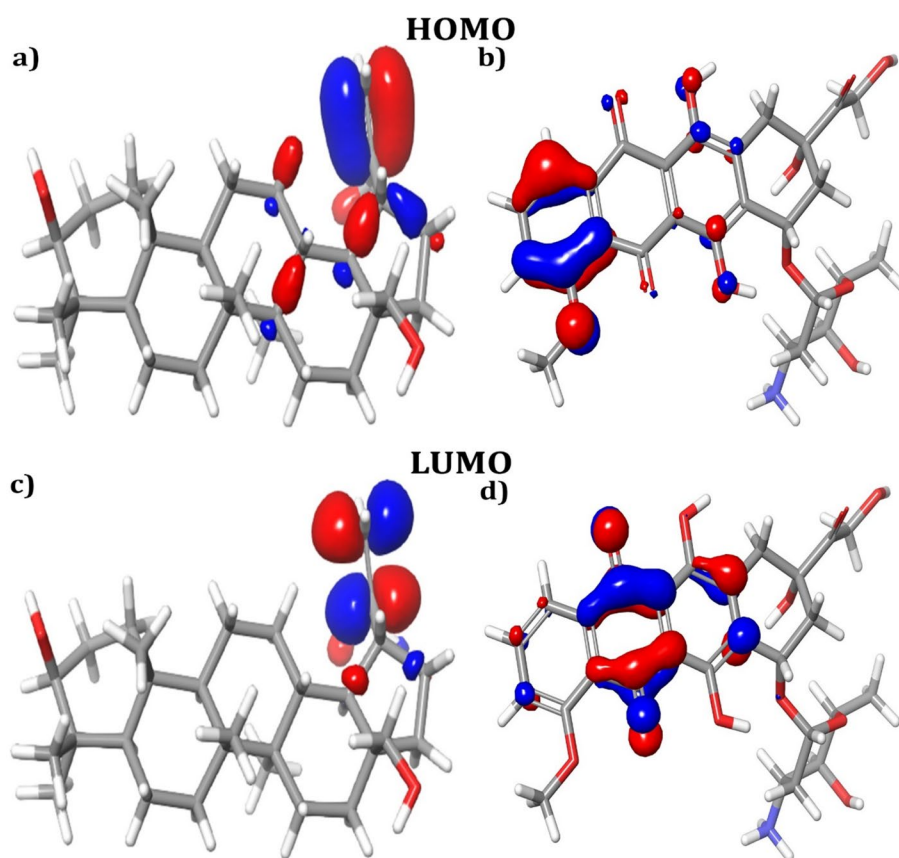
For charge transfer interactions with the epigenetic protein binding site, the orbital structures of the compounds play a crucial role. An available electron acceptor exists in a molecule with a high HOMO value. Furthermore, molecules intermolecular charge transfer and bioactivity are greatly affected by a more negligible energy difference between LUMO and HOMO energies. The low affinity of the inhibitors for epigenetic proteins is due to the massive energy gap in the compounds, which negatively affects the electron

traveling from the HOMO to the LUMO. The electronic and molecular properties of the pilot molecules were calculated using density functional theory. LUMO values represent the electron-accepting ability and a distinct energy gap that shows its electron affinity, whereas HOMO values denote the ability to donate electrons. The HOMO orbital energy of the BE molecule was  $-0.231397$  eV, and the LUMO orbital energy was  $0.023250$  eV. The expected energy gap for BE molecules was  $0.254647$  eV. Whereas, the HOMO orbital energy of DOX was  $-0.290605$  eV, and LUMO orbital energy was  $-0.159686$  eV. The expected energy gap for the DOX molecule was  $0.130909$  eV. The HOMO–LUMO energy gap determines lead molecules' chemical hardness, reactivity, and polarizability (Fig. 6). Due to the DFT studies' elucidation of electrophilic and nucleophilic reactivity zones in BE, these regions may be exploited to enhance the chemical reactivity and efficiency of the compound (Fig. 7).

### Cytotoxicity analysis

Following a preliminary screening analysis that included docking, modeling, and pharmacokinetics profiling, the cytotoxicity test results were validated using *In vitro* investigations. Treatment of Hela cells with varied doses of BE (ranging from 0.01 to 20  $\mu\text{g/ml}$ ) resulted in a substantial

**Fig. 7** **a** Betulin and Doxorubicin's boundary chemical orbitals (HOMO) and the accompanying transitioning energies. **b** Betulin and Doxorubicin's boundary chemicals orbitals (LUMO) and the accompanying transitioning energies



reduction in the viability of cervical cancer cells, with the inhibitory concentration ( $IC_{50}$ ) estimated to be roughly 15  $\mu\text{g}/\text{ml}$ . It is important to note that BE exhibited a low level of cytotoxicity toward normal cells, which suggests that it has the potential to be a selective therapy option for cervical cancer (Fig. 8).

## Discussion

Cervical cancer is one of the fourth leading causes of mortality among women in the world. The extent of malignancy of CCa can be classified based on stages of migration, invasion, and metastasis [30]. Metastatic lesion formation is promoted at stage III to IV transition, wherein stages IV A and B are categorized based on the type of malignant spread in and around the gynecological system. The incidence and prevalence of mortality rates of CCa across India have increased over the past few years [32]. In the present scenario, mortality is restricted to the genetic constituents, which are the key drivers of cellular reprogramming. This enables sustainment through intricate mechanisms and the presence of extra-genetic ailments termed epigenetics adds up complicity in terms of pathogenesis in CCa. Epigenetic elements represent an intriguing mode of action to regulate gene/protein expression patterns comprising manipulated cellular-physiological and biochemical processes [33]. Methylation, demethylation, acetylation, or deacetylation are some of the critical modifications enrolled by epigenetic ailments encompassing the tumorigenesis process in several cancers, including cervical. This has provoked the development of pharmaceuticals to target these epigenetic proteins, which have displayed robust anti-tumor activities against several cancers, including cervical cancer [34]. For instance, Takai et al. reported that HDAC inhibitors (HDACi) restricted cell proliferation by

inducing apoptosis and arresting the alteration of malignant phenotype expression against human cervical carcinoma [35]. In addition, these HDACi have exerted potentiating anti-tumor effects in vivo and clinical trials against cervical carcinoma [36]. Likewise, histone lysine methyltransferases (KMT) have been enthralling therapeutic targets in most cancers, including cervical cancer. One of the most potent natural products, curcumin, exerted influential anti-tumor activity against several cancers, which includes the alarming cervical cancer and breast. Among the existing signaling pathways, curcumin demonstrated anti-proliferative, anti-invasive, and anti-migrating properties via modulation of epigenetic markers in lungs (38), colon (39), and breast (40). DNMT3A, HDAC4, and KMT2C are critical nodes in the epigenetic regulatory network of cervical cancer [37]. A multifaceted approach to modulating gene expression patterns that promote oncogenesis and tumor progression is provided by targeting these proteins [38]. It is possible that the therapeutic efficacy of cervical cancer could be improved and resistance mechanisms could be overcome by combining inhibitors targeting DNMT3A, HDAC4, and strategies to restore KMT2C function synergistically [39]. The development of biomarkers for patient stratification and personalized treatment approaches in cervical cancer can be facilitated by an understanding of the molecular pathways involving these proteins [40]. Likewise, Paclitaxel, a triterpenoid, has served as one of the potent chemotherapeutic agents used to treat patients with advanced cervical cancer via the downregulation of ERK/JNK or NF-KB pathway [41].

Further, the combination of paclitaxel with bevacizumab has appeared as one of the gold standard therapeutic agents for metastatic cervical cancer. Triterpenoid, in combination with taxol, synergistically arrested cervical cancer cell proliferation via modulating reactive oxygen species (ROS) production and mitochondrial dysfunction [42]. BE, a terpenoid molecule, is reported as one of the efficacious phytochemicals against melanoma, leukemia, colon, lung, and cervical carcinomas [43]. In the same study, it was reported that BE exhibited potent anti-tumor effects against each cancer cell, with no cytotoxicity in normal cells, which was validated further using in vivo platform [44]. BE has been reported to induce apoptosis by downregulating PI3K/AKT and inducing mitochondria-dependent apoptosis in human cervical cancer cells (HeLa) [45].

Additionally, proteomic analysis of BE-treated cervical cells revealed that most of the differentially expressed genes were involved in ROS-mediated apoptosis induction in the HeLa [46]. The previously reported studies suggest Betulin shows promise as a therapeutic agent in cervical cancer due to its selective cytotoxicity and potential to modulate epigenetic markers associated with cancer progression. Molecular docking is a promising computational tool for identifying potential drug candidates. Thus, we conducted molecular docking

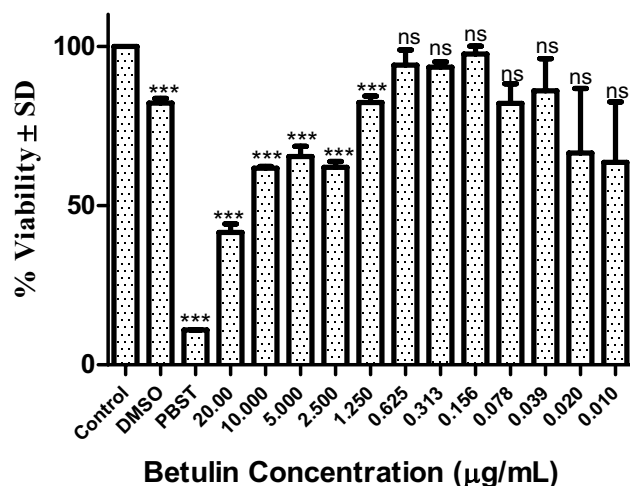


Fig. 8 Depicts the MTT assay result, and it shows  $IC_{50} = 15 \mu\text{g}/\text{ml}$



and virtual screening of 5000 phytochemicals targeting three important epigenetic proteins: Histone Deacetylase (HDAC4), DNA Methyltransferase 3A (DNMT3A), and Histone-lysine *N*-methyltransferase (KMT2C). Initially, the molecules were passed through the pre-filters using Lipinski's rule of five and finally, 364 confirmations generated in the ligand preparations process were screened on the substrate binding site of the three epigenetic proteins using the Glide score. We identified a list of ligands that had low binding energy based on the Glide score and low RMSD values between the ligand poses. Our molecular docking results showed that BE showed a high binding affinity with KMT2C (−9.8 kcal/mol) as compared to HDAC4 (−9.7 kcal/mol) and DNMT3A (−7.8 kcal/mol). The molecular interaction analysis depicted that the BE molecule has established stable hydrogen bonds with the active site residues of the target proteins. Moreover, the molecular docking of the control drug Doxorubicin with the epigenetic targets has shown a comparatively lower docking score than the test molecule BE. Further, the molecular dynamics simulations confirmed the stable binding and stability of the BE molecule within the active site of the epigenetic proteins. The toxicity evaluation through experimental techniques are expensive and time-consuming process. Based on the toxicity profile of 364 lead molecules, 11 molecules which are predicted to be non-toxic in nature were selected for further analysis. The ADME properties (QPlogPo/wb, QPlogS, QplogHERG, Rule of five, ClQPlogS, QPlogBB, QPlogKhsa, QPlogKp, and rule of three) of the hits predicted by Qikprop are shown to be in an acceptable range. The DFT studies depicted the electrophilic and nucleophilic reactivity regions on the BE identified against the three epigenetic proteins which can be potentially exploited to enhance the chemical reactivity and efficacy. Various computational studies have also reported BE as a potential inhibitor against cervical cancer through different *in silico* methods [47]. We have further validated the *in silico* results through the cytotoxicity studies using MTT Assay in HeLa cell lines, wherein BE exhibited significant cytotoxic effects at its respective IC<sub>50</sub> in comparison to the control. Our results suggested BE as a potential epigenetic inhibitor against cervical cancer as compared to the standard FDA-approved drug. Thus, BE can be considered a potential candidate drug candidate for further clinical studies. Nevertheless, we acknowledge that computational docking analysis has limitations and further detailed *in vitro* and *in vivo* studies are needed to validate the inhibitory effects of BE against these epigenetic targets as potential drugs for cervical cancer.

## Conclusion

We concluded that BE exhibited a strong affinity for the epigenetic proteins (HDAC4, DNMT3A, and KMT2C) and established stable hydrogen bonds and a water bridge

throughout the simulation, which improved protein inhibition and kept the complex stable. The present study's *in silico* results prove that BE has an epigenetic inhibitory function. In addition, the *in vitro* assay confirmed with *in silico* investigations wherein, BE had a low IC<sub>50</sub> value inhibited the proliferation of these cervical cancer cells via modulation of epigenetic proteins. The vivid investigations based on *in silico* experimental studies depicted that BE apprehended as a fascinating therapeutic target against epigenetic markers based on molecular docking and simulation results. The *in silico* result that BE forms persistent hydrogen bonds and water bridges to improve protein inhibition is consistent with the manner of competitive inhibition of epigenetic proteins. This is where our research can provide the groundwork for future cervical cancer treatments involving BE as powerful epigenetic protein inhibitors.

**Acknowledgements** We sincerely acknowledge Lovely Professional University, Jalandhar, India, Bioclues Organization, Hyderabad, India and Virchow Biotech Pvt Ltd, Manufacturing and R&D Facility, Gaggilapur Hyderabad, India. The authors thank the Center for Bioinformatics, KAHE, for providing a high-performance computing facility (NVIDIA DGX A100 server) to carry out the molecular dynamics' simulations.

**Author contributions** Sugunakar Vuree (SV) conceptualized the idea and methodology and proofread the initial and final draft. Satbir Kour (SK) wrote the first draft. Indrani Biswas (IB) edited the draft, and SK, Swati Arora and Sumit Sheoran (SS) analyzed the *In silico* Results. Anjuvan Singh (AS) and Smita C Pawar (SCP) proofreading. Shyam Perugu (SP) is supportive of docking and simulation. Dhamodharan Prabhu (DP) supported Docking, DFT calculations, and simulations.

**Conflict of interests** The authors declare no competing interests.

## References

- Golkar Z (2020) CRISPR: a journey of gene-editing based medicine. *Genes Genom* 42(12):1369–1380
- Jeong HM, Kwon MJ, Shin YK (2014) Overexpression of cancer-associated genes via epigenetic derepression mechanisms in gynecologic cancer. *Front Oncol* 4:12
- Rhee I, Bachman KE, Park BH, Jair KW, Yen RW, Schuebel KE, Cui H, Feinberg AP, Lengauer C, Kinzler KW, Baylin SB (2002) DNMT1 and DNMT3b cooperate to silence genes in human cancer cells. *Nature* 416(6880):552–556
- Kaefer CM, Milner JA (2008) The role of herbs and spices in cancer prevention. *J Nutr Biochem* 19(6):347–361
- Quarta A, Gaballo A, Pradhan B, Patra S, Jena M, Ragusa A (2021) Beneficial oxidative stress-related trans-resveratrol effects in the treatment and prevention of breast cancer. *Appl Sci* 11(22):11041
- Vernousfaderani EK, Akhtari N, Rezaei S, Rezaee Y, Shiranirad S, Mashhadi M, Hashemi A, Khankandi HP, Behzad S (2021) Resveratrol and colorectal cancer: a molecular approach to clinical researches. *Curr Top Med Chem* 21(29):2634–2646
- Udenigwe CC, Ramprasath VR, Aluko RE, Jones PJ (2008) The potential of resveratrol in anticancer and anti-inflammatory therapy. *Nutr Rev* 66(8):445–454

8. Sak K (2014) Characteristic features of cytotoxic activity of flavonoids on human cervical cancer cells. *Asian Pac J Cancer Prev* 15(19):8007–8018
9. Mehta P, Pawar A, Mahadik K, Bothiraja C (2018) Emerging novel drug delivery strategies for bioactive flavonol fisetin in biomedicine. *Biomed Pharmacother* 106:1282–1291
10. Khamjan NA, Beigh S, Algaissi A, Megha K, Lohani M, Darraj M et al (2023) Natural and synthetic drugs and formulations for intra-vaginal HPV clearance. *J Infect Public Health* 16(9):1471–1480
11. Patra KC, Pareta SK, Harwansh RK, Kumar KJ (2010) Traditional approaches towards standardisation of herbal medicines—a review. *J Pharm Sci Technol* 2(11):372–379
12. Brooijmans N, Kuntz ID (2003) Molecular recognition and docking algorithms. *Ann Rev Biophys Biomolec Struct* 32(1):335–373
13. Krasutsky PA (2006) Birch bark research and development. *Nat Prod Rep* 23:919–942
14. Dehelean CA, Feflea S, Molnár J, Zupko I, Soica C (2012) Betulin as an anti-tumour agent tested in vitro on A431, HeLa and MCF7 and as an angiogenic inhibitor in vivo in the CAM assay. *Nat Prod Commun* 7(8). <https://doi.org/10.1177/1934578X1200700805>.
15. Soica CM, Dehelean CA, Peev C, Aluas M, Zupko I, Kása P Jr, Alexa E (2012) Physico-chemical comparison of betulinic acid, Betulin and birch bark extract and in vitro investigation of their cytotoxic effects towards skin epidermoid carcinoma (A431), breast carcinoma (MCF7) and cervix adenocarcinoma (HeLa) cell lines. *Nat Prod Res* 26(10):968–974
16. Zhao J, Li R, Pawlak A, Henklewska M, Sysak A, Wen L, Yi JE, Obmińska-Mrukowicz B (2018) Anti-tumor activity of betulinic acid and Betulin in canine cancer cell lines. *In Vivo* 32(5):1081–1088
17. Sundaram MK, Ansari MZ, Al Mutery A, Ashraf M, Nasab R, Rai S, Rais N, Hussain A (2018) Genistein induces alterations of epigenetic modulatory signatures in human cervical cancer cells. *Anti-Cancer Agents Med Chem (Formerly Current Medicinal Chemistry-Anti-Cancer Agents)* 18(3):412–421.
18. Das SK, Mahanta S, Tanti B, Tag H, Hui PK (02) Identification of phytocompounds from *Houttuynia cordata* Thunb. as potential inhibitors for SARS-CoV-2 replication proteins through GC–MS/LC–MS characterisation, molecular docking and molecular dynamics simulation. *Molecular Divers* 26(1):365–388.
19. Rose PW, Prlić A, Altunkaya A, Bi C, Bradley AR, Christie CH, Costanzo LD, Duarte JM, Dutta S, Feng Z, Green RK (2016) The RCSB protein data bank: an integrative view of protein, gene and 3D structural information. *Nucleic Acids Res*, gkw1000.
20. Repasky MP, Murphy RB, Banks JL, Greenwood JR, Tubert-Brohman I, Bhat S, Friesner RA (2012) Docking performance of the glide program evaluated on the Astex and DUD datasets: a complete set of glide SP results and selected results for a new scoring function integrating WaterMap and glide. *J Comput Aided Mol Des* 26:787–799
21. Meng XY, Zhang HX, Mezei M, Cui M (2011) Molecular docking: a powerful approach for structure-based drug discovery. *Curr Comput Aided Drug Des* 7(2):146–157
22. Guo Z, Mohanty U, Noehre J, Sawyer TK, Sherman W, Krilov G (2010) Probing the  $\alpha$ -helical structural stability of stapled p53 peptides: molecular dynamics simulations and analysis. *Chem Biol Drug Des* 75(4):348–359
23. Schrödinger Release 2021–2: Desmond Molecular Dynamics System, D. E. Shaw Research, New York, NY, 2021. Maestro-Desmond Interoperability Tools, Schrödinger, New York, NY, 2021.
24. Demeule M, Régina A, Jodoin J, Laplante A, Dagenais C, Berthelot F, Moghrabi A, Béliveau R (2002) Drug transport to the brain: key roles for the efflux pump P-glycoprotein in the blood–brain barrier. *Vascul Pharmacol* 38(6):339–348
25. Montavon G, Rupp M, Gobre V, Vazquez-Mayagoitia A, Hansen K, Tkatchenko A, Müller KR, Von Lilienfeld OA (2013) Machine learning of molecular electronic properties in chemical compound space. *New J Phys* 15(9):095003
26. Palanivel S, Yli-Harja O, Kandhavelu M (2022) Molecular interaction study of novel indoline derivatives with EGFR-kinase domain using multiple computational analysis. *J Biomol Struct Dyn* 40(16):7545–7554
27. Kour S, Biswas I, Sheoran S, Arora S, Sheela P, Duppal SK et al (2023) Artificial intelligence and nanotechnology for cervical cancer treatment: Current status and future perspectives. *J Drug Deliv Sci Technol* 83:104392
28. Novel Chemotherapy using Histone Deacetylase Inhibitors in Cervical Cancer (2011) *Asian Pacific J Cancer Prevent* 12(3):575–580.
29. Psilopatis I, Garmis N, Garmis A, Vrettou K, Sarantis P, Koustas E et al (2023) The emerging role of histone deacetylase inhibitors in cervical cancer therapy. *Cancers (Basel)* 15(8):2222
30. Sun R, Qin C, Jiang B, Fang S, Pan X, Peng L, Liu Z, Li W, Li Y, Li G (2016) Down-regulation of MALAT1 inhibits cervical cancer cell invasion and metastasis by inhibition of epithelial–mesenchymal transition. *Mol BioSyst* 12(3):952–962
31. Rezasoltani S, Asadzadeh-Aghdaei H, Nazemalhosseini-Mojarad E, Dabiri H, Ghanbari R, Zali MR (2017) Gut microbiota, epigenetic modification and colorectal cancer. *Iran J Microbiol* 9(2):55
32. Hagemann T, Bozanovic T, Hooper S, Ljubac A, Slettenaar VI, Wilson JL, Singh N, Gayther SA, Shepherd JH, Van Trappen PO (2007) Molecular profiling of cervical cancer progression. *Br J Cancer* 96(2):321–328
33. Sindelar RD (2024) Genomics, other “OMIC” technologies, precision medicine, and additional biotechnology-related techniques. In: *Pharmaceutical biotechnology: fundamentals and applications*. Springer, Cham, pp 209–254
34. Aman MN (xxx) The role of extracellular matrix in tumor progression and treatment response (Doctoral dissertation).
35. Ming T, Tao Q, Tang S, Zhao H, Yang H, Liu M et al (2022) Curcumin: an epigenetic regulator and its application in cancer. *Biomed Pharmacother* 156:113956
36. Eum DY, Byun JY, Yoon CH, Seo WD, Park KH, Lee JH et al (2011) Triterpenoid pristimerin synergises with taxol to induce cervical cancer cell death through reactive oxygen species-mediated mitochondrial dysfunction. *Anticancer Drugs* 22(8):763–773
37. Jones PA, Baylin SB (2002) The fundamental role of epigenetic events in cancer. *Nat Rev Genet* 3(6):415–428. <https://doi.org/10.1038/nrg962>
38. Laguer G, O’Carroll D, Rembold M et al (2002) Essential function of histone deacetylase 1 in proliferation control and CDK inhibitor repression. *EMBO J* 21(11):2672–2681. <https://doi.org/10.1093/emboj/21.11.2672>
39. Guo C, Chen LH, Huang Y et al (2013) KMT2D maintains neoplastic cell proliferation and global histone H3 lysine 4 monomethylation. *Oncotarget* 4(12):2144–2153. <https://doi.org/10.18632/oncotarget.1525>.
40. Mansouri H, Alcaraz LB, Mollevi C, Mallavialle A, Jacot W, Boissière-Michot F, Simony-Lafontaine J, Laurent-Matha V, Roger P, Liaudet-Coopman E, Guiu S (2020) Co-expression of androgen receptor and cathepsin D defines a triple-negative breast cancer subgroup with poorer overall survival. *Cancers* 12(5):1244
41. Xu T, Pang Q, Wang Y, Yan X (2017) Betulinic acid induces apoptosis by regulating PI3K/Akt signaling and mitochondrial pathways in human cervical cancer cells. *Int J Mol Med* 40(6):1669–1678
42. Xu T, Pang Q, Zhou D, Zhang A, Luo S, Wang Y et al (2014) Proteomic investigation into betulinic acid-induced apoptosis of human cervical cancer HeLa cells. *PLoS ONE* 9(8):e105768

43. Kumar A, Rathi E, Kini SG (2019) E-pharmacophore modelling, virtual screening, molecular dynamics simulations and in-silico ADME analysis for identification of potential E6 inhibitors against cervical cancer. *J Mol Struct* 1189:299–306
44. Liu R (xxx) Pharmacology and toxicology of Echinacea, Souroubea and Platanus spp. Doctoral dissertation, Université d'Ottawa/University of Ottawa.
45. Abdalla M, Mohapatra RK, Sarangi AK, Mohapatra PK, Eltayb WA, Alam M, El-Arabey AA, Azam M, Al-Resayes SI, Seidel V, Dhama K (2021) In silico studies on phytochemicals to combat the emerging COVID-19 infection. *J Saudi Chem Soc* 25(12):101367
46. Jorgensen WL, Chandrasekhar J, Madura JD, Impey RW, Klein ML (1983) Comparison of simple potential functions for simulating liquid water. *J Chem Phys* 79(2):926–935
47. Pęcak P, Świtalska M, Chrobak E, Boryczka G, Bębenek E (2022) Betulin acid ester derivatives inhibit cancer cell growth by inducing apoptosis through caspase cascade activation: a comprehensive in vitro and in silico study. *Int J Mol Sci* 24(1):196
48. Yang IV, Schwartz DA (2011) Epigenetic control of gene expression in the lung. *Am J Respir Crit Care Med* 183(10):1295–1301
49. Abdel-Hafiz HA, Horwitz KB (2015) Role of epigenetic modifications in luminal breast cancer. *Epigenomics* 7(5):847–862
50. Voutchkova AM, Ferris LA, Zimmerman JB, Anastas PT (2010) Toward molecular design for hazard reduction—fundamental relationships between chemical properties and toxicity. *Tetrahedron* 66(5):1031–1039

**Publisher's Note** Springer Nature remains neutral with regard to jurisdictional claims in published maps and institutional affiliations.

Springer Nature or its licensor (e.g. a society or other partner) holds exclusive rights to this article under a publishing agreement with the author(s) or other rightsholder(s); author self-archiving of the accepted manuscript version of this article is solely governed by the terms of such publishing agreement and applicable law.



# Flavonoids as an Alternative Option to Treat Cancer

Swati Arora, Shefali Srivastava, Utkarsh Verma, Sumit Sheoran, and Neeraj Kumar

## Abstract

Cancer continues to be a leading cause of mortality worldwide, with rising prevalence linked to genetic abnormalities, epigenetic alterations, detrimental lifestyle choices, and an aging demographic. Conventional cancer treatments, such as chemotherapy, radiation, and immunotherapy, while somewhat successful, sometimes entail significant adverse effects, drug resistance, and restricted access to tumor tissues, especially in advanced-stage tumors. These problems have exacerbated the quest for alternative and complementary therapy. Flavonoids, a category of naturally occurring polyphenolic chemicals present in several fruits, vegetables, and medicinal plants, have garnered significant interest for their anticancer properties. Compounds such as kaempferol, quercetin, apigenin, and diosmin demonstrate several modes of action, including antioxidant properties, reduction of tumor cell growth, activation of apoptosis, and suppression of angiogenesis and metastasis. Moreover, flavonoids have demonstrated the capacity to regulate critical signaling pathways implicated in cancer advancement, including the PI3K/Akt, mTOR, and JAK/STAT pathways. Recent

---

First Equal contributing authors: Swati Arora, Sumit Sheoran.

---

S. Arora · S. Sheoran (✉)

Lovely Professional University, Jalandhar, Punjab, India

Thyme Phyto BioMed Pvt. Ltd, Hisar, Haryana, India

e-mail: [sumit.12009083@lpu.in](mailto:sumit.12009083@lpu.in)

S. Srivastava

Shambhunanth Institute of Pharmacy, Jhalwa, Prayagraj, Uttar Pradesh, India

U. Verma

Faculty of Pharmacy, United University, Prayagraj, Uttar Pradesh, India

N. Kumar

Bhupal's Noble College of Pharmacy, Udaipur, Rajasthan, India

breakthroughs in nanotechnology have improved the bioavailability and targeted distribution of flavonoids, hence enhancing their medicinal efficiency. This chapter underscores the potential of flavonoids in cancer prevention and treatment, examines the incorporation of flavonoid-based nanoparticles in augmenting cancer therapy, and stresses the necessity for additional research to assess their safety, pharmacokinetics, and synergistic interactions with standard therapies.

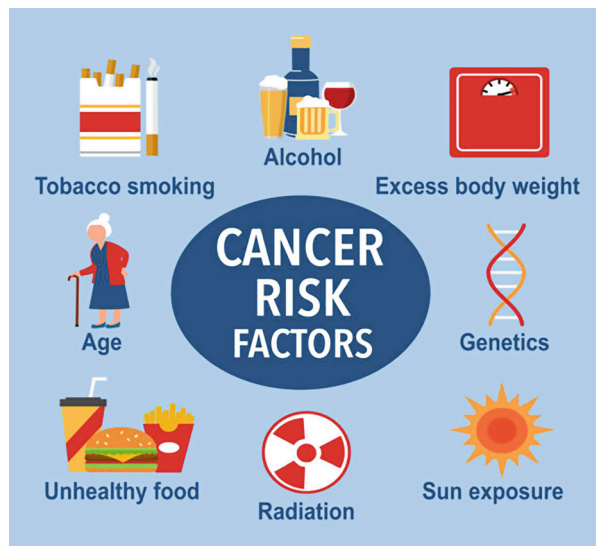
## Keywords

Cancer · Diosmetin · Diosmin · Flavonoids · Nanoformulations · Quercetin

## 1 Introduction

Cancer is currently the leading cause of mortality worldwide, significantly impacting life expectancy in the twenty-first century (Cao et al. 2017). Various factors contribute to the increasing number of cancer-related deaths; these include genetic predisposition, changes in epigenetic markers, rapid population growth leading to increased cancer incidence, an aging population with higher cancer risk, and unhealthy lifestyle choices like smoking, lack of physical activity, and consumption of Western dietary patterns (Fig. 1) (Mbemi et al. 2020). These factors particularly exacerbate the cancer burden in developing countries due to their influence on cancer incidence and mortality. Conventional cancer treatments, such as chemotherapy, radiotherapy, and immunotherapy, face challenges such as limited access to tumor

**Fig. 1** Various risk factors associated with cancer



tissues and side effects from high doses and non-targeted therapies (Debela et al. 2021; Kciuk et al. 2023) (Arora et al. 2023; Sheoran et al. 2022a, 2023a, b, c, 2024; Thesis et al. 2019).

Phytochemicals from plants, such as resveratrol, which targets the cell cycle; sulforaphane, which activates detoxification enzymes; and berberine, which stops tumor growth pathways, have become very promising cancer treatments (Wang et al. n.d.). Their ability to modulate multiple molecular pathways while maintaining a favorable safety profile makes them valuable in cancer treatment (Hashem et al. 2022). Researchers have found that flavonoids such as kaempferol, EGCG, curcumin, and others can help combat various types of cancer. These chemicals, acting as anticarcinogenic agents, stop pro-carcinogens and the enzymes that turn them on. They also prevent carcinogens from functioning and shield DNA from oxidative stress-induced damage (Amjad et al. 2022).

Despite extensive research on their potential to fight cancer, we have not thoroughly assessed the safety profiles of these flavonoids. Safety evaluations typically involve in vitro studies, animal models, and clinical trials to determine the toxicity, pharmacokinetics, and potential interactions of these compounds. Some studies suggest that in specific situations, these flavonoids may act as pro-oxidants and interact with other medications through biotransformation enzymes (Khan et al. 2021). For example, concurrent use of flavonoids with certain chemotherapy drugs may lead to altered drug metabolism and efficacy, emphasizing the importance of understanding these interactions. The advent of nanotechnology has facilitated the development of drug delivery systems that selectively target tumor-specific tissues. Nanocarriers offer advantages such as enhanced drug accumulation at the tumor site, controlled release of therapeutic agents, and reduced systemic toxicity, making them promising tools in cancer therapy (Chehelgerdi et al. 2023). Nanocarriers can enhance the pharmacokinetics and pharmacodynamics of incorporated drugs, allowing for greater accumulation at tumor sites and potentially improving treatment efficacy (Al-Thani et al. 2024). Currently, research is exploring the use of nanotechnologies to deliver multiple drugs simultaneously, which holds significant promise in cancer treatment. For instance, clinical trials are evaluating the co-delivery of chemotherapy agents and immunotherapeutic drugs using nanocarriers to enhance treatment outcomes and reduce drug resistance (Elumalai et al. 2024).

Cancer cells have special biological traits that help them grow and turn cancerous in a number of ways, such as by disrupting cell signaling pathways, avoiding immune surveillance, encouraging blood vessel growth, and being resistant to apoptosis (programmed cell death). These characteristics contribute to the aggressiveness and treatment resistance of cancer. Some of these include keeping proliferative signaling going, avoiding growth suppressors and immune system damage, maintaining immortal replication, encouraging blood vessel growth, and fighting cell death. Such characteristics are a result of epigenetic reprogramming and genomic instability caused by repeated mutations in regulatory genes. Understanding these fundamental cancer characteristics is critical for developing successful treatments.

A key challenge in treating cancer is the resistance of tumor cells to multiple drugs, known as multidrug resistance (MDR). This resistance happens for a number of reasons, such as increased activity of drug efflux transporters like P-glycoprotein, activation of antiapoptotic pathways, and changes in drug targets (Duan et al. 2023). This makes it difficult to kill cancer cells effectively. Tumors trigger physiological responses that fight back, including avoiding drug-induced cell death, initiating detoxification pathways, absorbing drugs less efficiently, and enhancing DNA repair systems (Talib et al. 2021). Natural products have demonstrated potential in clinical trials to overcome these resistance mechanisms, offering the possibility of more effective treatment combinations with fewer side effects (Chunarkar-Patil et al. 2024).

Moreover, abnormal changes in gene activity, such as DNA methylation and histone modifications, play a crucial role in initiating and advancing tumors (Yang et al. 2022). Researchers are recognizing the potential of natural phenolic compounds found in plants as epigenetic agents that regulate these modifications in cancer therapy. Combining them with traditional chemotherapy drugs or other natural compounds often enhances their effectiveness (El Omari et al. 2021).

This chapter focuses on the utilization of flavonoids and nanoformulations in the treatment and prevention of cancer, underscoring the importance of investigating their safety and mechanisms to improve therapeutic strategies.

---

## 2 Therapeutic Potential of Flavonoids in Cancer Treatment

Targeted cancer medicines have markedly enhanced patient survival rates; yet, managing advanced-stage metastatic malignancies continues to pose a considerable challenge (Debela et al. 2021). Continued endeavors aim to identify safe and effective pharmaceuticals to enhance the efficacy of cancer therapy and reduce expenses. The utilization of plant-derived chemicals (Table 1) for chemoprevention and therapy is increasingly gaining prominence (Chaachouay and Zidane 2024). Plant-derived pharmaceuticals are employed to treat several acute and chronic ailments, including **paclitaxel** and **vincristine** (Cragg and Pezzuto 2016). Moreover, the intake of some fruits has been associated with a decreased risk of cancer occurrence. Despite the potential of plant-based chemicals in cancer treatment, the scientific comprehension of their molecular processes remains inadequate.

Recent breakthroughs in drug discovery, supported by advanced experimental and molecular biology tools, allow researchers to explore the efficacy of these phytochemicals in the treatment and prevention of cancer, inflammatory illnesses, and cardiovascular problems (Chihomvu et al. 2024). Of the roughly 250,000 recognized plant species, hardly 10% have undergone investigation for their medicinal properties in relation to various ailments.

Phytoconstituents (Fig. 2), especially secondary metabolites present in diverse plant components such as roots, leaves, bark, stems, fruits, and seeds, exhibit multiple pharmacological effects. Compounds such as alkaloids, saponins, flavonoids,



**Table 1** Flavonoids with anticancer properties

S.No.	Flavonoids	MOA	References
1.	Silybin	Inhibits mTOR signaling pathway	Garcia-Maceira and Mateo (2009)
2.	Apigenin	Demonstrates anticancer effects by activating both the JAK-STAT and Wnt/ $\beta$ -catenin signaling pathways	Ozbey et al. (2019)
3.	Modified flavonoids derivatives of silybin, such as 2,3-dehydrosilybin (DHS), 7-O-methylsilybin (7OM), 7-O-galloylsilybin (7OG), 7,23-disulphatesilybin (DSS), 7-O-palmitoylsilybin (7OP), and 23-O-palmitoylsilybin (23OP)	Exhibits growth inhibition and promotes apoptotic cell death	Agarwal et al. (2013)
4.	Luteolin	Induces autophagy and triggers apoptosis in MCF-7, ANA-1, and ACS gastric cells through the Akt, JNK, and p38 signaling cascades	Liao et al. (2018)
5.	Silybin nanosuspension	Causes growth inhibition in PC-3 cells and induces apoptosis in the G1 phase	Zheng et al. (2011)
6.	Tangeritin	Leads to cell cycle arrest via Cyp1A1 and Cyp1B1-mediated metabolism, particularly in MCF-7 and MDA-MB-468 breast cancer cell lines	Surichan et al. (2018)
7.	Silibinin	Inhibits rapamycin signaling, which reduces translation initiation	Lin et al. (2009)
8.	Kaempferol	Promotes apoptosis and induces autophagy by increasing the expression of miR-340 microRNA in colon cancer (HCT-116, HCT15, and SW480) and human lung cancer (A549) cell lines. Promotes apoptosis and induces autophagy by increasing the expression of miR-340 microRNA in colon cancer (HCT-116, HCT15, and SW480) and human lung cancer (A549) cell lines	Han et al. (2018)
9.	Quercetin	Triggers the mitochondrial-mediated apoptotic pathway, thus inhibiting the growth of metastatic ovarian cancer cells	Teekaraman et al. (2019)

(continued)



**Table 1** (continued)

S.No.	Flavonoids	MOA	References
10.	Myricetin	Suppresses metastasis by preventing cell migration, as observed in prostate cancer	Kumar et al. (2023)
11.	Hesperetin	Induces apoptosis in H522 lung cancer cells	Elango et al. (2018)
12.	Galangin	Reduces cellular proliferation by initiating apoptosis via the PI3K/Akt/mTOR signaling pathway in human kidney (A498) cancer cells	Zhou et al. (2018)
13.	Naringenin	Decreases cancer metastasis through voltage-gated sodium channels and initiates apoptosis at both early and late stages in prostate cancer	Aktas and Akgun (2018)
14.	Epigallocatechin gallate	Enhances chemoprevention and induces apoptosis through the Abl/Bcr-mediated p38-JAK2/STAT3/Akt and MAPK/JNK pathways in chronic myeloid leukemia and glioblastoma cells, respectively	Grube et al. (2018)
15.	Taxifolin	Inhibits carcinogenesis via the mTOR/PTEN axis and CYP1B1-mediated pathways	Haque et al. (2018)
16.	Catechin	Suppresses cancer growth by promoting programmed cell death	Xiao et al. (2019)
17.	Delphinidin	Promotes apoptosis and autophagy in HER2-positive MDA-MB-453 cancer cells	Chen et al. (2018)
18.	Cyanidin	Reduces angiogenesis in MCF-7 cells through the STAT3/VEGF signaling pathway	Ma and Ning (2019)
19.	Genistein	Increases apoptosis and inhibits cellular proliferation in human laryngeal cancer and melanoma cells expressing Mcl-1 and EP3, respectively	Ma et al. (2018)

terpenes, and glycosides have shown efficacy in cancer chemoprevention (Rabizadeh et al. 2022).

Their capacity to combat cancer is believed to stem from their capability to inhibit certain cellular enzymes and proteins that are crucial to metabolism (Fig. 3) (Park et al. 2020). Furthermore, these substances may initiate certain DNA repair processes or signaling pathways, which encompasses phosphatidylinositol 3-kinase (PI3K) and the mammalian target of rapamycin (mTOR), or enhance protective

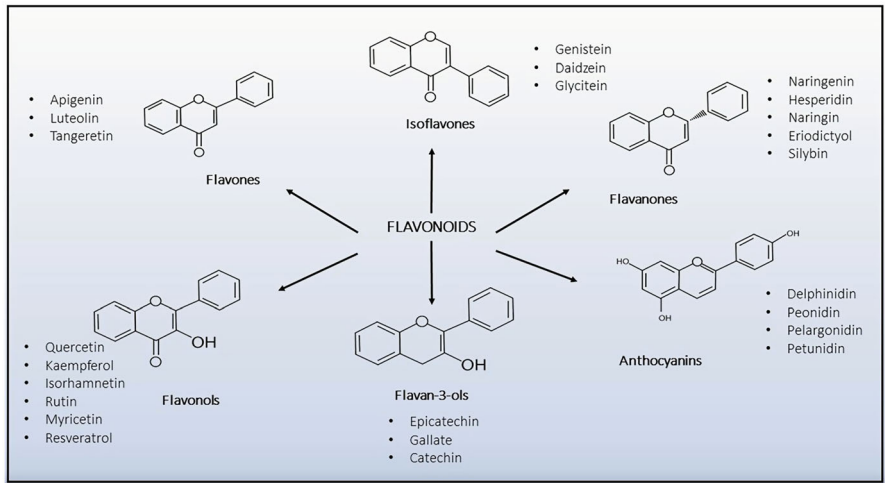


Fig. 2 Flavonoids and its characterization

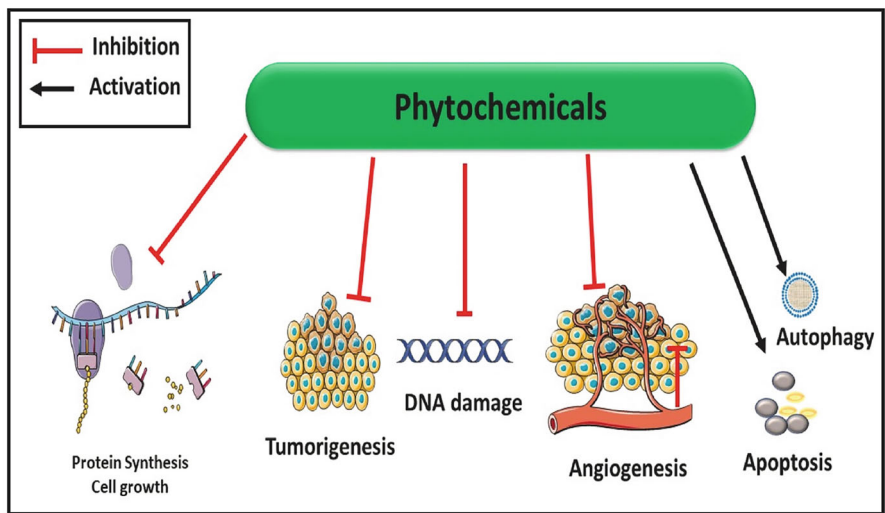
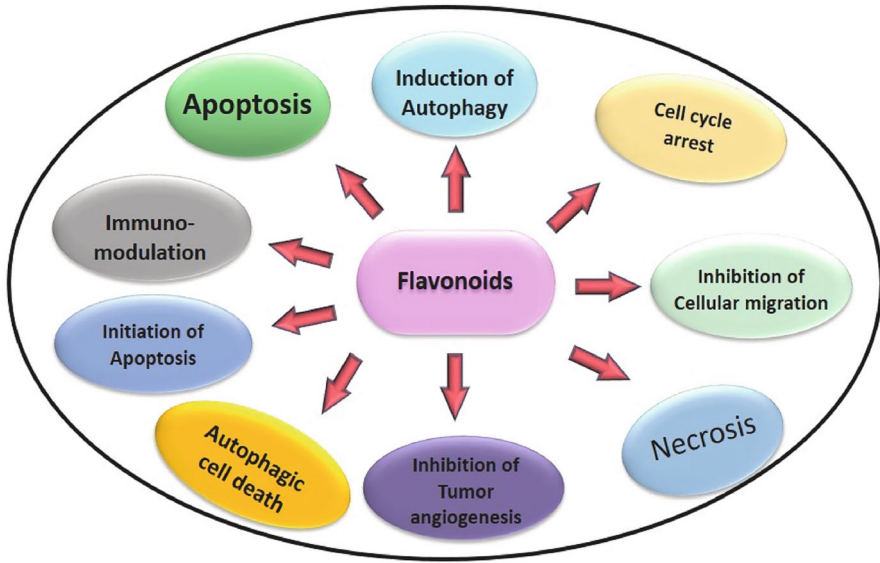


Fig. 3 Multifaceted mechanisms through which phytochemicals exert their anticancer effects

enzymes like caspases (Roy et al. 2023). These bioactive compounds can enhance the activity of antioxidant enzymes such as catalase, glutathione peroxidase, and superoxide dismutase, hence augmenting their potential as cancer preventive agents.

### Phytochemicals in Cancer Therapy: A Multifunctional Approach

Flavonoids, natural chemicals prevalent in several plant-based diets including tea, vegetables, fruits, soybeans, and grains (Shen et al. 2022). They are recognized for



**Fig. 4** Schematic representation of the diverse mechanistic pathways underlying the anticancer potential of flavonoids

their many attributes, including antioxidant benefits and anti-inflammatory activities (Fig. 4). Their structure comprises aromatic rings, and alterations in hydroxylation, polymerization, and other replacements influence their chemical behavior. Flavonoids exhibit variability in their chemical composition and are categorized according to the atomic arrangement in their structures, including the quantity and positioning of particular components. The impact of flavonoids on the body is dictated by their structure, including the core framework and particular constituents, which affect their ability to neutralize detrimental compounds and bind to metal ions.

Research demonstrates that flavonoids exhibit therapeutic promise for a wide range of ailments, including cancer, cardiovascular problems, and immunological issues (Farhan et al. 2023). Studies indicate that they can inhibit cellular proliferation and facilitate programmed cell death mechanisms such as apoptosis and autophagy. Furthermore, they can trigger cell death via necrosis, impede cell cycle progression, and inhibit cellular migration, invasion, or angiogenesis in malignancies (Fig. 4). This suggests that they may assist in overcoming or preventing chemotherapy resistance by altering enzymes that neutralize detrimental reactive oxygen species, thus enhancing the effectiveness of cancer treatment (Jiang et al. 2023). Furthermore, flavonoids possess the capacity to eradicate detrimental free radicals, mitigate oxidative stress, and modulate cellular metabolism (Panche et al. 2016). Flavonoids are acknowledged as eco-friendly and economical substances. Numerous flavonoids have been demonstrated to be safe and beneficial for diverse purposes, including

**Table 2** Flavonoids and its cancer type

Flavonoids	Cancer types	References
Artemisinin	Breast cancer, pancreatic cancer, and liver cancer	Efferth (2017)
EGCG, epigallocatechin	Breast, bladder, lung, skin, and prostate cancer	Iqbal et al. (2017)
Ginkgetin, ginkgolide A & B	Liver, hepatocarcinoma, prostate, and colon cancer	Xiong et al. (2016)
Solasonine, solamargine	Breast, skin, and lung cancer	Al Sinani et al. (2016)
Doxorubicin, rutin, and quercetin	Breast and lung cancer	Jaradat et al. (2016)
Licochalcone and licochalcone-A	Kidney, breast, stomach, and prostate cancer	Zhang et al. (2016)
Psoralidin	Prostate and stomach cancer	Pahari et al. (2016)
Xanthium	Lymphocyte leukemia cancer	Thangapazham et al. (2016)
Vicenin 2	Prostate cancer	Nagaprashantha et al. (2011)
Withaferin D and withaferin A	Breast, cervical, prostate, and colon, cancer	Lee and Choi (2016)
Gingerol	Liver, urinary, cervix, colon, and ovary cancer	Rastogi et al. (2015a)
Luteolin	Colorectal cancer	Osman et al. (2015)
Podophyllotoxin	Non-small cell lung carcinoma	Choi et al. (2015)
Procyanidins	Colon cancer	Cheah et al. (2014)
Emodin and alexin B	Stomach cancer	Shalabi et al. (2015)
Crocetin	Lung and hippocampal cancer	Bakshi et al. (2009)
Allylmercaptocysteine and allicin	Cervical and lymphoma cancer	Karmakar et al. (2011)
Bilobalide	Human colon cancer	Suzuki et al. (2004)
Cannabinoid	Female breast, colorectal, prostate, and lung cancer	Appendino et al. (2011)
Saffron	Pancreatic, lung, and liver cancer	Ververidis et al. (2007)
Crocetin, safranal, Picrocrocin, and crocin	Oral and sarcoma cancers	Hoshyar and Mollaei (2017)
Gingerol	Ovarian and colon cancers	Rastogi et al. (2015b)
6-Shogaol	Ovarian cancer	Ghasemzadeh et al. (2015)

cosmetic products, nutritional supplements, and pharmaceutical formulations (Amawi et al. 2017; Chahar et al. 2011; Dias et al. 2021; Falcone Ferreyra et al. 2012; Kühnau 1976; Woo et al. n.d.) (Table 2).

## 2.1 Key Phytochemicals in Cancer Treatment

### 2.1.1 Diosmin

Diosmin (Ds), the flavonoid, is a methoxy flavonoid (3,5,7-trihydroxy-4-methoxyflavone-7-rhamnoglucoside), which can be obtained from the plant *Abies nephrolepis*, *Scrophularia nodosa* L (Li and Du 2018) and the peels of some citrus fruits. Ds is a flavonoid glycoside with two glycosidic moieties in its structure and is synthesized from another bioflavonoid, hidrosmin (Ramelet 2011).

### Diosmin and Cancer

Anna Lewinska and their team (Lewinska et al. 2017) worked on 30 feeding flavonoids in vitro to check anticancer activities and selected Diosmin, a citrus flavonoid, due to its ability to diminish breast tumor cell activity at minimal micromolar concentrations. This study demonstrated that exposure to diosmin resulted in accelerated cellular aging and apoptosis, characterized by oxidative stress, DNA damage, and alterations in global DNA methylation patterns. The cellular response to diosmin was notably influenced by variations in the p53 status, expression levels of ERK1/2, and diosmin-induced autophagy in breast cancer cell lines MCF-7, MDA-MB-231, and SK-BR-3 [84][85].

Furthermore, the effects of diosmin on specific methylation markers were assessed in these breast carcinoma cell lines, revealing significant changes in DNA methylation and the expression of key methyltransferases, including DNMT1, DNMT2, DNMT3a, and DNMT3b. Diosmin exhibited a hypomethylating effect on DNA in MCF-7 cells, whereas it induced hypermethylation in SK-BR-3 cells. In contrast, MDA-MB-231 cells displayed no significant alterations in global DNA methylation levels.

For comparative analysis, 5-aza-2'-deoxycytidine (5-azadC) was employed as a reference compound for DNA methylation inhibition. Treatment with 5-aza-dC resulted in reductions of global DNA methylation by 33%, 25%, and 23% in MCF-7, MDA-MB-231, and SK-BR-3 cells, respectively. Notably, levels of DNMT1, a housekeeping transcription factor, remained unchanged in response to alterations in global DNA methylation. However, significant increases in the expression of de novo methyltransferases, particularly DNMT3a, were observed following diosmin treatment, suggesting a complex regulatory mechanism underlying its effects on DNA methylation dynamics. MCF-7 and SK-BR-3 cells treated with this showed a boost in DNMT3b (Lewinska et al. 2017).

Kilit et al. (2021) stated that it has cytotoxic, antiangiogenic, and antibacterial properties. Further, in a concentration and time-dependent approach, reduced cell growth in MDAMB-231 cells, with poor cytotoxic toward healthy human epithelium cells in vitro, caused apoptosis by raising the *Bax/Bcl-2* ratio or active caspase-3 levels. It was shown to be liable for morphological alterations and damage to DNA in MDA-MB-231 breast cancer (BC) cell lines. However, in addition to in vitro analysis, in vivo studies employing laboratory animals of tumorigenesis should be conducted to assess the therapeutic performance and define the mechanism and state it as a possible active drug for BC medicaments. Ds could be effective in the

treatment of melanoma (Kilit et al. 2021). The molecule was evaluated for anti-inflammatory activity, and the biochemical reduction of myeloperoxidase activity confirmed the inflammatory activity. It inhibits colonic MDA production and inhibits LTB<sub>4</sub> synthesis, preventing colonic inflammation through oxidation (Crespo et al. 1999). Diosmin is effective against hepatocellular carcinoma by attenuating the 2-AAF-induced hepatotoxicity and initial tumor promoters like *ODC*, *PCNA*, and *Ki67*. Ds inhibits cell proliferation, and it has shown chemopreventive activity and prevents hepatocarcinogenesis (Tahir et al. 2013). It also offers anti-inflammatory, antihyperglycemic, antioxidant, and antiproliferative characteristics, which mainly regulates cell proliferation by inducing apoptosis in oral cancer. It shows that the antiproliferative associated with the *STAT-3* pathway also creates an imbalance ratio in Bax/Bcl-2 ratio, which triggers the caspase cascade and favors the apoptosis. *IL-6/STAT-3* signaling pathway, which is the potent developer of tumor cells, is inhibited by Ds (Rajasekar et al. 2016). It induces apoptosis in DU145 prostate cancer cells by inducing oxidative stress intracellular total reactive oxygen species based on the superoxide formation, stimulating the DNA and breaking the double strand, producing the micronuclei further that induce apoptosis (Lewinska et al. 2015). It is also active against hepatocellular carcinoma HA22T and inhibits cell proliferation. This influences the cell cycle arrest in the G2/M stage due to P53 activation and the PI3K-Akt-MDM2 signaling pathway (Dung et al. 2012b). Rajamanickam Buddhan and their team (Buddhan and Manoharan 2017) investigated Diosmin's in vitro cytotoxic activity in A431 skin cancerous cells. The cytostatic potential of this molecule was investigated in A431 cells using the MTT test, twofold staining, and dichloro-dihydro-fluorescein diacetate assay (reactive oxygen species [ROS] generation). DNA fragment decreased the survival of A431 cells dose sensitively, with an inhibitory concentration of 50% reaching at 45 g/ml using the MTT test. Diosmin at 45 g/ml produced increased ROS in A431 cells compared to the untreated control. In A431 cells, it increased the transcription of p53, caspases-3 and 9, while decreasing the transcription of Bcl-2, matrix metalloproteinases-2 and 9. Its carcinogenic or anti-cell proliferation ability is related to its ROS-mediated apoptosis induction potential and its involvement in inhibiting penetration in A431 cells (Dung et al. 2012a) (Fig. 5).

At varying concentrations, certain flavonoids have been shown to induce premature senescence and increased mortality in MCF-7 breast cancer cells. Among various breast cancer cell lines tested, including MDA-MB-231 and SKBR-3, MCF-7 demonstrated the highest sensitivity. The treatment with these flavonoids led to G2/M phase cell cycle arrest, accompanied by elevated levels of tumor suppressor proteins p53, p21, and p27. Additionally, there was a significant increase in senescence-associated  $\beta$ -galactosidase (SA- $\beta$ -gal) activity, oxidative stress markers, and DNA damage in MCF-7 cells at lower concentrations indicative of senescence. At higher concentrations, these compounds resulted in increased nitric oxide production, elevated levels of reactive oxygen species (ROS), total superoxide, enhanced mitochondrial biogenesis, and protein carbonylation, ultimately leading to cellular mortality.

The pro-apoptotic effects of these flavonoids were further established in the androgen-independent prostate cancer cell line DU145, where the transcriptomic

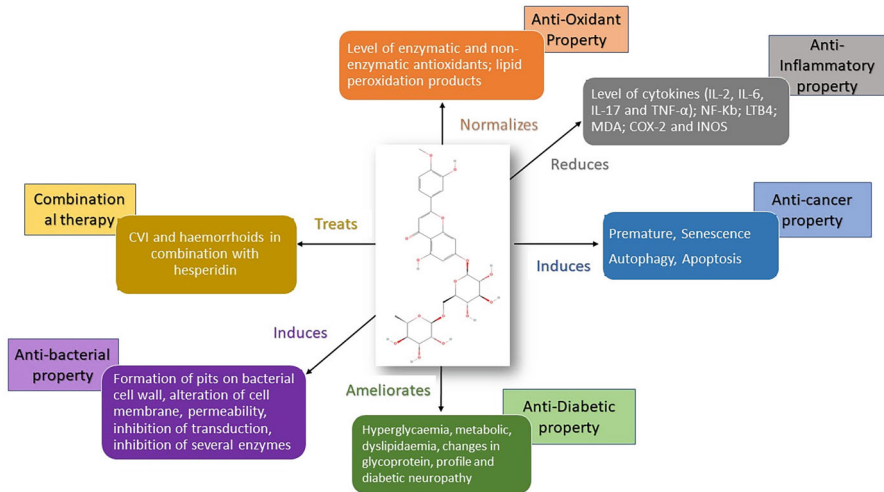


**Fig. 5** Therapeutic nature of diosmin. (Adopted from Huwait and Mobashir 2022)

profile and toxicity of diosmin, naringin, and hesperidin were evaluated. Diosmin exhibited the most significant cytotoxic effects among the three. The phytochemicals induced lipid peroxidation and disrupted cellular redox homeostasis in DU145 cells, resulting in alterations to the mitochondrial membrane potential and subsequent apoptotic cell death. Notably, diosmin treatment significantly increased ROS production and was associated with a higher frequency of DNA double-strand breaks and micronuclei formation, indicating genotoxicity. Kuntz et al. [95] reported that diosmin has an antiproliferative effect on various human colon cancer cell lines, further supporting its potential as a therapeutic agent in cancer treatment.

Tanaka et al. observed that diosmin had a chemoprotective impact on cancer development caused by azoxymethane in men F344 rats (Tanaka et al. 1997a, b). Further, oral therapy decreased colon tumorigenesis, as shown by reduced incidences of colorectal cancer. They speculated that blocking ornithine decarboxylase (ODC), a rate-limiting enzyme in polyamine synthesis, was indeed the cause of the reduction in colonic malignancies (Tanaka, Makita, Kawabata, Mori, Kakumoto, Satoh, Hara, Sumida, Tanaka, et al., 1997). If ODC is blocked, damage to DNA causes apoptotic cell death [26]. ODC levels have been found to elevate in several tissues after chemical exposure. ODC activity was also increased in the colonic mucosa of rats given azoxymethane. According to Buddhan et al. (2017), it has a dose-dependent cytotoxic capacity for A431 melanoma cancerous cells. It suppresses A431 cellular invasiveness by causing mortality via a ROS-mediated mechanism (Eraslan et al. 2017; Perumal et al. 2018). With Ds therapy, A431 cells showed DNA breakage, upregulation of p53, caspase-3 and caspase-9 genes, and reduced expression of Bcl-2, matrix metalloproteinases-2 and 9 genes. The IC<sub>50</sub> value of Diosmin was found to be 45 g/mL, creating substantial ROS (Baskar et al. 2014). In male F344 rats, it inhibited oral tumorigenesis caused by 4-nitroquinoline

1-oxide (4-NQO). They believed that the molecule might fight cancer through a variety of methods. One of those strategies was ornithine decarboxylase (ODC) suppression. Drugs that reduce ODC activity have been demonstrated to limit tumor development. Another proposed method suppresses DT-diaphorase function, essential for 4-NQO to cause cancer (Tanaka, Makita, Kawabata, Mori, Kakumoto, Satoh, Hara, Sumida, Fukutani, et al., 1997; Tanaka, Makita, Kawabata, Mori, Kakumoto, Satoh, Hara, Sumida, Tanaka, et al., 1997). It is much more effective than diosmetin (the aglycone form of diosmin) at suppressing oral tumorigenesis (Browning et al. 2005; Walle et al. 2005). In male ICR mice, oral therapy with 1,000 ppm of the molecule reduced urinary bladder tumorigenesis caused by N-butyl-N-(4-hydroxybutyl) nitrosamine. A count of silver-stained nucleolar-organizer-region-associated enzymes (AgNORs) and a 5-bromodeoxyuridine (BUDR)-labeling index validated these findings. The anticarcinogenic actions of molecules may be attributed to a reduction in cell proliferation (Sahu et al. 2016). Diosmin exhibited a comparable impact on stomach cancer produced by N-methyl-N-amylnitrosamine in male Wistar rats (MNAN). Figure 6 summarizes its chemopreventive effect on several types of cancer or cell lines.

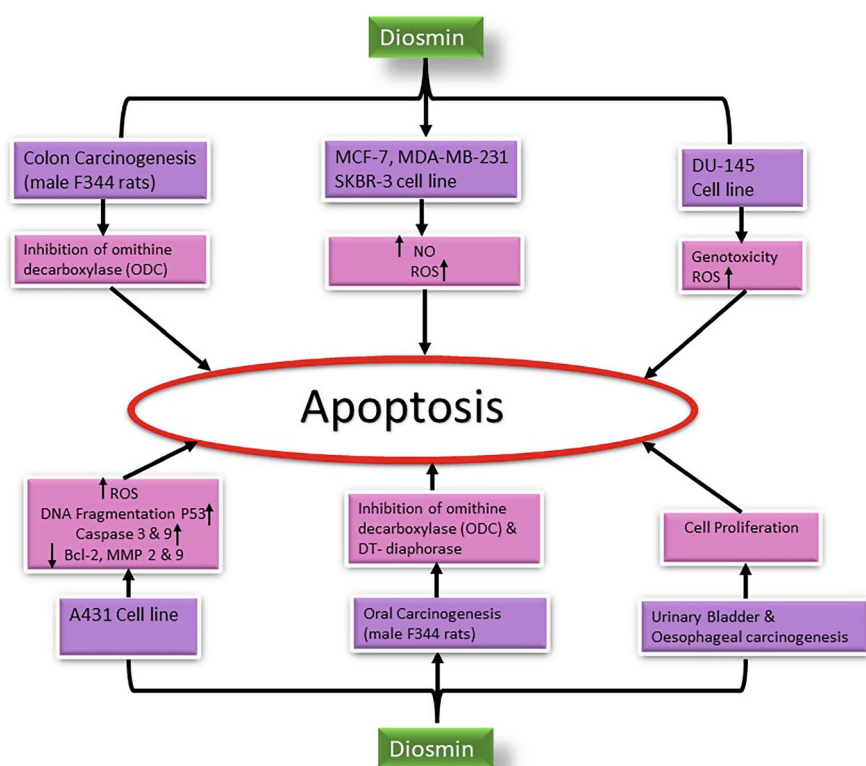


**Fig. 6** Various anticancer activities of diosmin. (Huwait and Mobashir 2022)



Diosmin also possesses antimetastatic effects in patients with lung carcinoma (B16F10) (Martinez et al. 2005; Martínez Conesa et al. 2005). Further, it decreases the number of metastasis lesions, the proportion of implants, and the penetration index in micro- and macroscopic studies. Diosmin works with IFN to cure patients with lung carcinoma (Alvarez et al. 2009). Further, it inhibited HA22T cell growth in nude rodent models by interrupting the PI3K-Akt-MDM2 transcription factor and actuating G2/M cell cycle arrest via p53 activation (Dung et al. 2012b).

### 2.1.2 Diosmetin

Diosmetin, commonly called 5,7,3'-trihydroxy-4'-methoxy flavone, is an O-methylated flavone with three OH groups found in Caucasian vetch, limes, and the legumes *Acacia farnesiana*. It was identified as a gentle TrkB binding site agonist and had various biological activities as shown in Fig. 7.

The biosynthetic pathway of the molecule begins with the step-by-step evaporation of three molecules of malonyl CoA and one molecule of 4-coumaryl CoA, accompanied by a stereoselective cyclization that results in a flavanone. During the existence of chalcone synthase (CHS), it generates calcone, and in the reality of chalcone isomerase, it generates naringenin (CHI). Naringenin creates eriodictiol in the presence of F3H, while eriodictiol produces lutein in the context of FNS. Finally, the end product of this reaction is Diosmetin (Fig. 8).

### Diosmetin and Cancer

Xu Zhijie and colleagues (2017) demonstrated that the molecule, an aglycone of the flavonoid glycoside found in olive leaves, limes, as well as some herbal remedies, does have a positive potential on radiation therapy hypersensitivity and can induce G1 phase arrest, thereby increasing radiosensitivity of radioresistant A549/IR lung

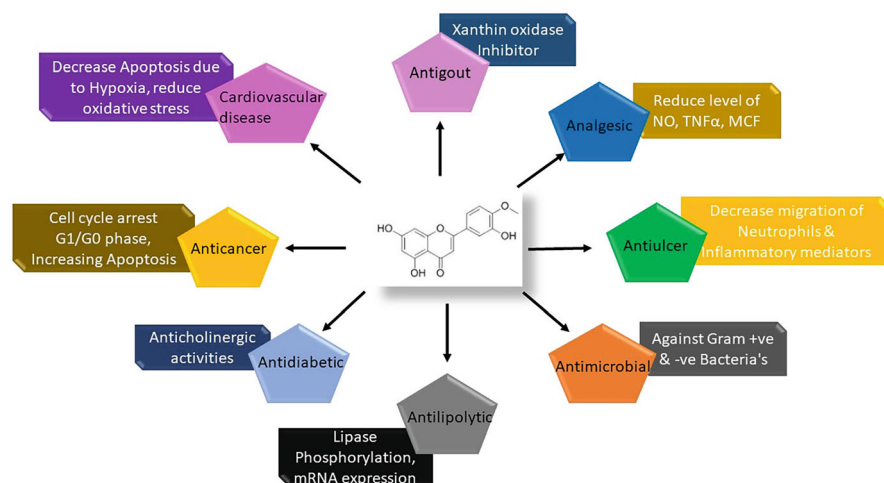


**Fig. 7** Pharmacological characteristics and action mechanism of diosmetin

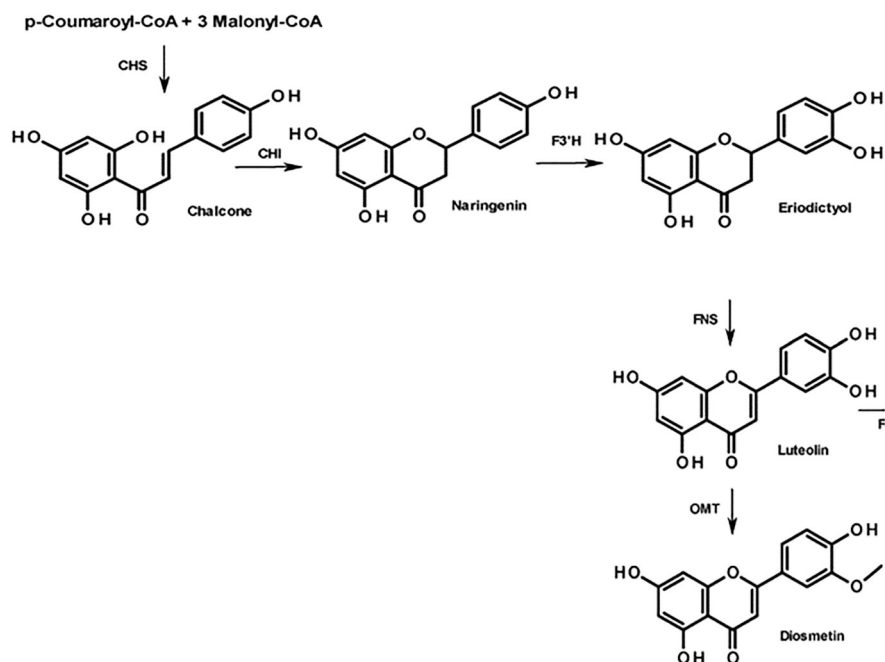


**Fig. 8** Diosmetin biogenesis involves the enzymes chalcone isomerase (CHI), chalcone synthase (CHS), flavanone 3'-hydroxylase (F3'H), flavone synthase (FNS), and flavone O-methyltransferase (FNS) (OMT) [37]

cancer cells. It inhibits IR-induced DNA damage repair by blocking the active Akt signaling pathway (Xu et al. 2017). Combining Akt inhibitor and therapy effectively inhibited the growth of A549/IR cancer cells (Xu et al. 2017). Christine Oak and colleagues (Oak et al. 2018) discovered that the molecule treatments of LNCaP and PC 3 prostate cancer cells caused a significant drop in cyclin D1, Cdk2, and Cdk4 expression levels (these proteins remained functional in the G0 and G1 stages of the cell). Such alterations are followed by a reduction in c-Myc and Bcl-2 expression and a rise in Bax, p27Kip1, and FOXO3a protein production, indicating that it may modulate protein formation. It activated an apoptosis mechanism in prostate cancer cells by suppressing the X-linked regulator of mortality (XIAP) and raising cleavage PARP and cleavage caspase-3 protein expression. Overall, the results of this investigation offer such an assessment of the molecular pathways held to account for the molecule's regulation effects on essential proteins that disrupt cellular proliferation to restrict tumor development and recommend that it as an efficient antitumor drug for long-term application in the management of prostate cancer (Oak et al. 2018).

Xiangcui Chen and colleagues (Chen et al. 2019) sought to characterize its impact, a natural flavonoid, on NSCLC cells with its capacity to increase the antitumor effect of paclitaxel. They discovered that Dm preferentially caused death

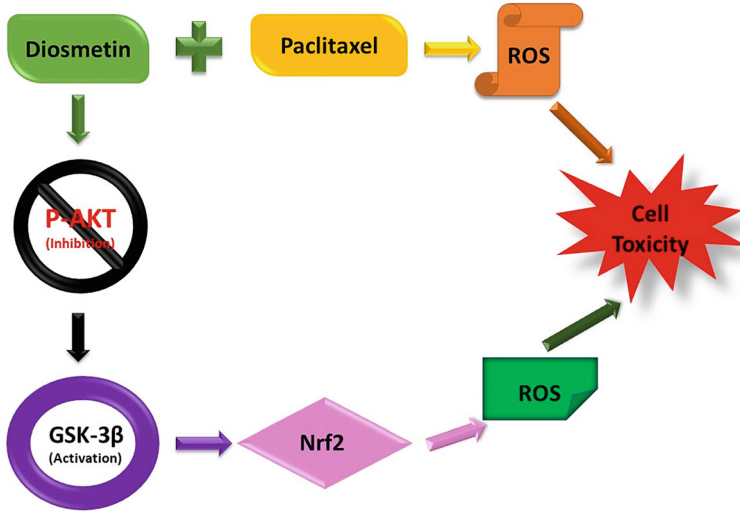


**Fig. 9** MOA of diosmetin. (Adopted from Chen et al. 2019)

and increased the effectiveness of paclitaxel in NSCLC cells via rattle or disturbing the PI3K/Akt/GSK-3/Nrf2 cascade (Fig. 9). As a result, the molecule could be a viable supplemental therapy for NSCLC (Chen et al. 2019).

Sanaz Koosha and colleagues (n.d.) studied its putative signaling events in the colorectal (CRC) cancer cell line HCT-116. Utilizing micro sequence and transcriptomic analyzer element techniques, we supervised the survivability of HCT-116 cells in it. We explored the principle against HCT-116 molecules at the protein and gene tiers. Their results indicated that it had a more considerable lethal impact on HCT-116 CRC cells ( $IC_{50} = 3.58 \pm 0.58$  g/ml) than on normal colon CCD-841 cells ( $IC_{50} = 51.95 \pm 0.11$  g/ml). Arrests of G2/M cells demonstrate the presence of mitosis disturbance via the molecule (Koosha et al. n.d.). The induction of mortality markers, including Fas and Bax, just at protein and gene levels, as well as the release of cytochrome from mitochondria and caspase cascade cleavage, shows the existence of turbulence in diosmetin-treated cells (Koosha et al. n.d.). Furthermore, it suppressed NF- $\kappa$ B translocation in cells. Their findings show it may impact HCT-116 cells via mitosis breakdown and apoptotic activation. Ageing Ma and colleagues (A. Ma and Zhang 2020; Management and Zhang 2020) discovered that it could reduce cellular proliferation, enhance apoptotic cell death, and induce G2/M cell cycle arrest in HepG2 cells by targeting Chk2 (Ma and Zhang 2020). Zhiyi Hu and colleagues (Hu et al. 2020) show how it inhibits homologous recombination mechanisms, decreasing cell growth and increasing the susceptibility of endometriosis (EC) to radiation. Colony formation studies demonstrated that combining the molecule and X-ray dramatically reduced the survival of EC cells compared to treated cells with it or X-ray separately (Hu et al. 2020). Whenever 0.4 Gy X-ray and 4 M molecule were combined, the surviving proportion of EC cells

dropped to 40%; nevertheless, every therapy itself only killed around 15% and 22% of cancerous cells. Following the development of DNA double-strand breaks, it blocked the recruiting of RPA2 and RAD51, two essential factors involved in the HR repair pathway (Hu et al. 2020).

Feijie Zhao and colleagues (2021) aimed to look into the impact of molecules on solid tumors A2780 and SKOV3 cells and the causative factors. According to our findings, it decreased cell growth, motility, and penetration while causing cell death. Furthermore, it raised the levels of Bax, cleaved caspase-3, and PARP while reducing the level of Bcl2 (Zhao et al. 2021). Moreover, they discovered that the former molecule reduced Nrf2 and increased the generation of ROS. The ROS scavenger N-acetyl-L-cysteine (NAC) inhibited its inhibitory impact on ovarian cancer cell growth. Furthermore, Nrf2 overexpression partly reduced molecule-induced apoptosis and proliferation suppression in these cells (Zhao et al. 2021). Such results show that the molecule has an antitumor effect through increasing ROS levels and suppressing Nrf2, implying that the molecule is a potential chemotherapy choice for treating tumors (Zhao et al. 2021).

According to Rende et al. 2021 (Ning et al. 2021), it has anti-osteosarcoma actions by decreasing cell growth and causing death by blocking the stimulation of the STAT3/c-Myc signaling cascade, suggesting that it might be a chemotherapeutic option for sarcoma. Substantially, it decreased cells, caused G2/M cycle arrest, encouraged apoptotic cell death, including both Saos-2 and U2SO cells, and negatively regulated the interpretation of antiapoptotic protein Bcl-xL whilst also raising the levels of pro-apoptotic enzymes such as bisected caspase-3, cleaved-PARP, and Bax.

Moreover, it blocked STAT3 phosphorylation, decreased the production of its regulatory protein c-Myc, and hampered STAT3-STAT3 coupling (Ning et al. 2021). Kamran et al. (2022) study the synergistic effect of the molecule and 5-fluorouracil (FU) on HCT116 and HT29 colorectal cancer cells and the combination's lethal action. The MTT test evaluated cell viability after monotherapy and combinatorial treatment (Kamran et al. 2022). In HCT116 cells, the mixture of 5-FU and the molecule had a beneficial influence with an average CI value of 0.66 0.4 and an adhesive in HT29 cells with a CI value of 1.0 0.2. Compared to monotherapy, the dose reduction index (DRI) of 5-FU in HCT116 cells was three times less in the combined treatment of 5-FU (Kamran et al. 2022). Acridine orange (AO)/propidium iodide (PI) microscopic inspection and Annexin V findings implied that perhaps the combination-treated cultures contained more significant cellular damage than the monotherapy-treated cell lines, indicating that suicide was primarily induced via the intrinsic induction of apoptosis. Mitotic arrest in the G2/M phase verified HCT116 cell damage. These findings imply that combining 5-FU and molecule has a synergic effect on HCT116 cancer cells, possibly reducing the undesirable side effects of 5-FU while increasing antitumor efficiency by triggering death and interfering with mitosis (Kamran et al. 2022). Additional study is required to confirm the combination's anti-tumorigenic properties in a xenograft animal study.

**Fig. 10** MTT experiment to determine the influence of diosmetin on the vitality of HCC827 and A549 cells. (Song et al. 2022)

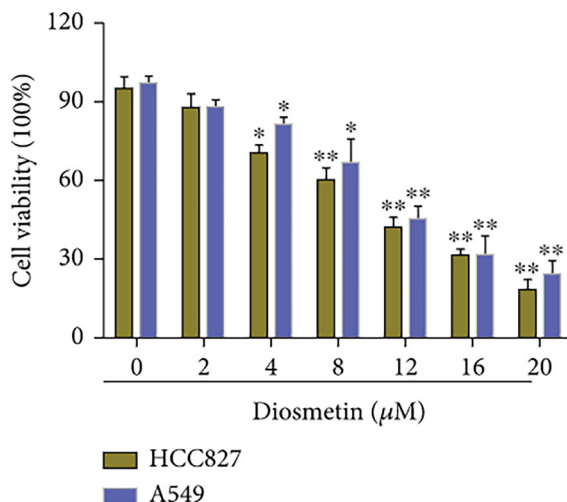
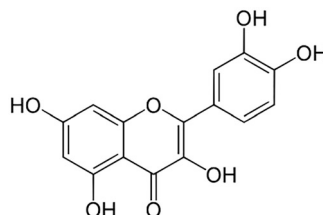


**Fig. 11** Structure of quercetin



Song et al. (2022) wanted to see how it affected gene expression in lung adenocarcinoma (LUAD) cells (Fig. 10). Further, it decreased HCC827 and A549 cell growth and colony formation (Song et al. 2022).

It can upregulate or inhibit the activity and overall production of mRNAs, microRNAs, and LncRNAs in A549 and HCC827 cells compared to the control group, according to differentially expressed genes (Song et al. 2022). Furthermore, the three top possibilities in each RNA group were cross-validated using RT-qPCR, and a single peak in the melted curve was seen, indicating high sensitivity and specificity (Song et al. 2022).

### 2.1.3 Quercetin

It is an important flavonoid that belongs to the group flavanols. It contains five hydroxyl groups at 3,5,7,3' and 4 of the basic skeleton of flavonols (Fig. 11).

Few of these hydroxyl groups are glycosylated to various molecule glycosides and are distributed among multiple fruits and vegetables (Magar and Sohng 2020). Their diverse biological activities are shown in Fig. 12.

It has been synthesized via phenylpropanoid metabolic pathway (Fig. 13). Phenylalanine produces cinnamic acid with the crucial enzyme phenylalanine

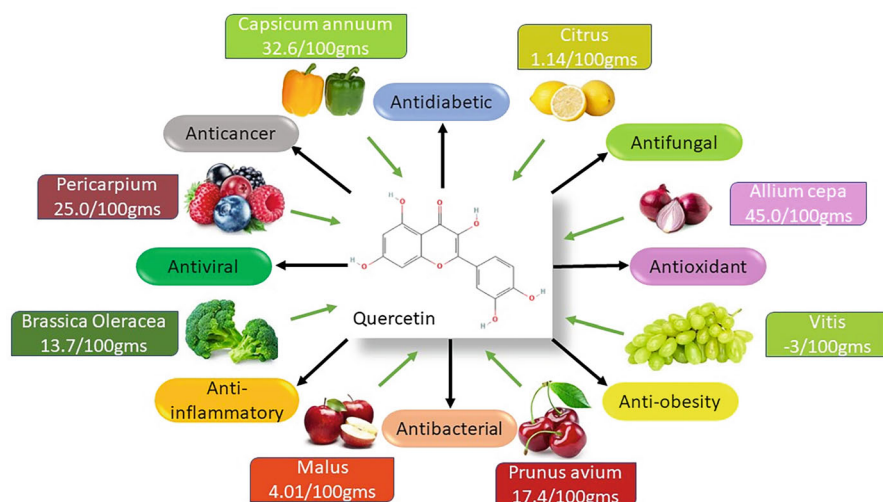


**Fig. 12** Biological activity of quercetin

ammonia ligase (PAL). Cinnamic acid produces p-coumaric acid with the enzyme cinnamate-4-hydroxylase (C4H). P-coumaric acid having a carboxylic group made 4-coumaroyl-CoA by ligation with CoA. The enzyme p-coumarate CoA ligase catalyzes this reaction. One p-coumaroyl CoA produces naringenin chalcone in the presence of the enzyme chalcone synthase (CHS).

On the other hand, three malonyl-CoA makes A and B rings of flavonoid skeleton. The hydroxylation of naringenin in the presence of enzyme flavonone 3 $\beta$  hydroxylase (F3H) produces dihydro kaempferol. On the other hand, hydroxylation of dihydro kaempferol in the presence of flavanol 3' hydroxylase makes dihydroquercetin, another enzyme flavanol synthase, the former molecule.

### Quercetin and Cancer

It is one of the essential free-radical scavenging antioxidants. Further, it possesses many hydroxyl groups and conjugated  $\pi$  orbitals by which it can donate electrons or hydrogen and scavenge  $H_2O_2$  and superoxide anion (Shirai et al. 2006). It is practically indigestible fiber in its aglycone form, although it is exposed to conjugated events such as glucuronidation and sulfation (Nam 2006), with a few intermediates retaining antioxidant activity (Dihal n.d.). In plants, glycosylation deactivates its biological action, with rutin (Qu-3-O-rutinoside) among the most prevalent quercetin glycosides. As it is consumed as glycosides in food sources, assessing them is more practicable than considering them alone. At least two chemopreventive investigations in the rat colon have been conducted utilizing it and rutin (Volate et al. 2005). Volate et al. (Femia et al. 2003) exposed rats to a carcinogen, azoxymethane, and gave them 0–3% former molecule or rutin. Though several hypotheses (Fig. 14) seeking to explain its molecular activity have been

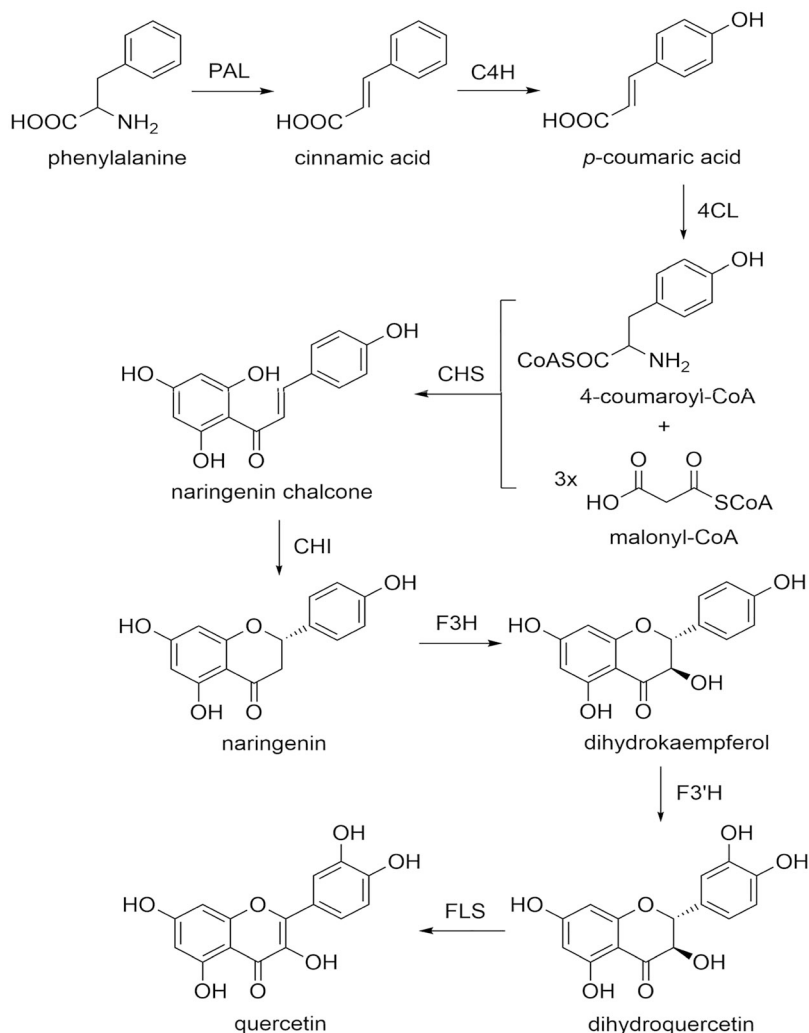


**Fig. 13** A- and B-rings unite to make an aryl ring, cyclized by isomerase to generate flavonone, which is utilized to synthesize other flavonoids. Various alterations are blameworthy for the formation of significant structural and functional variations. PAL catalyses the synthesis of cinnamic acid from phenylalanine, and the resulting cinnamic acid is further transformed into p-coumaric acid by C4H. The produced p-coumaric acid reacts with 4-CL, resulting in the formation of 4-coumaroyl-CoA, and the following action of CHS over one 4-coumaroyl-CoA molecule of three malonyl-CoA molecules yields the naringenin chalcone. Lastly, the FLS is involved in the synthesis of the molecule. Enzyme abbreviations: *PAL* phenylalanine ammonia lyase, *C4H* cinnamate 4-hydroxylase, *4-CL* p-coumarate: CoA ligase, *CHS* chalcone synthase, *CHI* chalcone isomerase, *F3H* flavone 3-hydroxylase, *F3' H* flavonol 3'-hydroxylase, *FLS* flavonol synthase

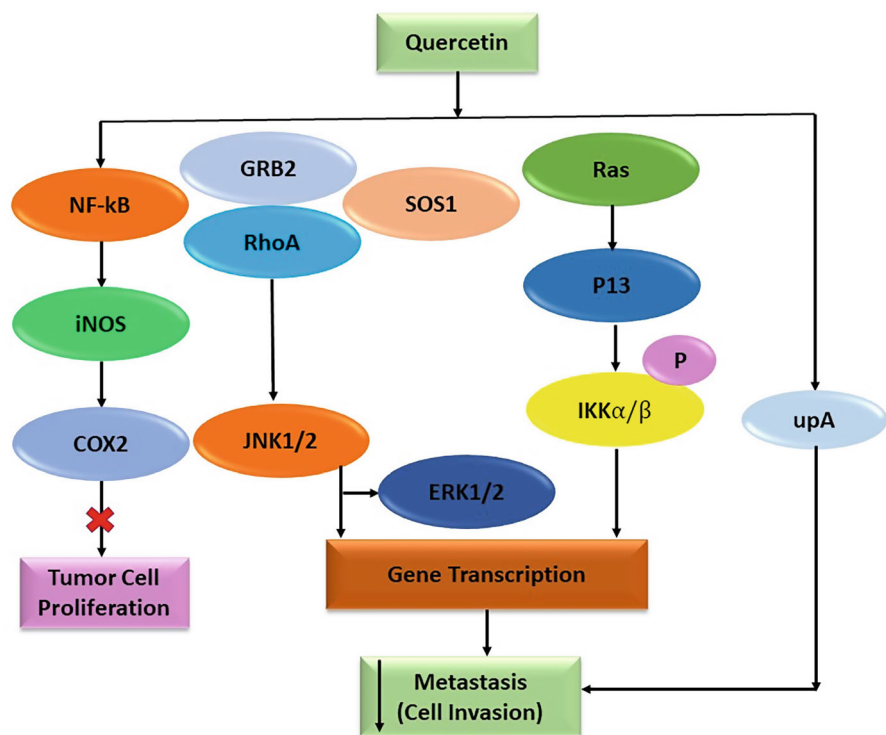


**Fig. 14** Quercetin mechanism of action in cancer

addressed, the mechanism by which it exerts an anti-inflammatory, pro-apoptotic, and chemopreventive function is still not entirely known. One of these hypotheses posits that it inhibits nuclear factor-B (NF-B) via the PI3K/Akt/IKK/NF-B signaling pathway. Flavonoids are NF-B inhibitors that are present in nature, as is commonly known (Bremner and Heinrich 2002; Kwon et al. 2005).

The transcriptional element NF-B has generated significant attention because of its peculiar and complicated management, the wide variety of triggers that engage it, its potential role in a diverse range of human disorders, the varied genes and biochemical characteristics that it controls, and the impressive evolutionary preservation of its function and structure across family members. Recently, NF-B has been demonstrated as a viable target for novel drug development, increasing interest in molecules derived from raw natural sources (Min et al. 2007; Perkins 2007). NF-B has a significant impact on carcinogenesis and cancer formation. The NF-B inhibitor IB keeps the predominant type of NF-B, known as RelA (the heterodimer p50/p65), in a latent state. NF-B is activated by phosphorylation of IB by IB kinase (IKK), which is powered by the IKK, IKK, and IKK subunits. IKK is the major kinase that phosphorylates IB's amino-(NH)-terminus in vivo, while IKK is a critical regulatory component known as NF-B significant modulation or NEMO. It has been found to



have anticancer activity, both in vitro and in vivo, with many of these effects attributed to its direct or indirect action on various molecular actors involved in carcinogenesis. Further, it inhibits NF- $\kappa$ B. However, this function may imply multiple effects in a pro- or antiapoptotic direction, given that NF- $\kappa$ B also controls p53 by acting on the p53 gene (Schneider and Krämer 2011). Several studies have been conducted to evaluate the pro-apoptotic effect of it in cancer cells, which, like many other flavonoids, contributes to the chemopreventive action of diet (Chen et al. 2005; Kim and Lee 2007). The fact that it is a potentially genotoxic chemical is intriguing for integrative medicine. Although its mutagenicity and chemical toxicity have not been verified in vivo, it may activate the p53 signal—which HDM2 inversely controls. This molecule requires Akt activation and works as an E3 ubiquitin ligase-promoting p53 proteolysis (Wang et al. 2011); low doses of the molecule, in the context of hormesis, allow this polyphenol to act protectively. However, the position of the former molecule particle in the NF- $\kappa$ B-p53 cross-talk is still unknown. Although the connection between it and p53 has also been evaluated lately (Gupta et al. 2010), it seems capable of inducing cell death irrespective of the p53 signaling pathway (Vargas et al. 2011). Moreover, this also inhibits the PI3K/Akt/IKK/NF- $\kappa$ B pathway in human salivary adenoid cystic cancer, causing cell death via a mitochondria-dependent pathway (Kong et al. 2011). The PI3K/Akt/IKK/NF- $\kappa$ B signaling pathway (Fig. 14) avoids cell death in such cells; it accelerates cancer cell apoptosis by inhibiting PI3K/Akt upstream of NF- $\kappa$ B signaling (Hou and Kumamoto 2010). Because several flavonoids, especially the former molecule, suppress various PI3K isoforms and the PI3K/Akt axis, PI3K is a putative biological targeting for it. Apart from PI3K and NF- $\kappa$ B, it can suppress a wide range of some of the other kinases and enzymes (Bulzomi et al. 2012). Furthermore, flavonol could have a favorable effect on kinase/suppressor factors, resulting in indirect kinase suppression. It does not suppress Akt and ERK1/2, but it can raise the onco-suppressor PTEN, which enhances the inhibition activity on PI3K activity.

### 3 Nanotechnology in Flavonoid-Based Cancer Therapy

The use of nanotechnology in cancer therapy has created new opportunities for enhancing the therapeutic effectiveness of bioactive substances like flavonoids. Traditional delivery strategies for flavonoids are frequently constrained by their inadequate bioavailability, fast metabolism, and low solubility, which impede their therapeutic use. Nanotechnology provides novel answers to these issues by augmenting the pharmacokinetic and pharmacodynamic characteristics of flavonoids, therefore boosting their therapeutic efficacy in cancer treatment (Sharma et al. 2022).

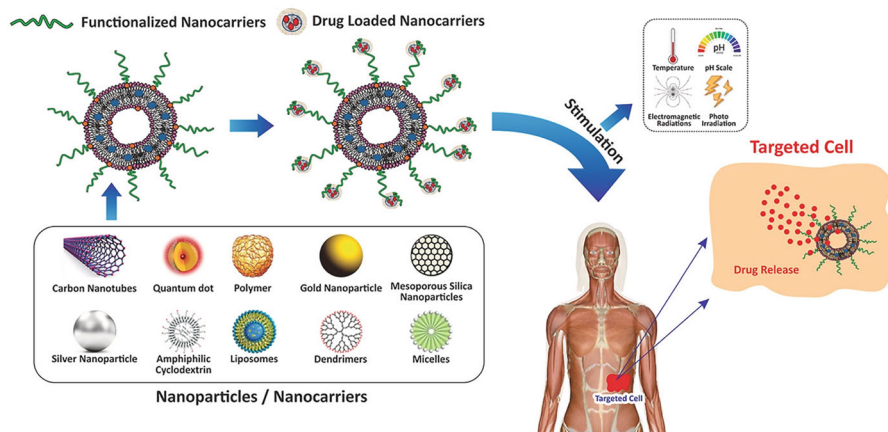


**Fig. 15** Various nanoformulations for drug delivery system

### 3.1 Nanocarriers for Targeted Drug Delivery

Nanocarriers, including liposomes, dendrimers, polymeric nanoparticles, and solid lipid nanoparticles, have been engineered to encapsulate flavonoids, safeguarding them from degradation and enabling targeted delivery to tumor tissues (Fig. 15). These nanocarriers may be designed to preferentially accumulate at the tumor site via increased permeability and retention (EPR) effects, which are typical of the abnormal vasculature found in malignancies. By selectively targeting cancer cells, nanocarriers mitigate harm to healthy tissues, therefore diminishing the negative effects typically associated with chemotherapy. Nanoparticles loaded with flavonoids have demonstrated encouraging outcomes in preclinical investigations. Quercetin-loaded nanoparticles exhibit heightened cytotoxicity against cancer cells, especially in lung and prostate malignancies, by increasing the intracellular concentration of quercetin and triggering apoptosis more efficiently than free quercetin. Nanoformulations of diosmin and kaempferol have demonstrated enhanced anticancer activity by improving drug solubility and bioavailability, as well as facilitating regulated drug release over time.

### 3.2 Synergistic Delivery of Flavonoids with Chemotherapeutic Agents

Nanotechnology enables the simultaneous administration of flavonoids with traditional chemotherapeutic drugs, providing synergistic benefits that can improve total therapy success (Fig. 16). Integrating flavonoids and chemotherapeutic chemicals inside a single nanocarrier enables researchers to facilitate coordinated delivery to cancer cells, hence enhancing the cytotoxic efficacy of chemotherapy and

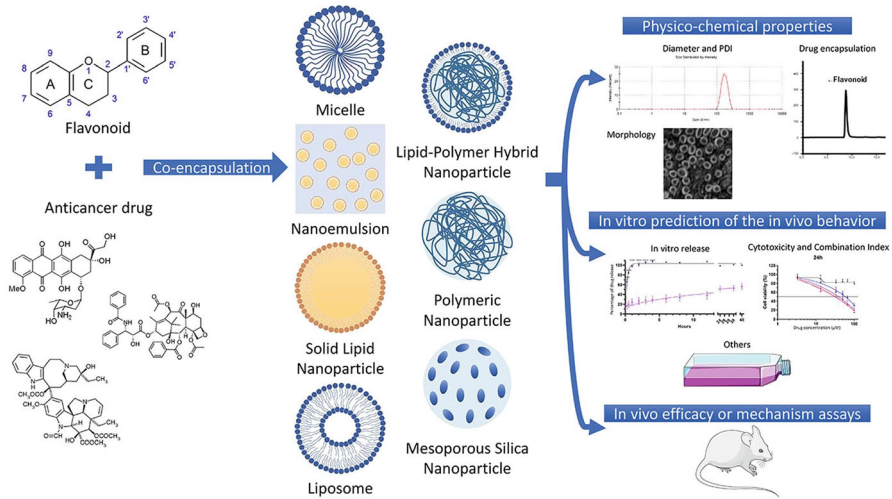


**Fig. 16** Synergistic effects of flavonoids with anticancer drugs

minimizing the necessary dosage of harmful substances. This method enhances therapy efficacy while simultaneously alleviating negative side effects [139].

Flavonoid-based nanoparticles that co-deliver doxorubicin and quercetin have demonstrated enhanced therapeutic efficacy in breast cancer models by circumventing multidrug resistance (MDR) pathways, a major impediment to successful cancer therapy. The flavonoid component enhances the sensitivity of cancer cells to chemotherapy by regulating drug efflux pumps and apoptotic pathways, hence improving the effectiveness of the chemotherapeutic agent.

### 3.3 Overcoming Drug Resistance and Enhancing Bioavailability

A significant benefit of employing nanotechnology in flavonoid-based cancer treatment is its capacity to surmount multidrug resistance (MDR) [142]. Cancer cells frequently acquire resistance to chemotherapy by activating efflux transporters such as P-glycoprotein (Fig. 17), which extrude medicines from the cell, diminishing the efficacy of therapies [143]. Flavonoid-encapsulated nanoparticles can circumvent these resistance mechanisms by directly administering the active component into cancer cells and improving intracellular retention [144].

The encapsulation of flavonoids in nanoparticles enhances their bioavailability, enabling lower dosages to provide therapeutic benefits. Nanoformulations such as quercetin or kaempferol-loaded nanocarriers have shown a considerable enhancement in drug accumulation at tumor sites, attributed to their reduced size and enhanced penetration into malignant tissues. The enhanced bioavailability facilitates the extended release of flavonoids, essential for sustaining therapeutic concentrations in the body and attaining maximum anticancer effects (Dwivedi et al. 2023).

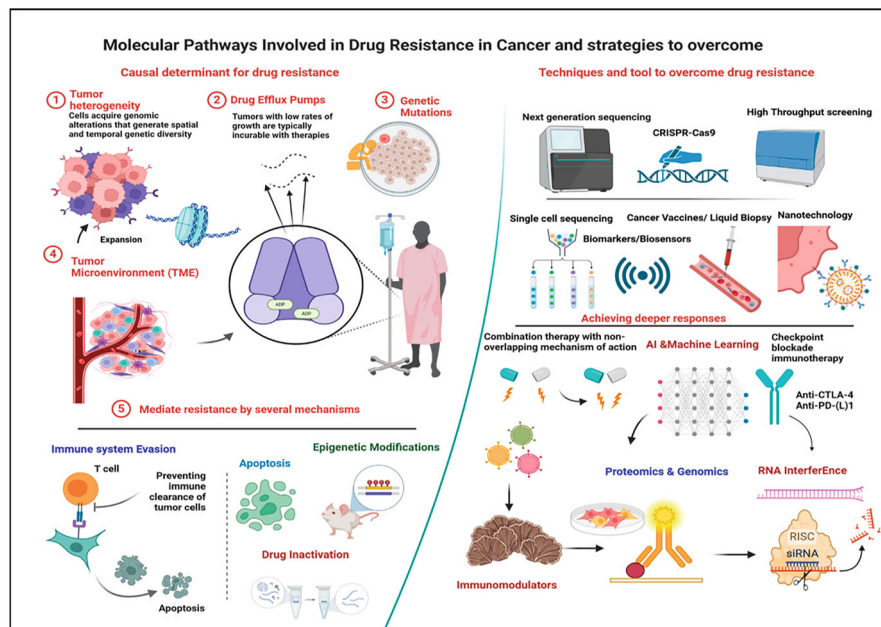


**Fig. 17** Drug resistance pathways in cancer

### 3.4 Future Directions and Clinical Potential

Notwithstanding the encouraging outcomes from preclinical investigations, the clinical utilization of flavonoid-based nanocarriers continues to encounter several obstacles. These encompass the necessity for extensive production, comprehension of the long-term safety of nanocarriers, and the mitigation of possible immunological reactions. As research advances, the creation of advanced nanocarrier systems, including stimuli-responsive nanoparticles that release medications in reaction to particular triggers in the tumor microenvironment (e.g., pH, temperature, or enzymes), has considerable potential.

Nanotechnology offers a promising avenue for addressing the constraints of flavonoid-based medicines and realizing their complete promise in cancer therapy (Sheoran et al. 2022b, 2024). Nanotechnology has the potential to augment the delivery and efficacy of flavonoids, therefore transforming them into potent agents in cancer treatment, providing more effective and less hazardous therapeutic alternatives in the future.

## 4 Conclusion

Flavonoids, owing to their varied biological functions, have surfaced as intriguing candidates for cancer prevention and treatment. Their capacity to address several hallmarks of cancer, including unchecked cell proliferation, evasion of apoptosis, angiogenesis, and metastasis, positions them as leading natural chemicals with anticancer efficacy. Flavonoids, including quercetin, kaempferol, and diosmin, have shown considerable effectiveness in preclinical trials, including processes such as the management of oxidative stress, regulation of cell cycle checkpoints, and activation of pro-apoptotic signaling pathways. The advancement of nanoformulations has enhanced the therapeutic use of flavonoids by enhancing their solubility, stability, and targeted delivery to tumor sites, therefore minimizing systemic toxicity. This novel methodology has demonstrated potential in addressing the shortcomings of traditional cancer treatments, including drug resistance and off-target effects. Notwithstanding these advancements, the practical use of flavonoid-based medicines encounters several obstacles. The intricate pharmacokinetics of flavonoids, possible interactions with other pharmaceuticals, and heterogeneity in absorption continue to pose substantial challenges. Furthermore, although several flavonoids demonstrate anticancer properties *in vitro* and in animal studies, their efficacy in human clinical trials requires additional confirmation. To fully exploit the potential of flavonoids in cancer therapy, it is imperative to undertake thorough investigations on their safety profiles, appropriate doses, and long-term effects. Future study ought to investigate flavonoid combinations with current chemotherapeutic drugs and their implications in personalized medicine to formulate more effective, low-toxicity cancer therapy options. Flavonoid-based medicines have the potential to transform cancer care by connecting natural product research with clinical applications, providing more sustainable and less detrimental therapy alternatives for patients.

## References

- Agarwal C, Wadhwa R, Deep G, Biedermann D, Gažák R, Křen V, Agarwal R (2013) Anti-cancer efficacy of silybin derivatives-a structure-activity relationship. *PLoS One* 8(3):e60074
- Aktas HG, Akgun T (2018) Naringenin inhibits prostate cancer metastasis by blocking voltage-gated sodium channels. *Biomed Pharmacother* 106:770–775
- Al Sinani SS, Eltayeb EA, Coomber BL, Adham SA (2016) Solamargine triggers cellular necrosis selectively in different types of human melanoma cancer cells through extrinsic lysosomal mitochondrial death pathway. *Cancer Cell Int* 16:1–12
- Al-Thani AN, Jan AG, Abbas M, Geetha M, Sadasivuni KK (2024) Nanoparticles in cancer theragnostic and drug delivery: A comprehensive review. In: *Life sciences*, vol 352. Elsevier Inc., p 122899. <https://doi.org/10.1016/j.lfs.2024.122899>
- Alvarez N, Vicente V, Martinez C (2009) Synergistic effect of diosmin and interferon- $\alpha$  on metastatic pulmonary melanoma. *Cancer Biother Radiopharm* 24(3):347–352
- Amawi H, Ashby CR, Tiwari AK (2017) Cancer chemoprevention through dietary flavonoids: what's limiting? *Chin J Cancer* 36(1):50. <https://doi.org/10.1186/s40880-017-0217-4>

- Amjad E, Sokouti B, Asnaashari S (2022) A systematic review of anti-cancer roles and mechanisms of kaempferol as a natural compound. In: *Cancer cell international*, vol 22, Issue 1. BioMed Central Ltd. <https://doi.org/10.1186/s12935-022-02673-0>
- Appendino G, Chianese G, Tagliatalata-Scafati O (2011) Cannabinoids: occurrence and medicinal chemistry. *Curr Med Chem* 18(7):1085–1099
- Arora S, Sheoran S, Basu T, Subbarao N, Upadhyay AK, Vuree S (2023) Abstract 5343: evaluating the screened polyphenolics molecules as potential chemosensitizers against the oncogenic signalling proteins in lung cancer. *Cancer Res* 83(7\_Suppl):5343. <https://doi.org/10.1158/1538-7445.AM2023-5343>
- Bakshi HA, Sam S, Feroz A, Ravesh Z, Shah GA, Sharma M (2009) Crocin from Kashmiri saffron (*Crocus sativus*) induces in vitro and in vivo xenograft growth inhibition of Dalton's lymphoma (DLA) in mice. *Asian Pac J Cancer Prev* 10(5):887–890
- Baskar R, Dai J, Wenlong N, Yeo R, Yeoh K-W (2014) Biological response of cancer cells to radiation treatment. *Front Mol Biosci* 1:24
- Bremner P, Heinrich M (2002) Natural products as targeted modulators of the nuclear factor-kappaB pathway. *J Pharm Pharmacol* 54(4):453–472. <https://doi.org/10.1211/0022357021778637>
- Browning AM, Walle UK, Walle T (2005) Flavonoid glycosides inhibit oral cancer cell proliferation—role of cellular uptake and hydrolysis to the aglycones. *J Pharm Pharmacol* 57(8):1037–1041
- Buddhan R, Manoharan S (2017) Diosmin reduces cell viability of A431 skin cancer cells through apoptotic induction. *J Cancer Res Ther* 13(3):471–476. <https://doi.org/10.4103/0973-1482.183213>
- Bulzomi P, Galluzzo P, Bolli A, Leone S, Acconcia F, Marino M (2012) The pro-apoptotic effect of quercetin in cancer cell lines requires ER $\beta$ -dependent signals. *J Cell Physiol* 227(5):1891–1898. <https://doi.org/10.1002/jcp.22917>
- Cao B, Bray F, Beltrán-Sánchez H, Ginsburg O, Soneji S, Soerjomataram I (2017) Benchmarking life expectancy and cancer mortality: global comparison with cardiovascular disease 1981–2010. *BMJ (Online)* 357. <https://doi.org/10.1136/bmj.j2765>
- Chaachouay N, Zidane L (2024) Plant-derived natural products: a source for drug discovery and development. *Drugs Drug Candidates* 3(1):184–207. <https://doi.org/10.3390/ddc3010011>
- Chahar MK, Sharma N, Dobhal MP, Joshi YC (2011) Flavonoids: A versatile source of anticancer drugs. *Pharmacogn Rev* 5(9):1–12. <https://doi.org/10.4103/0973-7847.79093>
- Cheah KY, Howarth GS, Bindon KA, Kennedy JA, Bastian SEP (2014) Low molecular weight procyanidins from grape seeds enhance the impact of 5-fluorouracil chemotherapy on Caco-2 human colon cancer cells. *PLoS One* 9(6):e98921
- Chehelgerdi M, Chehelgerdi M, Allela OQB, Pecho RDC, Jayasankar N, Rao DP, Thamaraikani T, Vasanthan M, Viktor P, Lakshmaiya N, Saadh MJ, Amajd A, Abo-Zaid MA, Castillo-Acobo RY, Ismail AH, Amin AH, Akhavan-Sigari R (2023) Progressing nanotechnology to improve targeted cancer treatment: overcoming hurdles in its clinical implementation. In: *Molecular cancer*, vol 22, Issue 1, BioMed Central Ltd. <https://doi.org/10.1186/s12943-023-01865-0>
- Chen J-C, Ho F-M, Chao P-DL, Chen C-P, Jeng K-CG, Hsu H-B, Lee S-T, Wu WT, Lin W-W (2005) Inhibition of iNOS gene expression by quercetin is mediated by the inhibition of IkappaB kinase, nuclear factor-kappa B and STAT1, and depends on heme oxygenase-1 induction in mouse BV-2 microglia. *Eur J Pharmacol* 521(1–3):9–20. <https://doi.org/10.1016/j.ejphar.2005.08.005>
- Chen J, Zhu Y, Zhang W, Peng X, Zhou J, Li F, Han B, Liu X, Ou Y, Yu X (2018) Delphinidin induced protective autophagy via mTOR pathway suppression and AMPK pathway activation in HER-2 positive breast cancer cells. *BMC Cancer* 18:1–13
- Chen X, Wu Q, Chen Y, Zhang J, Li H, Yang Z, Yang Y, Deng Y, Zhang L, Liu B (2019) Diosmetin induces apoptosis and enhances the chemotherapeutic efficacy of paclitaxel in



- non-small cell lung cancer cells via Nrf2 inhibition background and purpose: non-small-cell lung cancer (NSCLC) accounts for up to, vol 176, p 2079. <https://doi.org/10.1111/bph.14652>
- Chihomvu P, Ganesan A, Gibbons S, Woollard K, Hayes MA (2024) Phytochemicals in drug discovery—a confluence of tradition and innovation. *Int J Mol Sci* 25(16):8792. <https://doi.org/10.3390/ijms25168792>
- Choi JY, Hong WG, Cho JH, Kim EM, Kim J, Jung C-H, Hwang S-G, Um H-D, Park JK (2015) Podophyllotoxin acetate triggers anticancer effects against non-small cell lung cancer cells by promoting cell death via cell cycle arrest, ER stress and autophagy. *Int J Oncol* 47(4):1257–1265
- Chunarkar-Patil P, Kaleem M, Mishra R, Ray S, Ahmad A, Verma D, Bhayye S, Dubey R, Singh HN, Kumar S (2024) Anticancer drug discovery based on natural products: from computational approaches to clinical studies. *Biomedicines* 12(1) Multidisciplinary Digital Publishing Institute (MDPI). <https://doi.org/10.3390/biomedicines12010201>
- Cragg GM, Pezzuto JM (2016) Natural products as a vital source for the discovery of cancer chemotherapeutic and Chemopreventive agents. *Med Princ Pract* 25(2):41–59. <https://doi.org/10.1159/000443404>
- Crespo ME, Galvez J, Cruz T, Ocete MA, Zarzuelo A (1999) Anti-inflammatory activity of diosmin and hesperidin in rat colitis induced by TNBS. *Planta Med* 65(07):651–653
- Debela DT, Muzazu SGY, Heraro KD, Ndalama MT, Mesele BW, Haile DC, Kitui SK, Manyazewal T (2021) New approaches and procedures for cancer treatment: current perspectives. In: SAGE open medicine, vol 9. SAGE. <https://doi.org/10.1177/20503121211034366>
- Dias MC, Pinto DCGA, Silva AMS (2021) Plant flavonoids: chemical characteristics and biological activity. *Molecules* (Basel, Switzerland) 26(17). <https://doi.org/10.3390/molecules26175377>
- Dihal AA (n.d.) Biomarkers of quercetin-mediated modulation of colon carcinogenesis
- Duan C, Yu M, Xu J, Li BY, Zhao Y, Kankala RK (2023) Overcoming cancer multi-drug resistance (MDR): reasons, mechanisms, nanotherapeutic solutions, and challenges. *Biomed Pharmacother* 162). Elsevier Masson s.r.l. <https://doi.org/10.1016/j.biopha.2023.114643>
- Dung TD, Lin C-H, Binh TV, Hsu H-H, Su C-C, Lin Y-M, Tsai C-H, Tsai F-J, Kuo W-W, Chen L-M (2012a) Diosmin induces cell apoptosis through protein phosphatase 2A activation in HA22T human hepatocellular carcinoma cells and blocks tumour growth in xenografted nude mice. *Food Chem* 132(4):2065–2073
- Dung TD, Day CH, Binh TV, Lin C-H, Hsu H-H, Su C-C, Lin Y-M, Tsai F-J, Kuo W-W, Chen L-M (2012b) PP2A mediates diosmin p53 activation to block HA22T cell proliferation and tumor growth in xenografted nude mice through PI3K–Akt–MDM2 signaling suppression. *Food Chem Toxicol* 50(5):1802–1810
- Dwivedi K, Mandal AK, Afzal O, Altamimi ASA, Sahoo A, Alossaimi MA, Almalki WH, Alzahrani A, Barkat MA, Almeleebia TM, Mir Najib Ullah SN, Rahman M (2023) Emergence of Nano-based formulations for effective delivery of flavonoids against topical infectious disorders. *Gels* 9(8) Multidisciplinary Digital Publishing Institute (MDPI). <https://doi.org/10.3390/gels9080671>
- Efferth T (2017) From ancient herb to modern drug: Artemisia annua and artemisinin for cancer therapy. *Semin Cancer Biol* 46:65–83
- El Omari N, Bakrim S, Bakha M, Lorenzo JM, Rebezov M, Shariati MA, Aboulaghra S, Balahbib A, Khayrullin M, Bouyahya A (2021) Natural bioactive compounds targeting epigenetic pathways in cancer: A review on alkaloids, terpenoids, quinones, and isothiocyanates. *Nutrients* 13(11) MDPI. <https://doi.org/10.3390/nu13113714>
- Elango R, Athinayanan J, Subbarayan VP, Lei DKY, Alshatwi AA (2018) Hesperetin induces an apoptosis-triggered extrinsic pathway and a p53-independent pathway in human lung cancer H522 cells. *J Asian Nat Prod Res* 20(6):559–569
- Elumalai K, Srinivasan S, Shanmugam A (2024) Review of the efficacy of nanoparticle-based drug delivery systems for cancer treatment. *Biomed Technol* 5:109–122). KeAi Communications Co. <https://doi.org/10.1016/j.bmt.2023.09.001>
- Eraslan G, Sarica ZS, Bayram LÇ, Tekeli MY, Kanbur M, Karabacak M (2017) The effects of diosmin on aflatoxin-induced liver and kidney damage. *Environ Sci Pollut Res* 24(36):27931–27941

- Falcone Ferreyra ML, Rius SP, Casati P (2012) Flavonoids: biosynthesis, biological functions, and biotechnological applications. *Front Plant Sci* 3:222. <https://doi.org/10.3389/fpls.2012.00222>
- Farhan M, Rizvi A, Aatif M, Ahmad A (2023) Current understanding of flavonoids in cancer therapy and prevention. *Metabolites* 13(4) MDPI. <https://doi.org/10.3390/metabo13040481>
- Femia AP, Caderni G, Ianni M, Salvadori M, Schijlen E, Collins G, Bovy A, Dolara P (2003) Effect of diets fortified with tomatoes or onions with variable quercetin-glycoside content on azoxymethane-induced aberrant crypt foci in the colon of rats. *Eur J Nutr* 42(6):346–352. <https://doi.org/10.1007/s00394-003-0431-5>
- Garcia-Maceira P, Mateo J (2009) Silibinin inhibits hypoxia-inducible factor-1 $\alpha$  and mTOR/p70S6K/4E-BP1 signalling pathway in human cervical and hepatoma cancer cells: implications for anticancer therapy. *Oncogene* 28(3):313–324
- Ghasemzadeh A, Jaafar HZE, Rahmat A (2015) Optimization protocol for the extraction of 6-gingerol and 6-shogaol from *Zingiber officinale* var. *rubrum* Theilade and improving antioxidant and anticancer activity using response surface methodology. *BMC Complement Altern Med* 15:1–10
- Grube S, Ewald C, Kögler C, Lawson McLean A, Kalff R, Walter J (2018) Achievable central nervous system concentrations of the green tea catechin EGCG induce stress in glioblastoma cells in vitro. *Nutr Cancer* 70(7):1145–1158
- Gupta SC, Kim JH, Prasad S, Aggarwal BB (2010) Regulation of survival, proliferation, invasion, angiogenesis, and metastasis of tumor cells through modulation of inflammatory pathways by nutraceuticals. *Cancer Metastasis Rev* 29(3):405–434. <https://doi.org/10.1007/s10555-010-9235-2>
- Han X, Liu C-F, Gao N, Zhao J, Xu J (2018) RETRACTED: Kaempferol suppresses proliferation but increases apoptosis and autophagy by up-regulating microRNA-340 in human lung cancer cells, vol 108. Elsevier, p 809
- Haque MW, Bose P, Siddique MUM, Sunita P, Lapenna A, Pattanayak SP (2018) Taxifolin binds with LXR ( $\alpha$  &  $\beta$ ) to attenuate DMBA-induced mammary carcinogenesis through mTOR/Maf-1/PTEN pathway. *Biomed Pharmacother* 105:27–36
- Hashem S, Ali TA, Akhtar S, Nisar S, Sageena G, Ali S, Al-Mannai S, Therachiyil L, Mir R, Elfaki I, Mir MM, Jamal F, Masoodi T, Uddin S, Singh M, Haris M, Macha M, Bhat AA (2022) Targeting cancer signaling pathways by natural products: exploring promising anti-cancer agents. *Biomed Pharmacother* 150. Elsevier Masson s.r.l. <https://doi.org/10.1016/j.biopha.2022.113054>
- Hoshyar R, Mollaei H (2017) A comprehensive review on anticancer mechanisms of the main carotenoid of saffron, crocin. *J Pharm Pharmacol* 69(11):1419–1427
- Hou D-X, Kumamoto T (2010) Flavonoids as protein kinase inhibitors for cancer chemoprevention: direct binding and molecular modeling. *Antioxid Redox Signal* 13(5):691–719. <https://doi.org/10.1089/ars.2009.2816>
- Hu Z, Cai B, Wang M, Wen X, Geng A, Hu X, Xue R, Mao Z, Jiang Y, Wan X (2020) Diosmetin enhances the sensitivity of radiotherapy by suppressing homologous recombination in endometrial cancer. *Cell Cycle* 19(22):3115–3126. <https://doi.org/10.1080/15384101.2020.1831257>
- Huwait E, Mobashir M (2022) Potential and therapeutic roles of Diosmin in human diseases. *Biomedicines* 10(5). <https://doi.org/10.3390/biomedicines10051076>
- Iqbal J, Abbasi BA, Mahmood T, Kanwal S, Ali B, Shah SA, Khalil AT (2017) Plant-derived anticancer agents: A green anticancer approach. *Asian Pac J Trop Biomed* 7(12):1129–1150
- Jaradat NA, Al-Ramahi R, Zaid AN, Ayesh OI, Eid AM (2016) Ethnopharmacological survey of herbal remedies used for treatment of various types of cancer and their methods of preparations in the West Bank-Palestine. *BMC Complement Altern Med* 16:1–12
- Jiang H, Zuo J, Li B, Chen R, Luo K, Xiang X, Lu S, Huang C, Liu L, Tang J, Gao F (2023) Drug-induced oxidative stress in cancer treatments: angel or devil? In: *Redox biology*, vol 63, Elsevier B.V. <https://doi.org/10.1016/j.redox.2023.102754>



- Kamran S, Sinniah A, Chik Z, Alshawsh MA (2022) Diosmetin exerts synergistic effects in combination with 5-fluorouracil in colorectal cancer cells. *Biomedicines* 10(3). <https://doi.org/10.3390/biomedicines10030531>
- Karmakar S, Roy Choudhury S, Banik L, N., & K Ray, S. (2011) Molecular mechanisms of anti-cancer action of garlic compounds in neuroblastoma. *Anti-Cancer Agents Med Chem* 11(4): 398–407
- Kciuk M, Yahya EB, Mohamed Ibrahim Mohamed M, Rashid S, Iqbal MO, Kontek R, Abdulsamad MA, Allaq AA (2023) Recent advances in molecular mechanisms of cancer immunotherapy. *Cancers*. MDPI 15(10). <https://doi.org/10.3390/cancers15102721>
- Khan H, Ullah H, Martorell M, Valdes SE, Belwal T, Tejada S, Sureda A, Kamal MA (2021) Flavonoids nanoparticles in cancer: treatment, prevention and clinical prospects. *Semin Cancer Biol* 69:200–211. <https://doi.org/10.1016/j.semcancer.2019.07.023>
- Kilit AC, Köse EO, Imir NG, Aydemir E (2021) Anticancer and antimicrobial activities of diosmin. *Genet Mol Res* 20(1):1–18. <https://doi.org/10.4238/gmr18752>
- Kim Y-H, Lee YJ (2007) TRAIL apoptosis is enhanced by quercetin through Akt dephosphorylation. *J Cell Biochem* 100(4):998–1009. <https://doi.org/10.1002/jcb.21098>
- Kong D, Zhang Y, Yamori T, Duan H, Jin M (2011) Inhibitory activity of flavonoids against class I phosphatidylinositol 3-kinase isoforms. *Molecules (Basel, Switzerland)* 16(6):5159–5167. <https://doi.org/10.3390/molecules16065159>
- Koosha S, Mohamed Z, Sinniah A, Alshawsh MA (n.d.) Investigation into the molecular mechanisms underlying the anti-proliferative and anti-tumorigenesis activities of Diosmetin against HCT-116 human colorectal cancer. 9. <https://doi.org/10.1038/s41598-019-41685-1>
- Kühnau J (1976) The flavonoids. A class of semi-essential food components: their role in human nutrition. *World Rev Nutr Diet* 24:117–191
- Kumar S, Swamy N, Tuli HS, Rani S, Garg A, Mishra D, Abdulabbas HS, Sandhu SS (2023) Myricetin: a potential plant-derived anticancer bioactive compound—an updated overview. *Naunyn Schmiedeberg's Arch Pharmacol* 396(10):2179–2196
- Kwon KH, Murakami A, Tanaka T, Ohigashi H (2005) Dietary rutin, but not its aglycone quercetin, ameliorates dextran sulfate sodium-induced experimental colitis in mice: attenuation of pro-inflammatory gene expression. *Biochem Pharmacol* 69(3):395–406. <https://doi.org/10.1016/j.bcp.2004.10.015>
- Lee I-C, Choi BY (2016) Withaferin-A—a natural anticancer agent with pleiotropic mechanisms of action. *Int J Mol Sci* 17(3):290
- Lewinska A, Siwak J, Rzesutek I, Wnuk M (2015) Diosmin induces genotoxicity and apoptosis in DU145 prostate cancer cell line. *Toxicol In Vitro* 29(3):417–425
- Lewinska A, Adamczyk-Grochala J, Kwasniewicz E, Deręgowska A, Wnuk M (2017) Diosmin-induced senescence, apoptosis and autophagy in breast cancer cells of different p53 status and ERK activity. *Toxicol Lett* 265:117–130. <https://doi.org/10.1016/j.toxlet.2016.11.018>. Epub 2016 Nov 24. PMID: 27890807
- Li C, Du GH (2018) Diosmin. *Natural Small Mol Drugs Plants* 9(3):65–70. [https://doi.org/10.1007/978-981-10-8022-7\\_10](https://doi.org/10.1007/978-981-10-8022-7_10)
- Liao Y, Xu Y, Cao M, Huan Y, Zhu L, Jiang Y, Shen W, Zhu G (2018) Luteolin induces apoptosis and autophagy in mouse macrophage ANA-1 cells via the Bcl-2 pathway. *J Immunol Res* 2018(1):4623919
- Lin C-J, Sukarieh R, Pelletier J (2009) Silibinin inhibits translation initiation: implications for anticancer therapy. *Mol Cancer Ther* 8(6):1606–1612
- Ma X, Ning S (2019) Cyanidin-3-glucoside attenuates the angiogenesis of breast cancer via inhibiting STAT3/VEGF pathway. *Phytother Res* 33(1):81–89
- Ma A, Zhang R (2020) Diosmetin inhibits cell proliferation, induces cell apoptosis and cell cycle arrest in liver cancer. *Cancer Manag Res* 12:3537–3546. <https://doi.org/10.2147/CMAR.S240064>

- Ma C, Zhang Y, Tang L, Yang X, Cui W, Han C, Ji W (2018) MicroRNA-1469, a p53-responsive microRNA promotes Genistein induced apoptosis by targeting Mcl1 in human laryngeal cancer cells. *Biomed Pharmacother* 106:665–671
- Magar RT, Sohng JK (2020) A review on structure, modifications and structure-activity relation of quercetin and its derivatives. *J Microbiol Biotechnol* 30(1):11–20. <https://doi.org/10.4014/jmb.1907.07003>
- Management C, Zhang R (2020) Diosmetin inhibits cell proliferation, induces cell apoptosis and cell cycle arrest in liver. *Cancer* 12:3537–3546
- Martínez Conesa C, Vicente Ortega V, Yáñez Gascón MJ, Alcaraz Baños M, Canteras Jordana M, Benavente-García O, Castillo J (2005) Treatment of metastatic melanoma B16F10 by the flavonoids tangeretin, rutin, and diosmin. *J Agric Food Chem* 53(17):6791–6797
- Martínez C, Vicente V, Yáñez J, Alcaraz M, Castells Mora MT, Canteras M, Benavente-García García O, Castillo J (2005) The effect of the flavonoid diosmin, grape seed extract and red wine on the pulmonary metastatic B16F10 melanoma. *Histol Histopathol*
- Mbemi, A., Khanna, S., Njiki, S., Yedjou, C. G., & Tchounwou, P. B. (2020). Impact of gene–environment interactions on cancer development. *Intl J Environ Res Pub Health*. MDPI AG<https://doi.org/10.3390/ijerph17218089>, 17 21 1–15
- Min Y-D, Choi C-H, Bark H, Son H-Y, Park H-H, Lee S, Park J-W, Park E-K, Shin H-I, Kim S-H (2007) Quercetin inhibits expression of inflammatory cytokines through attenuation of NF-kappaB and p38 MAPK in HMC-1 human mast cell line. *Inflammat Res* 56(5):210–215. <https://doi.org/10.1007/s00011-007-6172-9>
- Nagaprashantha LD, Vatsyayan R, Singhal J, Fast S, Roby R, Awasthi S, Singhal SS (2011) Anti-cancer effects of novel flavonoid vicenin-2 as a single agent and in synergistic combination with docetaxel in prostate cancer. *Biochem Pharmacol* 82(9):1100–1109. <https://doi.org/10.1016/j.bcp.2011.07.078>
- Nam N-H (2006) Naturally occurring NF-kappaB inhibitors. *Mini Rev Med Chem* 6(8):945–951. <https://doi.org/10.2174/138955706777934937>
- Ning R, Chen G, Fang R, Zhang Y, Zhao W, Qian F (2021) Diosmetin inhibits cell proliferation and promotes apoptosis through STAT3/c-Myc signaling pathway in human osteosarcoma cells. *Biol Res* 54(1):40. <https://doi.org/10.1186/s40659-021-00363-1>
- Oak C, Khalifa OA, Isali I, Bhaskaran N, Walker E, Shukla S (2018) Diosmetin suppresses human prostate cancer cell proliferation through the induction of apoptosis and cell cycle arrest. *Int J Oncol* 53(2):835–843. <https://doi.org/10.3892/ijo.2018.4407>
- Osman NHA, Said UZ, El-Waseef AM, Ahmed ESA (2015) Luteolin supplementation adjacent to aspirin treatment reduced dimethylhydrazine-induced experimental colon carcinogenesis in rats. *Tumour Biol* 36:1179–1190
- Ozbezy U, Attar R, Romero MA, Alhewairini SS, Afshar B, Sabitaliyevich UY, Hanna-Wakim L, Ozcelik B, Farooqi AA (2019) Apigenin as an effective anticancer natural product: spotlight on TRAIL, WNT/β-catenin, JAK-STAT pathways, and microRNAs. *J Cell Biochem* 120(2):1060–1067
- Pahari P, Saikia UP, Das TP, Damodaran C, Rohr J (2016) Synthesis of Psoralidin derivatives and their anticancer activity: first synthesis of Lespeflorin II. *Tetrahedron* 72(23):3324–3334. <https://doi.org/10.1016/j.tet.2016.04.066>
- Panche AN, Diwan AD, Chandra SR (2016) Flavonoids: an overview. *J Nutr Sci* 5:e47. <https://doi.org/10.1017/jns.2016.41>
- Park JH, Pyun WY, Park HH (2020) Cancer metabolism: phenotype, signaling and therapeutic targets. *Cells* 9(10):1–31. <https://doi.org/10.3390/cells9102308>
- Perkins ND (2007) Integrating cell-signalling pathways with NF-κB and IKK function. *Nat Rev Mol Cell Biol* 8(1):49–62. <https://doi.org/10.1038/nrm2083>
- Perumal S, Langeswaran K, Selvaraj J, Ponnulakshmi R, Shyamaladevi B, Balasubramanian MP (2018) Effect of diosmin on apoptotic signaling molecules in N-nitrosodiethylamine-induced hepatocellular carcinoma in experimental rats. *Mol Cell Biochem* 449(1):27–37

- Rabizadeh F, Mirian MS, Doosti R, Kiani-Anbouhi R, Eftekhari E (2022) Phytochemical classification of medicinal plants used in the treatment of kidney disease based on traditional Persian medicine. In: Evidence-based complementary and alternative medicine, vol 2022. Hindawi Limited. <https://doi.org/10.1155/2022/8022599>
- Rajasekar M, Suresh K, Sivakumar K (2016) Diosmin induce apoptosis through modulation of STAT-3 signaling in 7, 12 dimethylbenz (a) anthracene induced hamster buccal pouch carcinogenesis. *Biomed Pharmacother* 83:1064–1070
- Ramelet AA (2011) Veno-active drugs
- Rastogi N, Duggal S, Singh SK, Porwal K, Srivastava VK, Maurya R, Bhatt MLB, Mishra DP (2015a) Proteasome inhibition mediates p53 reactivation and anti-cancer activity of 6-gingerol in cervical cancer cells. *Oncotarget* 6(41):43310
- Rastogi N, Duggal S, Singh SK, Porwal K, Srivastava VK, Maurya R, Bhatt MLB, Mishra DP (2015b) Proteasome inhibition mediates p53 reactivation and anti-cancer activity of 6-gingerol in cervical cancer cells. *Oncotarget* 6(41):43310
- Roy T, Boateng ST, Uddin MB, Banang-Mbeumi S, Yadav RK, Bock CR, Folahan JT, Siwe-Noundou X, Walker AL, King JA, Buerger C, Huang S, Chamcheu JC (2023) The PI3K-Akt-mTOR and associated signaling pathways as molecular drivers of immune-mediated inflammatory skin diseases: update on therapeutic strategy using natural and synthetic compounds. *Cells* 12(12) MDPI. <https://doi.org/10.3390/cells12121671>
- Sahu N, Soni D, Chandrashekhar B, Satpute DB, Saravanadevi S, Sarangi BK, Pandey RA (2016) Synthesis of silver nanoparticles using flavonoids: hesperidin, naringin and diosmin, and their antibacterial effects and cytotoxicity. *Int Nano Lett* 6(3):173–181
- Schneider G, Krämer OH (2011) NFκB/p53 crosstalk-a promising new therapeutic target. *Biochim Biophys Acta* 1815(1):90–103. <https://doi.org/10.1016/j.bbcan.2010.10.003>
- Shalabi M, Khilo K, Zakaria MM, Elsebaei MG, Abdo W, Awadin W (2015) Anticancer activity of Aloe vera and Calligonum comosum extracts separately on hepatocellular carcinoma cells. *Asian Pac J Trop Biomed* 5(5):375–381
- Sharma T, Singh D, Mahapatra A, Mohapatra P, Sahoo S, Sahoo SK (2022) Advancements in clinical translation of flavonoid nanoparticles for cancer treatment. In: *OpenNano*, vol 8. Elsevier Inc., p 100074. <https://doi.org/10.1016/j.onano.2022.100074>
- Shen N, Wang T, Gan Q, Liu S, Wang L, Jin B (2022) Plant flavonoids: classification, distribution, biosynthesis, and antioxidant activity. *Food Chem* 383:132531. <https://doi.org/10.1016/j.foodchem.2022.132531>
- Sheoran S, Arora S, Pilli G (2022a) Lipid based nanoparticles For treatment of cancer. *Heliyon* e09403:e09403
- Sheoran S, Arora S, Samsonraj R, Govindaiah P, vuree, S. (2022b) Lipid-based nanoparticles for treatment of cancer. *Heliyon* 8(5):e09403. <https://doi.org/10.1016/j.heliyon.2022.e09403>
- Sheoran, S., Arora, S., Basu, T., Negi, S., Subbarao, N., Kumar, A., Singh, H., Prabhu, D., Kumar, A., Kumar, N., & Vuree, S. (2023a). In silico analysis of Diosmetin as an effective chemopreventive agent against prostate cancer : molecular docking , validation , dynamic simulation and pharmacokinetic prediction-based studies. *J Biomol Struct Dyn*, 0(0), 1–13. <https://doi.org/10.1080/07391102.2023.2250451>
- Sheoran S, Arora S, Basu T, Subbarao N, Upadhyay AK, Vuree S (2023b) Abstract 5342: assessment of polyphenolic secondary metabolites and small molecules against the xenobiotic metabolic and cell cycle regulatory proteins in prostate cancer. *Cancer Res* 83(7\_Suppl):5342. <https://doi.org/10.1158/1538-7445.AM2023-5342>
- Sheoran S, Arora S, Singh H, Kumar A, Vuree S (2023c) Characterisation, development and validation of UV spectrophotometric technique for the determination of Diosmetin in bulk and nanoformulations. *Results Chem* 100972. <https://doi.org/10.1016/j.rechem.2023.100972>
- Sheoran S, Arora S, Velingkar A, Pawar SC, Vuree S (2024) Chapter 10 – empowering treatment strategies for pancreatic cancer by employing lipid nanoparticle-driven drug delivery. In: Kesharwani P, Gupta N (eds) *Recent advances in nanocarriers for pancreatic cancer therapy*. Academic Press, pp 239–266. <https://doi.org/10.1016/B978-0-443-19142-8.00016-4>

- Shirai M, Kawai Y, Yamanishi R, Kinoshita T, Chuman H, Terao J (2006) Effect of a conjugated quercetin metabolite, quercetin 3-glucuronide, on lipid hydroperoxide-dependent formation of reactive oxygen species in differentiated PC-12 cells. *Free Radic Res* 40(10):1047–1053. <https://doi.org/10.1080/10715760600794287>
- Song C, Deng S, Hu H, Zheng Z, Shen B, Wu X, Huang M, Wang J, Wang Z (2022) Diosmetin affects gene expression on human lung adenocarcinoma cells. *J Oncol* 2022:5482148. <https://doi.org/10.1155/2022/5482148>
- Surichan S, Arroo RR, Tsatsakis AM, Androutsopoulos VP (2018) Tangeretin inhibits the proliferation of human breast cancer cells via CYP1A1/CYP1B1 enzyme induction and CYP1A1/CYP1B1-mediated metabolism to the product 4'-hydroxy tangeretin. *Toxicol In Vitro* 50: 274–284
- Suzuki R, Kohno H, Sugie S, Sasaki K, Yoshimura T, Wada K, Tanaka T (2004) Preventive effects of extract of leaves of ginkgo (*Ginkgo biloba*) and its component bilobalide on azoxymethane-induced colonic aberrant crypt foci in rats. *Cancer Lett* 210(2):159–169
- Tahir M, Rehman MU, Lateef A, Khan AQ, Khan R, Qamar W, O'Hamiza O, Ali F, Hasan SK, Sultana S (2013) Diosmin abrogates chemically induced hepatocarcinogenesis via alleviation of oxidative stress, hyperproliferative and inflammatory markers in murine model. *Toxicol Lett* 220(3):205–218
- Talib WH, Alsayed AR, Barakat M, Abu-Taha MI, Mahmood AI (2021) Targeting drug chemoresistance in cancer using natural products. *Biomedicines*. MDPI 9(10). <https://doi.org/10.3390/biomedicines9101353>
- Tanaka T, Makita H, Kawabata K, Mori H, Kakumoto M, Satoh K, Hara A, Sumida T, Fukutani K, Tanaka T (1997a) Modulation of N-methyl-N-aminonitrosamine-induced rat oesophageal tumorigenesis by dietary feeding of diosmin and hesperidin, both alone and in combination. *Carcinogenesis* 18(4):761–769
- Tanaka T, Makita H, Kawabata K, Mori H, Kakumoto M, Satoh K, Hara A, Sumida T, Tanaka T, Ogawa H (1997b) Chemoprevention of azoxymethane-induced rat colon carcinogenesis by the naturally occurring flavonoids, diosmin and hesperidin. *Carcinogenesis* 18(5):957–965
- Teekaraman D, Elayapillai SP, Viswanathan MP, Jagadeesan A (2019) Quercetin inhibits human metastatic ovarian cancer cell growth and modulates components of the intrinsic apoptotic pathway in PA-1 cell line. *Chem Biol Interact* 300:91–100
- Thangapazham RL, Sharad S, Maheshwari RK (2016) Phytochemicals in wound healing. *Adv Wound Care* 5(5):230–241
- Thesis D, To S, Partial IN, For F, Degree THE, Sheoran S (2019) Antioxidants and antimicrobial activity of some
- Vargas AJ, Sittadjody S, Thangasamy T, Mendoza EE, Limesand KH, Burd R (2011) Exploiting tyrosinase expression and activity in melanocytic tumors: quercetin and the central role of p53. *Integr Cancer Ther* 10(4):328–340. <https://doi.org/10.1177/1534735410391661>
- Ververidis F, Trantas E, Douglas C, Vollmer G, Kretzschmar G, Panopoulos N (2007) Biotechnology of flavonoids and other phenylpropanoid-derived natural products. Part I: chemical diversity, impacts on plant biology and human health. *Biotechnol J Healthc Nutr Technol* 2(10): 1214–1234
- Volate SR, Davenport DM, Muga SJ, Wargovich MJ (2005) Modulation of aberrant crypt foci and apoptosis by dietary herbal supplements (quercetin, curcumin, silymarin, ginseng and rutin). *Carcinogenesis* 26(8):1450–1456. <https://doi.org/10.1093/carcin/bgi089>
- Walle T, Browning AM, Steed LL, Reed SG, Walle UK (2005) Flavonoid glucosides are hydrolyzed and thus activated in the oral cavity in humans. *J Nutr* 135(1):48–52. <https://doi.org/10.1093/jn/135.1.48>
- Wang K, Liu R, Li J, Mao J, Lei Y, Wu J, Zeng J, Zhang T, Wu H, Chen L, Huang C, Wei Y (2011) Quercetin induces protective autophagy in gastric cancer cells: involvement of Akt-mTOR- and hypoxia-induced factor 1 $\alpha$ -mediated signaling. *Autophagy* 7(9):966–978. <https://doi.org/10.4161/auto.7.9.15863>

- Wang, H., Shu, L., Su, Z., Fuentes, F., Lee, J.-H., & Kong, A.-N. T. (n.d.). Plants against cancer: A review on natural phytochemicals in preventing and treating cancers and their Druggability
- Woo H-H, Ryong Jeong B, Hawes MC (n.d.) Flavonoids: from cell cycle regulation to biotechnology. <https://doi.org/10.1007/s10529-005-1521-7>
- Xiao X, Jiang K, Xu Y, Peng H, Wang Z, Liu S, Zhang G (2019) (–)-Epigallocatechin-3-gallate induces cell apoptosis in chronic myeloid leukaemia by regulating Bcr/Abl-mediated p38-MAPK/JNK and JAK 2/STAT 3/AKT signalling pathways. *Clin Exp Pharmacol Physiol* 46(2):126–136
- Xiong M, Wang L, Yu H, Han H, Mao D, Chen J, Zeng Y, He N, Liu Z, Wang Z (2016) Ginkgetin exerts growth inhibitory and apoptotic effects on osteosarcoma cells through inhibition of STAT3 and activation of caspase-3/9. *Oncol Rep* 35(2):1034–1040
- Xu Z, Yan Y, Xiao L, Dai S, Zeng S, Qian L, Wang L, Yang X, Xiao Y, Gong Z (2017) Radiosensitizing effect of diosmetin on radioresistant lung cancer cells via Akt signaling pathway. *PLoS One* 12(4):e0175977
- Yang Y, Zhang M, Wang Y (2022) The roles of histone modifications in tumorigenesis and associated inhibitors in cancer therapy. *J Nat Cancer Center* 2(4):277–290. Chinese National Cancer Center. <https://doi.org/10.1016/j.jncc.2022.09.002>
- Zhang Y-Y, Huang C-T, Liu S-M, Wang B, Guo J, Bai J-Q, Fan X-J, Jia Y-S (2016) Licochalcone A exerts antitumor activity in bladder cancer cell lines and mice models. *Trop J Pharm Res* 15(6):1151–1157
- Zhao F, Hong X, Li D, Wei Z, Ci X, Zhang S (2021) Diosmetin induces apoptosis in ovarian cancer cells by activating reactive oxygen species and inhibiting the Nrf2 pathway. *Med Oncol* 38(5): 54. <https://doi.org/10.1007/s12032-021-01501-1>
- Zheng D, Wang Y, Zhang D, Liu Z, Duan C, Jia L, Wang F, Liu Y, Liu G, Hao L (2011) In vitro antitumor activity of silybin nanosuspension in PC-3 cells. *Cancer Lett* 307(2):158–164
- Zhou X, Zhu Y, Rao Q, Zhang X (2018) Galangin induced antitumor effects in human kidney tumor cells mediated via mitochondrial mediated apoptosis, inhibition of cell migration and invasion and targeting PI3K/ AKT/mTOR signalling pathway. *JBUON* 23(3):795–799